Alkene Functionalization via a Dication Pool Strategy

by

Diana J. Wang

A dissertation submitted in partial fulfillment of

the requirements for the degree of

Doctor of Philosophy

(Chemistry)

at the

UNIVERSITY OF WISCONSIN-MADISON

2023

Date of final oral examination: 2/16/2023

The dissertation is approved by the following members of the Final Oral Committee:

Zachary K. Wickens, Professor, Organic Chemistry
Jennifer M. Schomaker, Professor, Organic Chemistry
Daniel J. Weix, Professor, Organic Chemistry
Heike Hofstetter, Associate Director of Magnetic Resonance Facility

This work is dedicated to people who inspired me to be a better scientist,

and more importantly, a better person.

Abstract

Oxidative alkene functionalization is an attractive transformation to form value-added products by leveraging readily accessible alkene starting materials to rapidly build and diversify molecular complexity. However, these reactions traditionally use high-energy, electrophilic reagents (ex.: iminoiodinanes as nitrene precursors, diazo compounds as carbene precursors, etc.) that place strict limitations on substituents installed on the final product. My thesis work describes a distinct "dication pool strategy" that couples abundant, unactivated alkenes and diverse nucleophiles via electrochemically generated dicationics. Key to this strategy is the decoupling of alkene activation and substitution which enables use of a wide variety of oxidatively sensitive nucleophiles as demonstrated in the synthesis of *N*-alkyl aziridines, polysubstituted cyclopropanes, and *(Z)*-allylic alkylamines.

The first section of this work entails an overview of recent developments on sulfonium electrophiles derived from unactivated alkenes (**Chapter 1**). Discussion will focus on recent advances in the synthesis of these sulfonium electrophiles and their use in various alkene functionalization reactions.

The second part of this work will describe synthetic methodologies developed via the "dication pool" strategy, focusing specifically on alkene aziridination (**Chapter 2**), allylic amination (**Chapter 3**), and cyclopropanation (**Chapter 4**).

Acknowledgements

Graduate school really is a time that pushes you to be the best that you can be but will also show you the worser sides of yourself in the face of continued challenge. The highs are excitingly high, and the lows are gruelingly low. And while that discomfort is necessary and welcome for growth and learning, I am grateful for all the support that got me through.

To my loving family who is always there for me unconditionally. To my mom, who is my most enthusiastic cheerleader, always believing in me, pushing me forward, and keeping my sights eagerly on the bright future ahead. To my dad, who taught me how to be there for people by always being there for me, even if that means dropping everything in the moment. To my sister, Jenny, who keeps me grounded with both light-hearted, silly banter and much-needed tough love.

To my friends that got me through. To Marco, who's been with me every step of the way. I always marvel at your capacity to love and be kind to everyone around you. I'm so happy to have watched you be your true authentic self. Thank you for the meandering weekend walks, the early mornings at the gym, the chemistry napkin doodles at McDonalds, and so many hours of belting harmonies on roadtrip karoke sessions. To Seoyoung, who has been my role model these five years. Thank you so much for taking care of me and listening to me. You let me be myself and accepted me completely for who I am. Thank you for the hour long conversations over boba, after seminars, in front of Shain elevators, and generally anywhere we happened to meet. I'm so happy we got to jam, and I'm excited for more jam sessions in the future! And lastly, to Joe, who always made me laugh with your dark, biting humor. Underneath the sarcasm was a heart of gold that cared about his friends over everything.

To all members of the Wickens group, both past and present, thank you for pushing me and expediting my growth. Thank you especially to earlier members who were pivotal in building up a group with growth at its core and values that we all firmly stood behind. I'm excited to see where the group goes! To Zach, who took a chance on me and took me into his lab at such a momentous time. You've done so much to facilitate my growth and have fundamentally shaped who I am as both a scientist and a person. From you, I've learned to lead by positivity and excitement and to always let curiosity get the better of

you. I've learned to never be satisfied and to keep pushing on both your strengths and weaknesses as you strive to be better than the day before. Thank you for being my mentor and for choosing to be my mentor for life. I'll continue working hard to make you proud.

I would like to thank my committee members, Jen and Dan, who've always taken the time to offer their insight and suggestions, pushing me to continuously improve at every graduate school milestone. Lastly, to Heike who's been such a strong source of support and an amazingly patient mentor that teaches you by meeting you where you're at and lifting you up. She in turn has taught me the joys of teaching.

Table of Contents

Chapter 4

Diastereoselective Synthesis of Cyclopropanes from Carbon Pronucleophiles and Alkenes

Appendix A

Supporting Information for Chapter 2 (Aziridine synthesis by coupling amines and alkenes via an electrogenerated dication)

Appendix B

Supporting Information for Chapter 3 (Electrochemical Synthesis of Allylic Amines from Terminal Alkenes and Secondary Amines)

Appendix C

Supporting Information for Chapter 4 (Diastereoselective Synthesis of Cyclopropanes from Carbon Pronucleophiles and Alkenes)

Abbreviations and Acronyms

Aq	aqueous
Ar	aryl
Bn	benzyl
Boc	*tert*-butyl carbamate
Cp*	1,2,3,4,5-pentamethylcyclopentadiene
CV	cyclic voltammetry
Cy	cyclohexyl
d.r.	diastereomeric ratio
dba	Bis(dibenzylideneacetone)
DBU	1,8-Diazabicycl[5.4.0]undec-7-ene
DCM	dichloromethane
DIPEA	N,N-Diisopropylethylamine
DMF	dimethyl formamide
DMSO	dimethyl sulfoxide
EtOAc	ethyl acetate
EtOH	ethanol
EWG	electron withdrawing group
GC	gas chromatography
HAT	hydrogen atom transfer
HFIP	hexafluoroisopropanol
Me	methyl
MeCN	acetonitrile
MeOH	methanol
Naph	Naphthyl group

NBS	*N*-bromosuccinimide
n-Bu_4	tetrabutyl
n-Hex	hexyl
NMO	N-methylmorpholine N-oxide
n-Oct_4	tetraoctyl
NPhth	phthalimide
n-Pr	propyl
Nuc	nucleophile
OAc	acetate
o-tol	ortho-toluene
Ph	phenyl
PTFE	polytetrafluoroethylene
RVC	reticulated vitreous carbon
S_N2	biomolecular nucleophilic substitution
TBAB	tetrabutylammonium bromide
*t*Bu	*tert*-butyl
TEA	triethylamine
Tf	triflyl
TFA	trifluoroacetic acid
TFAA	trifluoroacetic anhydride
THF	tetrahydrofuran
TLC	thin layer chromatography
Ts	toluenesulfonamide
TT	thianthrene
TT=O	thianthrene-*S*-oxide

Chapter 1: Sulfonium Electrophiles from Unactivated Alkenes

1.1 Introduction

Oxidative alkene functionalization is an attractive approach to form value-added products from readily accessible alkene starting materials to rapidly build and diversify molecular complexity. However, due to the nucleophilicity of the alkene π-bond, many alkene functionalization reactions rely on use of electrophilic reagents, poised as both oxidant and group transfer reagent, for necessary polarity matching (Figure 1.1). (For example, iminoiodinanes are commonly used in concert with transition metals to form electrophilic metal nitrenoids used for alkene aziridination[1,2] and allylic amination[3]. Similarly, diazo compounds decompose with transition metals to form electrophilic metal carbenoids used for alkene cyclopropanation.[4]) However, the requisite balance of stability and reactivity of these electrophilic reagents often requires electron-withdrawing groups, limits the diversity of substituents that can be installed on the desired product.[4,5]

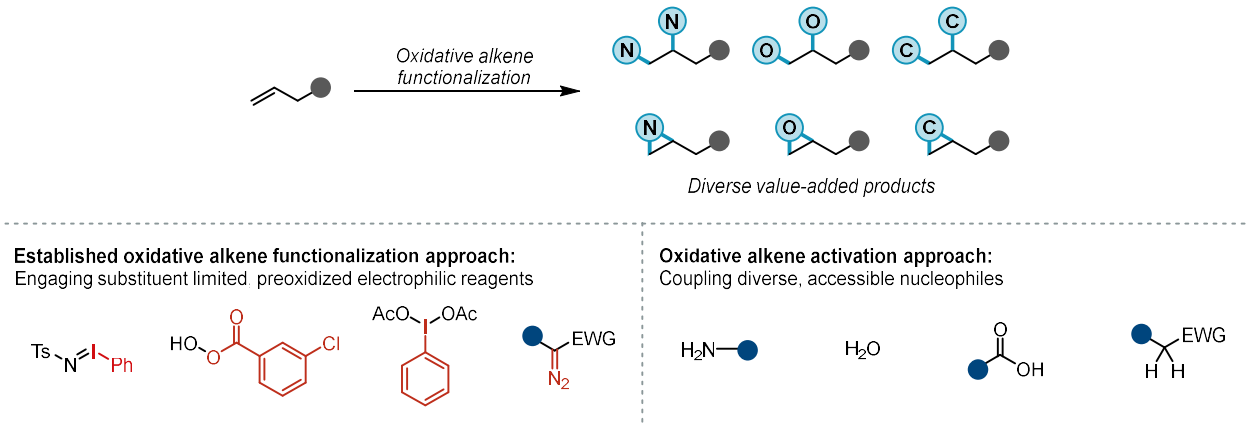

Figure 1.1. Comparison between different approaches to oxidative alkene functionalization.

Alternatively, an oxidative alkene activation strategy that transform alkenes into dielectrophiles with the desired downstream reactivity could engage the wide pool of innate nucleophiles for a more modular approach to alkene functionalization. Dihalogenation is a well-established reaction for transforming alkenes into dielectrophiles. However, due to their propensity to undergo elimination reactions, vicinal dihalides are not viable for coupling with basic nucleophiles.[6] The appeal of this alkene

activation strategy holds strong however, with many protocols pivoting towards a roundabout sequence anchoring on initial alkene oxidation with robust epoxidation/dihydroxylation reactions that then rely on iterative activation and substitution steps with nucleophiles to achieve the overall alkene functionalization.[7,8] This multistep, synthetic workaround exists in part due to the lack of a general method to convert alkenes into a vicinal dielectrophile capable of productive iterative engagement with nucleophiles.

1.2 Advances in the Synthesis of Sulfonium Electrophiles from Unactivated Alkenes

Alkenylsulfonium salts stand out as a class of sulfonium electrophiles that have been extensively studied for reactivity with diverse nucleophiles.[9,10] However, the lull in their general adaptation in synthetic application can be in part due to limitations of alkenyl substituents on the sulfonium salt, stemming from lack of generality in their synthetic preparations. The handful of viable substituents derive from different starting materials and strategies that are largely classified into 3 reaction classes: 1) methylation/phenylation of vinyl sulfides[11–13], 2) sulfide substitution of vicinal dielectrophiles followed by subsequent elimination,[14,15] and 3) an interrupted Pummerer reaction (featuring in-situ sulfoxide activation with anhydride (commonly Tf_2O or TFAA)) followed by displacement with alkenes[16,17] (Figure 1.2). Of the three, the interrupted Pummerer reaction is an attractive approach to engage alkene as a broader class of starting materials, but due to the need for a stabilizing group proximal to the carbocation generated upon attack of the alkene to the activated sulfoxide, this reaction is limited to only styrenyl substrates. Vicinal dielectrophiles are also accessible via alkene starting materials and can be paired with sulfide displacement as seen with the use of Br_2/Me_2S with styrene substrates to form α-aryl vinylsulfonium salts.[15,18] But unfortunately, this method doesn't extend well to non-styrene alkenes presumably due to uncontrolled elimination from bromoethylsulfonium intermediates when other acidic protons are present.

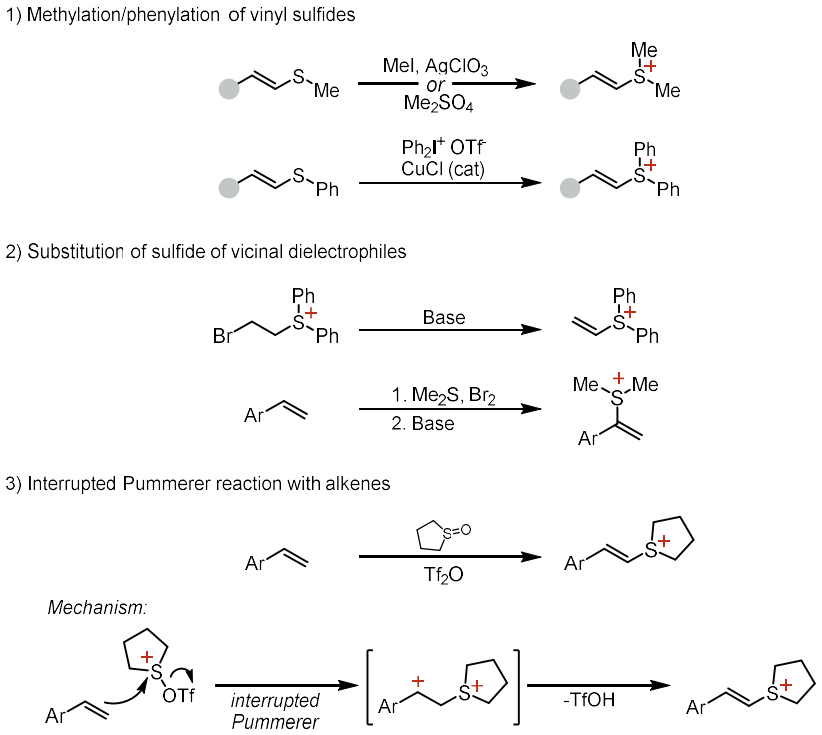

Figure 1.2. Main reaction classes for the formation of alkenylsulfonium salts.

Recently, there has been a renewed interest in alkenylsulfonium salts due to method developments greatly extended their synthesis to engage unactivated alkenes. Key to this synthetic advancement is the unique structure and reactivity of thianthrene. Initial insight of this reactivity came from Shine and co-workers who extensively studied the reactivity of thianthrene radical cation salts with various functional groups. Between 1979–1999, they found that exposure of thianthrene radical cation to various unactivated alkenes formed unexpected alkene-thianthrene adducts (which they termed *mono* and *bis* adducts) (Scheme 1.1).[19–21] Importantly, these adducts underwent facile elimination in the presence of base to form alkenylthianthrenium salts. While few substitution studies were done with these adducts,[22] the full synthetic potential of this system for alkene functionalization was not explored.

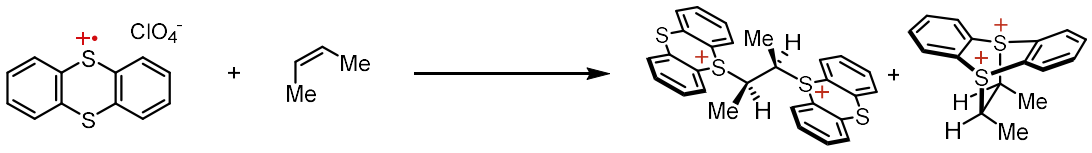

Scheme 1.1. Shine's study of stereospecific adduct formation with cis-2-butene and thianthrene radical cation.

The key linking this discovery to expansion of alkenylsulfonium synthesis to unactivated alkenes was the recognition that adduct formation was occurring through unique mechanisms allowing stereospecific retention of the alkene stereochemistry.[21] This led to Shine's initial proposal of a concerted cycloaddition between alkene and thianthrene radical cation for formation of *mono* adduct. Ritter[23] and Wickens[6] later proposed thianthrenium dication (generated via heterolytic cleavage of TT^{+}-TFA or disproportionation of thianthrene radical cation, respectively) as the actual intermediate involved in an inverse-electron-demand hetero-Diels Alder cycloaddition with alkene based on CV and time course studies (see Chapter 2 for further discussion) (Figure 1.3). The above study also supported sequential thianthrene radical cation addition into alkene for *bis* adduct formation. Crucially, these unique mechanisms enabled by oxidized thianthrene allowed access to dicationic adducts as a versatile means to generate diverse alkenylthianthrenium salts. There was no longer a need for carbocation stabilizing groups requisite by the interrupted Pummerer reaction, thus opening unactivated alkenes as an amenable class for alkenylsulfonium formation.

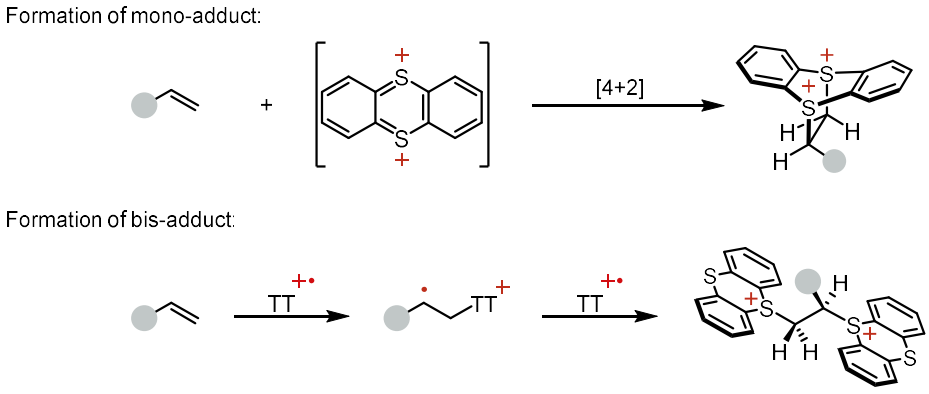

Figure 1.3. Proposed mechanisms for the formation of mono- and bis-adduct

Currently there are two synthetically relevant methods to form these key dicationic adduct intermediates. In 2020, Ritter and coworkers showcased a simple, breakthrough method using in situ activation of thianthrene *S*-oxide with trifluoracetic anhydride, previously used for their site-selective aromatic C(sp^2)–H thianthrenation reaction and adapted towards thianthrenation of olefins (Figure 1.4). This reactivity was unique for activation of thianthrene scaffolds as similar sulfoxides (such as

dibenzothiophene sulfoxide and phenoxathiine-*S*-oxide) failed to give good yields. Formation of both *mono* adduct and subsequent elimination to alkenylthianthrenium occurred in a stereospecific manner. For all terminal alkenes investigated, there was exclusive regioselectivity for formation of the 1,2-disubstituted alkenylthianthrenium products. In addition to the diversely substituted alkenes demonstrated (terminal, internal, tri-substitued), a huge synthetic advantage of this method is the robust functional group tolerance, enabling alkene thianthrenation even for molecularly complex substrates.

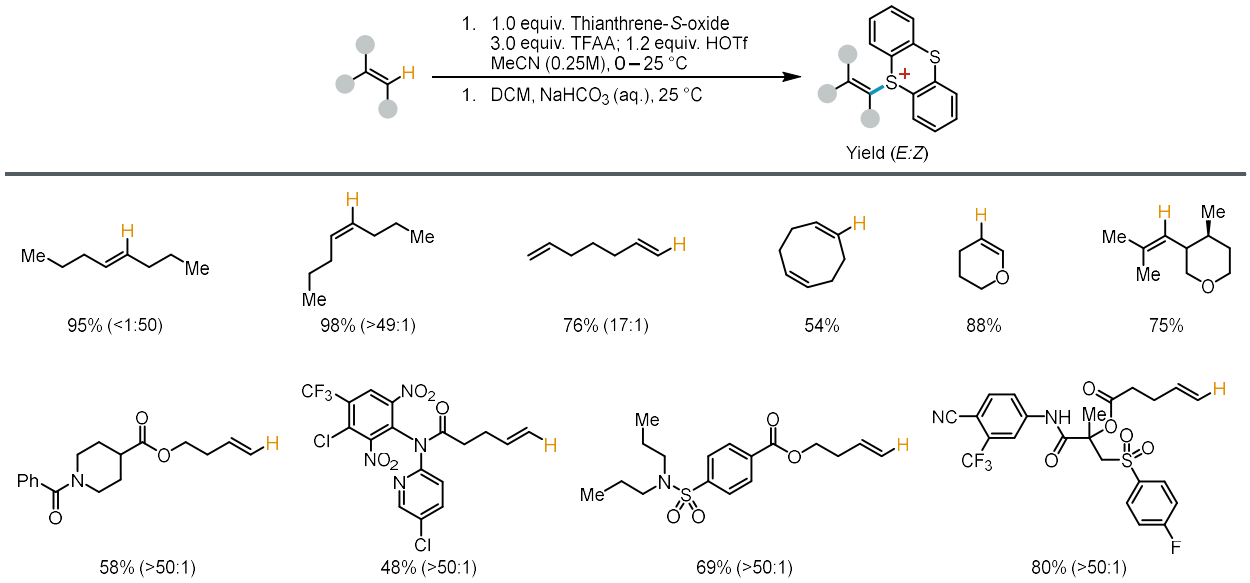

Figure 1.4. Method and scope of Ritter's regio- and stereoselective olefin thianthrenation

The second practical method to generate dicationic alkene-thianthrenium adducts is an electrochemical platform for alkene activation. In 2021, Wickens and coworkers disclosed their "dication pool" strategy (Figure 1.5) (see Chapter 2 for further discussion).[6] This approach uses the mild, anodic oxidation of thianthrene to transform terminal alkenes into dicationic mono- and bis-adduct that pool in solution during electrolysis. As these adducts are metastable in solution, an "ex-cell" strategy (heavily influenced by the work of Yoshida and his "cation pool" strategy) can then be applied wherein electrolysis is terminated before additional reagents are added, triggering addition chemical steps that can occur in the absence of electrochemical current. This strategic decoupling of alkene activation and functionalization is imperative for the use of oxidatively sensitive bases and nucleophiles, and the 1-pot, 2-step process enables the formal coupling of alkenes and diverse nucleophiles. Follow up reports from

the initial disclosure support rapid elimination of adducts to alkenylthianthrenium as the key on-path intermediate for all substitution reactions disclosed so far.

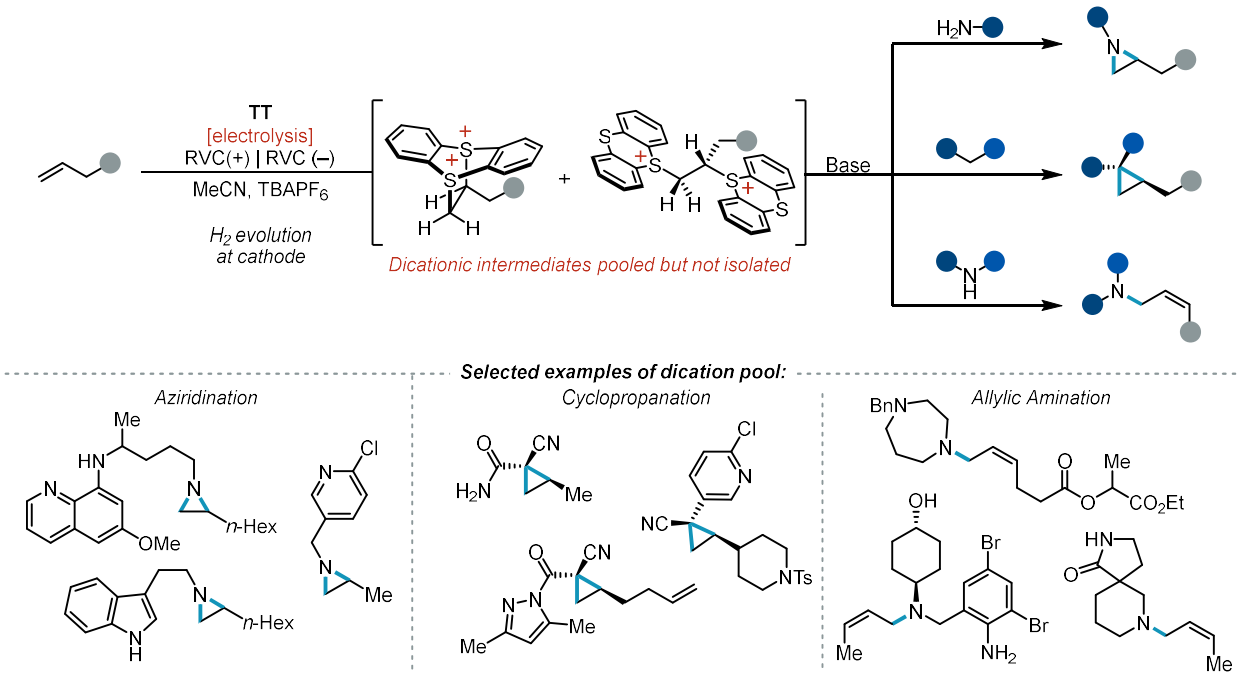

Figure 1.5. Alkene functionalization reactions of the dication pool strategy enabling formal coupling of alkenes and nucleophiles.

The following chapter sections includes recent synthetic applications enabled by these two methods generating sulfonium electrophiles from unactivated alkenes.

1.3 Difunctionalization Reactivity

Oxidative alkene difunctionalization reactions are powerful transformations geared towards the rapid buildup of molecular complexity from simple starting materials. In addition to the variety of carbon bond formations (C–C, C–O, C–N, C–X, etc.) possible with the introduction of different functional groups, product diversity also stems from different connectivity patterns introducing either the same (homodifunctionalization) or two distinct functional groups (heterodifunctionalization) across the carbon–carbon double bond. While many strategies exist for these transformations, there is no general strategy that engages diverse classes of nucleophiles for alkene difunctionalization.

In 2021, Wickens and coworkers first demonstrated the selective reactivity of alkene-thianthrenium adducts as unique vicinal dielectrophiles for alkene difunctionalization (Figure 1.6) (see Chapter 2 for further discussion).[6] Their dication pool strategy enabled the formal coupling of unactivated

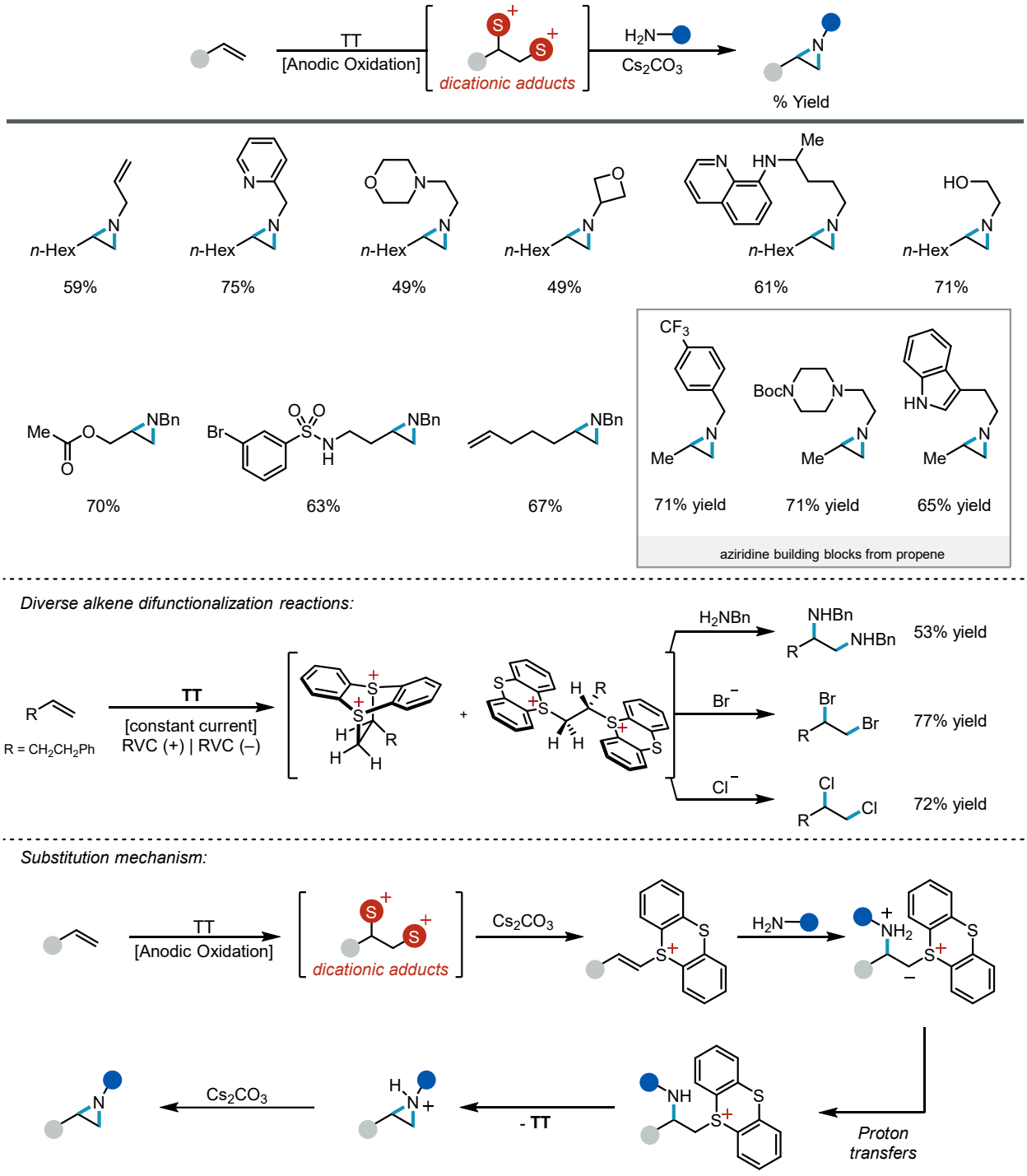

Figure 1.6. Synthesis of *N*-alkyl aziridines via the dication pool strategy.

alkenes and primary amine nucleophiles for the synthesis of *N*-alkyl azirdines. This obviated the need for high energy electrophilic nitrogen reagents traditionally used in concert with transition metals for alkene aziridination and instead leveraged the innate nucleophilicity inherent in the over 1 million commercially available primary amine nucleophiles. As substitution was decoupled from alkene activation, both oxidatively-sensitive amine starting materials and products were safe from anodic decomposition. Even substrates bearing Lewis basic moieties (such as pyridine, morpholine, and piperazine) were demonstrated, despite traditionally being challenging to use with transition metal methodologies. The fact that alkenes are also readily accessible starting materials greatly enhanced the coupling capability of this method. Even propene, an abundant feedstock alkene, could be introduced with a simple balloon to form synthetically attractive aziridine building blocks. In addition, Wickens presented further generality of these thianthrenium adducts, showing their use in a diverse array of other difunctionalization reactions, such as dichlorination, dibromination, and diamination. Time-course study reveals rapid elimination of both mono- and bisaddut to alkenylthianthrenium, which is a productive on-path intermediate to aziridine product. The substitution of primary amine is thus mechanistically rationalized as proceeding via conjugate addition into alkenylsulfonium salts which are regularly used for their reactivity as Michael acceptors. Protonation of the generated sulfur ylide, followed by subsequent intramolecular cyclization, and final deprotonation furnishes the *N*-alkyl aziridine product.

In 2022, Shu and coworkers used alkenylthianthrenium salts to both expand the scope of aziridination and extend substitution reactivity to carbon pronucleophiles for analogous cyclopropanation product (Figure 1.7).[24] In addition to aliphatic primary amines, sulfonamides, carbamates, and amides also funneled to aziridine products. Malononitriles, 1,3-dicarbonyl compounds, and other complex acidic methylenes furnished cyclopropane products with some diastereoselectivity seen maxing at 2:1 d.r. Incredibly, expansion in alkene scope showed that acyclic and cyclic, symmetric internal alkenes as well as styrene starting materials worked for both reactions in efficient yields. Further synthetic practicality of this method was demonstrated by scaling up aziridine and cyclopropane procedures to >1.0 g, and a one-pot sequence starting from alkene was developed. Following deuteration studies, Shu proposed a

mechanism wherein alkenylthianthrenium reversibly forms monoadduct, and site-selective ring-opening by intermolecular attack of either amine or carbon nucleophile and subsequent intramolecular cyclization would afford their 3-membered cyclic products.

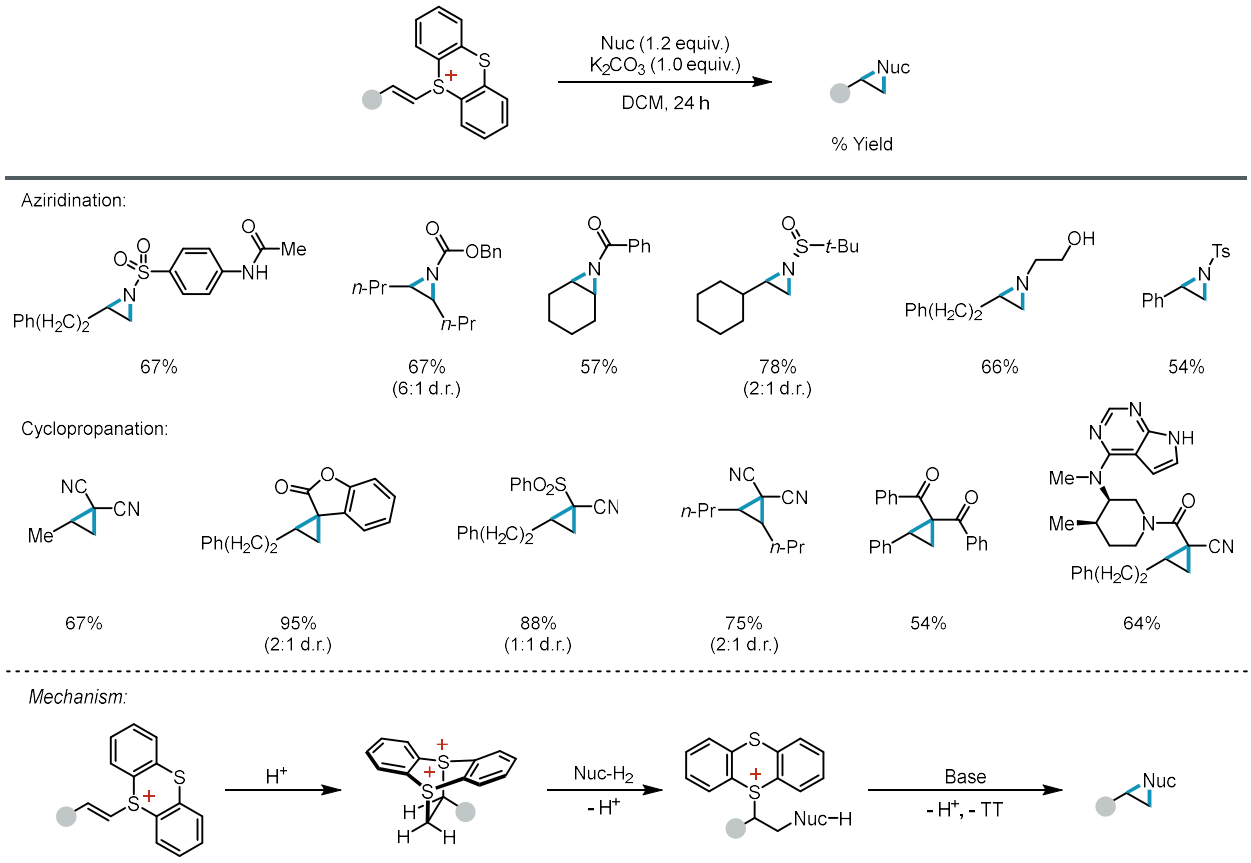

Figure 1.7. Aziridination and cyclopropanation of alkenylthianthrenium salts.

1.4 Alkenylation Reactivity

Alkenes are synthetically versatile functional groups with myriad opportunities for further diversification via robust reactions such as epoxidation, dihydroxylation, metathesis, and beyond.[25] Thus, targeted installation of alkenyl groups into molecules is a strategic endeavor when building molecular complexity. The direct functionalization of unactivated alkenyl C–H bonds represents the most straightforward path to access valuable alkenes from simpler ones, with the Heck reaction being a powerful representation on the utility of this transformation.[26] With general, simple methods now

available to generate alkenyl electrophiles directly from unactivated alkenes via regioselective C(sp^2)–thianthrenation,[6,23] formal olefinic C–H functionalization now expands to include reactivity classic to alkenylsulfoniums, such as oxidative addition of transition metals as well as conjugate addition-elimination sequences enabled by their reactivity as Michael acceptors.

In their 2020 report, Ritter and coworkers initially demonstrated the utility of alkenylthianthrenium salts by tapping into the ability of C(sp^2)–substituted sulfonium salts to serve as electrophiles in transition-metal catalyzed coupling reactions.[23] In addition to precedented nickel-catalyzed Negishi coupling,[17,18] other C–C bond forming reactions were demonstrated by exploiting Sonogashira and Heck reaction conditions. These salts were also coupled with various nucleophiles via ruthenium catalysis for C–Cl, C–Br, and C–SCF_3 bond formation, showcasing opposite regioselectivity to that seen with nucleophiles classically undergoing conjugate addition when engaging alkenylsulfoniums as Michael acceptors.

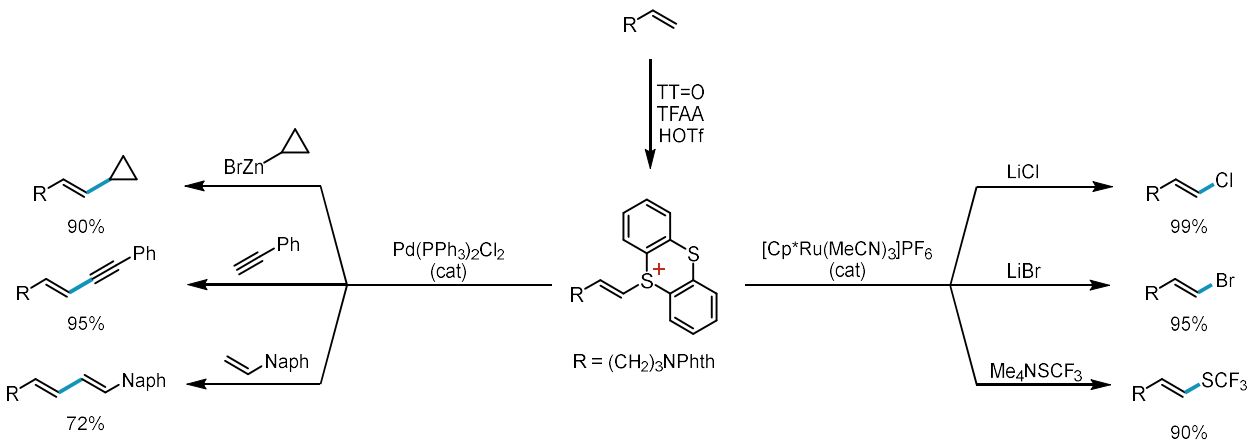

Figure 1.8. Metal-catalyzed alkenylation reactions of alkenylthianthrenium salts.

Later in 2021, Ritter further pushed the practicality of activating unactivated alkenes into potent sulfonium electrophiles by repurposing inexpensive, feedstock ethylene as an effective, electrophilic vinylating reagent (Figure 1.9).[27] Thianthrene *S*-oxide activation with a simple balloon of ethylene afforded ethylene-thianthrene monoadduct on multigram scale (50 mmol), which eliminated to vinylthianthrenium upon basic workup. This salt was precipitated as a bench-stable, crystalline, non-

hygroscopic reagent for easy handling. Unique from other common vinylating reagents, vinylthianthrenium was efficient at the alkenylation of both N-heterocycles (operating as a Michael acceptor for nucleophilic addition) as well as aryl boronic acids (operating as a electrophile for oxidative addition towards Suzuki coupling).

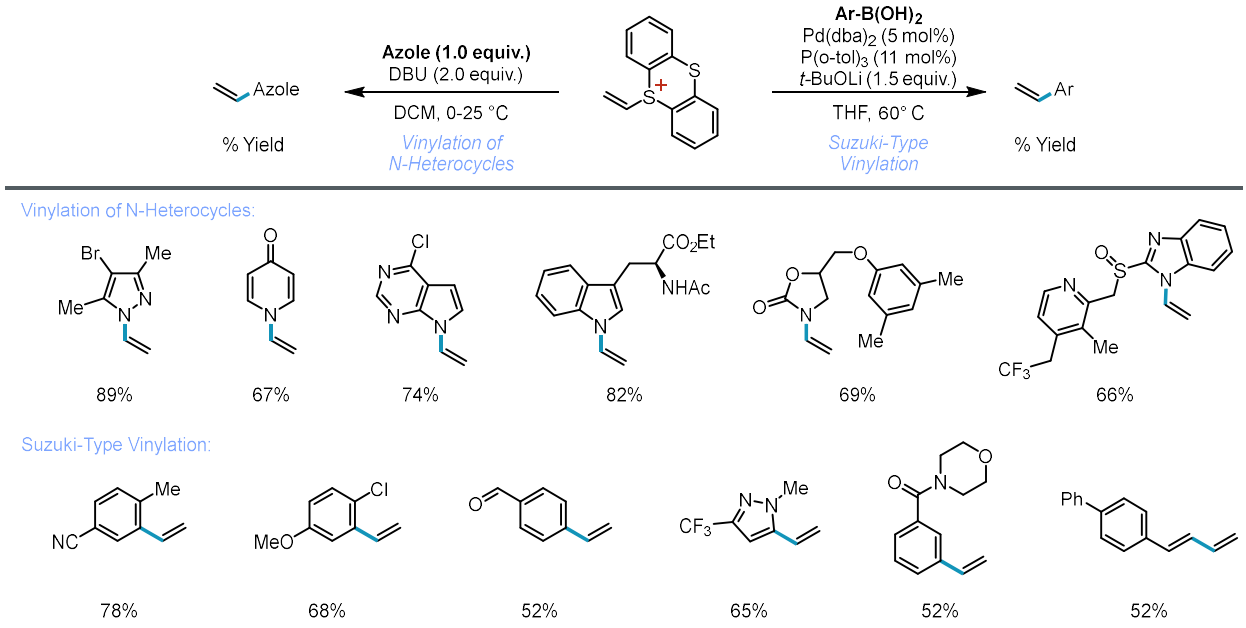

Figure 1.9. Vinylation reactions of vinylthianthrenium salts via reactivity as Michael acceptor and oxidative addition electrophile.

1.5 Allylation Reactivity

Unlike the reactivity discussed thus far focusing on functionalization directly across the alkene carbons, another distinct reactivity opportune to alkene transformations is allylic functionalization. While many methods exist that deliver allylic products (SN_2 displacement[28,29] and transition metal catalyzed π-allyl activation[30,31] of prefunctionalized allylic precursors are two established strategies), direct C–H allylic functionalization is an attractive approach due to the accessibility of alkene starting materials. However, this oxidative mode of alkene functionalization often faces challenges stemming from requisite use of electronically deactivated pronucleophiles compatible with exogenous chemical oxidants or electrophilic, preoxidized coupling partners, both of which limits accessible products to oxidant-compatible, electron-withdrawing substituents.

Great efforts have been made towards direct access of oxidatively sensitive allylic products from alkenes, culminating in the first report of direct C–H allylic amination furnishing aliphatic allylic amine products. In 2020, Ritter and co-workers used iminothianthrenes as electrophilic aminating reagents for C–H allylic amination (Figure 1.10).[32] These robust sulfilimine reagents were generated in a single step from primary amines and thianthrene-S-oxide activated by triflic acid described similarly to the method in section 1.2. Overall, 8 different iminothianthrene reagents were prepared and used in photocatalytic formation of secondary (E)-allylic amine products from unactivated terminal and internal alkenes.

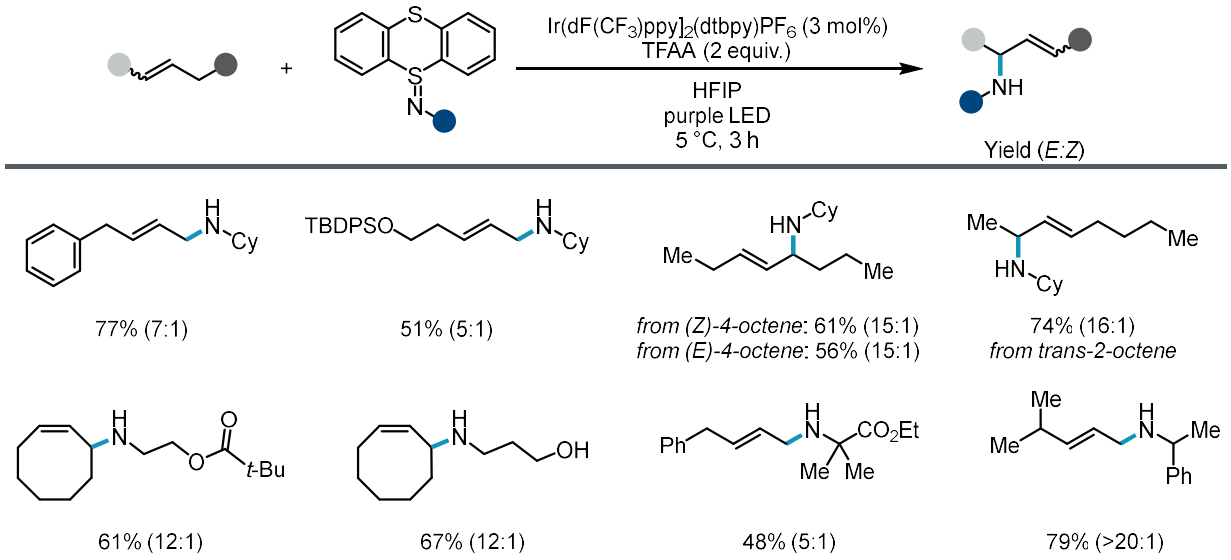

Figure 1.10. Allylic amination using photoactivation of iminothianthrene to deliver aliphatic allylic amines.

Coincidentally, the second report of direct C–H allylic amination also leverages thianthrene but with a switch in substrate activation. Instead of using thianthrene to activate the amine to preform an electrophilic aminating reagent, in 2021, the Wickens group used their dication pool strategy, wherein thianthrene activates the alkene to form a dicationic adducts that engages with diverse, aliphatic secondary amine nucleophiles to form linear, tertiary (Z)-allylic amine products (Figure 1.11) (see chapter 3 for further discussion). This dication pool strategy allows the formal coupling of unactivated alkenes and amines in a one pot-two step procedure.

Alkenes with diverse functional groups and steric profiles tolerated mild anodic activation, forming allylamine products with even with homoallylic and allylic functional groups. Of note, the Z:E

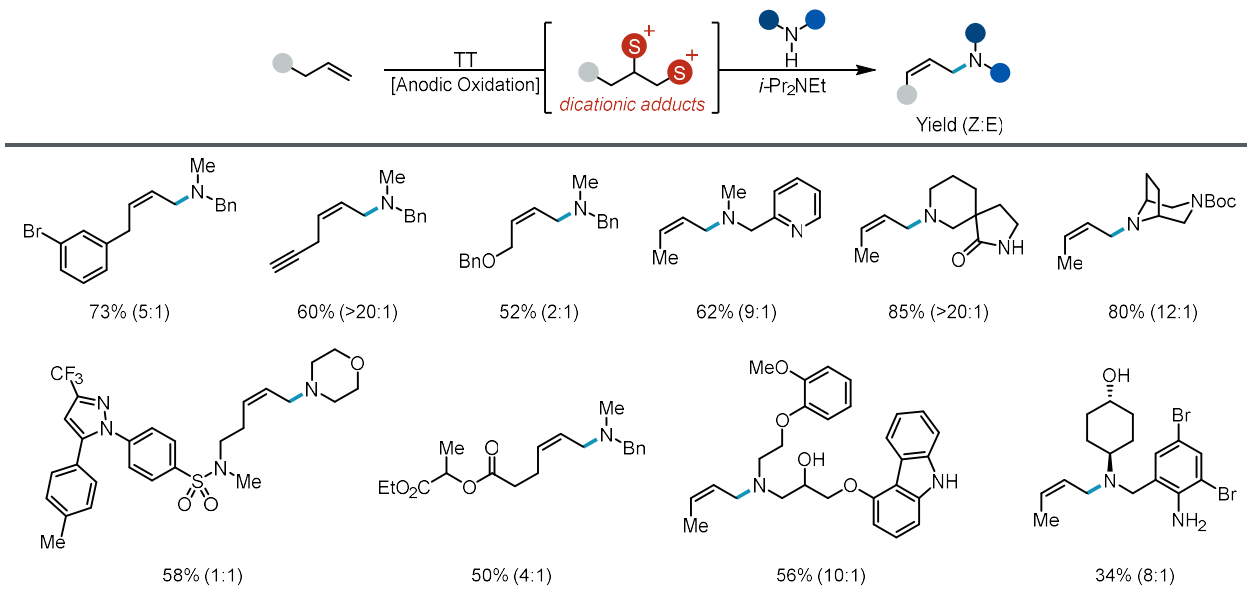

Figure 1.11. Allylic amination via the dication pool strategy to deliver aliphatic allylic amines. selectivity was observed to be heavily influenced by the alkene coupling partner (ranging from >20:1 to 2:1 Z:E) with one example of 1,4-pentadiene favoring formation of conjugated (E)-allylamine product in 1:3 Z:E. Feedstock alkenes such as propene and isobutene formed allyl- and methallyamine products, respectively. Surprisingly, butene resulted in consistently high Z:E (≥10:1) for the allylamine product, pushing forward the idea of butene as a (Z)-crotylation reagent. Due to the decoupling of alkene activation and subsequent substitution, a variety of acyclic and cyclic secondary amines were coupled in this overall oxidative transformation without worry of detrimental oxidation of either amine starting material or allylamine product. This was further demonstrated with the introduction of pendant saturated heterocycles (pyridine, piperidine, pyrrolidine, morpholine, piperazine, etc.) into allylic amine product, which shows distinct reactivity to that of classic transition-metal catalyzed C–H allylic amination methods which suffer from challenges with Lewis basic moieties due to deleterious metal ligation. This method was also amenable to late-stage functionalization of both complex alkenes and amines, seen by allylic amine products formed with substrates derived from celecoxib, carvedilol, ambroxol, and others.

Currently, the mechanism of allylic functionalization from the dication pool strategy remains unknown. With an unexpected change in reactivity selectivity from the other dication pool work undergoing formal iterative substitution (aziridination and cyclopropanation), the proposed reactivity

selectivity which now pivots towards formal substitution-elimination for allylic functionalization anchors on the increased steric bulk of secondary amines. (Allylic amination was also observed for sterically encumbered primary *tert*-butylamine.) The steric profile of the base also needed to be carefully tuned: *i*-Pr_2NEt was shown to be an optimal base with smaller tertiary alkylamine bases (such as NEt_3) directly adding to form Z-selective quaternary allylic ammonium salts and larger tertiary alkylamine bases (such as *i*-Bu_3N) forming alkenyl-thianthrenium salt as an elimination side-product. Isolation and subjection of the observed alkenyl-thianthrenium side-product to substitution conditions recapitulated allylamine formation in similar yields as Z-selectivity, suggesting alkenyl-thianthrenium to be an on-path intermediate. This inspired the initial mechanistic model wherein alkenyl-thianthrenium undergoes base-induced isomerization to form a transient allylic thianthrenium intermediate that can be trapped by amine nucleophile (Figure 1.12). Mechanistic investigations are currently underway to probe this hypothesis and build deeper understanding of the stereoselectivity-determining step.

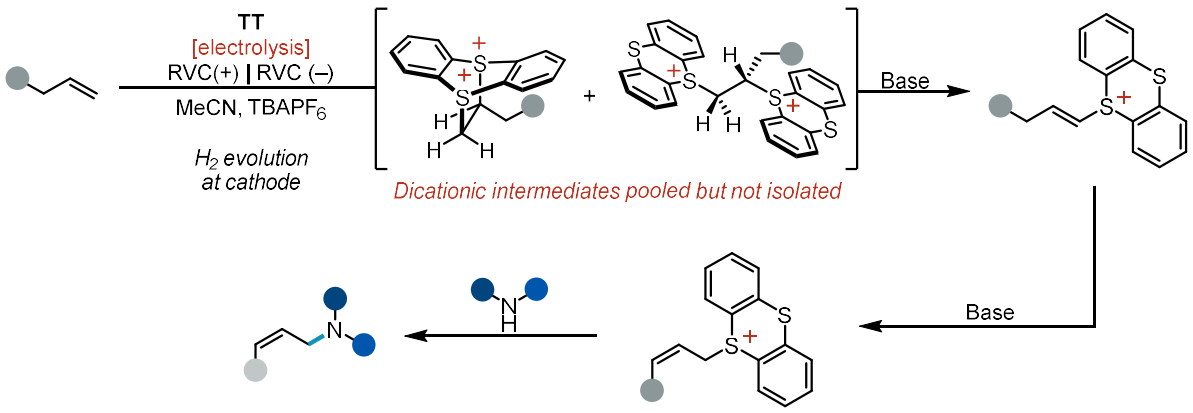

Figure 1.12. Proposed mechanism for Z-selective allylic amination via the dication pool strategy.

Contemporarily to the dication pool approach, Shu and coworkers also demonstrated that alkenyl-thianthrenium salts (isolated directly from S-oxide activation) could undergo allylic functionalization, forming a wide array of allylic esters (Figure 1.13). The same unexpected selectivity for the (Z)-allylic product (ranging 2:1–3:1 Z:E), was also observed. In addition, demonstrations of diverse nucleophiles (such as ethers, thiols, arenes, and sulfonamides) were demonstrated, greatly expanding this strategy as a more general method of allylic functionalization. Primary, secondary, and tertiary amines were all

competent for allylic amination giving (Z)-allylamine products in 2:1–5:1 Z:E ratio. Interestingly, the use of sterically hindered pentamethyldiethylenetriamine trialkylamine base in place of K_2CO_3 was used to increase Z-selectivity for select substrates. This simple, practical method could even be pivoted into a one-pot procedure starting from accessible alkene starting material without any workup or immediate purification of the alkenyl-thianthrenium intermediate, furnishing allylamine product in similar yields as the 2-step procedures.

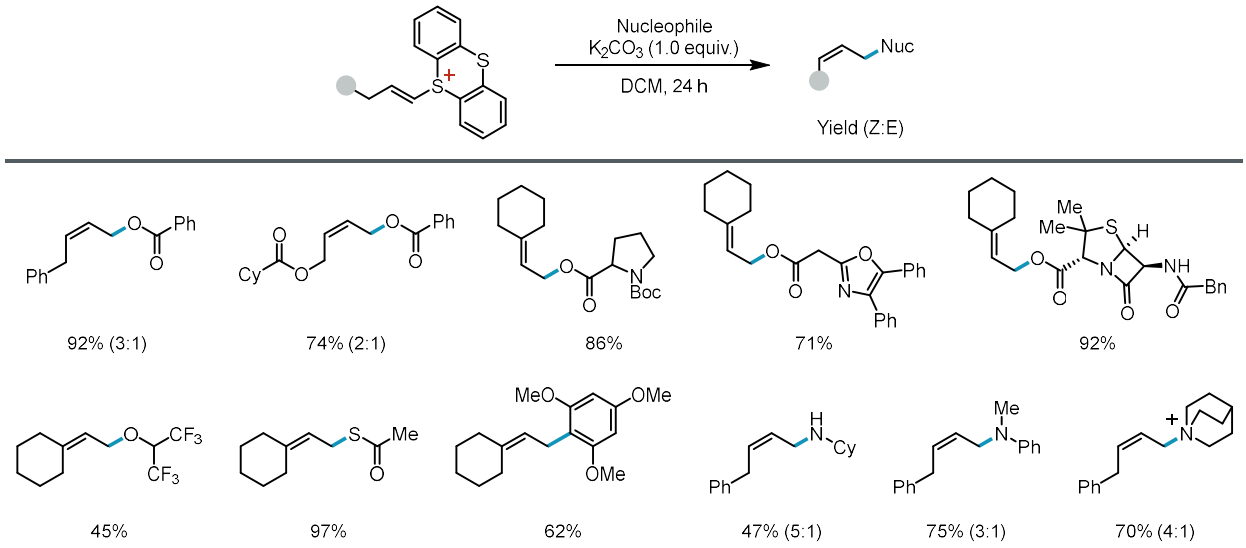

Figure 1.13. Allylic functionalization of alkenylthianthrenium salts.

Shu's origin of Z-selective allylic functionalization differs significantly from that of Wickens and coworkers. Subjecting dicationic monoadduct to their reaction conditions gave similar yield and diastereoselectivity for the final allylic product. This led to the proposal that alkenyl thianthrenium can convert to dicationic mono-adduct, which is then the key intermediate interacting directly with nucleophile via a site-selective ring-opening (Figure 1.14). Subsequent syn-elimination promoted by carbonate coordination to cationic sulfur then gives the finally allylic product favoring the Z-isomer.

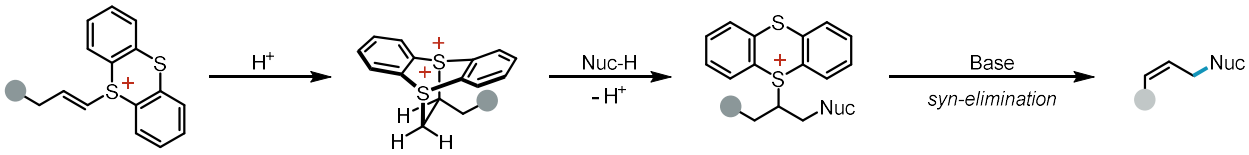

Figure 1.14. Alternative proposed mechanism for Z-selective allylic functionalization from alkenylthianthrenium salts.

Soós and coworkers in 2022 expanded (Z)-selective allylation reactivity to deliver (Z)-α,β-unsaturated carbonyls by cleverly leveraging Kornblum oxidation with alkenyl-thianthrenium reactivity (Figure 1.15).[33] Using either DMSO or NMO (Ganem modification), these weak nucleophiles undergo substitution of the putative allyl-thianthrenium intermediate, forming allyloxysulphonium or allyloxyammonium, respectively, which then undergoes β-elimination to give α,β-unsaturated carbonyls in similar Z-selectivity observed for previous allylic functionalization reports. While reported as a two-step procedure starting from purified alkenyl-thianthrenium, this method was adapted for a one-pot procedure starting from the original alkene starting material using both telescoping from S-oxide and electrochemical activation.

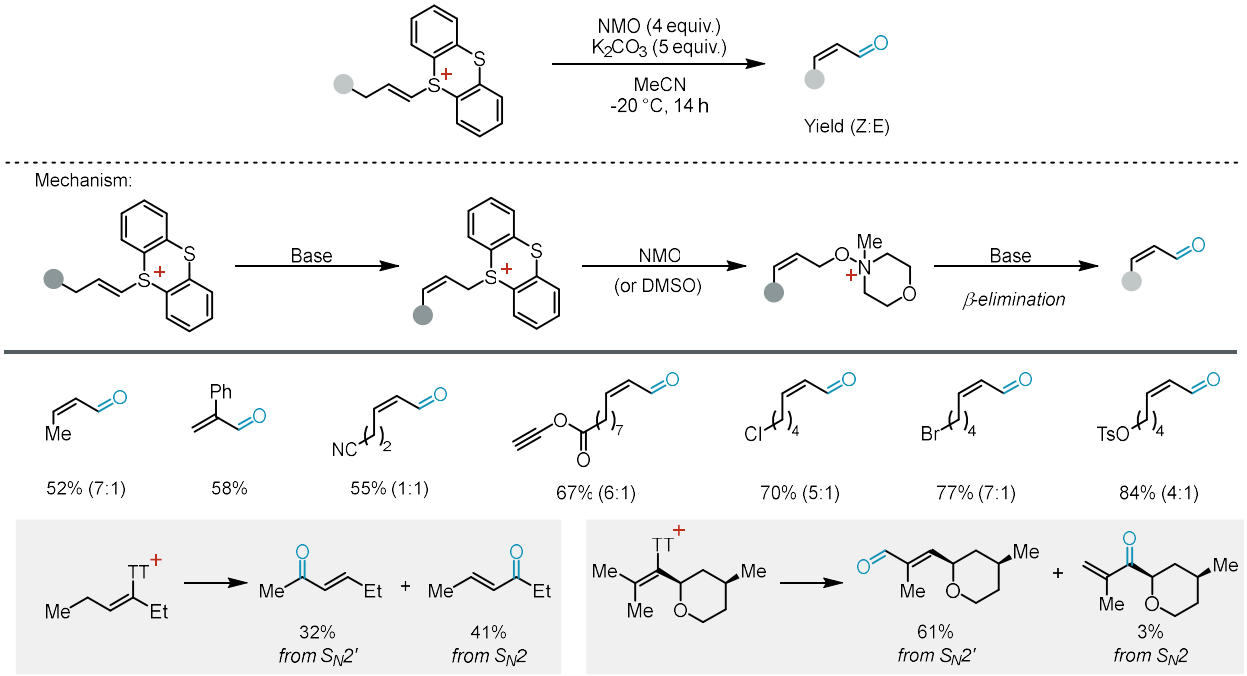

Figure 1.15. Kornblum/Ganem oxidation of alkenylthianthrenium salts for formal double oxidation of alkenes to (*Z*)-unsaturated aldehydes.

A variety of different functional groups were tolerated, including pendant chloride, bromide, and tosylate, which demonstrate the increased relative electrophilicity of allylic thianthrenium as a leaving group. Expansion of this method to acyclic internal alkenes did suffer from site selectivity issues due to competitive S_N2 and S_N2' reactivity though steric proximity proves a useful parameter for biasing product selectivity. One particularly useful application of this method is the tunability between the kinetically

preferred (Z)-enal and the thermodynamically preferred (E)-enal simply by simply increasing temperature and reaction duration. This switch was exploited and coupled with downstream Wittig chemistry for streamlining the stereoselective synthesis of diene-type pheromone and kairomone.

Concurrent to these reports in Chapter 1.5, 2022 saw continued efforts in designing oxidative methods to convert alkenes to aliphatic allylamines directly using amines as coupling reagents. Many of these methods still focus on palladium-catalyzed π-allyl reactivity but target creative solutions to overcome deleterious catalyst deactivation instigated by unwanted coordination of lewis basic nitrogen. These solutions involve the slow release of basic amine from amine-HBF_4 salts,[34] the use of bidentate phosphine ligand to inhibit amine-palladium coordination,[35] and the merge of photochemistry for homolytic allylic C-H cleavage and subsequent trapping by radical-polar crossover with Pd(I) radical[36]. Another clever solution bypassing palladium altogether targets photochemical generation of aminium radical cations that undergo olefin addition and leverage site selective HAT to selectively furnish allylic amines with high regioselectivity.[37] All these reports still favor select generation of (E)-allylamine products, in contrast to the preferred formation of the contrathermodynamic (Z)-allylamine product with alkene-derived sulfonium electrophiles. Overall, the continued pursuit of a formal coupling of unactivated alkenes with amine nucleophiles for aliphatic amine product further supports the desirability of this transformation.

1.6 References

(1) Li, Z.; Conser, K. R.; Jacobsen, E. N. Asymmetric Alkene Aziridination with Readily Available Chiral Diimine-Based Catalysts. *J. Am. Chem. Soc.* **1993**, *115* (12), 5326–5327. https://doi.org/10.1021/ja00065a067.

(2) Evans, D. A.; Faul, M. M.; Bilodeau, M. T.; Anderson, B. A.; Barnes, D. M. Bis(Oxazoline)-Copper Complexes as Chiral Catalysts for the Enantioselective Aziridination of Olefins. *J. Am. Chem. Soc.* **1993**, *115* (12), 5328–5329. https://doi.org/10.1021/ja00065a068.

(3) Ide, T.; Feng, K.; Dixon, C. F.; Teng, D.; Clark, J. R.; Han, W.; Wendell, C. I.; Koch, V.; White, M. C. Late-Stage Intermolecular Allylic C–H Amination. *J. Am. Chem. Soc.* **2021**, *143* (37), 14969–14975. https://doi.org/10.1021/jacs.1c06335.

(4) Davies, H. M. L.; Antoulinakis, E. G. Intermolecular Metal-Catalyzed Carbenoid Cyclopropanations. In *Organic Reactions*; American Cancer Society, 2004; pp 1–326. https://doi.org/10.1002/0471264180.or057.01.

(5) Dauban, P.; Dodd, R. H. Iminoiodanes and C-NBond Formation in Organic Synthesis. *Synlett* **2003**, No. 11, 1571–1586. https://doi.org/10.1055/s-2003-41010.

(6) Holst, D. E.; Wang, D. J.; Kim, M. J.; Guzei, I. A.; Wickens, Z. K. Aziridine Synthesis by Coupling Amines and Alkenes via an Electrogenerated Dication. *Nature* **2021**, *596* (7870), 74–79. https://doi.org/10.1038/s41586-021-03717-7.

(7) Moschona, F.; Savvopoulou, I.; Tsitopoulou, M.; Tataraki, D.; Rassias, G. Epoxide Syntheses and Ring-Opening Reactions in Drug Development. *Catalysts* **2020**, *10* (10), 1117. https://doi.org/10.3390/catal10101117.

(8) Jakubowska, A.; Żuchowski, G.; Kulig, K. Cyclic Sulfates as Useful Tools in the Asymmetric Synthesis of 1-Aminocyclopropane-1-Carboxylic Acid Derivatives. *Tetrahedron: Asymmetry* **2015**, *26* (21), 1261–1267. https://doi.org/10.1016/j.tetasy.2015.09.013.

(9) Mondal, M.; Chen, S.; Kerrigan, N. Recent Developments in Vinylsulfonium and Vinylsulfoxonium Salt Chemistry. *Molecules* **2018**, *23* (4), 738. https://doi.org/10.3390/molecules23040738.

(10) Kaiser, D.; Klose, I.; Oost, R.; Neuhaus, J.; Maulide, N. Bond-Forming and -Breaking Reactions at Sulfur(IV): Sulfoxides, Sulfonium Salts, Sulfur Ylides, and Sulfinate Salts. *Chem. Rev.* **2019**, *119* (14), 8701–8780. https://doi.org/10.1021/acs.chemrev.9b00111.

(11) Lowe, P. A. Synthesis of Sulphonium Salts. In *The Sulphonium Group (1981)*; John Wiley & Sons, Ltd, 1981; pp 267–312. https://doi.org/10.1002/9780470771648.ch11.

(12) Takaki, K.; Agawa, T. Synthesis of Acylcyclopropanes and Oxiranes from Vinylsulfonium Salts and Lithium Enolates. *J. Org. Chem.* **1977**, *42* (20), 3303–3304. https://doi.org/10.1021/jo00440a024.

(13) Hanamoto, T. Fluorinated Vinyl Sulfonium Salts and Their Synthetic Utilization. *The Chemical Record n/a* (n/a), e202200270. https://doi.org/10.1002/tcr.202200270.

(14) Matlock, J. V.; Aggarwal, V. K.; McGarrigle, E. M. (2-Bromoethyl)Diphenylsulfonium Trifluoromethanesulfonate. In *Encyclopedia of Reagents for Organic Synthesis*; John Wiley & Sons, Ltd, 2016; pp 1–5. https://doi.org/10.1002/047084289X.rn01921.

(15) Matlock, J. V.; Fritz, S. P.; Harrison, S. A.; Coe, D. M.; McGarrigle, E. M.; Aggarwal, V. K. Synthesis of α-Substituted Vinylsulfonium Salts and Their Application as Annulation Reagents in the Formation of Epoxide- and Cyclopropane-Fused Heterocycles. *J. Org. Chem.* **2014**, *79* (21), 10226–10239. https://doi.org/10.1021/jo501885z.

(16) Yamanaka, H.; Matsuo, J.; Kawana, A.; Mukaiyama, T. New Methods for the Preparations of 2-Aryl Aziridines, α-Imido Styrenes, and Allyl Amines from Olefins via Diphenylvinylsulfonium Triflates. *Arkivoc* **2003**, *2004* (3), 42–65. https://doi.org/10.3998/ark.5550190.0005.306.

(17) Aukland, M. H.; Talbot, F. J. T.; Fernández-Salas, J. A.; Ball, M.; Pulis, A. P.; Procter, D. J. An Interrupted Pummerer/Nickel-Catalysed Cross-Coupling Sequence. *Angewandte Chemie International Edition* **2018**, *57* (31), 9785–9789. https://doi.org/10.1002/anie.201805396.

(18) Srogl, J.; Allred, G. D.; Liebeskind, L. S. Sulfonium Salts. Participants Par Excellence in Metal-Catalyzed Carbon−Carbon Bond-Forming Reactions. *J. Am. Chem. Soc.* **1997**, *119* (50), 12376–12377. https://doi.org/10.1021/ja9726926.

(19) Shine, H. J.; Bandlish, B. K.; Mani, S. R.; Padilla, A. G. Ion Radicals. 43. Addition of Thianthrene and Phenoxathiin Cation Radicals to Alkenes and Alkynes. *J. Org. Chem.* **1979**, *44* (6), 915–917. https://doi.org/10.1021/jo01320a004.

(20) Lee, W. K.; Liu, B.; Park, C. W.; Shine, H. J.; Whitmire, K. H. Addition of Thianthrene Cation Radical to Cycloalkenes. An Unexpected Monoadduct. *J. Org. Chem.* **1999**, *64* (25), 9206–9210. https://doi.org/10.1021/jo9911241.

(21) Qian, D.-Q.; Shine, H. J.; Guzman-Jimenez, I. Y.; Thurston, J. H.; Whitmire, K. H. Mono- and Bisadducts from the Addition of Thianthrene Cation Radical Salts to Cycloalkenes and Alkenes. *J. Org. Chem.* **2002**, *67* (12), 4030–4039. https://doi.org/10.1021/jo0104633.

(22) Iwai, K.; Shine, H. J. Ion Radicals. 46. Reactions of the Adducts of Thianthrene and Phenoxathiin Cation Radicals and Cyclohexene with Nucleophiles. *J. Org. Chem.* **1981**, *46* (2), 271–276. https://doi.org/10.1021/jo00315a009.

(23) Chen, J.; Li, J.; Plutschack, M. B.; Berger, F.; Ritter, T. Regio- and Stereoselective Thianthrenation of Olefins To Access Versatile Alkenyl Electrophiles. *Angewandte Chemie International Edition* **2020**, *59* (14), 5616–5620. https://doi.org/10.1002/anie.201914215.

(24) Liu, M.-S.; Du, H.-W.; Cui, J.-F.; Shu, W. Intermolecular Metal-Free Cyclopropanation and Aziridination of Alkenes with XH2 (X=N, C) by Thianthrenation**. *Angewandte Chemie International Edition* **2022**, *61* (41), e202209929. https://doi.org/10.1002/anie.202209929.

(25) Patai, S. *The Chemistry of Alkenes*, 1st ed.; John Wiley & Sons, Ltd, 1964. https://doi.org/10.1002/9780470771044.

(26) Beletskaya, I. P.; Cheprakov, A. V. The Heck Reaction as a Sharpening Stone of Palladium Catalysis. *Chem. Rev.* **2000**, *100* (8), 3009–3066. https://doi.org/10.1021/cr9903048.

(27) Juliá, F.; Yan, J.; Paulus, F.; Ritter, T. Vinyl Thianthrenium Tetrafluoroborate: A Practical and Versatile Vinylating Reagent Made from Ethylene. *J. Am. Chem. Soc.* **2021**, *143* (33), 12992–12998. https://doi.org/10.1021/jacs.1c06632.

(28) Taylor, A. R.; Katritzky, R. J. K. Comprehensive Organic Functional Group Transformations II. In *Comprehensive Organic Functional Group Transformations II.*; Elsevier; pp 255–300.

(29) Sen, S. E.; Roach, S. L. A Convenient Two-Step Procedure for the Synthesis of Substituted Allylic Amines from Allylic Alcohols. *Synthesis* **1995**, *1995* (07), 756–758. https://doi.org/10.1055/s-1995-4012.

(30) Trost, B. M.; Crawley, M. L. Asymmetric Transition-Metal-Catalyzed Allylic Alkylations: Applications in Total Synthesis. *Chem. Rev.* **2003**, *103* (8), 2921–2944. https://doi.org/10.1021/cr020027w.

(31) Sundararaju, B.; Achard, M.; Bruneau, C. Transition Metal Catalyzed Nucleophilic Allylic Substitution: Activation of Allylic Alcohols via π-Allylic Species. *Chem. Soc. Rev.* **2012**, *41* (12), 4467–4483. https://doi.org/10.1039/C2CS35024F.

(32) Cheng, Q.; Chen, J.; Lin, S.; Ritter, T. Allylic Amination of Alkenes with Iminothianthrenes to Afford Alkyl Allylamines. *J. Am. Chem. Soc.* **2020**, *142* (41), 17287–17293. https://doi.org/10.1021/jacs.0c08248.

(33) Angyal, P.; Kotschy, A. M.; Dudás, Á.; Varga, S.; Soós, T. Intertwining Olefin Thianthrenation with Kornblum/Ganem Oxidations: Ene-Type Oxidation to Furnish α,β-Unsaturated Carbonyls. *Angewandte Chemie International Edition* **2023**, *62* (2), e202214096. https://doi.org/10.1002/anie.202214096.

(34) Ali, S. Z.; Budaitis, B. G.; Fontaine, D. F. A.; Pace, A. L.; Garwin, J. A.; White, M. C. Allylic C–H Amination Cross-Coupling Furnishes Tertiary Amines by Electrophilic Metal Catalysis. *Science* **2022**, *376* (6590), 276–283. https://doi.org/10.1126/science.abn8382.

(35) Jin, Y.; Jing, Y.; Li, C.; Li, M.; Wu, W.; Ke, Z.; Jiang, H. Palladium-Catalysed Selective Oxidative Amination of Olefins with Lewis Basic Amines. *Nat. Chem.* **2022**, *14* (10), 1118–1125. https://doi.org/10.1038/s41557-022-01023-x.

(36) Pak Shing Cheung, K.; Fang, J.; Mukherjee, K.; Mihranyan, A.; Gevorgyan, V. Asymmetric Intermolecular Allylic C–H Amination of Alkenes with Aliphatic Amines. *Science* **2022**, *378* (6625), 1207–1213. https://doi.org/10.1126/science.abq1274.

(37) Wang, S.; Gao, Y.; Liu, Z.; Ren, D.; Sun, H.; Niu, L.; Yang, D.; Zhang, D.; Liang, X.; Shi, R.; Qi, X.; Lei, A. Site-Selective Amination towards Tertiary Aliphatic Allylamines. *Nat Catal* **2022**, *5* (7), 642–651. https://doi.org/10.1038/s41929-022-00818-y.

Chapter 2: Aziridine synthesis by coupling amines and alkenes via an electrogenerated dication

This chapter has been published and adapted with permission from:

Holst, D. E.*; **Wang, D. J.***; Kim, M. J.; Guzei, I. A.; Wickens, Z. K. Aziridine Synthesis by Coupling Amines and Alkenes via an Electrogenerated Dication. *Nature* **2021**, *596* (7870), 74–79. *Indicates co-first authorship

2.1 Abstract

Aziridines, the nitrogen congener of epoxides, are fundamentally important synthetic targets. Their significant ring strain and resultant proclivity towards ring opening reactions makes them versatile precursors to diverse amine products[1-3] and, in some cases, the aziridine functional group itself imbues important biological (e.g. anti-tumor) activity[4-6]. A deceptively straightforward strategy to access aziridines would be through the coupling of amines and alkenes, liberating H_2 as a benign byproduct (Fig. 2.1a). Unfortunately, this strain-inducing oxidative reaction is thermodynamically uphill (>30 kcal/mol) and thus this idealized transformation is not feasible. In theory, the aziridine formation could be coupled to the quenching of a chemical oxidant rather than formation of H_2. However, sufficiently strong oxidants to render this aziridination favorable are incompatible with most amine coupling partners as well as many functional groups[7]. Herein, we demonstrate that unactivated alkenes can be electrochemically transformed into a metastable, dicationic intermediate that undergoes aziridination with primary amines under basic conditions. This new approach dramatically expands the scope of readily accessible *N*-alkyl aziridine products relative to state-of-the-art methods. A key strategic advantage of this new approach is that oxidative alkene activation is decoupled from the aziridination step, allowing a broad range of

commercially available but oxidatively sensitive amines to act as coupling partners for this strain-inducing transformation. This new aziridination methodology will find immediate application in organic synthesis and, more broadly, lay the foundation for a diverse array of challenging difunctionalization reactions that leverage oxidatively sensitive coupling partners using this dication pool approach.

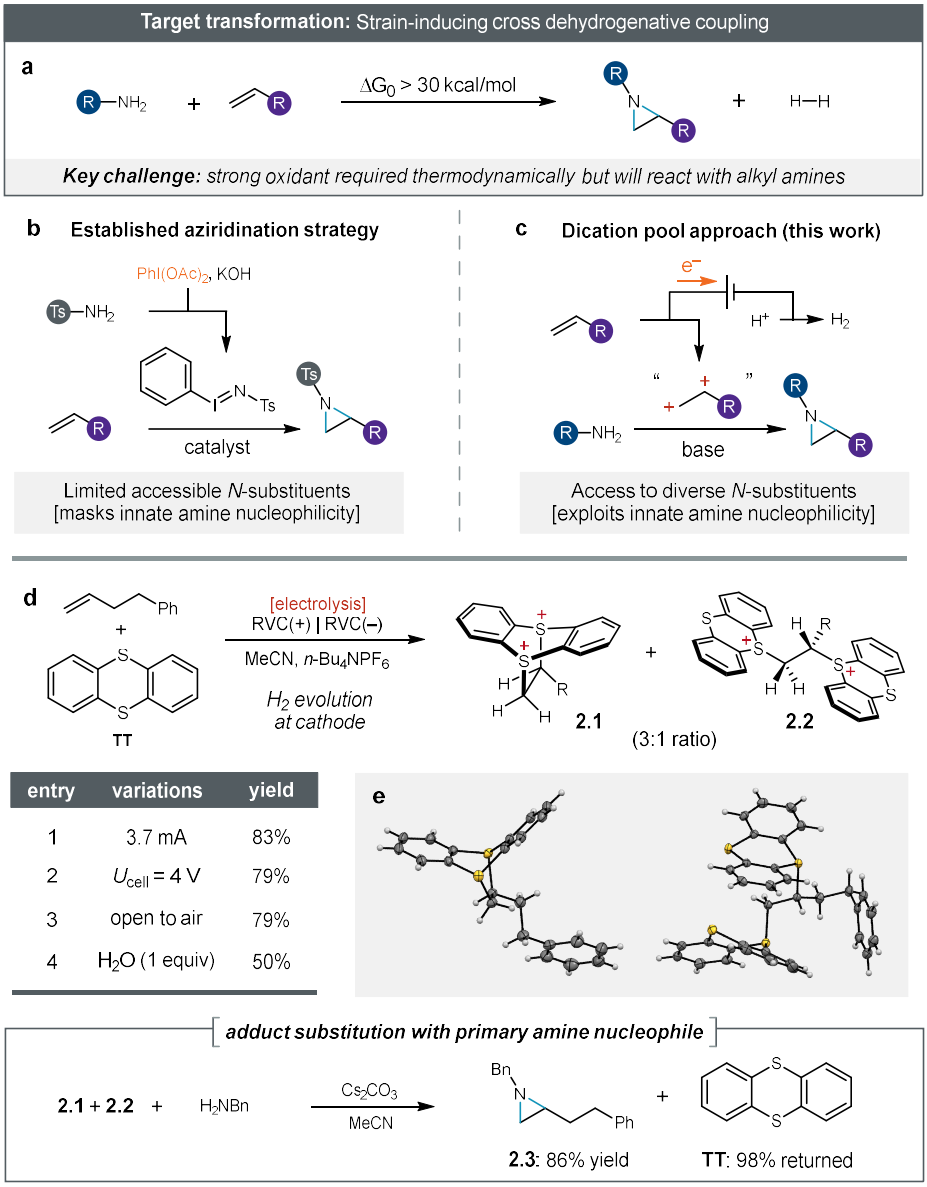

Figure 2.1. Development of an oxidative coupling strategy for aziridine synthesis. **a**, Thermodynamic challenges associated with ideal aziridine synthesis. **b**, Representative example of previous strategies for alkene aziridination rely on electrophilic nitrogen reagents that limit the accessible *N*-substituents. **c**, Our proposed electrochemical aziridine synthesis, involving the coupling of structurally diverse amines and alkenes through a strategic dicationic intermediate. **d**, Development of our electrochemical reaction. Bottom, aziridination with a model primary amine. **e**, Adducts characterized by X-ray crystallography. All yields were determined by ^{1}H-NMR. Ph, phenyl; R, $(CH_2)_2Ph$; RVC, reticulated vitreous carbon; Ts, toluenesulfonyl.

2.2 Introduction

Despite tremendous progress in aziridine synthesis over the past decade, diverse *N*-substituted aziridine products remain difficult to efficiently access. Established alkene aziridination methodologies employ a high energy electrophilic nitrogen reagent (e.g. iminoiodinane) or nitrene precursor (e.g. organoazide) that serves both as the stoichiometric oxidant and the nitrogen source[1,8-10]. These reagents typically bear electron-withdrawing *N*-substituents to strike the requisite balance of reactivity and reagent stability (Fig. 2.1b). As a consequence, there is a paucity of general strategies to transform alkenes into aziridines bearing *N*-alkyl substituents despite the utility of these aziridines in the construction of diverse aliphatic amine products and their presence in biologically active molecules. Buchwald and coworkers recently reported an intramolecular aziridination methodology that provides access to a broader range of *N*-alkyl-substituted aziridine products via copper hydride chemistry; however, multistep synthesis to access the appropriately activated allylic amine substrate is required[11]. Pioneering recent advances have introduced electrophilic reagents to furnish N–H aziridines[12-15] but analogous reagents to access diverse *N*-alkyl aziridines through intermolecular reaction with alkenes have been slow to follow. Indeed, despite substantial effort, there are only a handful of electrophilic nitrogen reagents capable of delivering *N*-alkyl aziridines or even the corresponding vicinal aminohalide precursors from simple alkenes (<10 unique *N*-substituents). Furthermore, each new reagent requires multistep *de novo* synthesis[16,17], and only isolated examples of *in situ* generation of electrophilic nitrogen reagents to form *N*-alkyl aziridine products have been reported[18].

In principle, transformation of an alkene into a dielectrophile–reversing the conventional strategy of pre-oxidizing the amine–could leverage intrinsic amine nucleophilicity rather than masking it. Given that there are over one million commercially available primary amines[19], this complementary approach would dramatically expand the scope of readily accessible *N*-alkyl aziridines. Dibromination is a well-established reaction to transform alkenes into dielectrophiles; however, the vast majority of vicinal dihalides do not undergo substitution with primary amines and undesired elimination reactions are

observed instead (see Supplementary Table A1). As a result, initial alkene oxygenation (epoxidation or dihydroxylation) followed by iterative stoichiometric activation and substitution steps remains the most commonly employed synthetic workaround to accomplish the net coupling of alkenes and primary amines to form *N*-alkyl aziridines[20-22].

We envisioned that electrochemistry could enable the clean, efficient, and scalable transformation of alkenes into a metastable dielectrophile of sufficient reactivity to be leveraged for aziridine synthesis (Fig. 2.1c). Pioneering work in electroorganic synthesis has illustrated that electrochemistry can replace chemical redox agents with safer and more environmentally benign conditions and, in some cases, enable reactivity that would be impractical to otherwise access[23-27]. Unfortunately, despite recent progress in other electrochemical alkene oxidation reactions[28,29], electrochemical aziridinations still depend on direct oxidation of the coupling partners and, consequently, remain limited to electron-rich styrene derivatives, specific nucleophiles, or both[30-33]. To address the implicit limitations of prior approaches, we drew inspiration from Yoshida's stabilized cation pool strategy wherein a potent cationic electrophile is anodically generated from a hydrocarbon and subsequently treated with an oxidatively sensitive nucleophile in a one-pot process[34,35]. Unfortunately, extension of this strategy to alkene functionalization has proven difficult. Instead of direct oxidation of the alkene substrate, we targeted the anodic activation of a safe and inexpensive reagent *in situ* that would transform an alkene into a potent dielectrophile. To this end, we were attracted to the dicationic adducts first prepared by Shine through the reaction of thianthrene radical cation (**$TT^{+\bullet}$**) with alkenes[36,37]. While we suspected that these dicationic adducts might be potent dielectrophiles, little is known of their reactivity with organic nucleophiles[38]. In recent years, Ritter has illustrated the immense synthetic value of C(sp^2) thianthrenium salts, generated from C(sp^2)–H bonds, in a wide range of cross coupling reactions[39-41]. However, electrochemical methods to access thianthrenium salts from hydrocarbons are underdeveloped[42] and examples that generate C(sp^3) products through hydrocarbon thianthrenation are rare[43]. We hypothesized that dicationic thianthrenenium alkene adducts could be cleanly prepared electrochemically and would undergo efficient reaction with amines to

furnish *N*-alkyl aziridines. Given the expansive pool of commercially available primary amines as well as the fact that thianthrene (**TT**) is both safe[45] and inexpensive (<0.15 USD/mmol), this approach would dramatically expand the scope of readily accessible *N*-alkyl aziridine products. Herein, we validate that this new strategy allows us to take a significant step towards an ideal *N*-alkyl aziridine synthesis by coupling unactivated terminal alkenes and aliphatic primary amines using electricity to circumvent the need for a conventional chemical oxidant.

2.3 Results and Discussion

First, we probed the viability of electrochemical generation of the key electrophilic adduct between an alkene and thianthrene. Both constant current and constant cell potential electrolysis of a solution of 4-phenyl-1-butene, thianthrene, and electrolyte delivered a 3:1 mixture of dicationic adducts **2.1** and **2.2** in excellent combined yield (Fig. 2.1d, entries 1 and 2). Despite the presumably high reactivity of these species, we characterized both adducts **2.1** and **2.2** unambiguously through x-ray crystallography. We found that the electrochemical generation of these dicationic adducts is robust; the yield of adducts **2.1** and **2.2** is insensitive to exposure to air (entry 3) and even tolerated intentional addition of exogenous water (entry 4). Having established that electrochemistry can promote the oxidative coupling of thianthrene and an unactivated terminal alkene, we next evaluated the substitution chemistry of this presumably reactive intermediate. To our delight, exposure of the mixture of adducts **2.1** and **2.2** to benzylamine and a heterogeneous base fully consumed both adducts and delivered the desired aziridine (**2.3**) in excellent yield (86%). As expected, thianthrene was returned after substitution (98% returned). The aziridination of **2.1** and **2.2** could proceed either through direct iterative nucleophilic substitution or via elimination to form a transient vinyl thianthrenium salt that undergoes subsequent substitution[45]. The overall transformation employs trifluoroacetic acid (TFA) as the formal oxidant, producing H_2 and trifluoroacetate as stoichiometric byproducts. We translated these preliminary data into a simple one-pot, two-step procedure that could furnish synthetically useful yields of *N*-alkyl aziridine products using either limiting amine (68%) or limiting alkene (80%) with a modest excess (3–4 equivalents) of the other

coupling partner (see Supplementary Fig. A1). This reaction requires no expensive specialized electrochemical equipment; it can be conducted using a commercially available DC power supply (<100 USD) paired with cheap carbon electrodes in a simple glass divided cell.

We next probed the scope of the amines amenable to this process using 1-octene as a representative unactivated alkene. These experiments illustrated aziridine products to be accessible from a wide range of amine nucleophiles, dramatically expanding upon the limited range of viable aziridine *N*-substituents accessible from alkenes using conventional electrophilic nitrogen reagents (Fig. 2.2). Primary amines bearing diverse steric profiles (**2.4**–**2.8**) were well tolerated. Amines containing an alkene (**2.7**) and an alkyne (**2.8**) incorporated handles for further functionalization that would be difficult to install using conventional electrophilic nitrogen approaches. Diverse heterocycles are broadly represented in biologically active molecules, yet many of these species are oxidatively sensitive and/or poison the transition metal catalysts required for conventional aziridination reactions. In stark contrast, using the metal-free dication pool strategy outlined herein, aziridines bearing a range of both heteroaromatic and saturated heterocyclic groups could be efficiently accessed from inexpensive commercially available amines (**2.9**–**2.18**). We anticipate efficient access to these versatile heterocyclic building blocks will be of particularly high value in medicinal chemistry efforts. We were delighted to find primary amines bearing potential competing nucleophiles such as tryptamine, primaquine, and ethanolamine were each selectively transformed into aziridine products (**2.17**–**2.19**). Of note, each of the primary amines evaluated throughout this study were commercially available and inexpensive, illustrating the substantial benefit of this aziridination approach relative to multistep synthesis of novel electrophilic reagents for each distinct *N*-substituent.

Next, we turned our attention to the scope of alkene substrates. Under limiting alkene conditions, we found that modest steric hindrance about the alkene had a minimal impact on aziridine yield (**2.19**, **2.20**) and even an alkene bearing a hindered allylic quaternary carbon was transformed into the corresponding aziridine, albeit in diminished yield (**2.21**). However, disubstituted alkenes were not

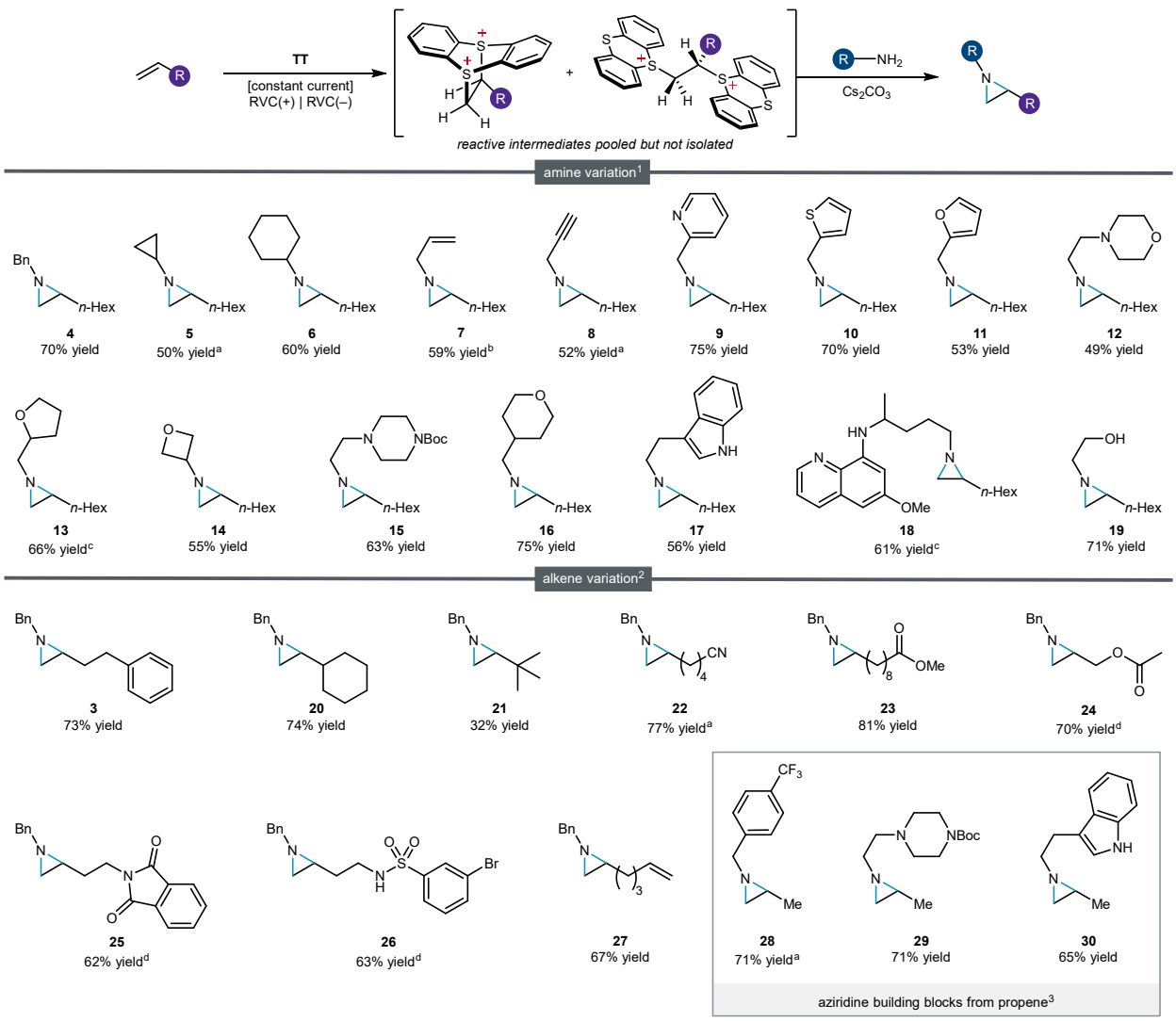

Figure 2.2. Scope of aziridination reaction. All yields, unless otherwise noted, are for isolated aziridine products. (1) Limiting amine conditions: 1-octene (1.2 mmol), thianthrene (1.8 mmol), 4 ml MeCN (0.2 M n-Bu_4NPF_6), I = 11.1 mA, 7 h (2.5 F mol^{-1} alkene); then amine (0.4 mmol) Cs_2CO_3 (3.2 mmol), 16 h. (2) Limiting alkene conditions: alkene (0.4 mmol), thianthrene (0.6 mmol), trifluoroacetic acid (0.8 mmol), 8 ml MeCN (0.2 M n-Bu_4NPF_6), I = 3.7 mA, 7 h (2.5 F mol^{-1} alkene); then benzylamine (1.6 mmol), Cs_2CO_3 (2.4 mmol), 16 h. (3) Propene conditions: thianthrene (1.8 mmol), 4 ml MeCN (0.2 M n-Bu_4NPF_6) under propene (1 atm), I = 11.1 mA, 7 h (2.5 F mol^{-1} alkene); then amine (0.4 mmol), Cs_2CO_3 (3.2 mmol), 16 h. [a]Yield determined by NMR spectroscopy. [b]Yield obtained using limiting alkene conditions (2) instead of limiting amine conditions (1). [c]Isolated in 1:1 diastereomeric ratio. [d]I = 12.0 mA, 2 h. See Appendix A for further experimental details.

compatible with this aziridination methodology. While 1,2-disubstituted thianthrenium adducts could be formed, attempted substitution delivered either vinyl thianthrenium salts or intractable mixtures (see Appendix A Fig. A2). While our initial efforts have focused on simple unactivated aliphatic alkenes, alkene substrates bearing functional groups such as esters, nitriles, sulfonamides, aryl halides and

phthalimides in both distal and proximal positions each furnished the desired aziridine products (**2.23**–**2.26**). Notably an unconjugated diene underwent selective monofunctionalization to provide a useful building block that contains two orthogonal sites for further functionalization (**2.27**). Finally, this oxidative coupling strategy is also amenable to functionalization of gaseous feedstock alkenes using primary amine nucleophiles. Electrolysis of thianthrene under one atmosphere of propene, followed by addition of base and amine, furnished a range of synthetically attractive but previously unknown aziridine building blocks from exceptionally inexpensive starting materials (**2.28**–**2.30**).

We envisioned that this newly realized oxidative aziridination methodology would streamline the synthesis of important complex amines, a class of compounds broadly represented in medicinally relevant molecules. Consistent with this proposal, we were able to prepare aziridine **2.31**, an intermediate in the synthesis of a collection of patented 5-HT1B, 5-HT2A, and D2 receptor agonists (Pfizer, CNS indication) from a commercially available primary amine and propene gas in high yield (Fig. 2.3a). In contrast, the previous route hinged on a low yielding (17%) aziridine *N*-alkylation reaction[46]. Beyond offering a substantial improvement in synthetic efficiency, the new oxidative coupling route enables rapid synthesis of analogs (**2.32**, **2.33**) because the alkene partner can be varied. Supporting its practical synthetic utility, we found this electrochemical transformation to be readily amenable to scale up (Fig. 2.3b). We employed a commercially available flow reactor to prepare 3.2 g (13.4 mmol) of aziridine **2.3** and recovery of thianthrene was straightforward (76% recovered). While the cost of thianthrene on even this scale was trivial (3.60 USD), we envision reisolation could be attractive for large scale industrial processes. Transformation of this aziridine provides facile access to diverse, valuable compounds through numerous selective ring-opening functionalization reactions (Fig. 2.3c). Derivatives of both vicinal amino alcohol isomers (**2.34**, **2.35**), aminoazides (**2.36**), and medicinally relevant phenethylamines (**2.37**) are each smoothly generated in a single step from the *N*-alkyl aziridine product. In addition to serving as versatile synthetic precursors to diverse amines, *N*-alkyl aziridines themselves can possess attractive biological activity[4]. Using the electrochemical methodology reported herein, we prepared an *N*-

cyclohexyl aziridine alkaloid natural product (**2.38**) from inexpensive starting materials (Fig. 2.3d). Finally, we probed whether this dication pool approach could be employed outside of the context of aziridine synthesis. We found that omission of exogeneous base under our aziridination conditions

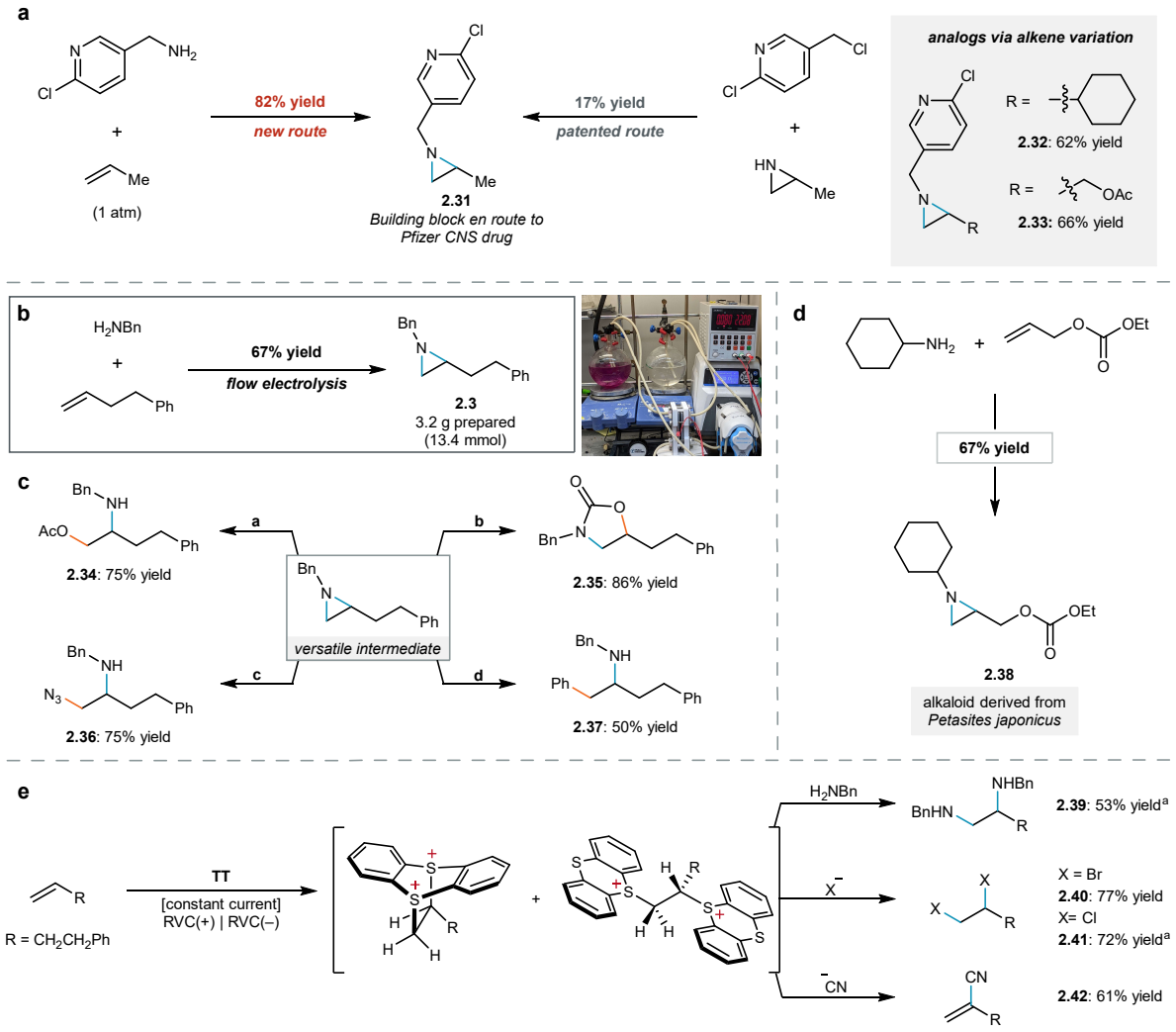

Figure 2.3. Synthetic applications of the dication pool strategy. All yields are isolated products, and electrochemical alkene activation was conducted using standard conditions (2) from Fig. 2.2 unless otherwise noted. See Supplementary Information for experimental details. **a**, Comparison of our new dicationic adduct aziridination approach with the patented N–H aziridine alkylation route in the synthesis of a patented pharmaceutical intermediate and new analogues. CNS, central nervous system. **b**, Multigram aziridination via electrochemical formation of dicationic adducts using constant current flow electrolysis and subsequent substitution. **c**, Synthetic versatility of N-alkylaziridine products. Diversification conditions: a, acetic acid (AcOH), dichlormethane (DCM), 72 h; b, LiI, CO_2 (1 atm.), tetrahydrofuran (THF), 44 h; c, trimethylsilyl azide ($TMSN_3$), AcOH, DCM, 48 h; d, lithium diphenyl cuprate (Ph_2CuLi), boron trifluoride etherate (BF_3OEt_2), THF, 4 h. **d**, Synthesis of an aziridine-containing natural product. **e**, Preliminary expansion of the dication pool strategy beyond aziridination. [a]Yield determined by ^{1}H-NMR. See Appendix A for experimental details.

resulted in direct diamination of alkenes (**2.39**), treatment of the adduct with halide salts resulted in dihalogenation (**2.40** and **2.41**), and addition of potassium cyanide furnished the vinyl nitrile (**2.42)**. Collectively, these data validate that the addition of this electrochemical alkene activation strategy to the synthetic lexicon will dramatically accelerate the preparation of diverse compounds containing the aliphatic amine moiety and beyond.

We next investigated the mechanism of the electrochemical process that generates electrophilic adducts such as **2.1** and **2.2**. In principle, either the thianthrene radical cation or its dication ($\mathbf{TT}^{2+}$) could react with an alkene to produce these dicationic adducts[41,47]. We found that standard constant current conditions operate slightly above the requisite voltage to oxidize **TT** ($E_{1/2}$(**TT**) = 0.8 V vs Fc/Fc^{+}) for the majority of the reaction and significantly below the voltage required to oxidize $\mathbf{TT}^{+\bullet}$ to the $\mathbf{TT}^{2+}$ ($E_{1/2}$ ($\mathbf{TT}^{+\bullet}$) = 1.4 V vs Fc/Fc^{+}) (Fig. 2.4a)[41,48]. However, we suspected that disproportionation of $\mathbf{TT}^{+\bullet}$ to provide the $\mathbf{TT}^{2+}$ *in situ* could be kinetically relevant (see Supplementary Fig. S4 for cyclic voltammetry experiments consistent with this hypothesis)[47,49,50]. Since disproportionation will become increasingly favored as **TT** is anodically consumed, we monitored the conversion of alkene over the course of a typical reaction. Following a brief induction period as $\mathbf{TT}^{+\bullet}$ is generated, alkene is slowly consumed in a pseudo 0^{th} order fashion but then the rate sharply increases mid-way through the reaction. Electrochemical analysis reveals that this inflection point occurs when sufficient charge has been passed to oxidize all of the neutral thianthrene to its radical cation congener (1 F/mol **TT**); however, no significant anodic voltage occurs in parallel with this rate change. Given that comproportionation processes will be minimized once **TT** has been anodically consumed, these data are consistent with the hypothesis that disproportionation to form $\mathbf{TT}^{2+}$ is responsible for the increased rate of adduct formation in this second regime. Furthermore, increasing initial thianthrene concentration but maintaining the same current delays the sharp rate increase but has no impact on the initial product forming regime of the reaction (Fig. 2.4b). This is consistent with addition of $\mathbf{TT}^{+\bullet}$ to the alkene dominating the reaction until **TT** is consumed. Given the prediction that these two phases of the reaction proceed through distinct mechanistic pathways, we evaluated the

selectivity for *mono,* **2.1**, *vs. bis*, **2.2**, adducts as a function of time. We found that exclusively *bis* adduct **2.2** is formed initially followed by rapid generation of *mono* adduct **2.1**, once the concentration of **TT** is low enough to render disproportionation kinetically relevant. This constitutes an unusual kinetic scenario, wherein two products are each formed in exceptionally high selectivity but at different stages of the reaction. To further evaluate the relevance of a transiently generated thianthrene dication, we compared our typical electrolysis conditions with an applied potential sufficient to anodically oxidize the radical cation to the dication without relying on disproportionation. These conditions resulted in an appreciable rate acceleration relative to standard constant current reaction conditions along with exclusive formation of *mono* adduct **2.1** (Fig. 2.4d, see Appendix A section 3). Based on these preliminary data, we propose that the *mono* adduct **2.1** is formed through the following sequence of steps under standard reaction conditions: (1) anodic oxidation of thianthrene to the radical cation; (2) disproportionation to generate the

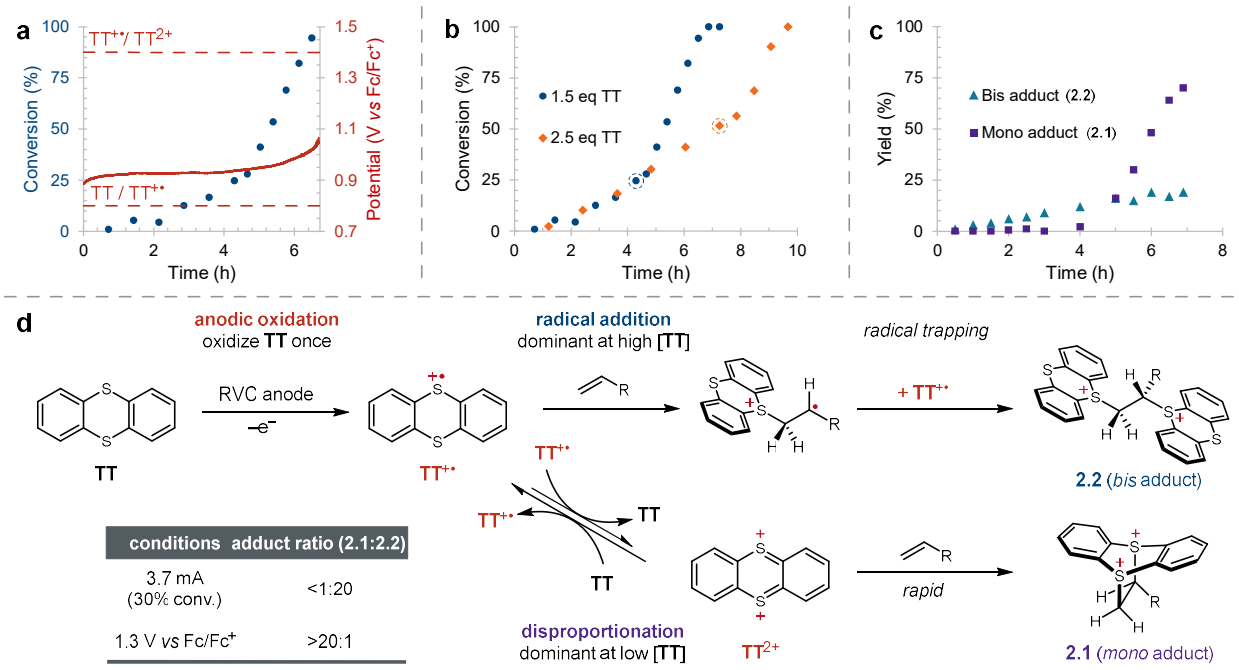

Figure 2.4. Mechanistic insight into adduct formation. a, Reaction profile under conditions of standard constant current for alkene conversion (left y-axis, blue) as a function of time (x-axis) overlaid with anodic working potential (right y-axis, red). **b**, Impact of increased thianthrene equivalents on alkene conversion under constant current electrolysis (3.7 mA). The dotted circle indicates the point at which 1 F mol^{-1} thianthrene has been passed. **c**, Formation of adducts **1** and **2** as a function of time during constant current electrolysis (3.7 mA). **d**, Plausible routes for the formation of mono and bis adducts. See Supplementary Information for full experimental details. Fc, ferrocene; R, $(CH_2)_2Ph$. Percentage yield and percentage conversion are relative to the alkene starting material.

thianthrenium dication; (3) formal cycloaddition with the alkene (Fig. 2.4d). The *bis* adduct **2.2** could be formed by direct radical addition of $\mathbf{TT}^{+\bullet}$ across the alkene followed by coupling between the transient distonic radical cation and the persistent thianthrene radical cation $\mathbf{TT}^{+\bullet}$.

2.4 Conclusion

Overall, we identified an electrochemical strategy to access a metastable, dicationic intermediate from alkenes. We found that, unlike conventional dielectrophiles (e.g. 1,2-dihalides), these species were cleanly transformed into aziridine products by simple treatment with base and amine. This method represents a new approach to generate *N*-alkyl aziridines by coupling widely available primary amine nucleophiles and unactivated alkene substrates. This scalable procedure unlocks efficient access to diverse aziridine building blocks bearing sensitive functional groups that are challenging to access through more conventional approaches. Reaction monitoring experiments revealed an unusual kinetic scenario wherein the mechanism of adduct formation changes sharply as **TT** is anodically consumed. We anticipate that this new electrochemical transformation will find immediate application in organic synthesis. Moreover, the results reported herein set the stage for the development of a wide range of alkene difunctionalization reactions that remain challenging to accomplish via more conventional approaches.

2.5 Acknowledgements

We thank A. Wendlandt, M. Levin and. D. Weix for suggestions and manuscript proofreading. We also acknowledge A. Hoque and F. Wang in the Stahl laboratory for the use of, and technical assistance with, the electrochemical flow reactor. Additionally, we thank the Weix, Stahl, Yoon and Schomaker groups for sharing their chemical inventories. B. J. Thompson is acknowledged for his assistance with the design and fabrication of the power supply. T. Drier is acknowledged for the fabrication of electrochemical glassware. A. M. Wheaton is acknowledged for assistance with crystallographic studies. We also acknowledge support and suggestions from all members of the Wickens group throughout the investigation of this project. This work was supported financially by the Office of

the Vice Chancellor for Research and Graduate Education at the University of Wisconsin–Madison, with funding from the Wisconsin Alumni Research Foundation. Spectroscopic instrumentation was supported by a gift from P. J. and M. M. Bender, by National Science Foundation (NSF) grant CHE-1048642, and by National Institutes of Health (NIH) grants 1S10OD020022-1 and S10 OD01225. This study also made use of the National Magnetic Resonance Facility at Madison, which is supported by NIH grants P41GM136463 (old number P41GM103399 (NIGMS)) and P41RR002301. Equipment was purchased with funds from the University of Wisconsin–Madison, the NIH (grants P41GM103399, S10RR02781, S10RR08438, S10RR023438, S10RR025062 and S10RR029220), the NSF (DMB-8415048, OIA-9977486 and BIR-9214394), and the US Department of Agriculture (USDA). The Bruker D8 VENTURE Photon III X-ray diffractometer was partially funded by NSF award CHE-1919350 to the University of Wisconsin–Madison Department of Chemistry.

2.6 Author Contribution

Z.K.W., D.E.H. and D.J.W. designed the project. D.E.H., D.J.W. and M.J.K. performed the experiments and collected the data. I.A.G. collected and analysed X-ray data to provide crystal structures. Z.K.W., D.E.H., D.J.W. and M.J.K. analysed the data and contributed to writing the manuscript. D.E.H. and D.J.W. contributed equally.

2.7 References

1. Sweeney, J. B. Aziridines: epoxides' ugly cousins? *Chem. Soc. Rev.* **31**, 247–258 (2002).
2. Stanković, S. *et al.* Regioselectivity in the ring opening of non-activated aziridines. *Chem. Soc. Rev.* **41**, 643–665 (2012).
3. Botuha, C., Chemla, F., Ferreira, F. & Pérez-Luna, A. Aziridines in Natural Product Synthesis. in *Heterocycles in Natural Product Synthesis* 1–39 (John Wiley & Sons, Ltd, 2011).
4. Ismail, F. M. D., Levitsky, D. O. & Dembitsky, V. M. Aziridine alkaloids as potential therapeutic agents. *Eur. J. Med. Chem.* **44**, 3373–3387 (2009).
5. Thibodeaux, C. J., Chang, W. & Liu, H. Enzymatic Chemistry of Cyclopropane, Epoxide, and Aziridine Biosynthesis. *Chem. Rev.* **112**, 1681–1709 (2012).
6. Lowden, P. A. S. Aziridine Natural Products – Discovery, Biological Activity and Biosynthesis. in *Aziridines and Epoxides in Organic Synthesis* 399–442 (John Wiley & Sons, Ltd, 2006).

7. Roth, H. G., Romero, N. A. & Nicewicz, D. A. Experimental and Calculated Electrochemical Potentials of Common Organic Molecules for Applications to Single-Electron Redox Chemistry. *Synlett* **27**, 714–723 (2016).
8. Evans, D. A., Faul, M. M. & Bilodeau, M. T. Copper-catalyzed aziridination of olefins by (N-(p-toluenesulfonyl)imino)phenyliodinane. *J. Org. Chem.* **56**, 6744–6746 (1991).
9. Sweeney, J. B. Synthesis of Aziridines. in *Aziridines and Epoxides in Organic Synthesis* 117–144 (John Wiley & Sons, Ltd, 2006).
10. Osborn, H. M. I. & Sweeney, J. The asymmetric synthesis of aziridines. *Tetrahedron: Asymmetry* **8**, 1693–1715 (1997).
11. Wang, H., Yang, J. C. & Buchwald, S. L. CuH-Catalyzed Regioselective Intramolecular Hydroamination for the Synthesis of Alkyl-Substituted Chiral Aziridines. *J. Am. Chem. Soc.* **139**, 8428–8431 (2017).
12. Legnani, L., Prina-Cerai, G., Delcaillau, T., Willems, S. & Morandi, B. Efficient access to unprotected primary amines by iron-catalyzed aminochlorination of alkenes. *Science* **362**, 434–439 (2018).
13. Jat, J. L. *et al.* Direct Stereospecific Synthesis of Unprotected N-H and N-Me Aziridines from Olefins. *Science* **343**, 61–65 (2014).
14. Ma, Z., Zhou, Z. & Kürti, L. Direct and Stereospecific Synthesis of N-H and N-Alkyl Aziridines from Unactivated Olefins Using Hydroxylamine-O-Sulfonic Acids. *Angew. Chem. Int. Ed.* **56**, 9886–9890 (2017).
15. Cheng, Q.-Q. *et al.* Organocatalytic nitrogen transfer to unactivated olefins via transient oxaziridines. *Nat. Catal.* **3**, 386–392 (2020).
16. Falk, E., Makai, S., Delcaillau, T., Gürtler, L. & Morandi, B. Design and Scalable Synthesis of N-Alkylhydroxylamine Reagents for the Direct Iron-Catalyzed Installation of Medicinally Relevant Amines. *Angew. Chem. Int. Ed.* **59**, 21064–21071 (2020).
17. Munnuri, S., Anugu, R. R. & Falck, J. R. Cu(II)-Mediated N–H and N-Alkyl Aryl Amination and Olefin Aziridination. *Org. Lett.* **21**, 1926–1929 (2019).
18. Govaerts, S. *et al.* Photoinduced Olefin Diamination with Alkylamines. *Angew. Chem. Int. Ed.* **59**, 15021–15028 (2020).
19. Commercial availability of primary amines: 1,054,553. Source: eMolecules database, accessed December 9th, 2020 using Elsevier REAXYS.
20. Lohray, B. B., Gao, Y. & Sharpless, K. B. One pot synthesis of homochiral aziridines and aminoalcohols from homochiral 1,2-cyclic sulfates. *Tetrahedron Lett.* **30**, 2623–2626 (1989).
21. Wenker, H. The Preparation of Ethylene Imine from Monoethanolamine. *J. Am. Chem. Soc.* **57**, 2328–2328 (1935).
22. Li, X., Chen, N. & Xu, J. An Improved and Mild Wenker Synthesis of Aziridines. *Synthesis* **20**, 3423–3428 (2010).
23. Yan, M., Kawamata, Y. & Baran, P. S. Synthetic Organic Electrochemical Methods Since 2000: On the Verge of a Renaissance. *Chem. Rev.* **117**, 13230–13319 (2017).
24. Wiebe, A. *et al.* Electrifying Organic Synthesis. *Angew. Chem. Int. Ed.* **57**, 5594–5619 (2018).
25. Francke, R. & Little, R. D. Redox catalysis in organic electrosynthesis: basic principles and recent developments. *Chem. Soc. Rev.* **43**, 2492–2521 (2014).
26. Moeller, K. D. Using Physical Organic Chemistry To Shape the Course of Electrochemical Reactions. *Chem. Rev.* **118**, 4817–4833 (2018).
27. Yoshida, J., Kataoka, K., Horcajada, R. & Nagaki, A. Modern Strategies in Electroorganic Synthesis. *Chem. Rev.* **108**, 2265–2299 (2008).
28. Sauer, G. S. & Lin, S. An Electrocatalytic Approach to the Radical Difunctionalization of Alkenes. *ACS Catal.* **8**, 5175–5187 (2018).
29. Doobary, S., Sedikides, A. T., Caldora, H. P., Poole, D. L. & Lennox, A. J. J. Electrochemical Vicinal Difluorination of Alkenes: Scalable and Amenable to Electron-Rich Substrates. *Angew. Chem. Int. Ed.* **59**, 1155–1160 (2020).

30. Siu, T. & Yudin, A. K. Practical Olefin Aziridination with a Broad Substrate Scope. *J. Am. Chem. Soc.* **124**, 530–531 (2002).
31. Oseka, M. *et al.* Electrochemical Aziridination of Internal Alkenes with Primary Amines. *Chem* **7**, 255-266 (2020)
32. Chen, J. *et al.* Electrocatalytic Aziridination of Alkenes Mediated by n-Bu4NI: A Radical Pathway. *Org. Lett.* **17**, 986–989 (2015).
33. Li, J. *et al.* Electrochemical Aziridination by Alkene Activation Using a Sulfamate as the Nitrogen Source. *Angew. Chem. Int. Ed.* **57**, 5695–5698 (2018).
34. Yoshida, J., Shimizu, A. & Hayashi, R. Electrogenerated Cationic Reactive Intermediates: The Pool Method and Further Advances. *Chem. Rev.* **118**, 4702–4730 (2018).
35. Hayashi, R., Shimizu, A. & Yoshida, J. The Stabilized Cation Pool Method: Metal- and Oxidant-Free Benzylic C–H/Aromatic C–H Cross-Coupling. *J. Am. Chem. Soc.* **138**, 8400–8403 (2016).
36. Shine, H. J., Bandlish, B. K., Mani, S. R. & Padilla, A. G. Ion radicals. 43. Addition of thianthrene and phenoxathiin cation radicals to alkenes and alkynes. *J. Org. Chem.* **44**, 915–917 (1979).
37. Shine, H. J. *et al.* Adducts of Phenoxathiin and Thianthrene Cation Radicals with Alkenes and Cycloalkenes. *J. Org. Chem.* **68**, 8910–8917 (2003).
38. Rangappa, P. & Shine, H. J. An overview of some reactions of thianthrene cation radical. Products and mechanisms of their formation. *J. Sulfur Chem*. **27**, 617–664 (2006).
39. Berger, F. *et al.* Site-selective and versatile aromatic C−H functionalization by thianthrenation. *Nature* **567**, 223–228 (2019).
40. Engl, P. S. *et al.* C–N Cross-Couplings for Site-Selective Late-Stage Diversification via Aryl Sulfonium Salts. *J. Am. Chem. Soc.* **141**, 13346–13351 (2019).
41. Chen, J., Li, J., Plutschack, M. B., Berger, F. & Ritter, T. Regio- and Stereoselective Thianthrenation of Olefins To Access Versatile Alkenyl Electrophiles. *Angew. Chem. Int. Ed.* **59**, 5616–5620 (2020).
42. Houmam, A., Shukla, D., Kraatz, H.-B. & Wayner, D. D. M. Electrosynthesis of Mono- and Bisthianthrenium Salts. *J. Org. Chem.* **64**, 3342–3345 (1999).
43. Iwai, K. & Shine, H. J. Ion radicals. 46. Reactions of the adducts of thianthrene and phenoxathiin cation radicals and cyclohexene with nucleophiles. *J. Org. Chem.* **46**, 271–276 (1981).
44. Mitchell, S. C. & Waring, R. H. Fate of thianthrene in biological systems. *Xenobiotica* **47**, 731–740 (2017).
45. Kaiser, D., Klose, I., Oost, R., Neuhaus, J. & Maulide, N. Bond-Forming and -Breaking Reactions at Sulfur(IV): Sulfoxides, Sulfonium Salts, Sulfur Ylides, and Sulfinate Salts. *Chem. Rev.* **119**, 8701–8780 (2019).
46. Bright, G. M., Brodney, M. A. & Wlodecki, B. Pyridyloxymethyl and Benzisoxazole Azabicyclic Derivatives. WO/2004/081007 (Pfizer, 2004).
47. Qian, D.-Q., Shine, H. J., Guzman-Jimenez, I. Y., Thurston, J. H. & Whitmire, K. H. Mono- and Bisadducts from the Addition of Thianthrene Cation Radical Salts to Cycloalkenes and Alkenes. *J. Org. Chem.* **67**, 4030–4039 (2002).
48. Speer, M. E. *et al.* Thianthrene-functionalized polynorbornenes as high-voltage materials for organic cathode-based dual-ion batteries. *Chem. Commun.* **51**, 15261–15264 (2015).
49. Murata, Y. & Shine, H. J. Ion radicals. XVIII. Reactions of thianthrenium perchlorate and thianthrenium trichlorodiiodide. *J. Org. Chem.* **34**, 3368–3372 (1969).
50. Sandford, C. et al. A synthetic chemist's guide to electroanalytical tools for studying reaction mechanisms. *Chem. Sci.* **10**, 6404–6422 (2019).

Chapter 3: Electrochemical Synthesis of Allylic Amines from Terminal Alkenes and Secondary Amines

This chapter has been published and adapted with permission from:

Wang, D. J.; Targos, K.; Wickens, Z. K. Electrochemical Synthesis of Allylic Amines from Terminal Alkenes and Secondary Amines. *J. Am. Chem. Soc.* **2021**, *143* (51), 21503–21510.

3.1 Abstract

Allylic amines are valuable synthetic targets en route to diverse biologically active amine products. Current allylic C–H amination strategies remain limited with respect to the viable *N*-substituents. Herein we disclose a new electrochemical process to prepare aliphatic allylic amines by coupling two abundant starting materials: secondary amines and unactivated alkenes. This oxidative transformation proceeds via electrochemical generation of an electrophilic adduct between thianthrene and the alkene substrates. Treatment of these adducts with aliphatic amine nucleophiles and base provides allylic amine products in high yield. This synthetic strategy is also amenable to functionalization of feedstock gaseous alkenes at one atmosphere. In the case of 1-butene, high *Z*-selective crotylation is observed. This strategy, however, is not limited to the synthesis of simple building blocks; complex biologically active molecules are suitable as both alkene and amine coupling partners. Preliminary mechanistic studies implicate vinylthianthrenium salts as key reactive intermediates.

3.2 Introduction

Aliphatic amines are prevalent in pharmaceuticals, natural products, and other biologically active molecules.[1–3] Thus, the development of strategies to rapidly construct C–N bonds is of longstanding synthetic importance. Allylic amines are particularly valuable building blocks due to their synthetic

versatility.[4–8] A deceptively simple strategy to prepare alkyl allylic amines would be the oxidative coupling of alkenes and aliphatic amines (Fig. 3.1, top). Such a reaction would be an attractive complement to classic amine allylation strategies such as S_N2[9–16] and π-allyl substitution reactions[17–24] that rely on prefunctionalized electrophiles.[25] However, successful realization of such a transformation requires a strategy to promote the desired oxidative C–N bond-forming process without undesired oxidation of the aliphatic amine starting materials or the aliphatic allylic amine products (0.8 – 1.1 V *vs* SCE).[26] As a consequence, generation of aliphatic allylic amines by oxidative coupling of alkenes and amines has remained elusive.[27–36] Instead, pioneering reports have established powerful C–H functionalization protocols to construct allylic C–N bonds using oxidatively stable nitrogen sources in diverse intermolecular amination reactions.[37–46] These reaction manifolds primarily take advantage of electronically deactivated nitrogen pronucleophiles[47–59] and nitrene precursors.[60–74] As a direct result, these established approaches offer limited access to aliphatic allylic amine products and instead furnish

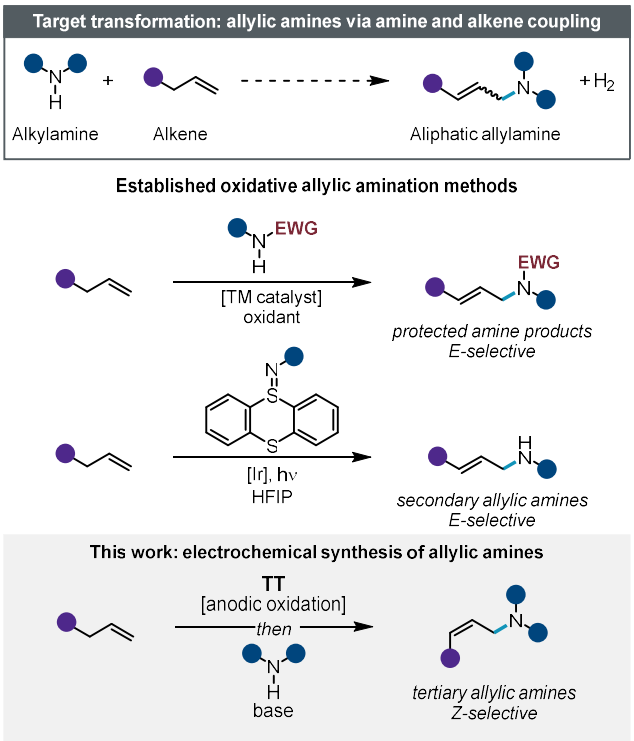

Figure 3.1. Project overview. Idealized transformation to access alkyl allylic amines (top); representative established allylic C–H amination reactions (middle); schematic overview of this work (bottom). **TT** = thianthrene.

products with electron-deficient nitrogen atoms, such as allylic sulfonamides and carbamates (Fig. 3.1, middle).

Despite the significant progress in other oxidative amination reactions,[75–80] to date, there is a single intermolecular allylic C−H amination reaction that directly furnishes aliphatic allylic amine products.[27] This strategy, reported by Ritter and co-workers in 2020, exploits photochemically-activated sulfilimine reagents as nitrogen sources. While this is a landmark report in allylic C–H amination, installation of different *N*-substituents in the product requires preparation of unique electrophilic reagents. Additionally, this reagent design strategy is not readily amenable to tertiary amine synthesis. Accordingly, a complementary synthetic technology that generates allylic amines via an oxidative coupling of unactivated amine nucleophiles and alkenes remains poised to have a significant impact on organic synthesis. Such an approach would directly translate the >4 million commercially available aliphatic amines into versatile allylic amine building blocks.[81]

We recently developed an electrochemical strategy to engage oxidatively sensitive nucleophiles in net oxidative alkene difunctionalization reactions.[80] Our approach draws inspiration from Yoshida's pioneering cation pool work[82–84] and contributes to a rapidly growing body of literature exploiting oxidized thianthrene derivatives as synthetic intermediates.[85–92] Specifically, we leveraged electrochemistry to cleanly generate dicationic adducts between unactivated alkenes and thianthrene (**TT**),[93,94] a safe[95] and inexpensive[96] reagent. This strategy circumvents the need for oxidatively stable coupling partners in net oxidative alkene functionalization reactions; the oxidative alkene activation event is decoupled from nucleophilic substitution. In our first report, we leveraged this approach to enable the formal coupling of primary amine nucleophiles with alkenes to furnish aziridine products through a one-pot, two-operation process. Herein, we report an electrochemical strategy to prepare linear, tertiary allylic amine products from aliphatic amines and alkenes with contrathermodynamic *Z*-selectivity. This is accomplished by diverting the reactivity of the dicationic alkene-thianthrene adducts down a formal substitution-elimination pathway.

3.3 Results and discussion

Our development of an allylic amination process began with an unexpected observation during the study of our dication pool aziridination reaction. We found that, upon exposure to excess tert-butylamine, the electrogenerated mixture of dicationic electrophiles **3.1** and **3.2** was transformed into the linear allylic amine product **3.3** in 3:1 *Z:E* ratio rather than the expected *N*-*tert*-butylaziridine (Scheme 3.1). We suspected this net substitution-elimination process may be a consequence of the increased steric bulk about the nitrogen nucleophile. This rationalization suggested that secondary amine nucleophiles may proceed down an analogous allyic amination pathway rather than forming aziridinium intermediates expected to lead to diamination products.[97] Such a reaction would furnish tertiary *(Z)*-allylic amine products and serve as an ideal complement to the recent secondary *(E)*-allylic amine synthesis developed by Ritter and co-workers.[27] To probe this hypothesis, we exposed an electrogenerated mixture of **3.1** and **3.2** to an excess of *N*-methylbenzylamine. To our delight, this resulted in conversion of the adduct to the corresponding allylic amine product **3.4** with 4:1 *Z*-selectivity. Next, we aimed to identify a suitable stoichiometric base to lower the necessary equivalents of amine (Table 3.1). We surveyed a range of bases and found *i*-Pr_2NEt promoted the desired allylic functionalization in 79% yield with a 1:1 stoichiometry of amine and alkene starting materials. Increasing the steric bulk of the amine base to triisobutylamine resulted in formation of a vinyl thianthrenium salt **3.5** alongside a reduced yield of allylic amine product (entry 2). Smaller amine bases, such as triethylamine, also resulted in reduced yield (40%) of the desired allylic amine product **3.4** due to competitive formation of an allylic ammonium salt **3.6** derived from the triethylamine base (entry 3). Alternative bases, such as Cs_2CO_3, promoted the desired allylic functionalization albeit in diminished *Z*-selectivity (entry 4). Weaker inorganic bases, such as $NaHCO_3$, provided vinyl thianthrenium product **3.5** alongside traces of the desired allylic amine (entry 5). Overall, this method provides an appealing one-pot synthesis of allylic amine building blocks. With optimized conditions in hand, we next investigated the alkene scope for this allylic amination process, employing *N*-methylbenzylamine as a model secondary amine nucleophile (Table 3.2).

Allylic amination of 4-phenyl-1-butene and an aryl bromide derivative provided the desired *(Z)*-allylic amine products (**3.4**, **3.7**) without detectable arene thianthrenation. Likewise, selective alkene

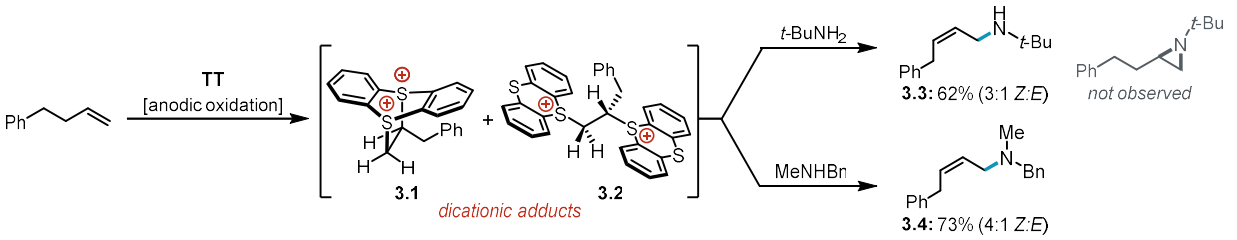

aReactions were conducted using alkene (0.15 mmol), TT (0.23 mmol), 3 mL MeCN (0.2 M n-Bu4NPF6), I = 4.0 mA, 2.5 h (2.5 F mol−1 alkene); then amine (1.2 mmol), 16 h. Yields and Z:E ratios were determined by 1H NMR analysis. See the Supporting Information (SI) for details)

Scheme 3.1. Initial observations of allylic amination from dicationic adducts.

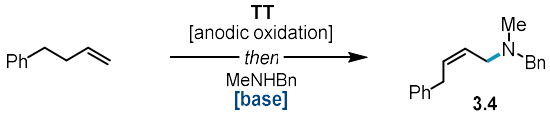

entry	base	yield **3.4** (*Z*:*E*)	yield **3.5**
1	*i*-Pr_2NEt	79% (6:1)	n.d.
2	*i*-Bu_3N	27% (5:1)	52%[a]
3	Et_3N	40% (3:1)	n.d.
4	Cs_2CO_3	61% (3:1)	n.d.
5	$NaHCO_3$	<5%	67%[b]

Observed side products

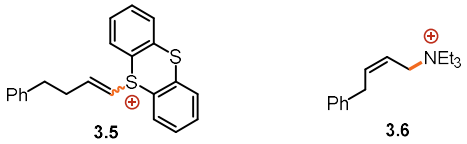

Reactions were conducted using alkene (0.15 mmol), TT (0.23 mmol), 3 mL MeCN (0.2 M n-Bu4NPF6), I = 4.0 mA, 2.5 h (2.5 F mol−1 alkene); then base (1.1 mmol), amine (0.30 mmol), 16 h. Yields and Z:E ratios were determined by 1H NMR analysis. See the Supporting Information (SI) for details. n.d. = not detected. [a]1:5 Z:E ratio. [b]1:6 Z:E ratio.

Table 3.1. Base evaluation for the allylic amination reaction

functionalization in the presence of an unconjugated alkyne was obtained with high *Z*-selectivity (**3.8**). This result, alongside with tolerance of aromatic substrates (**3.4, 3.7**), illustrates the exquisite chemoselectivity for adduct formation between oxidized thianthrene and alkene over previously observed thianthrenation of arenes[85] and alkynes.[98] Unconjugated dienes underwent selective monofunctionalization to provide *(Z)*-unconjugated diene **3.9** and *(E)*-conjugated diene **3.10** building

blocks. Alkenes bearing a variety of proximal functional groups, such as nitrile (**3.11**), acetate (**3.12**), ether (**3.13**), and phthalimide (**3.14**) each efficiently delivered the desired allylic amine products. These examples illustrate the viability of accessing allylic amine building blocks with a secondary homoallylic

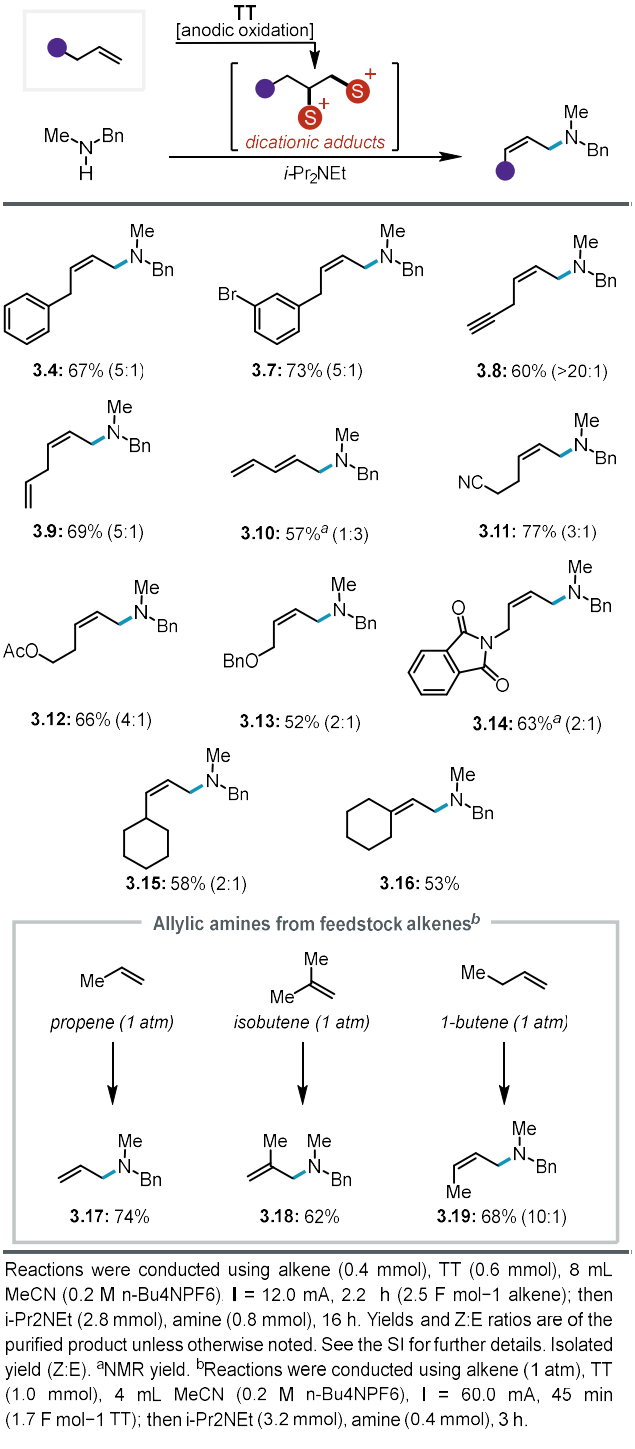

Reactions were conducted using alkene (0.4 mmol), TT (0.6 mmol), 8 mL MeCN (0.2 M n-Bu4NPF6). I = 12.0 mA, 2.2 h (2.5 F mol−1 alkene); then i-Pr2NEt (2.8 mmol), amine (0.8 mmol), 16 h. Yields and Z:E ratios are of the purified product unless otherwise noted. See the SI for further details. Isolated yield (Z:E). [a]NMR yield. [b]Reactions were conducted using alkene (1 atm), TT (1.0 mmol), 4 mL MeCN (0.2 M n-Bu4NPF6), I = 60.0 mA, 45 min (1.7 F mol−1 TT); then i-Pr2NEt (3.2 mmol), amine (0.4 mmol), 3 h.

Table 3.2. Scope of alkenes for allylic amination via dication pool strategy

(**3.11, 3.12**) or allyic (**3.13**, **3.14**) functional group handle for further elaboration. Allylcyclohexane underwent allylic amination to furnish the sterically hindered vinylcyclohexane product **3.15**.[99] Finally, vinylcyclohexane underwent allylic amination to form trisubstituted allylic amine **3.16**.[100]

We next probed whether this oxidative coupling strategy is also amenable to functionalization of commodity feedstock alkenes derived from steam cracking and related petroleum refinery processes (Table 3.2).[101,102] Electrolysis of thianthrene under one atmosphere of propene and isobutene each generated the desired dicationic adducts. Treatment of these reaction mixtures with *i*-Pr_2NEt and *N*-methylbenzylamine resulted in allyl- and methallylamine products (**3.17, 3.18**) in high yields relative to the amine starting material. Traditional methods to produce these products rely on S_N2 displacement of the corresponding allylic halides, which are carcinogenic and also industrially derived from the same feedstock alkenes through a multistep oxidation-halogenation sequence.[103,104] In contrast, this electrochemical method offers an appealing alternative protocol that produces H_2 gas as the stoichiometric byproduct since thianthrene can be recycled and reused.[105] Notably, 1-butene—the simplest alkene to form stereoisomeric allylic amine products—gave allylic amine **3.19** with high *Z*-selectivity. This highlights the value of this new transformation beyond a green chemistry context; crotylhalides are only readily available as an *(E)*-dominant mixture.

Next, we probed the scope of the amine nucleophile, employing 1-butene as the alkene coupling partner (Table 3). These transformations furnish synthetically attractive *(Z)*-crotylamine building blocks that are not straightforward to access using conventional alkylation chemistry. Simple, acyclic dialkylamines **(3.20–3.23)** resulted in high yields and *Z*-selectivity. Of note, even sterically hindered amines delivered the corresponding (*Z)*-crotylamine product **3.21**, albeit with a diminished yield. Heteroaromatic and saturated heterocycles are tolerated both as pendant functional groups (**3.22**, **3.23**) or as the nucleophile itself (**3.24–3.28**). Amine nucleophiles bearing potential competing nucleophiles were also selectively transformed into *(Z)*-allylic amine products (**3.24, 3.26**), preserving the unprotected functional groups for further derivatization. In addition to spirocyclic piperidine **(3.24)**, other bicyclic heterocycles with morpholine **(3.27)** and piperazine **(3.28)** cores underwent *Z*-selective crotylation.

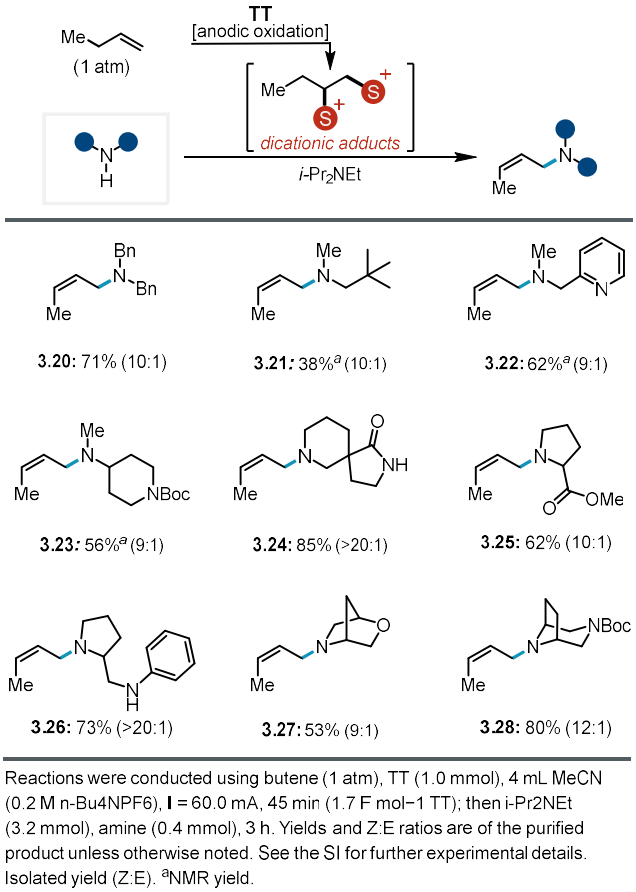

Reactions were conducted using butene (1 atm), TT (1.0 mmol), 4 mL MeCN (0.2 M n-Bu4NPF6), I = 60.0 mA, 45 min (1.7 F mol−1 TT); then i-Pr2NEt (3.2 mmol), amine (0.4 mmol), 3 h. Yields and Z:E ratios are of the purified product unless otherwise noted. See the SI for further experimental details. Isolated yield (Z:E). [a]NMR yield.

Table 3.3. Scope of (*Z*)-crotylamine building blocks.

In addition to the efficient formation of simple, allylic amine building blocks, we envisioned that this newly realized oxidative allylic amination methodology would also streamline the synthesis of more complex amine products (Table 3.4). With this in mind, we next evaluated a range of drug-like compounds as both alkene and amine coupling partners. Due to their structural complexity, these substrates each contain numerous functional groups expected to be liabilities for typical oxidative allylic amination procedures. Lewis basic heterocycles, such as pyridine (**3.29**) and pyrazole (**3.30**) as well as oxidatively sensitive electron-rich aromatic systems (**3.31–3.33**),[26] each delivered the desired allylic amine products. Additionally, allylic amines could be obtained from substrates bearing a variety of saturated heterocycles, including piperidine (**3.29**), morpholine (**3.30**), homopiperazine (**3.34**), and piperizine (**3.35**). Of note, the homopiperazine (**3.34**) and piperizine substrates (**3.35**), each contain a competent tertiary amine nucleophile yet produce the desired allylic amine products in synthetically

useful yield. This chemoselectivity extended to other nucleophilic functional groups; unprotected alcohols and arylamines (**3.31**, **3.32**) did not compete with the secondary amine under these allylation conditions, leaving them as synthetic handles for further functionalization. An array of different aryl halides were well tolerated, including both medicinally relevant fluorinated groups (**3.30**, **3.33**, **3.35**) as well as aryl bromides (**3.32**) and chlorides (**3.29**) that readily participate in cross-coupling reactions.

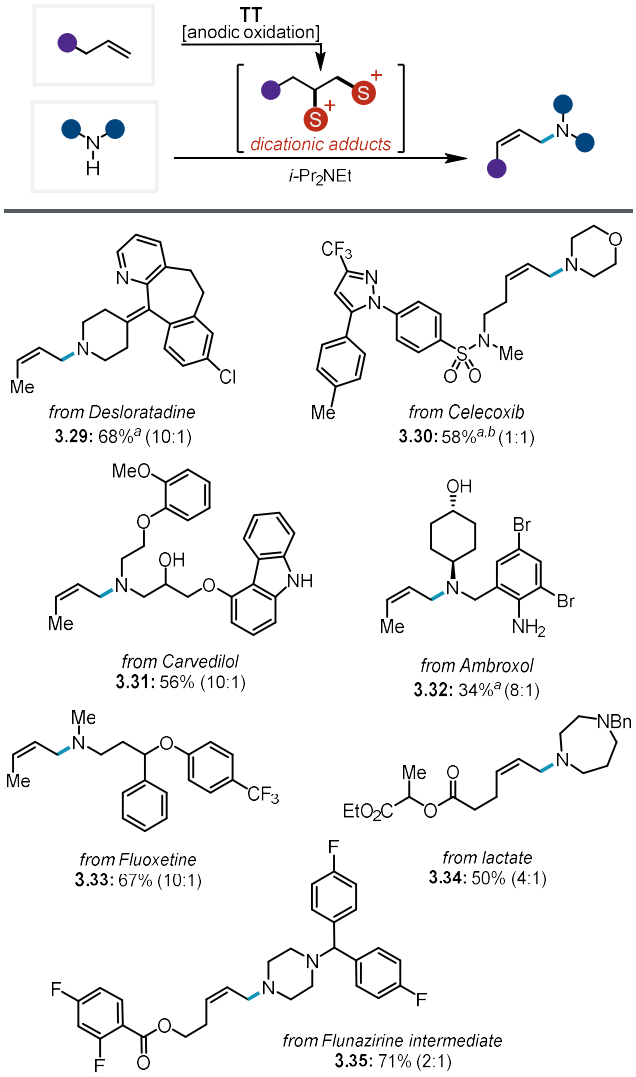

Limiting amine reactions were conducted using alkene (1 atm), TT (1.0 mmol), 4 mL MeCN (0.2 M n-Bu4NPF6), I = 60.0 mA, 45 min (1.7 F mol−1 TT); then i-Pr2NEt (3.2 mmol), amine (0.4 mmol), 3 h. Limiting alkene reactions were conducted using alkene (0.4 mmol), TT (0.6 mmol), 8 mL MeCN (0.2 M n-Bu4NPF6), I = 12.0 mA, 2.2 h (2.5 F mol−1 alkene); then i-Pr2NEt (2.8 mmol), amine (0.4 mmol), 16 h. Yields and Z:E ratios are of the purified product unless otherwise noted. See the SI for further details. Isolated yield (Z:E). [a]NMR yield. [b]0.8 mmol amine.

Table 3.4. Oxidative coupling of complex bioactive molecules

Next, we aimed to provide some preliminary mechanistic insight into this new process. Monitoring the transformation of dicationic adducts to allylic amine over time revealed that the adducts are rapidly consumed and a vinylthianthrenium salt is generated. Given the basic conditions, we suspected that the vinylthianthrenium salt was likely a key intermediate en route to the observed allylic amine product rather than an off-cycle reservoir. To probe this specific question, we directly prepared vinylthianthrenium salt **3.36** by base-induced elimination of the electrochemically generated dicationic adducts between 1-butene and thianthrene. We then subjected this isolated vinylthianthrenium **3.36** to otherwise standard substitution conditions (see Appendix B for experimental details). Under these conditions, the allyic amine product **3.19** was formed in 75% yield and identical stereoselectivity to what is observed under standard conditions (Eq. 3.1). This is consistent with the vinyl thianthrenium salt

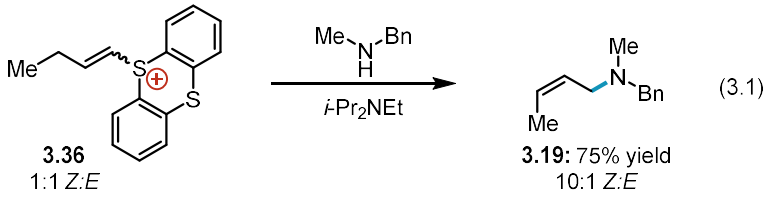

(3.1)

serving as an on pathway intermediate. Based on these data, we have constructed a working mechanistic model wherein the vinylthianthrenium salt undergoes a base-induced isomerization to an allylic thianthrenium intermediate. This species is then rapidly trapped with the amine nucleophile. Indeed, there is a single report of vinylsulfonium salts being converted to allylic amines.[106] Studies are underway to clarify the mechanistic details of this reaction, particularly the stereodetermining step for the process. Beyond the mechanistic implications, however, these data also indicate that vinylthianthrenium salts prepared through chemical means[86] can be engaged as an electrophile for this transformation. We envision this may be valuable for practicing synthetic chemists in a small-scale research and development setting where electrochemistry offers a less significant advantage relative to more traditional synthetic tactics.

3.4 Conclusion

Overall, we developed an electrochemical synthesis of allylic amines from terminal alkenes and secondary amines. This represents the first example of a formal C–H functionalization approach to furnish tertiary aliphatic allylic amines as well as the first example of a strategy for oxidative allylic C–H functionalization that provides *Z*-selectivity. This linear-selective process exhibits good functional group tolerance and is attractive for substrates ranging from feedstock gas functionalization to derivatization of complex molecules. Furthermore, the conditions are operationally simple; no precautions to exclude air or moisture are necessary. Preliminary mechanistic studies indicate that vinylthianthrenium salts are key intermediates. We anticipate that this new electrochemical transformation will find immediate application in organic synthesis given the established synthetic utility of allylic amine building blocks. Moreover, we anticipate that the results reported herein set the stage for the development of a wide range of *Z*-selective allylic functionalization reactions that remain challenging to accomplish via more conventional approaches.

3.5 Acknowledgments

We thank Prof. Mark Levin for helpful discussions regarding this manuscript. We thank the Weix, Stahl, Yoon and Schomaker groups for sharing their chemical inventories. In addition, we would like to thank Prof. Samuel Gellman and the entire Gellman group for hosting the authors of this work during a temporary closure of our labs. Along this line, we also thank the staff of the Paul Bender Chemistry Instrumentation Center for enabling NMR and MS sample analysis during building construction. B. J. Thompson is acknowledged for his assistance with the design and fabrication of the power supply. T. Drier is acknowledged for the fabrication of electrochemical glassware. We also acknowledge support and suggestions from all members of the Wickens group throughout the investigation of this project. This work was financially supported by the Office of the Vice Chancellor for Research and Graduate Education at the University of Wisconsin-Madison, with funding from the Wisconsin Alumni Research

Foundation. This material is based upon work supported by the National Science Foundation Graduate Research Fellowship Program under Grant No. DGE-1747503 (K.T.). Any opinions, findings, and conclusions or recommendations expressed in this material are those of the author(s) and do not necessarily reflect the views of the National Science Foundation. Spectroscopic instrumentation was supported by a generous gift from Paul J. and Margaret M. Bender, the National Science Foundation (CHE-1048642), and the National Institutes of Health (S10OD012245 and 1S10OD020022-1).

3.6 Author Contributions

Z.K.W. and D.J.W. designed the project. All authors performed the experiments and collected the data. D.J.W. designed and implemented the mechanistic experiments. All authors contributed to writing the manuscript.

3.7 References

(1) Trowbridge, A.; Walton, S. M.; Gaunt, M. J. New Strategies for the Transition-Metal Catalyzed Synthesis of Aliphatic Amines. *Chem. Rev.* **2020**, *120* (5), 2613–2692. https://doi.org/10.1021/acs.chemrev.9b00462.

(2) Richter, M. F.; Drown, B. S.; Riley, A. P.; Garcia, A.; Shirai, T.; Svec, R. L.; Hergenrother, P. J. Predictive Compound Accumulation Rules Yield a Broad-Spectrum Antibiotic. *Nature* **2017**, *545* (7654), 299–304. https://doi.org/10.1038/nature22308.

(3) Vitaku, E.; Smith, D. T.; Njardarson, J. T. Analysis of the Structural Diversity, Substitution Patterns, and Frequency of Nitrogen Heterocycles among U.S. FDA Approved Pharmaceuticals. *J. Med. Chem.* **2014**, *57* (24), 10257–10274. https://doi.org/10.1021/jm501100b.

(4) For examples of synthetic strategies that exploit allylic amines as key intermediates, see references 5-8.

(5) Johannsen, M.; Jørgensen, K. A. Allylic Amination. *Chem. Rev.* **1998**, *98* (4), 1689–1708. https://doi.org/10.1021/cr970343o.

(6) Wang, M.; Xiao, F.; Bai, Y.; Hu, X. Reactions of Tertiary Allylic Amines and Dichlorocarbenes. *Synth. Commun.* **2015**, *45* (19), 2259–2265. https://doi.org/10.1080/00397911.2015.1075218.

(7) DeLuca, R. J.; Sigman, M. S. Anti-Markovnikov Hydroalkylation of Allylic Amine Derivatives via a Palladium-Catalyzed Reductive Cross-Coupling Reaction. *J. Am. Chem. Soc.* **2011**, *133* (30), 11454–11457. https://doi.org/10.1021/ja204080s.

(8) Weiner, B.; Baeza, A.; Jerphagnon, T.; Feringa, B. L. Aldehyde Selective Wacker Oxidations of Phthalimide Protected Allylic Amines: A New Catalytic Route to B3-Amino Acids. *J. Am. Chem. Soc.* **2009**, *131* (27), 9473–9474. https://doi.org/10.1021/ja902591g.

(9) Allylic S_N2 reactions can suffer from numerous problems such as poor regioselectivity between branched and linear products. In the case of amination, competitive overallylation of tertiary amine products can be a major challenge. For specific examples of these issues, see references 10-12.

(10) Mitsunobu, O. In *Comprehensive Organic Synthesis*; Trost, B. M., Fleming, I., Winterfeldt, E., Eds.; Pergamon Press: Oxford, 1991; Vol. 6, pp 22-28.
(11) Sen, S. E.; Roach, S. L. A Convenient Two-Step Procedure for the Synthesis of Substituted Allylic Amines from Allylic Alcohols. *Synthesis* **1995**, *1995* (07), 756–758. https://doi.org/10.1055/s-1995-4012.
(12) Solomons, T.W.G.S.; Fryhle, C.B.; Snyder S. A. In *Organic Chemistry*; Wiley: New York, 2016, pp 901-908.
(13) For selected successful examples of SN_2-type reactions, see references 14-16.
(14) Roughley, S. D.; Jordan, A. M. The Medicinal Chemist's Toolbox: An Analysis of Reactions Used in the Pursuit of Drug Candidates. *J. Med. Chem.* **2011**, *54* (10), 3451–3479. https://doi.org/10.1021/jm200187y.
(15) Brown, D. G.; Boström, J. Analysis of Past and Present Synthetic Methodologies on Medicinal Chemistry: Where Have All the New Reactions Gone? Miniperspective. *J. Med. Chem.* **2016**, *59* (10), 4443–4458. https://doi.org/10.1021/acs.jmedchem.5b01409.
(16) Taylor, A. R.; Katritzky, R. J. K. In *Comprehensive Organic Functional Group Transformations II.*; Elsevier; pp 255–300.
(17) For examples of amination of transition metal π-allyl intermediates derived from allylic electrophiles, see references 18-24.
(18) Trost, B. M.; Van Vranken, D. L. Asymmetric Transition Metal-Catalyzed Allylic Alkylations. *Chem. Rev.* **1996**, *96* (1), 395–422. https://doi.org/10.1021/cr9409804.
(19) Graening, T.; Schmalz, H.-G. Pd-Catalyzed Enantioselective Allylic Substitution: New Strategic Options for the Total Synthesis of Natural Products. *Angew. Chem. Int. Ed.* **2003**, *42* (23), 2580–2584. https://doi.org/10.1002/anie.200301644.
(20) Grange, R. L.; Clizbe, E. A.; Evans, P. A. Recent Developments in Asymmetric Allylic Amination Reactions. *Synthesis* **2016**, *48* (18), 2911-2968.
(21) Yamashita, Y.; Gopalarathnam, A.; Hartwig, J. F. Iridium-Catalyzed, Asymmetric Amination of Allylic Alcohols Activated by Lewis Acids. *J. Am. Chem. Soc.* **2007**, *129* (24), 7508–7509. https://doi.org/10.1021/ja0730718.
(22) You, S.-L.; Zhu, X.-Z.; Luo, Y.-M.; Hou, X.-L.; Dai, L.-X. Highly Regio- and Enantioselective Pd-Catalyzed Allylic Alkylation and Amination of Monosubstituted Allylic Acetates with Novel Ferrocene P,N-Ligands. *J. Am. Chem. Soc.* **2001**, *123* (30), 7471–7472. https://doi.org/10.1021/ja016121w.
(23) Takeuchi, R.; Ue, N.; Tanabe, K.; Yamashita, K.; Shiga, N. Iridium Complex-Catalyzed Allylic Amination of Allylic Esters. *J. Am. Chem. Soc.* **2001**, *123* (39), 9525–9534. https://doi.org/10.1021/ja0112036.
(24) Sundararaju, B.; Achard, M.; Bruneau, C. Transition Metal Catalyzed Nucleophilic Allylic Substitution: Activation of Allylic Alcohols via π-Allylic Species. *Chem. Soc. Rev.* **2012**, *41* (12), 4467–4483. https://doi.org/10.1039/C2CS35024F.
(25) While reductive amination is a classic approach for the synthesis of aliphatic amines, the reductive amination α,β-unsaturated aldehydes is substantially less common, presumably due to rapid 1,4-addition processes.
(26) Roth, H.; Romero, N.; Nicewicz, D. Experimental and Calculated Electrochemical Potentials of Common Organic Molecules for Applications to Single-Electron Redox Chemistry. *Synlett* **2015**, *27* (05), 714–723. https://doi.org/10.1055/s-0035-1561297.
(27) Cheng, Q.; Chen, J.; Lin, S.; Ritter, T. Allylic Amination of Alkenes with Iminothianthrenes to Afford Alkyl Allylamines. *J. Am. Chem. Soc.* **2020**, *142* (41), 17287–17293. https://doi.org/10.1021/jacs.0c08248.
(28) Substantial progress has been made in redox-neutral hydroamination processes that furnish aliphatic amine products. See references 29-36.
(29) Wiese, S.; Badiei, Y. M.; Gephart, R. T.; Mossin, S.; Varonka, M. S.; Melzer, M. M.; Meyer, K.; Cundari, T. R.; Warren, T. H. Catalytic C–H Amination with Unactivated Amines through

Copper(II) Amides. *Angew. Chem. Int. Ed.* **2010**, *49* (47), 8850–8855. https://doi.org/10.1002/anie.201003676.

(30) Beller, M.; Trauthwein, H.; Eichberger, M.; Breindl, C.; Herwig, J.; Müller, T. E.; Thiel, O. R. The First Rhodium-Catalyzed Anti-Markovnikov Hydroamination: Studies on Hydroamination and Oxidative Amination of Aromatic Olefins. *Chem. - Eur. J.* **1999**, *5* (4), 1306–1319. https://doi.org/10.1002/(SICI)1521-3765(19990401)5:4<1306::AID-CHEM1306>3.0.CO;2-4.

(31) Utsunomiya, M.; Hartwig, J. F. Intermolecular, Markovnikov Hydroamination of Vinylarenes with Alkylamines. *J. Am. Chem. Soc.* **2003**, *125* (47), 14286–14287. https://doi.org/10.1021/ja0375535.

(32) Al-Masum, M.; Meguro, M.; Yamamoto, Y. The Two Component Palladium Catalyst System for Intermolecular Hydroamination of Allenes. *Tetrahedron Lett.* **1997**, *38* (34), 6071–6074. https://doi.org/10.1016/S0040-4039(97)01370-1.

(33) Kuchenbeiser, G.; Shaffer, A. R.; Zingales, N. C.; Beck, J. F.; Schmidt, J. A. R. Palladium(II) 3-Iminophosphine (3IP) Complexes: Active Precatalysts for the Intermolecular Hydroamination of 1,2-Dienes (Allenes) and 1,3-Dienes with Aliphatic Amines under Mild Conditions. *J. Organomet. Chem.* **2011**, *696* (1), 179–187. https://doi.org/10.1016/j.jorganchem.2010.08.033.

(34) Ickes, A. R.; Ensign, S. C.; Gupta, A. K.; Hull, K. L. Regio- and Chemoselective Intermolecular Hydroamination of Allyl Imines for the Synthesis of 1,2-Diamines. *J. Am. Chem. Soc.* **2014**, *136* (32), 11256–11259. https://doi.org/10.1021/ja505794u.

(35) Liu, R. Y.; Buchwald, S. L. CuH-Catalyzed Olefin Functionalization: From Hydroamination to Carbonyl Addition. *Acc. Chem. Res.* **2020**, *53* (6), 1229–1243. https://doi.org/10.1021/acs.accounts.0c00164.

(36) Gui, J.; Pan, C.-M.; Jin, Y.; Qin, T.; Lo, J. C.; Lee, B. J.; Spergel, S. H.; Mertzman, M. E.; Pitts, W. J.; La Cruz, T. E.; Schmidt, M. A.; Darvatkar, N.; Natarajan, S. R.; Baran, P. S. Practical Olefin Hydroamination with Nitroarenes. *Science* **2015**, *348* (6237), 886–891. https://doi.org/10.1126/science.aab0245.

(37) Ramirez, T. A.; Zhao, B.; Shi, Y. Recent Advances in Transition Metal-Catalyzed sp^3 C–H Amination Adjacent to Double Bonds and Carbonyl Groups. *Chem. Soc. Rev.* **2012**, *41* (2), 931–942. https://doi.org/10.1039/C1CS15104E.

(38) Liron, F.; Oble, J.; Lorion, M. M.; Poli, G. Direct Allylic Functionalization Through Pd-Catalyzed C-H Activation: Direct Allylic Functionalization by Pd-Catalyzed C-H Activation. *Eur. J. Org. Chem.* **2014**, *2014* (27), 5863–5883. https://doi.org/10.1002/ejoc.201402049.

(39) Fernandes, R. A.; Nallasivam, J. L. Catalytic Allylic Functionalization *via* π-Allyl Palladium Chemistry. *Org. Biomol. Chem.* **2019**, *17* (38), 8647–8672. https://doi.org/10.1039/C9OB01725A.

(40) Wang, R.; Luan, Y.; Ye, M. Transition Metal–Catalyzed Allylic C(sp_3)–H Functionalization via η^3-Allylmetal Intermediate. *Chin. J. Chem.* **2019**, *37* (7), 720–743. https://doi.org/10.1002/cjoc.201900140.

(41) Fix, S. R.; Brice, J. L.; Stahl, S. S. Efficient Intramolecular Oxidative Amination of Olefins through Direct Dioxygen-Coupled Palladium Catalysis. *Angew. Chem. Int. Ed.* **2002**, *41* (1), 164–166. https://doi.org/10.1002/1521-3773(20020104)41:1<164::AID-ANIE164>3.0.CO;2-B.

(42) As an alternative to employing oxidatively stable nitrogen sources, a handful of examples have exploited amine oxidation (typically of N-aryl amines) to generate an iminium intermediate that undergoes a subsequent trapping with vinyl nucleophiles in a one-pot process. For examples, see references 43-46.

(43) Muramatsu, W.; Nakano, K.; Li, C.-J. Direct sp^3 C–H Bond Arylation, Alkylation, and Amidation of Tetrahydroisoquinolines Mediated by Hypervalent Iodine(III) under Mild Conditions. *Org. Biomol. Chem.* **2014**, *12* (14), 2189–2192. https://doi.org/10.1039/C3OB42354A.

(44) Barham, J. P.; John, M. P.; Murphy, J. A. One-Pot Functionalisation of N-Substituted Tetrahydroisoquinolines by Photooxidation and Tunable Organometallic Trapping of Iminium Intermediates. *Beilstein J. Org. Chem.* **2014**, *10* (1), 2981–2988. https://doi.org/10.3762/bjoc.10.316.

(45) Franz, J. F.; Kraus, W. B.; Zeitler, K. No Photocatalyst Required – Versatile, Visible Light Mediated Transformations with Polyhalomethanes. *Chem. Commun.* **2015**, *51* (39), 8280–8283. https://doi.org/10.1039/C4CC10270C.
(46) Barham, J. P.; John, M. P.; Murphy, J. A. Contra-Thermodynamic Hydrogen Atom Abstraction in the Selective C–H Functionalization of Trialkylamine N-CH_3 Groups. *J. Am. Chem. Soc.* **2016**, *138* (47), 15482–15487. https://doi.org/10.1021/jacs.6b09690.
(47) Burman, J. S.; Blakey, S. B. Regioselective Intermolecular Allylic C−H Amination of Disubstituted Olefins via Rhodium/π-Allyl Intermediates. *Angew. Chem. Int. Ed.* **2017**, *56* (44), 13666–13669. https://doi.org/10.1002/anie.201707021.
(48) Ma, R.; White, M. C. C–H to C–N Cross-Coupling of Sulfonamides with Olefins. *J. Am. Chem. Soc.* **2018**, *140* (9), 3202–3205. https://doi.org/10.1021/jacs.7b13492.
(49) Lei, H.; Rovis, T. Ir-Catalyzed Intermolecular Branch-Selective Allylic C–H Amidation of Unactivated Terminal Olefins. *J. Am. Chem. Soc.* **2019**, *141* (6), 2268–2273. https://doi.org/10.1021/jacs.9b00237.
(50) Liu, G.; Yin, G.; Wu, L. Palladium-Catalyzed Intermolecular Aerobic Oxidative Amination of Terminal Alkenes: Efficient Synthesis of Linear Allylamine Derivatives. *Angew. Chem. Int. Ed.* **2008**, *47* (25), 4733–4736. https://doi.org/10.1002/anie.200801009.
(51) Reed, S. A.; Mazzotti, A. R.; White, M. C. A Catalytic, Brønsted Base Strategy for Intermolecular Allylic C−H Amination. *J. Am. Chem. Soc.* **2009**, *131* (33), 11701–11706. https://doi.org/10.1021/ja903939k.
(52) Pattillo, C. C.; Strambeanu, I. I.; Calleja, P.; Vermeulen, N. A.; Mizuno, T.; White, M. C. Aerobic Linear Allylic C–H Amination: Overcoming Benzoquinone Inhibition. *J. Am. Chem. Soc.* **2016**, *138* (4), 1265–1272. https://doi.org/10.1021/jacs.5b11294.
(53) Yin, G.; Wu, Y.; Liu, G. Scope and Mechanism of Allylic C−H Amination of Terminal Alkenes by the Palladium/$PhI(OPiv)_2$ Catalyst System: Insights into the Effect of Naphthoquinone. *J. Am. Chem. Soc.* **2010**, *132* (34), 11978–11987. https://doi.org/10.1021/ja1030936.
(54) Harris, R. J.; Park, J.; Nelson, T. A. F.; Iqbal, N.; Salgueiro, D. C.; Bacsa, J.; MacBeth, C. E.; Baik, M.-H.; Blakey, S. B. The Mechanism of Rhodium-Catalyzed Allylic C–H Amination. *J. Am. Chem. Soc.* **2020**, *142* (12), 5842–5851. https://doi.org/10.1021/jacs.0c01069.
(55) Lei, H.; Rovis, T. A Site-Selective Amination Catalyst Discriminates between Nearly Identical C–H Bonds of Unsymmetrical Disubstituted Alkenes. *Nat. Chem.* **2020**, *12* (8), 725–731. https://doi.org/10.1038/s41557-020-0470-z.
(56) Ide, T.; Feng, K.; Dixon, C. F.; Teng, D.; Clark, J. R.; Han, W.; Wendell, C. I.; Koch, V.; White, M. C. Late-Stage Intermolecular Allylic C–H Amination. *J. Am. Chem. Soc.* **2021**, *143* (37), 14969–14975. https://doi.org/10.1021/jacs.1c06335.
(57) Gephart III, R. T.; Huang, D. L.; Aguila, M. J. B.; Schmidt, G.; Shahu, A.; Warren, T. H. Catalytic C–H Amination with Aromatic Amines. *Angew. Chem. Int. Ed.* **2012**, *51* (26), 6488–6492. https://doi.org/10.1002/anie.201201921.
(58) Wilken, M.; Ortgies, S.; Breder, A.; Siewert, I. Mechanistic Studies on the Anodic Functionalization of Alkenes Catalyzed by Diselenides. *ACS Catal.* **2018**, *8* (11), 10901–10912. https://doi.org/10.1021/acscatal.8b01236.
(59) Souto, J. A.; Zian, D.; Muñiz, K. Iodine(III)-Mediated Intermolecular Allylic Amination under Metal-Free Conditions. *J. Am. Chem. Soc.* **2012**, *134* (17), 7242–7245. https://doi.org/10.1021/ja3013193.
(60) Roizen, J. L.; Harvey, M. E.; Du Bois, J. Metal-Catalyzed Nitrogen-Atom Transfer Methods for the Oxidation of Aliphatic C–H Bonds. *Acc. Chem. Res.* **2012**, *45* (6), 911–922. https://doi.org/10.1021/ar200318q.
(61) Starkov, P.; Jamison, T. F.; Marek, I. Electrophilic Amination: The Case of Nitrenoids. *Chem. – Eur. J.* **2015**, *21* (14), 5278–5300. https://doi.org/10.1002/chem.201405779.
(62) Dauban, P.; Dodd, R. H. Iminoiodanes and C-N Bond Formation in Organic Synthesis. *Synlett* **2003**, *2003* (11), 1571–1586. https://doi.org/10.1055/s-2003-41010.

(63) Shimbayashi, T.; Sasakura, K.; Eguchi, A.; Okamoto, K.; Ohe, K. Recent Progress on Cyclic Nitrenoid Precursors in Transition-Metal-Catalyzed Nitrene-Transfer Reactions. *Chem. – Eur. J.* **2019**, *25* (13), 3156–3180. https://doi.org/10.1002/chem.201803716.

(64) Scriven, E. F. V.; Turnbull, K. Azides: Their Preparation and Synthetic Uses. *Chem. Rev.* **1988**, *88* (2), 297–368. https://doi.org/10.1021/cr00084a001.

(65) Shin, K.; Kim, H.; Chang, S. Transition-Metal-Catalyzed C–N Bond Forming Reactions Using Organic Azides as the Nitrogen Source: A Journey for the Mild and Versatile C–H Amination. *Acc. Chem. Res.* **2015**, *48* (4), 1040–1052. https://doi.org/10.1021/acs.accounts.5b00020.

(66) Lebel, H.; Huard, K.; Lectard, S. *N*-Tosyloxycarbamates as a Source of Metal Nitrenes: Rhodium-Catalyzed C−H Insertion and Aziridination Reactions. *J. Am. Chem. Soc.* **2005**, *127* (41), 14198–14199. https://doi.org/10.1021/ja0552850.

(67) Hennessy, E. T.; Betley, T. A. Complex N-Heterocycle Synthesis via Iron-Catalyzed, Direct C–H Bond Amination. *Science* **2013**, *340* (6132), 591–595. https://doi.org/10.1126/science.1233701.

(68) Hennessy, E. T.; Liu, R. Y.; Iovan, D. A.; Duncan, R. A.; Betley, T. A. Iron-Mediated Intermolecular N-Group Transfer Chemistry with Olefinic Substrates. *Chem. Sci.* **2014**, *5* (4), 1526–1532. https://doi.org/10.1039/C3SC52533C.

(69) Liang, C.; Collet, F.; Robert-Peillard, F.; Müller, P.; Dodd, R. H.; Dauban, P. Toward a Synthetically Useful Stereoselective C−H Amination of Hydrocarbons. *J. Am. Chem. Soc.* **2008**, *130* (1), 343–350. https://doi.org/10.1021/ja076519d.

(70) Collet, F.; Lescot, C.; Liang, C.; Dauban, P. Studies in Catalytic C–H Amination Involving Nitrene C–H Insertion. *Dalton Trans.* **2010**, *39* (43), 10401–10413. https://doi.org/10.1039/C0DT00283F.

(71) Fantauzzi, S.; Gallo, E.; Caselli, A.; Ragaini, F.; Casati, N.; Macchi, P.; Cenini, S. The Key Intermediate in the Amination of Saturated C–H Bonds: Synthesis, X-Ray Characterization and Catalytic Activity of Ru(TPP)$(NAr)_2$ (Ar = 3,5-$(CF_3)_2C_6H_3$). *Chem. Commun.* **2009**, No. 26, 3952–3954. https://doi.org/10.1039/B903238J.

(72) Leveraging ene reactions rather than nitrene insertion, other high oxidation state nitrogen sources have been used for allylic amination. See references 73-74.

(73) Bao, H.; Tambar, U. K. Catalytic Enantioselective Allylic Amination of Unactivated Terminal Olefins via an Ene Reaction/[2,3]-Rearrangement. *J. Am. Chem. Soc.* **2012**, *134* (45), 18495–18498. https://doi.org/10.1021/ja307851b.

(74) Bayeh, L.; Le, P. Q.; Tambar, U. K. Catalytic Allylic Oxidation of Internal Alkenes to a Multifunctional Chiral Building Block. *Nature* **2017**, *547* (7662), 196–200. https://doi.org/10.1038/nature22805.

(75) New strategies for alkene oxidation strategies towards N-alkyl aziridine synthesis have been recently developed, see references 76-80. In stark contrast, the synthesis of allylic amine building blocks from alkenes via net $C(sp_3)$–H amination transformations remains limited.

(76) Falk, E.; Makai, S.; Delcaillau, T.; Gürtler, L.; Morandi, B. Design and Scalable Synthesis of *N*-Alkylhydroxylamine Reagents for the Direct Iron-Catalyzed Installation of Medicinally Relevant Amines. *Angew. Chem. Int. Ed.* **2020**, *59* (47), 21064–21071. https://doi.org/10.1002/anie.202008247.

(77) Jat, J. L.; Paudyal, M. P.; Gao, H.; Xu, Q.-L.; Yousufuddin, M.; Devarajan, D.; Ess, D. H.; Kürti, L.; Falck, J. R. Direct Stereospecific Synthesis of Unprotected N–H and N–Me Aziridines from Olefins. *Science* **2014**, *343* (6166), 61–65. https://doi.org/10.1126/science.1245727.

(78) Ošeka, M.; Laudadio, G.; Leest, N. P. van; Dyga, M.; Bartolomeu, A. de A.; Gooßen, L. J.; Bruin, B. de; Oliveira, K. T. de; Noël, T. Electrochemical Aziridination of Internal Alkenes with Primary Amines. *Chem* **2021**, *7* (1), 255–266. https://doi.org/10.1016/j.chempr.2020.12.002.

(79) Govaerts, S.; Angelini, L.; Hampton, C.; Malet-Sanz, L.; Ruffoni, A.; Leonori, D. Photoinduced Olefin Diamination with Alkylamines. *Angew. Chem. Int. Ed.* **2020**, *59* (35), 15021–15028. https://doi.org/10.1002/anie.202005652.

(80) Holst, D. E.; Wang, D. J.; Kim, M. J.; Guzei, I. A.; Wickens, Z. K. Aziridine Synthesis by Coupling Amines and Alkenes via an Electrogenerated Dication. *Nature* **2021**, *596* (7870), 74–79. https://doi.org/10.1038/s41586-021-03717-7.
(81) 2,490,000 primary amines and 1,888,500 secondary amines, which totals 4,378,500 commerical amines to give aliphatic amine products. eMolecules (eMolecules Inc, accessed 7 November 2021); https://www.emolecules.com.
(82) Yoshida, J.; Shimizu, A.; Hayashi, R. Electrogenerated Cationic Reactive Intermediates: The Pool Method and Further Advances. *Chem. Rev.* **2018**, *118* (9), 4702–4730. https://doi.org/10.1021/acs.chemrev.7b00475.
(83) Hayashi, R.; Shimizu, A.; Yoshida, J. The Stabilized Cation Pool Method: Metal- and Oxidant-Free Benzylic C–H/Aromatic C–H Cross-Coupling. *J. Am. Chem. Soc.* **2016**, *138* (27), 8400–8403. https://doi.org/10.1021/jacs.6b05273.
(84) Yoshida, J.; Suga, S. Basic Concepts of "Cation Pool" and "Cation Flow" Methods and Their Applications in Conventional and Combinatorial Organic Synthesis. *Chem. – Eur. J.* **2002**, *8* (12), 2650–2658. https://doi.org/10.1002/1521-3765(20020617)8:12<2650::AID-CHEM2650>3.0.CO;2-S.
(85) Berger, F.; Plutschack, M. B.; Riegger, J.; Yu, W.; Speicher, S.; Ho, M.; Frank, N.; Ritter, T. Site-Selective and Versatile Aromatic C−H Functionalization by Thianthrenation. *Nature* **2019**, *567* (7747), 223–228. https://doi.org/10.1038/s41586-019-0982-0.
(86) Chen, J.; Li, J.; Plutschack, M. B.; Berger, F.; Ritter, T. Regio- and Stereoselective Thianthrenation of Olefins To Access Versatile Alkenyl Electrophiles. *Angew. Chem. Int. Ed.* **2020**, *59* (14), 5616–5620. https://doi.org/10.1002/anie.201914215.
(87) Alvarez, E. M.; Plutschack, M. B.; Berger, F.; Ritter, T. Site-Selective C–H Functionalization-Sulfination Sequence to Access Aryl Sulfonamides. *Org. Lett.* **2020**, *22* (12) 4593–4596. https://doi.org/10.1021/acs.orglett.0c00982.
(88) Juliá, F.; Yan, J.; Paulus, F.; Ritter, T. Vinyl Thianthrenium Tetrafluoroborate: A Practical and Versatile Vinylating Reagent Made from Ethylene. *J. Am. Chem. Soc.* **2021**, *143* (33), 12992–12998. https://doi.org/10.1021/jacs.1c06632.
(89) Chen, C.; Wang, M.; Lu, H.; Zhao, B.; Shi, Z. Enabling the Use of Alkyl Thianthrenium Salts in Cross-Coupling Reactions by Copper Catalysis. *Angew. Chem. Int. Ed.* **2021**, *60* (40), 21756–21760. https://doi.org/10.1002/anie.202109723.
(90) Chen, C.; Wang, Z.-J.; Lu, H.; Zhao, Y.; Shi, Z. Generation of Non-Stabilized Alkyl Radicals from Thianthrenium Salts for C–B and C–C Bond Formation. *Nat. Commun.* **2021**, *12* (1), 4526. https://doi.org/10.1038/s41467-021-24716-2.
(91) Jia, H.; Häring, A. P.; Berger, F.; Zhang, L.; Ritter, T. Trifluoromethyl Thianthrenium Triflate: A Readily Available Trifluoromethylating Reagent with Formal CF_3^+, CF_3•, and CF_3^- Reactivity. *J. Am. Chem. Soc.* **2021**, *143* (20), 7623–7628. https://doi.org/10.1021/jacs.1c02606.
(92) Antoni, P. W.; Mackenroth, A. V.; Mulks, F. F.; Rudolph, M.; Helmchen, G.; Hashmi, A. S. K. Dibenzothiophenesulfilimines: A Convenient Approach to Intermolecular Rhodium-Catalysed C−H Amidation. *Chem. – Eur. J.* **2020**, *26* (37), 8235–8238. https://doi.org/10.1002/chem.202002371.
(93) Shine, H. J.; Bandlish, B. K.; Mani, S. R.; Padilla, A. G. Ion Radicals. 43. Addition of Thianthrene and Phenoxathiin Cation Radicals to Alkenes and Alkynes. *J. Org. Chem.* **1979**, *44* (6), 915–917. https://doi.org/10.1021/jo01320a004.
(94) Shine, H. J.; Zhao, B.; Qian, D.-Q.; Marx, J. N.; Guzman-Jimenez, I. Y.; Thurston, J. H.; Ould-Ely, T.; Whitmire, K. H. Adducts of Phenoxathiin and Thianthrene Cation Radicals with Alkenes and Cycloalkenes. *J. Org. Chem.* **2003**, *68* (23), 8910–8917. https://doi.org/10.1021/jo030173h.
(95) Mitchell, S. C.; Waring, R. H. Fate of Thianthrene in Biological Systems. *Xenobiotica* **2017**, *47* (8), 731–740. https://doi.org/10.1080/00498254.2016.1222107.
(96) The cost of thianthrene is less than 0.15 USD mmol−1.
(97) When base was omitted from previously reported thianthrene-based aziridination conditions (reference 80), diamination was observed rather than aziridination. Preliminary mechanistic

evidence suggests this product proceeds via an aziridinium intermediate. Additionally, for a recent strategy generating diamine products via generation of aziridinium salts from secondary amines, see reference 79.

(98) Alkyne thianthrenation by chemically-generated thianthrene radical cation has been previously observed, see: Rangappa, P.; Shine, H. J.; Marx, J. N.; Ould-Ely, T.; Kelly, A. T.; Whitmire, K. H. Adducts of Thianthrene- and Phenoxathiin Cation Radical Tetrafluoroborates to 1-Alkynes. Structures and Formation of 1-(5-Thianthreniumyl)- and 1-(10-Phenoxathiiniumyl)Alkynes on Alumina Leading to α-Ketoylides and α-Ketols. *J. Org. Chem.* **2005**, *70* (24), 9764–9770. https://doi.org/10.1021/jo051317q.

(99) While stereoselectivity was attenuated in these examples bearing proximal branching or functional groups, the thermodynami-cally disfavored Z-isomer was still observed.

(100) Currently, this methodology is restricted to terminal alkenes. While adduct could be formed readily from internal alkenes, these adducts provided an intractable mixture upon treatment with the amine nucleophile (see SI for details).

(101) Zimmermann, H. Propene. In *Ullmann's Encyclopedia of Industrial Chemistry*; American Cancer Society, 2013; pp 00–00. https://doi.org/10.1002/14356007.a22_211.pub3.

(102) Geilen, F. M. A.; Stochniol, G.; Peitz, S.; Schulte-Koerne, E. Butenes. In *Ullmann's Encyclopedia of Industrial Chemistry*; American Cancer Society, 2014; pp 1–13. https://doi.org/10.1002/14356007.a04_483.pub3.

(103) Krähling, L.; Krey, J.; Jakobson, G.; Grolig, J.; Miksche, L. Allyl Compounds. In *Ullmann's Encyclopedia of Industrial Chemistry*; American Cancer Society, 2000. https://doi.org/10.1002/14356007.a01_425.

(104) By avoiding use of allylic halides, this methods also obviates need for disposal of halide waste.

(105) Our previous report shows 76% thianthrene recovery following substitution of the dicationic adducts upon scaleup. See reference 80.

(106) Yamanaka, H.; Matsuo, J.; Kawana, A.; Mukaiyama, T. A Convenient Method for the Synthesis of β,γ-Unsaturated Amines from Alkenes via α,β-Unsaturated Diphenylsulfonium Salts. *Chem. Lett.* **2003**, *32* (7), 626–627. https://doi.org/10.1246/cl.2003.626.

Chapter 4: Diastereoselective Synthesis of Cyclopropanes from Carbon Pronucleophiles and Alkenes

Kim, M. J.; **Wang, D. J.**; Targo, K.; Garcia, U. A.; Harris A. F.; Guzei, I. A.; Wickens, Z. K. Diastereoselective Synthesis of Cyclopropanes from Carbon Pronucleophiles and Alkenes.

4.1 Abstract

Cyclopropanes are desirable structural motifs with valuable applications in drug discovery and beyond. Established alkene cyclopropanation methods give rise to cyclopropanes with a limited array of substituents, are difficult to scale, or both. Herein, we disclose a new cyclopropane synthesis through the formal coupling of abundant carbon pronucleophiles and unactivated alkenes. This strategy relies on key dicationic adducts derived from anodic oxidation of thianthrene in the presence of alkene substrates. We find that these unusual dielectrophiles undergo cyclopropanation with methylene pronucleophiles via alkenyl thianthrenium intermediates. This protocol is scalable, proceeds with high diastereoselectivity, and tolerates diverse functional groups on both the alkene and pronucleophile coupling partners. Furthermore, cyclopropanation of gaseous feedstock alkenes enables access to stereochemically-defined cyclopropane building blocks from inexpensive precursors. To validate the utility of this new procedure, we prepared an array of substituted analogs of an established cyclopropane intermediate en route to multiple top selling pharmaceuticals.

4.2 Introduction

Cyclopropanes are important structural motifs with diverse applications as synthetic intermediates, mechanistic probes, and design elements of bioactive molecules.[1–10] In the context of medicinal chemistry, these three-membered carbocyclic rings are employed to increase potency, reduce off-target effects, and fine-tune metabolic stability.[10–12] Recognition of these strategic benefits has driven the number of approved small molecule drugs containing cyclopropanes to double over the last ten years.[13] Recently, other structurally rigid ring systems are emerging as an appealing design strategy to precisely control the

3D molecular geometry of drug candidates.[11,14–20] While in principle cyclopropanes offer a myriad of 3D shapes, 64% of the cyclopropane rings in active pharmaceutical ingredients are substituted at only a single carbon (Fig. 4.1, top).[13,21] This overrepresentation of a narrow subset of possible substitution patterns is, in part, due to the reactions used to construct cyclopropane rings. For example, cyclopropanes substituted at one carbon are straightforward to access on large scale via enolate alkylation using 1,2-dihaloethane dielectrophiles. However, vicinal dihalides bearing any additional substituents suffer inextricable elimination reactions, limiting access to more substituted analogs through this intermolecular disconnection.[22–25] The most well-studied approach to prepare more substituted cyclopropanes is alkene

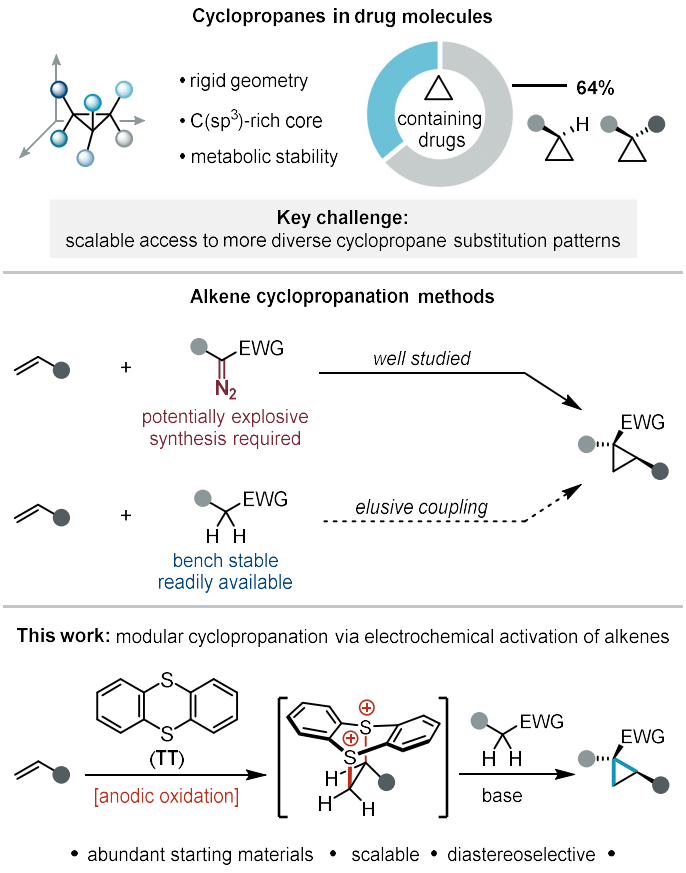

Figure 4.1. Project overview. Cyclopropanes in drug molecules (top); alkene cyclopropanation methods (middle); overview of this work (bottom).

cyclopropanation based on metal carbenoid reactivity (Fig. 1, middle).[26–36] While indisputably effective, the modularity of these methods is limited by the requisite synthesis of unique carbene

precursors to deliver each distinct substituent. Furthermore, hazardous diazo compounds are commonly required, which further complicates broad implementation due to safety concerns.[37–58] As a result, development of new approaches to prepare cyclopropane products is an area of contemporary interest.[59–62] Overall, a modular annulative cyclopropane synthesis that couples two abundant building blocks has remained elusive and is poised to substantially impact synthetic chemistry.

A deceptively straightforward strategy to access cyclopropanes in a modular fashion would be through the intermolecular oxidative coupling of carbon pronucleophiles and alkenes. Unfortunately, this idealized reaction has yet to be realized. In principle, the net transformation could be accomplished through conversion of an alkene to a dielectrophile that undergoes iterative substitution with a metylene pronucleophile rather than deleterious elimination. No established dielectrophile possesses the requisite selectivity profile to accomplish this in a general fashion.

Recent work has begun to explore the diverse and unique electrophilic reactivity of thianthrenium salts.[63–72] Our group recently developed an electrochemical strategy to generate dicationic adducts between unactivated alkenes and thianthrene (**TT**) that serve as dielectrophiles.[63,64] Specifically, these species underwent substitution by primary amine nucleophiles without deleterious elimination, unlocking a new approach to prepare *N*-alkyl aziridine products. However, the reactivity of these adducts with carbon nucleophiles remains largely unexplored and we anticipate elimination may pose a more substantial challenge for these more basic nucleophiles.[73] Furthermore, cyclopropanation also introduces the added challenge of controlling diastereoselectivity if a stereocenter is formed at the cyclopropane carbon derived from the nucleophile. Herein, we report the results of our investigations into the reactivity of dicationic thianthrene-alkene adducts with carbon pronucleophiles (Fig. 4.1, bottom). This led to a modular and diastereoselective cyclopropane synthesis from abundant precursors as well as key insights into the dicationic adduct substitution mechanism.

4.3 Results and Discussion

We initiated our investigations using nitrile pronucleophile **4.3.** This model pronucleophile was selected for two primary reasons: (1) we suspected that sterically differentiated carbanion stabilizing groups would maximize diastereoselectivity, and (2) basic nitrogen heterocycles are pervasive in medicinal chemistry but their coordinating ability can challenge many established alkene cyclopropanation procedures.[74–76] After initial optimization of reaction conditions (see Appendix C for details), we found this pronucleophile underwent base-promoted cyclopropanation with dicationic adducts (**4.1** and **4.2**) in high yield (Fig. 4.2, top). Consistent with our hypothesis, small nitrile substituent promotes high diastereoselectivity (≥20:1 d.r.). Indeed, conducting the same procedure with an analog of **4.3**, wherein the nitrile is replaced with an ester, furnished the product in diminished diastereoselectivity (2:1 d.r., see SI for details). Although these initial conditions were effective, they required a substantial

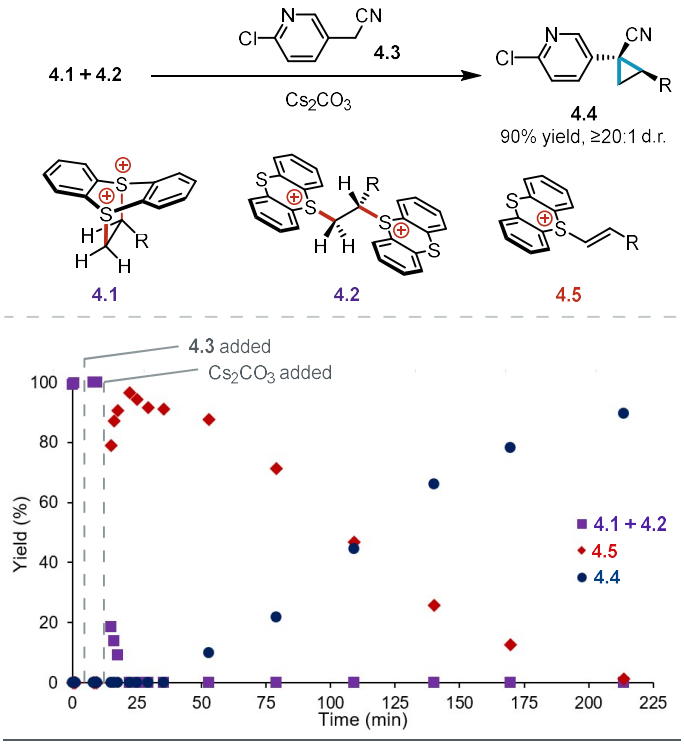

[a]Top reaction was conducted using alkene (0.15 mmol), TT (0.225 mmol), 3 mL of MeCN-*d3* (0.2 M KPF_6); then pronucleophile (0.15 mmol), Cs_2CO_3 (1.5 mmol), 2.5 h. Yields and d.r. are ^1H NMR analysis. See the SI for further details. R = CH_2CH_2Ph.

Figure 4.2. Initial experiments into cyclopropanation.

excess of Cs_2CO_3 base (10 equiv.) to favor the desired cyclopropane over the elimination product, an alkenyl thianthrenium salt (**4.5**). Given that initially we anticipated increased formation of elimination byproducts upon increasing base equivalents, we suspected that a more complex mechanistic pathway might be occurring rather than simple iterative substitution.

To investigate the mechanism of cyclopropanation, we monitored the substitution of dicationic adducts by ^{1}H NMR (Fig. 4.2, bottom). Intriguingly, the dicationic adducts are rapidly consumed to form alkenyl thianthrenium salt **4.5**. This elimination product is subsequently converted to cyclopropane product **4.4**. Overall, this timecourse analysis suggests that an alkenyl thianthrenium **4.5** is a key intermediate en route to cyclopropanation. This proposal is consistent with prior work on vinyl sulfonium salts, which undergo cyclopropanation reactions with malonates and related pronucleophiles. However, these previously reported transformations have been predominantly limited to unsubstituted vinyl sulfonium salts.[77–84] Only a handful of alkenyl sulfonium salts have been found to undergo cyclopropanation.[73,84–90] Given the relatively limited examples of cyclopropanation from unactivated alkenyl sulfonium salts similar to **4.5**, we validated this potential mechanism by isolating **4.5** and resubjecting it to the substitution conditions. This experiment afforded the cyclopropane product **4.4** in 89% yield, validating the kinetic competency of this species as an intermediate in cyclopropanation. This electrophilic elimination product also offers a plausible explanation for the distinct reactivity profile of the dicationic adducts relative to conventional dihalide dielectrophiles, since alkenyl halides do not undergo addition with nucleophiles. With this mechanism in mind, we streamlined access to the key alkenyl thianthrenium intermediate by passing the dicationic adduct solution through a short pad of basic alumina prior to addition of the pronucleophile and base. This modified procedure furnished the desired cyclopropane product **4.4** in 81% yield relative to alkene as a single diastereomer using one equivalent of pronucleophile and two equivalents of Cs_2CO_3.

With an optimized procedure in hand, we next examined the scope of this new cyclopropanation protocol. We found that this process enabled the formal coupling of a wide range of carbon

pronucleophiles and unactivated alkenes (Table 4.1). First, we probed a range of nitrile pronucleophiles substituted with a second strong electron withdrawing group. Alkylnitriles bearing amide (**4.6, 4.7**), ester (**4.8**), sulfone (**4.9**), benzophenone imine (**4.10**), and phosphonate (**4.11**) α-substituents each underwent efficient cyclopropanation. High diastereoselectivity was observed across the majority of these substrates. These stereochemically defined cyclopropane building blocks each bear distinct synthetic handles for further diversification. Furthermore, acidic cyclic pronucleophiles were converted into a range of architecturally complex spirocyclic building blocks (**4.12**–**4.14**) from simple precursors. Symmetrical pronucleophiles such as malonate and malononitrile were also suitable coupling partners and afforded the expected cyclopropane products (**4.15, 4.16**). We next explored the scope of this methodology with respect to less acidic pronucleophiles bearing diverse and medicinally-relevant (hetero)arenes as secondary withdrawing groups. We found that alkylnitrile pronucleophiles substituted with pyridines (**4.17, 4.18**), pyrimidines (**4.19**), thiophenes (**4.20**), thiazoles (**4.21**), and trifluorotoluene derivatives (**4.22**) each underwent efficient and diastereoselective cyclopropanation. Of note, established carbene-transfer-based approaches to related products deliver the opposite relative stereochemistry.[75] Hetereoarene substituted pronucleophiles with an ester instead of a nitrile furnished the final cyclopropane product in high yield, albeit with diminished diastereoselectivity (**4.23**). We also found that nitromethane, an inexpensive commodity chemical, could be employed to prepare 1,2-disubstituted cyclopropane (**4.24**) with high selectivity for the *trans* product. Throughout these studies, we found that variation of the alkene coupling partner provided access to cyclopropane building blocks bearing diverse pendant functional groups, such as acetates (**4.12**), carbonates (**4.22**), nitriles (**4.14**), phthalimides (**4.6, 4.13**), and sulfonamides (**4.8**). Additionally, steric hindrance about the alkene was well tolerated (**4.10, 4.14, 4.16, 4.18, 4.20**). Notably, unconjugated dienes (**4.7, 4.9**) and ene-ynes (**4.21**) both underwent selective cyclopropanation at a single site, leaving a pendant unsaturated π-system for subsequent derivatization. An alkene substrate containing an α,β-unsaturated ester (**4.17, 4.24**) underwent selective cyclopropanation at the more electron-rich alkene. This demonstrates high selectivity both in the generation of the key electrophilic alkenyl thianthrenium intermediate as well as for cyclopropanation over enolate 1,4-

addition. Taken together, these data validate that this modular cyclopropanation strategy is amenable to the synthesis of diverse and complex cyclopropanes that would have been difficult to prepare using more conventional methods.

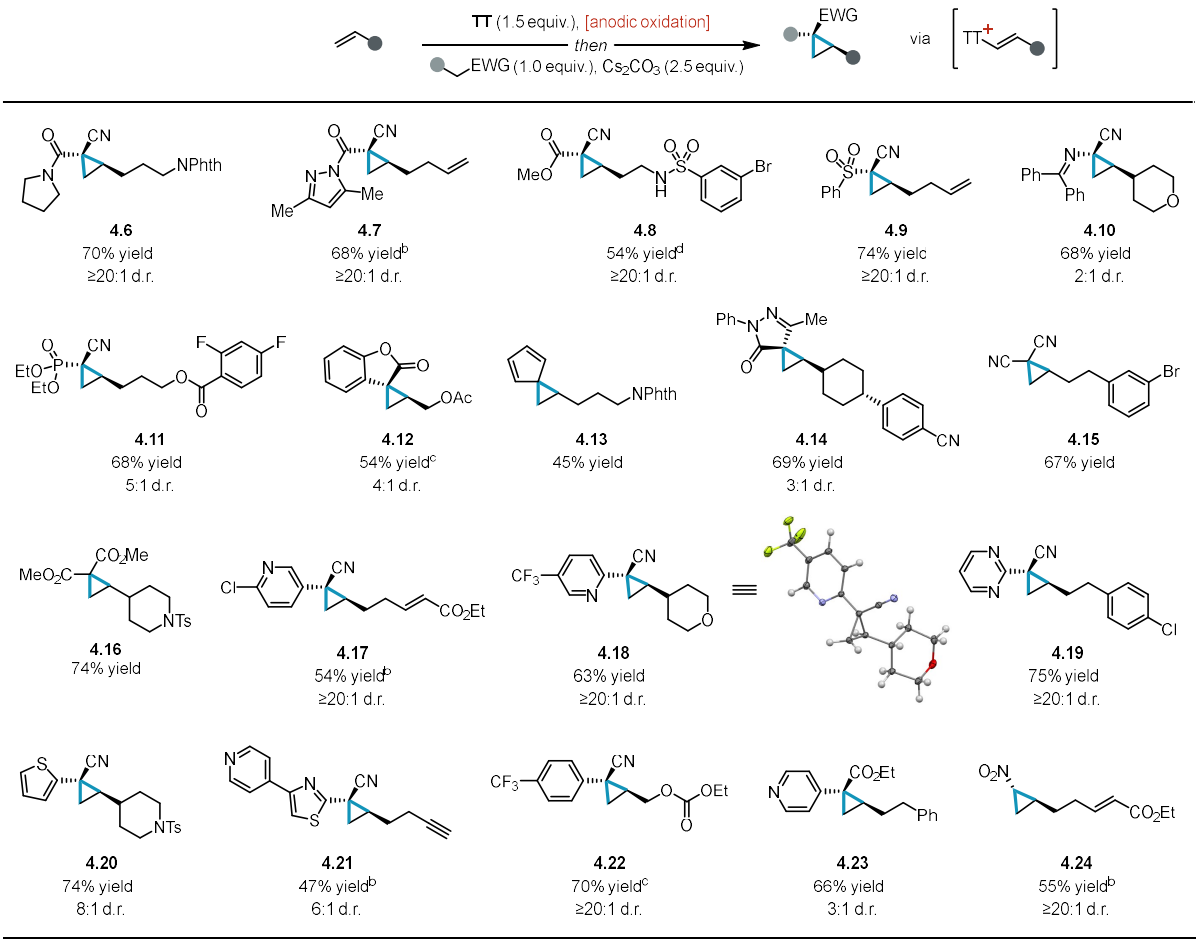

[a]Reactions were conducted using alkene (0.4 mmol), TT (0.6 mmol), 8 mL of MeCN (0.2 M *n*-Bu_4NPF_6); then pronucleophile (0.4 mmol), Cs_2CO_3 (1.0 mmol), 2 h. Yields and d.r. are of the purified product as a racemate unless otherwise noted. See the SI for further details. [b]NMR yield. [c]alkene (0.8 mmol), TT (1.2 mmol), 8 mL of MeCN (0.2 M *n*-Bu_4NPF_6). [d]alkene (0.6 mmol), TT (0.9 mmol), 8 mL of MeCN (0.2 M *n*-Bu_4NPF_6).

Table 4.1. Scope of Cyclopropanation via Dication Pool Strategy.

We next evaluated the viability of performing this process on preparative scale (Scheme 4.2). We synthesized product **4.25** on multigram scale (3.3 g, 72% yield, 7.9 mmol, ≥20:1 d.r.) using a 1:1 stoichiometry of the alkene and pronucleophile coupling partners. This representative example is illustrative of the power of this protocol in the synthesis of versatile cyclopropane building blocks. Specifically, compound **4.25** bears orthogonal handles for further functionalizations using robust reactions, such as S_NAr and Grignard addition. Of note, this practical batch electrolysis reaction setup is

comprised of a DC power supply, inexpensive electrodes, and a divided cell and does not require any precautions to exclude air or moisture. Combined with the low cost[91] low toxicitiy[92] and recyclability[63] of the thianthrene promoter, these results demonstrate the scalability of this electrochemical cyclopropanation protocol.

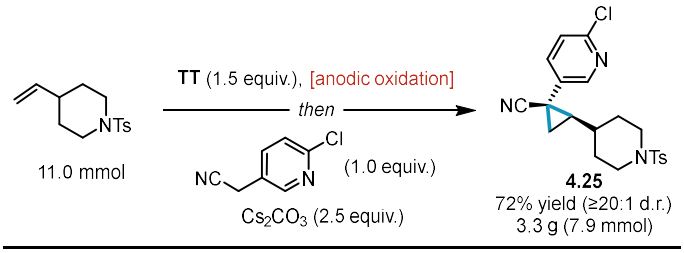

Reaction was conducted using alkene (11.0 mmol), TT (16.5 mmol), 110 mL of MeCN (0.2 M n-Bu_4NPF_6); then pronucleophile (11.0 mmol), Cs_2CO_3 (27.5 mmol), 16 h. Yield and d.r. are of the purified product.

Scheme 4.2. Preparative scale

We recognized that use of feedstock alkenes would enable access to cyclopropane building blocks from exceptionally inexpensive starting materials. Anodic oxidation of thianthrene under 1 atm of ethylene, propene, 1-butene, and 2-methyl-1-butene each delivered dicationic adducts that could be subsequently converted to the desired cyclopropane products (Table 4.2). When relevant, these reactions proceeded with high diastereoselectivity even in the case of propene (**4.27, 4.29, 4.30**), which bears a relatively small methyl substituent. These data illustrate how the high functional group tolerance of this method can be leveraged to prepare diverse cyclopropane building blocks for drug discovery from simple precursors.

We envisioned that this newly realized oxidative cyclopropanation methodology would have immediate utility through both the preparation of established cyclopropane targets as well as previously unknown derivatives. As an illustrative example, we prepared cyclopropane **4.34** from a commercially available benzylic nitrile and ethylene (1 atm) in high yield. Compound **4.34** is an established intermediate in the synthesis of two distinct small molecule components in the most common cystic fibrosis drugs (lumacaftor and tezacaftor; total sales in 2021 amounted to $6.9 B USD).[93] The established

route to **4.34** constructs the cyclopropane ring through an enolate dialkylation using 1,2-dihaloethane.[94,95] While circumventing this carcinogenic dihalide may offer strategic advantages in synthesis of **4.34**, we

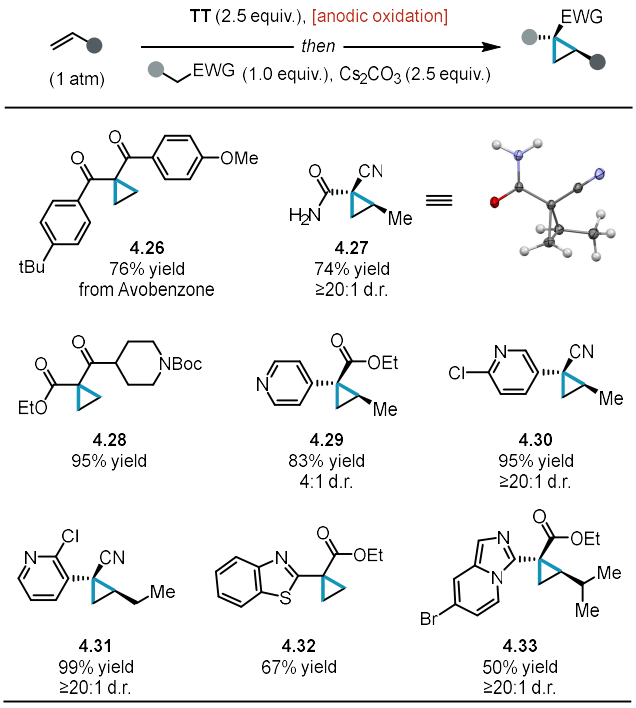

Reactions were conducted using alkene (1 atm), TT (1.0 mmol), 4 mL of MeCN (0.4 M *n*-Bu_4NPF_6); then pronucleophile (0.4 mmol), Cs_2CO_3 (1.0 mmol), 14-16 h. Yields and d.r. are of the purified product unless otherwise noted. See the SI for further details.

Table 4.2. Cyclopropane building blocks from feedstock alkenes.

anticipated that the true power of this oxidative coupling route would lie in the synthesis of new structural analogs to this key intermediate. Indeed, no analogs of intermediate **4.34** bearing additional substituents on the cyclopropane moiety have been previously reported, presumably due to the limitations associated with substituted dihalide dielectrophiles. To this end, we prepared a series of substituted analogs of **4.34** by varying the alkene coupling partner (**4.35**–**4.37**). This approach enabled both large structural changes, such as replacement of a cyclopropyl hydrogen with a piperidine ring (**4.35**), as well as small perturbations, accessing methylated analog **4.37**. Attempts to access the same products from analogous vicinal dihalide starting materials resulted in at most trace product. Taken together, these results illustrate how this new technology can impact the cyclopropane compounds prepared and studied in medicinal chemistry.

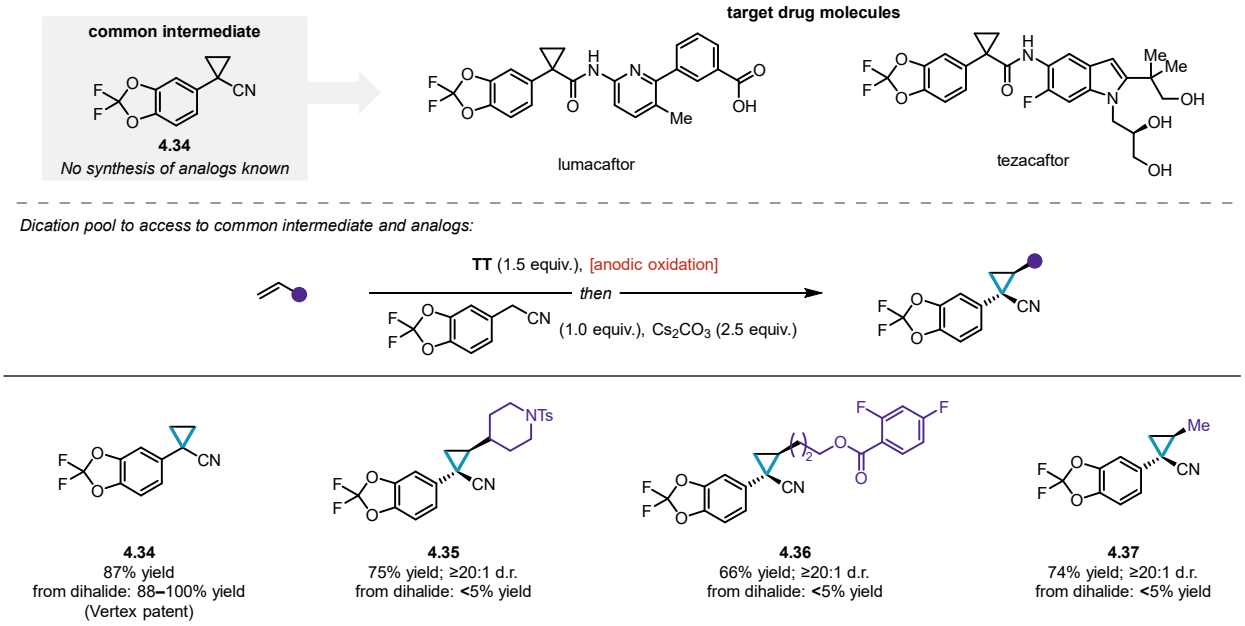

[a]Gaseous alkene reactions were conducted using alkene (1 atm), TT (1.0 mmol), 4 mL of MeCN (0.4 M *n*-Bu_4NPF_6); then pronucleophile (0.4 mmol), Cs_2CO_3 (1.0 mmol), 14-16 h. Reactions with non-gaseous alkenes were conducted using alkene (0.4 mmol), TT (0.6 mmol), 8 mL of MeCN (0.2 M *n*-Bu_4NPF_6); then pronucleophile (0.4 mmol), Cs_2CO_3 (1.0 mmol), 2 h. Yields and d.r. are of the purified product. See the SI for further details.

Scheme 4.3. Synthesis of drug intermediate and analogs.

4.4 Conclusion

Overall, we have developed a modular procedure to prepare cyclopropanes from abundant carbon pronucleophiles and alkenes via electrochemically-generated thianthrenium salts. Mechanistic studies revealed that the dicationic adducts underwent rapid elimination under the reaction conditions to form an alkenyl thianthrenium salt, which serves as a key electrophilic intermediate en route to cyclopropanes. This approach is amenable to generation of diverse cyclopropanes bearing medicinally-relevant functional groups and handles for further elaboration. This cyclopropanation strategy allows for highly diastereoselective synthesis of nitrile-substituted cyclopropanes and furnishes complementary relative stereochemistry when compared to conventional metal-catalyzed approaches. This method expands the scope of readily accessible cyclopropane building blocks using inexpensive coupling partners and reagents. We anticipate that this new transformation will find broad application in organic synthesis given the growing interest in cyclopropanes in medicinal chemistry and beyond.

4.5 Acknowledgement

We thank the Stahl, Weix, Yoon, and Schomaker groups for sharing their chemical inventory. This work was financially supported by the Office of the Vice Chancellor for Research and Graduate Education at the University of Wisconsin–Madison with funding from the Wisconsin Alumni Research Foundation. Spectroscopic instrumentation was supported by a generous gift from Paul J. and Margaret M. Bender, NSF (CHE-1048642), and NIH (S10OD012245 and 1S10OD020022-1). The Bruker D8 VENTURE Photon III X-ray diffractometer was partially funded by NSF Award #CHE-1919350 to the UW–Madison Department of Chemistry. This material is based upon work supported by the National Science Foundation Graduate Research Fellowship Program under grant no. DGE-1747503 (K.T.). Any opinions, findings, and conclusions or recommendations expressed in this material are those of the author(s) and do not necessarily reflect the views of the National Science Foundation. A.H. was supported by a Nicholas O'Connor Research Fellowship.

4.6 Author Contributions

Z.K.W., M.K. and D.J.W. designed the project. All authors performed the experiments and collected the data. M.K. designed and implemented the mechanistic experiments. I.A.G. collected and analyzed X-ray data to provide crystal structures. Z.K.W., M.K, D.J.W., K.T., and U.A.G. contributed to writing the manuscript.

4.7 References

(1) Wong, H. N. C.; Hon, M. Y.; Tse, C. W.; Yip, Y. C.; Tanko, J.; Hudlicky, T. Use of Cyclopropanes and Their Derivatives in Organic Synthesis. *Chem. Rev.* **1989**, *89* (1), 165–198. https://doi.org/10.1021/cr00091a005.

(2) Griller, D.; Ingold, K. U. Free-Radical Clocks. *Acc. Chem. Res.* **1980**, *13* (9), 317–323. https://doi.org/10.1021/ar50153a004.

(3) Pirenne, V.; Muriel, B.; Waser, J. Catalytic Enantioselective Ring-Opening Reactions of Cyclopropanes. *Chem. Rev.* **2021**, *121* (1), 227–263. https://doi.org/10.1021/acs.chemrev.0c00109.

(4) Ebner, C.; Carreira, E. M. Cyclopropanation Strategies in Recent Total Syntheses. *Chem. Rev.* **2017**, *117* (18), 11651–11679. https://doi.org/10.1021/acs.chemrev.6b00798.

(5) Faust, R. Fascinating Natural and Artificial Cyclopropane Architectures. *Angew. Chem. Int. Ed.* **2001**, *40* (12), 2251–2253. https://doi.org/10.1002/1521-3773(20010618)40:12<2251::AID-ANIE2251>3.0.CO;2-R.
(6) Wessjohann, L. A.; Brandt, W.; Thiemann, T. Biosynthesis and Metabolism of Cyclopropane Rings in Natural Compounds. *Chem. Rev.* **2003**, *103* (4), 1625–1648. https://doi.org/10.1021/cr0100188.
(7) Lamberth, C. Small Ring Chemistry in Crop Protection. *Tetrahedron* **2019**, *75* (33), 4365–4383. https://doi.org/10.1016/j.tet.2019.06.043.
(8) Ghosh, K.; Das, S. Recent Advances in Ring-Opening of Donor Acceptor Cyclopropanes Using C-Nucleophiles. *Org. Biomol. Chem.* **2021**, *19* (5), 965–982. https://doi.org/10.1039/D0OB02437F.
(9) Schneider, T. F.; Kaschel, J.; Werz, D. B. A New Golden Age for Donor–Acceptor Cyclopropanes. *Angew. Chem. Int. Ed.* **2014**, *53* (22), 5504–5523. https://doi.org/10.1002/anie.201309886.
(10) Talele, T. T. The "Cyclopropyl Fragment" Is a Versatile Player That Frequently Appears in Preclinical/Clinical Drug Molecules. *J. Med. Chem.* **2016**, *59* (19), 8712–8756. https://doi.org/10.1021/acs.jmedchem.6b00472.
(11) Taylor, R. D.; MacCoss, M.; Lawson, A. D. G. Rings in Drugs. *J. Med. Chem.* **2014**, *57* (14), 5845–5859. https://doi.org/10.1021/jm4017625.
(12) Novakov, I. A.; Babushkin, A. S.; Yablokov, A. S.; Nawrozkij, M. B.; Vostrikova, O. V.; Shejkin, D. S.; Mkrtchyan, A. S.; Balakin, K. V. Synthesis and Structure—Activity Relationships of Cyclopropane-Containing Analogs of Pharmacologically Active Compounds. *Russ. Chem. Bull.* **2018**, *67* (3), 395–418. https://doi.org/10.1007/s11172-018-2087-6.
(13) Wishart, D. S.; Feunang, Y. D.; Guo, A. C.; Lo, E. J.; Marcu, A.; Grant, J. R.; Sajed, T.; Johnson, D.; Li, C.; Sayeeda, Z.; Assempour, N.; Iynkkaran, I.; Liu, Y.; Maciejewski, A.; Gale, N.; Wilson, A.; Chin, L.; Cummings, R.; Le, D.; Pon, A.; Knox, C.; Wilson, M. DrugBank 5.0: A Major Update to the DrugBank Database for 2018. *Nucleic Acids Res.* **2018**, *46* (D1), D1074–D1082. https://doi.org/10.1093/nar/gkx1037.
(14) Hung, A. W.; Ramek, A.; Wang, Y.; Kaya, T.; Wilson, J. A.; Clemons, P. A.; Young, D. W. Route to Three-Dimensional Fragments Using Diversity-Oriented Synthesis. *Proc. Natl. Acad. Sci.* **2011**, *108* (17), 6799–6804. https://doi.org/10.1073/pnas.1015271108.
(15) Carreira, E. M.; Fessard, T. C. Four-Membered Ring-Containing Spirocycles: Synthetic Strategies and Opportunities. *Chem. Rev.* **2014**, *114* (16), 8257–8322. https://doi.org/10.1021/cr500127b.
(16) Zheng, Y.; Tice, C. M.; Singh, S. B. The Use of Spirocyclic Scaffolds in Drug Discovery. *Bioorg. Med. Chem. Lett.* **2014**, *24* (16), 3673–3682. https://doi.org/10.1016/j.bmcl.2014.06.081.
(17) Mykhailiuk, P. K. Saturated Bioisosteres of Benzene: Where to Go Next? *Org. Biomol. Chem.* **2019**, *17* (11), 2839–2849. https://doi.org/10.1039/C8OB02812E.
(18) Zhao, J.-X.; Chang, Y.-X.; He, C.; Burke, B. J.; Collins, M. R.; Del Bel, M.; Elleraas, J.; Gallego, G. M.; Montgomery, T. P.; Mousseau, J. J.; Nair, S. K.; Perry, M. A.; Spangler, J. E.; Vantourout, J. C.; Baran, P. S. 1,2-Difunctionalized Bicyclo[1.1.1]Pentanes: Long–Sought-after Mimetics for Ortho/Meta-Substituted Arenes. *Proc. Natl. Acad. Sci.* **2021**, *118* (28), e2108881118. https://doi.org/10.1073/pnas.2108881118.
(19) Zhang, X.; Smith, R. T.; Le, C.; McCarver, S. J.; Shireman, B. T.; Carruthers, N. I.; MacMillan, D. W. C. Copper-Mediated Synthesis of Drug-like Bicyclopentanes. *Nature* **2020**, *580* (7802), 220–226. https://doi.org/10.1038/s41586-020-2060-z.
(20) Gianatassio, R.; Lopchuk, J. M.; Wang, J.; Pan, C.-M.; Malins, L. R.; Prieto, L.; Brandt, T. A.; Collins, M. R.; Gallego, G. M.; Sach, N. W.; Spangler, J. E.; Zhu, H.; Zhu, J.; Baran, P. S. Strain-Release Amination. *Science* **2016**, *351* (6270), 241–246. https://doi.org/10.1126/science.aad6252.
(21) Analysis was conducted using the DrugBank database (accessed January 2023), see ref 13 for DrugBank details.
(22) Lavoisier, T.; Rodriguez, J. Practical Large Scale Preparation of Activated Cyclopropanes. *Synth. Commun.* **1996**, *26* (3), 525–530. https://doi.org/10.1080/00397919608003644.
(23) Časar, Z. Synthetic Approaches to Contemporary Drugs That Contain the Cyclopropyl Moiety. *Synthesis* **2020**, *52* (09), 1315–1345. https://doi.org/10.1055/s-0039-1690058.

(24) To circumvent these elimination issues, a multistep protocol has been developed involving initial dihydroxylation followed by sequential activation and substitution steps, for an example, see: Jakubowska, A.; Żuchowski, G.; Kulig, K. Cyclic Sulfates as Useful Tools in the Asymmetric Synthesis of 1-Aminocyclopropane-1-Carboxylic Acid Derivatives. Tetrahedron Asymmetry 2015, 26 (21), 1261–1267. https://doi.org/10.1016/j.tetasy.2015.09.013.
(25) Since failed experiments are not often reported, we validated the challenge of elimination by subjecting a substituted vicinal dibromide to malonate and base. These experiments resulted in formation of exclusively elimination products. See SI for details.
(26) Chen, D. Y.-K.; Pouwer, R. H.; Richard, J.-A. Recent Advances in the Total Synthesis of Cyclopropane-Containing Natural Products. *Chem. Soc. Rev.* **2012**, *41* (13), 4631–4642. https://doi.org/10.1039/C2CS35067J.
(27) Davies, H. M. L.; Antoulinakis, E. G. Intermolecular Metal-Catalyzed Carbenoid Cyclopropanations. In *Organic Reactions*; American Cancer Society, 2004; pp 1–326. https://doi.org/10.1002/0471264180.or057.01.
(28) Charette, A. B.; Beauchemin, A. Simmons-Smith Cyclopropanation Reaction. In *Organic Reactions*; American Cancer Society, 2004; pp 1–415. https://doi.org/10.1002/0471264180.or058.01.
(29) Gurmessa, G. T.; Singh, G. S. Recent Progress in Insertion and Cyclopropanation Reactions of Metal Carbenoids from α-Diazocarbonyl Compounds. *Res. Chem. Intermed.* **2017**, *43* (11), 6447–6504. https://doi.org/10.1007/s11164-017-3000-x.
(30) Wu, W.; Lin, Z.; Jiang, H. Recent Advances in the Synthesis of Cyclopropanes. *Org. Biomol. Chem.* **2018**, *16* (40), 7315–7329. https://doi.org/10.1039/C8OB01187G.
(31) Lebel, H.; Marcoux, J.-F.; Molinaro, C.; Charette, A. B. Stereoselective Cyclopropanation Reactions. *Chem. Rev.* **2003**, *103* (4), 977–1050. https://doi.org/10.1021/cr010007e.
(32) Brookhart, Maurice.; Studabaker, W. B. Cyclopropanes from Reactions of Transition Metal Carbene Complexes with Olefins. *Chem. Rev.* **1987**, *87* (2), 411–432. https://doi.org/10.1021/cr00078a008.
(33) Ford, A.; Miel, H.; Ring, A.; Slattery, C. N.; Maguire, A. R.; McKervey, M. A. Modern Organic Synthesis with α-Diazocarbonyl Compounds. *Chem. Rev.* **2015**, *115* (18), 9981–10080. https://doi.org/10.1021/acs.chemrev.5b00121.
(34) Doyle, M. P.; Forbes, D. C. Recent Advances in Asymmetric Catalytic Metal Carbene Transformations. *Chem. Rev.* **1998**, *98* (2), 911–936. https://doi.org/10.1021/cr940066a.
(35) Maas, G. Ruthenium-Catalysed Carbenoid Cyclopropanation Reactions with Diazo Compounds. *Chem. Soc. Rev.* **2004**, *33* (3), 183–190. https://doi.org/10.1039/B309046A.
(36) Simmons, H. E.; Smith, R. D. A NEW SYNTHESIS OF CYCLOPROPANES FROM OLEFINS. *J. Am. Chem. Soc.* **1958**, *80* (19), 5323–5324. https://doi.org/10.1021/ja01552a080.
(37) Green, S. P.; Wheelhouse, K. M.; Payne, A. D.; Hallett, J. P.; Miller, P. W.; Bull, J. A. Thermal Stability and Explosive Hazard Assessment of Diazo Compounds and Diazo Transfer Reagents. *Org. Process Res. Dev.* **2020**, *24* (1), 67–84. https://doi.org/10.1021/acs.oprd.9b00422.
(38) In some cases, diazo compounds can be generated in situ, for selected examples, see refs 39–42.
(39) Day, A. C.; Raymond, P.; Southam, R. M.; Whiting, M. C. The Preparation of Secondary Aliphatic Diazo-Compounds from Hydrazones. *J. Chem. Soc. C Org.* **1966**, No. 0, 467–469. https://doi.org/10.1039/J39660000467.
(40) Morandi, B.; Carreira, E. M. Iron-Catalyzed Cyclopropanation in 6 M KOH with in Situ Generation of Diazomethane. *Science* **2012**, *335* (6075), 1471–1474. https://doi.org/10.1126/science.1218781.
(41) Fulton, J. R.; Aggarwal, V. K.; de Vicente, J. The Use of Tosylhydrazone Salts as a Safe Alternative for Handling Diazo Compounds and Their Applications in Organic Synthesis. *Eur. J. Org. Chem.* **2005**, *2005* (8), 1479–1492. https://doi.org/10.1002/ejoc.200400700.
(42) Liu, Z.; Sivaguru, P.; Zanoni, G.; Bi, X. N-Triftosylhydrazones: A New Chapter for Diazo-Based Carbene Chemistry. *Acc. Chem. Res.* **2022**, *55* (12), 1763–1781. https://doi.org/10.1021/acs.accounts.2c00186.

(43) Alkene cyclopropanation using diazo compounds has been successfully executed for large scale manufacturing though numerous safety concerns must be considered, for selected examples, see refs 44–48.
(44) Simpson, J. H.; Kotnis, A. S.; Deshpande, R. P.; Kacsur, D. J.; Hamm, J.; Kodersha, G.; Merkl, W.; Domina, D.; Wang, S. Y. Development of a Multi-Kilogram Procedure To Prepare, Use, and Quench Ethyl Diazoacetate. In *Managing Hazardous Reactions and Compounds in Process Chemistry*; ACS Symposium Series; American Chemical Society, 2014; Vol. 1181, pp 235–244. https://doi.org/10.1021/bk-2014-1181.ch009.
(45) Proctor, L. D.; Warr, A. J. Development of a Continuous Process for the Industrial Generation of Diazomethane1. *Org. Process Res. Dev.* **2002**, *6* (6), 884–892. https://doi.org/10.1021/op020049k.
(46) Anthes, R.; Bello, O.; Benoit, S.; Chen, C.-K.; Corbett, E.; Corbett, R. M.; DelMonte, A. J.; Gingras, S.; Livingston, R.; Sausker, J.; Soumeillant, M. Kilogram Synthesis of a Selective Serotonin Reuptake Inhibitor. *Org. Process Res. Dev.* **2008**, *12* (2), 168–177. https://doi.org/10.1021/op700125z.
(47) Lathrop, S. P.; Mlinar, L. B.; Manjrekar, O. N.; Zhou, Y.; Harper, K. C.; Sacia, E. R.; Higgins, M.; Bogdan, A. R.; Wang, Z.; Richter, S. M.; Gong, W.; Voight, E. A.; Henle, J.; Diwan, M.; Kallemeyn, J. M.; Sharland, J. C.; Wei, B.; Davies, H. M. L. Continuous Process to Safely Manufacture an Aryldiazoacetate and Its Direct Use in a Dirhodium-Catalyzed Enantioselective Cyclopropanation. *Org. Process Res. Dev.* **2022**. https://doi.org/10.1021/acs.oprd.2c00288.
(48) Bien, J.; Davulcu, A.; DelMonte, A. J.; Fraunhoffer, K. J.; Gao, Z.; Hang, C.; Hsiao, Y.; Hu, W.; Katipally, K.; Littke, A.; Pedro, A.; Qiu, Y.; Sandoval, M.; Schild, R.; Soltani, M.; Tedesco, A.; Vanyo, D.; Vemishetti, P.; Waltermire, R. E. The First Kilogram Synthesis of Beclabuvir, an HCV NS5B Polymerase Inhibitor. *Org. Process Res. Dev.* **2018**, *22* (10), 1393–1408. https://doi.org/10.1021/acs.oprd.8b00214.
(49) Accessing metal carbenoid reactivity without diazo compounds is an area of considerable contemporary interest. For recent examples of progress in this domain, see refs 50–53.
(50) Zhang, L.; DeMuynck, B. M.; Paneque, A. N.; Rutherford, J. E.; Nagib, D. A. Carbene Reactivity from Alkyl and Aryl Aldehydes. *Science* **2022**. https://doi.org/10.1126/science.abo6443.
(51) Cao, L.-Y.; Wang, J.-L.; Wang, K.; Wu, J.-B.; Wang, D.-K.; Peng, J.-M.; Bai, J.; Zhuo, C.-X. Catalytic Asymmetric Deoxygenative Cyclopropanation Reactions by a Chiral Salen-Mo Catalyst. *J. Am. Chem. Soc.* **2023**. https://doi.org/10.1021/jacs.2c12225.
(52) Herndon, J. W. The Chemistry of the Carbon-Transition Metal Double and Triple Bond: Annual Survey Covering the Year 2017. *Coord. Chem. Rev.* **2018**, *377*, 86–190. https://doi.org/10.1016/j.ccr.2018.08.007.
(53) Zhu, D.; Ma, J.; Luo, K.; Fu, H.; Zhang, L.; Zhu, S. Enantioselective Intramolecular C−H Insertion of Donor and Donor/Donor Carbenes by a Nondiazo Approach. *Angew. Chem. Int. Ed.* **2016**, *55* (29), 8452–8456. https://doi.org/10.1002/anie.201604211.
(54) The Corey–Chaykovsky reaction offers an alternative method for polysubstituted cyclopropanes that eschews carbene intermediates but requires activated electron-deficient p-systems (e.g. a,b-unsaturated carbonyl compounds). For selected reviews and examples, see refs 55–58.
(55) Caiuby, C. A. D.; Furniel, L. G.; Burtoloso, A. C. B. Asymmetric Transformations from Sulfoxonium Ylides. *Chem. Sci.* **2022**, *13* (5), 1192–1209. https://doi.org/10.1039/D1SC05708A.
(56) Beutner, G. L.; George, D. T. Opportunities for the Application and Advancement of the Corey–Chaykovsky Cyclopropanation. *Org. Process Res. Dev.* **2022**. https://doi.org/10.1021/acs.oprd.2c00315.
(57) Gololobov, Yu. G.; Nesmeyanov, A. N.; lysenko, V. P.; Boldeskul, I. E. Twenty-Five Years of Dimethylsulfoxonium Ethylide (Corey's Reagent). *Tetrahedron* **1987**, *43* (12), 2609–2651. https://doi.org/10.1016/S0040-4020(01)86869-1.
(58) Li, A.-H.; Dai, L.-X.; Aggarwal, V. K. Asymmetric Ylide Reactions: Epoxidation, Cyclopropanation, Aziridination, Olefination, and Rearrangement. *Chem. Rev.* **1997**, *97* (6), 2341–2372. https://doi.org/10.1021/cr960411r.

(59) Johnson, J. D.; Teeples, C. R.; Akkawi, N. R.; Wilkerson-Hill, S. M. Efficient Synthesis of Orphaned Cyclopropanes Using Sulfones as Carbene Equivalents. *J. Am. Chem. Soc.* **2022**, *144* (32), 14471–14476. https://doi.org/10.1021/jacs.2c07063.
(60) Phelan, J. P.; Lang, S. B.; Compton, J. S.; Kelly, C. B.; Dykstra, R.; Gutierrez, O.; Molander, G. A. Redox-Neutral Photocatalytic Cyclopropanation via Radical/Polar Crossover. *J. Am. Chem. Soc.* **2018**, *140* (25), 8037–8047. https://doi.org/10.1021/jacs.8b05243.
(61) Fischer, D. M.; Lindner, H.; Amberg, W. M.; Carreira, E. M. Intermolecular Organophotocatalytic Cyclopropanation of Unactivated Olefins. *J. Am. Chem. Soc.* **2023**, *145* (2), 774–780. https://doi.org/10.1021/jacs.2c11680.
(62) Jie, L.-H.; Guo, B.; Song, J.; Xu, H.-C. Organoelectrocatalysis Enables Direct Cyclopropanation of Methylene Compounds. *J. Am. Chem. Soc.* **2022**, *144* (5), 2343–2350. https://doi.org/10.1021/jacs.1c12762.
(63) Holst, D. E.; Wang, D. J.; Kim, M. J.; Guzei, I. A.; Wickens, Z. K. Aziridine Synthesis by Coupling Amines and Alkenes via an Electrogenerated Dication. *Nature* **2021**, *596* (7870), 74–79. https://doi.org/10.1038/s41586-021-03717-7.
(64) Wang, D. J.; Targos, K.; Wickens, Z. K. Electrochemical Synthesis of Allylic Amines from Terminal Alkenes and Secondary Amines. *J. Am. Chem. Soc.* **2021**, *143* (51), 21503–21510. https://doi.org/10.1021/jacs.1c11763.
(65) Berger, F.; Plutschack, M. B.; Riegger, J.; Yu, W.; Speicher, S.; Ho, M.; Frank, N.; Ritter, T. Site-Selective and Versatile Aromatic C−H Functionalization by Thianthrenation. *Nature* **2019**, *567* (7747), 223–228. https://doi.org/10.1038/s41586-019-0982-0.
(66) Meng, H.; Liu, M.-S.; Shu, W. Organothianthrenium Salts: Synthesis and Utilization. *Chem. Sci.* **2022**, *13* (46), 13690–13707. https://doi.org/10.1039/D2SC04507A.
(67) Tang, S.; Zhao, X.; Yang, L.; Li, B.; Wang, B. Copper-Catalyzed Carboxylation of Aryl Thianthrenium Salts with CO2. *Angew. Chem. Int. Ed.* **2022**, *61* (47), e202212975. https://doi.org/10.1002/anie.202212975.
(68) Chen, J.; Li, J.; Plutschack, M. B.; Berger, F.; Ritter, T. Regio- and Stereoselective Thianthrenation of Olefins To Access Versatile Alkenyl Electrophiles. *Angew. Chem. Int. Ed.* **2020**, *59* (14), 5616–5620. https://doi.org/10.1002/anie.201914215.
(69) Liu, M.-S.; Du, H.-W.; Shu, W. Metal-Free Allylic C–H Nitrogenation, Oxygenation, and Carbonation of Alkenes by Thianthrenation. *Chem. Sci.* **2022**, *13* (4), 1003–1008. https://doi.org/10.1039/D1SC06577G.
(70) Angyal, P.; Kotschy, A. M.; Dudás, Á.; Varga, S.; Soós, T. Intertwining Olefin Thianthrenation with Kornblum/Ganem Oxidations: Ene-Type Oxidation to Furnish α,β-Unsaturated Carbonyls. *Angew. Chem. Int. Ed.* **2023**, *62* (2), e202214096. https://doi.org/10.1002/anie.202214096.
(71) Chen, C.; Wang, Z.-J.; Lu, H.; Zhao, Y.; Shi, Z. Generation of Non-Stabilized Alkyl Radicals from Thianthrenium Salts for C–B and C–C Bond Formation. *Nat. Commun.* **2021**, *12* (1), 4526. https://doi.org/10.1038/s41467-021-24716-2.
(72) Chen, C.; Wang, M.; Lu, H.; Zhao, B.; Shi, Z. Enabling the Use of Alkyl Thianthrenium Salts in Cross-Coupling Reactions by Copper Catalysis. *Angew. Chem. Int. Ed.* **2021**, *60* (40), 21756–21760. https://doi.org/10.1002/anie.202109723.
(73) During the preparation of this manuscript, Shu and co-workers reported a method preparing aziridines and cyclopropanes through the reaction of isolated alkenyl thianthrenium salt with sulfonamides, amides, carbamates, primary amines, as well as malonates and related nucleophiles. See: Liu, M.-S.; Du, H.-W.; Cui, J.-F.; Shu, W. Intermolecular Metal-Free Cyclopropanation and Aziridination of Alkenes with XH2 (X=N, C) by Thianthrenation. Angew. Chem. Int. Ed. 2022, 61 (41), e202209929. https://doi.org/10.1002/anie.202209929.
(74) For an example of transition metal-catalyzed cyclopropanation that tolerates Lewis basic heterocycles as well as a discussion of associated challenges, see refs 75–76.
(75) Sharland, J. C.; Wei, B.; Hardee, D. J.; Hodges, T. R.; Gong, W.; Voight, E. A.; Davies, H. M. L. Asymmetric Synthesis of Pharmaceutically Relevant 1-Aryl-2-Heteroaryl- and 1,2-

Diheteroarylcyclopropane-1-Carboxylates. *Chem. Sci.* **2021**, *12* (33), 11181–11190. https://doi.org/10.1039/D1SC02474D.

(76) Ye, Q.-S.; Li, X.-N.; Jin, Y.; Yu, J.; Chang, Q.-W.; Jiang, J.; Yan, C.-X.; Li, J.; Liu, W.-P. Synthesis, Crystal Structures and Catalytic Activity of Tetrakis(Acetato)Dirhodium(II) Complexes with Axial Picoline Ligands. *Inorganica Chim. Acta* **2015**, *434*, 113–120. https://doi.org/10.1016/j.ica.2015.05.017.

(77) Juliá, F.; Yan, J.; Paulus, F.; Ritter, T. Vinyl Thianthrenium Tetrafluoroborate: A Practical and Versatile Vinylating Reagent Made from Ethylene. *J. Am. Chem. Soc.* **2021**, *143* (33), 12992–12998. https://doi.org/10.1021/jacs.1c06632.

(78) Mondal, M.; Chen, S.; Kerrigan, N. J. Recent Developments in Vinylsulfonium and Vinylsulfoxonium Salt Chemistry. *Molecules* **2018**, *23* (4), 738. https://doi.org/10.3390/molecules23040738.

(79) Zhou, M.; En, K.; Hu, Y.; Xu, Y.; Shen, H. C.; Qian, X. Zinc Triflate-Mediated Cyclopropanation of Oxindoles with Vinyl Diphenyl Sulfonium Triflate: A Mild Reaction with Broad Functional Group Compatibility. *RSC Adv.* **2017**, *7* (7), 3741–3745. https://doi.org/10.1039/C6RA24985J.

(80) Zhou, M.; Hu, Y.; En, K.; Tan, X.; Shen, H. C.; Qian, X. Efficient Cyclopropanation of Aryl/Heteroaryl Acetates and Acetonitriles with Vinyl Diphenyl Sulfonium Triflate. *Tetrahedron Lett.* **2018**, *59* (14), 1443–1445. https://doi.org/10.1016/j.tetlet.2018.02.080.

(81) Nambu, H.; Ono, N.; Hirota, W.; Fukumoto, M.; Yakura, T. An Efficient Method for the Synthesis of 2′,3′-Nonsubstituted Cycloalkane-1,3-Dione-2-Spirocyclopropanes Using (2-Bromoethyl)Diphenylsulfonium Trifluoromethanesulfonate. *Chem. Pharm. Bull. (Tokyo)* **2016**, *64* (12), 1763–1768. https://doi.org/10.1248/cpb.c16-00625.

(82) Qin, H.; Miao, Y.; Zhang, K.; Xu, J.; Sun, H.; Liu, W.; Feng, F.; Qu, W. A Convenient Cyclopropanation Process of Oxindoles via Bromoethylsulfonium Salt. *Tetrahedron* **2018**, *74* (47), 6809–6814. https://doi.org/10.1016/j.tet.2018.09.042.

(83) Xie, C.; Han, D.; Hu, Y.; Liu, J.; Xie, T. Synthesis of Pyrrolidin-2-Ones via Tandem Reactions of Vinyl Sulfonium Salts under Mild Conditions. *Tetrahedron Lett.* **2010**, *51* (40), 5238–5241. https://doi.org/10.1016/j.tetlet.2010.07.108.

(84) Mao, Z.; Qu, H.; Zhao, Y.; Lin, X. A General Access to 1,1-Cyclopropane Aminoketones and Their Conversion into 2-Benzoyl Quinolines. *Chem. Commun.* **2012**, *48* (79), 9927–9929. https://doi.org/10.1039/C2CC35235D.

(85) Gosselck, J.; Béress, L.; Schenk, H. Reactions of Substituted Vinylsulfonium Salts with CH-Acidic Compounds. – A New Route to Polysubstituted Cyclopropanes. *Angew. Chem. Int. Ed. Engl.* **1966**, *5* (6), 596–597. https://doi.org/10.1002/anie.196605962.

(86) Braun, H.; Huber, G. Reaktionen von Butadienylsulfoniumsaltzen Mit Carbonionen. *Tetrahedron Lett.* **1976**, *17* (25), 2121–2124. https://doi.org/10.1016/S0040-4039(00)93135-6.

(87) Takaki, K.; Agawa, T. Synthesis of Acylcyclopropanes and Oxiranes from Vinylsulfonium Salts and Lithium Enolates. *J. Org. Chem.* **1977**, *42* (20), 3303–3304. https://doi.org/10.1021/jo00440a024.

(88) Lin, H.; Shen, Q.; Lu, L. β-(Trifluoromethyl)Vinyl Sulfonium Salts: Preparation and Reactions with Active Methylene and Methenyl Compounds. *J. Org. Chem.* **2011**, *76* (18), 7359–7369. https://doi.org/10.1021/jo2009033.

(89) Guo, S.; Zhang, N.; Tang, X.; Mao, Z.; Zhang, X.; Yan, M.; Xuan, Y. Cyclopropanation of Active Methylene Compounds with β-Alkoxycarbonyl Vinylsulfonium Salts. *Chin. Chem. Lett.* **2019**, *30* (2), 406–408. https://doi.org/10.1016/j.cclet.2018.08.021.

(90) Matlock, J. V.; Fritz, S. P.; Harrison, S. A.; Coe, D. M.; McGarrigle, E. M.; Aggarwal, V. K. Synthesis of α-Substituted Vinylsulfonium Salts and Their Application as Annulation Reagents in the Formation of Epoxide- and Cyclopropane-Fused Heterocycles. *J. Org. Chem.* **2014**, *79* (21), 10226–10239. https://doi.org/10.1021/jo501885z.

(91) Cost of thianthrene is less than 0.15 USD/mmol (Ambeed, Jan 2023).

(92) Mitchell, S. C.; Waring, R. H. Fate of Thianthrene in Biological Systems. *Xenobiotica* **2017**, *47* (8), 731–740. https://doi.org/10.1080/00498254.2016.1222107.
(93) McGrath, N. A.; Brichacek, M.; Njardarson, J. T. A Graphical Journey of Innovative Organic Architectures That Have Improved Our Lives. *J. Chem. Educ.* **2010**, *87* (12), 1348–1349. https://doi.org/10.1021/ed1003806.
(94) Ruah, S. H.; Hamilton, M.; Miller, M.; Grootenhuis, P. D. J.; Bear, B.; Mccarthy, J.; Zhou, J. Heterocyclic Modulators of Atp-Binding Cassette Transporters. WO2007056341A1, May 18, 2007. https://patents.google.com/patent/WO2007056341A1/en (accessed 2023-01-16).
(95) Tanoury, G. J.; Harrison, C.; Littler, B. J.; Rose, P. J.; Hughes, R. M.; Jung, Y. C.; Siesel, D. A.; Lee, E. C.; Belmont, D. T. Process of Producing Cycloalkylcarboxamido-Indole Compounds. WO2011133751A2, October 27, 2011. https://patents.google.com/patent/WO2011133751A2/en?oq=WO+2011133751 (accessed 2023-01-16).

Appendix A: Supporting Information for Chapter 1 (Aziridine synthesis by coupling amines and alkenes via an electrogenerated dication)

A.1 General Methods and Materials

Unless otherwise noted, reactions were performed under an inert N_2 atmosphere in an anhydrous solvent. MeCN, THF, DMF, and DCM were dried by passing through activated alumina columns. Tetrabutylammonium hexafluorophosphate was recrystallized three times from EtOAc prior to use. Lithium tetrafluoroborate was dried at 50 °C under vacuum prior to use. All liquid amines were distilled from CaH_2 prior to use. Thianthrene was recrystallized from acetone prior to use. Unless otherwise noted, other commercially-available reagents were used as received. Crude mixtures were evaluated by thin-layer chromatography using EMD/Merck silica gel 60 F254 pre-coated plates (0.25 mm) and were visualized by UV, Seebach, p-anisaldehyde, ninhydrin, or $KMnO_4$ staining. Flash chromatography was performed with a Biotage Isolera One automated chromatography system with re-packed silica columns (technical grade silica, pore size 60 Å, 230-400 mesh particle size, 40-63 particle size) or pre-packed Biotage SNAP Ultra columns unless otherwise noted. Purified materials were dried in vacuo (0.050 Torr) to remove trace solvent. ^{1}H, ^{13}C, ^{19}F Spectra were taken using a Bruker Avance-400 with a BBFO Probe, a Bruker Avance-500 with a DCH Cryoprobe, Bruker Avance III HD-500 with a TXO Cryoprobe, or a Bruker Avance-600 with a TCI-F cryoprobe. NMR data are reported relative to residual $CHCl_3$ (^{1}H, δ = 7.26 ppm), $CDCl_3$ (^{13}C, δ = 77.16 ppm) or residual C_6H_6 (^{1}H, δ = 7.16), C_6D_6 (^{13}C, δ = 128.06 ppm). Data for ^{1}H NMR spectra are reported as follows: chemical shift (δ ppm) (multiplicity, coupling constant (Hz), integration). Multiplicity and qualifier abbreviations are as follows: s = singlet, d = doublet, t = triplet, q = quartet, m = multiplet, br = broad. All NMR yields were determined via reference against an internal standard (dibromomethane or mesitylene for ^{1}H, trifluorotoluene for ^{19}F). GC traces were taken on an Agilent 7890A GC with dual DB-5 columns (20 m ×180 μμm × 0.18 μm), dual FID detectors, and hydrogen as the carrier gas. A sample volume of 1 μL was injected at a temperature of 300 °C and a 100:1 split ratio. The initial inlet pressure was 20.3 psi but varied as the column flow was held constant at 1.8 mL/min for the duration of the run, FID temperature was 325 °C. Mass spectrometry data was collected on a Thermo Scientific Q Exactive Plus Mass Spectrometer. The crystal evaluation and data collections were performed on a Bruker D8 VENTURE PhotonIII four-circle diffractometer with Cu Kα (λ = 1.54178 Å) radiation with the detector to crystal distance of 4.0 cm (Bruker-AXS (2018). APEX3. Version 2018.1-0. Madison, Wisconsin, USA.). The reflections were indexed by an automated indexing routine built in the APEX3 program. Mercury was used for structural visualization[1].

Abbreviations: Boc—tert-butyl carbamate, tBu—tert-butyl, CV—cyclic voltammetry, DCM—dichloromethane, DMF—dimethyl formamide, EtOAc—ethyl acetate, MeCN—acetonitrile, MeOH—methanol, RVC—reticulated vitreous carbon, Ph—phenyl, *n*-Hex—hexyl, *n*-Pr—propyl, DMSO—dimethylsulfoxide, THF— tetrahydrofuran, TEA—triethylamine, TFA—trifluoroacetic acid, GC— gas chromatography.

Electrochemical Methods and Materials

All chronoamperometric, chronopotentiometric, and cyclic voltammetry measurements were performed at room temperature using a Pine WaveNowXV. The CV experiments were carried out in a three-electrode cell configuration with a glassy carbon (GC) working electrode (3 mm diameter, unless otherwise stated) and a platinum wire counter electrode. Chronoamperometric and chronopotentiometric measurements were carried out in divided cells with RVC (8 × 6 × 6 mm, Ultramet, 80 ppi) as working and counter electrodes affixed to stainless steel wire or a graphite pencil/silver wire assembly (see below). The potentials were measured versus an $Ag/AgNO_3$ (0.01 M in MeCN with 0.1 M n-Bu_4N•PF_6) reference electrode (all electrodes from Pine Research) and externally referenced via the ferrocene/ferrocenium couple. Bulk constant current electrolysis experiments were driven with a Dr. Meter HY3005M-L DC Power Supply or a custom–made low current power supply (see Scheme below) which was externally calibrated with a multimeter using a 10 or 1–Ohm resistor.

Divided cell fabricated in house. Glass frit purchased from Ace Glass (7176-36). Anode electrode assembled via affixing end of the silver wire (Belden Hook-Up wire, item no. 83005 007100) around the pencil (JuneGold 2B graphite 2 mm) using conductive graphite adhesive (Alfa Aesar, 42465), wrapping in teflon tape to prevent exposure, then piercing RVC with pencil. Solvent exposed electrode surface area (2.1 cm^2) was calculated via manufacturer-supplied surface area/volume ratio measurements. PTFE tubing (Cole-Parmer; 1/32” ID, 1/16” OD, item number EW-06407-41) connects both sides of the divided cell to normalize pressure. Septa inner diameter 16 mm. Stainless steel purchased from Grainger; stainless steel lockwire, 0.025" diameter, item number 16Y043. Average cell resistance: 0.9 kΩ.

Low-current Power Supply [2]**:** Original design and fabrication by Dr. Blaise J. Thompson. Provides an operational range of ±0.01–9.99 mA, tunable by analog input, delivering power to multiple banana socket pairs. The power supply is limited to ±15 V for bulk electrolysis and is powered by an 18 V wall wart. Circuitry is housed within an aluminum enclosure.

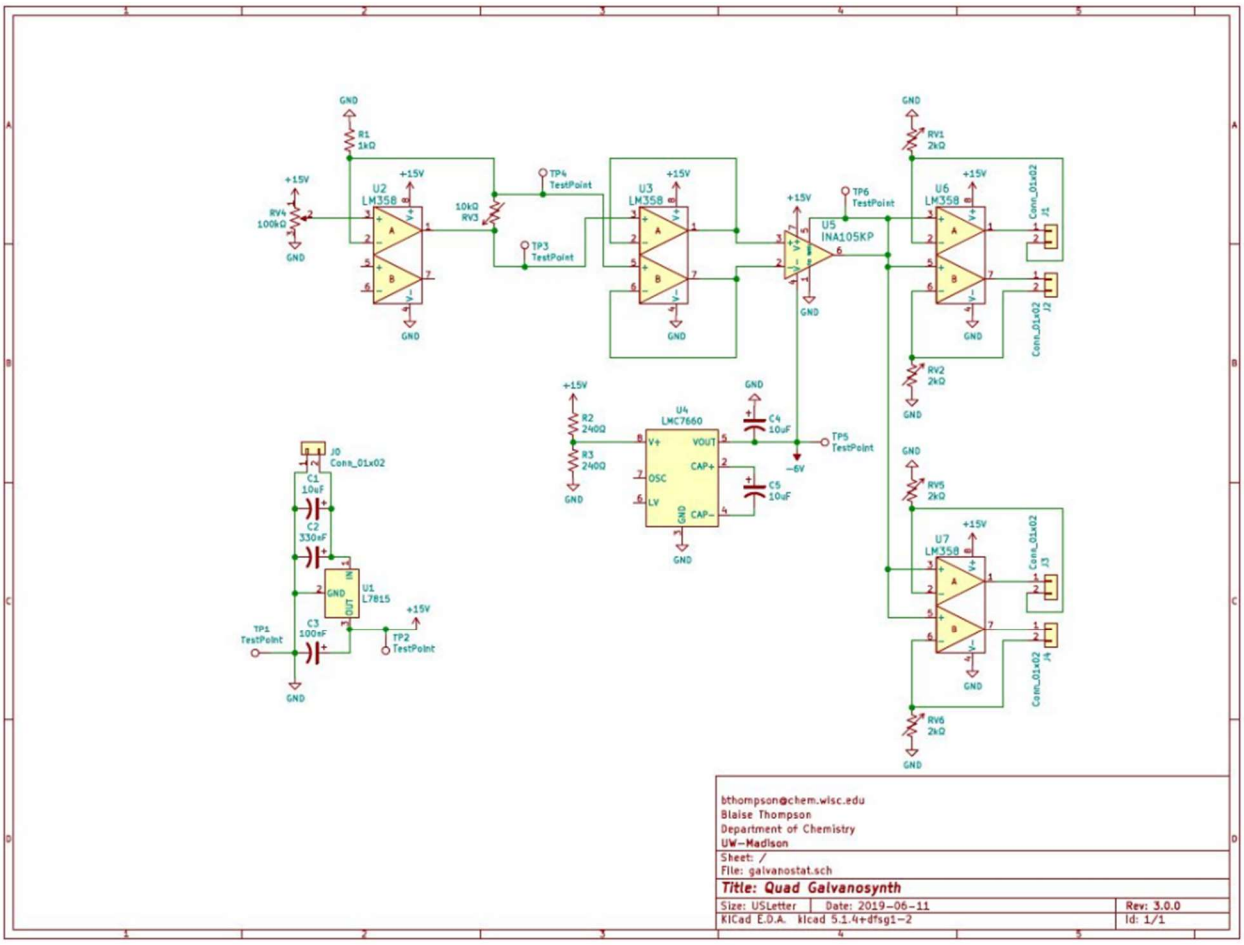

A.2 Supplementary Data

Dibromide substitution with a primary amine:

A literature survey revealed that the only examples of aziridine formation from vicinal dibromides were restricted to substitution of activated α-carbonyl vicinal dibromides. Reactivity of vicinal dibromides to form aziridines with primary amines was not found outside of these examples. We adapted a selection of precedent conditions from α-carbonyl vicinal dibromides[3–5] to the substitution reaction, as well as conditions similar to our scope procedures to probe aziridine formation directly from a 4-phenylbutene-derived dibromide. For comparison, substitution of the 4-phenylbutene-derived dicationic adduct results in 91% yield of the desired aziridine product.

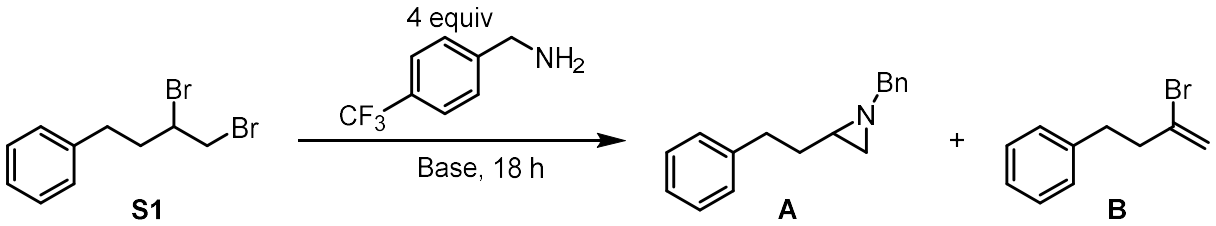

entry	Base (equiv)	Solvent	Temp (°C)	Conc. (M)	**A** (%)	**B** (%)	Dibromide Conv. (%)	Amine Conv. (%)	Source
1	Cs_2CO_3 (4)	MeCN*	20	0.05	0	51	100	12	this work
2	Cs_2CO_3 (6)	MeCN*	20	0.05	0	54	100	25	this work
3	TEA (3)	MeOH	20, 50	0.4	0	0	0	0	ref. 3
4	TEA (4)	toluene	80	0.35	0	0	0	0	ref. 4
5	TEA (2)	THF	20, 50	0.125	0	0	0	0	ref. 5

Table A1.

*0.2 M *n*-Bu_4NPF_6. Concentrations are in reference to the dibromide starting material. Entries 3 and 5 were heated to 50 °C following stirring at rt for 18 h and stirred for an additional 18 h. No change in the amount of dibromide or amine was observed upon heating. Under these conditions, substitution of a vicinal dibromide using a primary amine results in exclusively vinyl bromide or no reactivity.

Limiting Alkene and Amine Conditions:

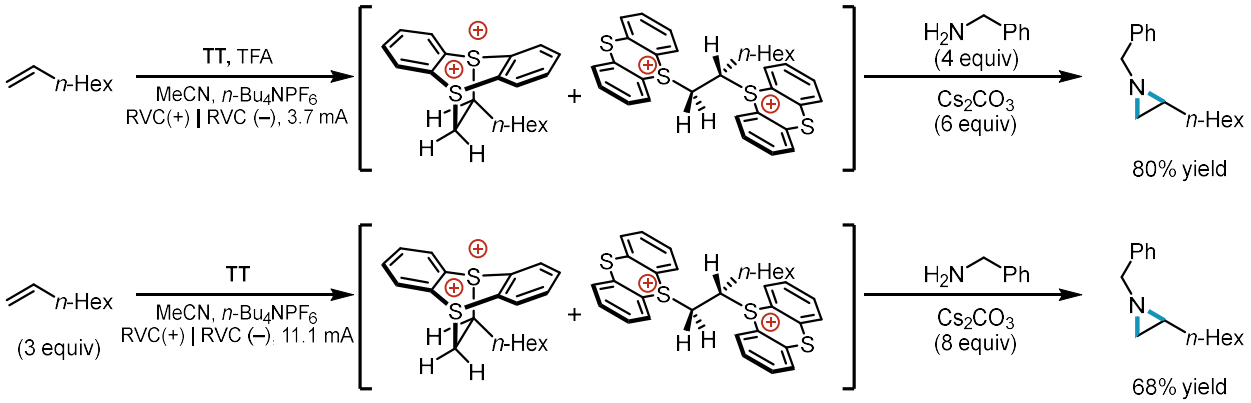

Fig. A1.

Limiting alkene (top, General Procedure E, NMR yield) and limiting amine (bottom, General Procedure D, isolated yield) conditions for aziridine formation

Internal Alkene Adduct Formation and Attempted Aziridination

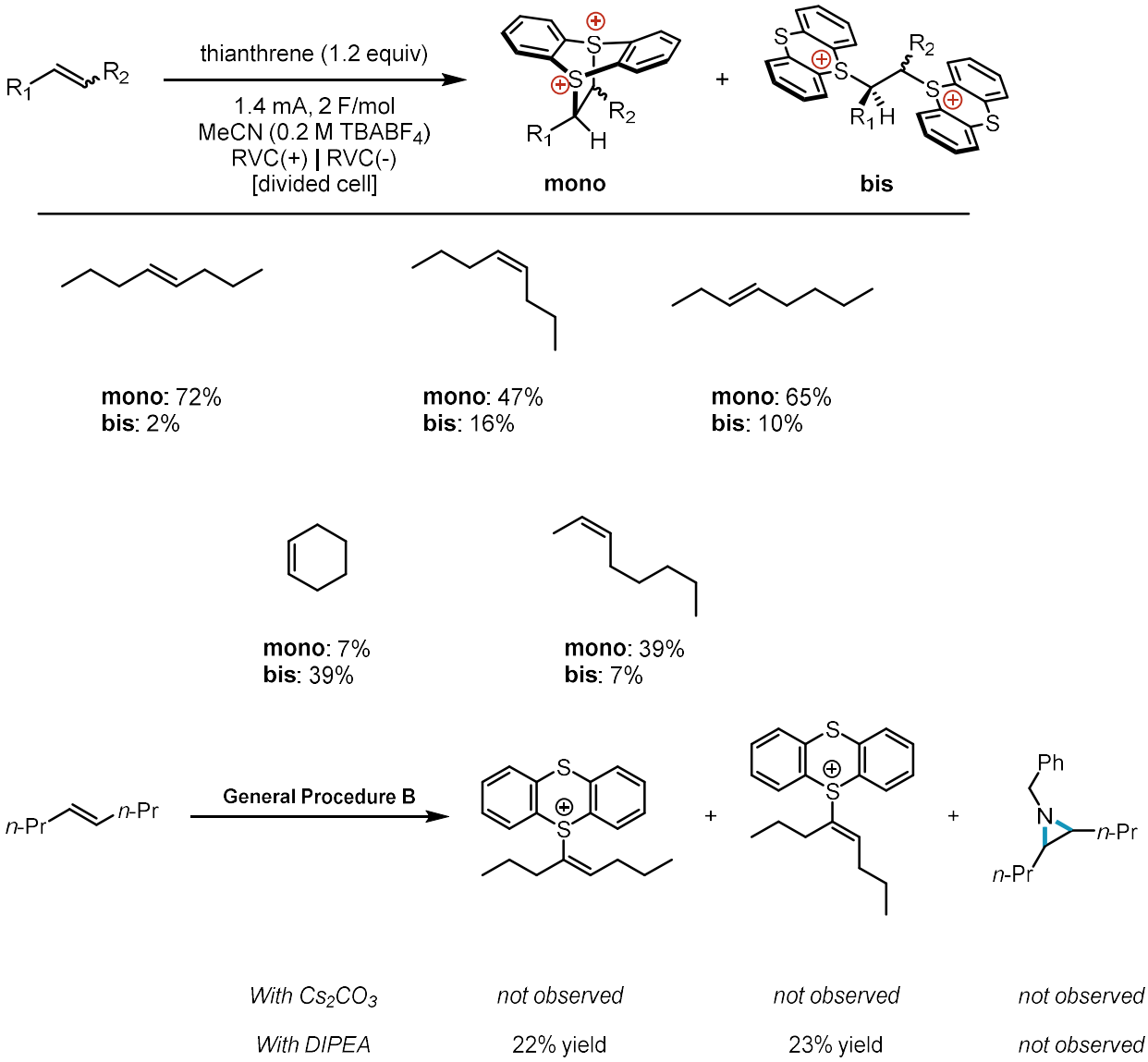

Fig. A2.

1,2-Disubstituted alkenes, which can form both mono- and bis- adduct under electrolysis in the presence of thianthrene, give intractable mixtures of products or eliminate to the internal vinyl thianthrenium salt but do not react further when subjected to standard aziridination conditions. Reactions performed on 0.15 mmol scale.

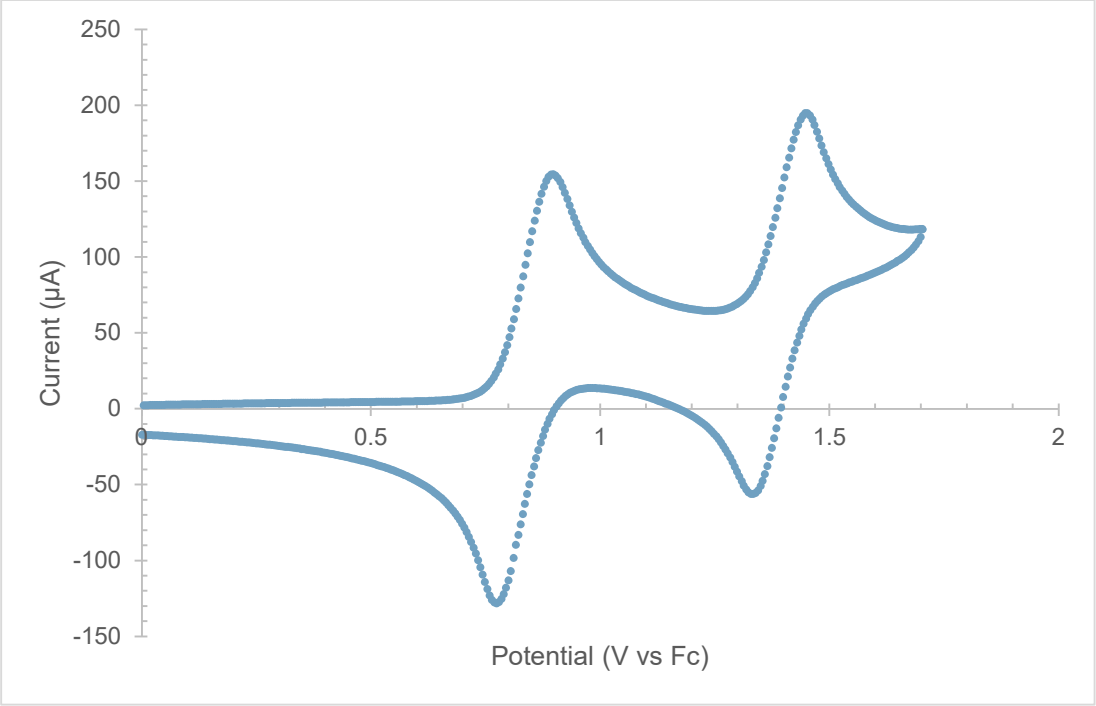

Fig. A3.

Cyclic voltammetry of thianthrene (5 mM) in MeCN (0.1 M BuN_4PF_6). Sweep rate: 100 mV/s. Externally referenced to the ferrocene/ferrocenium couple. 2% trifluoroacetic anhydride by volume was added to the solution as a dessicant before the CV measurement was taken to render the second oxidation peak reversible.

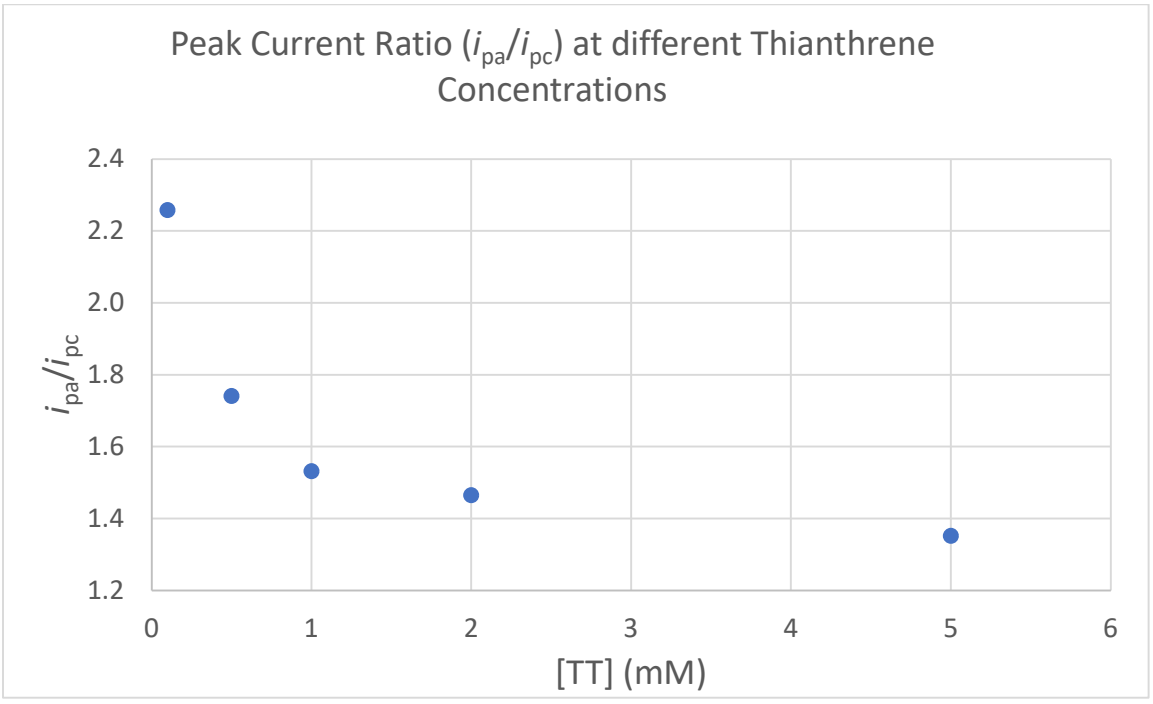

Fig. A4.

Peak current ratios (anodic over cathodic, i_{pa}/i_{pc}) from cyclic voltammetry of different concentrations of thianthrene (0.1 – 5 mM) in MeCN (0.1 M *n*-BuN_4PF_6). Sweep rate: 100 mV/s. Externally referenced to the ferrocene/ferrocenium couple. 2% trifluoroacetic anhydride by volume was added to the solution as a desiccant. As the thianthrene concentration is increased, disproportionation becomes disfavored relative to comproportionation, which should lower the ratio of peak currents since more thianthrene radical cation should remain in solution at cathodic peak.

A.3 Mechanistic Investigations

Conversion Time Courses Procedure

To an oven-dried divided electrochemical cell equipped with magnetic stir bars was added thianthrene (130 mg, 0.6 mmol, 1.5 equiv or 217 mg, 1.0 mmol, 2.5 equiv) to the anode compartment and *n*-Bu_4NPF_6 (620 mg, 1.6 mmol, 4 equiv) to both compartments. The cell was equipped with two septa containing a stainless steel wire/RVC cathode assembly and a pencil/RVC anode assembly connected together with a teflon tubing to equalize pressure. MeCN (8 mL) was added to the cathode compartment and the glass frit was allowed to become saturated (<1 min). MeCN (8 mL) was added to the anode compartment, followed by 4-phenylbutene (0.4 mmol, 1 equiv, 60 µL), benzonitrile (0.4 mmol, 1 equiv, 41 µL) and trifluoroacetic acid (61 µL, 0.8 mmol, 2 equiv). Trifluoroacetic acid (153 µL, 2.0 mmol, 5 equiv) was added to the cathode compartment and both sides of the cell were stirred and electrolyzed under a constant current of 3.7 mA (1.8 mA/cm^2) for 7.2 h (2.5 F/mol). At varying times, ~10 µL aliquots of the reaction mixture were removed via syringe and immediately diluted with a small amount of Et_2O and quenched by passing through a short pad of silica. The solution was transferred to a GC vial and the concentration of the 4-phenylbutene starting material was determined via GC using benzonitrile as the internal standard.

Adduct Yield Time Course Procedure

To an oven-dried divided electrochemical cell equipped with magnetic stir bars was added thianthrene (130 mg, 0.6 mmol, 1.5 equiv or 217 mg, 1.0 mmol, 2.5 equiv) to the anode compartment and n-Bu_4NPF_6 (620 mg, 1.6 mmol, 4 equiv) to both compartments. The cell was equipped with two septa containing a stainless steel wire/RVC cathode assembly and a pencil/RVC anode assembly connected together with a teflon tubing to equalize pressure. MeCN (8 mL) was added to the cathode compartment and the glass frit was allowed to become saturated (<1 min). MeCN (8 mL) was added to the anode compartment, followed by 4-phenylbutene (0.4 mmol, 1 equiv, 60 µL), dibromomethane (0.4 mmol, 1 equiv, 28 µL) and trifluoroacetic acid (61 µL, 0.8 mmol, 2 equiv). Trifluoroacetic acid (153 µL, 2.0 mmol, 5 equiv) was added to the cathode compartment and both sides of the cell were stirred and electrolyzed under a constant current of 3.7 mA (1.8 mA/cm^2) for 7.2 h (2.5 F/mol). At varying times, aliquots of the reaction mixture were removed via syringe (~50 µL for time points before 3 h, then ~10 µL afterwards) and transferred to an NMR tube and diluted with CD_3CN. The concentration of monoadduct **1** and bisadduct **2** were determined via NMR using dibromomethane as an internal standard.

Constant Potential Electrolysis at Potential of Second Oxidation of Thianthrene

To an oven-dried divided electrochemical cell equipped with magnetic stir bars was added thianthrene (66 mg, 0.3 mmol, 1.5 equiv or 109mg, 0.5 mmol, 2.5 equiv) to the anode compartment and Bu_4NPF_6 (775 mg, 2.0 mmol, 10 equiv) to both compartments. The cell was equipped with two septa containing a stainless steel wire/RVC cathode assembly and a pencil/RVC, reference electrode anode assembly connected together with a teflon tubing to equalize pressure. MeCN (4 mL) was added to the cathode compartment and the glass frit was allowed to become saturated (<1 min). MeCN (4 mL) was added to the anode compartment, followed by 4-phenylbutene (0.2 mmol, 1 equiv, 30 µL), benzonitrile (0.2 mmol, 1 equiv, 21 µL) and trifluoroacetic acid (31 µL, 0.4 mmol, 2 equiv). Trifluoroacetic acid (77 µL, 1.0 mmol, 5 equiv) was added to the cathode compartment and both sides of the cell were stirred and electrolyzed under a constant potential of 1.4V until so starting material remained as monitored by GC. At varying times, ~10 µL aliquots of the reaction mixture were removed via syringe and immediately diluted with a small amount of Et_2O and quenched by passing through a short pad of silica. The solution was transferred to a GC vial and the concentration of the 4-phenylbutene starting material was determined via GC using benzonitrile as the internal standard.

Time Course Full Data

Figure A4A 1.5 equiv thianthrene conversion:

	Time (h)	Conv (%)
t1	0.7	0.9
t2	1.4	5.3
t3	2.2	4.4
t4	2.9	12.6
t5	3.6	16.5
t6	4.3	24.6
t7	4.7	27.9
t8	5.0	41.1
t9	5.4	53.4
t10	5.8	69.0
t11	6.1	82.1
t12	6.5	94.5
t13	6.9	100.0
t14	7.3	100.0

Figure A4B 2.5 equiv thianthrene conversion:

	Time (h)	Conv (%)
t1	1.2	2.4
t2	2.4	10.2
t3	3.6	18.4
t4	4.8	30.4
t5	6.1	41.1
t6	7.3	51.6
t7	7.9	56.4
t8	8.5	68.7
t9	9.1	90.3
t10	9.7	100.0

Figure A4C monoadduct/bisadduct yield:

	time (h)	bisadduct (%)	monoadduct (%)
t1	0.5	1	0
t2	1	3	0
t3	1.5	4	0
t4	2	6	0.5
t5	2.5	7	1
t6	3	9	0
t7	4	12	2
t8	5	16	16
t9	5.5	15	30
t10	6	19	48
t11	6.5	17	64
t12	6.9	19	70

Constant Potential electrolysis at second oxidation potential of thianthrene conversion:

Figure A4D 1.5 equiv. thianthrene conversion:

	time (min)	Conv (%)
t1	2	0.3
t2	5	0.7
t3	9	0.2
t4	12	9.9
t5	15	24.1
t6	19	47.9
t7	23	73
t8	27	96.3
t9	32	100

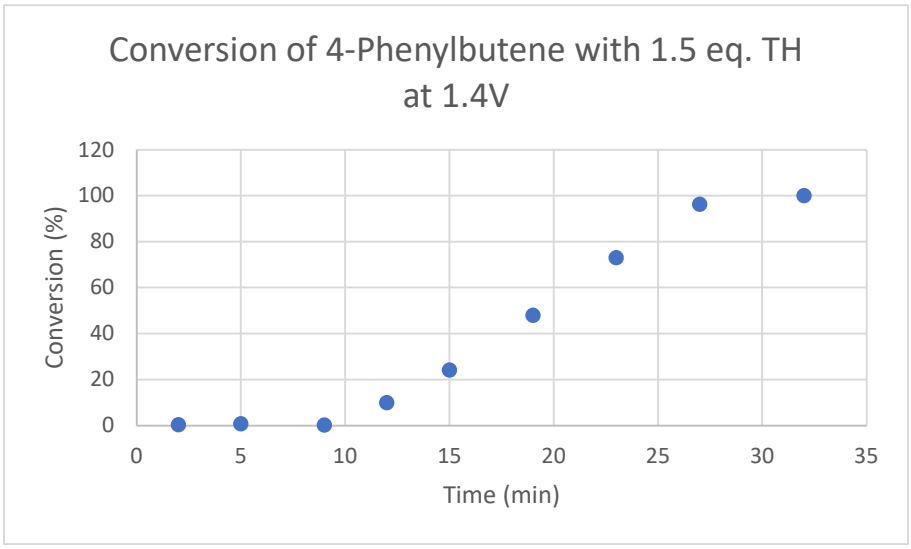

Figure A4D 2.5 equiv. thianthrene conversion:

	time (min)	Conv (%)
t1	2	2.3
t2	5	1.1
t3	9	3.5
t4	12	9.5
t5	15	14.5
t6	19	26.2
t7	23	39
t8	27	46.4
t9	32	66.7
t10	37	82.5
t11	42	95.8
t12	48	100

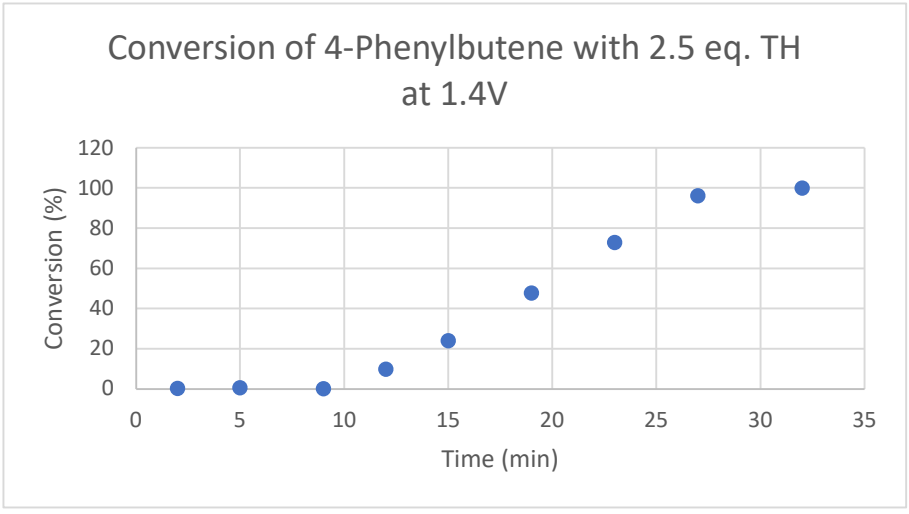

A.4 Substrate Preparation

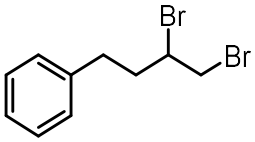

(3,4-dibromobutyl)benzene (A1): 4-phenylbutene (0.75 mL, 5.0 mmol, 1 equiv), DMSO (0.43 mL, 6.0 mmol, 1.2 equiv), and EtOAc (20 mL) were combined. The mixture was heated to 60 °C, and 48% HBr (1.4 mL, 12 mmol, 2.4 equiv) was added and the mixture was stirred for 1.5 h. After cooling to room temperature, the mixture was diluted with ~20 mL EtOAc and washed with water (20 mL x3). The organic layer was dried using anhydrous Na_2SO_4, filtered, and concentrated under reduced pressure. The residue was purified via flash column chromatography (0-20% EtOAc/hexanes) to yield 1.5 g (quant.) of **A1** as an oil. **^{1}H NMR** (400 MHz, $CDCl_3$) δ 7.37 – 7.21 (m, 5H), 4.14 (tdd, J = 9.6, 4.4, 2.9 Hz, 1H), 3.89 (dd, J = 10.3, 4.4 Hz, 1H), 3.68 (t, J = 10.0 Hz, 1H), 2.97 (ddd, J = 13.9, 9.3, 4.7 Hz, 1H), 2.78 (ddd, J = 13.7, 9.1, 7.2 Hz, 1H), 2.56 – 2.45 (m, 1H), 2.12 (dtd, J = 14.3, 9.3, 4.7 Hz, 1H). ^{13}C NMR Consistent with reported spectra[6].

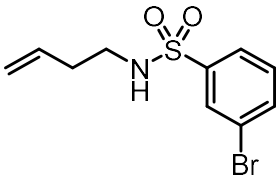

3-bromo-N-(but-3-en-1-yl)benzenesulfonamide (A2): To a solution of 3-bromobenzenesulfonyl chloride (1.41 g, 5.5 mmol, 1.1 equiv.) in DCM (5 mL) at 0 °C was added triethylamine (0.77 mL, 5.5 mmol, 1.1 equiv) followed by 3-buten-1-amine (0.46 mL, 5.0 mmol, 1 equiv). The mixture was allowed to warm to room temperature overnight. ~10 mL 1 M HCl was added to the reaction mixture and the layers were separated. The aqueous layer was extracted with DCM (~20 mL x3). The combined organic layers were dried with anhydrous Na_2SO_4, filtered, and evaporated under reduced pressure to give 1.44 g (99 % yield) of **A2** as a white fluffy solid. **^{1}H NMR** (500 MHz, $CDCl_3$) δ 7.94 (t, *J* = 1.8 Hz, 1H), 7.73 (dt, *J* = 8.1, 1.3 Hz, 1H), 7.65 (ddd, *J* = 8.0, 2.0, 1.0 Hz, 1H), 7.34 (t, *J* = 7.9 Hz, 1H), 5.56 (ddt, *J* = 17.1, 10.2, 6.9 Hz, 1H), 5.07 – 4.97 (m, 2H), 4.47 (t, *J* = 6.1 Hz, 1H), 2.99 (q, *J* = 6.5 Hz, 2H), 2.20 – 2.13 (m, 2H), 1.54 (brs, 1H); **^{13}C NMR** (126 MHz, $CDCl_3$) δ 142.12, 135.85, 134.04, 130.79, 130.17, 125.72, 123.27, 118.69, 42.26, 33.82; **HRMS** (ESI+) **Calc:** [M+Na]+ (C10H12BrNO2SNa) 311.96643; measured: 311.9660; 1.4 ppm difference.

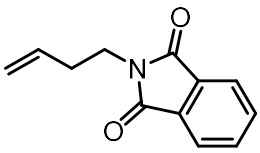

2-(but-3-en-1-yl)isoindoline-1,3-dione (A3): To a mixture of potassium phthalimide (741 mg, 4.0 mmol, 1 equiv) in DMF (8 mL) was added 4-bromo-1-butene (406 µL, 4 mmol, 1 equiv). The reaction mixture was heated to 60 °C and stirred overnight (16 h). At completion, the mixture was cooled to rt and poured into a saturated aqueous NaCl solution (~50 mL). The aqueous layer was extracted with Et_2O (3 x 100 mL). The combined organic layers were washed with aqueous 10% LiCl solution (2 x 10 mL), dried over anhydrous $MgSO_4$, filtered, and concentrated under reduced pressure. The residue was purified via flash column chromatography (0-45% EtOAc/hexanes) to give 492 mg (61% yield) of **A3** as a solid.

^{1}H NMR (500MHz, $CDCl_3$) δ 7.84 (dd, J = 5.4, 3.1 Hz, 2H), 7.71 (dd, J = 5.4, 3.0, 2H), 5.79 (ddt, J = 17.2, 10.2, 6.9 Hz, 1H), 5.07 (dd, J = 17.1, 1.7 Hz, 1H), 5.02 (dd, J = 10.3, 1.7 Hz, 1H), 3.77 (t, J = 7.1 Hz, 2H), 2.45 (q, J = 7.0 Hz, 2H); ^{13}C NMR consistent with reported spectra[7].

A.5 General Experimental Procedures

CAUTION: Although there is no known toxicology data on these dicationic adducts and no issues were encountered during these experiments, we suspect, based on analogy to other dielectrophiles[8], that these adducts are extremely toxic. Isolation or storage of the adducts was avoided, and all substitutions were carried out *in situ*.

Preparation of Basified Silica (Silica):

Following reported procedure[9], Silica gel (100 g) was added to 1 L of saturated aqueous $NaHCO_3$. The resulting slurry was stirred vigorously for 2 h. After stirring, the mixture was diluted with 100 mL acetone and filtered. The pad of silica gel was washed two times with 100 mL 1:1 water/acetone and once with 100 mL acetone. The filtrate was dried overnight under reduced pressure before use. Silica plates for crude mixture evaluation can be similarly basified.

General Procedure A: Limiting Amine

To an oven-dried divided electrochemical cell equipped with magnetic stir bars was added thianthrene (390 mg, 1.8 mmol, 4.5 equiv) to the anode compartment and n-Bu_4NPF_6 (310 mg, 0.8 mmol, 2 equiv) to both compartments. The cell was equipped with two septa containing a stainless steel wire/RVC cathode assembly and a pencil/RVC anode assembly connected together with a teflon tubing to equalize pressure. MeCN (4 mL) was added to the cathode compartment and the glass frit was allowed to become saturated (<1 min). MeCN (4 mL) was added to the anode compartment, followed by 1-octene (188 µL, 1.2 mmol, 3 equiv). (*Electrode depth: 2 cm).* Trifluoroacetic acid (460 µL, 6.0 mmol, 15 equiv) was added to the cathode compartment and both sides of the cell were stirred and electrolyzed under a constant current of 11.1 mA (5.4 mA/cm^2) for 7.2 h (2.5 F/mol alkene). At completion of electrolysis, the electrode leads were disconnected, septa removed, and the anode RVC was pushed off the pencil into the reaction mixture. Cs_2CO_3 (1.04 g, 3.2 mmol, 8 equiv) was added to the anode compartment followed by amine (0.4 mmol, 1 equiv). To the anode compartment was added a septum pierced with a needle to prevent pressurizing. After pressure equilibration, the needle was removed, and the cathode solution was removed from the cell via pipette. The anode solution was stirred in the cell for 16 h. At completion, the mixture was diluted with DCM (~60 mL) and water (150 mL). The aqueous layer was extracted with DCM (50 mL x 3). The combined organic layers were washed with saturated NaCl solution (40 mL), dried with anhydrous Na_2SO_4, filtered, and concentrated under reduced pressure. The residue was purified via flash column chromatography using basified silica gel to yield the pure aziridine product.

General Procedure B: Limiting Alkene

To an oven-dried divided electrochemical cell equipped with magnetic stir bars was added thianthrene (130 mg, 0.6 mmol, 1.5 equiv) to the anode compartment and *n*-Bu_4NPF_6 (620 mg, 1.6 mmol, 4 equiv) to both compartments. The cell was equipped with two septa containing a stainless steel wire/RVC cathode assembly and a pencil/RVC anode assembly connected together with a teflon tubing to equalize pressure. MeCN (8 mL) was added to the cathode compartment and the glass frit was allowed to become saturated (<1 min). MeCN (8 mL) was added to the anode compartment, followed by the alkene (0.4 mmol, 1 equiv) and trifluoroacetic acid (61 µL, 0.8 mmol, 2 equiv). (*Electrode depth: 2 cm).* Trifluoroacetic acid (153 µL, 2.0 mmol, 5 equiv) was added to the cathode compartment and both sides of the cell were stirred and electrolyzed under a constant current of 3.7 mA (1.8 mA/cm^2) for 7.2 h (2.5 F/mol). At completion of electrolysis, the electrode leads were disconnected, septa removed, and the anode RVC was pushed off the pencil into the reaction mixture. Cs_2CO_3 (782 mg, 2.4 mmol, 6 equiv) was added to the anode compartment followed by benzylamine (175 µL, 1.6 mmol, 4 equiv). To the anode compartment was added a septum pierced with a needle to prevent pressurizing. After pressure equilibration, the needle was removed, and the cathode solution was removed from the cell via pipette. The anode solution was stirred in the cell for 16 h. At completion, the mixture was diluted with DCM (~60 mL) and water (150 mL). The aqueous layer was extracted with DCM (50 mL x 3). The combined organic layers were washed with saturated NaCl solution (40 mL), dried with anhydrous Na_2SO_4, filtered, and concentrated under reduced pressure. The residue was purified via flash column chromatography using basified silica gel to yield the pure aziridine product.

General Procedure C: Propene Aziridination Procedure

To an oven-dried divided electrochemical cell equipped with magnetic stir bars was added thianthrene (390 mg, 1.8 mmol, 4.5 equiv) to the anode compartment and *n*-Bu_4NPF_6 (310 mg, 0.8 mmol, 2 equiv) to both compartments. The cell was equipped with two septa containing a stainless steel wire/RVC cathode assembly and a pencil/RVC anode assembly connected together with a teflon tubing to equalize pressure. In a separate 25 mL-round bottom flask, MeCN (12mL) was sparged with a balloon of propene for 12 mins. Propene-saturated MeCN (4mL) was delivered to cathode compartment via Teflon cannula and the glass frit was allowed to become saturated (<1). Propene-saturated MeCN (4 mL) was delivered to the anode compartment via Teflon cannula. (*Electrode depth: 2 cm).* The Teflon cannulae in both compartments were left attached to the 25-mL round bottom flask in order to maintain 1 atm atmosphere of propene. 1-octene (188 µL, 1.2 mmol, 3 equiv) was then added to the anode compartment. Trifluoroacetic acid (460 µL, 6.0 mmol, 15 equiv) was added to the cathode compartment and both sides of the cell were stirred and electrolyzed under a constant current of 11.1 mA (5.4 mA/cm^2) for 7.2 h. At completion of electrolysis, the electrode leads were disconnected, septa removed, and the anode RVC was pushed off the pencil into the reaction mixture. Cs_2CO_3 (1.04 g, 3.2 mmol, 8 equiv) was added to the anode compartment followed by amine (0.4 mmol, 1 equiv). To the anode compartment was added a septum pierced with a needle to prevent pressurizing. After pressure equilibration, the needle was removed, and the cathode solution was removed from the cell via pipette. The anode solution was stirred in the cell for 16 h. At completion, the mixture was diluted with DCM (~60 mL) and water (150 mL). The aqueous layer was extracted with DCM (50 mL x 3). The combined organic layers were washed with saturated NaCl solution (40 mL), dried with anhydrous Na_2SO_4, filtered, and concentrated under reduced pressure. The residue was purified via flash column chromatography using basified silica gel to yield the pure aziridine product.

General Procedure D: Limiting Amine NMR Yield

Following General Procedure A, but with the following modification: following stirring with benzylamine and Cs_2CO_3 for 16 h, aziridine product yield was determined via NMR using mesitylene or dibromomethane as an internal standard. Presence of aziridine product was further validated via HRMS analysis.

General Procedure E: Limiting Alkene NMR Yield

Following General Procedure B, but with the following modification: following stirring with benzylamine and Cs_2CO_3 for 16 h, aziridine product yield was determined via NMR using mesitylene or dibromomethane as an internal standard. Presence of aziridine product was further validated via HRMS analysis.

General Procedure F: Propene Aziridination Procedure NMR Yield

Following General Procedure C, but with the following modification: following stirring with amine and Cs_2CO_3 for 16 h, aziridine product yield was determined via 19F NMR using trifluorotoluene as an internal standard. Presence of aziridine product was further validated via HRMS analysis.

General Procedure G: Adduct Derivatization Procedure

To an oven-dried divided electrochemical cell equipped with magnetic stir bars was added thianthrene (130 mg, 0.6 mmol, 1.5 equiv) to the anode compartment and n-Bu_4NPF_6 (620 mg, 1.6 mmol, 4 equiv) to both compartments. The cell was equipped with two septa containing a stainless steel wire/RVC cathode assembly and a pencil/RVC anode assembly connected together with a teflon tubing to equalize pressure. MeCN (8 mL) was added to the cathode compartment and the glass frit was allowed to become saturated (<1 min). MeCN (8 mL) was added to the anode compartment, followed by 4-phenyl-butene (60 µL, 0.4 mmol, 1 equiv) and trifluoroacetic acid (61 µL, 0.8 mmol, 2 equiv). (*Electrode depth: 2 cm).* Trifluoroacetic acid (153 µL, 2.0 mmol, 5 equiv) was added to the cathode compartment and both sides of the cell were stirred and electrolyzed under a constant current of 3.7 mA (1.8 mA/cm^2) for 7.2 h (2.5 F/mol). At completion of electrolysis, the electrode leads were disconnected, septa removed, and the anode RVC was pushed off the pencil into the reaction mixture. The nucleophile was added to the anode compartment and the cell was capped with a septum pierced with a needle to prevent pressurizing. After pressure equilibration, the needle was removed, and the cathode solution was removed from the cell via pipette. The anode solution was stirred in the cell for 16 h. At completion, the mixture was diluted with DCM (~60 mL) and water (150 mL). The aqueous layer was extracted with DCM (50 mL x 3). The combined organic layers were washed with saturated NaCl solution (40 mL), dried with anhydrous Na_2SO_4, filtered, and concentrated under reduced pressure. The residue was purified via flash column chromatography to yield the pure difunctionalized product.

General Procedure H: Adduct Derivatization NMR Yield

Following General Procedure G, but with the following modification: following stirring with nucleophile for 16 h, product yield was determined via NMR using mesitylene or dibromomethane as an internal standard.

A.6 Aziridine Product Isolation and Characterization

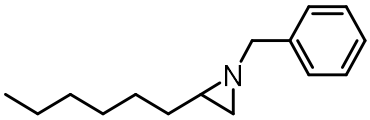

1-Benzyl-2-hexylaziridine (2.4): Following General Procedure B with 0-14% acetone/hexanes gradient, 60.7 mg (70% yield) obtained as an oil. ^{1}H NMR (400 MHz, $CDCl_3$) δ 7.30 – 7.14 (m, 5H), 3.41 (d, *J* = 13.3 Hz, 1H), 3.24 (d, *J* = 13.3 Hz, 1H), 1.53 (d, *J* = 3.3 Hz, 1H), 1.42 – 1.06 (m, 12H), 0.78 (t, *J* = 7.0 Hz, 3H). ^{13}C NMR consistent with reported spectra[10].

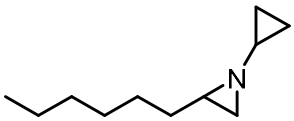

1-cyclopropyl-2-hexylaziridine (2.5): Following General Procedure D with the following modification: after stirring for 16 h, the mixture was diluted with DCM (~60 mL) and water (150 mL). The aqueous layer was extracted with DCM (50 mL x 3). The combined organic layers were washed with saturated NaCl solution (40 mL), dried with anhydrous Na_2SO_4, filtered, and concentrated under reduced pressure. Electrolyte was removed via flash column chromatography on basified silica (0-15% diethyl ether/hexanes gradient). Obtained 50% yield. **HRMS** (ESI+) Calc: [M+H]+ (C11H22N) 168.1747; measured: 168.1745; 1.2 ppm difference.

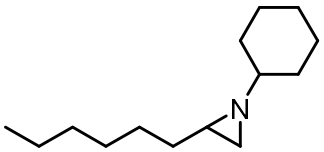

1-cyclohexyl-2-hexylaziridine (2.6): Following General Procedure A except with non-basified silica, 0-20% acetone/hexanes gradient, 60% yield obtained as a mixture with thianthrene S-oxide (127.7 mg, 1:1.4 pdt:S-oxide). **^{1}H NMR** (500 MHz, CDCl3) δ 1.81 – 1.63 (m, 4H), 1.58 – 1.51 (m, 1H), 1.44 – 1.02 (m, 18H), 0.93 (tt, J = 10.8, 3.8 Hz, 1H), 0.81 (t, J = 6.7 Hz, 3H). **^{13}C NMR** (126 MHz, CDCl3) δ 69.07, 38.42, 33.46, 33.08, 32.48, 32.44, 31.89, 29.24, 27.83, 26.14, 25.07, 25.05, 22.63, 14.09. **HRMS** (ESI+) Calc: [M+H]+ (C14H28N) 210.22163; measured: 210.2216; 0.1 ppm difference.

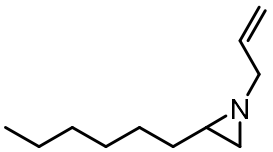

1-allyl-2-hexylaziridine (2.7): Following General Procedure B except with allylamine (120 µL, 1.6 mmol, 4 equiv) and non-basified silica with 0-15% acetone/hexanes gradient, 59% yield obtained as a mixture with thianthrene S-oxide (76.8 mg, 1:1 pdt:S-oxide). **^{1}H NMR** (500 MHz, CDCl3) δ 5.86 (ddt, J = 16.4, 10.3, 5.8 Hz, 1H), 5.12 (dd, J = 17.2, 1.8 Hz, 1H), 5.03 (dd, J = 10.3, 1.7 Hz, 1H), 2.77 (qd, J = 13.9, 6.0 Hz, 2H), 1.46 (d, J = 3.4 Hz, 1H), 1.40 – 1.18 (m, 12H), 1.17 (d, J = 6.3 Hz, 1H), 0.81 (t, J = 6.8 Hz, 3H). ^{13}C NMR consistent with reported spectra[11].

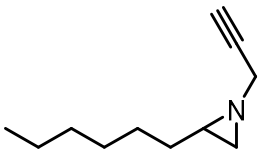

2-hexyl-1-(prop-2-yn-1-yl)aziridine (2.8): Following General Procedure D with the following modification: after stirring for 16 h, the mixture was diluted with DCM (~60 mL) and water (150 mL). The aqueous layer was extracted with DCM (50 mL x 3). The combined organic layers were washed with saturated NaCl solution (40 mL), dried with anhydrous Na_2SO_4, filtered, and concentrated under reduced pressure. Electrolyte was removed via flash column chromatography on basified silica (0-10% acetone/hexanes gradient). obtained 52% yield. **HRMS** (ESI+) Calc: [M+H]+ (C11H20N) 166.1590; measured: 166.1590; <0.1 ppm difference.

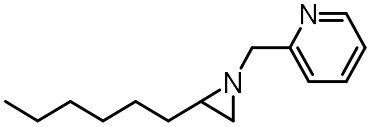

2-((2-hexylaziridin-1-yl)methyl)pyridine (2.9): Following General Procedure A with 0-50% acetone/diethyl ether gradient, 65.4mg (75% yield) obtained as an oil. **^{1}H NMR** (500MHz, $CDCl_3$) δ 8.45 (d, J = 2.3Hz, 2H), 8.42 (d, J = 4.8Hz, 1H), 7.63 (d, J = 7.7, 2.5Hz, 1H), 7.17 (m, 1H), 3.40 (d, J = 13.6Hz, 1H), 3.22 (d, J = 13.5Hz, 1H), 1.54 (d, J = 3.5Hz, 1H), 1.41-1.35 (m, 1H), 1.34-1.25 (m, 3H), 1.23-1.07 (m, 8H), 0.76 (t, J = 7.0Hz, 3H); **^{13}C NMR** (126 MHz, $CDCl_3$) δ 149.46, 148.49, 135.75, 134.83, 123.28, 62.22, 40.02, 34.18, 32.84, 31.71, 28.96, 27.32, 22.49, 14.00; **HRMS** (ESI+) Calc: [M+H]+ (C14H23N2) 219.1856; measured: 219.1854; 0.9 ppm difference.

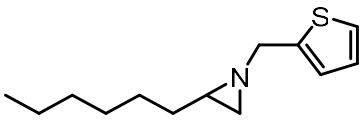

2-((2-hexylaziridin-1-yl)methyl)thiophene (2.10): Following General Procedure A with 0-15% EtOAc/hexanes gradient, 70% yield obtained as a mixture with thianthrene S-oxide (76.1 mg, 1:0.2 pdt:S-oxide). **1H NMR** (400 MHz, CDCl3) δ 7.21 (dd, J = 5.1, 1.3 Hz, 1H), 6.97-6.90 (m, 2H), 3.67 (d, J = 13.7 Hz, 1H), 3.47 (d, J = 13.7 Hz, 1H), 1.62 (d, J = 3.3 Hz, 1H), 1.51-1.18 (m, 12H), 0.86 (t, J = 6.8 Hz, 3H); **^{13}C NMR** (101 MHz, $CDCl_3$) δ 142.18, 126.44, 124.94, 124.37, 59.32, 40.05, 34.05, 32.89, 31.78, 29.00, 27.30, 2.54, 14.05; **HRMS** (ESI+) Calc: [M+H]+ (C13H22NS) 224.14675; measured: 224.1467; 0.2 ppm difference.

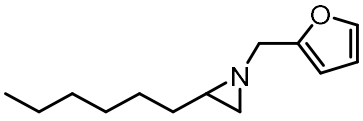

1-(furan-2-ylmethyl)-2-hexylaziridine (2.11): Following General Procedure A with 0-10% acetone/DCM gradient, 44.2mg (53% yield) obtained as an oil. **^{1}H NMR** (400 MHz, $CDCl_3$) δ 7.29 (d, J = 1.8 Hz, 1H), 6.24 (dd, J = 3.1, 1.9 Hz, 1H), 6.13 (d, J = 3.1 Hz, 1H), 3.35 (d, J = 13.9Hz, 1H), 3.28 (d, J = 13.9 Hz, 1H), 1.51 (d, J = 3.6 Hz, 1H), 1.44-1.38 (m, 11H), 0.80 (5, J = 6.9 Hz, 3H); **^{13}C NMR** (101 MHz, C_6D_6) δ 154.70, 142.42, 111.02, 107.75, 57.82, 40.16, 34.12, 33.94, 32.83, 30.07, 28.25, 23.59, 14.92 ; **HRMS** (ESI+) Calc: [M+H]+ (C13H22NO) 208.16959; measured: 208.1693; 1.4 ppm difference.

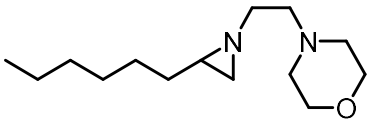

4-(2-(2-hexylaziridin-1-yl)ethyl)morpholine (2.12): Following General Procedure A with 10-40% acetone/hexanes gradient, 47 mg (49%) obtained as an oil. **1H NMR** (600 MHz, C_6D_6) δ 3.61 (t, *J* = 4.7 Hz, 4H), 2.48 (t, *J* = 6.9 Hz, 2H), 2.34 – 2.23 (m, 5H), 2.19 (dt, *J* = 11.5, 6.9 Hz, 1H), 1.51 – 1.23 (m, 11H), 1.07 (qd, *J* = 6.0, 3.3 Hz, 1H), 0.95 (d, *J* = 6.2 Hz , 1H), 0.90 (t, *J* = 7.0 Hz, 3H). **^{13}C NMR** (101 MHz, C_6D_6) δ 66.82, 59.07, 58.74, 54.28, 39.47, 33.21, 33.19, 31.92, 29.28, 27.51, 22.69, 13.98. **HRMS** (ESI+) Calc: [M+H]+ (C14H29N2O) 241.22744; measured: 241.2269; 2.2 ppm difference.

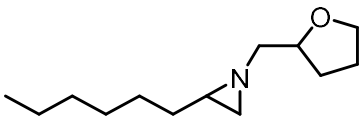

2-hexyl-1-((tetrahydrofuran-2-yl)methyl)aziridine (2.13): Following General Procedure A with 15-35% EtOAc/hexanes gradient, 55.4mg (66% yield) obtained as 1:1 mixture of diastereomers. **^{1}H NMR** (400 MHz, $CDCl_3$) δ 4.04-3.93 (m, 1H), 3.89-3.81 (m, 1H), 3.78-3.70 (m, 1H), 2.40-2.26 (m, 2H), 2.08-1.96 (m, 1H), 1.93-2.82 (m, 2H), 1.66-1.55 (m, 1H), 1.53 (dd, J = 6.0 2.4 Hz, 1H), 1.48-1.19 (m, 13H), 0.87 (t, J = 6.7 Hz, 3H); **^{13}C NMR** (101 MHz, C_6D_6) δ 79.04, 68.01, 67.69, 65.96, 65.86, 39.63, 39.59, 33.62, 33.57, 33.54, 32.32, 32.30, 30.19, 30.08, 29.66, 27.79, 27.78, 25.93, 23.07 14.37; **HRMS** (ESI+) Calc: [M+H]+ (C13H26NO) 212.20089; measured: 212.2007; 0.9 ppm difference.

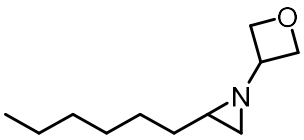

2-hexyl-1-(oxetan-3-yl)aziridine (2.14): Following General Procedure A with 35-75% EtOAc/hexanes gradient, 40.2mg (55% yield) obtained as an oil. **^{1}H NMR** (600 MHz, $CDCl_3$) δ 4.70 (dt, J = 13.4, 6.6 Hz, 2H), 4.61 (td, J = 5.9, 4.2 Hz, 2H), 3.02 (ddd, J = 12.2, 6.7, 5.5 Hz, 1H), 1.57 (d, J = 3.3 Hz, 1H), 1.49-1.41 (m, 2H), 1.38-1.24 (m, 10H), 0.88 (t, J = 7.0 Hz)z ; **^{13}C NMR** (151 MHz, $CDCl_3$) δ 67.93, 67.89, 67.84, 39.56, 36.22, 34.17, 33.09, 31.84, 31.64, 31.49, 29.13, 27.45, 22.59, 14.07 ; **HRMS** (ESI+) Calc: [M+H]+ (C11H22NO) 184.1696; measured: 184.1694; 1.1 ppm difference.

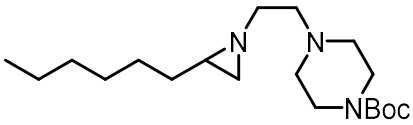

tert-butyl 4-(2-(2-hexylaziridin-1-yl)ethyl)piperazine-1-carboxylate (2.15): Following General Procedure A with 5-40% acetone/hexanes gradient, 87.6mg (63% yield) obtained as an oil. **^{1}H NMR** (400 MHz, $CDCl_3$) δ 3.36 (t, J = 5.1Hz, 4H), 2.50 (t, J = 7.0Hz, 2H), 2.44-2.31 (m, 5H), 2.22 (dt, J = 11.7, 7.1Hz, 1H), 1.45 (d, J = 3.0Hz, 1H), 1.42-1.13 (m, 22H), 0.81 (t, J = 6.6Hz, 3H) ; **^{13}C NMR** (101 MHz, $CDCl_3$) δ 154.56, 79.40, 58.38, 58.07, 53.31, 52.48, 39.69, 33.68, 32.93, 31.69, 28.99, 28.26, 27.39, 22.45, 13.94; **HRMS** (ESI+) Calc: [M+H]+ (C19H38N3O2) 340.29585; measured: 340.2958; 0.1 ppm difference.

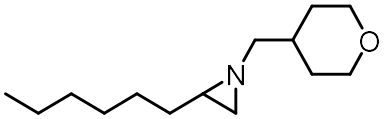

1-(tetrahydropyran-4-ylmethyl)-2-hexylaziridine (2.16): Following General Procedure A with 30-50% EtOAc/hexanes gradient followed by an additional flash column chromatography purification using 0-15% acetone/hexanes gradient, 86.4mg (75% yield) obtained as an oil. **^{1}H NMR** (400 MHz, $CDCl_3$) δ 4.00-3.92 (m, H), 3.44-3.35 (m, 2H), 2.19 (ddd, J = 11.8, 5.7, 1.7 Hz, 1H), 2.04 (ddd, J = 11.6, 5.7, 1.7 Hz, 1H), 1.86-1.73 (m, 2H), 1.66-1.59 (m, 1H), 1.51 (dd, J = 3.3, 1.9 Hz, 1H), 1.46-1.17 (m, 14H), 0.88 (t, J = 5.9Hz, 3H) ; **^{13}C NMR** (126 MHz, $CDCl_3$) δ 67.93, 67.89, 67.84, 39.56, 36.22, 34.17, 33.09, 31.84, 31.64, 31.49, 29.13, 27.45, 22.59, 14.07 ; **HRMS** (ESI+) Calc: [M+H]+ (C14H28NO) 226.21654; measured: 226.2162; 1.5 ppm difference.

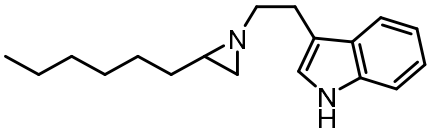

3-(2(2-hexylaziridin-1-yl)ethyl)-1H-indole (2.17): Following General Procedure A with 20-40% EtOAc/hexanes gradient, 60.8mg (56% yield) obtained as an oil. **^{1}H NMR** (600 MHz, $CDCl_3$) δ 8.38 (br s, 1H), 7.60 (d, J = 7.8Hz, 1H), 7.33 (d, J = 8.0Hz, 1H), 7.19 (t, J = 7.5 Hz, 1H), 7.19 (t, J = 7.5 Hz, 1H), 6.97 (d, J = 2.3 Hz, 1H), 3.13-2.99 (m, 2H), 2.67 (ddd, J = 11.4, 8.8, 6.8 Hz, 1H), 2.52 (ddd, J = 11.4, 9.2, 6.5 Hz, 1H), 1.57 (d, J = 3.2 Hz, 1H), 1.53-1.22 (m, 14H), 0.90 (t, J = 6.6 Hz, 3H); **^{13}C NMR** (151 MHz, $CDCl_3$) δ 136.41, 127.58, 122.00, 121.72, 119.27, 118.92, 114.30, 111.23, 62.14, 39.92, 33.98, 33.31, 32.00, 29.31, 27.70, 25.93, 22.76, 14.24; **HRMS** (ESI+) Calc: [M+H]+ (C18H27N2) 271.2166; measured: 271.2166; 1.1ppm difference.

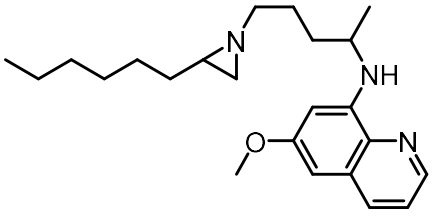

N-(5-(2-hexylaziridin-1-yl)pentan-2-yl)-6-methoxyquinolin-8-amine (2.18): Following General Procedure A using Primaquine phosphate (0.4 mmol, 1.0 equiv.) with 0-20% acetone/hexanes gradient followed by an additional flash column chromatography purification on non-basified silica using 0-10% MeOH/DCM gradient, 90.2 mg (61% yield) obtained as an 1:1 mixture of diastereomers. **^{1}H NMR** (600MHz, $CDCl_3$) δ 8.52 (dt, J = 4.1, 1.5 Hz, 1H), 7.91 (dd, J = 8.2, 1.7 Hz, 1H), 7.29 (dd, J = 8.2, 4.2 Hz, 1H), 6.32 (d, J = 2.5 Hz, 1H), 6.28 (d, J = 2.5Hz), 6.09-5.95 (m, 1H), 3.89 (s, 3H), 3.67-3.57 (m, 1H), 2.34-2.26 (m, 1H), 2.22-2.13 (m, 1H), 1.82-1.61 (m, 4H), 1.50 (d, J = 3.5 Hz), 1.46-1.20 (m, 14H), 1.17 (dd, J = 6.4, 4.0 Hz), 0.87 (5, J = 6.9 Hz, 3H); **^{13}C NMR** (126 MHz, $CDCl_3$) δ 159.61, 145.27, 144.38, 135.57, 134.85, 130.03, 121.93, 96.75, 91.64, 61.59, 61.52, 55.34, 48.30, 48.16, 39.81, 39.76, 34.78, 34.69, 33.25, 31.97, 29.29, 27.69, 27.68, 26.77, 26.64, 22.76, 20.64, 14.22; **HRMS** (ESI+) Calc: [M+H]+ (C23H36N3O) 370.2853; measured: 370.2850; 0.8ppm difference.

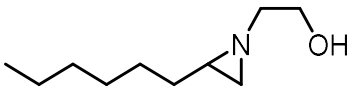

2-(2-hexylaziridin-1-yl)ethan-1-ol (19): Following General Procedure A except with the following purification modification: following flash column chromatography on basified silica (0-40% acetone/DCM), the product containing fractions were concentrated under reduced pressure, and the residue was dissolved into 5 mL pentane and filtered to yield 48.5 mg (71% yield) of **18** as an oil. **^{1}H NMR** (400 MHz, $CDCl_3$) δ 3.73 (t, J = 5.3Hz, 2H), 2.59-2.34 (m, 3H), 1.57 (d, J = 2.3Hz, 1H), 1.50-1.25 (m, 12H), 0.90 (t, J = 6.6Hz, 3H); **^{13}C NMR** (101 MHz, $CDCl_3$) δ 62.87, 62.16, 39.68, 33.80, 33.22, 31.99, 29.32, 27.62, 22.78, 14.25; **HRMS** (ESI+) Calc: [M+H]+ (C10H22NO) 172.1696; measured: 172.1696; <0.1 ppm difference. Connectivity confirmed by edited HSQC and HMBC.

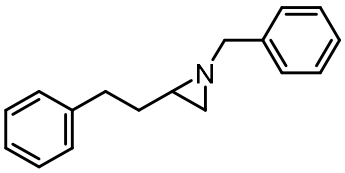

1-benzyl-2-phenethylaziridine (2.3): Following General Procedure B with 0-20% acetone/hexanes gradient, 73% yield obtained as a mixture with thianthrene-S-oxide (83 mg, 1:0.2 pdt:S-oxide). **^{1}H NMR** (600 MHz, $CDCl_3$) δ 7.30 – 7.22 (m, 4H), 7.20 – 7.13 (m, 3H), 7.11 – 7.05 (m, 1H), 7.04 – 7.00 (m, 2H), 3.41 (d, J = 13.2 Hz, 1H), 3.21 (d, J = 13.2 Hz, 1H), 2.57 (ddd, J = 14.9, 9.1, 6.1 Hz, 1H), 2.50 (ddd, J = 13.8, 9.0, 6.9 Hz, 1H), 1.64 (m, 2H), 1.55 (d, J = 3.5 Hz, 1H), 1.43 – 1.38 (m, 1H), 1.31 (d, J = 6.4 Hz, 1H). **^{13}C NMR** (151 MHz, CDCl3) δ 141.93, 139.41, 128.48, 128.40, 128.32, 128.27, 127.11, 125.78, 64.97, 39.23, 34.78, 34.13, 33.74.. **HRMS** (ESI+) Calc: [M+H]+ (C17H20N) 238.1590; measured: 238.1588; 0.8 ppm difference.

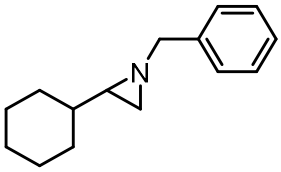

1-Benzyl-2-cyclohexylaziridine (2.20): Following General Procedure B with 0-10% acetone/hexanes, 63.4 mg (74% yield) obtained as an oil. **^{1}H NMR** (500 MHz, $CDCl_3$) δ 7.36-7.30 (m, 4H), 7.27-7.23 (m, 1H), 3.50 (d, J = 13.0Hz, 1H), 3.25 (d, J = 13.0Hz, 1H), 1.71-1.56 (m, 6H), 1.36 (d, J = 6.5Hz, 1H), 1.25 (ddd, J = 7.6, 6.4, 3.6Hz), 1.03-0.87 (m, 3H); **^{13}C NMR** (126 MHz, $CDCl_3$) δ 139.44, 128.45, 128.25, 127.00, 65.42, 45.24, 41.10, 33.09, 31.24, 30.29, 26.44, 25.96, 25.78; **HRMS** (ESI+) Calc: [M+H]+ (C15H22N) 216.1747; measured: 216.1747; < 0.1 ppm difference.

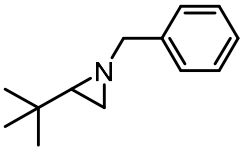

1-Benzyl-2-*t*-butylaziridine (2.21): Following General Procedure B with 0-20% acetone/hexanes, 24.5 mg (32% yield) obtained as an oil. **^{1}H NMR** (500 MHz, $CDCl_3$) δ 7.38-7.29 (m, 4H), 7.27-7.22 (m, 1H),

3.66 (d, J = 13.0Hz, 1H), 3.13 (d, J = 13.0Hz), 1.74 (d, J = 3.7Hz, 1H), 1.28 (dd, J = 6.6, 3.7Hz, 1H), 1.23 (d, J = 6.6Hz, 1H), 0.76 (s, 9H); ^{13}C NMR consistent with reported spectra[12].

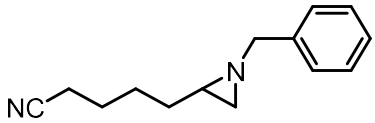

5-(1-benzylaziridin-2-yl)pentanenitrile (2.22): Following General Procedure E, obtained 77% yield. **HRMS** (ESI+) Calc: [M+H]+ (C14H19N2) 215.1543; measured: 215.1542; 0.5 ppm difference.

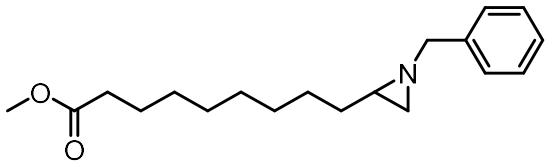

Methyl 9-(1-benzylaziridin-2-yl)nonanoate (2.23): Following General Procedure B with 0-15% acetone/hexanes gradient, 81% yield obtained as a mixture with thianthrene-S-oxide (110.7 mg, 1:0.1 pdt:S-oxide). **^{1}H NMR** (500 MHz, CDCl3) δ 7.28 – 7.14 (m, 5H), 3.58 (s, 3H), 3.42 (d, *J* = 13.3 Hz, 1H), 3.22 (d, *J* = 13.3 Hz, 1H), 2.21 (t, *J* = 7.6 Hz, 2H), 1.57 – 1.48 (m, 3H), 1.40 – 1.10 (m, 14H).**; ^{13}C NMR** (126 MHz, $CDCl_3$) δ 174.27, 139.46, 128.27, 128.18, 126.95, 65.03, 51.40, 39.76, 34.09, 34.07, 32.99, 29.36, 29.26, 29.12, 29.10, 27.39, 24.93; **HRMS** (ESI+) Calc: [M+H]+ (C19H30NO2) 304.22711; measured: 304.2266; 1.7 ppm difference.

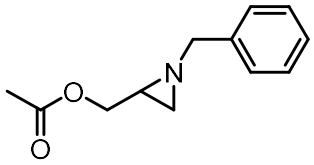

1-Benzyl-2-acetoxymethylaziridine (2.24): Following General Procedure B except with 12.0 mA (5.8 mA/cm^2), with 20-40% EtOAc/hexanes gradient, 57.3 mg (70% yield) obtained as an oil. **^{1}H NMR** (500 MHz, $CDCl_3$) δ 7.37-7.31 (m, 4H), 7.29-7.24 (m, 1H), 4.19 (dd, J = 11.7, 4.5Hz, 1H), 3.82 (dd, J = 11.7, 7.5 Hz, 1H), 3.60 (d, J = 13.4Hz, 1H), 3.32 (d, J = 13.4Hz, 1H), 1.97 (s, 3H), 1.87 (dddd, J = 7.7, 6.6, 4.5, 3.4 Hz, 1H), 1.53 (d, J = 6.5Hz, 1H); ^{13}C NMR consistent with reported spectra[13].

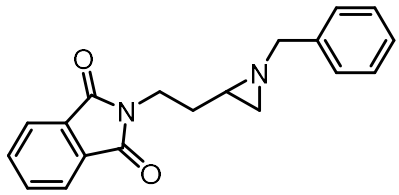

1-Benzyl-2-ethylpthalimidoaziridine (2.25): Following General Procedure B except with 12.0 mA (5.8 mA/cm^2), with 30-50% EtOAc/hexanes gradient, 75.4 mg (62% yield) obtained as an oil. **^{1}H NMR** (400 MHz, $CDCl_3$) δ 7.86-7.82 (m, 2H), 7.73-7.68 (m, 2H), 7.31-7.26 (m, 4H), 7.24-7.20 (m, 1H), 3.75 (t, J = 6.9Hz, 2H), 3.55 (d, J = 13.3Hz, 1H), 3.24 (d, J = 13.3Hz, 1H), 1.86-1.74 (m, 2H), 1.60 (d, J = 3.4Hz, 1H), 1.58-1.52 (m, 1H), 1.38 (d, J = 6.3Hz); **^{13}C NMR** (126 MHz, $CDCl_3$) δ 168.49, 139.33, 134.04, 132.30, 128.46, 128.22, 127.13, 123.34, 64.81, 37.23, 36.37, 33.64, 31.08; **HRMS** (ESI+) Calc: [M+H]+ (C19H19N2O2) 307.1441; measured: 307.1438; 1.0 ppm difference.

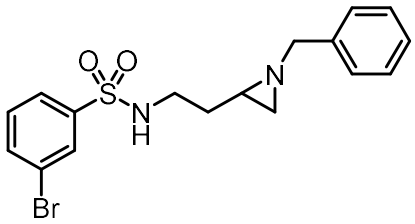

N-(2-(1-benzylaziridin-2-yl)ethyl)-3-bromobenzenesulfonamide (2.26): Following General Procedure B except with 12.0 mA (5.8 mA/cm^2), with 0-40% acetone/hexanes gradient, 99.2 mg (63% yield) obtained as a powder. **^{1}H NMR** (400 MHz, $CDCl_3$) δ 7.91 (t, J = 1.8 Hz, 1H), 7.69-7.63 (m, 2H), 7.40-7.29 (m, 6H), 5.71 (t, J = 4.9Hz, 1H), 3.50 (d, J = 12.9 Hz, 1H), 3.23 (d, J = 12.9 Hz, 1H), 2.98 (ddd, J = 12.6, 10.9, 5.9Hz, 1H), 2.79 (ddt, J = 13.0, 8.8, 4.2 Hz, 1H), 1.92 (ddt, J = 13.4, 8.6, 4.1 Hz, 1H), 1.67-1.59 (m, 2H), 1.44-1.32 (m, 2H); **^{13}C NMR** (126 MHz, $CDCl_3$) δ 142.28, 138.79 135.51, 130.62, 130.07, 128.87, 128.47, 127.72, 125.65, 123.08, 64.85, 41.16, 37.20, 32.51, 29.68; **HRMS** (ESI+) Calc: [M+H]+ (C17H20BrN2O2S) 395.04234; measured: 395.0420; 0.9 ppm difference.

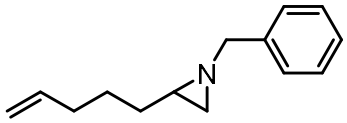

1-Benzyl-2-pent-4-eneaziridine (2.27): Following General Procedure B with 0-20% acetone/hexanes gradient, 55.3mg (67% yield) obtained as an oil. **^{1}H NMR** (500 MHz, $CDCl_3$) δ 7.36-7.30 (m, 4H), 7.28-7.24 (m, 1H), 5.75 (ddt, J = 16.9, 10.2, 6.6Hz, 1H), 4.98-4.89 (m, 2H), 3.50 (d, J = 13.3Hz, 1H), 3.32 (d, J = 13.2Hz, 1H), 2.04-1.97 (m, 2H), 1.62 (d, J = 3.3Hz), 1.48-1.35 (m, 6H); **^{13}C NMR** (126 MHz, $CDCl_3$) δ 139.44, 138.75, 128.32, 128.19, 126.99, 114.41, 65.00, 39.58, 34.09, 33.44, 32.49, 26.70; **HRMS** (ESI+) Calc: [M+H]+ (C14H20N) 202.1590.; measured: 202.1589; 0.5 ppm difference.

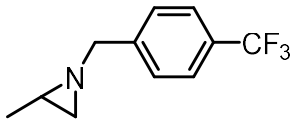

1-Trifluoromethylbenzyl-2-methylaziridine (2.28): Following General Procedure F, 71% yield obtained. **HRMS** (ESI+) Calc: [M+H]+ (C11H13F3N) 216.09946; measured: 216.0994; 0.3 ppm difference.

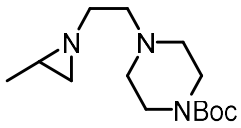

tert-butyl 4-(2-(2-methylaziridin-1-yl)ethyl)piperazine-1-carboxylate (2.29): Following General Procedure C with 10-50% acetone/hexanes gradient, 76.2 mg (71% yield) obtained as an oil. **^{1}H NMR** (500 MHz, $CDCl_3$) δ 3.45-3.37 (m, 4H), 2.60-2.51 (m, 2H), 2.45-2.32 (m, 6H), 1.47 (d, J = 3.6 Hz, 1H), 1.44 (s, 9H), 1.38-1.32 (m, 1H), 1.21 (d, J = 6.3 Hz, 1H), 1.16 (d, J = 5.5 Hz, 3H); **^{13}C NMR** (126 MHz, $CDCl_3$) δ 154.91, 79.73, 58.75, 58.43, 53.66, 34.86, 34.82, 29.45, 28.59, 18.51; **HRMS** (ESI+) Calc: [M+H]+ (C14H28N3O2) 270.21760; measured: 270.2175; 0.4 ppm difference.

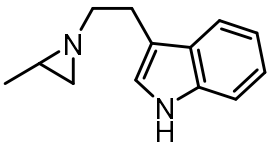

3-(2-(2-methylaziridin-1-yl)ethyl)-1H-indole (2.30): Following General Procedure C with 0-30% acetone/hexanes gradient followed by an additional flash column chromatography purification using 0-30% acetone/DCM gradient, 52.3 mg (65% yield) obtained as an oil. **^{1}H NMR** (500 MHz, $CDCl_3$) δ 8.06 (br s, 1H), 7.60 (dd, J = 7.9, 1.1 Hz, 1H), 7.35 (d, J = 8.1 Hz, 1H), 7.18 (ddd, J = 8.2, 6.9Hz, 1.2 Hz, 1H), 7.11 (ddd, J = 8.0, 7.0, 1.0 Hz, 1H), 7.01 (d, J = 2.3 Hz, 1H), 3.04 (t, J = 7.7 Hz, 2H), 2.62-2.52 (m, 2H), 1.50 (d, J = 3.5 Hz, 1H), 1.36-1.29 (m, 1H), 1.23 (d, J = 6.3 Hz, 1H), 1.15 (d, J = 5.4 Hz, 3H); **^{13}C NMR** (126 MHz, $CDCl_3$) δ 136.44, 127.61, 122.05, 121.79, 119.32, 118.99, 114. 46, 111.24, 62.02, 34.78, 34.73, 26.02, 18.62; **HRMS** (ESI+) Calc: [M+H]+ (C13H17N2) 201.13863; measured: 201.1386; 0.1 ppm difference.

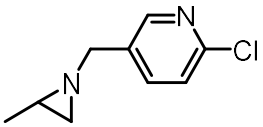

2-chloro-5-((2-methylaziridin-1-yl)methyl)pyridine (2.31): Following General Procedure C with 20-50% 1:3 acetone:DCM/hexanes gradient, 60.1 mg (82% yield) obtained as an oil. **^{1}H NMR** (500 MHz, $CDCl_3$) δ 8.31 (d, J = 2.5 Hz, 1H), 7.69 (dd, J = 8.2, 2.5 Hz, 1H), 7.29 (d, J = 8.1 Hz, 1H), 3.37 (d, J = 14.0 Hz, 1H), 3.41 (d, J = 14.0 Hz, 1H), 1.59 (d, J = 3.6 Hz, 1H), 1.55-1.49 (m, 1H), 1.37 (d, J = 6.4 Hz, 1H), 1.19 (d, J = 5.5 Hz, 3H); **^{13}C NMR** (126 MHz, $CDCl_3$) δ 150.21, 149.05, 138.53, 134.13, 124.15, 61.26, 35.37, 35.11, 18.31; **HRMS** (ESI+) Calc: [M+H]+ (C9H11ClN2) 183.06835; measured: 183.0684; 0.3 ppm difference.

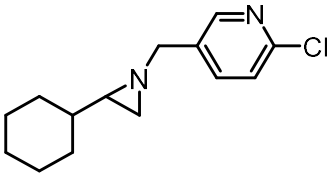

2-chloro-5-((2-cyclohexylaziridin-1-yl)methyl)pyridine (2.32): Following General Procedure B except with (6-chloropyridin-3-yl)methanamine (228 mg, 1.6 mmol, 4 equiv) and isolated using 0-50% EtOAc/hexanes, followed by an additional flash column chromatography purification using 0-45% acetone/hexanes gradient, 61.9 mg (62% yield) obtained as an oil. **^{1}H NMR** (500 MHz, C_6D_6) δ 8.19 (d, J = 2.4 Hz, 1H), 7.20 (dd, J = 8.2, 2.5 Hz, 1H), 6.85 (d, J = 8.1 Hz, 1H), 2.84 (d, J = 13.5 Hz, 1H), 2.69 (d, J = 13.5 Hz, 1H), 1.65 – 1.51 (m, 5H), 1.38 (d, J = 3.1 Hz, 1H), 1.08 (m, 3H), 0.90 – 0.78 (m, 5H).; **^{13}C NMR** (126 MHz, C_6D_6) δ 150.91, 149.85, 138.85, 134.65, 124.13, 61.78, 45.60, 41.07, 32.71, 31.47, 30.64, 26.97, 26.50, 26.36.; **HRMS** (ESI+) Calc: [M+H]+ (C14H20ClN2) 251.13095; measured: 251.1309; 0.2 ppm difference.

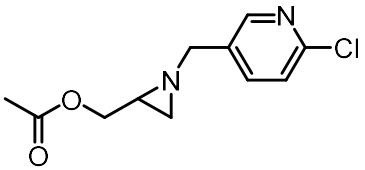

(1-((6-chloropyridin-3-yl)methyl)aziridin-2-yl)methyl acetate (2.33): Following General Procedure A except with 35 mA (17 mA/cm^2), Bu_4NPF_6 (620 mg, 1,6 mmol, 4 equiv), allyl acetate (129 µL, 1.2 mmol, 3 equiv), and the following purification modification: following flash column chromatography on basified silica (35-75% EtOAc/hexanes), the product containing fractions were concentrated under reduced pressure, and the residue was dissolved into 5 mL 1:1 EtOAc/hexanes and filtered to yield 64 mg (66%) as an oil. **^{1}H NMR** (500 MHz, C_6D_6) δ 8.15 (d, *J* = 2.4 Hz, 1H), 7.13 (dd, *J* = 8.2, 2.5 Hz, 1H), 6.84 (d, *J* = 8.2 Hz, 1H), 4.01 (dd, *J* = 11.6, 4.3 Hz, 1H), 3.60 (dd, *J* = 11.6, 7.4 Hz, 1H), 2.81 (d, *J* = 13.9 Hz, 1H), 2.55 (d, *J* = 13.9 Hz, 1H), 1.64 (s, 3H), 1.34 – 1.27 (m, 2H), 0.77 (d, *J* = 6.4 Hz, 1H).; **^{13}C NMR** (126 MHz, C_6D_6) δ 170.17, 150.89, 149.62, 138.49, 134.03, 124.07, 66.66, 60.47, 37.57, 31.64, 20.53. **HRMS** (ESI+) Calc: [M+H]+ (C11H14ClN2O2) 241.0738; measured: 241.0737; 0.4 ppm difference.

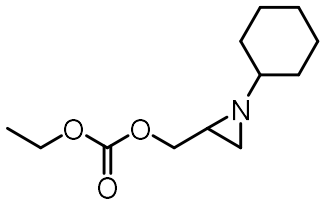

(1-cyclohexylaziridin-2-yl)methyl ethyl carbonate (2.38): Following General Procedure B except with 12 mA (5.8 mA/cm^2) and cyclohexylamine (183 µL, 1.6 mmol, 4 equiv), with 0-30% acetone/hexanes gradient followed by an additional flash column chromatography purification on non-basified silica using 40-70% 1:11 acetone:DCM/hexanes gradient, 60.6mg (67% yield) obtained as an oil. **^{1}H NMR** (500 MHz, $CDCl_3$) δ 4.20 (q, J = 7.1 Hz, 2H), 4.11 (dd, J = 11.4, 5.0 Hz, 1H), 3.95 (dd, J = 11.4, 7.2 Hz, 1H), 1.87-1.64 (m, 6H), 1.63-1.54 (m, 1H), 1.41-1.05 (m, 11H); **^{13}C NMR** (126 MHz, $CDCl_3$) δ 155.29, 70.33, 68.74, 64.15, 35.59, 32.88, 32.58, 30.57, 26.17 24.99, 24.92, 14.44; **HRMS** (ESI+) Calc: [M+H]+ (C12H22NO3) 228.1594*;* measured: 228.1591; 1.3 ppm difference.

A.7 Scale-Up Flow Electrolysis Set-Up and Procedure

Electrochemical flow reactor and setup:

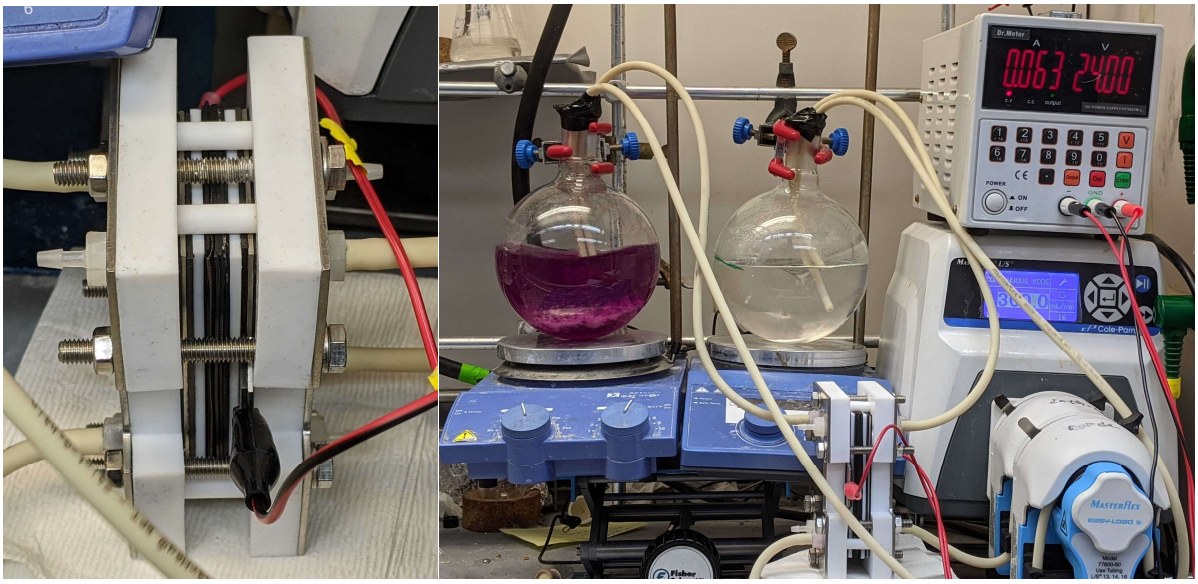

Left: Divided flow cell assembly (Electrocell Micro Flow Cell). Electrode plates area: 10 cm^2. In addition to the plates, a 32 x 32 x 8 mm graphite felt electrode (AvCarb Style G600A) was placed in each electrode compartment. The anode and cathode chambers were separated using a Nafion frit and the entire system sealed using rubber gaskets.

Right: Full flow assembly (pictured during first 30 mins of electrolysis). Cole Parmer Masterflex L/S digital peristaltic pump (2x Masterflex Easy-Load 3 pump heads, item no. 77800-60, PharMed® BPT, L/S 16 tubing item no. 06508-16), flow rate: 250 mL/min. Driven using DC power supply (see above). For each electrode compartment, the solution is pumped from the bulk, through the pump head and into the bottom inlet of the flow cell, through the flow cell making contact with the electrode, then flows out of the top outlet and back into the bulk solution.

Scale-Up Flow Electrolysis Procedure

To an oven-dried 1 L round-bottom flask was added thianthrene (6.5 g, 30 mmol, 1.5 equiv), $LiBF_4$ (7.5 g, 80 mmol, 4 equiv), and MeCN (400 mL), followed by 4-phenylbutene (3.0 mL, 20 mmol, 1 equiv) and trifluoroacetic acid (3.0 mL, 40 mmol, 2 equiv). Both ends of the anode pump tubing were submerged in the solution (see picture). To a separate oven-dried 1 L round-bottom flask was added *n*-Bu_4NPF_6 (15.5 g, 40 mmol, 2 equiv) and MeCN (400 mL) followed by trifluoroacetic acid (7.65 mL, 100 mmol, 5 equiv). Both ends of the cathode pump tubing were submerged into the solution. An argon balloon was added to the anode flask. Both flasks were stirred, a flow rate of 250 mL/min was applied using the peristaltic pump, and the reaction was electrolyzed at 60 mA (4.2 mA/cm^2) for 24 h (2.7 F/mol). Following electrolysis, the balloon was removed, and the pump tubing was held above the solution while pumping to expel solution from the flow cell. Once the cell was emptied, Cs_2CO_3 (39.1 g, 120 mmol, 6 equiv) was added to the anode solution, followed by benzylamine (8.75 mL, 80 mmol, 4 equiv). The solution was vigorously stirred for an additional 22 h. After this time, the mixture was diluted with DCM (500 mL) and divided into two portions. Water (500 mL) was added to each individual portion, and the organic layer

was separated and washed with additional water (500 mL). Each aqueous portion was individually extracted with DCM (100 mL x 3). The combined organic layers were dried with anhydrous Na_2SO_4, filtered, and concentrated under reduced pressure. The residue was divided into two portions, and each portion was filtered onto a silica column to remove thianthrene and purified individually using flash column chromatography (0-60% EtOAc/hexanes). Mixed fractions from both portions were combined and repurified (0-45% EtOAc/hexanes). All pure fractions were combined to obtain 3.2 g (67% yield, 13.4 mmol) of **2.3** as an oil.

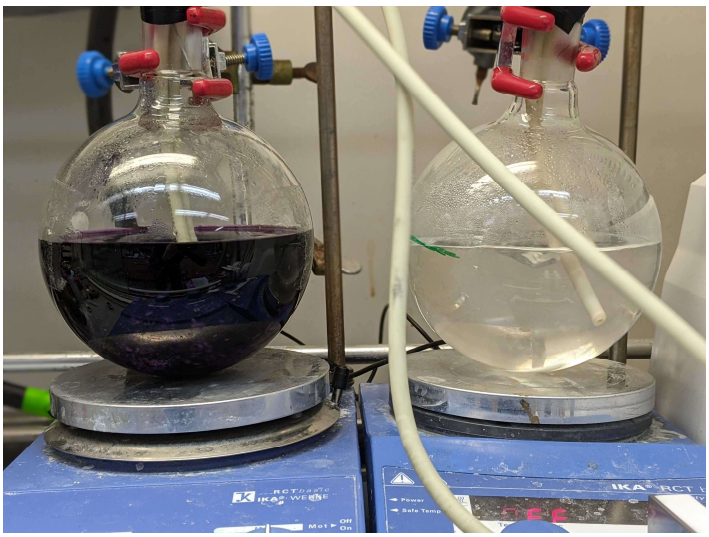

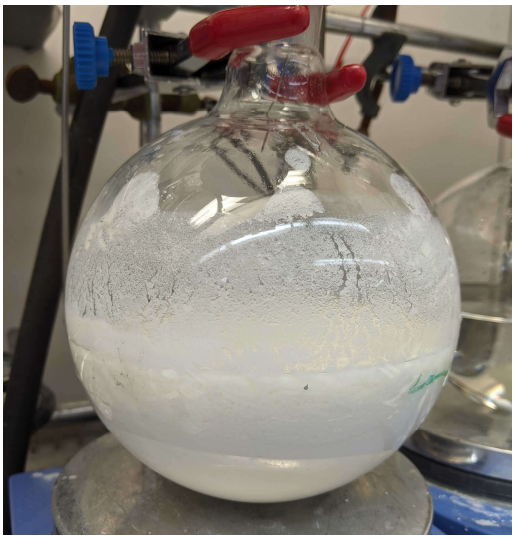

Left: anode solution (left) and cathode solution (right) after 2 h of electrolysis. **Right:** anode solution after complete substitution of dicationic adduct.

A.8 Aziridine and Adduct Derivatization Reactions

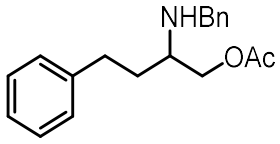

2-(benzylamino)-4-phenylbutyl acetate (2.34): To an oven-dried septum capped 2 dram vial equipped with a stir bar under nitrogen atmosphere was added aziridine **2.20 (**95 mg, 0.4 mmol, 1 equiv) via syringe, followed by DCM (0.8 mL). Acetic acid (114 µL, 2 mmol, 5 equiv) was added dropwise to the solution. The reaction was stirred at rt for 72 h before being quenched by addition of saturated aqueous $NaHCO_3$ (10 mL) and diluted with EtOAc (10 mL). The aqueous layer was separated and extracted with EtOAc (20 mL x 3). The combined organic layers were washed with saturated aqueous NaCl solution (10 mL), dried with anhydrous Na_2SO_4, filtered, and concentrated under reduced pressure. The residue was purified via flash column chromatography (10-60% EtOAc to yield 89 mg (75% yield) as an oil. **^{1}H NMR**

(600 MHz, $CDCl_3$) δ 7.30 – 7.17 (m, 7H), 7.15 – 7.09 (m, 3H), 4.13 (dd, J = 11.2, 4.4 Hz, 1H), 4.02 (dd, J = 11.2, 5.7 Hz, 1H), 3.77 (d, J = 13.1 Hz, 1H), 3.73 (d, J = 13.1 Hz, 1H), 2.79 (qd, J = 6.1, 4.5 Hz, 1H), 2.70 – 2.60 (m, 2H), 2.01 (s, 3H), 1.78 – 1.71 (m, 2H), 1.47 (bs, 1H); **^{13}C NMR** (151 MHz, $CDCl_3$) δ 171.12, 141.95, 140.45, 128.46, 128.44, 128.38, 128.18, 127.04, 125.92, 65.98, 55.09, 51.09, 33.63, 32.09, 20.99. **HRMS** (ESI+) Calc: [M+H]+ (C19H24NO2) 298.1802; measured: 298.1800; 0.7 ppm difference.

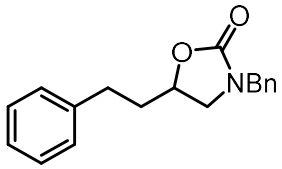

3-benzyl-5-phenethyloxazolidin-2-one (2.35): An oven-dried 2 dram vial equipped with a stir bar was transferred into a nitrogen-filled glovebox and anhydrous LiI (54 mg, 0.4 mmol, 1 equiv) was added. The vial was sealed with septum cap and transferred out of the glovebox. The atmosphere was immediately evacuated and replaced with 1 atm CO_2 using two balloons filled with CO_2. Aziridine **2.20** (95 mg, 0.4 mmol, 1 equiv) was added via syringe followed by THF (2 mL). The reaction mixture was warmed to 40 °C and stirred for 24 h, at which point the deflated balloon was replaced with an additional balloon of CO_2. The reaction mixture was stirred for an additional 20 h. The reaction mixture was cooled to rt and diluted with EtOAc (10 mL) and water (10 mL). The aqueous layer was separated and extracted with EtOAc (10 mL x 3). The combined organic layers were washed with saturated aqueous NaCl solution (10 mL), dried with anhydrous Na_2SO_4, filtered, and concentrated under reduced pressure. The residue was purified via flash column chromatography (0-50% acetone/hexanes) to yield 97 mg (86% yield) as a 16:1 mixture of regioisomers (major isomer depicted). **^{1}H NMR** (500 MHz, CDCl3) δ 7.31 – 7.18 (m, 7H), 7.15 – 7.07 (m, 3H), 4.42 – 4.34 (m, 2H), 4.32 (d, *J* = 14.8 Hz, 1H), 3.37 (t, *J* = 8.5 Hz, 1H), 2.94 (dd, *J* = 8.6, 7.0 Hz, 1H), 2.73 (ddd, *J* = 14.4, 9.3, 5.3 Hz, 1H), 2.64 (ddd, *J* = 13.8, 8.9, 7.3 Hz, 1H), 1.98 (dtd, *J* = 14.0, 8.7, 5.3 Hz, 1H), 1.79 (dddd, *J* = 13.9, 9.2, 7.3, 4.6 Hz, 1H).; **^{13}C NMR** (126 MHz, $CDCl_3$) δ 158.07, 140.47, 135.78, 128.86, 128.58, 128.46, 128.13, 127.99, 126.27, 72.60, 49.23, 48.33, 36.87, 30.95. **HRMS** (ESI+) Calc: [M+H]+ (C18H20NO2) 282.14886; measured: 282.1484; 1.6 ppm difference. Connectivity confirmed by edited HSQC and HMBC.

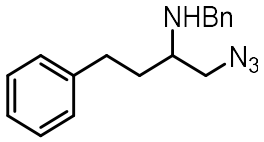

1-azido-N-benzyl-4-phenylbutan-2-amine (2.36):

CAUTION: Organic azides and hydrazoic acid are known to be potentially explosive compounds. While no issue was encountered during this synthesis, proper precautions were taken. All azidation reactions should be performed behind a blast shield, and aqueous layers should be kept basic. Once isolated, organic azides should be stored below room temperature and away from sources of heat, light, pressure and shock.

To an oven-dried septum capped 2 dram vial equipped with a stir bar under nitrogen atmosphere was added $TMSN_3$ (265 µL, 2.0 mmol, 5 equiv), followed by DCM (1 mL). Acetic acid (114 µL, 2 mmol, 5 equiv) was added dropwise. The reaction mixture was stirred at rt for 20 min. A solution of aziridine **2.20 (**95 mg, 0.4 mmol, 1 equiv) in DCM (1 mL) was added via syringe, and the reaction mixture was stirred at rt for 48 h. At completion, the reaction mixture was quenched using slow addition of saturated aqueous $NaHCO_3$ solution (10 mL). The aqueous layer was separated and extracted with EtOAc (10 mL x 3). The

combined organic layers were dried with anhydrous Na_2SO_4, filtered, and concentrated under reduced pressure. The residue was purified via flash column chromatography (0-45% EtOAc/hexanes) to yield 83.8 mg (75% yield) as an oil. **^{1}H NMR** (500 MHz, CDCl3) δ 7.26 (dd, *J* = 4.4, 1.3 Hz, 3H), 7.23 – 7.17 (m, 4H), 7.14 – 7.07 (m, 3H), 3.76 (d, *J* = 13.0 Hz, 1H), 3.70 (d, *J* = 12.7 Hz, 1H), 3.39 (dd, *J* = 12.3, 4.5 Hz, 1H), 3.22 (dd, *J* = 12.3, 5.5 Hz, 1H), 2.71 (p, *J* = 5.4 Hz, 1H), 2.61 (t, *J* = 7.9 Hz, 2H), 1.82 – 1.67 (m, 2H), 1.37 (bs, 1H); **^{13}C NMR** (126 MHz, $CDCl_3$) δ 141.73, 140.29, 128.49, 128.35, 128.17, 127.10, 125.98, 56.15, 54.32, 51.15, 34.20, 32.11. **HRMS** (ESI+) Calc: [M+H]+ (C17H21N4) 281.17607; measured: 281.1759; 0.6 ppm difference.

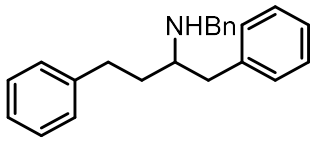

N-benzyl-1,4-diphenylbutan-2-amine (2.37): An oven-dried 50 mL three-necked round bottom flask equipped with a stir bar was charged with CuI (230 mg, 1.2 mmol, 3 equiv). The atmosphere was evacuated and refilled with nitrogen three times. THF (5 mL) was added and the flask was cooled to -40 °C. PhLi (1.9 M in dibutyl ether, 1.25 mL, 2.4 mmol, 6 equiv) was added via syringe and the reaction mixture was stirred at -40 °C for 30 min. The resulting black mixture was then cooled to -78 °C and a solution of aziridine **2.20** (95 mg, 0.4 mmol, 1 equiv) in THF (1 mL) was added, followed by dropwise addition of BF_3OEt_2 (152 µL, 1.2 mmol, 3 equiv). The reaction mixture was stirred at -78 °C for 30 min, then removed from the bath and allowed to warm to rt while stirring for 4 h. The reaction mixture was then quenched via addition of NH_4OH (10 mL) and saturated aqueous NH_4Cl (10 mL) and diluted with Et_2O (10 mL). The dark blue aqueous layer was separated, basified via the addition of 10% aqueous Na_2CO_3 (~20 mL), and extracted with Et_2O (20 mL x 3). The combined organic layers were washed with saturated aqueous NaCl (20 mL), dried with anhydrous Na_2SO_4, filtered, and concentrated under reduced pressure. The residue was purified via flash column chromatography (0-45% acetone/hexanes followed by 0-35% acetone/hexanes on basified silica) to yield 63.5 mg (50% yield) as an oil. **^{1}H NMR** (500 MHz, CDCl3) δ 7.24 – 7.03 (m, 15H), 3.71 (d, *J* = 13.2 Hz, 1H), 3.67 (d, *J* = 13.2 Hz, 1H), 2.84 – 2.57 (m, 5H), 1.70 (td, *J* = 8.1, 5.8 Hz, 2H), 1.35 – 1.26 (bs, 1H); **^{13}C NMR** (126 MHz, $CDCl_3$) δ 142.51, 140.67, 139.36, 129.33, 128.42, 128.40, 128.35, 128.09, 126.82, 126.18, 125.72, 57.69, 51.09, 40.67, 35.63, 32.04. **HRMS** (ESI+) Calc: [M+H]+ (C23H26N) 316.2060; measured: 316.2058; 0.6 ppm difference. Connectivity confirmed by edited HSQC and HMBC.

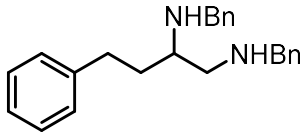

N^1,N^2-dibenzyl-4-phenylbutane-1,2-diamine (2.39): Following General Procedure H with benzylamine (310 µL, 2.8 mmol, 7 equiv) as the nucleophile, 53% yield obtained.

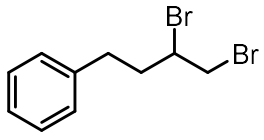

(3,4-dibromobutyl)benzene (2.40): Following General Procedure G with *n*-Bu_4NBr (645 mg, 2.0 mmol, 5 equiv) as the nucleophile, with 0-5% acetone/hexanes gradient, 89.9 mg (77% yield) obtained as an oil.

^{1}H NMR (500 MHz, CDCl3) δ 7.42 – 7.29 (m, 5H), 4.18 (tdd, *J* = 9.8, 4.5, 2.9 Hz, 1H), 3.93 (dd, *J* = 10.3, 4.3 Hz, 1H), 3.72 (t, *J* = 10.0 Hz, 1H), 3.02 (ddd, *J* = 13.7, 9.2, 4.6 Hz, 1H), 2.83 (ddd, *J* = 13.7, 9.2, 7.2 Hz, 1H), 2.60 – 2.50 (m, 1H), 2.16 (dtd, *J* = 14.5, 9.4, 4.7 Hz, 1H). ^{13}C NMR Consistent with reported spectra[6].

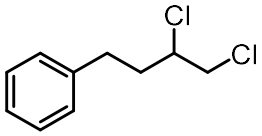

(3,4-dichlorobutyl)benzene (2.41): Following General Procedure H with $BnMe_3NCl$ (371 mg, 2.0 mmol, 5 equiv) as the nucleophile, 72% yield obtained.

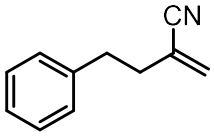

2-methylene-4-phenylbutanenitrile (2.42): Following General Procedure G with KCN (130 mg 2.0 mmol, 5 equiv) as the nucleophile, with 0-5% acetone/hexanes gradient, 38.8 mg (61% yield) obtained as an oil. **^{1}H NMR** (500 MHz, CDCl3) δ 7.36 (dd, *J* = 8.2, 6.8 Hz, 2H), 7.27 (m, 3H), 5.88 (s, 1H), 5.69 (s, 1H), 2.97 – 2.88 (m, 2H), 2.62 (t, *J* = 7.8 Hz, 2H). ^{13}C NMR consistent with reported spectra[14].

A.9 X-Ray Crystallography Data

Data Collection for 2.1

A colorless crystal with approximate dimensions 0.09 × 0.05 × 0.04 mm^3 was selected under oil under ambient conditions and attached to the tip of a MiTeGen MicroMount©. The crystal was mounted in a stream of cold nitrogen at 100(1) K and centered in the X-ray beam by using a video camera.

The crystal evaluation and data collection were performed on a Bruker D8 VENTURE PhotonIII four-circle diffractometer with Cu Kα (λ = 1.54178 Å) radiation and the detector to crystal distance of 4.0 cm[15].

The initial cell constants were obtained from a 180° φ scan conducted at a 2θ = 50° angle with the exposure time of 1 second per frame. The reflections were successfully indexed by an automated indexing routine built in the APEX3 program. The final cell constants were calculated from a set of 9088 strong reflections from the actual data collection.

The data were collected by using the full sphere data collection routine to survey the reciprocal space to the extent of a full sphere to a resolution of 0.78 Å. A total of 136275 data were harvested by collecting 44 sets of frames with 1.0º scans in ω and φ with an exposure time 1–3 sec per frame. These highly redundant datasets were corrected for Lorentz and polarization effects. The absorption correction was based on fitting a function to the empirical transmission surface as sampled by multiple equivalent measurements[16].

Structure Solution and Refinement

The systematic absences in the diffraction data were consistent for the space groups $P\bar{1}$ and $P1$. The *E*-statistics strongly suggested the centrosymmetric space group $P\bar{1}$ that yielded chemically reasonable and computationally stable results of refinement[17–22].

A successful solution by the direct methods provided most non-hydrogen atoms from the *E*-map. The remaining non-hydrogen atoms were located in an alternating series of least-squares cycles and difference Fourier maps. All non-hydrogen atoms were refined with anisotropic displacement coefficients unless indicated otherwise. All hydrogen atoms were included in the structure factor calculation at idealized positions and were allowed to ride on the neighboring atoms with relative isotropic displacement coefficients.

There are two sulfur-containing dications and four BF_4^- anions in the asymmetric unit. The crystallized compound is a racemate. The chiral dications have identical chemical composition and connectivity, but different handedness – chiral center C13 is *S*, whereas C13A is *R*.

Two BF_4^- anions exhibit positional disorder. Tetrafluroborate B3 is disordered over three positions in a 0.718(3) : 0.147(2) : 0.135(2) ratio. Tetrafluroborate B4 is disordered over three positions in a 0.699(3) : 0.154(3) : 0.147(3) ratio. The four minor disorder components were refined isotropically with an idealized geometry[23] and atomic displacement parameter constraints.

The final least-squares refinement of 897 parameters against 13706 data resulted in residuals R (based on F2 for $I \geq 2\sigma$) and wR (based on F2 for all data) of 0.0399 and 0.1037, respectively. The final difference Fourier map was featureless.

Data Collection for 2.2

Two separate data collections were carried out on two different colorless crystals with approximate dimensions of 0.07 x 0.06 x 0.05 mm^3 and 0.04 x 0.04 x 0.04 mm^3 in a similar fashion. Unless otherwise specified, the data collection parameters were similar for both crystals and therefore we report only the procedural details for the first.

The crystal was selected under oil under ambient conditions and attached to the tip of a MiTeGen MicroMount©. The crystal was mounted in a stream of cold nitrogen at 100(1) K and centered in the X-ray beam by using a video camera.

The crystal evaluation and data collections were performed on a Bruker D8 VENTURE PhotonIII four-circle diffractometer with Cu Kα (λ = 1.54178 Å) radiation with the detector to crystal distance of 4.0 cm[15].

The initial cell constants were obtained from a 180° φ scan conducted at a 2θ = 50° angle with an exposure time of 1 second per frame. The reflections were successfully indexed by an automated indexing routine built in the APEX3 program. The final cell constants were calculated from a set of 8035 strong reflections from the actual data collection.

The data were collected by using a full sphere data collection routine to survey reciprocal space to the extent of a full sphere to a resolution of 0.79 Å. For the crystal with dimensions of 0.07 x 0.06 x 0.05 mm^3, a total of 25205 data were harvested by collecting 14 sets of frames with 0.9º scans in ω and φ with exposure times of 3 – 22 sec per frame; for the crystal with dimensions of 0.04 x 0.04 x 0.04 mm^3, a total of 22269 data were harvested by collecting 13 sets of frames with 0.9º scans in ω and φ with exposure times of 1-15 sec per frame. The two datasets were then merged and corrected for Lorentz and polarization effects. The absorption correction was based on fitting a function to the empirical transmission surface as sampled by multiple equivalent measurements[16].

Structure Solution and Refinement

The diffraction data were consistent with the space groups $P\bar{1}$ and $P1$. The *E*-statistics strongly suggested the centrosymmetric space group $P\bar{1}$ which yielded chemically reasonable and computationally stable results of refinement[17–22].

A successful solution by direct methods provided most non-hydrogen atoms from the *E*-map. The remaining non-hydrogen atoms were located with an alternating series of least-squares cycles and difference Fourier maps. Unless otherwise specified, all non-hydrogen atoms were refined with anisotropic displacement coefficients. All hydrogen atoms were included in the structure factor calculation at idealized positions and were allowed to ride on the neighboring atoms with relative isotropic displacement coefficients.

The structure consists of one sulfur-containing dication, two PF_6^- anions, and one molecule of solvate acetonitrile. Both PF_6^- anions and the dication were disordered over two positions. However, the position for the minor component for atoms C15-C22 of the dication could not be located in the difference map; thus, atoms C15-C22 (and the H atoms bound to those C atoms) were refined at a 100 % occupancy to ensure a chemically reasonable structural formula. Atom H14 (bound to atom C14) was refined at a 100 % occupancy while no H atoms were assigned to atom C14A.

The major disorder component has a 90.9(2) % occupancy. The atoms in the minor disorder component were refined isotopically. For the dication, the atoms in the minor disorder component were refined with geometric and atomic displacement parameter constraints, as well as 1,2 and 1,3 distance restraints. For the PF_6^- anions, the atoms in the minor component were refined with geometric and atomic displacement parameter constraints[23].

The structure crystallizes as a racemate. The absolute configuration of the arbitrarily chosen enantiomer shown in Figure 3 is C14 – *R*.

The final least-squares refinement of 413 parameters against 5794 data resulted in residuals *R* (based on F^2 for $I \geq 2\sigma$) and *wR* (based on F^2 for all data) of 0.0378 and 0.1004, respectively. The final difference Fourier map was featureless.

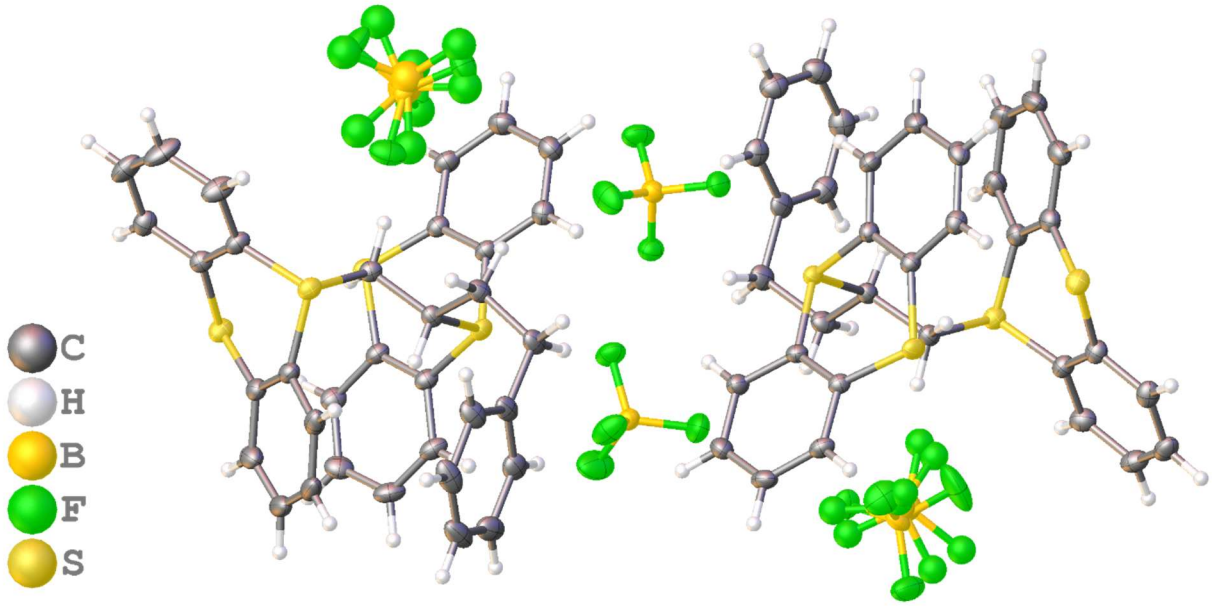

Fig. A5. A molecular drawing of the unit cell content of 2.1 shown with 50% probability ellipsoids. All disorder components are shown.

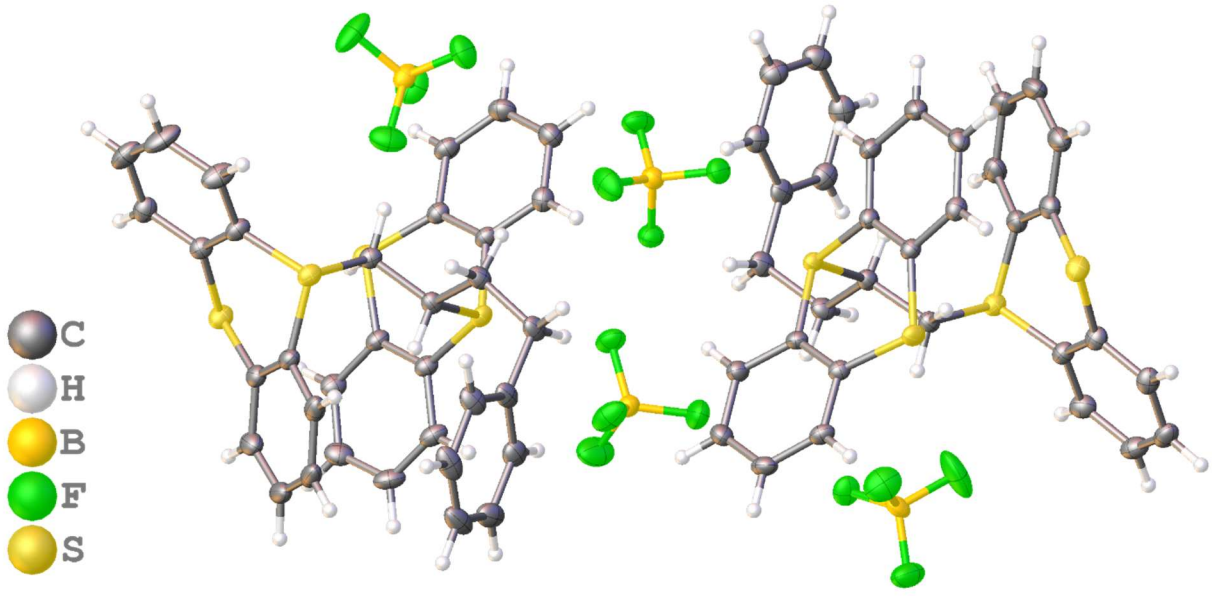

Fig A6. A molecular drawing of the unit cell content of 2.1 shown with 50% probability ellipsoids. All minor disorder components are omitted.

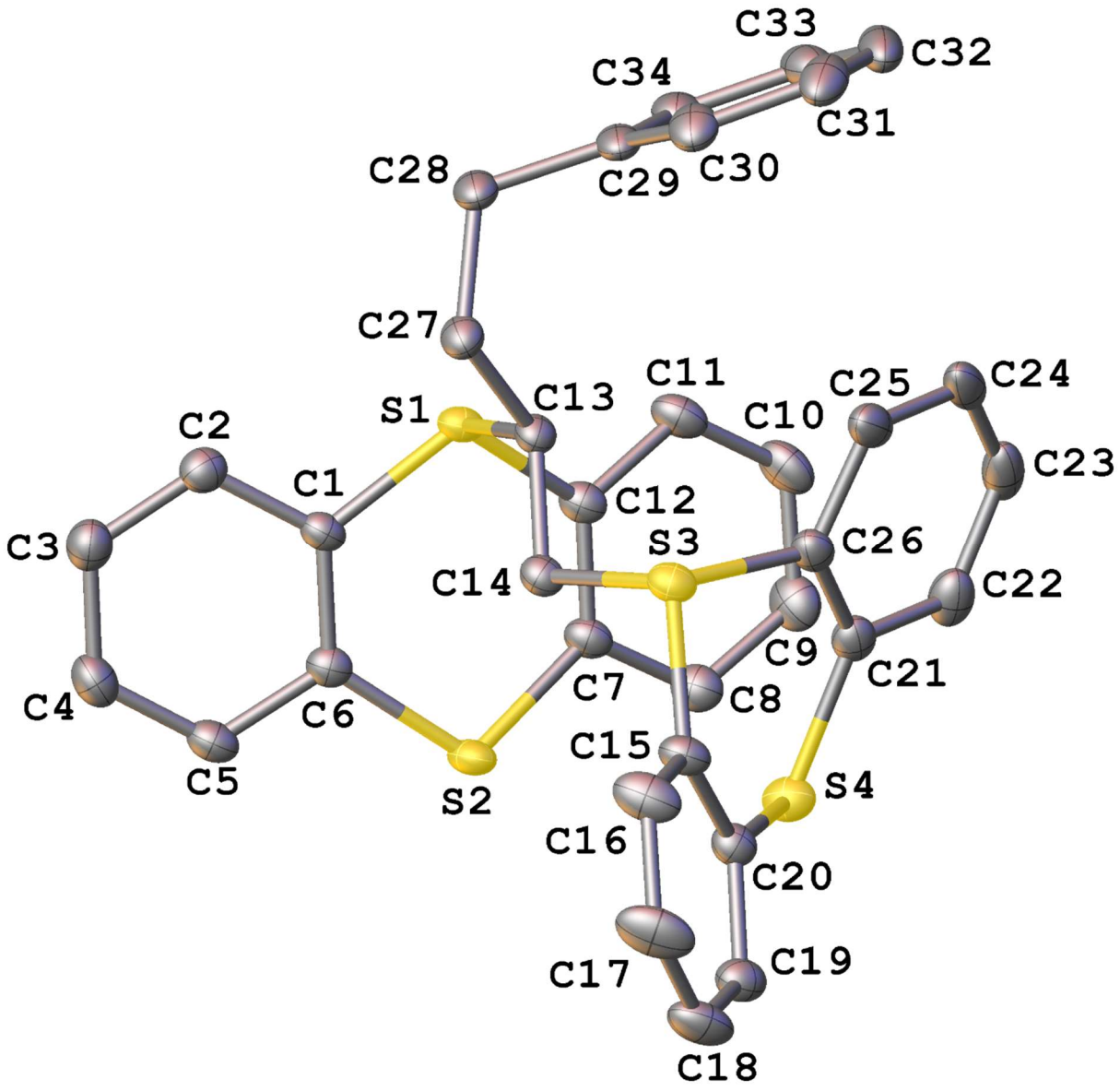

Fig. A7. A molecular drawing of the *S* enantiomer in 2.1 shown with 50% probability ellipsoids. All H atoms are omitted.

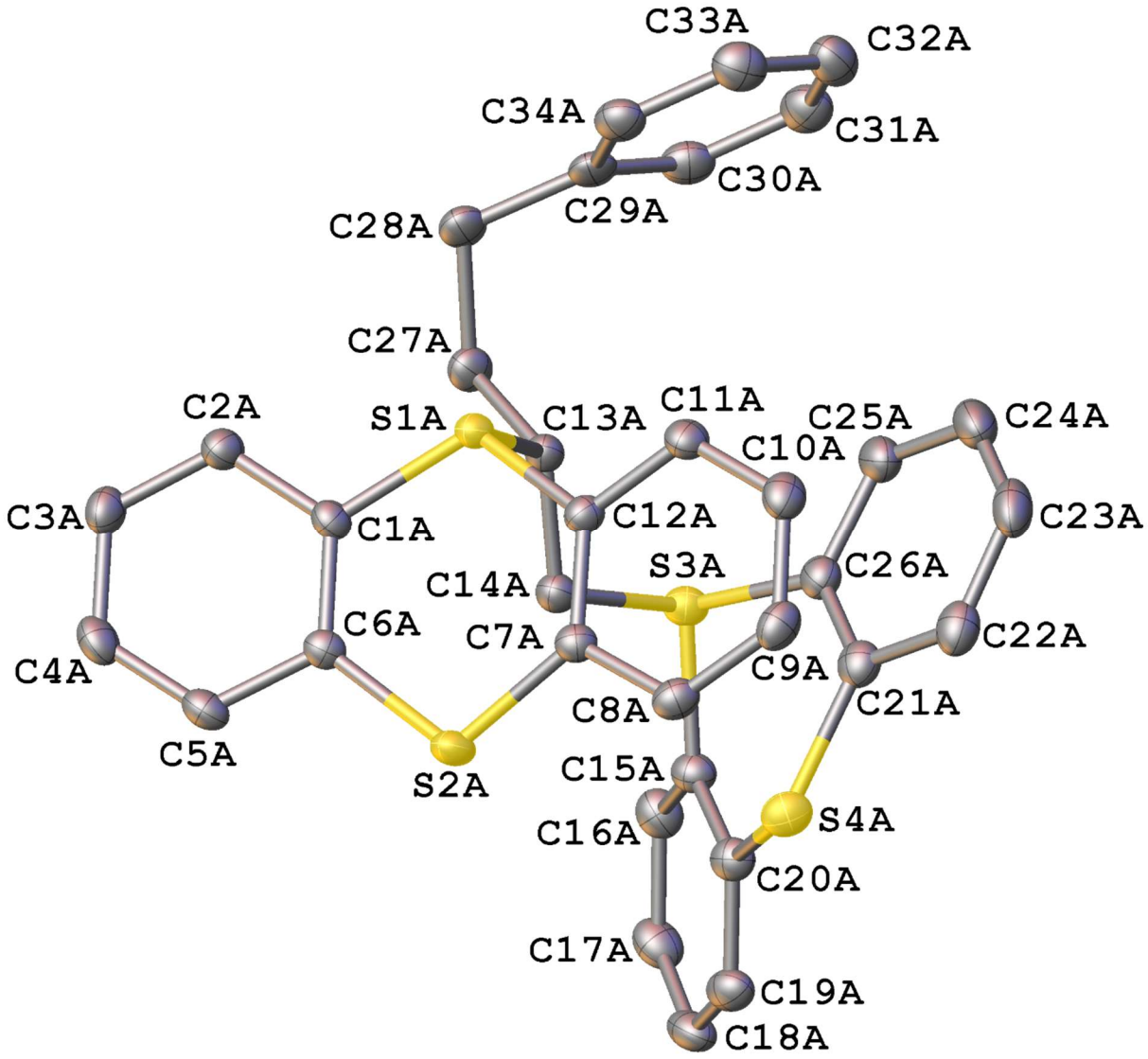

Fig. A8. A molecular drawing of the *R* enantiomer in 2.1 shown with 50% probability ellipsoids. All H atoms are omitted.

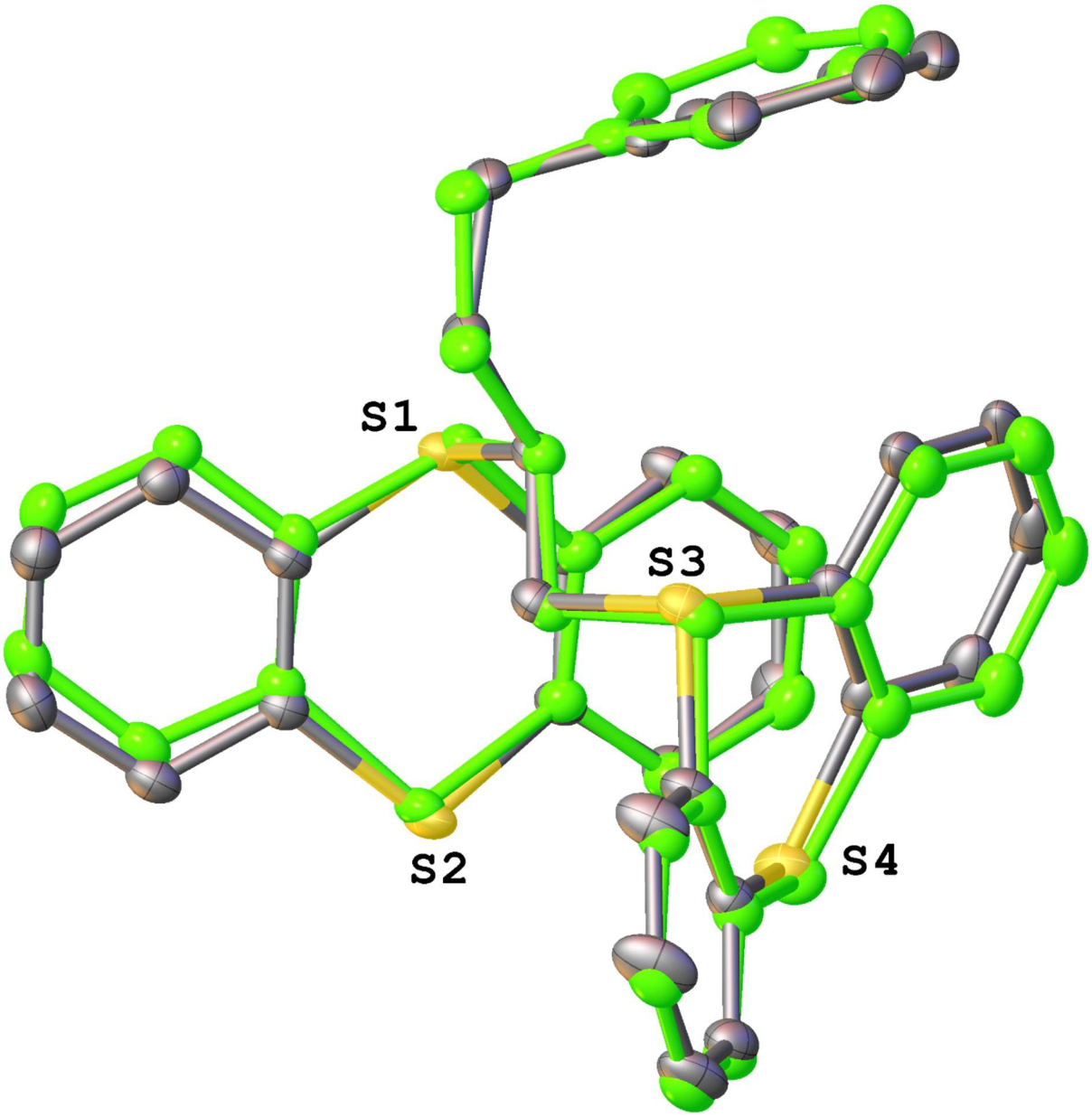

Fig. A9. A superposition of the two enantiomers in 2.1 shown with 50% probability ellipsoids (one of them is inverted). All H atoms are omitted.

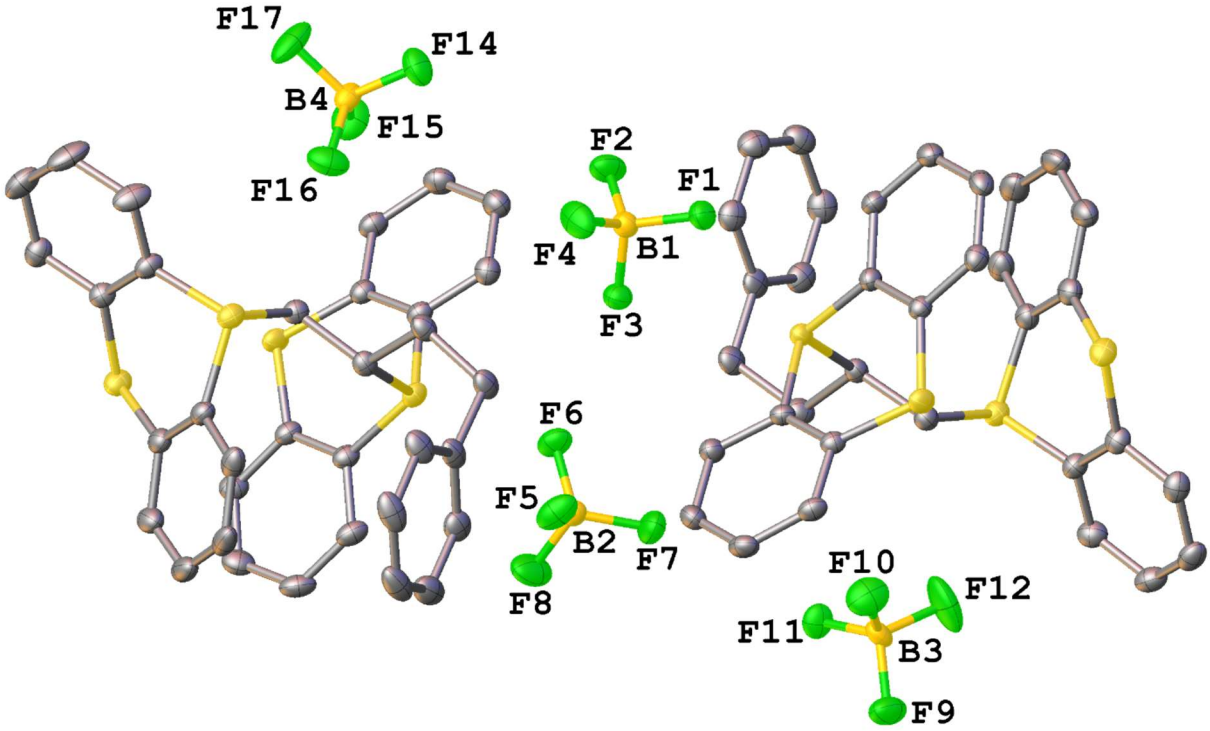

Fig. A10. A molecular drawing of 2.1 shown with 50% probability ellipsoids. All H atoms and minor disorder components are omitted. Only the B and F atoms are labelled.

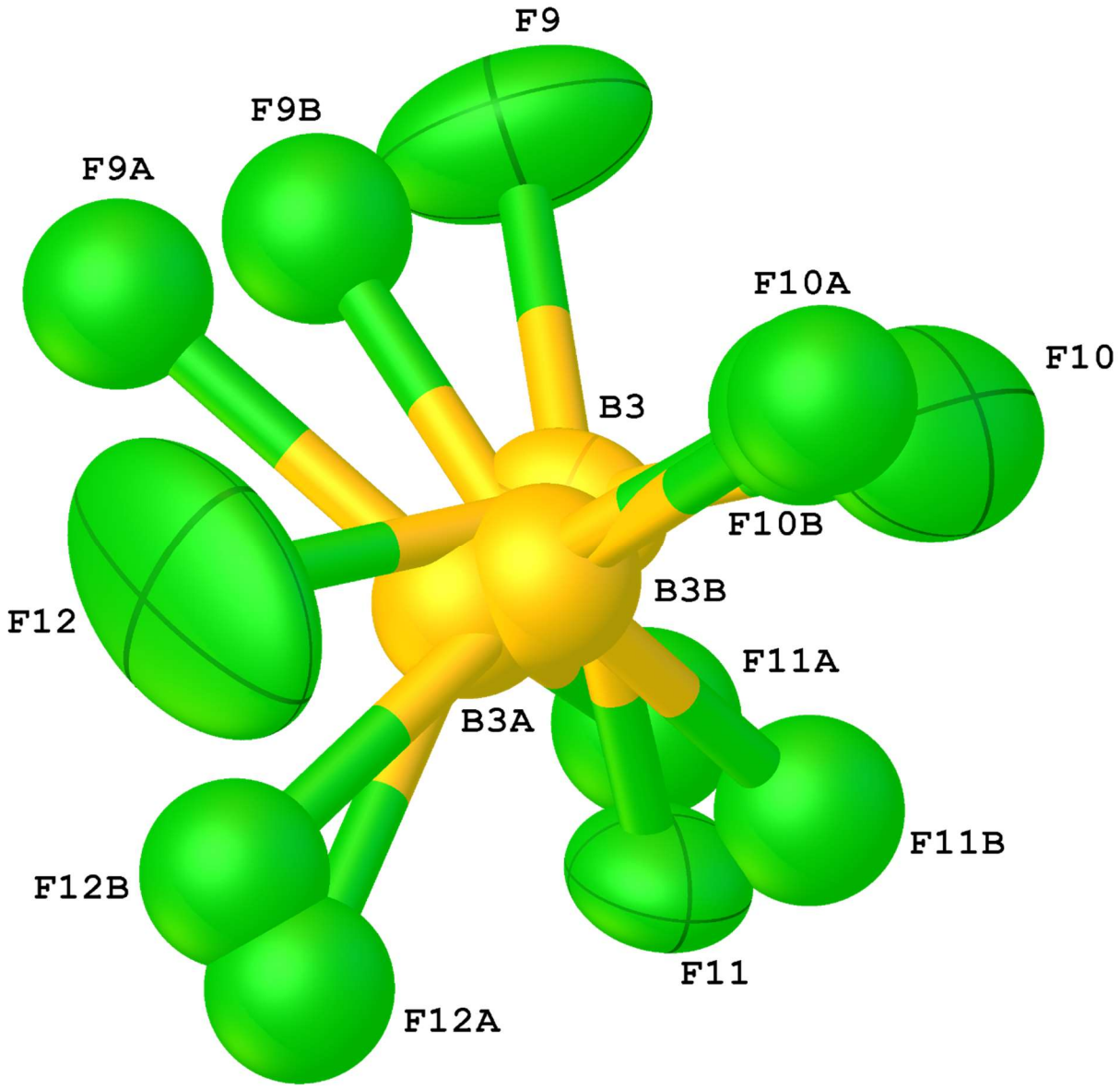

Fig. A11. A molecular drawing of the B3 anion in 2.1 shown with 50% probability ellipsoids. All disorder positions are shown.

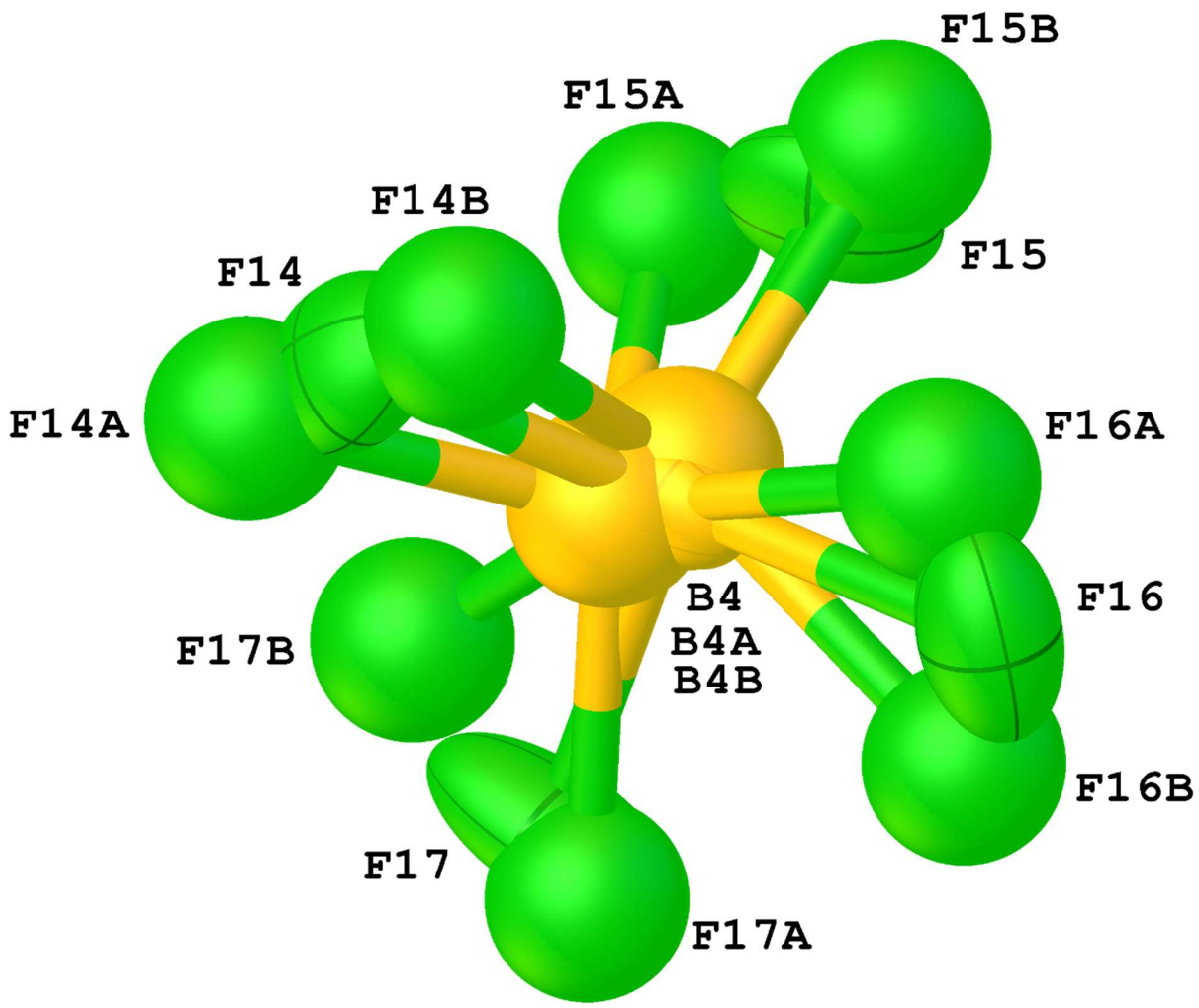

Fig. A12. A molecular drawing of the B4 anion in 2.1 shown with 50% probability ellipsoids. All disorder positions are shown.

Table A2. Crystal data and structure refinement for 2.1.

Identification code	1
Empirical formula	$[C_{34}H_{28}S_4][BF_4]_2$
Formula weight	738.42
Temperature/K	100
Crystal system	triclinic
Space group	$P\bar{1}$

a/Å	10.334(3)
b/Å	14.268(2)
c/Å	21.678(9)
α/°	87.734(14)
β/°	89.78(4)
γ/°	81.333(16)
Volume/$Å^3$	3157.3(16)
Z	4
$\rho_{calc}g/cm^3$	1.553
μ/mm^{-1}	3.423
F(000)	1512.0
Crystal size/mm^3	0.09 × 0.05 × 0.04
Radiation	CuKα (λ = 1.54178)
2Θ range for data collection/°	4.08 to 162.552
Index ranges	$-13 \leq h \leq 13$, $-18 \leq k \leq 18$, $-27 \leq l \leq 27$
Reflections collected	136275
Independent reflections	13706 [R_{int} = 0.0557, R_{sigma} = 0.0259]
Data/restraints/parameters	13706/2/897
Goodness-of-fit on F^2	1.042
Final R indexes [I>=2σ (I)]	R_1 = 0.0399, wR_2 = 0.1009
Final R indexes [all data]	R_1 = 0.0441, wR_2 = 0.1037
Largest diff. peak/hole / e $Å^{-3}$	0.76/-0.40

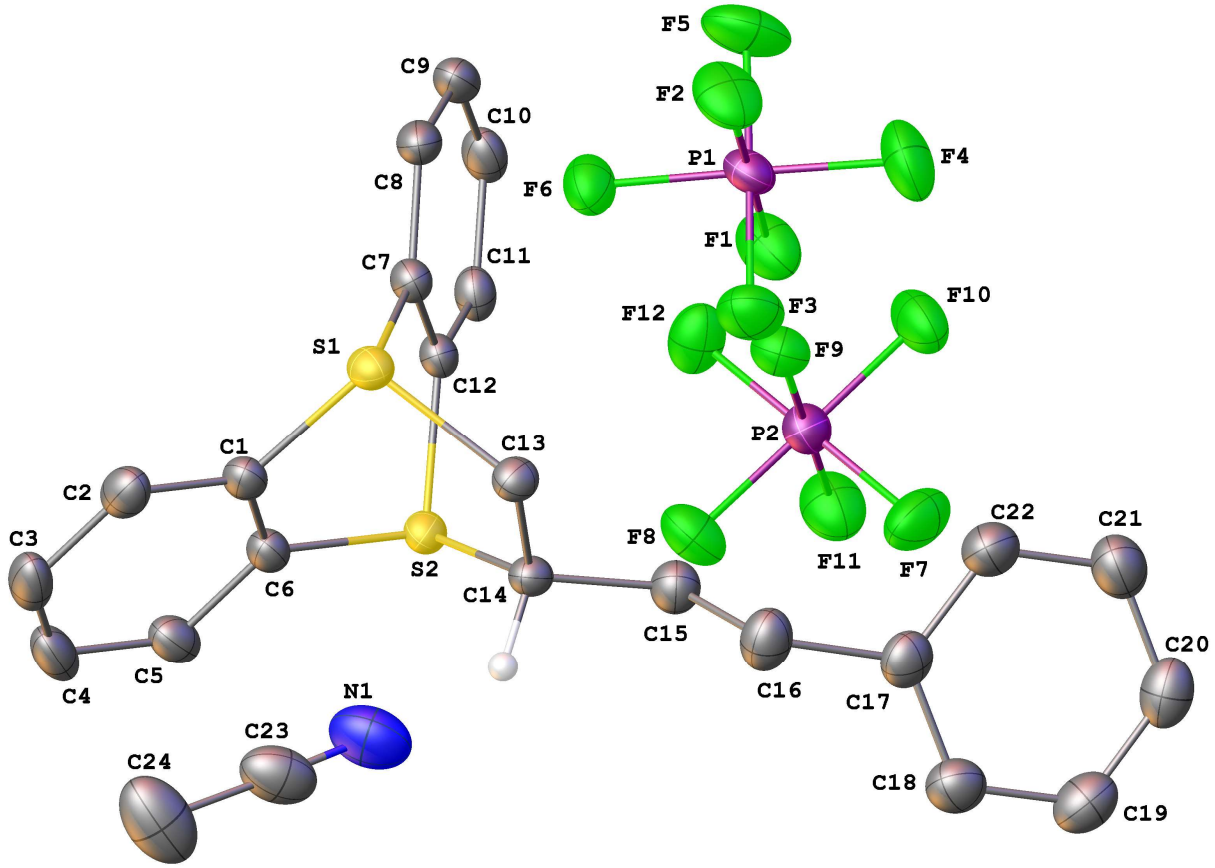

Fig. A13. A molecular drawing of 2.2 shown with 50% probability ellipsoids. All H atoms (except the H atom bound to C14) and minor disorder components are omitted.

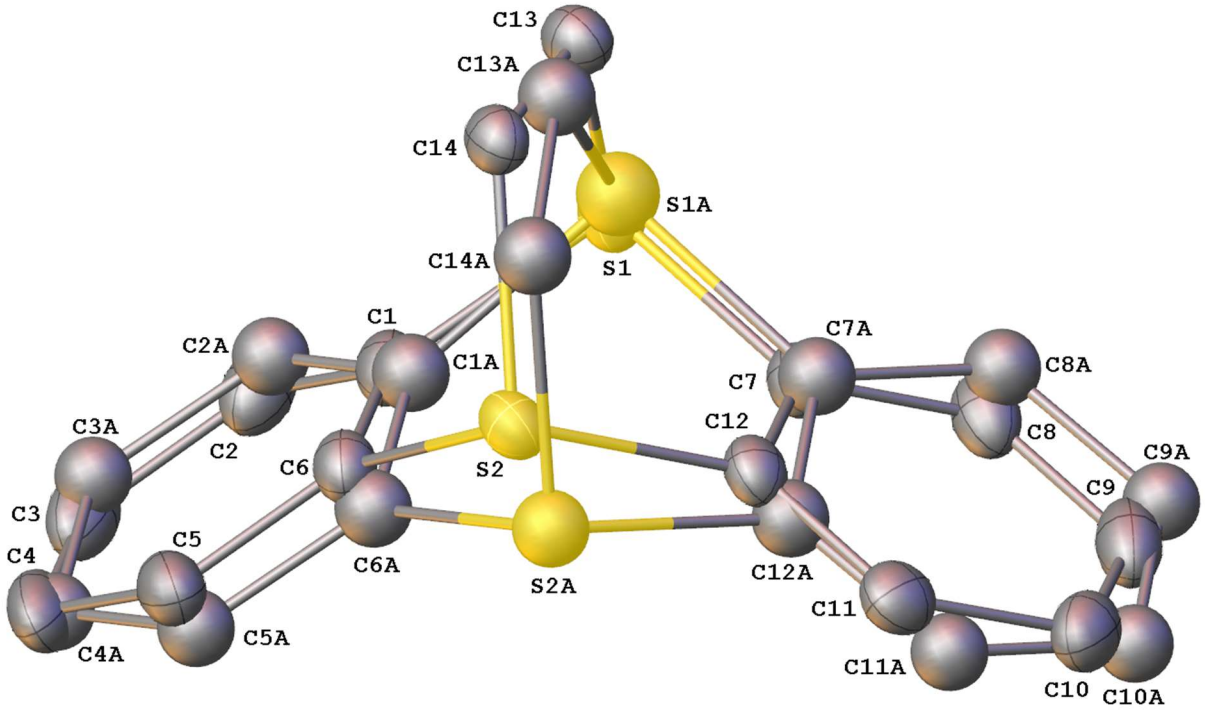

Fig. A14. A molecular drawing of the two disordered components of the sulfur-containing dication in 2.2 shown with 50 % probability ellipsoids. Atoms C15 – C22 and all H atoms have been omitted for clarity. In addition, the atomic radii of the atoms in the minor disorder component are shown at 80 % of their original value for clarity.

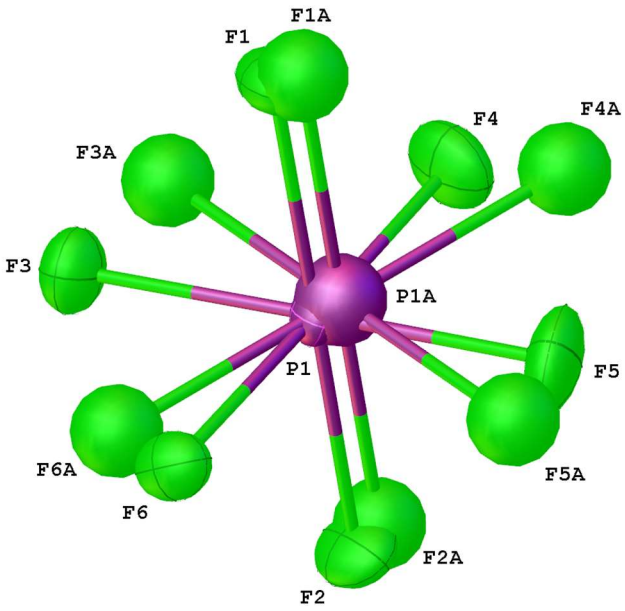

Fig. A15. A molecular drawing of the two disordered components in the first PF_6^- anion in 2.2 shown with 50 % probability ellipsoids; the atomic radii of the atoms in the minor component are shown at 60 % of their original value for clarity.

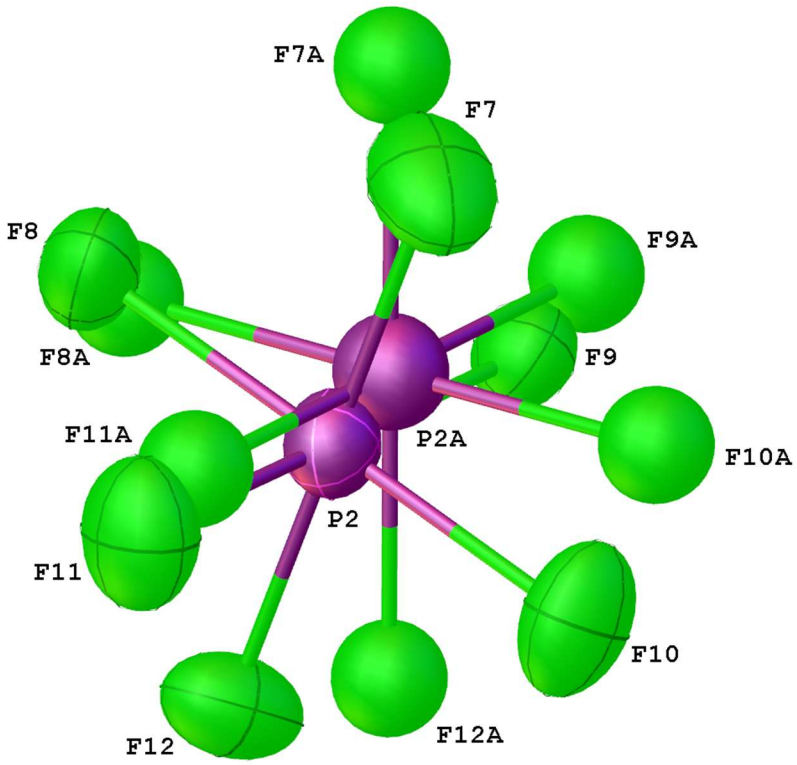

Fig. A16. A molecular drawing of the two disordered components in the second PF_6^- anion in 2.2 shown with 50 % probability ellipsoids; the atomic radii of the atoms in the minor component are shown at 70 % of their original value for clarity.

Table S3. Crystal data and structure refinement for 2.2.

Identification code	2
Empirical formula	$[C_{24}H_{23}S_2][PF_6]_2 \cdot CH_3CN$
Formula weight	679.49
Temperature/K	100.0
Crystal system	triclinic
Space group	$P\bar{1}$
a/Å	9.4023(15)
b/Å	9.8774(13)
c/Å	16.295(2)
α/°	92.640(8)

β/°	105.034(8)
γ/°	108.174(6)
Volume/Å^3	1375.3(3)
Z	2
ρ_{calc}g/cm^3	1.641
μ/mm^{-1}	3.784
F(000)	688.0
Crystal size/mm^3	0.04 × 0.04 × 0.04
Radiation	CuKα (λ = 1.54178)
2Θ range for data collection/°	5.67 to 157.86
Index ranges	-11 ≤ h ≤ 11, -12 ≤ k ≤ 12, -20 ≤ l ≤ 19
Reflections collected	29750
Independent reflections	5794 [R_{int} = 0.0460, R_{sigma} = 0.0305]
Data/restraints/parameters	5794/47/413
Goodness-of-fit on F^2	1.071
Final R indexes [I>=2σ (I)]	R_1 = 0.0378, wR_2 = 0.0984
Final R indexes [all data]	R_1 = 0.0405, wR_2 = 0.1004
Largest diff. peak/hole / e Å^{-3}	0.44/-0.34

A.10 References

1. C. F. Macrae, P. R. Edgington, P. McCabe, E. Pidcock, G. P. Shields, R. Taylor, M. Towler, J. van de Streek, Mercury: Visualization and analysis of crystal structures. J. Appl. Cryst. 39, 453–457 (2006). doi:10.1107/S002188980600731X.
2. Cowper, N. G. W., Chernowsky, C. P., Williams, O. P. & Wickens, Z. K. Potent Reductants via Electron-Primed Photoredox Catalysis: Unlocking Aryl Chlorides for Radical Coupling. *J. Am. Chem. Soc.* **142**, 2093–2099 (2020).
3. van Greunen, D. G. *et al.* Targeting Alzheimer's disease by investigating previously unexplored chemical space surrounding the cholinesterase inhibitor donepezil. *Eur. J. Med. Chem.* **127**, 671–690 (2017).
4. Glunz, P. W. *et al.* Cyclic Ureas as Inhibitors of Rock. (2016).
5. Brunetti, F. G. *et al.* Reversible Microwave-Assisted Cycloaddition of Aziridines to Carbon Nanotubes. *J. Am. Chem. Soc.* **129**, 14580–14581 (2007).
6. Song, S., Li, X., Sun, X., Yuan, Y. & Jiao, N. Efficient bromination of olefins, alkynes, and ketones with dimethyl sulfoxide and hydrobromic acid. *Green Chem.* **17**, 3285–3289 (2015).
7. Zhao, W., Wurz, R. P., Peters, J. C. & Fu, G. C. Photoinduced, Copper-Catalyzed Decarboxylative C–N Coupling to Generate Protected Amines: An Alternative to the Curtius Rearrangement. *J. Am. Chem. Soc.* **139**, 12153–12156 (2017).
8. CDC - Immediately Dangerous to Life or Health Concentrations (IDLH): Ethylene dibromide - NIOSH Publications and Products. https://www.cdc.gov/niosh/idlh/106934.html (2018).
9. Nagy, V., Agócs, A., Turcsi, E. & Deli, J. Isolation and purification of acid-labile carotenoid 5,6-epoxides on modified silica gels. *Phytochem. Anal.* **20**, 143–148 (2009).
10. Sternativo, S. *et al.* One-pot synthesis of aziridines from vinyl selenones and variously functionalized primary amines. *Tetrahedron* **66**, 6851–6857 (2010).
11. Besev, M. & Engman, L. Pyrrolidines from β-Aminoselenides via Radical Cyclization. Diastereoselectivity Control by the N-Substituent. *Org. Lett.* **2**, 1589–1592 (2000).
12. Miniejew, C., Outurquin, F. & Pannecoucke, X. New phenylselanyl group activation: synthesis of aziridines and oxazolidin-2-ones. *Org. Biomol. Chem.* **2**, 1575–1576 (2004).
13. Davoli, P. *et al.* Lipase-catalyzed resolution and desymmetrization of 2-hydroxymethylaziridines. *J. Chem. Soc. Perkin 1* **0**, 1948–1953 (2002).
14. Gao, D.-W. *et al.* Direct Access to Versatile Electrophiles via Catalytic Oxidative Cyanation of Alkenes. *J. Am. Chem. Soc.* **140**, 8069–8073 (2018).
15. APEX3 v. 2018.1-0 (Bruker AXS, Madison, Wisconsin, USA, 2018).
16. Krause, L., Herbst-Irmer, R., Sheldrick, G. M. & Stalke, D. Comparison of silver and molybdenum microfocus X-ray sources for single-crystal structure determination. *J. Appl. Cryst.* **48**, 3-10 (2015).
17. XPREP v. 2013/1 (Univeristy of Göttingen, Göttingen, Germany, 2013).
18. Sheldrick, G. M. *The SHELX homepage*, <http://shelx.uni-ac.gwdg.de/SHELX/> (2013).
19. Sheldrick, G. M. *Acta Cryst. A*, Integrated space-group and crystal-structure determination, **A71**, 3-8 (2015).
20. Sheldrick, G. M. *Acta Cryst. C*, Crystal structure refinement with SHELXL. **C71**, 3-8 (2015).
21. Dolomanov, O. V., Bourhis, L. J., Gildea, R. J., Howard, J. A. K. & Puschmann, H. OLEX2: a complete structure solution, refinement and analysis program. *J. Appl. Crystallogr.* **42**, 339-341 (2009).
22. Programs Gn (Madison, Wisconsin, USA, 2007-2013).
23. Guzei, I. A. An idealized molecular geometry library for refinement of poorly behaved molecular fragments with constraints. *J. Appl. Cryst.* **47**, 806-809 (2014).

A.11 NMR Spectra

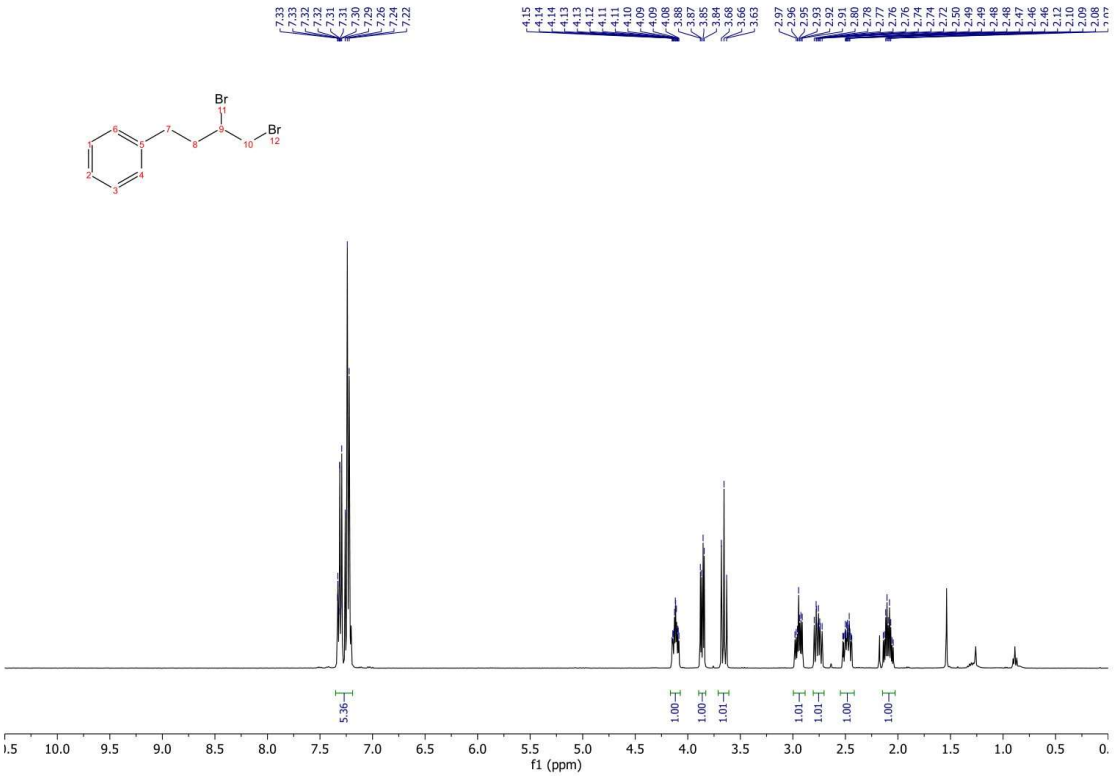

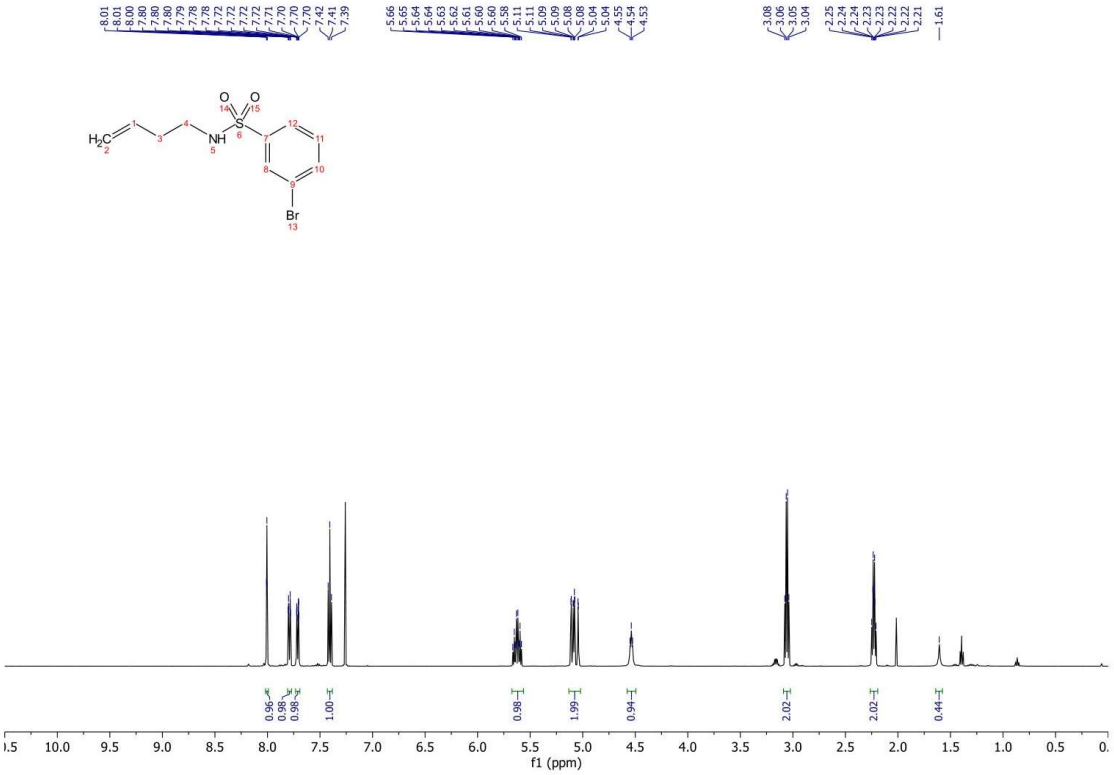

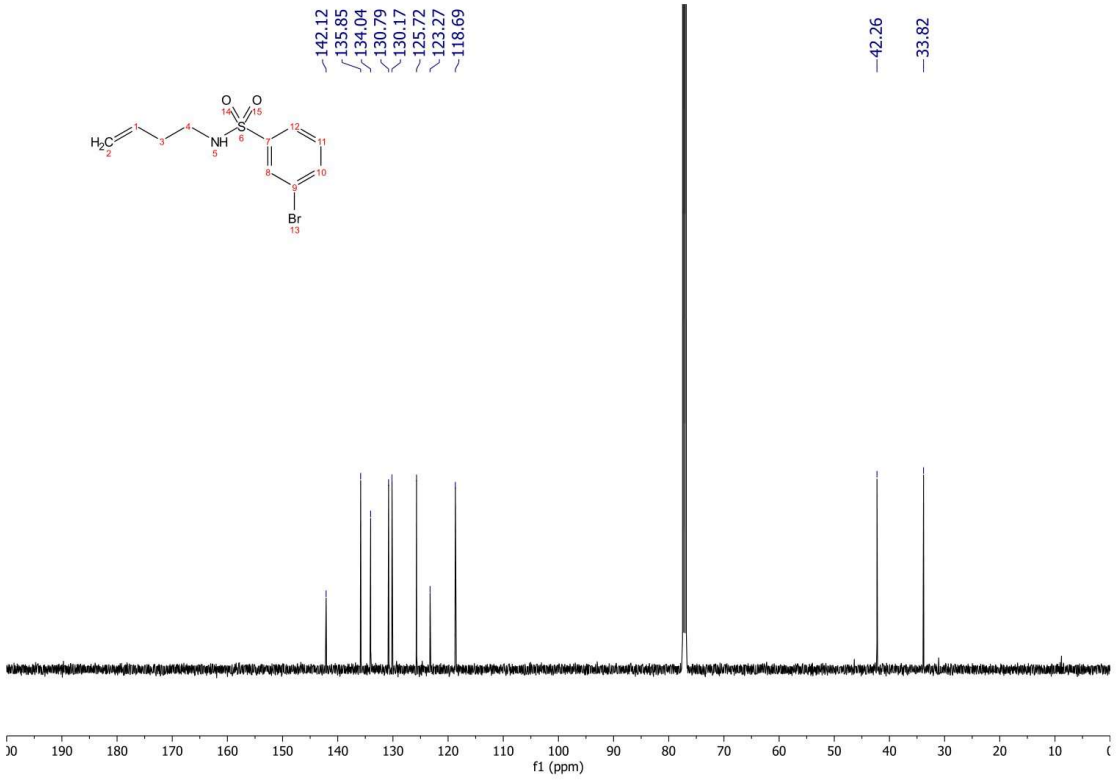
142.12
135.85
134.04
130.79
130.17
125.72
123.27
118.69
42.26
33.82
f1 (ppm)

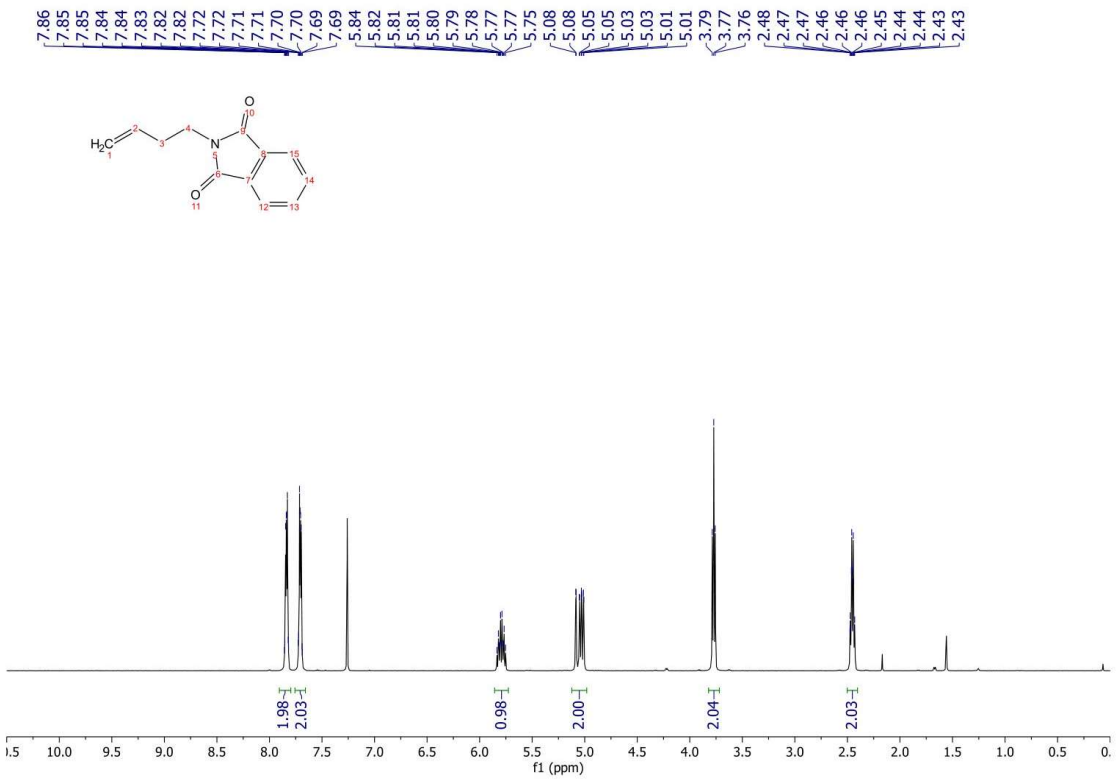
7.86
7.85
7.85
7.84
7.84
7.84
7.83
7.82
7.82
7.72
7.72
7.71
7.71
7.71
7.70
7.70
7.69
7.69
5.84
5.82
5.81
5.81
5.80
5.79
5.78
5.77
5.77
5.75
5.08
5.08
5.05
5.05
5.03
5.03
5.01
5.01
3.79
3.77
3.76
2.48
2.47
2.47
2.46
2.46
2.46
2.45
2.44
2.44
2.43
2.43
1.98
2.03
0.98
2.00
2.04
2.03
f1 (ppm)

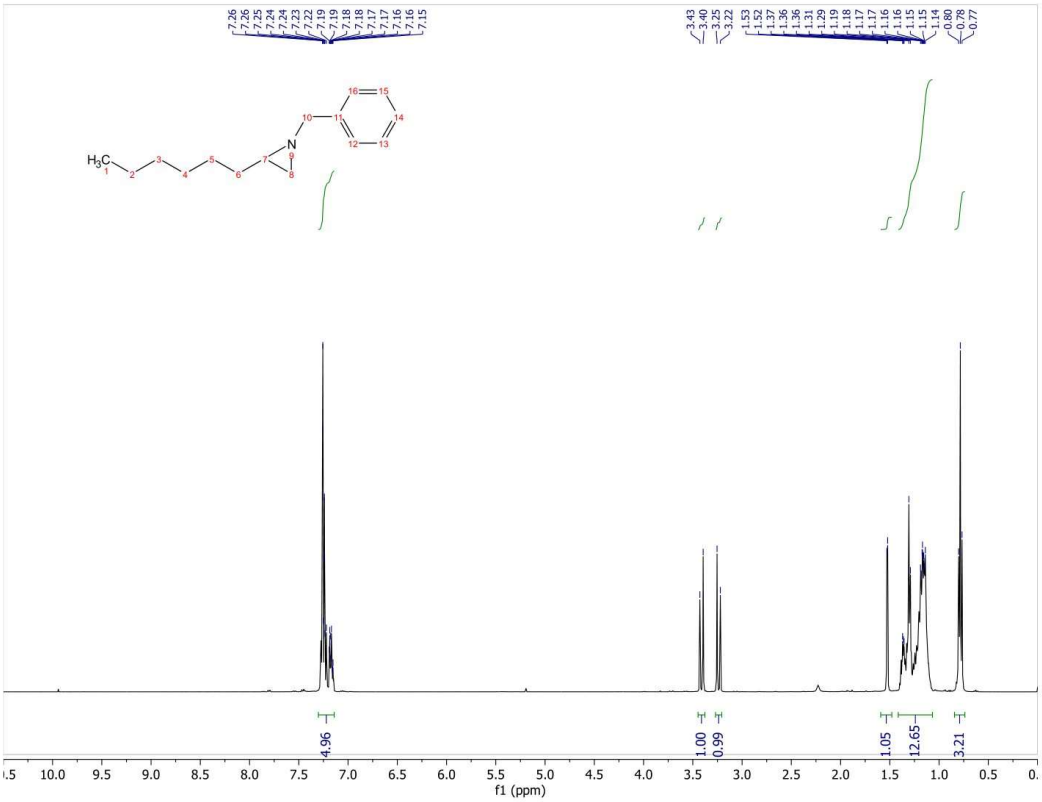
4.96
1.00
0.99
1.05
12.65
3.21
f1 (ppm)

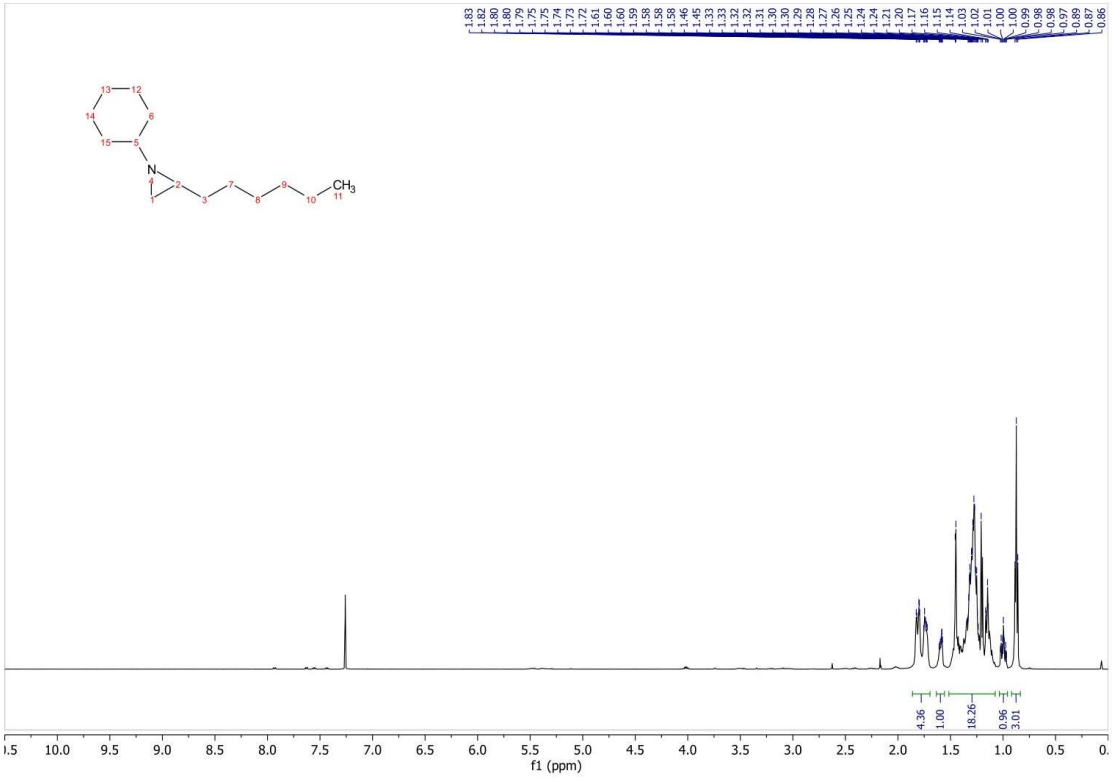
4.36
1.00
18.26
0.96
3.01
f1 (ppm)

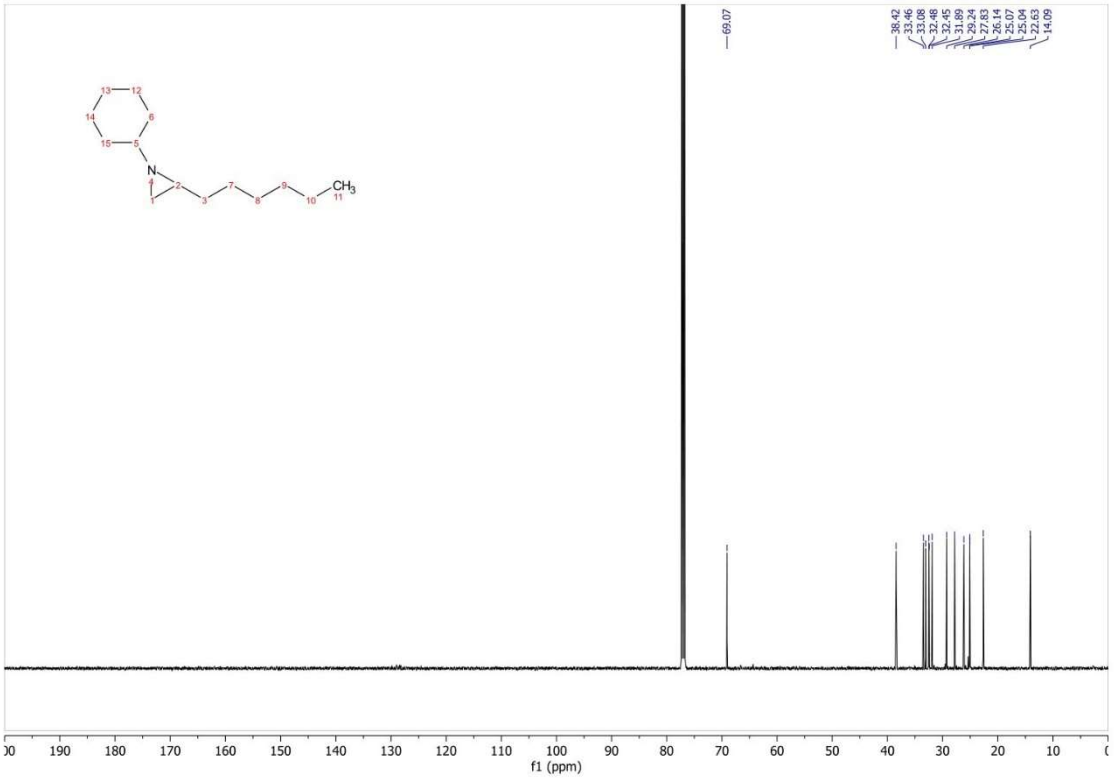
69.07
38.42
33.46
33.08
32.48
32.45
31.89
31.34
27.83
26.14
25.07
25.04
22.63
14.09
f1 (ppm)

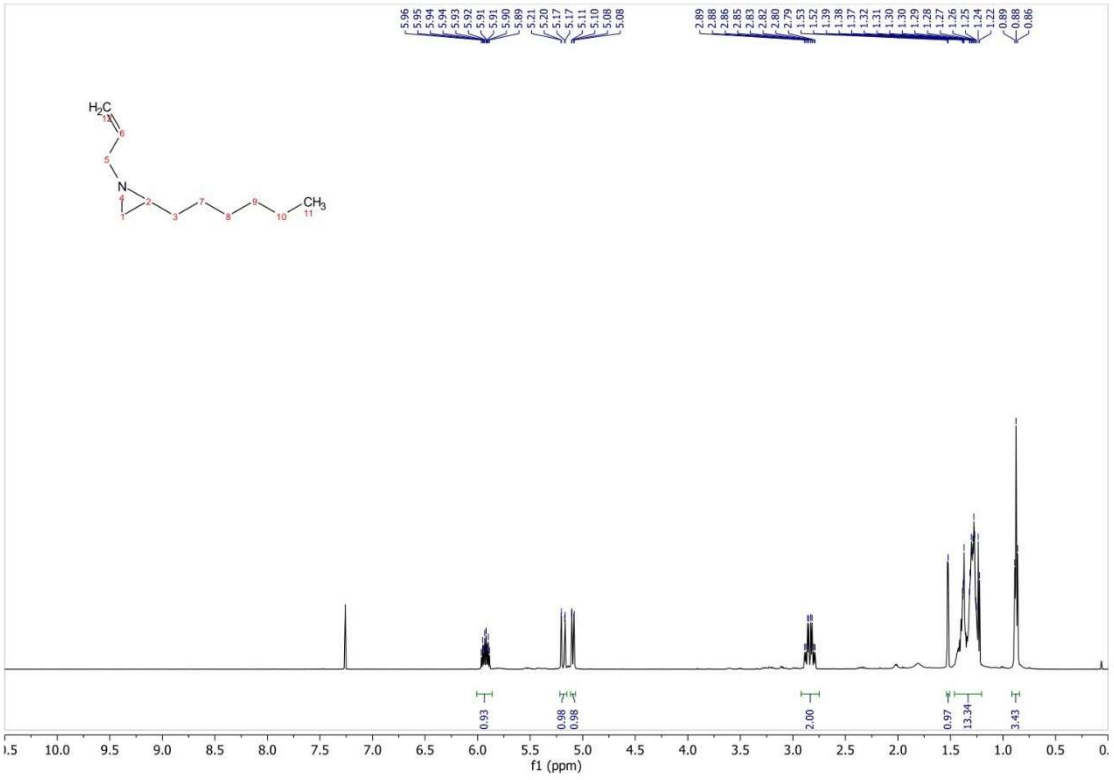
5.96
5.95
5.94
5.94
5.93
5.92
5.91
5.90
5.89
5.21
5.20
5.17
5.17
5.11
5.10
5.08
5.08
2.89
2.88
2.86
2.85
2.83
2.82
2.80
2.79
1.53
1.52
1.39
1.38
1.37
1.32
1.31
1.30
1.30
1.29
1.28
1.27
1.26
1.25
1.24
1.22
0.89
0.88
0.86
0.93
0.98
0.98
2.00
0.97
13.34
3.43
f1 (ppm)

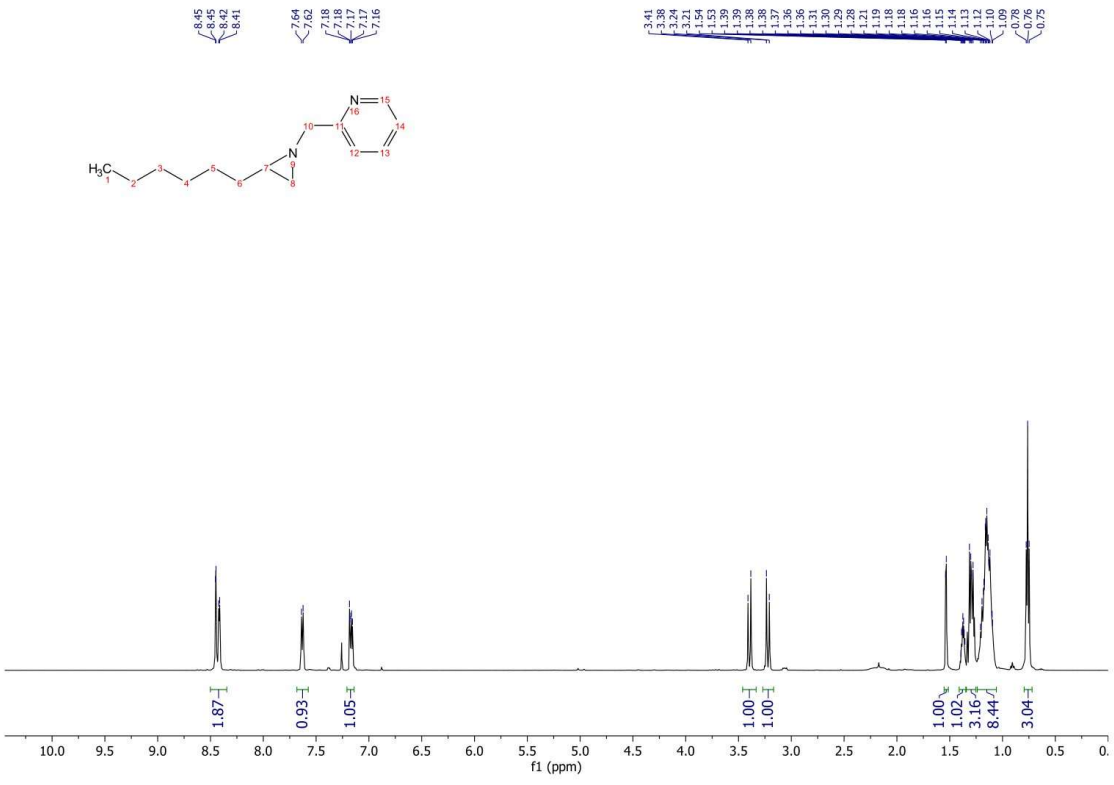
8.45
8.45
8.42
8.41
7.64
7.62
7.18
7.18
7.17
7.17
7.16
3.41
3.38
3.24
3.21
1.54
1.53
1.39
1.39
1.38
1.38
1.37
1.36
1.36
1.31
1.30
1.29
1.28
1.21
1.19
1.18
1.16
1.16
1.15
1.14
1.13
1.12
1.10
1.09
0.78
0.76
0.75
N
15
16
10
11
14
12
13
N
9
H3C
1
2
3
4
5
6
7
8
1.87
0.93
1.05
1.00
1.00
1.00
1.02
3.16
8.44
3.04
10.0
9.5
9.0
8.5
8.0
7.5
7.0
6.5
6.0
5.5
5.0
4.5
4.0
3.5
3.0
2.5
2.0
1.5
1.0
0.5
f1 (ppm)

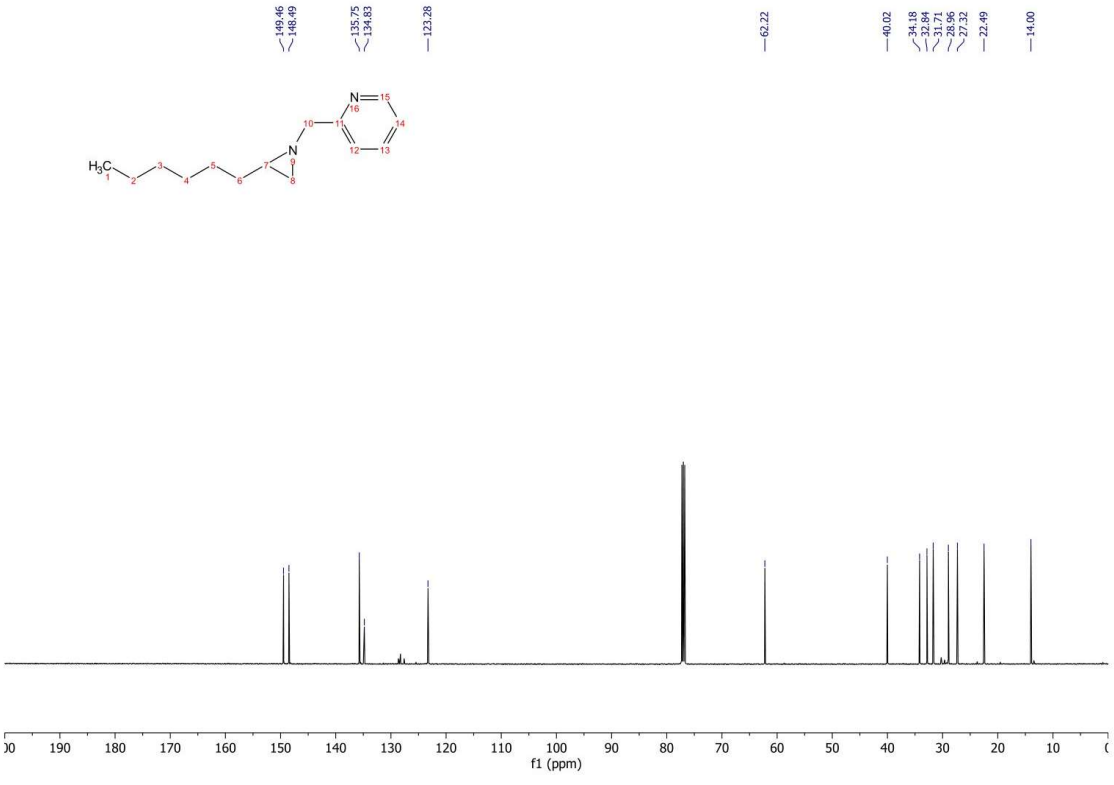
149.46
148.49
135.75
134.83
123.28
62.22
40.02
34.18
32.84
31.71
28.96
27.32
22.49
14.00
N
15
16
10
11
14
12
13
N
9
H3C
1
2
3
4
5
6
7
8
190
180
170
160
150
140
130
120
110
100
90
80
70
60
50
40
30
20
10
f1 (ppm)

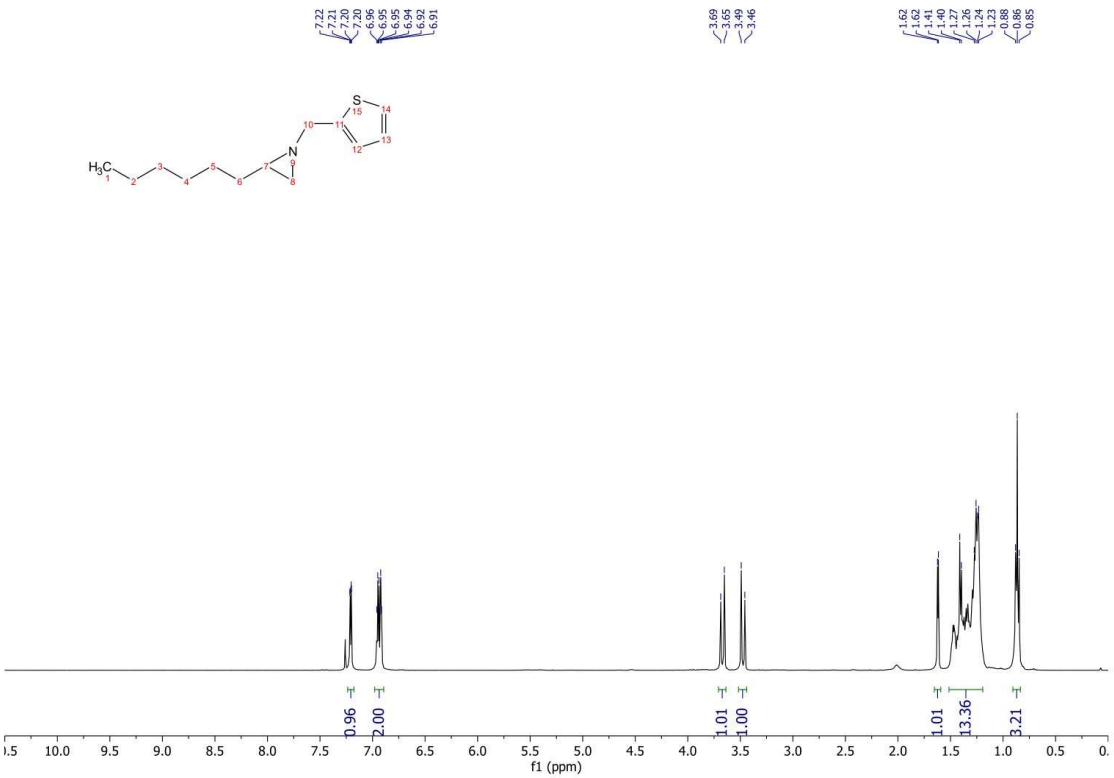
7.22
7.21
7.20
7.20
6.96
6.95
6.95
6.94
6.92
6.91
3.69
3.65
3.49
3.46
1.62
1.62
1.41
1.40
1.27
1.26
1.24
1.23
0.88
0.86
0.85
S
N
H3C
0.96
2.00
1.01
1.00
1.01
13.36
3.21
f1 (ppm)

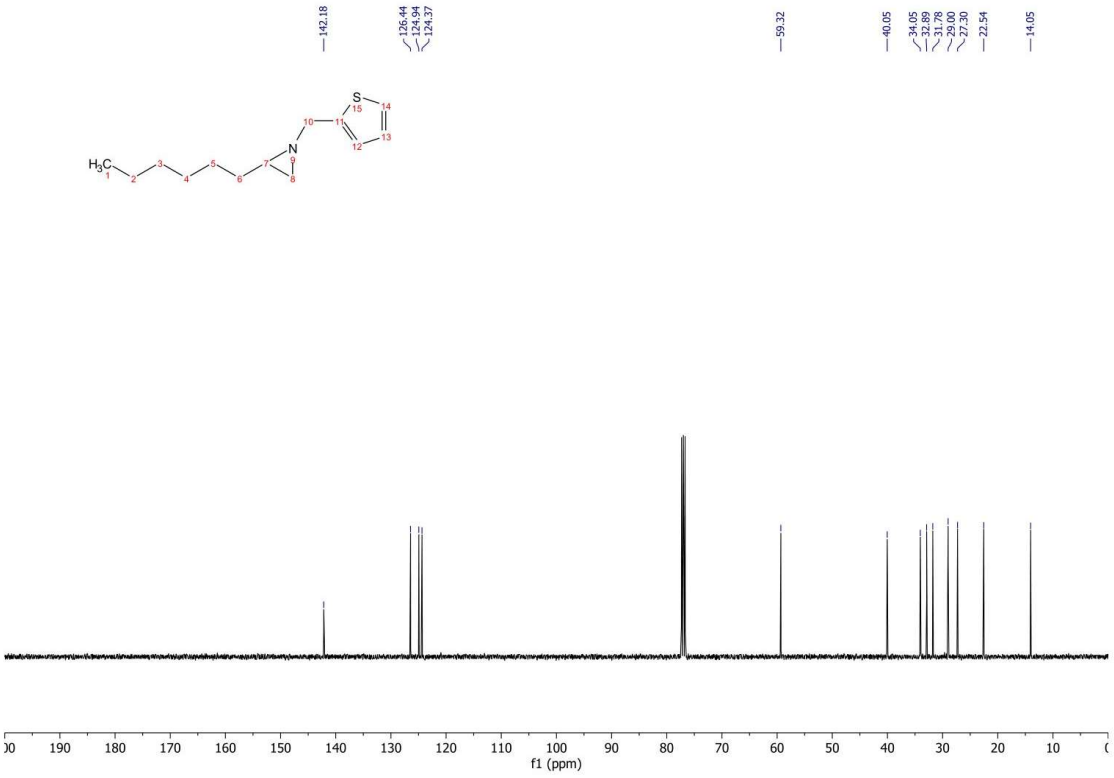
142.18
126.44
124.94
124.37
59.32
40.05
34.05
32.89
31.78
29.00
27.30
22.54
14.05
S
N
H3C
f1 (ppm)

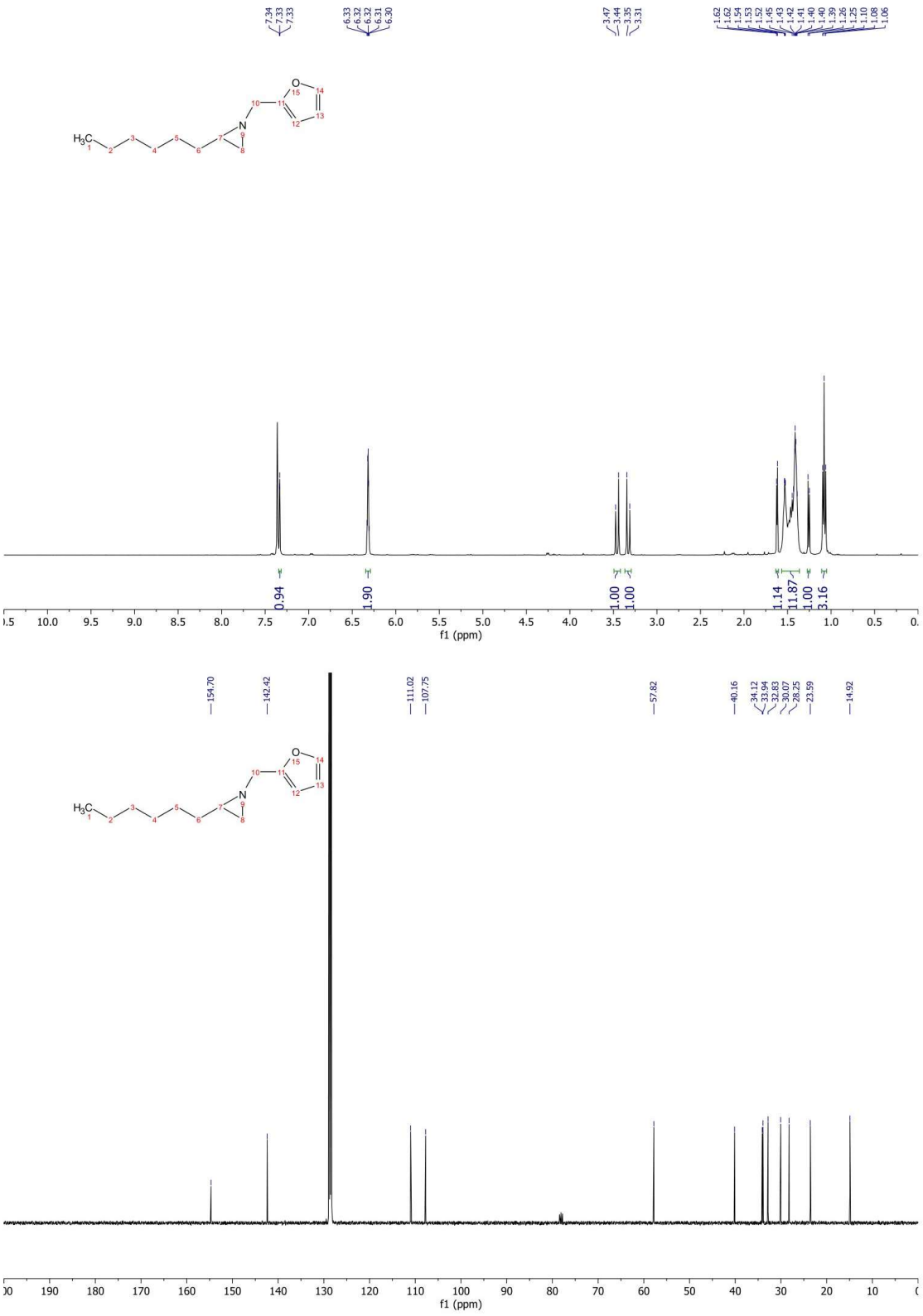
7.34
7.33
7.33
6.33
6.32
6.32
6.31
6.30
3.47
3.44
3.35
3.31
1.62
1.62
1.54
1.53
1.53
1.45
1.43
1.42
1.41
1.40
1.40
1.39
1.26
1.25
1.10
1.08
1.06
0.94
1.90
1.00
1.00
1.14
11.87
1.00
3.16
f1 (ppm)
154.70
142.42
111.02
107.75
57.82
40.16
34.12
33.94
32.83
30.07
28.25
23.59
14.92
f1 (ppm)

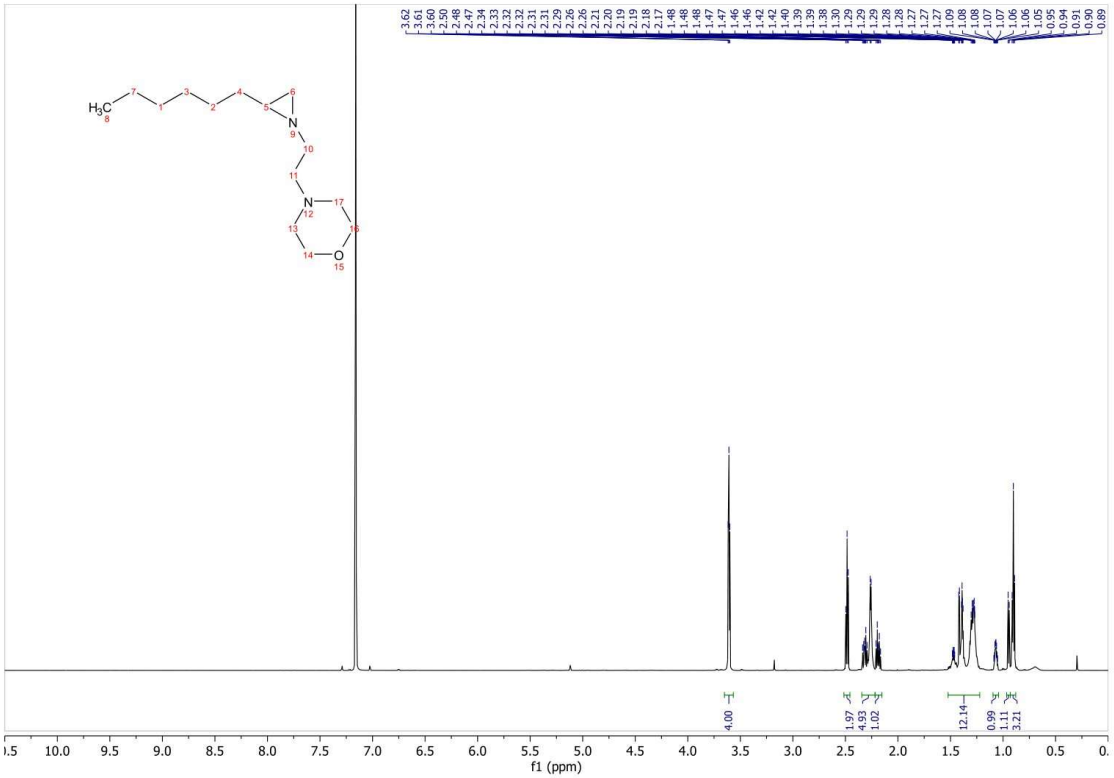
f1 (ppm)

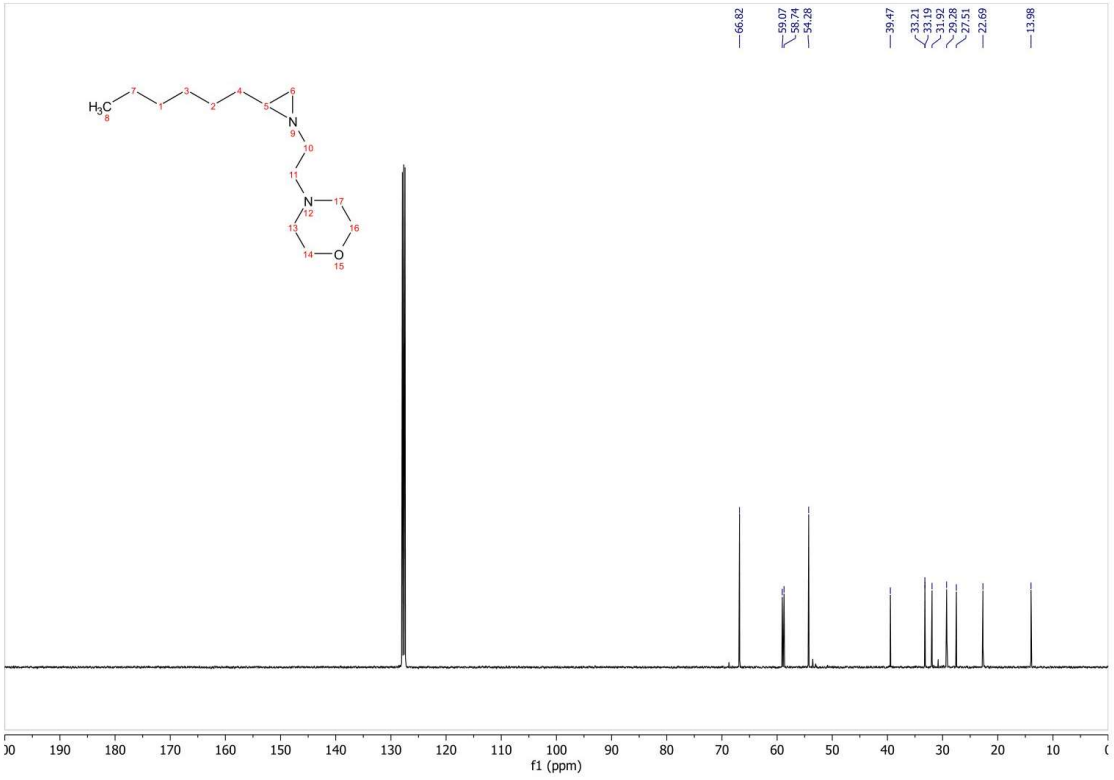
f1 (ppm)

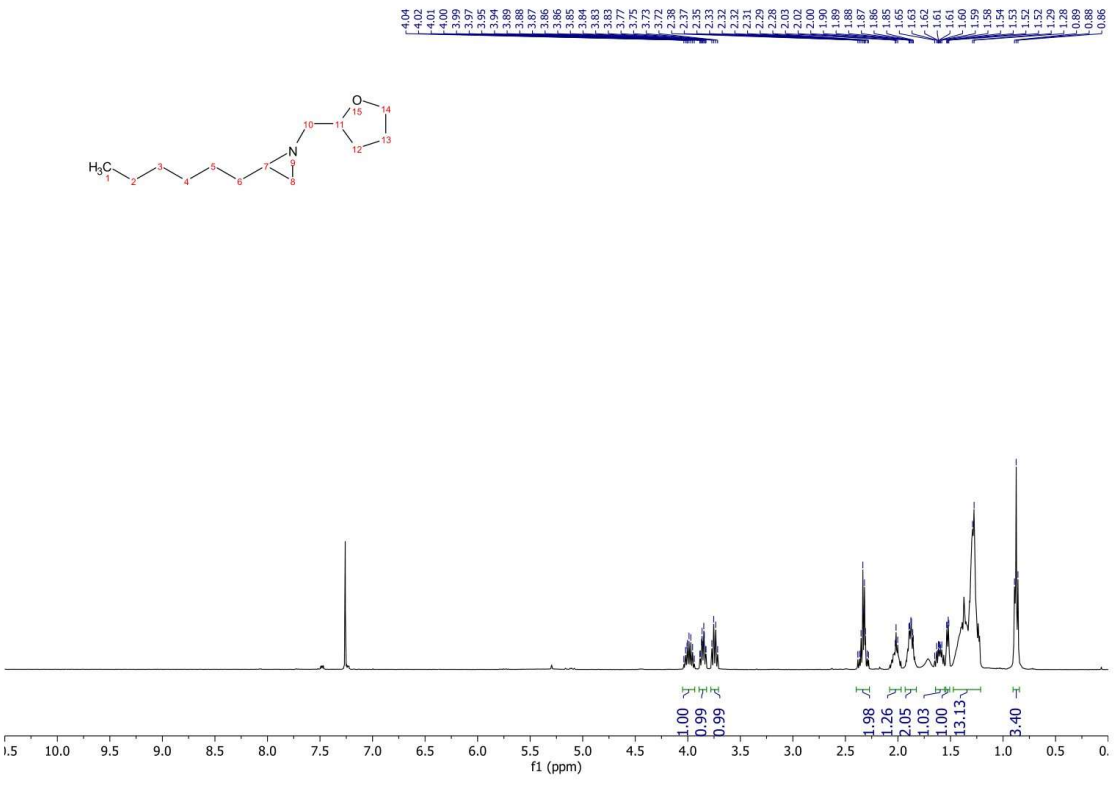
4.04 4.02 4.01 4.00 3.99 3.97 3.95 3.94 3.89 3.88 3.87 3.86 3.86 3.85 3.84 3.83 3.83 3.77 3.75 3.73 3.72 2.38 2.37 2.35 2.33 2.32 2.31 2.29 2.28 2.03 2.02 2.00 1.90 1.89 1.88 1.87 1.86 1.85 1.65 1.63 1.62 1.61 1.61 1.60 1.59 1.58 1.54 1.53 1.52 1.52 1.29 1.28 0.89 0.88 0.86
O 15 14 10 11 12 13 N 9 8 H3C 1 2 3 4 5 6 7
1.00 0.99 0.99 1.98 1.26 2.05 1.03 1.00 13.13 3.40
10.0 9.5 9.0 8.5 8.0 7.5 7.0 6.5 6.0 5.5 5.0 4.5 4.0 3.5 3.0 2.5 2.0 1.5 1.0 0.5
f1 (ppm)

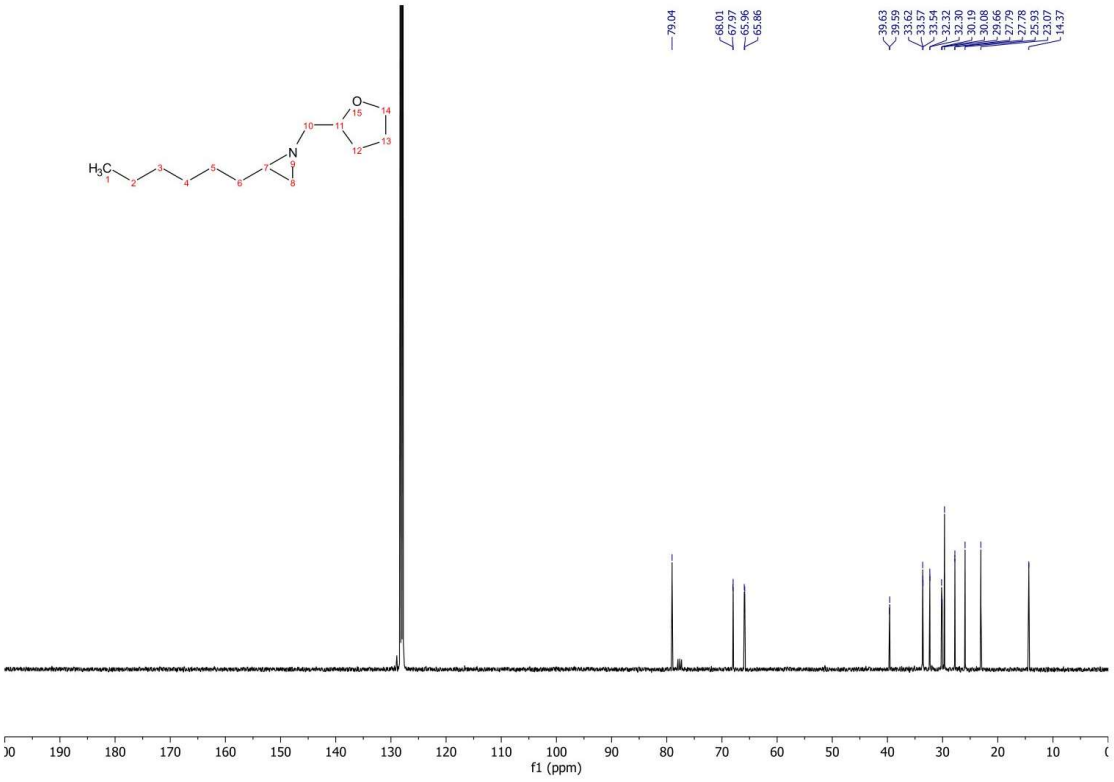
79.04 68.01 67.97 65.96 65.86 39.63 39.59 33.62 33.57 33.54 32.32 32.19 30.19 30.08 29.66 27.79 27.78 25.93 23.07 14.37
O 15 14 10 11 12 13 N 9 8 H3C 1 2 3 4 5 6 7
190 180 170 160 150 140 130 120 110 100 90 80 70 60 50 40 30 20 10
f1 (ppm)

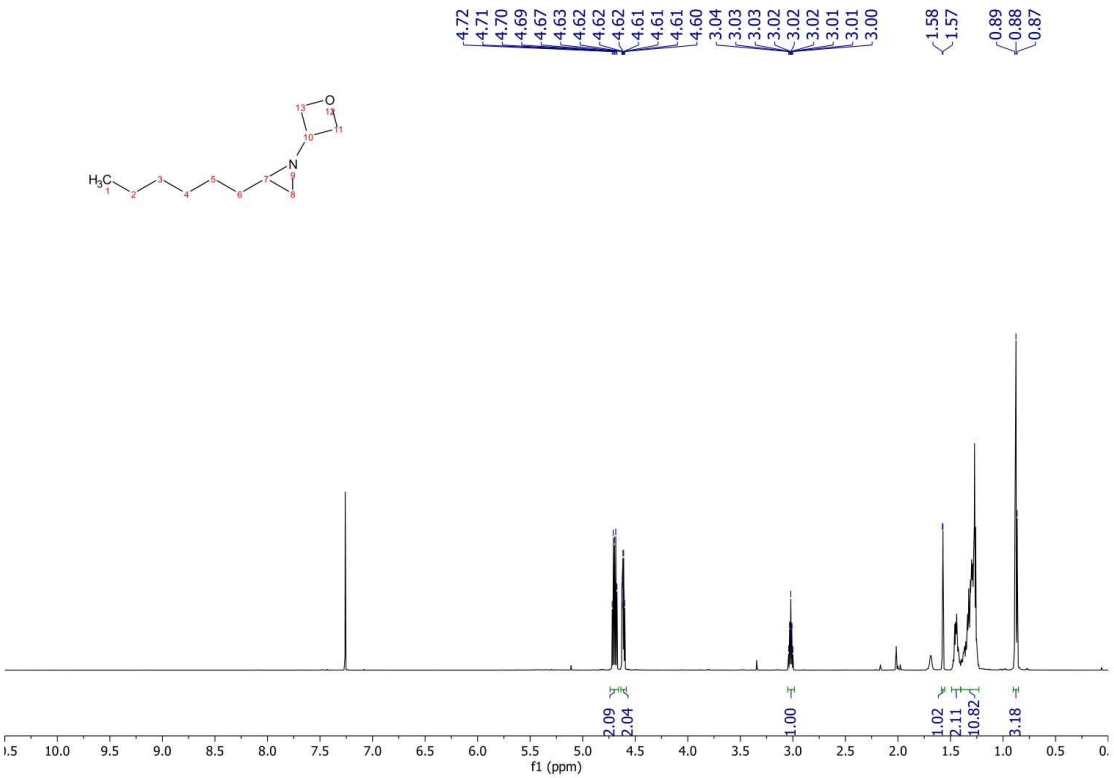
4.72
4.71
4.70
4.69
4.67
4.63
4.62
4.62
4.62
4.61
4.61
4.61
4.60
3.04
3.03
3.03
3.02
3.02
3.02
3.01
3.01
3.00
1.58
1.57
0.89
0.88
0.87
2.09
2.04
1.00
1.02
2.11
10.82
3.18
f1 (ppm)

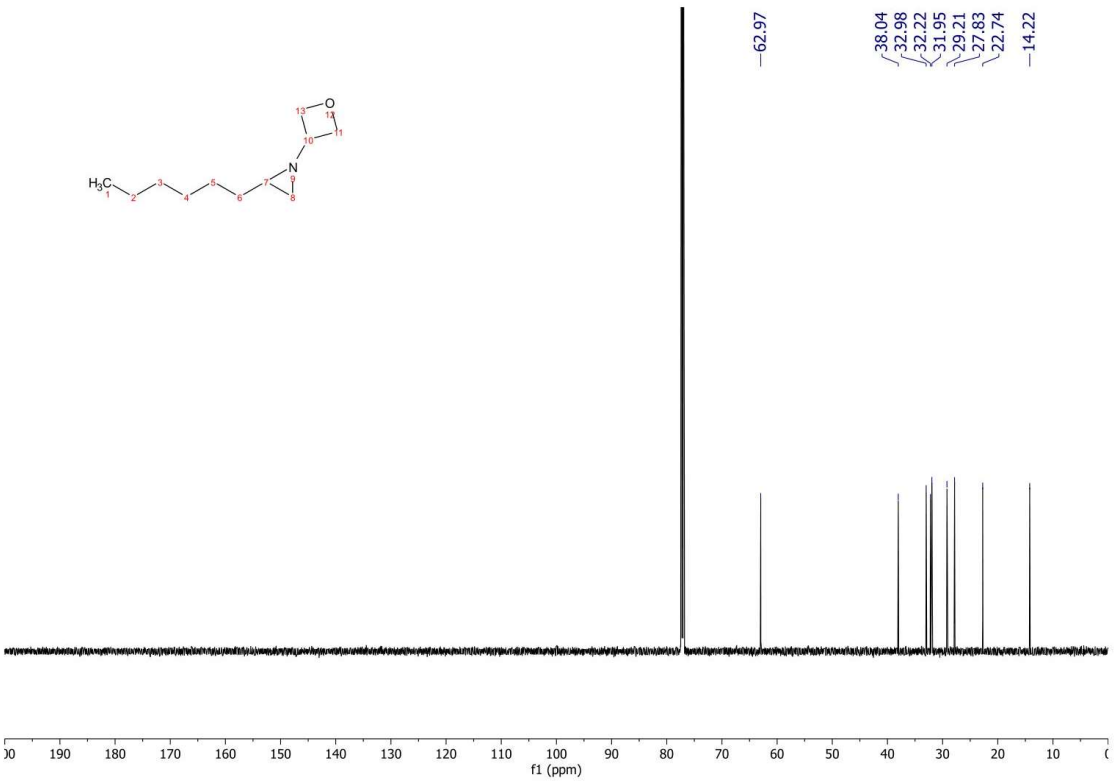
62.97
38.04
32.98
32.22
31.95
29.21
27.83
22.74
14.22
f1 (ppm)

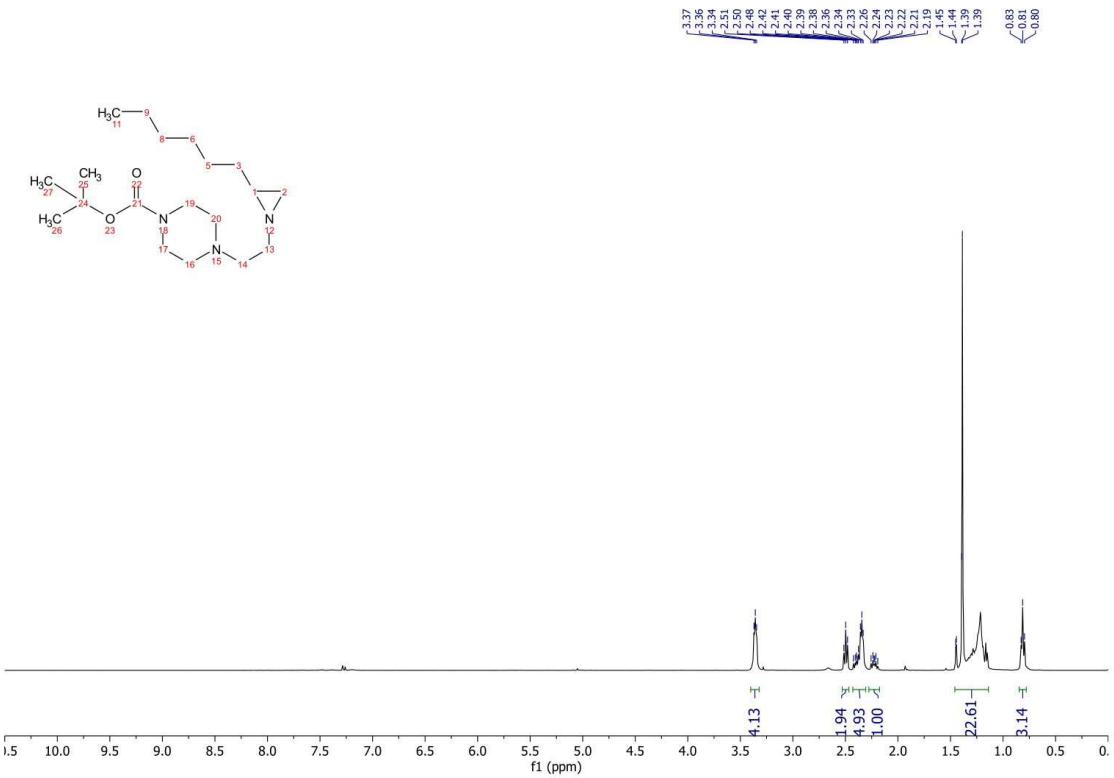
3.37
3.36
3.34
2.51
2.50
2.48
2.42
2.41
2.40
2.39
2.38
2.36
2.34
2.33
2.26
2.24
2.23
2.22
2.21
2.19
1.45
1.44
1.39
1.39
0.83
0.81
0.80
4.13
1.94
4.93
1.00
22.61
3.14
f1 (ppm)

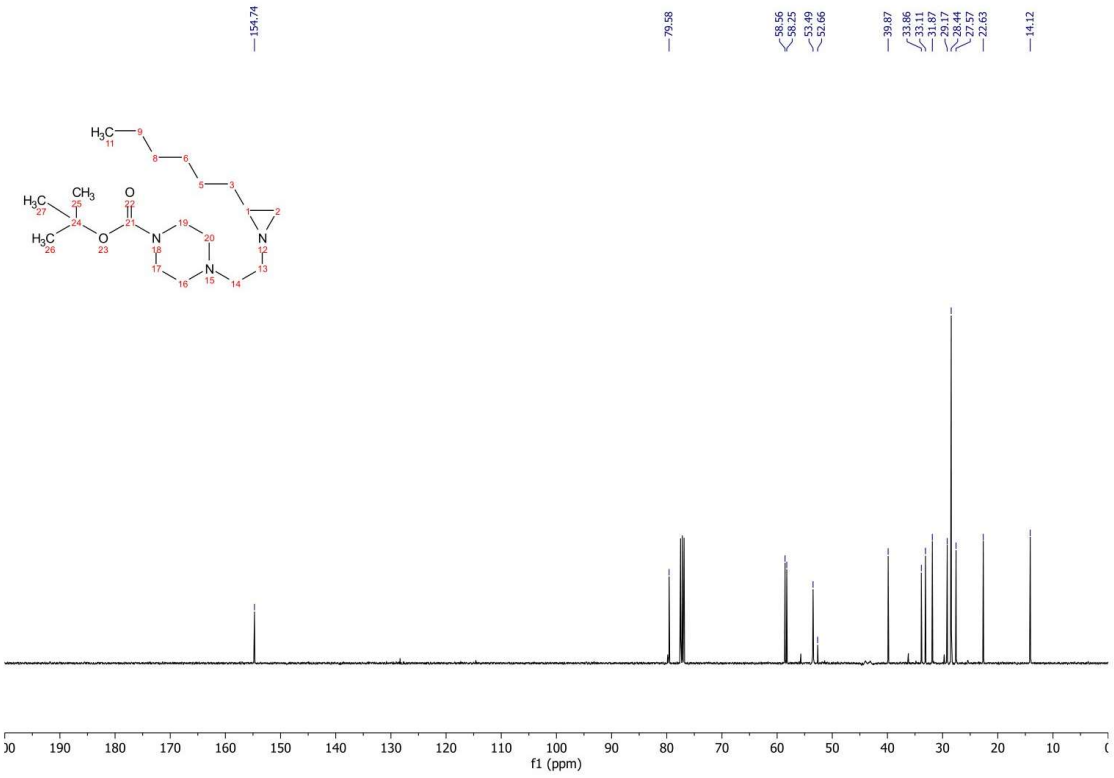
154.74
79.58
58.56
58.25
53.49
52.66
39.87
33.86
33.11
31.67
29.37
28.44
27.57
22.63
14.12
f1 (ppm)

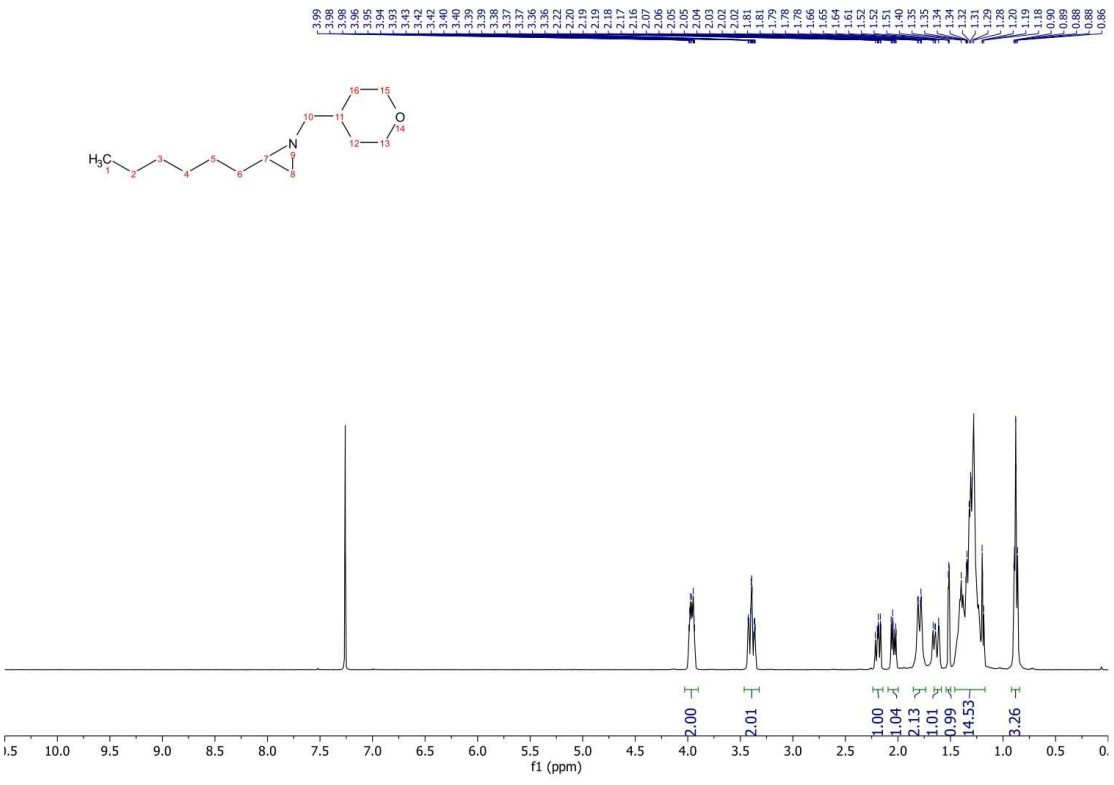
f1 (ppm)

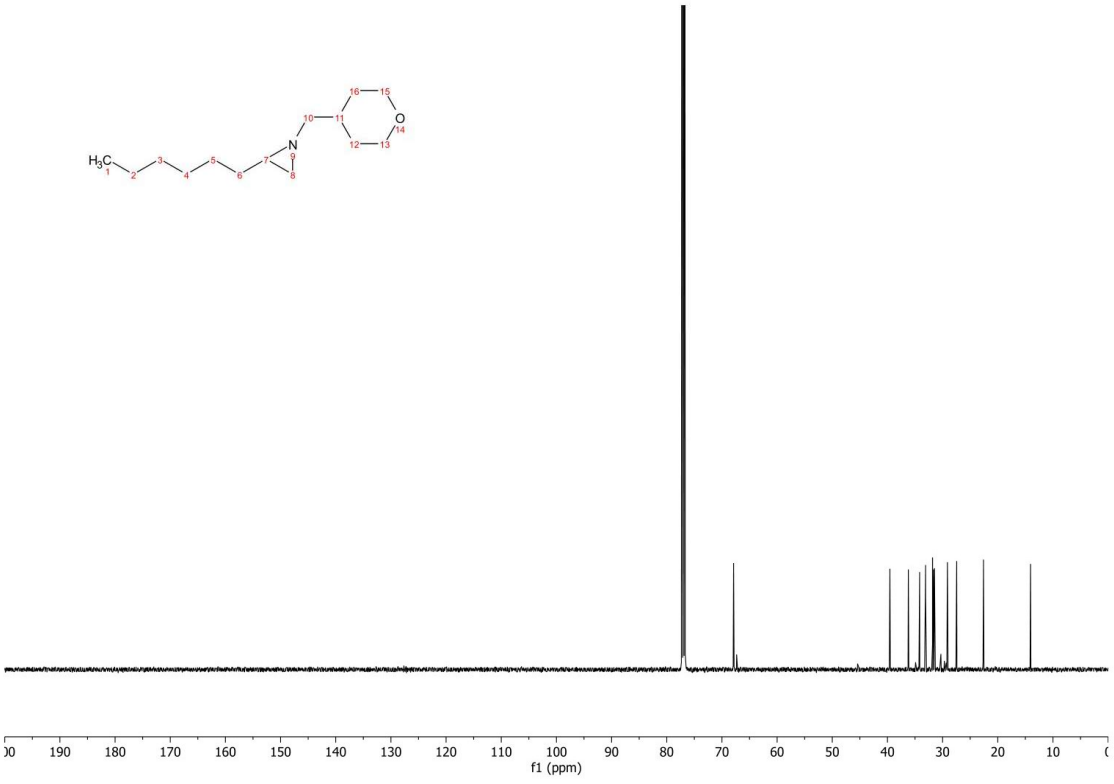
f1 (ppm)

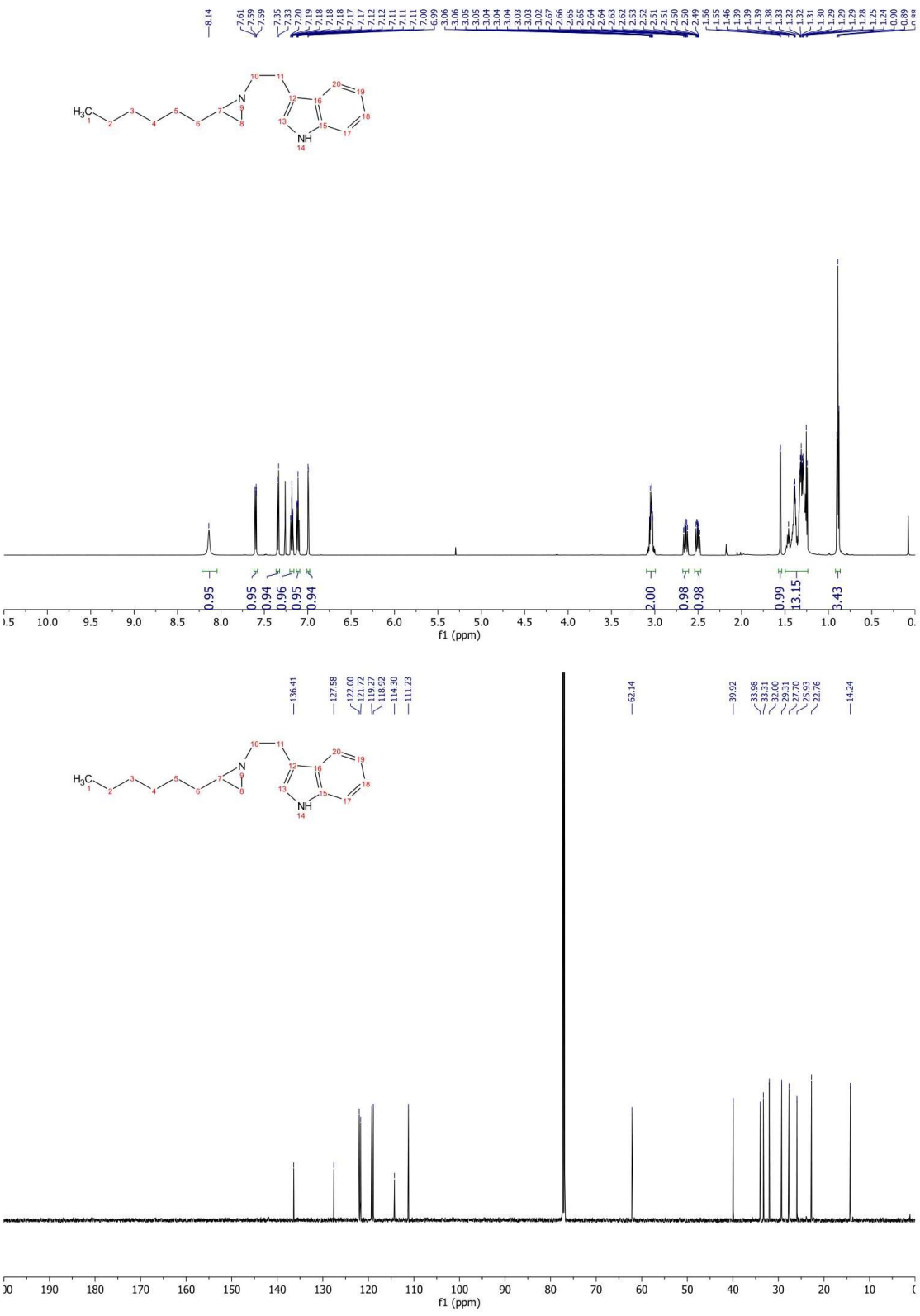
8.14
7.61
7.59
7.59
7.35
7.33
7.20
7.19
7.18
7.18
7.18
7.17
7.17
7.12
7.12
7.11
7.11
7.11
7.00
6.99
3.06
3.06
3.05
3.05
3.04
3.04
3.04
3.03
3.03
3.02
2.67
2.66
2.65
2.65
2.64
2.64
2.63
2.62
2.53
2.52
2.51
2.51
2.50
2.50
2.49
1.56
1.55
1.46
1.39
1.39
1.39
1.39
1.38
1.33
1.32
1.32
1.31
1.30
1.29
1.29
1.29
1.28
1.25
1.24
0.90
0.89
H3C
N
NH
0.95
0.95
0.94
0.96
0.95
0.94
2.00
0.98
0.98
0.99
13.15
3.43
f1 (ppm)
136.41
127.58
122.00
121.72
119.27
118.92
114.30
111.23
62.14
39.92
33.98
33.31
32.00
29.31
27.70
25.93
22.76
14.24
f1 (ppm)

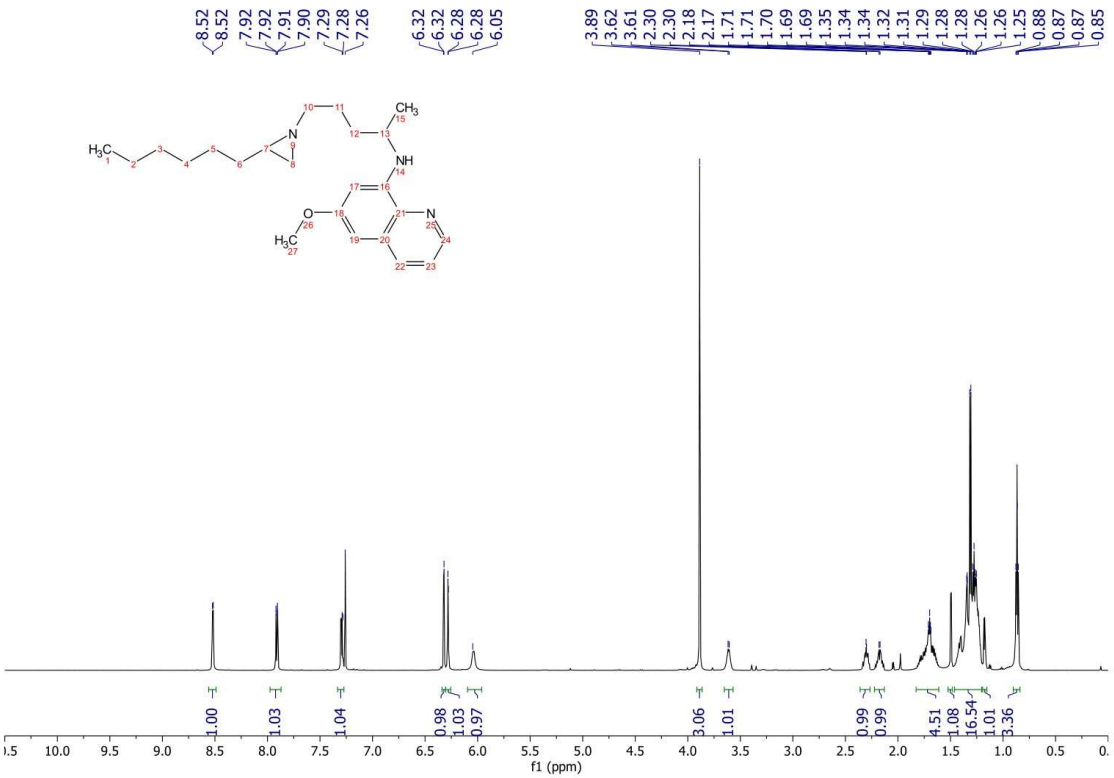
8.52
8.52
7.92
7.92
7.91
7.90
7.29
7.28
7.26
6.32
6.32
6.28
6.28
6.05
3.89
3.62
3.61
2.30
2.18
2.17
1.71
1.71
1.70
1.69
1.69
1.35
1.34
1.34
1.32
1.31
1.29
1.28
1.28
1.26
1.26
1.25
0.88
0.87
0.87
0.85
1.00
1.03
1.04
0.98
1.03
0.97
3.06
1.01
0.99
0.99
4.51
1.08
16.54
1.01
3.36
f1 (ppm)

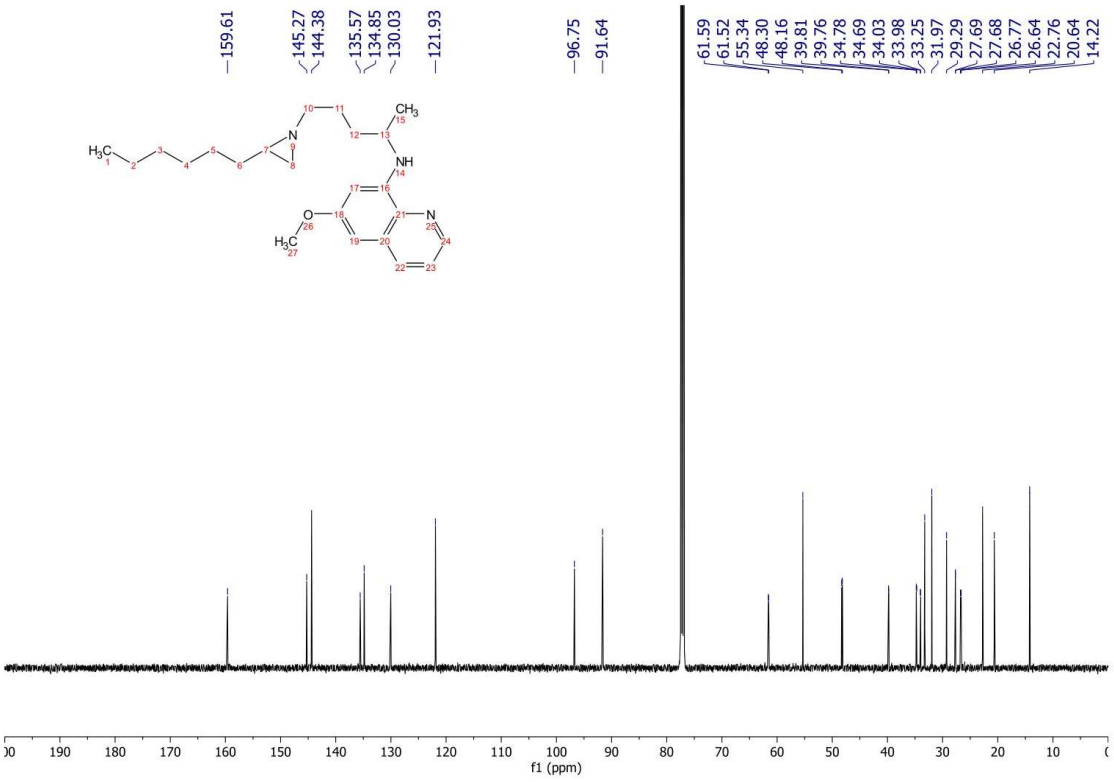
159.61
145.27
144.38
135.57
134.85
130.03
121.93
96.75
91.64
61.59
61.52
55.34
48.30
48.16
39.81
39.76
34.78
34.69
34.03
33.98
33.25
31.97
29.29
27.69
27.68
26.77
26.64
22.76
20.64
14.22
f1 (ppm)

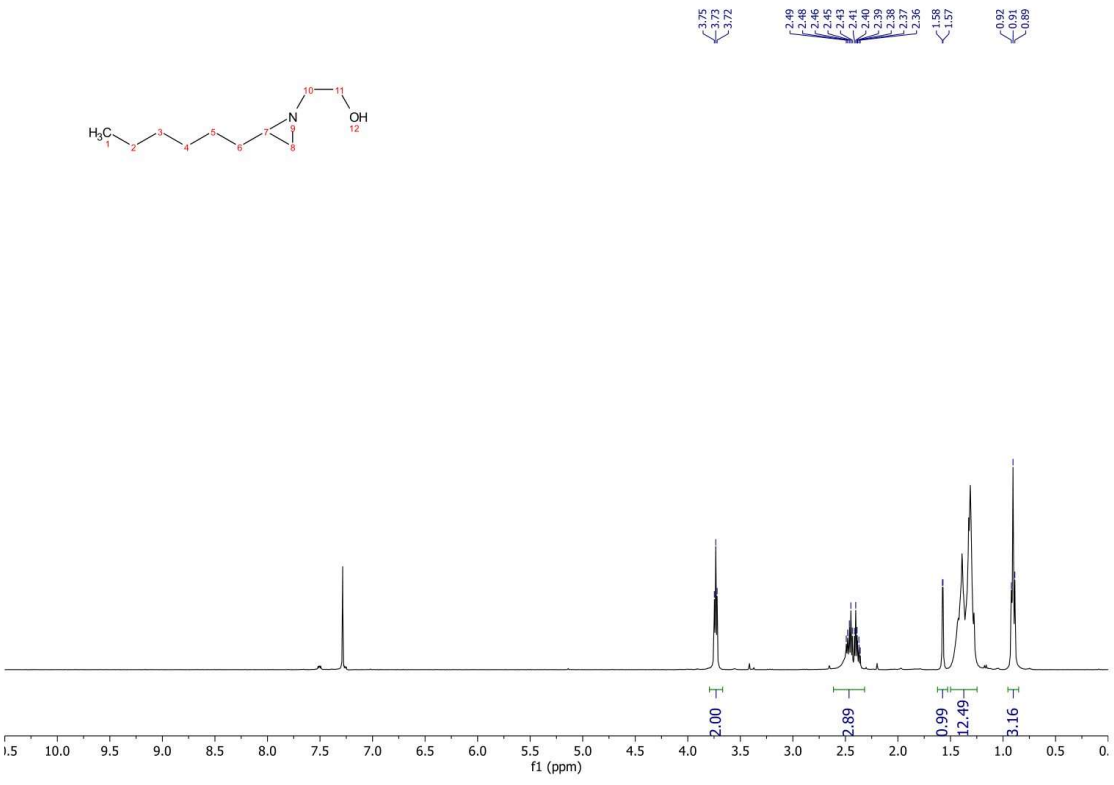
3.75
3.73
3.72
2.49
2.48
2.46
2.45
2.43
2.41
2.40
2.39
2.38
2.37
2.36
1.58
1.57
0.92
0.91
0.89
H3C
N
OH
2.00
2.89
0.99
12.49
3.16
f1 (ppm)

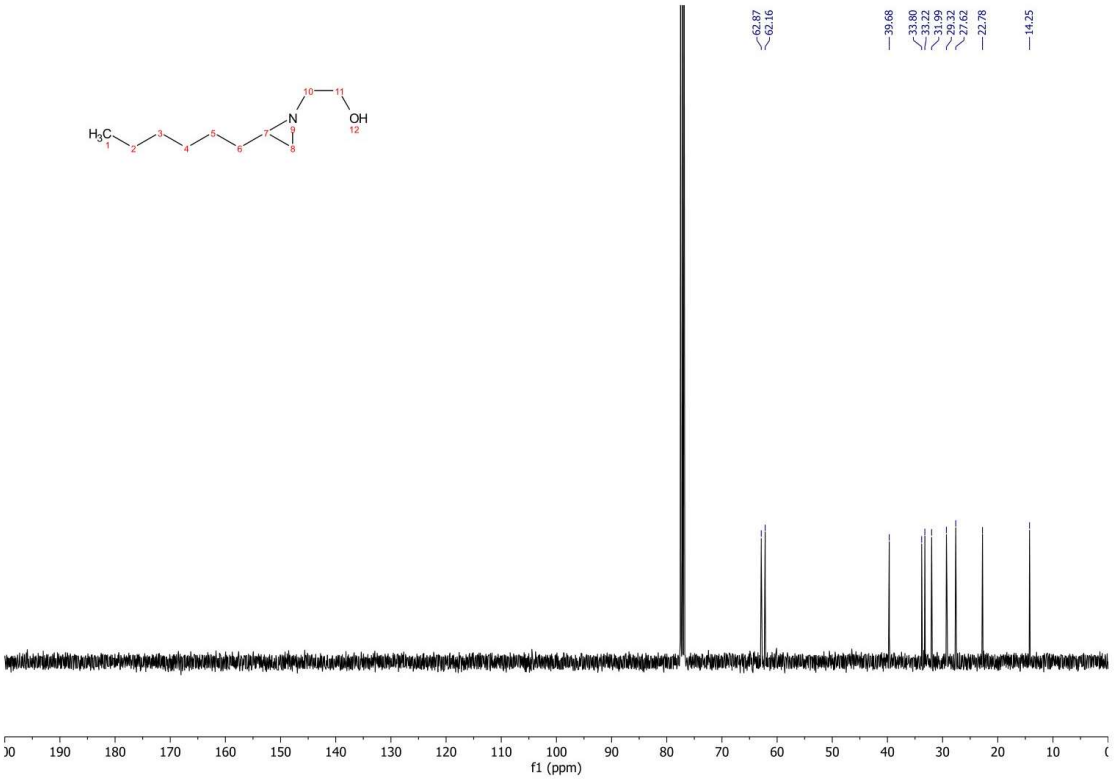
62.87
62.16
39.68
33.80
33.22
31.99
29.32
27.62
22.78
14.25
H3C
N
OH
f1 (ppm)

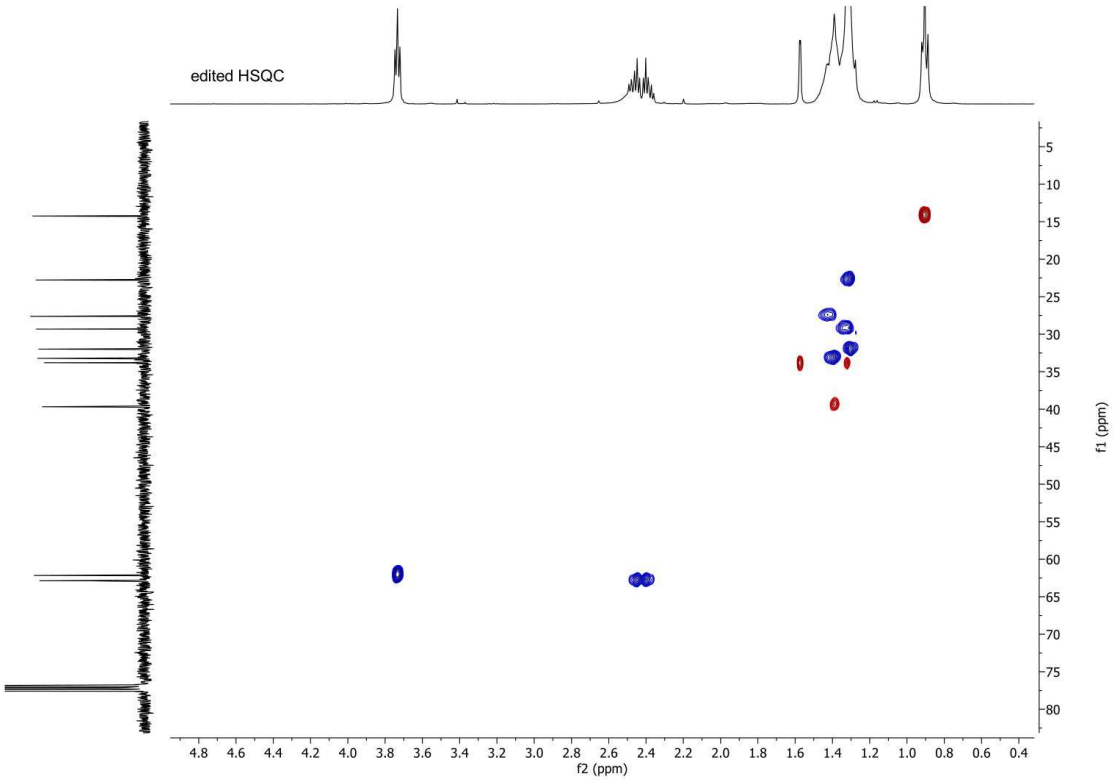
edited HSQC
f2 (ppm)
f1 (ppm)

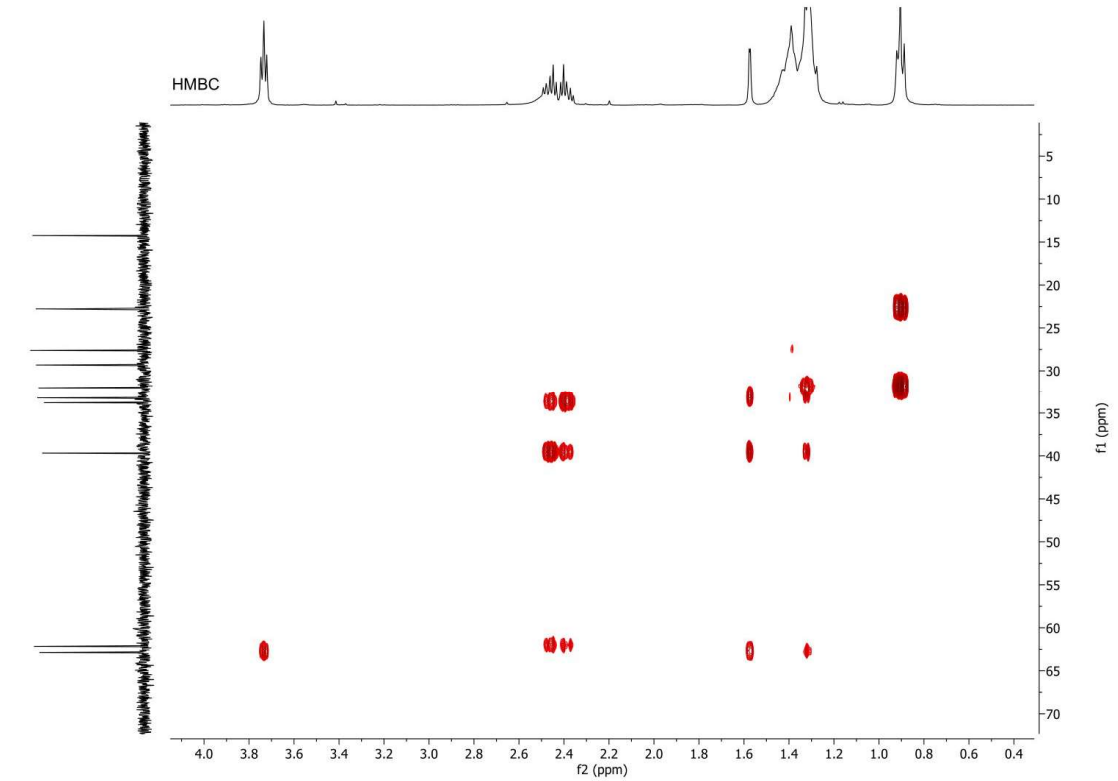
HMBC
f2 (ppm)
f1 (ppm)

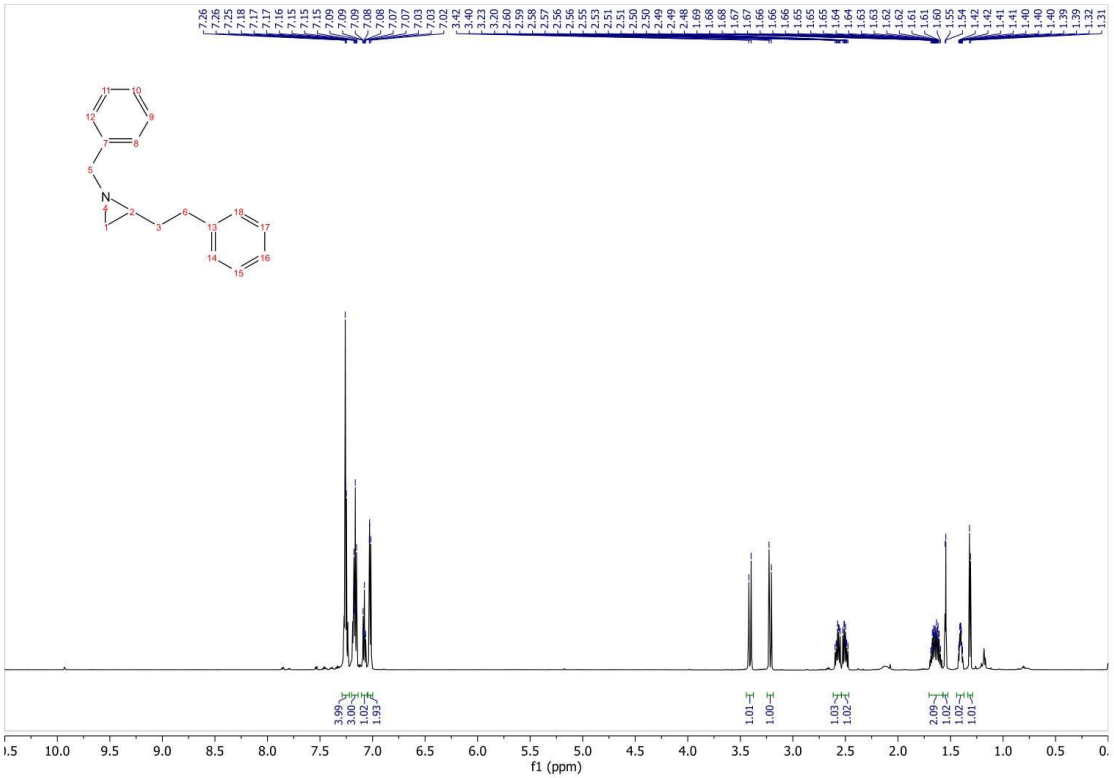
f1 (ppm)

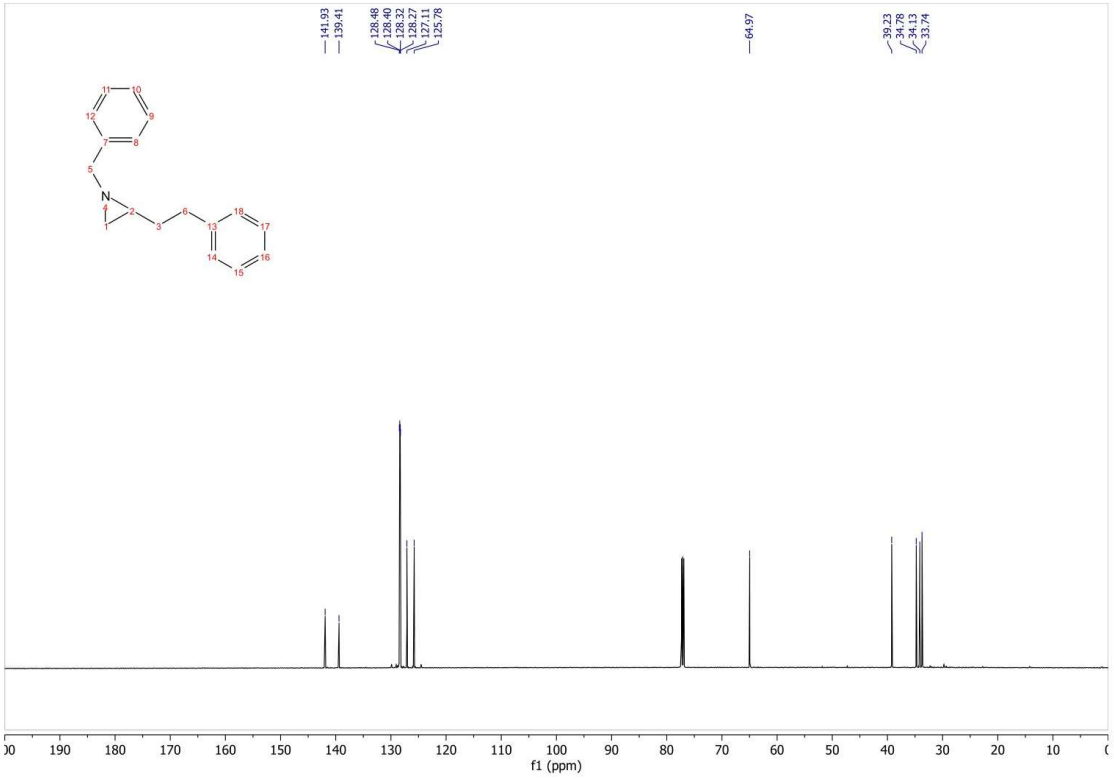
f1 (ppm)

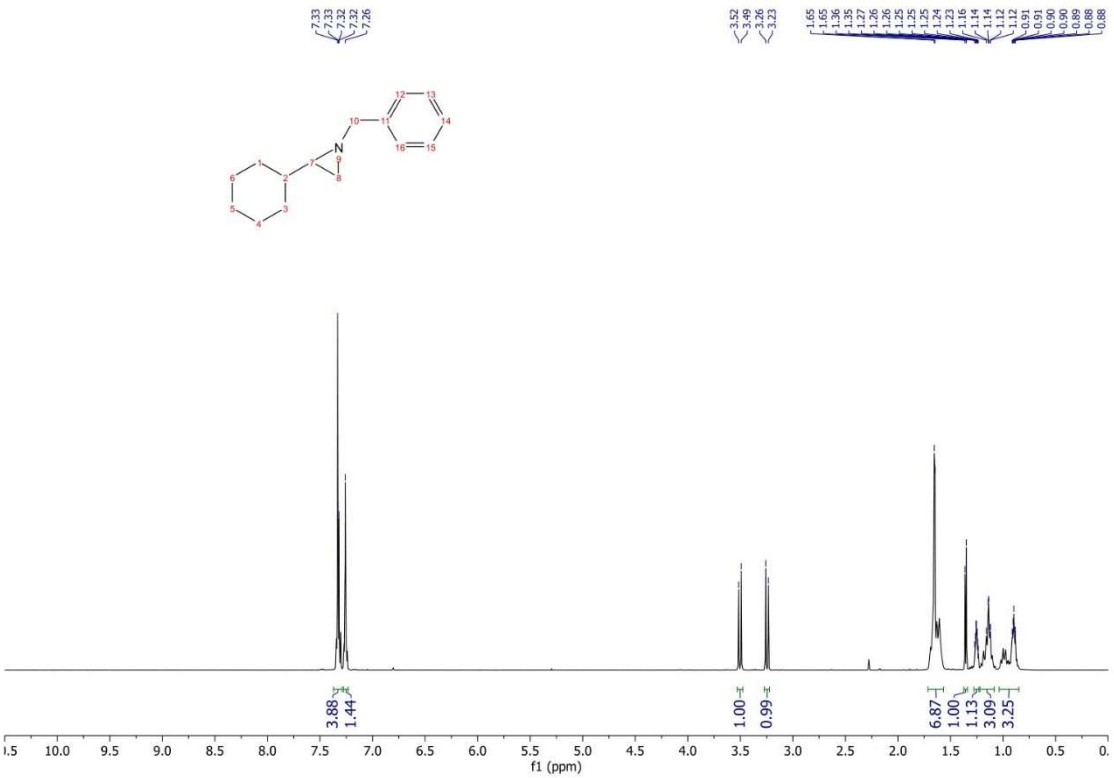
7.33
7.33
7.32
7.32
7.26
3.52
3.49
3.26
3.23
1.65
1.65
1.36
1.35
1.27
1.26
1.26
1.25
1.25
1.25
1.24
1.23
1.16
1.14
1.14
1.12
1.12
0.91
0.91
0.90
0.90
0.89
0.88
0.88
3.88
1.44
1.00
0.99
6.87
1.00
1.13
3.09
3.25
f1 (ppm)

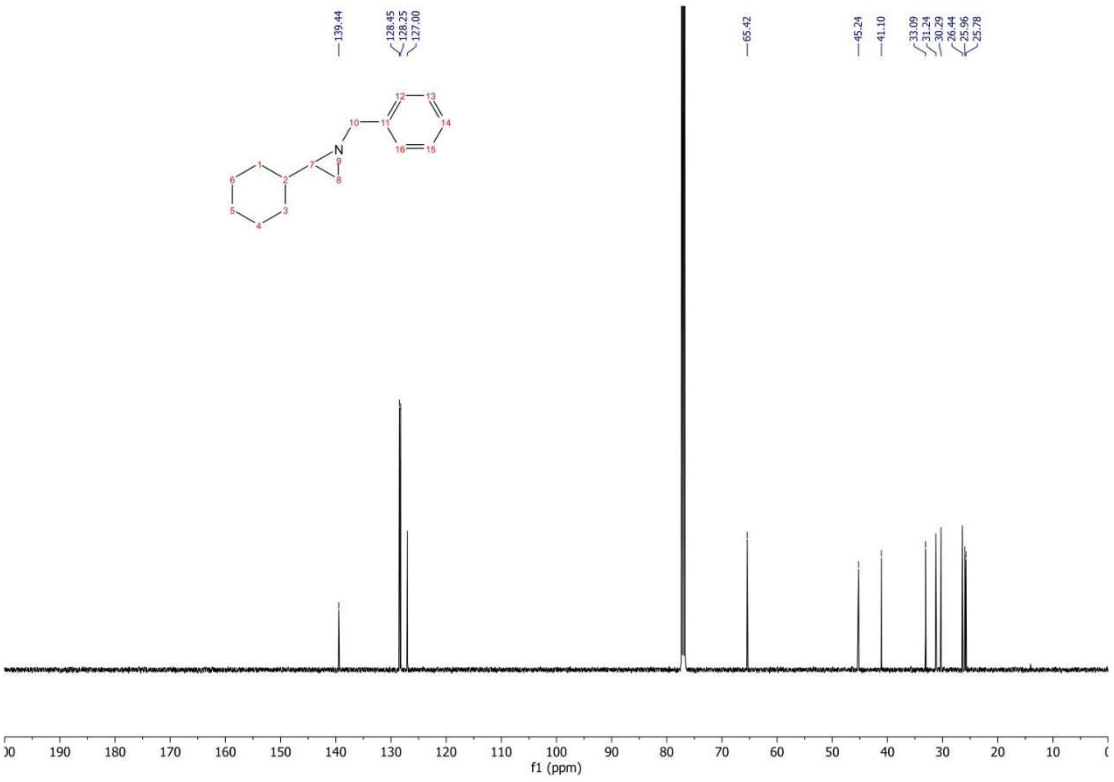
139.44
128.45
128.25
127.00
65.42
45.24
41.10
33.09
31.24
30.29
26.44
25.96
25.78
f1 (ppm)

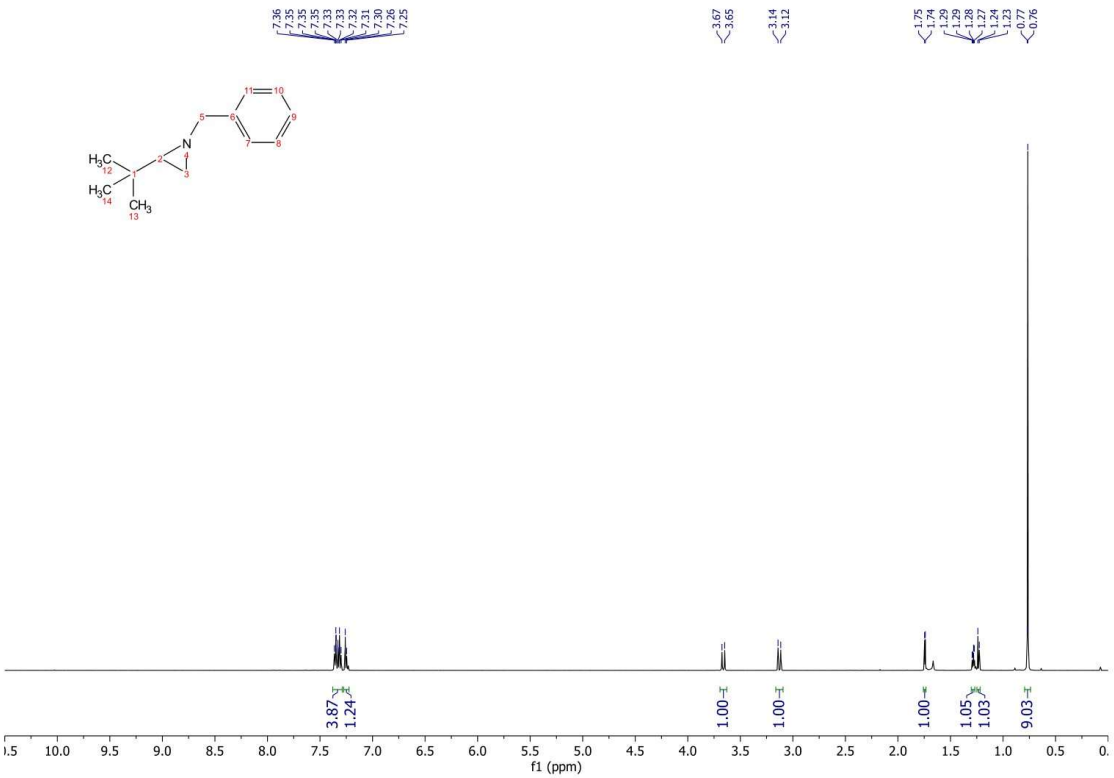
7.36
7.35
7.35
7.35
7.33
7.32
7.31
7.30
7.26
7.25
3.67
3.65
3.14
3.12
1.75
1.74
1.29
1.28
1.27
1.24
1.23
0.77
0.76
3.87
1.24
1.00
1.00
1.00
1.05
1.03
9.03
f1 (ppm)

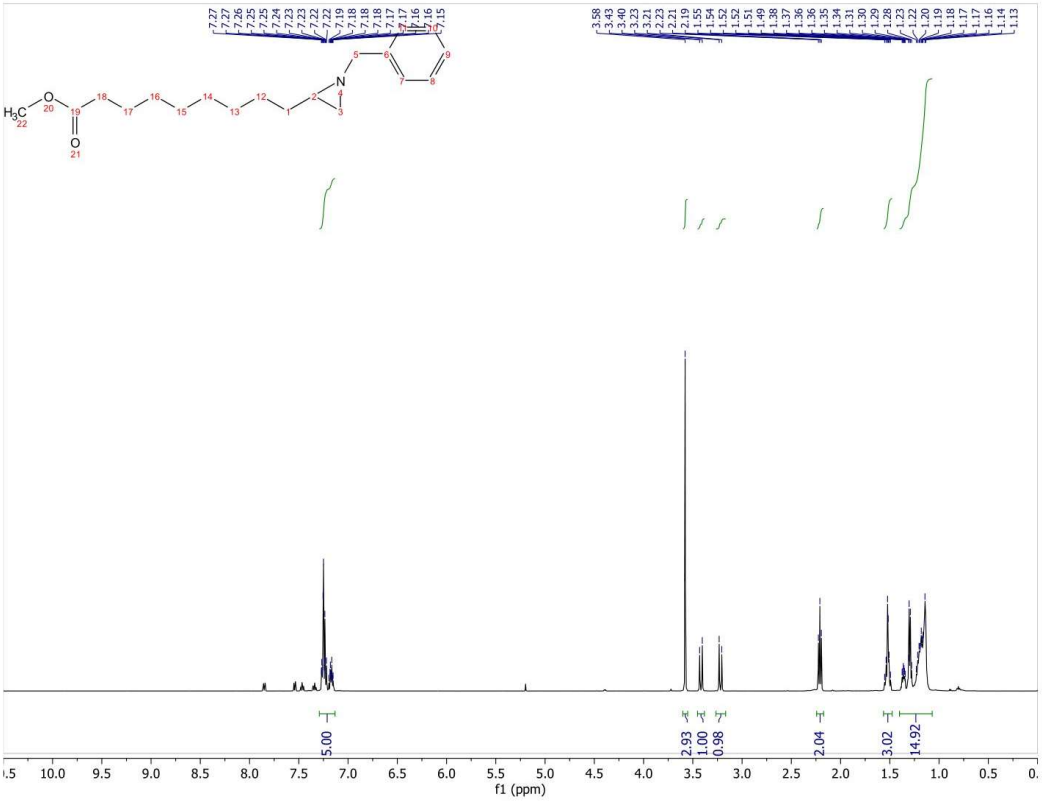
5.00
2.93
1.00
0.98
2.04
3.02
14.92
f1 (ppm)

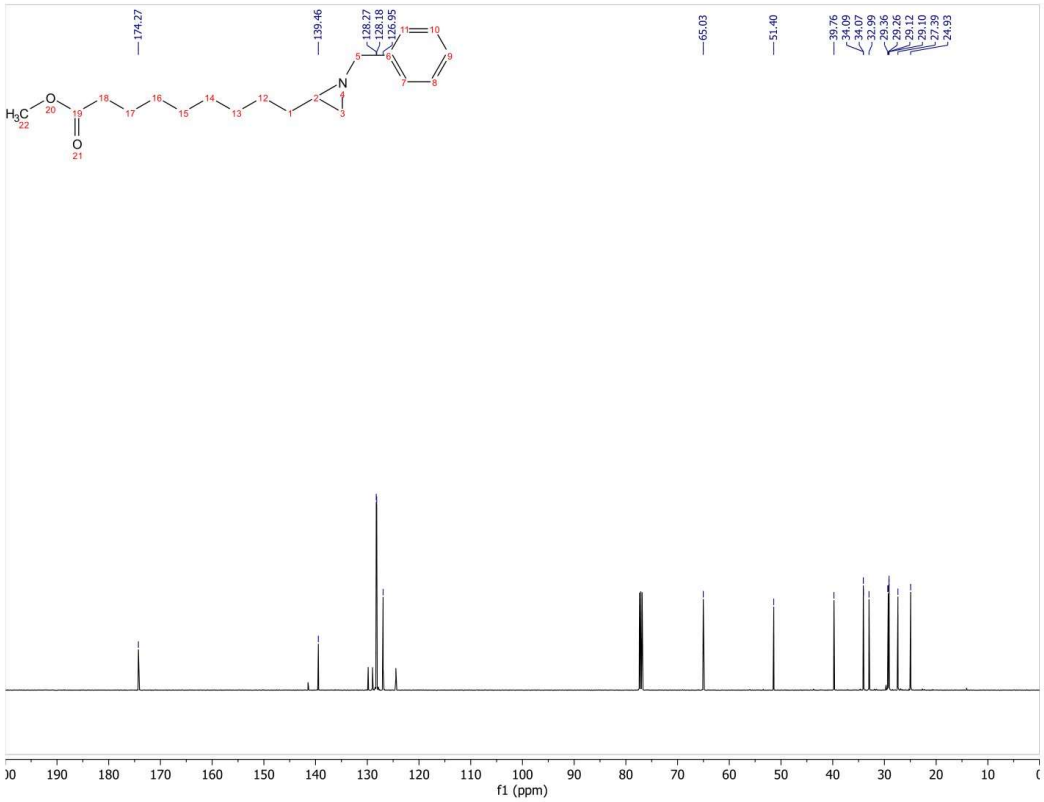
174.27
139.46
128.27
128.18
126.55
65.03
51.40
39.76
34.09
34.07
32.99
29.36
29.26
29.12
29.10
27.39
24.93
f1 (ppm)

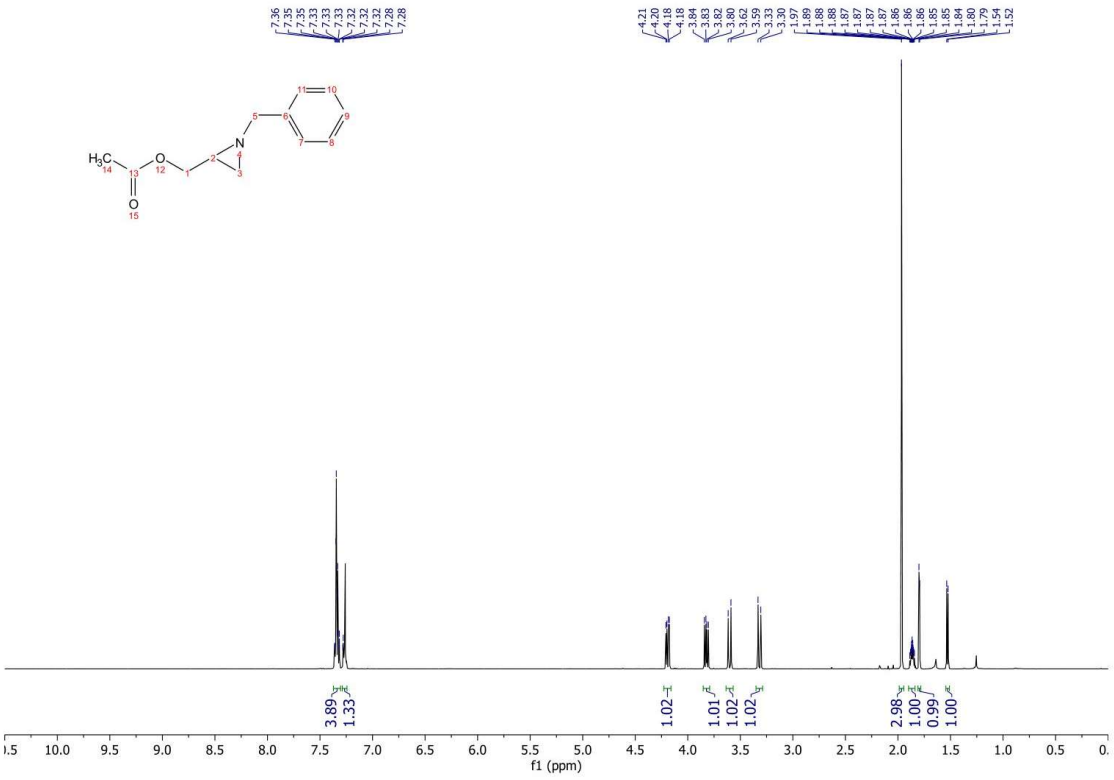
7.36
7.35
7.35
7.33
7.33
7.33
7.32
7.32
7.32
7.28
7.28
4.21
4.20
4.18
4.18
3.84
3.83
3.82
3.80
3.62
3.59
3.33
3.30
1.97
1.89
1.88
1.88
1.87
1.87
1.87
1.87
1.87
1.86
1.86
1.86
1.85
1.85
1.84
1.80
1.79
1.54
1.52
3.89
1.33
1.02
1.01
1.02
1.02
2.98
1.00
0.99
1.00
f1 (ppm)

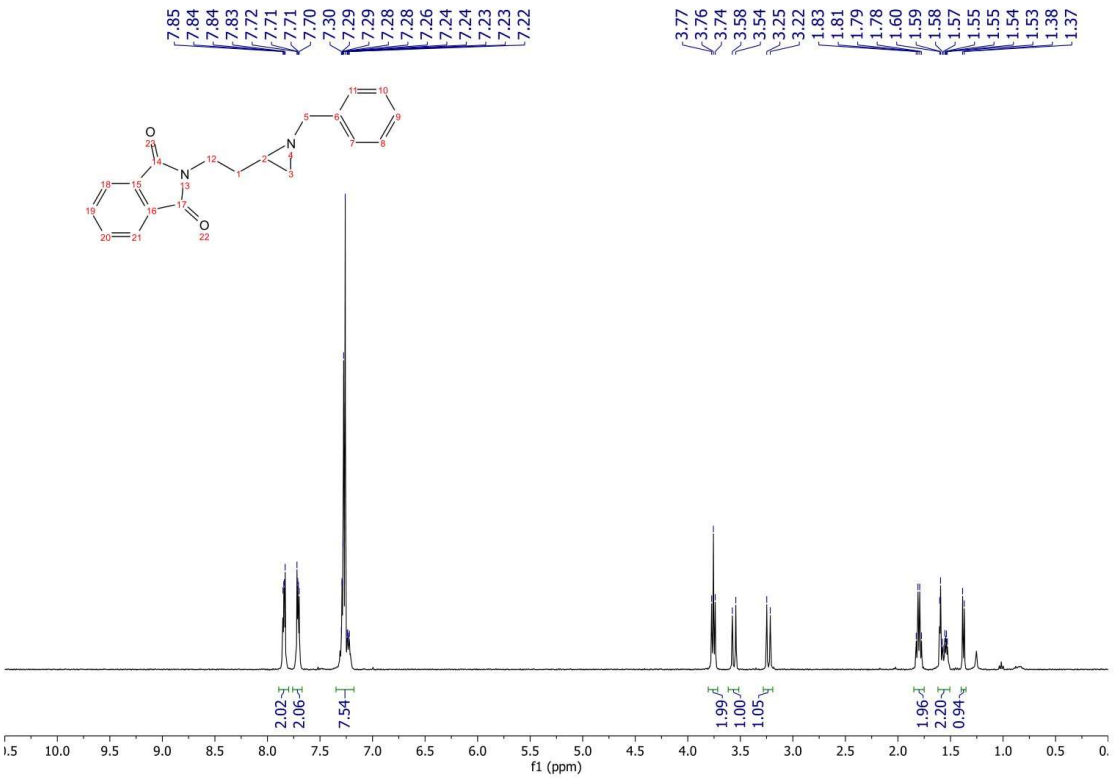
7.85
7.84
7.84
7.83
7.72
7.71
7.71
7.70
7.30
7.29
7.29
7.28
7.28
7.26
7.24
7.24
7.23
7.23
7.22
3.77
3.76
3.74
3.58
3.54
3.25
3.22
1.83
1.81
1.79
1.78
1.60
1.59
1.58
1.57
1.55
1.55
1.54
1.53
1.38
1.37
2.02
2.06
7.54
1.99
1.00
1.05
1.96
2.20
0.94
f1 (ppm)

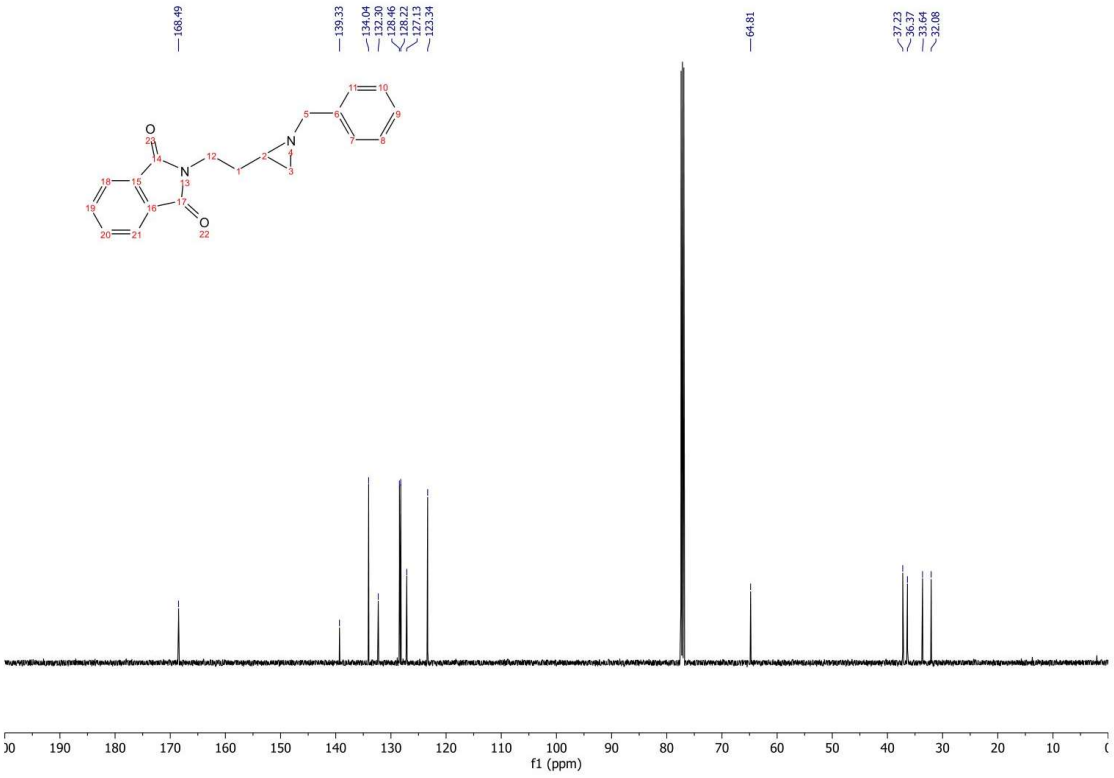
168.49
139.33
134.04
132.30
128.46
128.22
127.13
123.34
64.81
37.23
36.37
33.64
32.08
f1 (ppm)

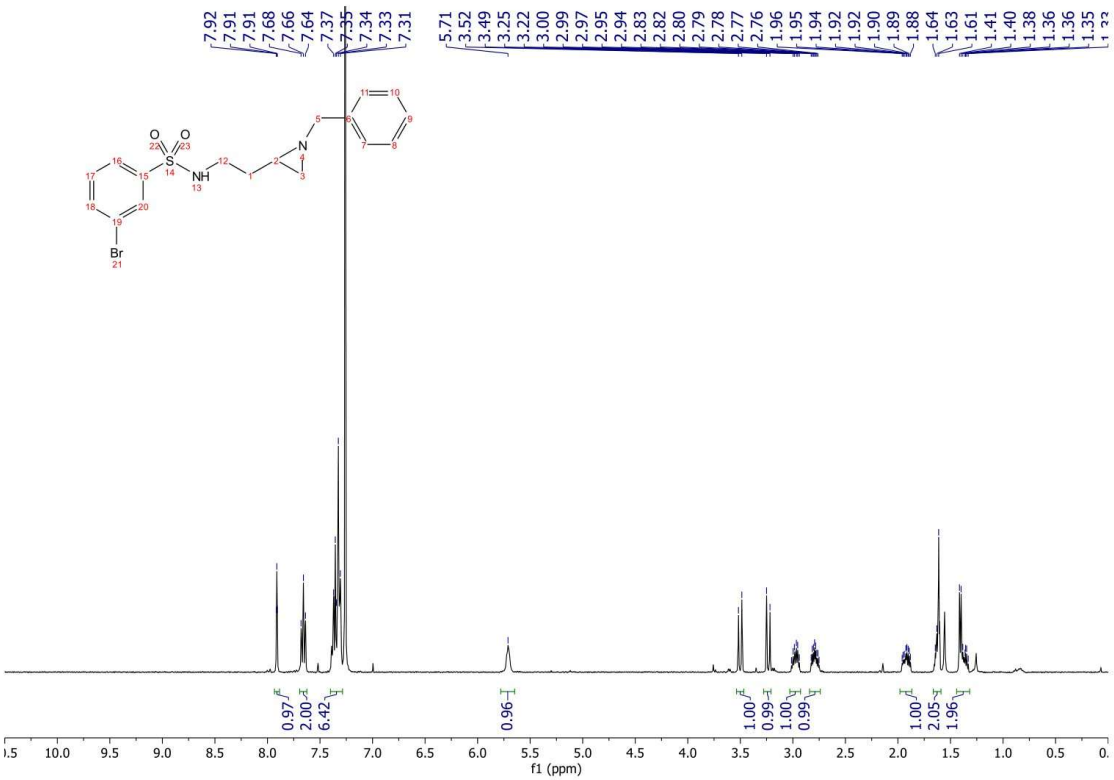
7.92
7.91
7.91
7.68
7.66
7.64
7.37
7.35
7.34
7.33
7.31
5.71
3.52
3.49
3.25
3.22
3.00
2.99
2.97
2.95
2.94
2.83
2.82
2.80
2.79
2.78
2.77
2.76
1.96
1.95
1.94
1.92
1.92
1.90
1.89
1.88
1.64
1.63
1.61
1.41
1.40
1.38
1.36
1.36
1.35
0.97
2.00
6.42
0.96
1.00
0.99
1.00
0.99
1.00
2.05
1.96
f1 (ppm)

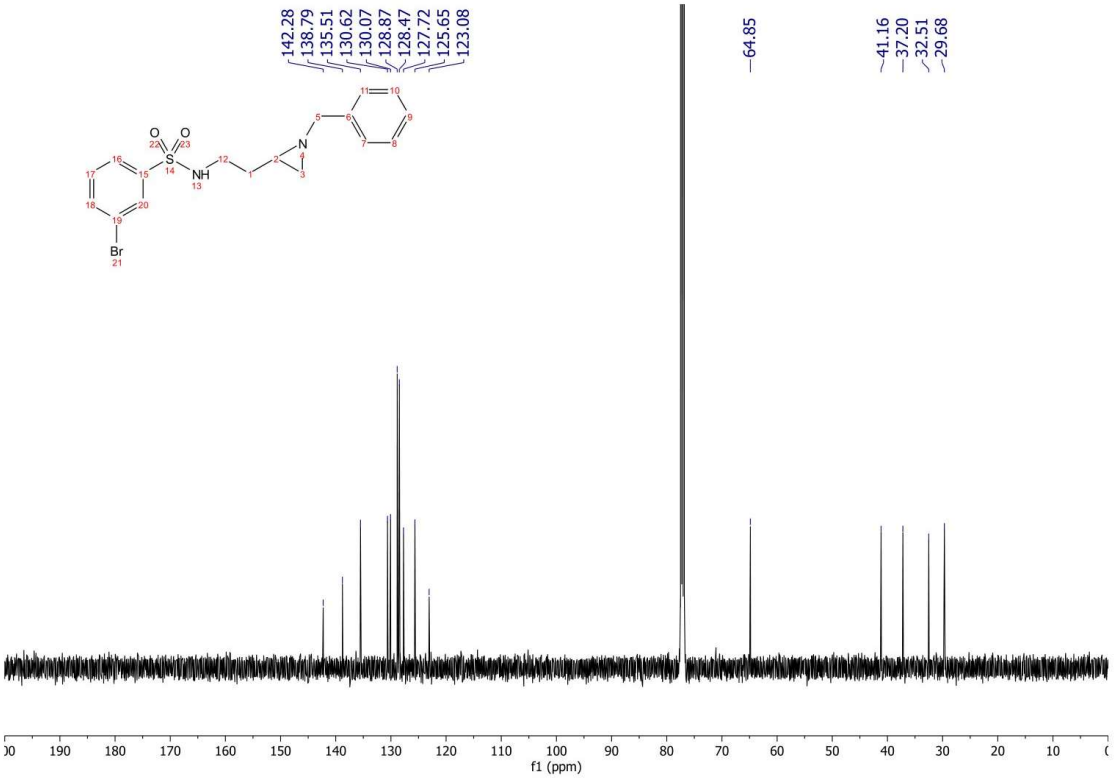
142.28
138.79
135.51
130.62
130.07
128.87
128.47
127.72
125.65
123.08
64.85
41.16
37.20
32.51
29.68
f1 (ppm)

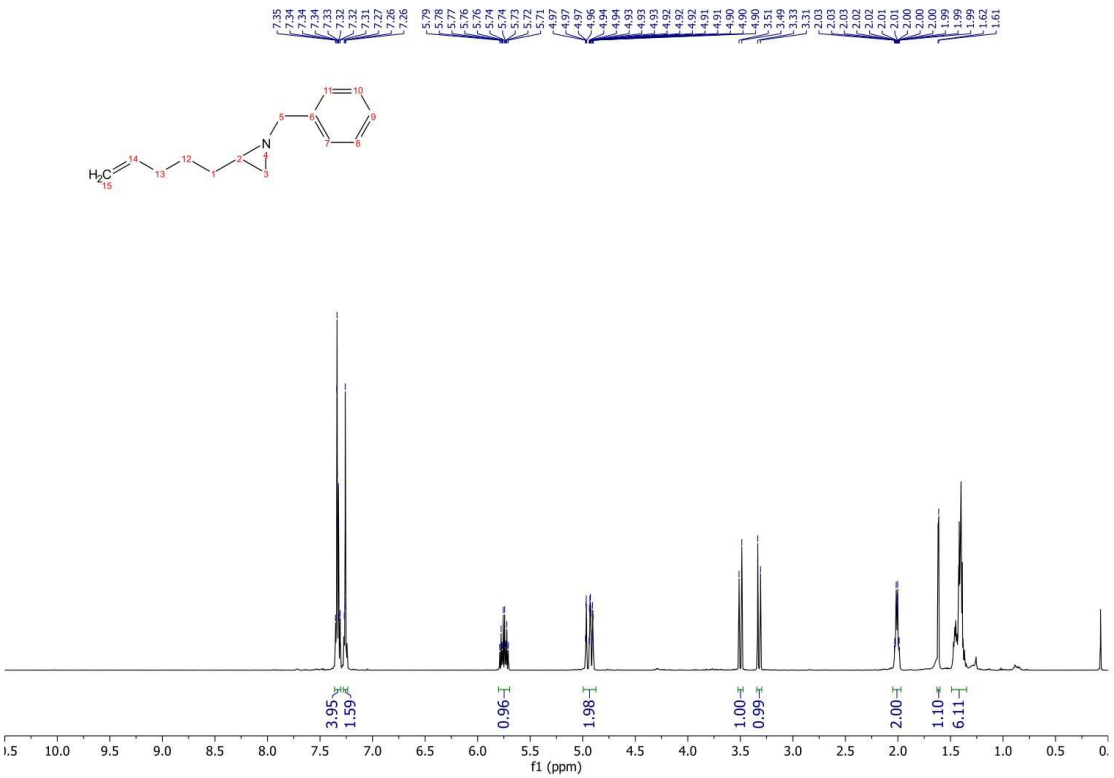
7.35 7.34 7.34 7.34 7.33 7.32 7.32 7.31 7.27 7.26 7.26
5.79 5.78 5.77 5.76 5.76 5.74 5.74 5.73 5.72 5.71 4.97 4.97 4.96 4.94 4.94 4.93 4.93 4.92 4.92 4.91 4.91 4.90 4.90 4.90 3.51 3.49 3.33 3.31 2.03 2.03 2.02 2.02 2.01 2.00 2.00 2.00 1.99 1.99 1.62 1.61
3.95
1.59
0.96
1.98
1.00
0.99
2.00
1.10
6.11
f1 (ppm)

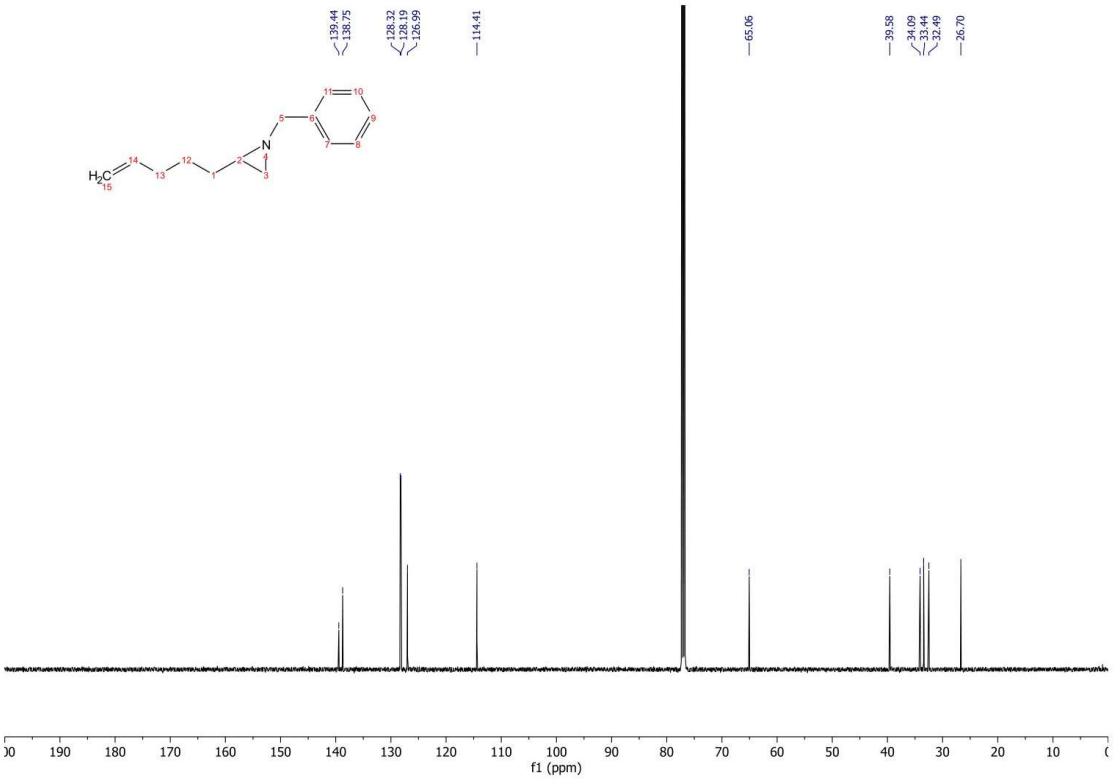
139.44
138.75
128.32
128.19
126.99
114.41
65.06
39.58
34.09
33.44
32.49
26.70
f1 (ppm)

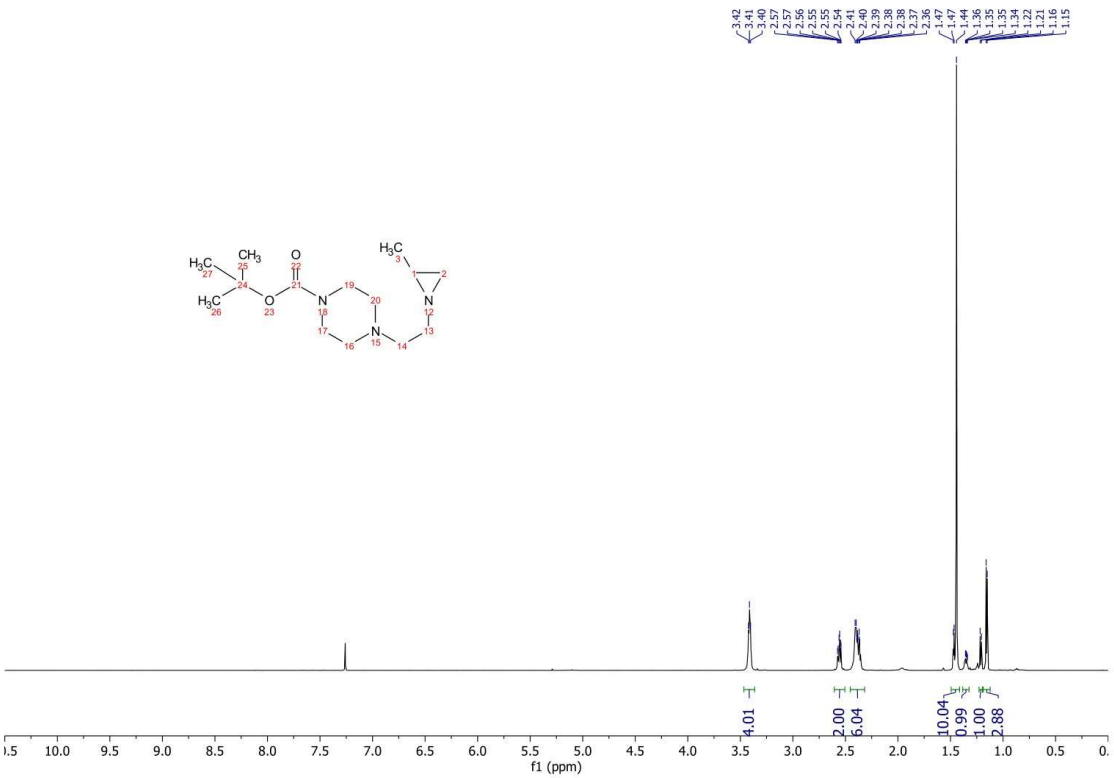
3.42
3.41
3.40
2.57
2.56
2.55
2.55
2.54
2.41
2.40
2.39
2.38
2.37
2.36
1.47
1.47
1.44
1.36
1.35
1.35
1.24
1.22
1.21
1.16
1.15
4.01
2.00
6.04
10.04
0.99
1.00
2.88
f1 (ppm)

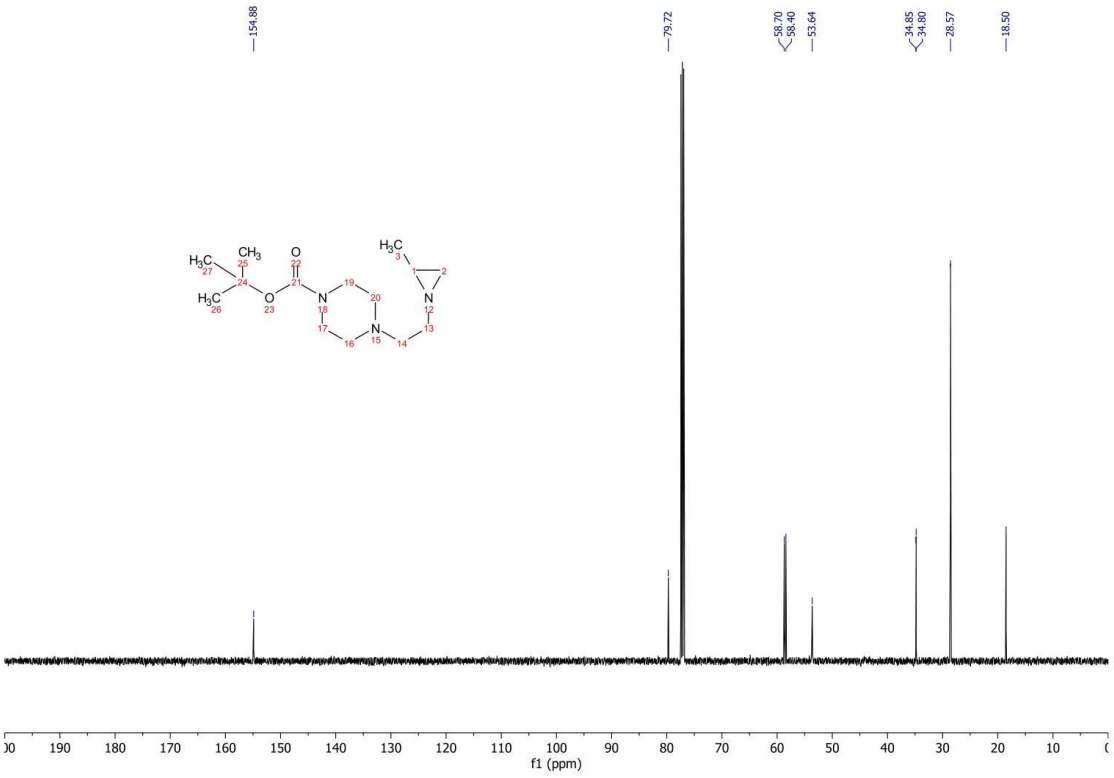
154.88
79.72
58.70
58.40
53.64
34.85
34.80
28.57
18.50
f1 (ppm)

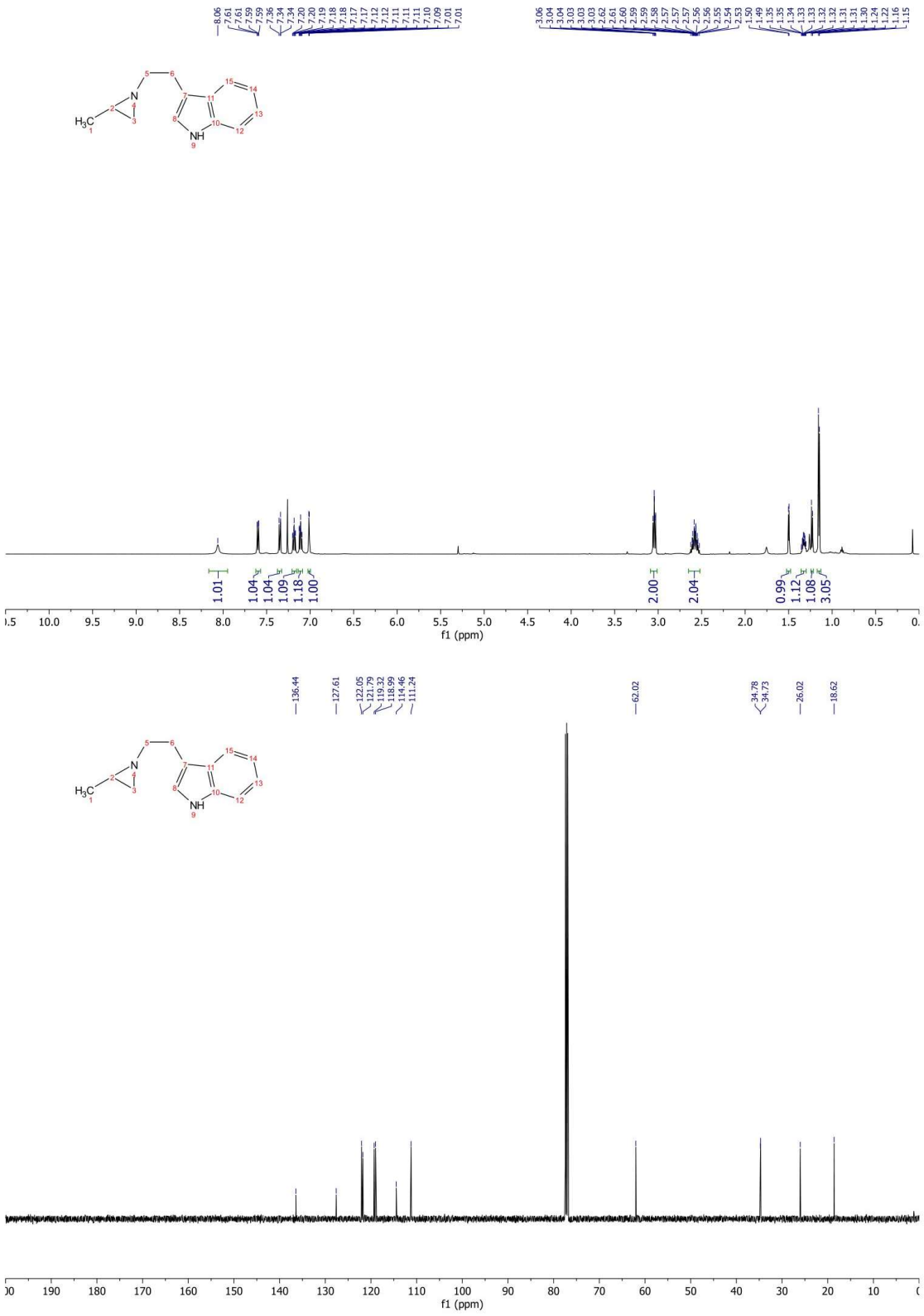
8.06
7.61
7.61
7.59
7.59
7.36
7.34
7.34
7.20
7.20
7.19
7.18
7.18
7.17
7.17
7.12
7.12
7.11
7.11
7.11
7.10
7.09
7.01
7.01
3.06
3.04
3.04
3.03
3.03
3.03
2.62
2.61
2.60
2.59
2.59
2.58
2.57
2.57
2.57
2.56
2.56
2.55
2.54
2.53
1.59
1.49
1.35
1.35
1.34
1.33
1.33
1.32
1.32
1.31
1.31
1.30
1.24
1.22
1.16
1.15
1.01
1.04
1.04
1.09
1.18
1.00
2.00
2.04
0.99
1.12
1.08
3.05
f1 (ppm)
136.44
127.61
122.05
121.79
119.32
118.99
114.46
111.24
62.02
34.78
34.73
26.02
18.62
f1 (ppm)

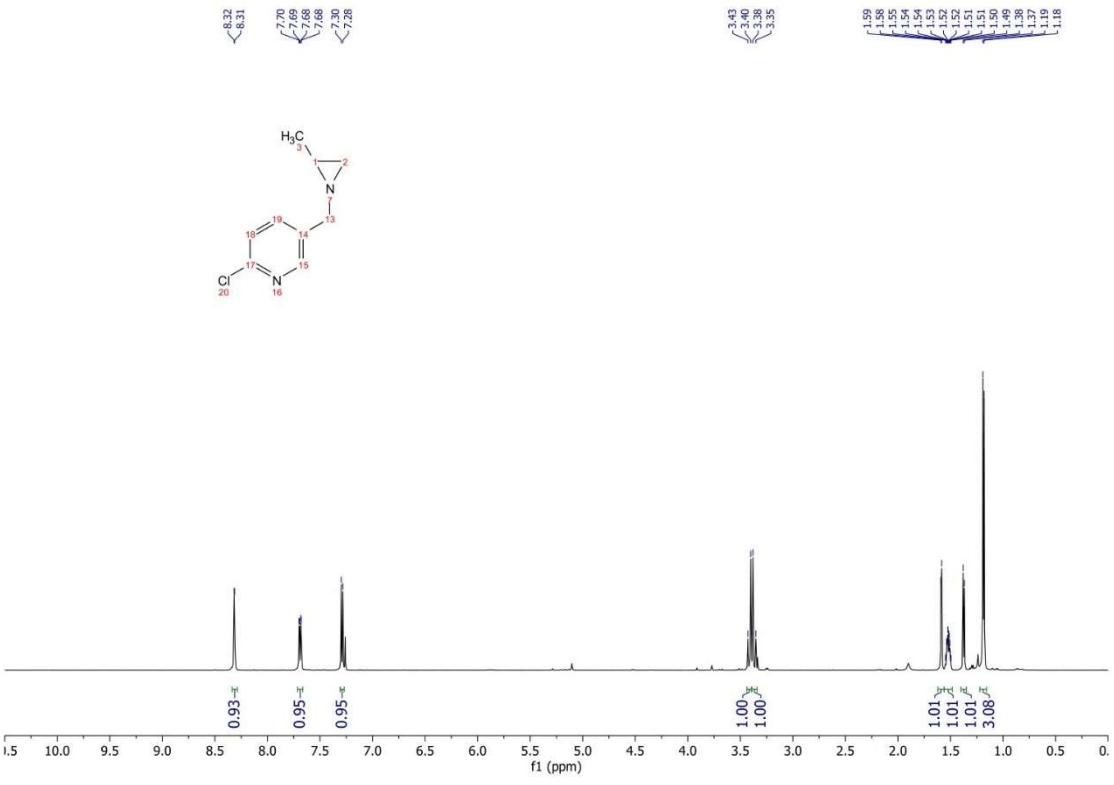
8.32
8.31
7.70
7.69
7.68
7.68
7.30
7.28
3.43
3.40
3.38
3.35
1.59
1.58
1.55
1.54
1.54
1.53
1.52
1.52
1.51
1.51
1.50
1.49
1.38
1.37
1.19
1.18
H3C
N
Cl
0.93
0.95
0.95
1.00
1.00
1.01
1.01
1.01
3.08
f1 (ppm)

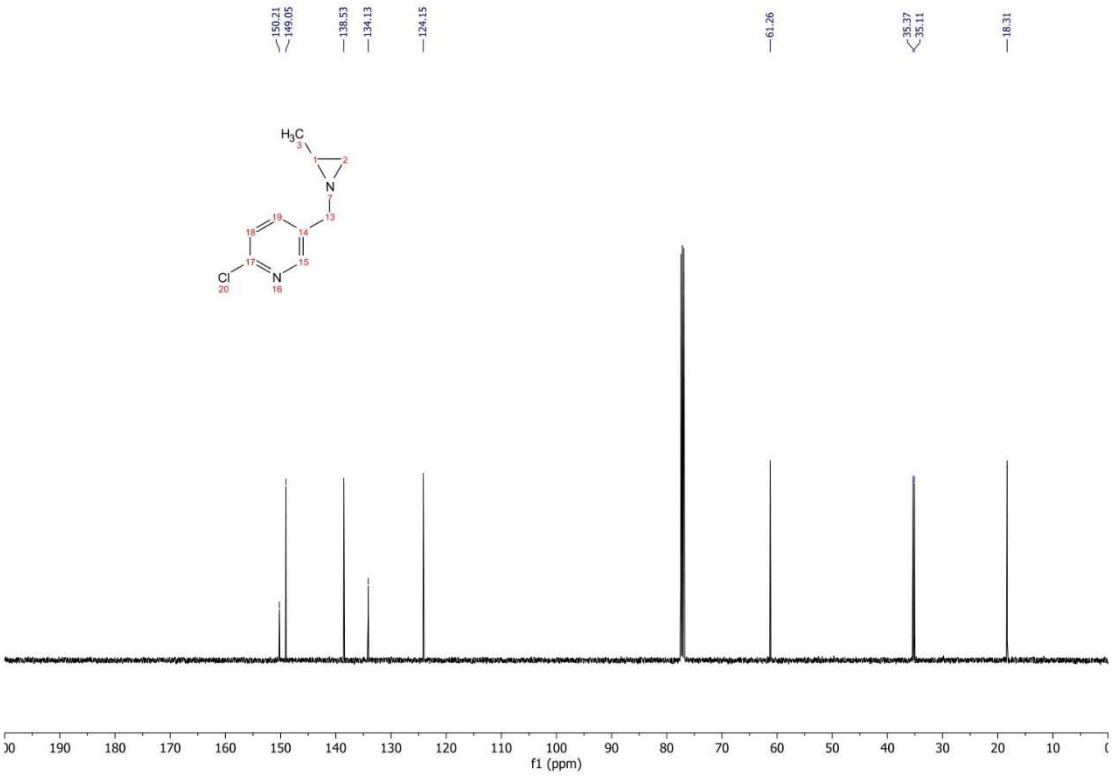
150.21
149.05
138.53
134.13
124.15
61.26
35.37
35.11
18.31
H3C
N
Cl
f1 (ppm)

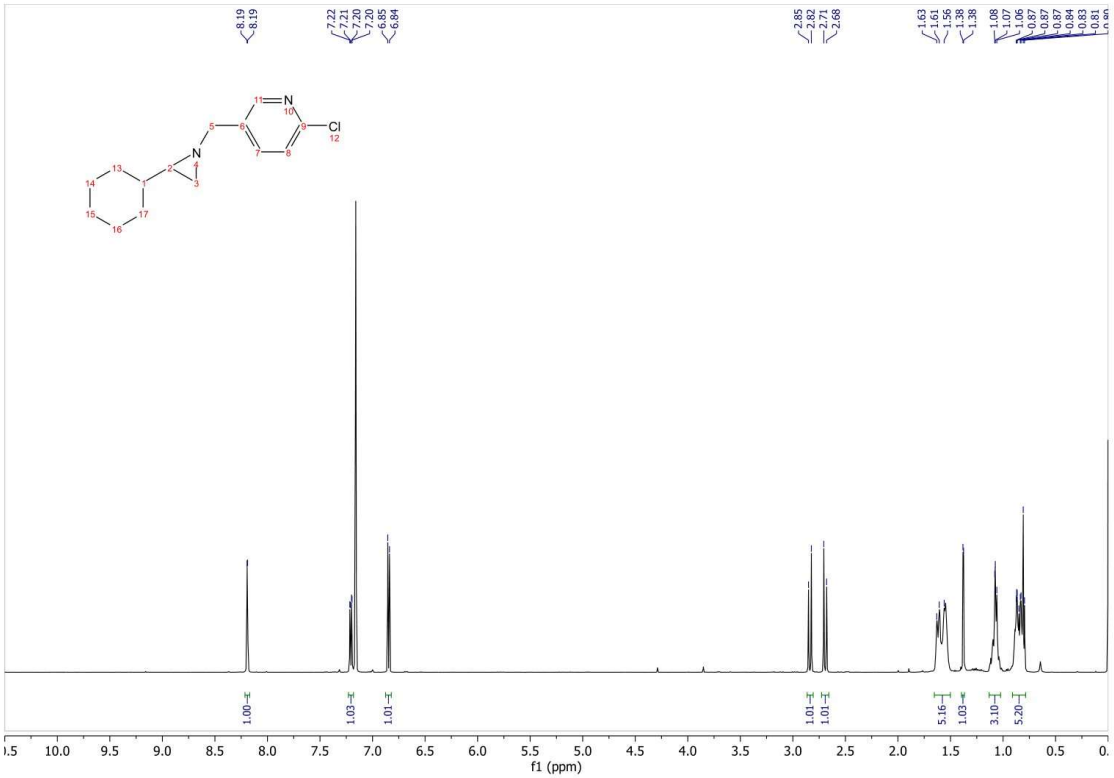
8.19
8.19
7.22
7.21
7.20
7.20
6.85
6.84
2.85
2.82
2.71
2.68
1.63
1.61
1.56
1.38
1.38
1.08
1.07
1.06
0.87
0.87
0.87
0.84
0.83
0.81
1.00
1.03
1.01
1.01
1.01
5.16
1.03
3.10
5.20
f1 (ppm)

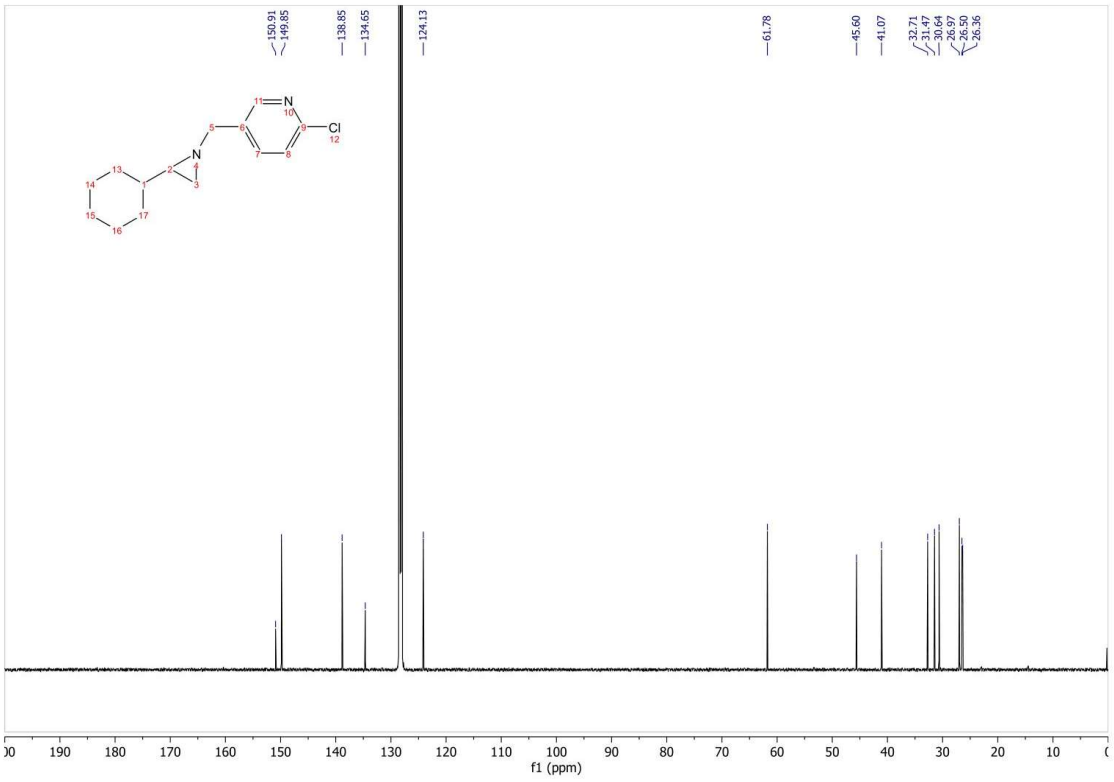
150.91
149.85
138.85
134.65
124.13
61.78
45.60
41.07
32.71
31.47
30.64
26.97
26.50
26.36
f1 (ppm)

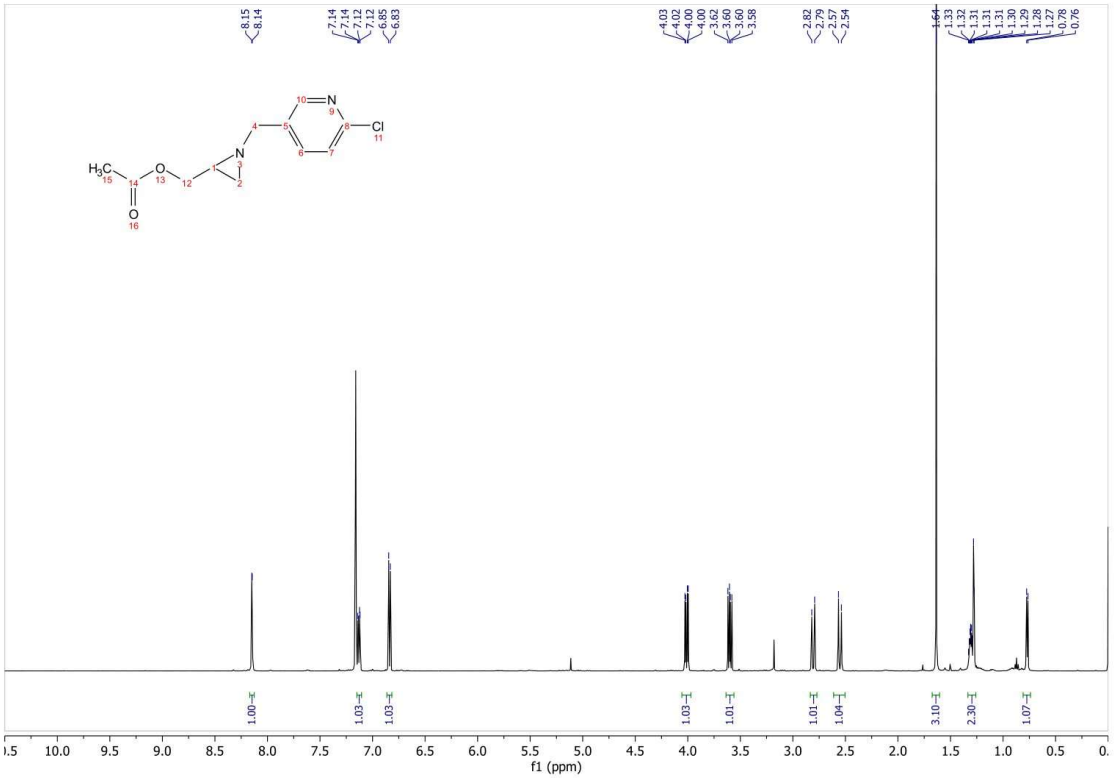
8.15
8.14
7.14
7.14
7.12
7.12
6.85
6.83
4.03
4.02
4.00
4.00
3.62
3.60
3.60
3.58
2.82
2.79
2.57
2.54
1.64
1.33
1.32
1.31
1.31
1.31
1.30
1.29
1.28
1.27
0.78
0.76
1.00
1.03
1.03
1.03
1.01
1.01
1.04
3.10
2.30
1.07
f1 (ppm)

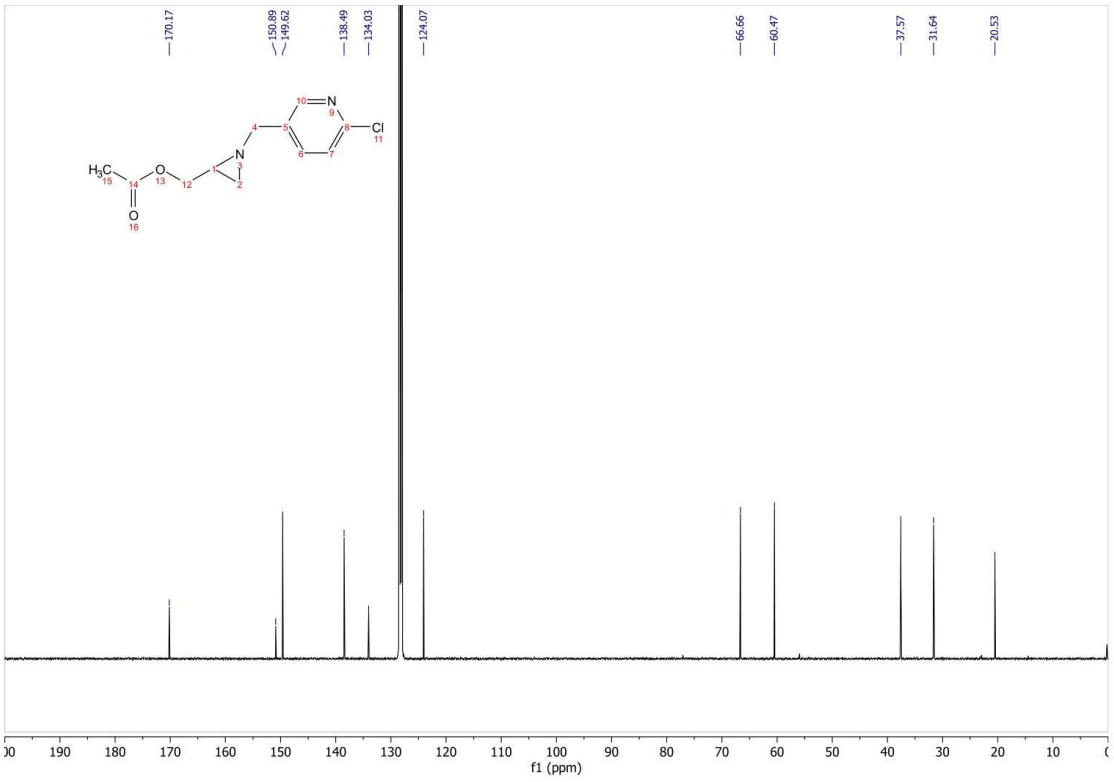
170.17
150.89
149.62
138.49
134.03
124.07
66.66
60.47
37.57
31.64
20.53
f1 (ppm)

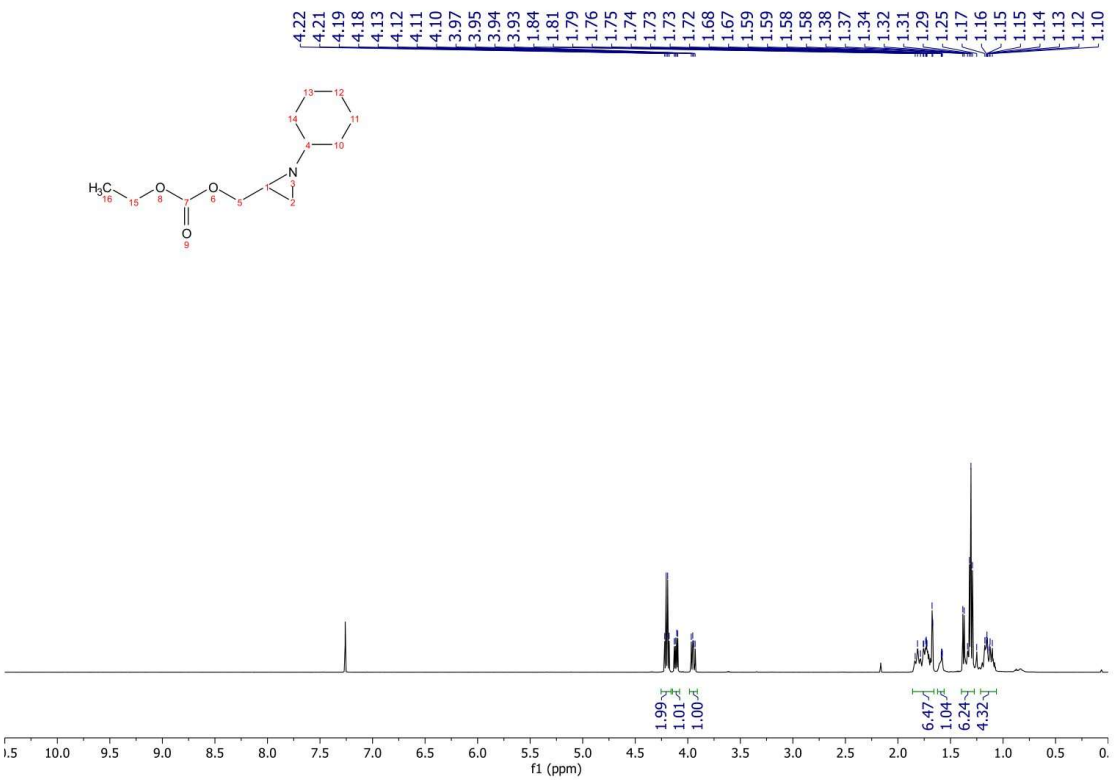
4.22
4.21
4.19
4.18
4.13
4.12
4.11
4.10
3.97
3.95
3.94
3.93
1.84
1.81
1.79
1.76
1.75
1.74
1.73
1.73
1.72
1.68
1.67
1.59
1.59
1.58
1.58
1.38
1.37
1.34
1.32
1.31
1.29
1.25
1.17
1.16
1.15
1.15
1.14
1.13
1.12
1.10
1.99
1.01
1.00
6.47
1.04
6.24
4.32
f1 (ppm)

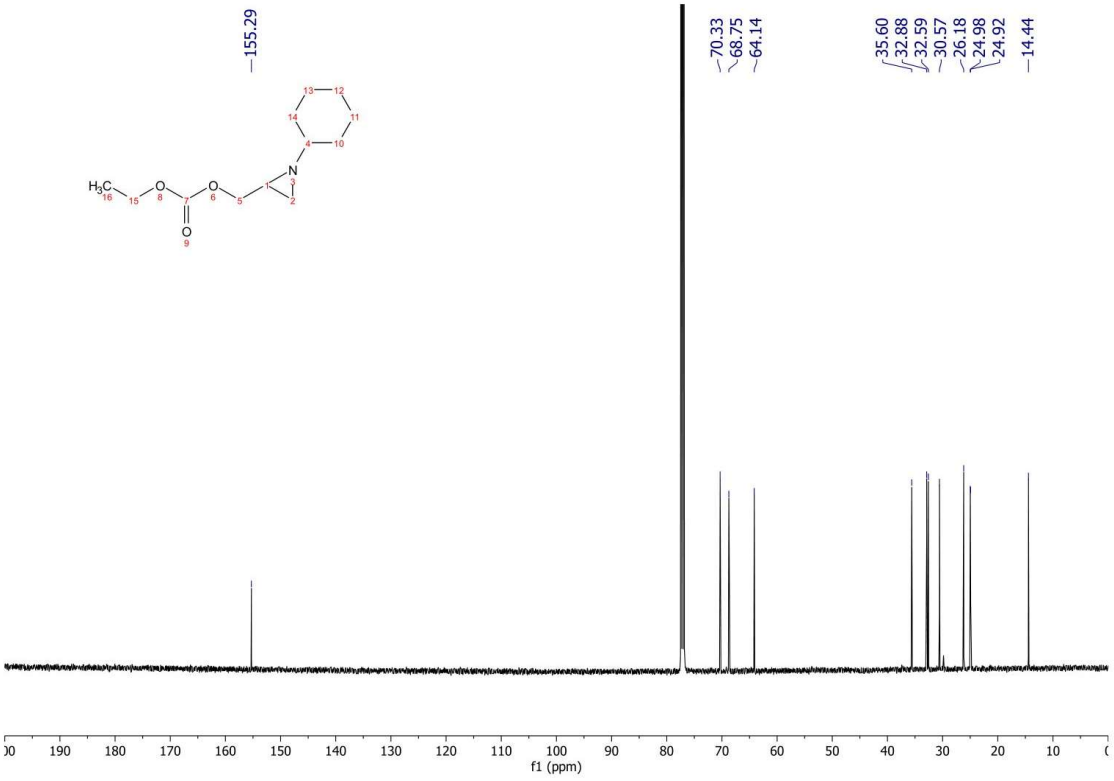
155.29
70.33
68.75
64.14
35.60
32.88
32.59
30.57
26.18
24.98
24.92
14.44
f1 (ppm)

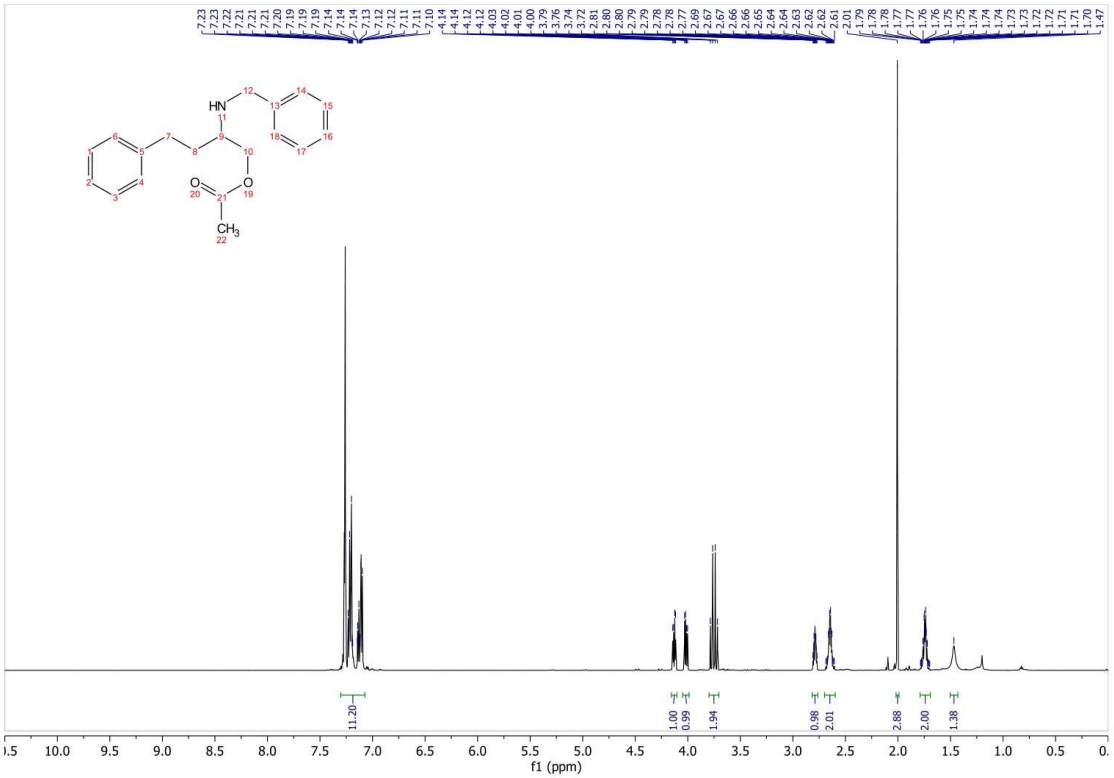
HN
O
O
CH3
11.20
1.00
0.99
1.94
0.98
2.01
2.88
2.00
1.38
f1 (ppm)

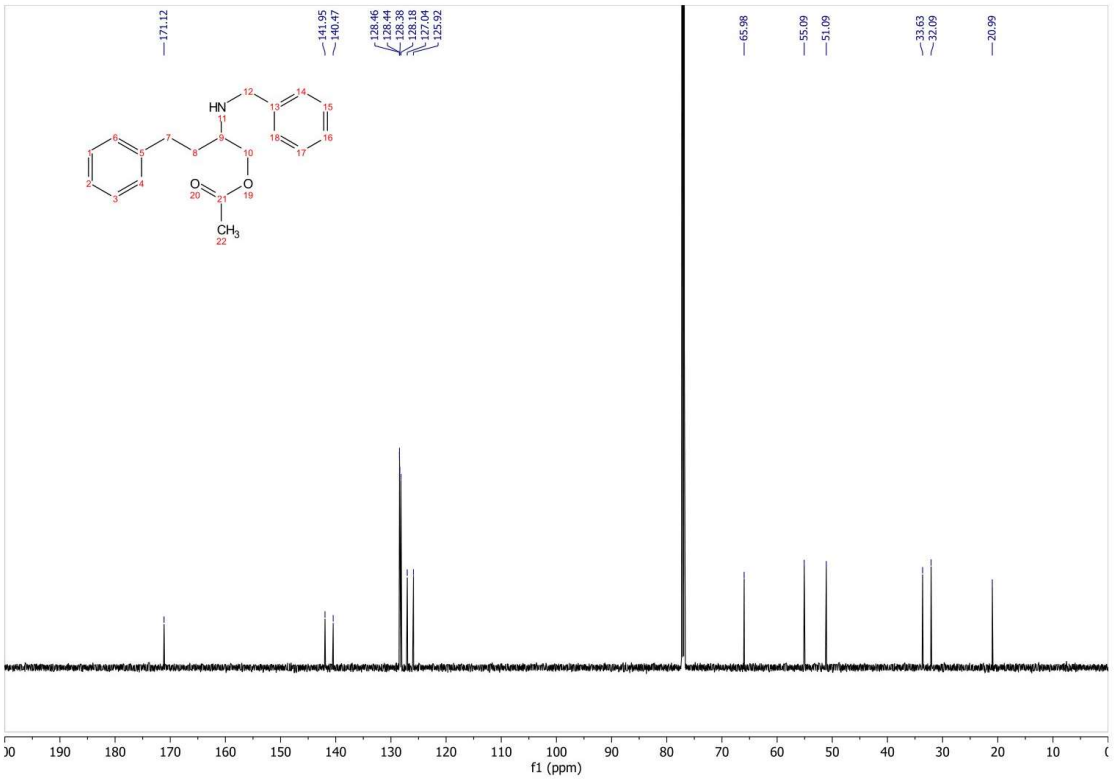
171.12
141.95
140.47
128.46
128.44
128.38
128.18
127.04
125.92
65.98
55.09
51.09
33.63
32.09
20.99
HN
O
O
CH3
f1 (ppm)

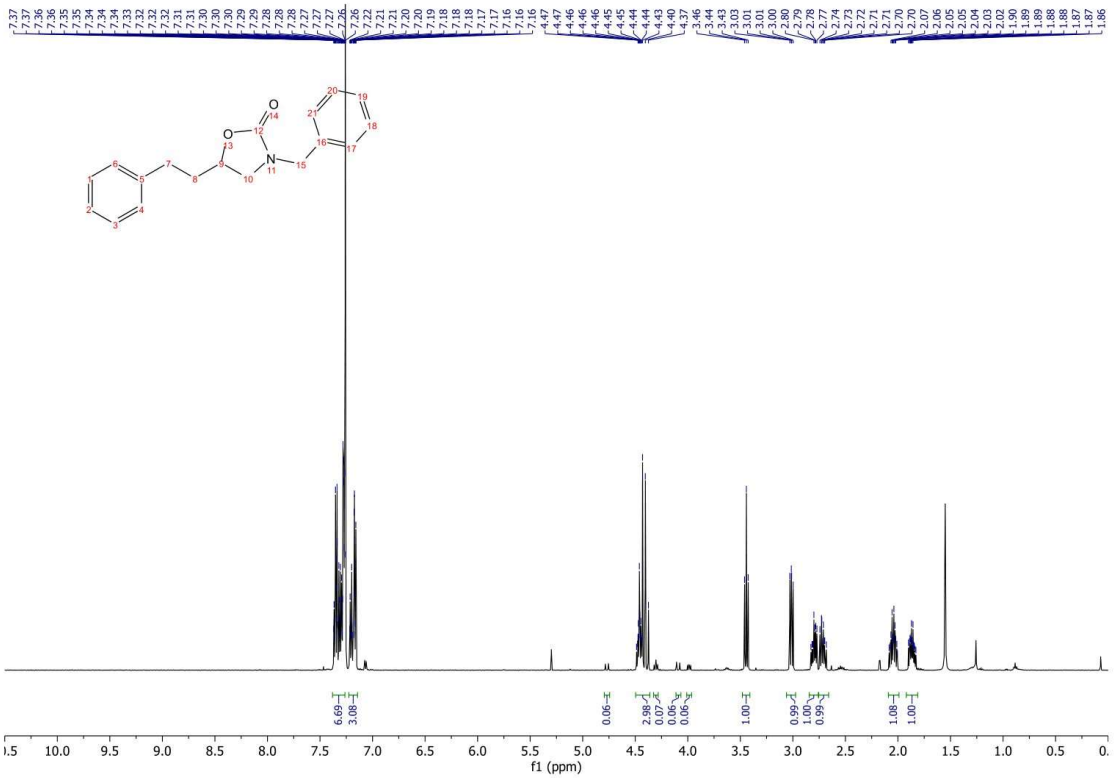
f1 (ppm)

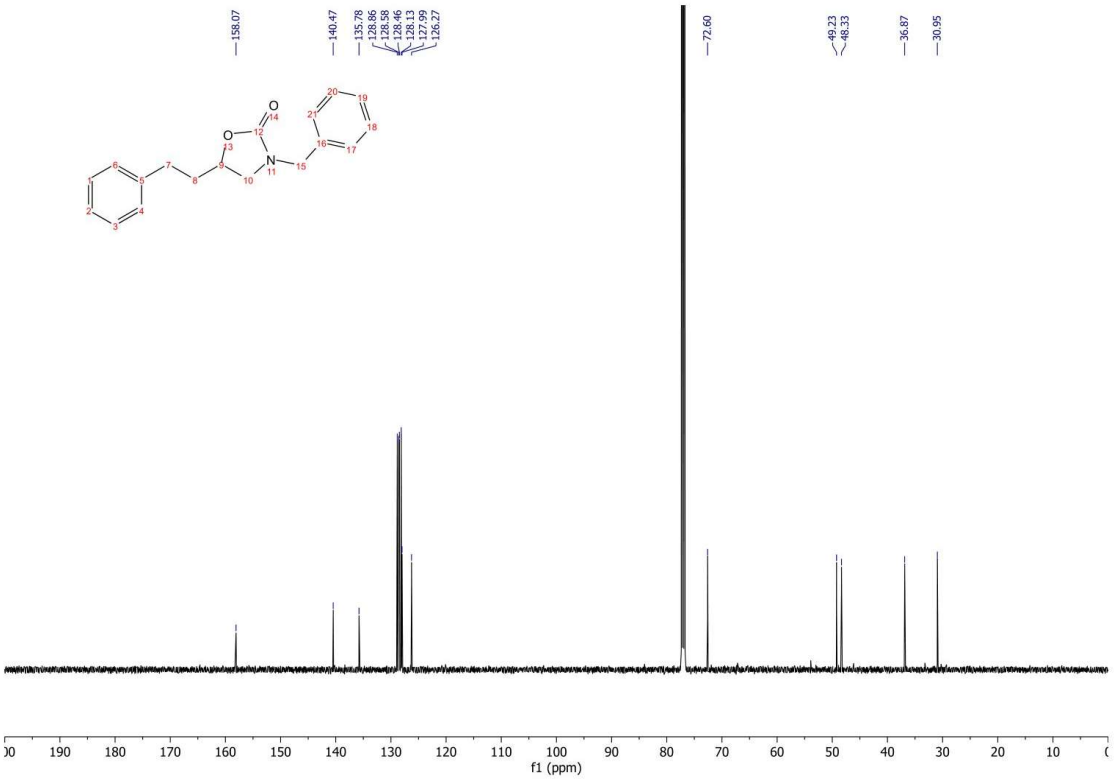
158.07
140.47
135.78
128.86
128.58
128.46
128.13
127.99
126.27
72.60
49.23
48.33
36.87
30.95
f1 (ppm)

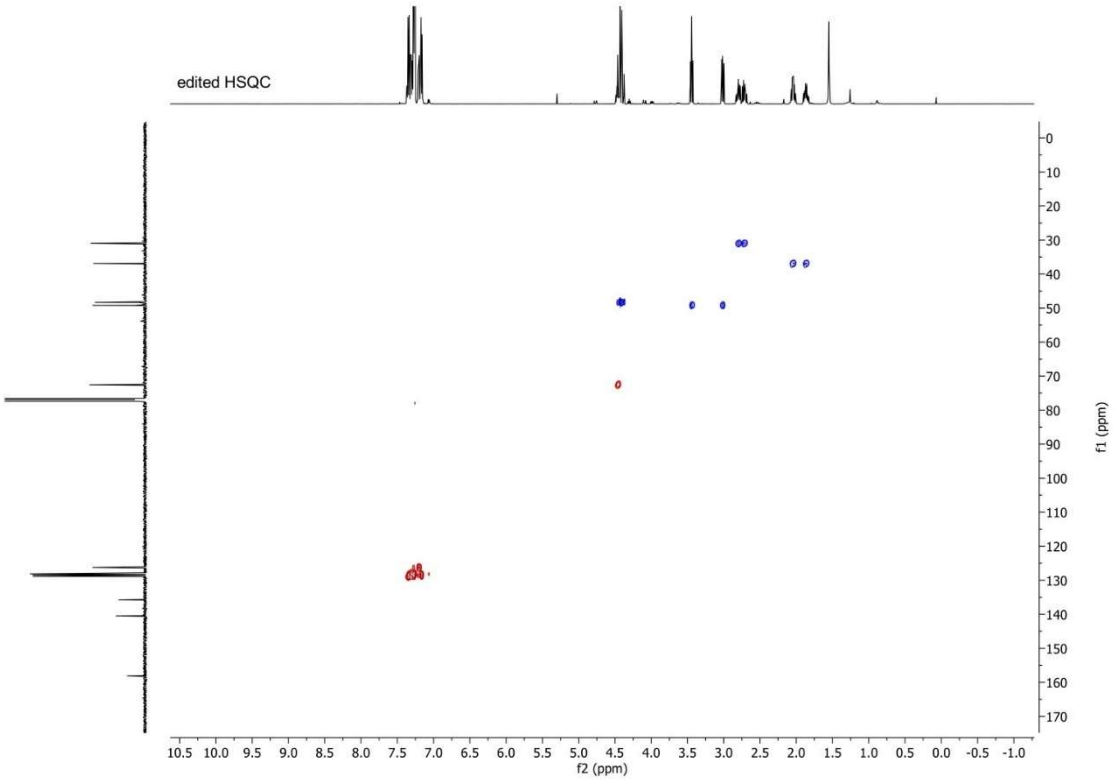
edited HSQC
f1 (ppm)
f2 (ppm)

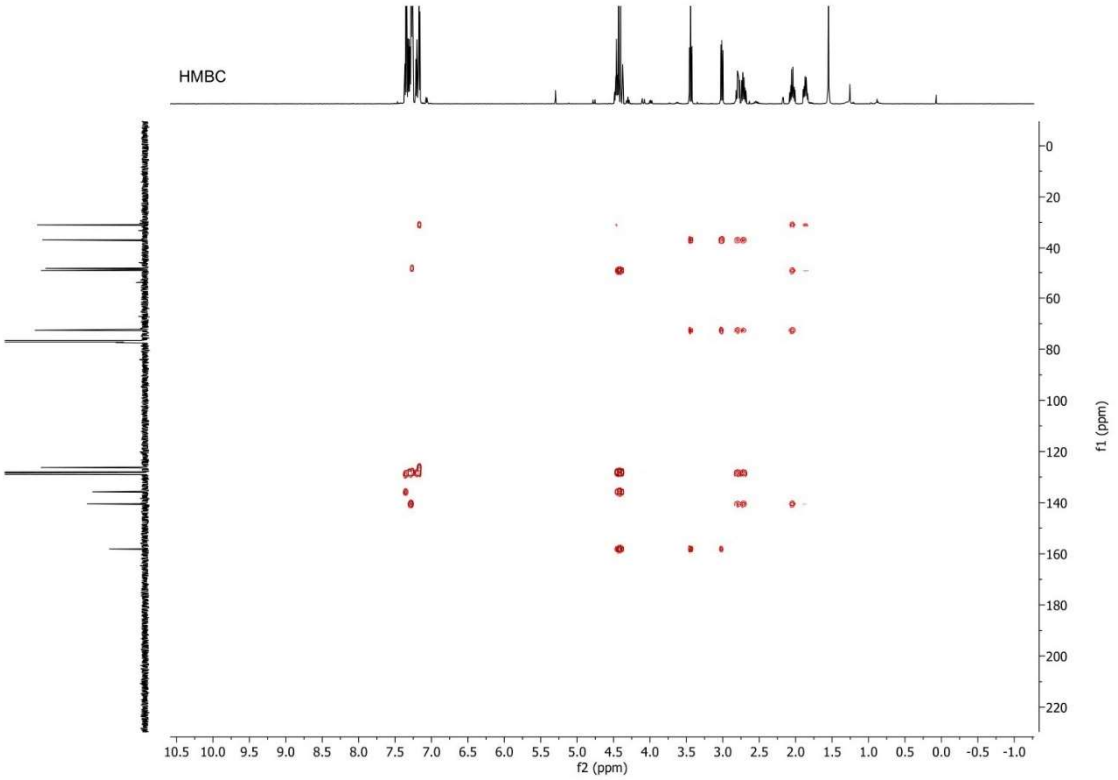
HMBC
f1 (ppm)
f2 (ppm)

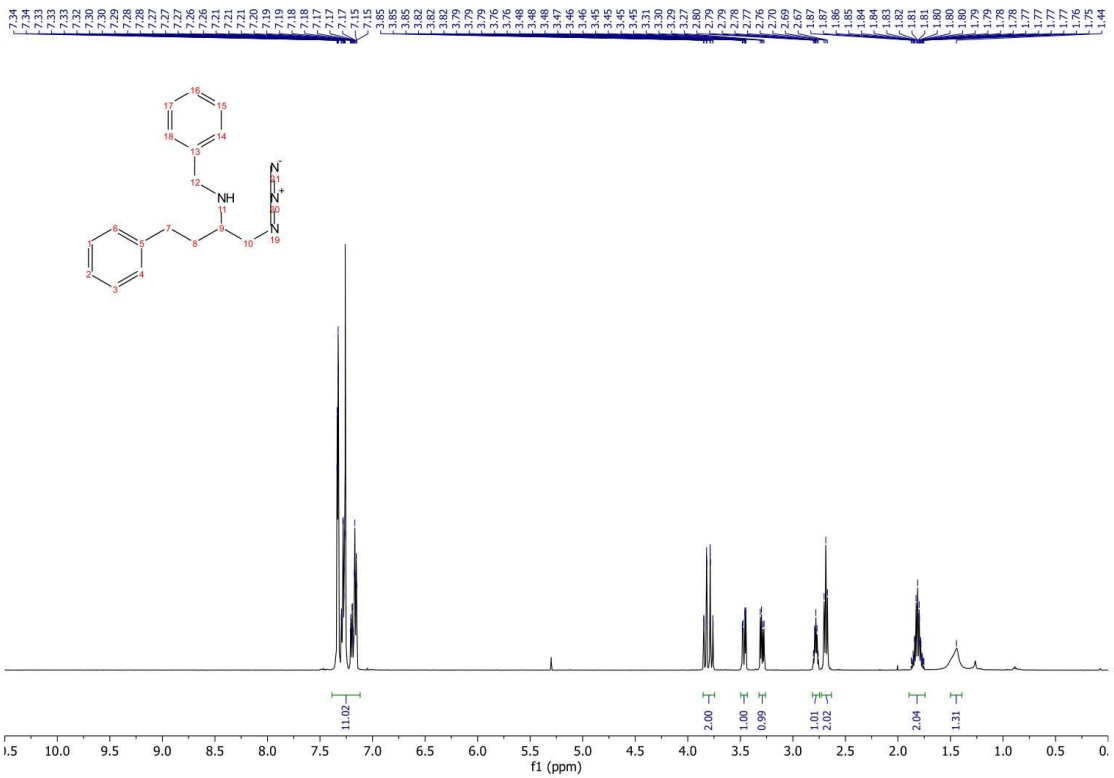
11.02
2.00
1.00
0.99
1.01
2.02
2.04
1.31
f1 (ppm)

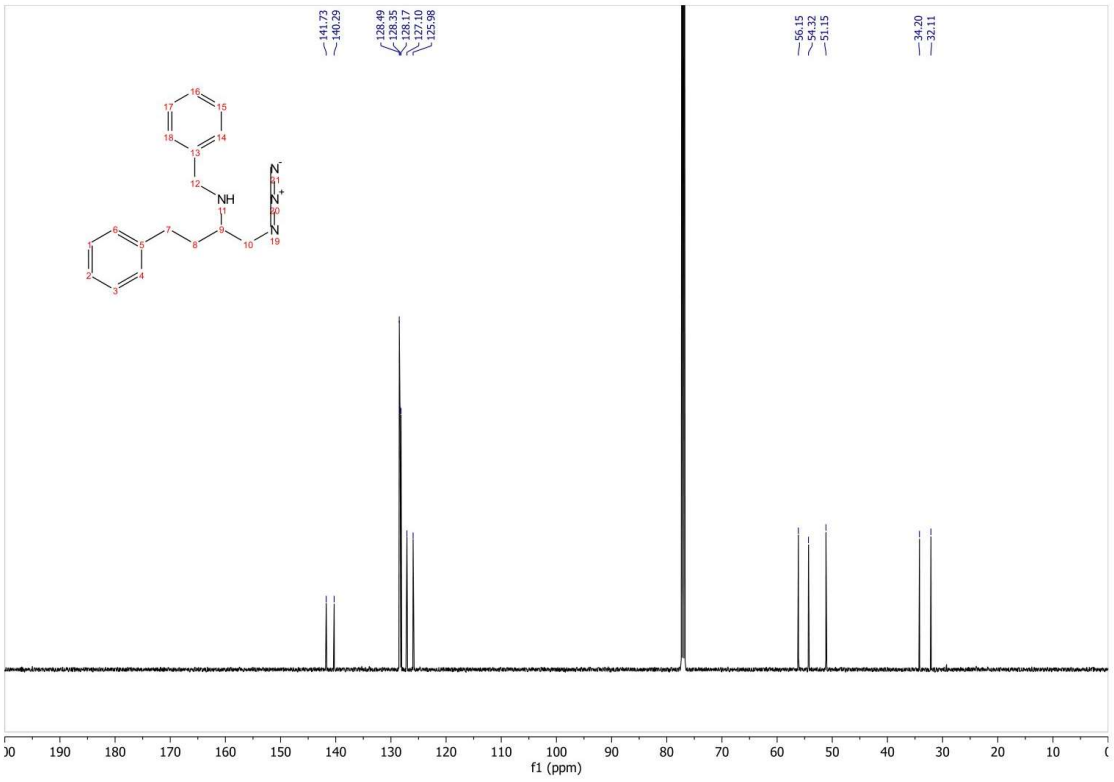
141.73
140.29
128.49
128.35
128.17
127.10
125.98
56.15
54.32
51.15
34.20
32.11
f1 (ppm)

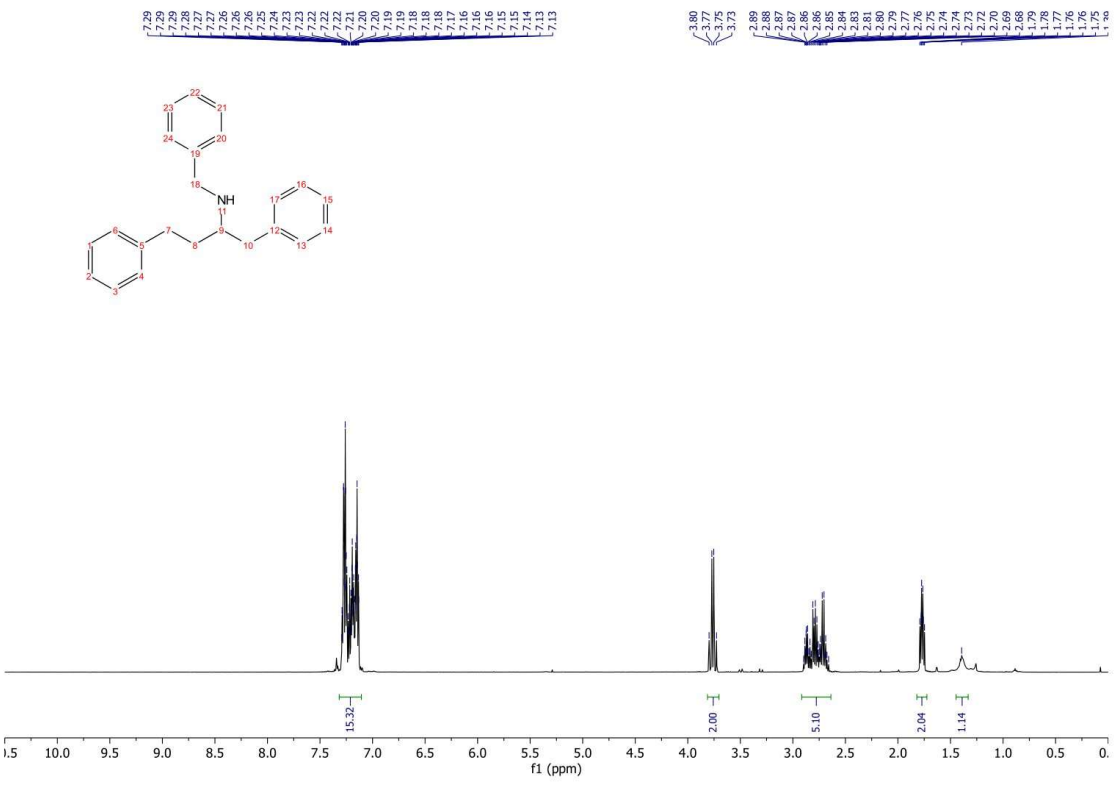
NH
15.32
2.00
5.10
2.04
1.14
f1 (ppm)

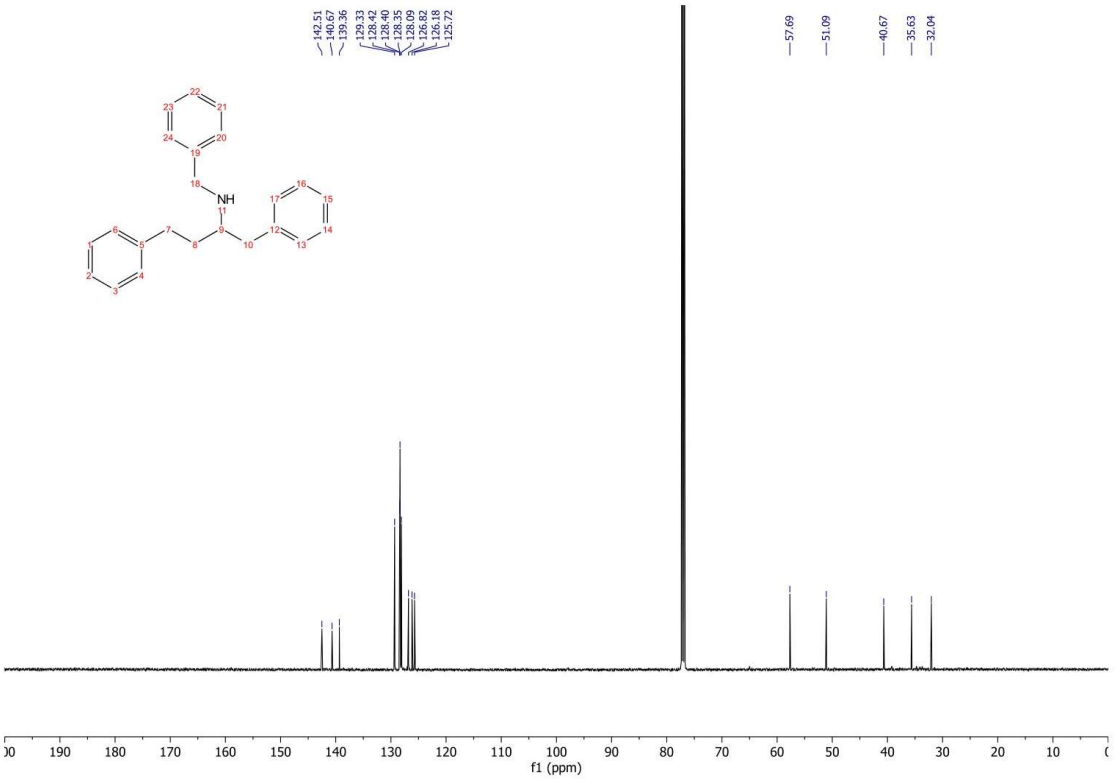
NH
142.51
140.67
139.36
129.33
128.42
128.40
128.35
128.09
126.82
126.18
125.72
57.69
51.09
40.67
35.63
32.04
f1 (ppm)

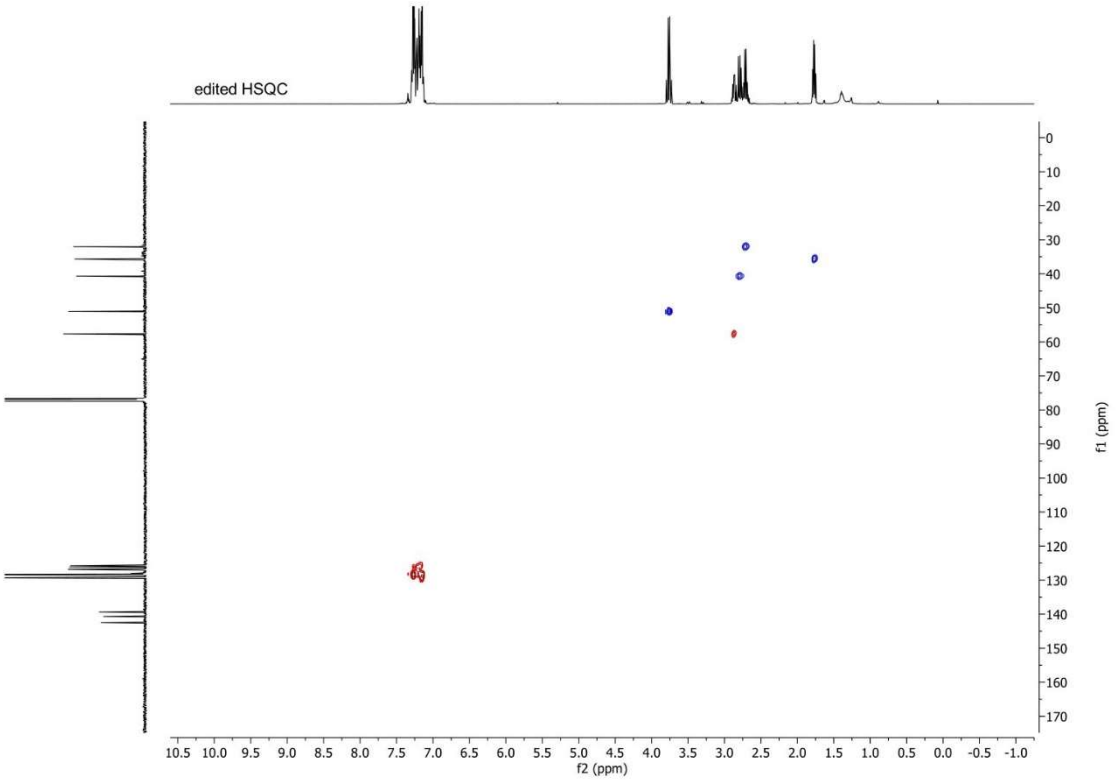
edited HSQC
f1 (ppm)
f2 (ppm)

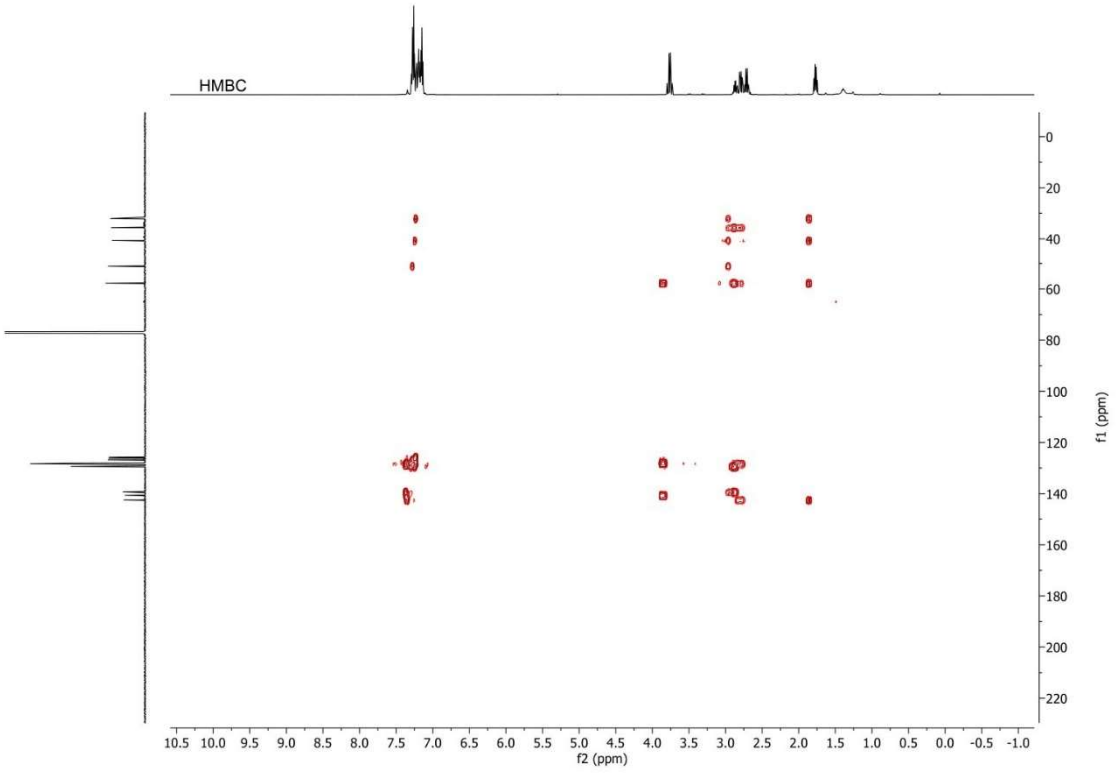
HMBC
f1 (ppm)
f2 (ppm)

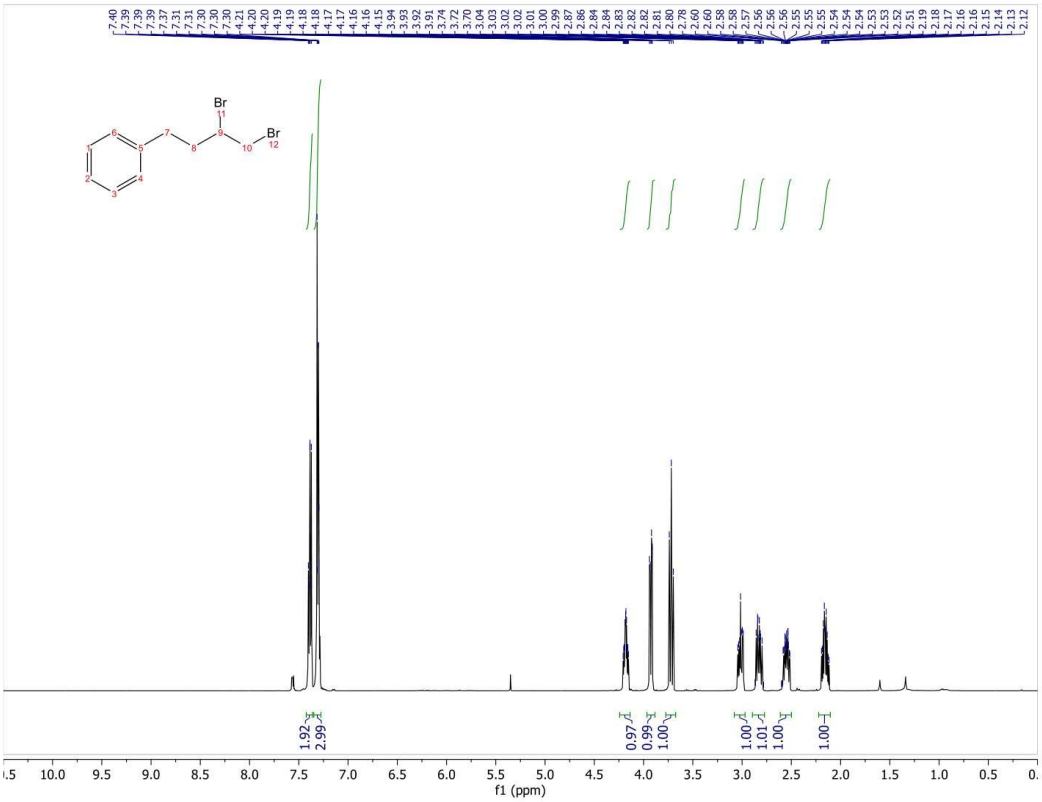
Br
Br
1.92
2.99
0.97
0.99
1.00
1.00
1.01
1.00
1.00
f1 (ppm)

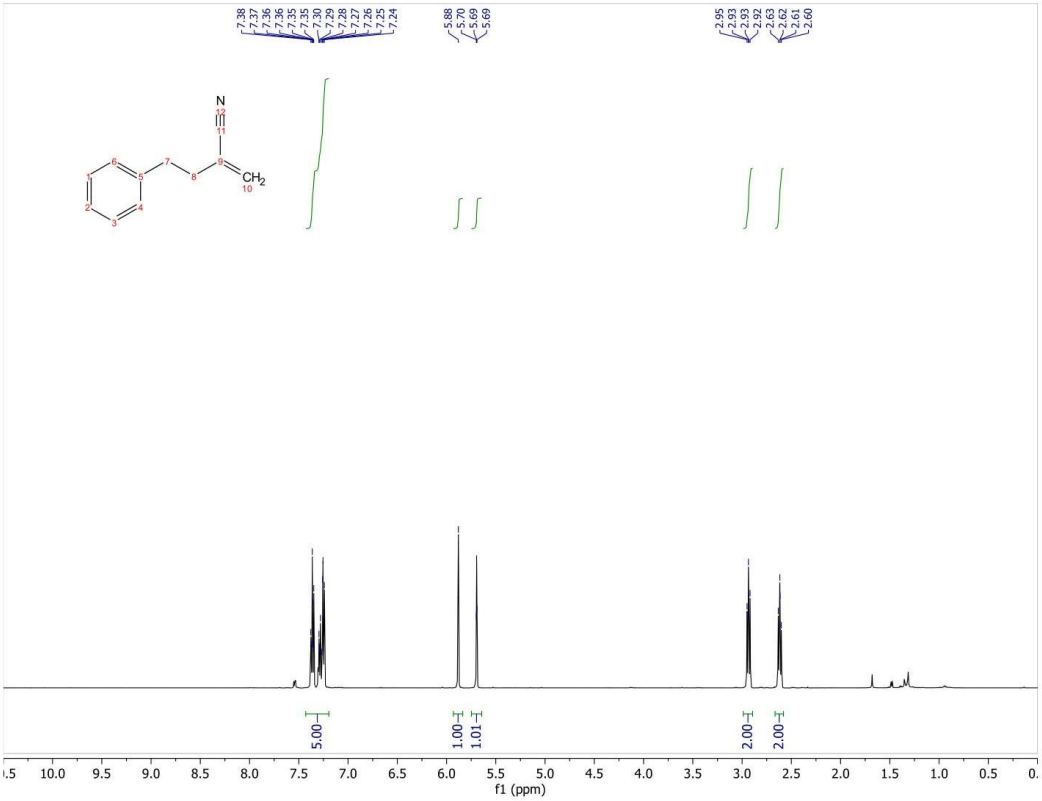
N
CH2
5.00
1.00
1.01
2.00
2.00
f1 (ppm)

Appendix B: Supporting Information for Chapter 3 (Electrochemical Synthesis of Allylic Amines from Terminal Alkenes and Secondary Amines)

B.1 General Methods and Materials

MeCN, DMF, and DCM were dried by passing through activated alumina columns. Tetrabutylammonium hexafluorophosphate was recrystallized three times from EtOAc prior to use. All liquid amines were distilled from CaH_2 prior to use. Thianthrene was recrystallized from acetone prior to use. Unless otherwise noted, other commercially-available reagents were used as received. Crude mixtures were evaluated by thin-layer chromatography using EMD/Merck silica gel 60 F254 pre-coated plates (0.25 mm) and were visualized by UV, Seebach, and/or $KMnO_4$ staining. Flash chromatography was performed with a Biotage Isolera One automated chromatography system with re-packed silica columns (technical grade silica, pore size 60 Å, 230-400 mesh particle size, 40-63 particle size) or pre-packed Biotage SNAP Ultra and Biotage Sfär Silica HC columns unless otherwise noted. Purified materials were dried in vacuo (0.050 Torr) to remove trace solvent. ^{1}H, ^{13}C, ^{19}F Spectra were taken using a Bruker Avance-400 with a BBFO Probe, a Bruker Avance-500 with a DCH Cryoprobe. NMR data are reported relative to residual $CHCl_3$ (^{1}H, δ = 7.26 ppm), $CDCl_3$ (^{13}C, δ = 77.16 ppm). Data for ^{1}H NMR spectra are reported as follows: chemical shift (δ ppm) (multiplicity, coupling constant (Hz), integration). Multiplicity and qualifier abbreviations are as follows: s = singlet, d = doublet, t = triplet, q = quartet, m = multiplet, br = broad. All NMR yields were determined via reference against an internal standard (dibromomethane or mesitylene for ^{1}H NMR). Mass spectrometry data was collected on a Thermo Scientific Q Exactive Plus Mass Spectrometer and a Waters Acquity™ LCMS.

Abbreviations: Bn—benzyl, Boc—tert-butyl carbamate, *t*-Bu—tert-butyl, DCM—dichloromethane, DIPEA—N,N-Diisopropylethylamine, DMF—dimethyl formamide, EtOAc—ethyl acetate, MeCN—acetonitrile, MeOH—methanol, RVC—reticulated vitreous carbon, Ph—phenyl, TEA—triethylamine, TFA—trifluoroacetic acid.

Electrochemical Methods and Materials

All chronoamperometric and chronopotentiometric measurements were performed at room temperature using a Pine WaveNowXV. Chronoamperometric and chronopotentiometric measurements were carried out in divided cells with RVC (8 × 6 × 6 mm, Ultramet, 80 ppi) as working electrodes affixed to a graphite pencil/silver wire assembly and with nickel foam (1.4 mm x 1.4 mm, MTI Corporation, Surface density: 350g/m^2) as counter electrodes affixed to stainless steel wire (see below). The potentials were measured versus an $Ag/AgNO_3$ (0.01 M in MeCN with 0.1 M n-Bu_4N•PF_6) reference electrode (all electrodes from Pine Research) and externally referenced via the ferrocene/ferrocenium couple. Bulk constant current electrolysis experiments were driven with a Dr. Meter HY3005M-L DC Power Supply or a custom–made low current power supply (see Scheme below) which was externally calibrated with a multimeter using a 10 or 1–Ohm resistor.

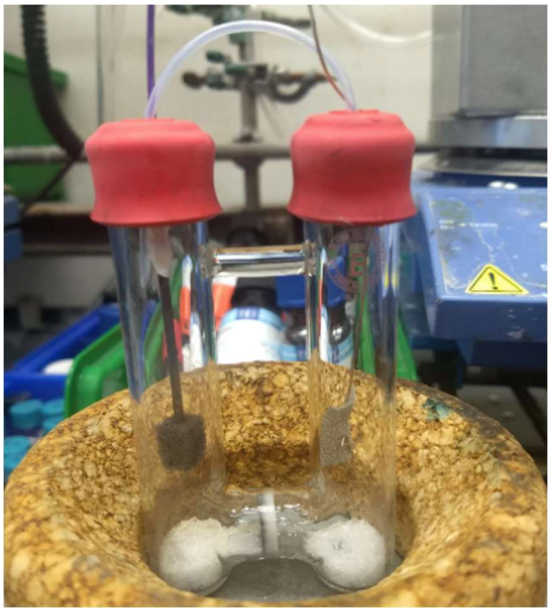

Figure B1. Large divided cell with electrodes.

Divided cell fabricated in-house. Glass frit purchased from Ace Glass (7176-36). Anode electrode assembled via affixing end of the silver wire (Belden Hook-Up wire, item no. 83005 007100) around the pencil (JuneGold 2B graphite 2 mm) using conductive graphite adhesive (Alfa Aesar, 42465), wrapping in teflon tape to prevent exposure, then piercing RVC with pencil. Solvent exposed electrode surface area (2.1 cm^2) was calculated via manufacturer-supplied surface area/volume ratio measurements. PTFE tubing (Cole-Parmer; 1/32" ID, 1/16" OD, item number EW-06407-41) connects both sides of the divided cell to normalize pressure. Septa inner diameter 16 mm. Stainless steel purchased from Grainger; stainless steel lockwire, 0.025" diameter, item number 16Y043.

Low-current Power Supply: Original design and fabrication by Dr. Blaise J. Thompson. Provides an operational range of ±0.01– 14.99 mA, tunable by variable resistor, delivering power to banana socket pair. The power supply is limited to ±15 V for bulk electrolysis and is powered by an 18 V wall wart. Circuitry is housed within an aluminum enclosure. For additional specifications, see: *J. Am. Chem. Soc.* **2020** 142, 2093–2099 and *Nature* **2021** 596, 74–79.

B.2 Reaction Optimization

Experimental Procedure – To an oven-dried divided electrochemical cell equipped with magnetic stir bars was added thianthrene (48.7 mg, 0.225 mmol, 1.5 equiv) to the anode compartment and *n*-Bu_4NPF_6 (232 mg, 0.6 mmol) to both compartments. The cell was equipped with two septa containing a stainless steel wire/Ni foam cathode assembly and a pencil/RVC anode assembly connected together with a teflon tubing to equalize pressure. MeCN (3 mL) was added to the cathode and anode compartments. Alkene (0.15 mmol, 1 equiv) was added to the anode compartment. Trifluoroacetic acid (116 µL, 1.5 mmol, 10 equiv) was added to the cathode compartment and both sides of the cell were stirred at ambient temperature and electrolyzed under a constant current of 4.0 mA (5.8 mA/cm^2) for 2.5 h (2.5 F/mol). At completion of electrolysis, the electrode leads were disconnected, septa removed, and the anode RVC was pushed off the pencil into the reaction mixture. Base (1.05 mmol, 7 equiv) was added to the anode

compartment followed by amine (either 0.4 mmol, 1 equiv or 0.8 mmol, 2 equiv). To the anode compartment was added a septum pierced with a needle to prevent pressurizing. After pressure equilibration, the needle was removed, and the cathode solution was removed from the cell via pipette. The anode solution was stirred in the cell for 16 h.

For NMR analyses – Following electrolysis, add dibromomethane internal standard to the anodic compartment. Upon substitution reaction completion, take up the solution in an NMR tube. Allylic amine coupling product yield was determined via ^{1}H NMR using dibromomethane as an internal standard.

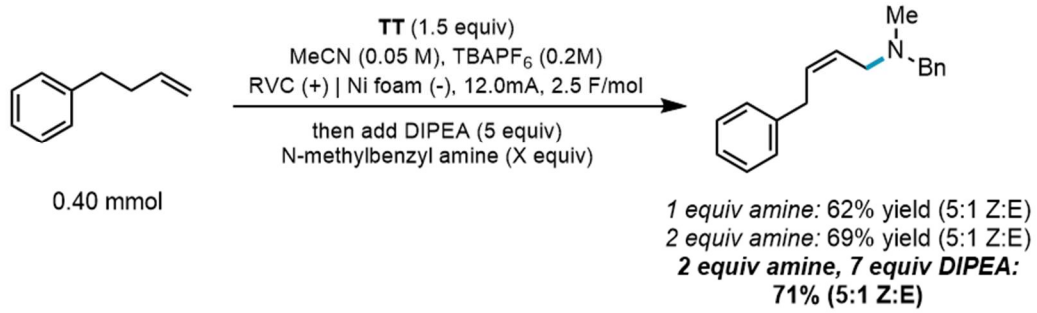

Scheme B1. Amine nucleophile and base equivalent optimization for limiting alkene 0.40 mmol scale reactions.

Internal Alkene Adduct Formation and Attempted Allylic Amination

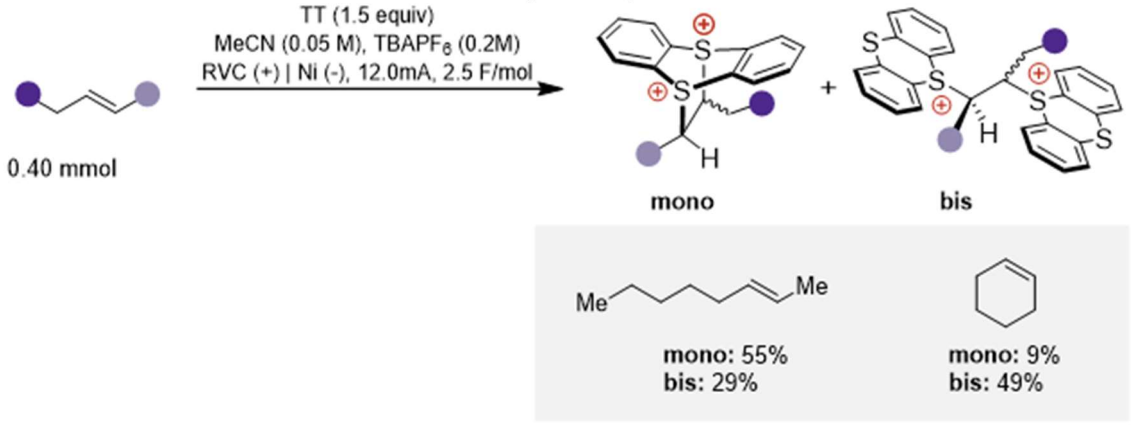

Fig. B2. 1,2-Disubstituted alkenes, which can form both mono- and bis- adduct under electrolysis in the presence of thianthrene, give intractable mixtures of products or eliminate to the internal vinylthianthrenium salt but do not react further when subjected to standard allylic amination conditions. Reactions performed on 0.4 mmol scale.

B.3 Substrate Preparations

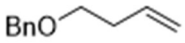

((but-3-en-1-yloxy)methyl)benzene (B1). To a suspension of NaH (60 % dispersion in mineral oil, 1.49 g, 37.2 mmol, 2 equiv) in DMF (30 mL) at 0°C was added but-3-en-1-ol (1.34 g, 15.0 mmol, 1.60 mL, 1 equiv) under inert atmosphere. After stirring for 45 min, (bromomethyl)benzene (2.5 g, 16.5 mmol, 2.43 mL, 1.1 equiv) was added dropwise. The temperature was slowly increased to room temperature and the reaction was stirred overnight (16 h). The reaction was then quenched with saturated NH_4Cl solution (~30 mL), diluted with water (~80 mL), and extracted with Et_2O (2x ~80 mL). The combined organic layer were washed with brine solution (~50 mL), dried over anhydrous MgSO4, filtered, and concentrated under reduced pressure. The residue was purified via flash column chromatography (EtOAc/hexanes) to give 1.92 g (64% yield) of **B1** as an oil. **^{1}H NMR** (500 MHz, $CDCl_3$) δ 7.39 (m, 4H), 7.32 (ddd, J = 8.7, 4.6, 2.2 Hz, 1H), 5.95 – 5.82 (m, 1H), 5.16 (dq, J = 17.2, 1.9 Hz, 1H), 5.13 – 5.07 (m, 1H), 4.57 (s, 2H), 3.58 (td, J = 6.7, 1.5 Hz, 2H), 2.43 (qd, J = 6.8, 1.6 Hz, 2H); consistent with reported spectra (*J. Am. Chem. Soc.* **2018**, 140, 49, 16976–16981).

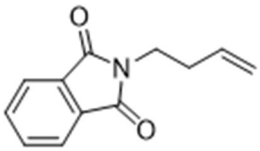

2-(but-3-en-1-yl)isoindoline-1,3-dione (B2). To a mixture of potassium phthalimide (741 mg, 4.0 mmol, 1 equiv) in DMF (8 mL) was added 4-bromo-1-butene (406 µL, 4 mmol, 1 equiv). The reaction mixture was heated to 60 °C and stirred overnight (16 h). At completion, the mixture was cooled to rt and poured into a saturated aqueous NaCl solution (~50 mL). The aqueous layer was extracted with Et2O (3 x 100 mL). The combined organic layers were washed with aqueous 10% LiCl solution (2 x 10 mL), dried over anhydrous MgSO4, filtered, and concentrated under reduced pressure. The residue was purified via flash column chromatography (EtOAc/hexanes) to give 492 mg (61% yield) of **B2** as a solid. **^{1}H NMR** (500 MHz, $CDCl_3$) δ 7.84 (dd, J = 5.4, 3.1 Hz, 2H), 7.71 (dd, J = 5.4, 3.0, 2H), 5.79 (ddt, J = 17.2, 10.2, 6.9 Hz, 1H), 5.07 (dd, J = 17.1, 1.7 Hz, 1H), 5.02 (dd, J = 10.3, 1.7 Hz, 1H), 3.77 (t, J = 7.1 Hz, 2H), 2.45 (q, J = 7.0 Hz, 2H); consistent with reported spectra (*J. Am. Chem. Soc.* **2017**, 139, 12153–12156).

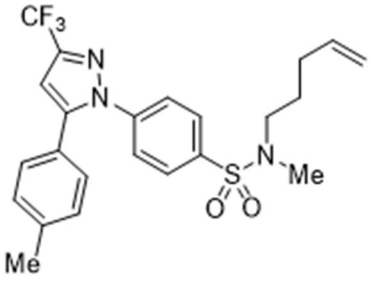

N-methyl-N-(pent-4-en-1-yl)-4-(5-(p-tolyl)-3-(trifluoromethyl)-1H-pyrazol-1-yl)benzenesulfonamide (B3). 4-(3-(p-tolyl)-5-(trifluoromethyl)-3H-2l4-pyrazol-2-yl)benzenesulfonamide (765 mg, 2.0 mmol, 1.0 equiv), 5-bromopent-1-ene (328 mg, 2.2 mmol, 261 µL, 1.1 equiv), K_2CO_3 (553 mg, 4.0 mmol, 2.0 equiv) were combined and placed under an atmosphere of nitrogen. The solids were then dissolved in acetone (2 mL) and reaction mixture was stirred at 60 ºC. Upon completion of the reaction (12 h), the solution was cooled to room temperature, filtered, rinsed with EtOAc, and concentrated under reduced pressure. The residue was purified via flash column chromatography (EtOAc/hexanes) to give 620.5 mg (69% yield) of N-(pent-4-en-1-yl)-4-(3-(p-tolyl)-5-(trifluoromethyl)-3H-2l4-pyrazol-2-yl)benzenesulfonamide as a solid.

^{1}H NMR (500 MHz, $CDCl_3$) δ 7.86 – 7.82 (m, 2H), 7.51 – 7.43 (m, 2H), 7.20 – 7.15 (m, 2H), 7.13 – 7.08 (m, 2H), 6.74 (s, 1H), 5.71 (ddt, J = 17.0, 10.2, 6.7 Hz, 1H), 5.00 (dq, J = 12.2, 1.5 Hz, 1H), 4.98 – 4.96 (m, 1H), 4.40 (t, J = 6.2 Hz, 1H), 3.03 – 2.91 (m, 2H), 2.38 (s, 3H), 2.17 – 1.96 (m, 2H), 1.65 – 1.53 (m, 2H); consistent with reported spectra (*J. Am. Chem. Soc.* **2021**, 143, 29, 11251–11261).

N-(pent-4-en-1-yl)-4-(3-(p-tolyl)-5-(trifluoromethyl)-3H-2l4-pyrazol-2-yl)benzenesulfonamide (430 mg, 957 µmol, 1.0 equiv) was dissolved in DMF (3.2 mL) and potassium carbonate (264 mg, 1.9 mmol, 2.0 equiv) was added, followed by methyl iodide (149 mg, 1.1 mmol, 65.5 µL, 1.1 equiv). The solution was heated to 50 °C in a vial without a vent and stirred at that temperature overnight (16 h). Upon completion, the reaction mixture was partitioned between 20 mL water and 10 mL EtOAc. The layers were separated, and the aqueous phase was extracted with EtOAc. The combined organic phases were washed 3x with 10% LiCl solution, dried over $MgSO_4$, and concentrated under reduced pressure. The residue was purified via flash column chromatography (EtOAc/hexanes) to give 421.2 mg (95% yield) of **B3** as a solid. **^{1}H NMR** (500 MHz, $CDCl_3$) δ 7.94 – 7.89 (m, 2H), 7.66 – 7.60 (m, 2H), 7.35 – 7.29 (m, 2H), 7.28 – 7.22 (m, 2H), 6.90 (s, 1H), 5.93 (ddt, J = 16.9, 10.2, 6.6 Hz, 1H), 5.19 (dq, J = 17.1, 1.7 Hz, 1H), 5.14 (dq, J = 10.2, 1.4 Hz, 1H), 3.18 – 3.12 (m, 2H), 2.87 (s, 3H), 2.53 (s, 3H), 2.28 – 2.20 (m, 2H), 1.78 (p, J = 7.4 Hz, 2H). **^{13}C NMR** (126 MHz, $CDCl_3$) δ 145.41, 144.26 (q, J = 38.5 Hz), 142.56, 139.95, 137.40, 129.88, 128.85, 128.45, 125.80, 125.73, 121.20 (q, J = 269.1 Hz), 115.65, 106.35, 106.33, 49.81, 34.80, 30.66, 26.94, 21.45. **^{19}F NMR** (377 MHz, $CDCl_3$) δ -62.44. **HRMS** (ESI+) Calc: $[M+H]^+$ ($C_{23}H_{25}F_3N_3O_2S$) 464.1614; measured: 464.1609 = 1.1 ppm difference.

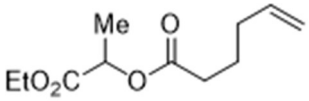

1-ethoxy-1-oxopropan-2-yl hex-5-enoate (B4). A mixture of hex-5-enoic acid (970 mg, 8.5 mmol, 1.00 mL, 1 equiv), N-(3-Dimethylaminopropyl)-N′-ethylcarbodiimide hydrochloride (2.12 g, 11.1 mmol, 1.3 equiv), and 4-(dimethylamino)pyridine (104 mg, 0.85 mmol, 0.1 equiv) in DCM (32 mL) was stirred at 0 °C for 20 min. Ethyl (R)-2-hydroxypropanoate (1.20 g, 10.2 mmol, 1.17 mL, 1.1 equiv) was added and the reaction mixture was allowed to warm to room temperature. At completion as monitored by TLC, the mixture was diluted with DCM and extracted with 1M HCl solution (~80 mL). The organic layer was washed with brine solution (~50 mL), dried over anhydrous MgSO4, filtered, and concentrated under reduced pressure. The residue was purified via flash column chromatography (EtOAc/hexanes) to give 1.17 g (64% yield) of **B4** as an oil. **^{1}H NMR** (500MHz, $CDCl_3$) δ 5.76 (ddt, J = 17.0, 10.2, 6.7 Hz, 1H), 5.04 (q, J = 7.1 Hz, 1H), 5.01 (dq, J = 16.4, 1.6 Hz, 1H), 4.97 (ddt, J = 10.2, 2.1, 1.2 Hz, 1H), 4.18 (qd, J = 7.2, 1.0 Hz, 2H), 2.45 – 2.30 (m, 2H), 2.10 (dtt, J = 7.9, 6.6, 1.4 Hz, 2H), 1.80 – 1.68 (m, 2H), 1.46 (d, J = 7.1 Hz, 3H), 1.25 (t, J = 7.1 Hz, 3H). **^{13}C NMR** (126 MHz, $CDCl_3$) δ 173.02, 170.95, 137.71, 115.51, 68.58, 61.38, 33.29, 33.02, 24.04, 17.01, 14.18. **HRMS** (ESI+) Calc: $[M+H]^+$ ($C_{11}H_{19}O_4$) 215.1278; measured: 215.1275 = 1.3 ppm difference.

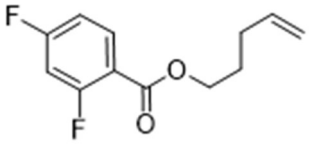

Pent-4-en-1-yl 2,4-difluorobenzoate (B5). A mixture of 2,4-difluorobenzoic acid (1.11 g, 7.0 mmol, 1 equiv), N-(3-Dimethylaminopropyl)-N′-ethylcarbodiimide hydrochloride (1.74 g, 9.1 mmol, 1.3 equiv), and 4-(dimethylamino)pyridine (86 mg, 0.7 mmol, 0.1 equiv) in DCM (28 mL) was stirred at 0 °C for 20 min. Pent-4-en-1-ol (724 mg, 8.4 mmol, 0.87 mL, 1.1 equiv) was added and the reaction mixture was allowed to warm to room temperature. At completion as monitored by TLC, the mixture was diluted with DCM and extracted with 1M HCl solution (~80 mL). The organic layer was washed with brine solution

(~50 mL), dried over anhydrous MgSO4, filtered, and concentrated under reduced pressure. The residue was purified via flash column chromatography (EtOAc/hexanes) to give 1.14 g (72% yield) of **B5** as an oil. **^{1}H NMR** (500MHz, $CDCl_3$) δ 7.95 (td, J = 8.5, 6.5 Hz, 1H), 6.91 (dddd, J = 8.7, 7.6, 2.5, 1.0 Hz, 1H), 6.85 (ddd, J = 11.1, 8.9, 2.5 Hz, 1H), 5.82 (ddt, J = 16.9, 10.2, 6.6 Hz, 1H), 5.05 (dq, J = 17.1, 1.7 Hz, 1H), 5.01 – 4.96 (m, 1H), 4.32 (t, J = 6.5 Hz, 2H), 2.24 – 2.15 (m, 2H), 1.84 (dq, J = 8.1, 6.6 Hz, 2H). **^{13}C NMR** (126 MHz, $CDCl_3$) δ 165.74 (dd, J = 256.1, 11.9 Hz), 163.64 (d, J = 4.2 Hz), 162.92 (dd, J = 263.2, 12.6 Hz), 137.43, 133.97 (dd, J = 10.4, 2.4 Hz), 115.51 (dd, J = 10.5, 3.7 Hz), 115.49, 111.60 (dd, J = 21.5, 4.0 Hz), 105.27 (dd, J = 26.2, 25.2 Hz), 64.82, 30.13, 27.87. **^{19}F NMR** (377 MHz, $CDCl_3$) δ -102.21 (d, J = 12.6 Hz), -103.89 (d, J = 12.3 Hz). **HRMS** (ESI+) Calc: $[M+H]^+$ ($C_{12}H_{13}F_2O_2$) 227.0878; measured: 227.0875 = 1.4 ppm difference.

B.4 General Experimental Procedures

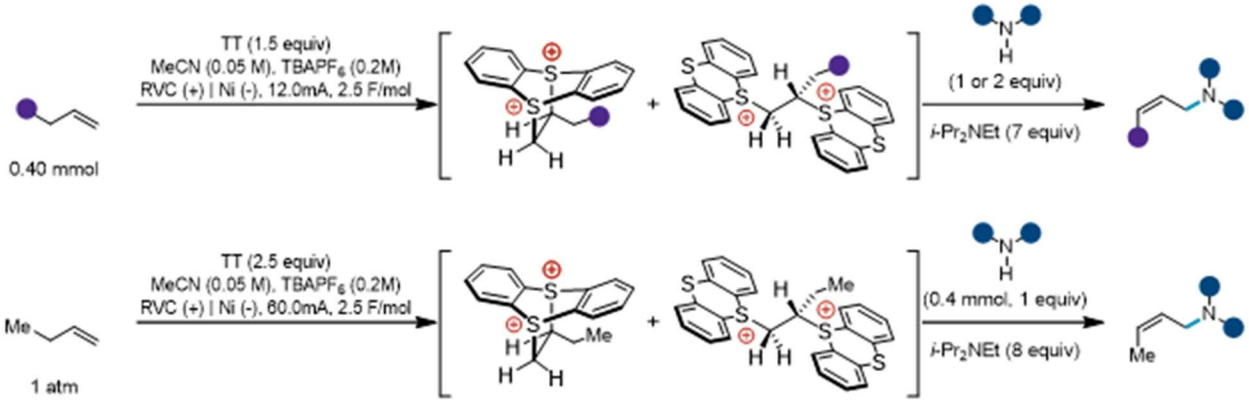

Fig. B3. Limiting amine (bottom, General Procedure B, 1-butene as representative alkene) and limiting alkene (top, General Procedure A) conditions for tertiary allylic amine formation.

CAUTION: Although there is no known toxicology data on these dicationic adducts and no issues were encountered during these experiments, we suspect, based on analogy to other dielectrophiles, that these adducts are extremely toxic. Isolation or storage of the adducts was avoided, and all substitutions were carried out *in situ*.

Note on reproducibility of conditions: undistilled DIPEA was used for substitution reactions. We found distilling both base and amine nucleophile resulted in quantitative conversion of alkene adduct to vinyl thianthrenium with no detected allylic amine product. Addition of 1 equivalent of water to distilled materials can recapitulate reactivity. We hypothesize that the role of water involves quenching of excess thianthrene radical cation. Mechanistic studies are ongoing.

General Procedure A: Limiting Alkene

To an oven-dried divided electrochemical cell equipped with magnetic stir bars was added thianthrene (130 mg, 0.6 mmol, 1.5 equiv) to the anode compartment and *n*-Bu_4NPF_6 (620 mg, 1.6 mmol) to both compartments. The cell was equipped with two septa containing a stainless steel wire/Ni foam cathode assembly and a pencil/RVC anode assembly connected together with a teflon tubing to equalize pressure. MeCN (8 mL) was added to the cathode and anode compartments. Alkene (0.4 mmol, 1 equiv) was added

to the anode compartment. Trifluoroacetic acid (308 μL, 4.0 mmol, 10 equiv) was added to the cathode compartment and both sides of the cell were stirred at 30 ˚C and electrolyzed under a constant current of 12.0 mA (5.8 mA/cm^2) for 2.2 h (2.5 F/mol). Average cell resistance = 0.9 kΩ. At completion of electrolysis, the electrode leads were disconnected, septa removed, and the anode RVC was pushed off the pencil into the reaction mixture. DIPEA (488 μL, 2.8 mmol, 7 equiv) was added to the anode compartment followed by amine (0.8 mmol, 2 equiv). To the anode compartment was added a septum pierced with a needle to prevent pressurizing. After pressure equilibration, the needle was removed, and the cathode solution was removed from the cell via pipette. The anode solution was stirred in the cell for 16 h. At completion, either workup A or workup B was followed to yield the pure allylamine product.

General Procedure B: Limiting Amine

To an oven-dried divided electrochemical cell equipped with magnetic stir bars was added thianthrene (216 mg, 1.0 mmol, 2.5 equiv) to the anode compartment and *n*-Bu_4NPF_6 (310 mg, 0.8 mmol) to both compartments. The cell was equipped with two septa containing a stainless steel wire/Ni foam cathode assembly and a pencil/RVC anode assembly connected together with a teflon tubing to equalize pressure. In a separate 25 mL-round bottom flask, MeCN (8mL) was sparged with a balloon of gaseous alkene for 8 mins. Alkene-saturated MeCN (4mL) was delivered to the cathode and anode compartments via Teflon cannula. Trifluoroacetic acid (460 μL, 6.0 mmol, 15 equiv) was added to the cathode compartment and both sides of the cell were stirred at ambient temperature and electrolyzed under a constant current of 60.0 mA (29 mA/cm^2) for 45 min (1.7 F/mol **TT**). Average cell resistance = 1.6 kΩ. At completion of electrolysis, the electrode leads were disconnected, septa removed, and the anode RVC was pushed off the pencil into the reaction mixture. DIPEA (560 μL, 3.2 mmol, 8 equiv) was added to the anode compartment followed by amine (0.4 mmol, 1 equiv). To the anode compartment was added a septum pierced with a needle to prevent pressurizing. After pressure equilibration, the needle was removed, and the cathode solution was removed from the cell via pipette. The anode solution was stirred in the cell for 3 h. At completion, two different workup procedures were followed depending on product sensitivity to acid.

Hydrochloride salts of amines (with an additional equivalent of DIPEA) were also used directly for substitution of electrochemically generated dicationic adducts.

Workup A:

The reaction mixture was diluted with ether (100 mL) and 6M HCl (30 mL). The organic layer was washed with 6M HCl (20 mL x 2). The combined aqueous layers were neutralized slowly with NaOH and extracted with DCM (60 mL x 3). The combined organic layers were dried with anhydrous $MgSO_4$, filtered, and concentrated under reduced pressure. The residue was purified via flash column chromatography to yield the pure allylamine product.

Workup B:

The reaction mixture was diluted with DCM (~60 mL) and 1M NaOH (150 mL). The aqueous layer was extracted with DCM (60 mL x 3). The combined organic layers were dried with anhydrous $MgSO_4$, filtered, and concentrated under reduced pressure. The residue was purified via flash column chromatography to yield the pure allylamine product.

Workup C:

The reaction mixture was diluted with DCM (~60 mL) and sat. $NaHCO_3$ (150 mL). The aqueous layer was extracted with DCM (60 mL x 3). The combined organic layers were dried with anhydrous $MgSO_4$,

filtered, and concentrated under reduced pressure. The residue was purified via flash column chromatography to yield the pure allylamine product.

General Procedure C: Limiting Alkene NMR Yield

Following General Procedure B, but with the following modification: following stirring with *N*-benzylmethylamine and DIPEA for 16 h, allylamine product yield was determined via ^{1}H NMR using mesitylene or dibromomethane as an internal standard.

General Procedure D: Limiting Amine NMR Yield

Following General Procedure A, but with the following modification: following stirring with amine and DIPEA for 3 h, allylic amine product yield was determined via NMR using dibromomethane as an internal standard.

Determination Z:E Selectivity – reported selectivity ratios were determined by ^{1}H NMR analysis of isolated or partially isolated compounds. See details below regarding assignment of major stereoisomer.

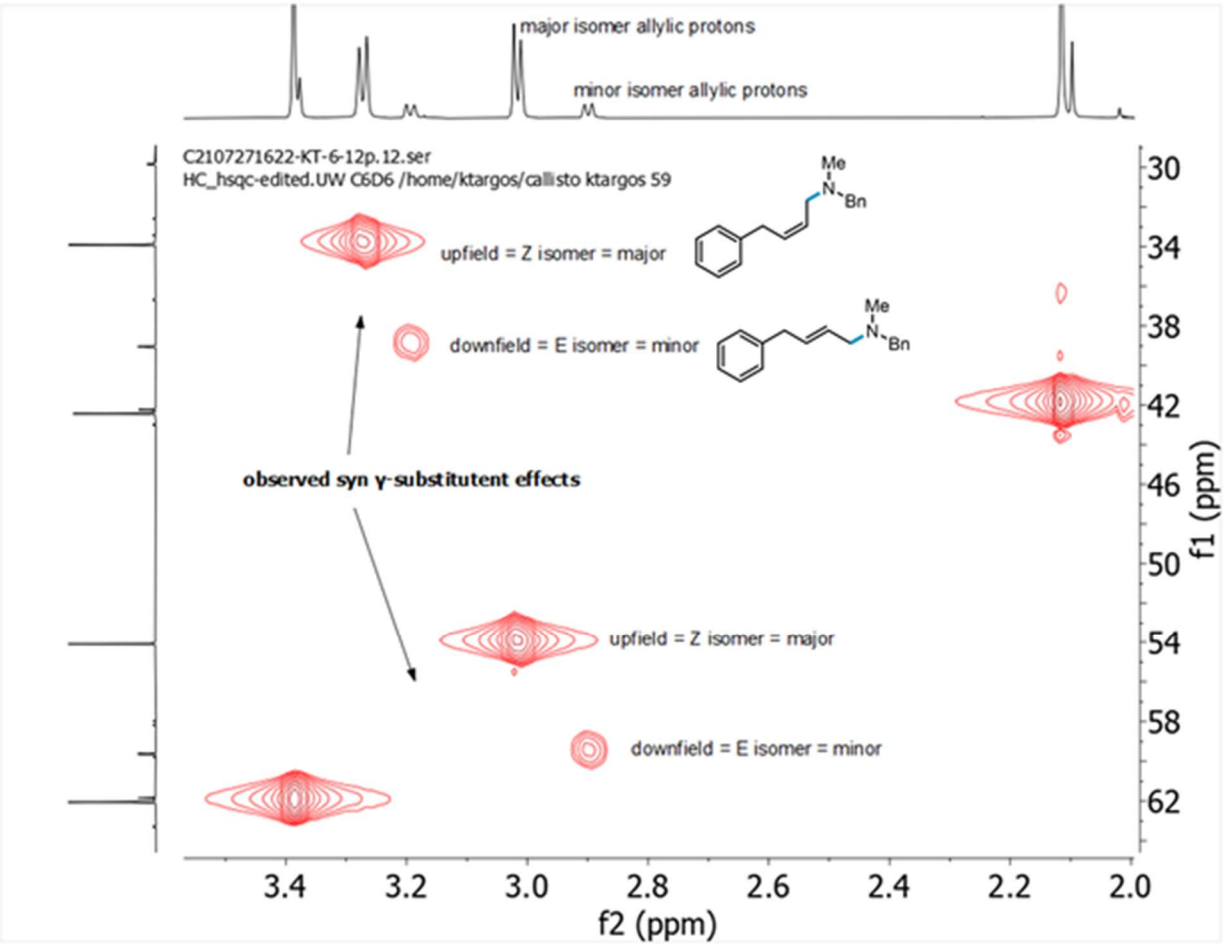

Fig. B4. Assignment was validated by ^{13}C-^{1}H NMR experiments using the correlation of the allyic protons to allylic carbon signal for which syn γ-substitutent effects of allylic carbon signals from *cis* isomers of alkenes are lower frequency (upfield). For a theoretical analysis see: Kleinpeter, E.; Seidl, P. R. *J. Phys. Org. Chem.* **2005**, 18, 272.

Additionally, authentic (Z)-N-benzyl-N-methylnon-2-en-1-amine was synthesized following literature precedent (*J. Am. Chem. Soc.* 2001, *123* (39), 9525–9534.).

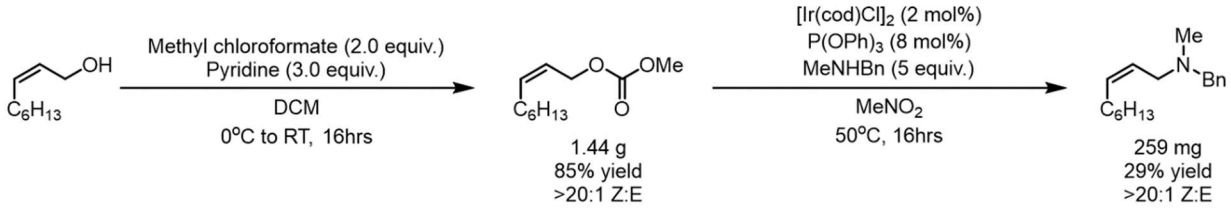

The synthesized authentic sample was doped into a crude reaction mixture of thianthrene promoted allylic amination coupling nonene and N-methylbenzylamine. Via ^{1}H NMR, observation of growth of major allylic signal confirms (Z)-allylic amine as major stereoisomer formed (see Figure **B5**).

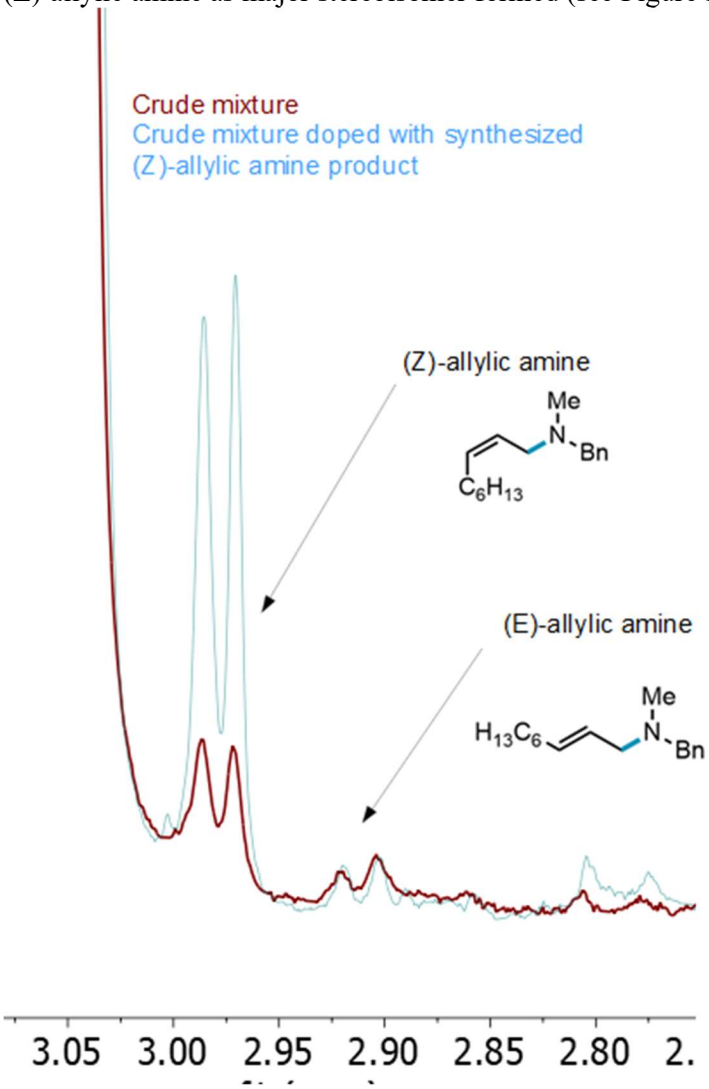

Fig. B5. Doping experiment to confirm (Z)-selective allylic amination.

B.5 Allylamine Product Isolation and Characterization

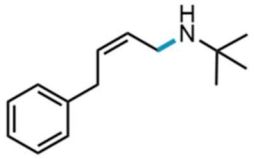

(Z)-N-(tert-butyl)-4-phenylbut-2-en-1-amine (3.3). Prepared from but-3-en-1-ylbenzene and tert-butylamine; 62% NMR yield (3:1 Z:E) obtained by following General Procedure C (using excess *tert*-butylamine in place of DIPEA). **HRMS** (ESI+) Calc: $[M+H]^+$ ($C_{14}H_{21}N$) 204.1747; measured: 204.1744 = 1.5 ppm difference.

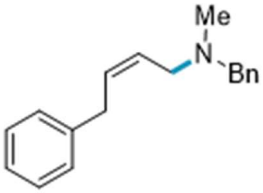

(Z)-N-benzyl-N-methyl-4-phenylbut-2-en-1-amine (3.4). Prepared from but-3-en-1-ylbenzene and N-methyl-1-phenylmethanamine; 67.8 mg (67% yield, 5:1 Z:E) obtained as an oil following General Procedure A and Workup B. **^{1}H NMR** (500 MHz, $CDCl_3$) δ 7.29 – 7.14 (m, 7H), 7.14 – 7.04 (m, 3H), 5.72 – 5.64 (m, 1H), 5.64 – 5.57 (m, 1H), 3.44 (s, 2H), 3.33 (d, J = 7.2 Hz, 2H), 3.07 (dd, J = 6.6, 1.4 Hz, 2H), 2.15 (s, 3H). Distinct minor *(E)*-isomer signals observed at δ 5.57 – 5.49 (m, 1H), 3.40 (s, 2H), 3.30 (d, J = 6.8 Hz, 2H), 2.92 (dd, J = 6.6, 1.2 Hz, 2H), 2.10 (s, 3H). **^{13}C NMR** (126 MHz, $CDCl_3$) δ 140.79, 139.19, 131.17, 129.21, 128.57, 128.44, 128.35, 128.10, 127.09, 126.08, 62.06, 54.09, 42.42, 33.90. Distinct minor *(E)*-isomer signals observed at δ 140.57, 139.21, 132.65, 128.97, 128.64, 128.53, 128.32, 127.04, 126.13, 61.85, 59.62, 42.22, 39.04. **HRMS** (ESI+) Calc: $[M+H]^+$ ($C_{18}H_{22}N$) 252.1747; measured: 252.1744 = 1.1 ppm difference.

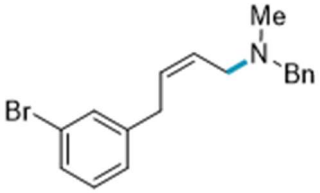

(Z)-N-benzyl-4-(3-bromophenyl)-N-methylbut-2-en-1-amine (3.7). Prepared from 1-bromo-3-(but-3-en-1-yl)benzene and N-methyl-1-phenylmethanamine; 95.9 mg (73% yield, 5:1 Z:E) obtained as an oil following General Procedure A and Workup A. **^{1}H NMR** (500 MHz, CDCl3) δ 7.28 – 7.23 (m, 6H), 7.19 (td, J = 5.8, 5.1, 2.8 Hz, 1H), 7.10 – 7.00 (m, 2H), 5.70 – 5.60 (m, 2H), 3.45 (s, 2H), 3.32 (d, J = 5.7 Hz, 2H), 3.06 (d, J = 5.2 Hz, 2H), 2.17 (s, 3H). Distinct minor *(E)*-isomer signals observed at δ 5.59 – 5.52 (m, 2H), 3.42 (s, 2H), 3.28 (d, J = 6.6 Hz, 2H), 2.95 (dd, J = 6.5, 1.2 Hz, 2H), 2.13 (s, 3H). **^{13}C NMR** (126 MHz, $CDCl_3$) δ 13C NMR (126 MHz, CDCl3) δ 143.12, 139.08, 131.54, 130.22, 130.11, 129.23, 129.22, 128.85, 128.39, 127.16, 127.10, 122.66, 62.11, 54.00, 42.45, 33.49. Distinct minor *(E)*-isomer signals observed at δ 142.92, 139.10, 131.73, 131.67, 130.09, 129.76, 129.29, 128.36, 127.32, 122.63, 61.90, 59.49, 42.25, 38.61. **HRMS** (ESI+) Calc: $[M+H]^+$ ($C_{18}H_{21}BrN$) 330.0852; measured: 330.0847 = 1.5 ppm difference.

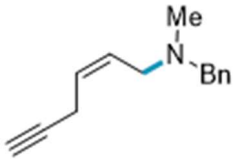

(Z)-N-benzyl-N-methylhex-2-en-5-yn-1-amine (3.8). Prepared from hex-1-en-5-yne and N-methyl-1-phenylmethanamine; 48.0 mg (60% yield, >20:1 Z:E) obtained as an oil following General Procedure A

and Workup A. **^{1}H NMR** (500 MHz, $CDCl_3$) δ 7.37 – 7.30 (m, 4H), 7.29 – 7.22 (m, 1H), 5.73 – 5.53 (m, 2H), 3.51 (s, 2H), 3.06 (d, J = 6.2 Hz, 2H), 2.98 (dd, J = 6.0, 2.4 Hz, 2H), 2.22 (s, 3H), 2.00 (t, J = 2.7 Hz, 1H). Distinct minor *(E)*-isomer signals observed at δ 5.95 – 5.80 (m, 2H), 2.21 (s, 3H). **^{13}C NMR** (126 MHz, $CDCl_3$) δ 139.02, 129.27, 129.20, 128.37, 127.15, 126.67, 82.44, 68.41, 61.97, 53.79, 42.37, 17.34. Distinct minor *(E)*-isomer signals observed at δ 129.70 128.34, 70.30, 61.86, 59.20, 42.22. **HRMS** (ESI+) Calc: $[M+H]^+$ ($C_{14}H_{18}N$) 200.1434 measured: 200.1433 = 0.5 ppm difference.

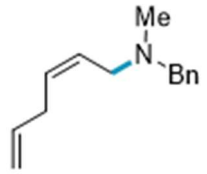

(Z)-N-benzyl-N-methylhexa-2,5-dien-1-amine (3.9). Prepared from hexa-1,5-diene and N-methyl-1-phenylmethanamine; 48.5 mg (69% yield, 5:1 Z:E) obtained as an oil following General Procedure A and Workup A. **^{1}H NMR** (500 MHz, $CDCl_3$) δ 7.31 – 7.26 (m, 4H), 7.24 – 7.17 (m, 1H), 5.86 – 5.71 (m, 1H), 5.00 (dq, J = 17.2, 1.8 Hz, 1H), 4.95 (dq, J = 10.2, 1.7 Hz, 1H), 5.08 – 4.85 (m, 2H), 3.45 (s, 2H), 3.02 (d, J = 6.0 Hz, 2H), 2.79 (t, J = 6.3 Hz, 2H), 2.16 (s, 3H). Distinct minor *(E)*-isomer signals observed at δ 2.97 (d, J = 5.8 Hz, 2H), 2.15 (s, 3H). **^{13}C NMR** (126 MHz, $CDCl_3$) δ 139.21, 136.60, 129.80, 129.21, 128.32, 128.31, 128.22, 128.17, 127.06, 115.03, 61.97, 53.97, 42.35, 31.89. Distinct minor *(E)*-isomer signals observed at δ 139.25, 136.92, 131.50, 128.64, 127.02, 115.34, 61.81, 59.70, 42.16, 36.67. **HRMS** (ESI+) Calc: $[M+H]^+$ ($C_{14}H_{20}N$) 202.1590; measured: 202.1590 = <0.1 ppm difference.

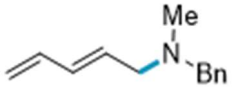

(E)-N-benzyl-N-methylpenta-2,4-dien-1-amine (3.10). Prepared from penta-1,4-diene and N-methyl-1-phenylmethanamine; 57% NMR yield (1:3 Z:E) obtained by following General Procedure C and Workup B. Peaks assigned partial isolation and ^{1}H-^{1}H COSY NMR analysis; stereochemistry determined using vinyl proton J_{HH} coupling values and ^{13}C-^{1}H HSQC NMR analysis. **HRMS** (ESI+) Calc: $[M+H]^+$ ($C_1H_{18}N$) 188.1434; measured: 188.1432 = 1.1 ppm difference.

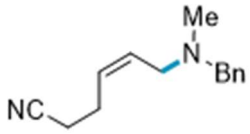

(Z)-6-(benzyl(methyl)amino)hex-4-enenitrile (3.11). Prepared from hex-5-enenitrile and N-methyl-1-phenylmethanamine; 66.0 mg (77% yield, 3:1 Z:E) obtained as an oil following General Procedure A and Workup B. **^{1}H NMR** (500 MHz, $CDCl_3$) δ 7.33 – 7.27 (m, 4H), 7.26 – 7.21 (m, 1H), 5.76 – 5.64 (m, 1H), 5.64 – 5.49 (m, 1H), 3.48 (s, 2H), 3.03 (dd, J = 6.9, 1.6 Hz, 2H), 2.41 – 2.29 (m, 4H), 2.19 (s, 3H). Distinct minor *(E)*-isomer signals observed at δ 3.02 – 2.98 (m, 2H), 2.18 (s, 3H). **^{13}C NMR** (126 MHz, $CDCl_3$) δ 138.90, 130.80, 129.11, 128.34, 128.11, 127.15, 119.29, 62.06, 53.78, 42.36, 23.62, 17.43. Distinct minor *(E)*-isomer signals observed at δ 138.96, 131.08, 129.12, 128.31, 127.07, 61.84, 59.21, 42.17, 28.26, 17.50. **HRMS** (ESI+) Calc: $[M+H]^+$ ($C_{14}H_{19}N_2$) 215.1543 measured: 215.1541 = 0.8 ppm difference.

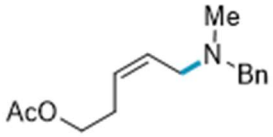

(Z)-5-(benzyl(methyl)amino)pent-3-en-1-yl acetate (3.12). Prepared from pent-4-en-1-yl acetate and N-methyl-1-phenylmethanamine; 65.7 mg (66% yield, 4:1 Z:E) obtained as an oil following General Procedure A and Workup B. **^{1}H NMR** (500 MHz, $CDCl_3$) δ 7.30 – 7.23 (m, 4H), 7.23 – 7.18 (m, 1H), 5.69 – 5.60 (m, 1H), 5.57 – 5.46 (m, 1H), 4.03 (t, J = 6.9 Hz, 2H), 3.45 (s, 2H), 3.01 (dd, J = 6.8, 1.6 Hz,

2H), 2.45 – 2.30 (m, 2H), 2.15 (s, 3H), 1.98 (s, 3H). Distinct minor *(E)*-isomer signals observed at δ 4.07 (t, J = 6.9 Hz, 2H), 3.44 (s, 2H), 2.98 – 2.92 (m, 2H), 2.13 (s, 3H). **^{13}C NMR** (126 MHz, $CDCl_3$) δ 171.12, 139.08, 130.02, 129.15, 128.32, 127.64, 127.08, 63.79, 61.97, 54.03, 42.29, 27.23, 21.02. Distinct minor *(E)*-isomer signals observed at δ 130.38, 129.02, 128.30, 127.04, 63.84, 61.71, 59.56, 42.09, 31.89, 23.69, 19.67. **HRMS** (ESI+) Calc: $[M+H]^+$ ($C_{15}H_{22}NO_2$) 248.1645 measured: 248.1643 = 0.8 ppm difference.

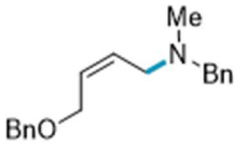

(Z)-N-benzyl-4-(benzyloxy)-N-methylbut-2-en-1-amine (3.13). Prepared from ((but-3-en-1-yloxy)methyl)benzene (**B1**) and N-methyl-1-phenylmethanamine; 58.5 mg (52% yield, 2:1 Z:E) obtained as an oil following General Procedure A and Workup B. **^{1}H NMR** (500 MHz, $CDCl_3$) δ 7.43 – 7.23 (m, 10H), 5.89 – 5.73 (m, 2H), 4.52 (s, 2H), 4.10 (d, J = 5.4 Hz, 2H), 3.49 (s, 2H), 3.05 (d, J = 5.7 Hz, 2H), 2.21 (s, 3H). Distinct minor *(E)*-isomer signals observed at δ 4.53 (s, 2H), 4.05 (d, J = 5.2 Hz, 2H), 3.52 (s, 2H), 3.07 (d, J = 5.8 Hz, 2H), 2.22 (s, 3H). **^{13}C NMR** (126 MHz, $CDCl_3$) δ 138.91, 138.30, 130.48, 129.67, 129.10, 128.43, 128.26, 127.80, 127.66, 127.05, 72.31, 65.90, 61.88, 54.06, 42.24. Distinct minor *(E)*-isomer signals observed at δ 139.00, 138.37, 131.15, 129.67, 129.16, 129.08, 128.41, 127.78, 127.61, 127.00, 72.07, 70.46, 61.79, 59.19, 42.19. **HRMS** (ESI+) Calc: $[M+H]^+$ ($C_{19}H_{24}NO$) 282.1852 measured: 282.1852 = <0.1 ppm difference.

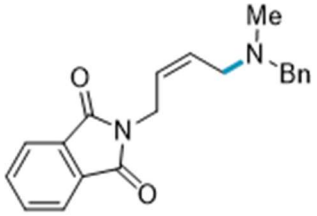

(Z)-2-(4-(benzyl(methyl)amino)but-2-en-1-yl)isoindoline-1,3-dione (3.14). Prepared from 2-(but-3-en-1-yl)isoindoline-1,3-dione (**B2**) and N-methyl-1-phenylmethanamine; 63% NMR yield (2:1 Z:E) obtained by following General Procedure C and Workup B. Peaks assigned by analogy to **3.13**.

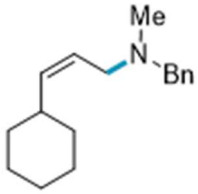

(Z)-N-benzyl-3-cyclohexyl-N-methylprop-2-en-1-amine (3.15). Prepared from allylcyclohexane and N-methyl-1-phenylmethanamine; 56.8 mg (58% yield, 2:1 Z:E) obtained as an oil following General Procedure A and Workup A. **^{1}H NMR** (500 MHz, $CDCl_3$) δ 7.32 – 7.20 (m, 4H), 7.20 – 7.14 (m, 1H), 5.40 – 5.28 (m, 2H), 3.42 (s, 2H), 2.98 (d, J = 5.7 Hz, 2H), 2.22 – 2.15 (m, 1H), 2.13 (s, 3H), 1.63 (ddt, J = 12.9, 6.8, 3.2 Hz, 2H), 1.59 – 1.49 (m, 2H), 1.25 – 1.14 (m, 3H), 1.13 – 1.05 (m, 1H), 1.05 – 0.93 (m, 2H). Distinct minor *(E)*-isomer signals observed at δ 5.56 – 5.40 (m, 2H), 3.41 (s, 2H), 2.90 (d, J = 6.3 Hz, 2H), 2.10 (s, 3H). **^{13}C NMR** (126 MHz, $CDCl_3$, mixture of major and minor stereoisomers) δ 140.40, 139.13, 138.99, 129.21, 129.14, 128.21, 128.20, 126.95, 126.93, 124.75, 124.29, 61.74, 61.48, 59.78, 54.15, 42.20, 41.92, 40.55, 36.55, 33.16, 33.01, 26.22, 26.06, 26.03, 25.89. **HRMS** (ESI+) Calc: $[M+H]^+$ ($C_{17}H_{26}N$) 244.2060 measured: 244.2058 = 0.7 ppm difference.

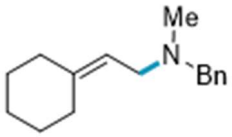

N-benzyl-2-cyclohexylidene-N-methylethan-1-amine (3.16). Prepared from vinylcyclohexane and N-methyl-1-phenylmethanamine; 48.4 mg (53% yield) obtained as an oil following a modified General Procedure A (4.0 mA instead of 12.0 mA current, and add 2 equiv of TFA to the anodic chamber) and Workup B. **^{1}H NMR** (500 MHz, $CDCl_3$) δ 7.36 – 7.27 (m, 4H), 7.27 – 7.22 (m, 1H), 5.25 (tt, J = 7.1, 1.2 Hz, 1H), 3.49 (s, 2H), 3.00 (d, J = 7.1 Hz, 2H), 2.18 (s, 3H), 2.15 (ddd, J = 14.7, 7.3, 3.3 Hz, 4H), 1.67 – 1.46 (m, 6H). **^{13}C NMR** (126 MHz, $CDCl_3$) δ 143.24, 139.39, 129.13, 128.17, 126.85, 118.39, 61.81, 54.02, 42.12, 37.35, 28.97, 28.67, 27.70, 26.86. **HRMS** (ESI+) Calc: $[M+H]^+$ ($C_{16}H_{24}N$) 230.1903 measured: 230.1901 = 1.0 ppm difference.

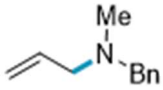

N-benzyl-N-methylprop-2-en-1-amine (3.17). Prepared from propene and N-methyl-1-phenylmethanamine; 47.9 mg (74% yield) obtained as an oil following General Procedure B and Workup B. **^{1}H NMR** (500 MHz, $CDCl_3$) δ 7.37 – 7.30 (m, 4H), 7.25 (m, J = 5.4, 4.2, 3.6 Hz, 1H), 5.92 (ddt, J = 16.8, 10.2, 6.4 Hz, 1H), 5.21 (m, 1H), 5.16 (ddt, J = 10.2, 2.2, 1.2 Hz, 1H), 3.50 (s, 2H), 3.04 (d, J = 6.5 Hz, 1H), 2.20 (s, 3H). **^{13}C NMR** (126 MHz, $CDCl_3$) δ 139.18, 136.09, 129.21, 128.35, 127.08, 117.59, 61.82, 60.68, 42.22. **HRMS** (ESI+) Calc: $[M+H]^+$ ($C_{11}H_{15}N$) 162.1277; measured: 162.1275 = 1.2 ppm difference.

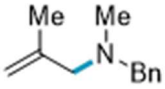

N-benzyl-N,2-dimethylprop-2-en-1-amine (3.18). Prepared from isobutene and N-methyl-1-phenylmethanamine; 43.3 mg (62% yield) obtained as an oil following General Procedure B and Workup B. **^{1}H NMR** (500 MHz, $CDCl_3$) δ 7.37 – 7.29 (m, 4H), 7.28 – 7.21 (m, 1H), 4.93 (dd, J = 2.3, 1.1 Hz, 1H), 4.90 – 4.82 (m, 1H), 3.45 (s, 2H), 2.90 (s, 2H), 2.14 (s, 3H), 1.79 (s, 3H). **^{13}C NMR** (126 MHz, $CDCl_3$) δ 143.82, 139.62, 128.82, 128.17, 126.80, 112.69, 64.62, 61.75, 42.24, 20.73. **HRMS** (ESI+) Calc: $[M+H]^+$ ($C_{12}H_{18}N$) 176.1434; measured: 176.1434 = <0.1 ppm difference.

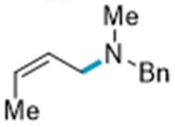

(Z)-*N*-Benzyl-*N*-methyl-1-buten-1-ylamine (3.19). Prepared from butene and N-methyl-1-phenylmethanamine; 47.9 mg (68% yield, 12:1 Z:E) obtained as an oil following General Procedure B and Workup A. **^{1}H NMR** (500 MHz, $CDCl_3$) δ 7.27 – 7.22 (m, 4H), 7.34 – 7.28 (m, 4H), 5.69 – 5.53 (m, 2H), 3.50 (s, 3H), 3.05 (dt, J = 6.7, 1.2 Hz, 2H), 2.20 (s, 3H), 1.66 – 1.62 (m, 3H). Distinct minor *(E)*-isomer signals observed at δ 3.48 (s, 3H), 2.97 (dd, J = 6.4, 1.31 Hz, 2H), 2.17 (s, 3H), 1.70 – 1.72 (m, 3H). **^{13}C NMR** (126 MHz, $CDCl_3$) δ 139.24, 129.27, 128.32, 127.73, 127.13, 127.05, 61.94, 53.72, 42.29, 13.27. Distinct minor *(E)*-isomer signals observed at δ 135.71, 128.86, 128.83, 128.52, 127.80, 127.59.83, 01, 61.76, 42.11, 17.96. **HRMS** (ESI+) Calc: $[M+H]^+$ ($C_{12}H_{17}N$) 176.1434; measured: 176.1433 = 0.6 ppm difference.

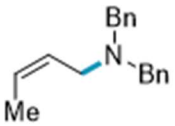

(Z)-N,N-dibenzylbut-2-en-1-amine (3.20). Prepared from butene and dibenzylamine; 71.6 mg (71% yield, 10:1 Z:E) obtained as an oil following General Procedure B and Workup A. **^{1}H NMR** (500 MHz,

$CDCl_3$) δ 7.40 (d, J = 6.6 Hz, 4H), 7.33 (t, J = 7.6 Hz, 4H), 7.25 (ddt, J = 8.8, 6.7, 1.5 Hz, 2H), 5.69 – 5.58 (m, 2H), 3.59 (s, 4H), 3.10 (d, J = 6.2 Hz, 2H), 1.60 (dd, J = 6.2, 1.2 Hz, 3H). Distinctive minor *(E)*-isomer signals observed at δ 3.57 (s, 4H), 3.03 (d, J = 6.2 Hz, 2H), 1.72 (dd, J = 5.9, 1.1 Hz, 3H). **^{13}C NMR** (126 MHz, $CDCl_3$) δ 139.96, 128.96, 128.27, 127.91, 127.08, 126.89, 58.09, 49.783 13.33. Distinctive minor *(E)*-isomer signals observed at δ 140.03, 128.91, 126.85, 57.80, 55.63, 18.02. **HRMS** (ESI+) Calc: $[M+H]^+$ ($C_{18}H_{21}N$) 252.1747; measured: 252.1744 = 1.2 ppm difference.

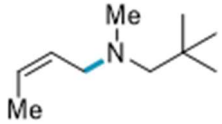

(Z)-N-methyl-N-neopentylbut-2-en-1-amine (3.21). Prepared from butene and N,2,2-trimethylpropan-1-amine; 38% NMR yield (10:1 Z:E) obtained by following General Procedure D and Workup A. **HRMS** (ESI+) Calc: $[M+H]^+$ ($C_{10}H_{21}N$) 156.1747; measured: 156.1746 = 0.6 ppm difference.

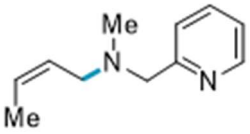

(Z)-N-methyl-N-(pyridin-2-ylmethyl)but-2-en-1-amine (3.22). Prepared from butene and N-methyl-1-(pyridin-2-yl)methanamine; 62% NMR yield (9:1 Z:E) obtained by following General Procedure D and Workup A. **HRMS** (ESI+) Calc: $[M+H]^+$ ($C_{11}H_{16}N_2$) 177.1386; measured: 177.1385 = 0.6 ppm difference.

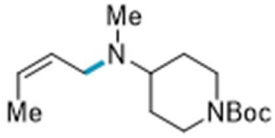

tert-butyl (Z)-4-(but-2-en-1-yl(methyl)amino)piperidine-1-carboxylate (3.23). Prepared from butene and tert-butyl 4-(methylamino)piperidine-1-carboxylate; 56% NMR yield (9:1 Z:E) obtained following General Procedure D and Workup B. **HRMS** (ESI+) Calc: $[M+H]^+$ ($C_{15}H_{28}N_2O_2$) 269.2224; measured: 269.2219 = 1.9 ppm difference.

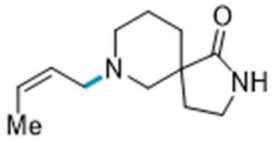

(Z)-8-(but-2-en-1-yl)-1,8-diazaspiro[4.5]decan-2-one (3.24). Prepared from butene and 1,8-diazaspiro[4.5]decan-2-one HCl salt; 71.1 mg (85% yield, >20:1 Z:E) obtained as an oil following General Procedure B and Workup C. **^{1}H NMR** (500 MHz, $CDCl_3$) δ 7.20 (br s, 1H), 5.61 – 5.53 (m, 1H), 5.43 – 5.36 (m, 1H), 3.27 (dt, J = 8.8, 5.6 Hz, 2H), 3.01 – 2.91 (m, 2H), 2.84 (d, J = 10.3 Hz, 1H), 2.59 (d, J = 11.1 Hz, 1H), 2.25 (ddd, J = 13.4, 8.0, 5.7 Hz, 1H), 2.05 (d, J = 11.1 Hz, 1H), 2.01 – 1.92 (m, 2H), 1.65 – 1.54 (m, 6H), 1.48 – 1.42 (m, 1H). **^{13}C NMR** (126 MHz, $CDCl_3$) δ 181.71, 127.38, 126.91, 58.58, 55.09, 54.00, 53.48, 44.60, 39.27, 31.82, 30.71, 22.33, 13.19. **HRMS** (ESI+) Calc: $[M+H]^+$ ($C_{12}H_{20}N_2O$) 209.1648; measured: 209.1645 = 1.4 ppm difference.

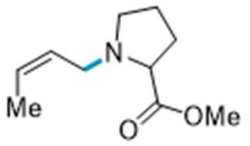

Methyl (Z)-but-2-en-1-yl-L-prolinate (3.25). Prepared from butene and methyl L-prolinate; 45.3 mg (62% yield, 10:1 Z:E) obtained as an oil following General Procedure B and Workup C. **^{1}H NMR** (500 MHz,

Acetone-d_6) δ 5.48 – 5.28 (m, 2H), 3.50 (s, 3H), 3.24 – 3.14 (m, 1H), 3.06 (dd, J = 8.9, 5.6 Hz, 1H), 3.02 – 2.97 (m, 1H), 2.87 (ddd, J = 8.7, 7.3, 3.7 Hz, 1H), 2.28 (dt, J = 8.7, 7.7 Hz, 1H), 1.98 – 1.85 (m, 3H), 1.82 – 1.55 (m, 3H), 1.55 – 1.41 (m, 3H). Distinctive minor *(E)*-isomer signals observed at δ 3.49 (s, 3H). **^{13}C NMR** (126 MHz, $CDCl_3$) δ 174.71, 128.54, 126.78, 65.43, 58.52, 53.56, 51.53, 50.47, 23.87, 13.12. Distinctive minor *(E)*-isomer signals observed at δ 129.72, 128.07, 65.35, 56.72, 51.50, 29.80, 17.81. **HRMS** (ESI+) Calc: $[M+H]^+$ ($C_{10}H_{17}NO_2$) 184.1332; measured: 184.1331; 0.5 ppm difference.

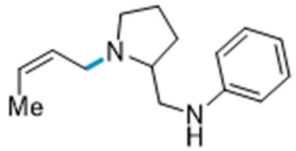

(Z)-N-((1-(but-2-en-1-yl)pyrrolidin-2-yl)methyl)aniline (3.26). Prepared from butene and (S)-N-(pyrrolidin-2-ylmethyl)aniline; 66.8 mg (73% yield, >20:1 Z:E) obtained as an oil following General Procedure B and Workup C. **^{1}H NMR** (500 MHz, $CDCl_3$) δ 7.25 – 7.15 (m, 2H), 6.72 (tt, J = 7.3, 1.1 Hz, 1H), 6.68 – 6.58 (m, 2H), 5.75 – 5.51 (m, 2H), 4.27 (s, 1H), 3.41 (dd, J = 13.7, 5.9 Hz, 0H), 3.30 – 3.11 (m, 3H), 3.02 (dd, J = 13.6, 7.2 Hz, 1H), 2.76 (dtd, J = 8.9, 5.4, 3.0 Hz, 1H), 2.39 – 2.25 (m, 1H), 2.06 – 1.88 (m, 1H), 1.87 – 1.74 (m, 3H), 1.71 – 1.64 (m, 3H). **^{13}C NMR** (126 MHz, $CDCl_3$) δ 148.97, 129.36, 127.57, 126.61, 117.01, 112.86, 62.61, 54.43, 50.24, 45.46, 28.83, 22.90, 13.21. **HRMS** (ESI+) Calc: $[M+H]^+$ ($C_{15}H_{22}N_2$) 231.1856; measured: 231.1853; 1.3 ppm difference.

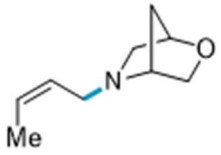

(1R,4R)-5-((Z)-but-2-en-1-yl)-2-oxa-5-azabicyclo[2.2.1]heptane (3.27). Prepared from butene and (1R,4R)-2-oxa-5-azabicyclo[2.2.1]heptane HCl salt; 32.4 mg (53% yield, 9:1 Z:E) obtained as an oil following General Procedure B and Workup B. **^{1}H NMR** (500 MHz, Acetone-d_6) δ 6.06 – 5.98 (m, 1H), 5.78 – 5.68 (m, 1H), 4.76 (t, J = 2.1 Hz, 1H), 4.59 (t, J = 2.3 Hz, 1H), 4.30 (dd, J = 10.0, 1.1 Hz, 1H), 4.18 (dd, J = 13.8, 7.3 Hz, 1H), 4.02 (dd, J = 13.7, 7.3 Hz, 1H), 3.89 (dd, J = 10.0, 2.0 Hz, 1H), 3.48 – 3.39 (m, 1H), 2.50 (d, *J* = 11.9 Hz, 2H), 2.22 (dt, J = 11.9, 2.6 Hz, 1H), 1.78 (dd, J = 7.0, 1.8 Hz, 3H). Distinct minor *(E)*-isomer signals observed at δ 2.43 (d, *J* = 12.1 Hz, 2H). **^{13}C NMR** (126 MHz, $CDCl_3$) δ 135.21, 127.94, 118.52, 114.09, 74.72, 63.79, 63.73, 55.61, 13.52. Distinct minor *(E)*-isomer signals observed at δ 119.49, 61.75, 56.12, 12.58. **HRMS** (ESI+) Calc: $[M+H]^+$ ($C_9H_{16}NO$) 154.1226; measured: 154.1226 = <0.1 ppm difference.

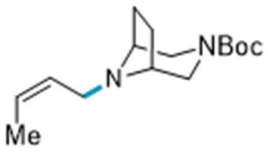

***tert*-butyl (1R,5S)-8-((Z)-but-2-en-1-yl)-3,8-diazabicyclo[3.2.1]octane-3-carboxylate (28).** Prepared from butene and *tert*-butyl (1R,5S)-3,8-diazabicyclo[3.2.1]octane-3-carboxylate; 85.6 mg (80% yield, 12:1 Z:E) obtained as an oil following General Procedure B and Workup B. **^{1}H NMR** (500 MHz, $CDCl_3$) δ 5.63 – 5.53 (m, 1H), 5.52 – 5.42 (m, 1H), 3.70 (d, J = 12.5 Hz, 1H), 3.57 (d, J = 12.4 Hz, 1H), 3.16 (s, 1H), 3.10 (s, 1H), 3.02 (d, J = 12.4 Hz, 1H), 2.97 (dt, J = 6.8, 1.2 Hz, 2H), 2.93 (d, J = 12.4 Hz, 1H), 1.95 – 1.78 (m, 2H), 1.61 – 1.56 (m, 5H), 1.41 (s, 9H). Distinct minor *(E)*-isomer signals observed at δ 2.86 (d, J = 6.0 Hz, 2H). **^{13}C NMR** (126 MHz, $CDCl_3$) δ 156.10, 127.86, 126.81, 79.42, 58.48, 58.47, 50.93, 49.77, 49.19, 28.52, 25.34, 25.16, 13.23. Distinct minor *(E)*-isomer signals observed at δ 128.56, 128.48, 58.17, 55.17, 30.40, 29.77, 17.88. **HRMS** (ESI+) Calc: $[M+H]^+$ ($C_{15}H_{27}N_2O_2$) 267.2067; measured: 267.2064 = 1.1 ppm difference.

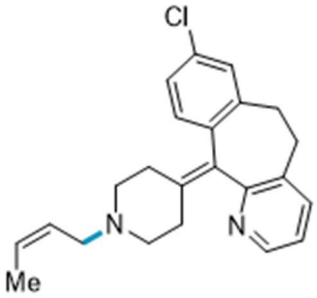

(Z)-11-(1-(but-2-en-1-yl)piperidin-4-ylidene)-8-chloro-6,11-dihydro-5H-benzo[5,6]cyclohepta[1,2-b]pyridine (3.29). Prepared from butene and Desloratadine; 68% NMR yield (10:1 Z:E) obtained by following General Procedure D and Workup A. **HRMS** (ESI+) Calc: $[M+H]^+$ ($C_{23}H_{25}ClN_2$) 365.1779; measured: 365.1776 = 0.8 ppm difference.

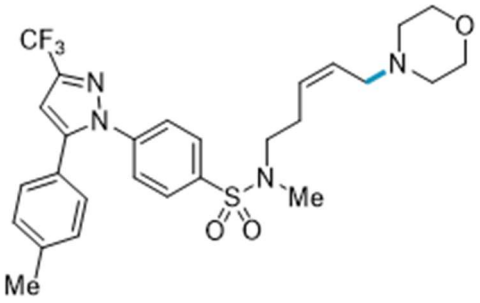

(Z)-N-methyl-N-(5-morpholinopent-3-en-1-yl)-4-(5-(p-tolyl)-3-(trifluoromethyl)-1H-pyrazol-1-yl)benzenesulfonamide (3.30). Prepared from N-methyl-N-(pent-4-en-1-yl)-4-(5-(p-tolyl)-3-(trifluoromethyl)-1H-pyrazol-1-yl)benzenesulfonamide (**B3**) and morpholine; 58% NMR yield (1:1 Z:E) obtained by following General Procedure C and Workup B. **HRMS** (ESI+) Calc: $[M+H]^+$ ($C_{27}H_{31}F_3N_4O_3S$) 549.2142 measured: 549.2140 = 0.4 ppm difference.

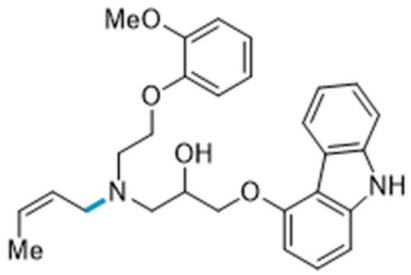

(Z)-1-((9H-carbazol-4-yl)oxy)-3-(but-2-en-1-yl(2-(2-methoxyphenoxy)ethyl)amino)propan-2-ol (3.31). Prepared from butene and Carvedilol; 103.3 mg (56% yield, 10:1 Z:E) obtained as a powder following General Procedure B and Workup C. **^{1}H NMR** (500 MHz, $CDCl_3$) δ 7.77 (d, J = 8.3, 1H), 8.26 (s, 1H), 7.39 – 7.33 (m, 2H), 7.29 (t, J = 8.0, 1H), 7.20 (ddd, J = 8.0, 5.8, 2.5 Hz, 1H), 7.00 (d, J = 8.1 Hz, 1H), 6.87 – 6.98 (m, 4H), 6.65 (d, J = 7.9 Hz, 1H), 5.53 – 5.73 (m, 2H), 4.28-4.34 (m, 2H), 4.21-4.26 (m, 1H), 4.11 – 4.18 (m, 2H), 3.83 (s, 3H), 3.38 (d, J = 6.7Hz, 2H), 3.15 (dt, J = 13.8, 6.1 Hz, 2H), 2.95 – 3.03 (m, 2H), 2.90 (dd, J = 13.0, 8.5 Hz, 1H), 1.64 – 1.68 (m, 3H). Distinctive minor *(E)*-isomer signals observed at δ 3.32 (d, J = 5.8 Hz, 2H). **^{13}C NMR** (126 MHz, $CDCl_3$) δ 155.36, 149.61, 149.58, 148.30, 141.06, 138.85, 129.49, 127.72, 126.88, 126.68, 123.13, 122.65, 121.45, 120.93, 119.56, 113.49, 112.74, 111.97, 111.91, 111.89, 110.08, 103.82, 101.12, 70.23, 67.37, 67.21, 57.69, 55.83, 53.43, 51.52, 13.23. Distinctive minor *(E)*-isomer signals observed at δ 124.94, 127.47, 123.07, 121.40, 119.60, 113.41, 70.27, 67.27, 57.55, 53.12, 17.90. **HRMS** (ESI+) Calc: $[M+Na]^+$ ($C_{28}H_{32}N_2O_4$) 469.2098; measured: 469.2021; 1.4 ppm difference.

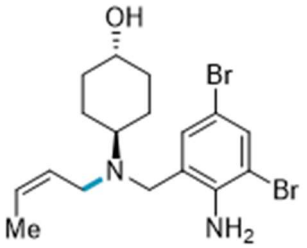

(1R,4R)-4-((2-amino-3,5-dibromobenzyl)((Z)-but-2-en-1-yl)amino)cyclohexan-1-ol (3.32). Prepared from butene and Ambroxol HCl; 38% NMR yield obtained by following General Procedure D and Workup C. No distinct minor isomers signals were observed by NMR spectroscopy. However, approximate selectivity of (8:1 Z:E) was determined using LC-MS analysis. **HRMS** (ESI+) Calc: $[M+H]^+$ ($C_{17}H_{24}Br_2N_2O$) 431.0328; measured: 431.0322 = 1.4 ppm difference.

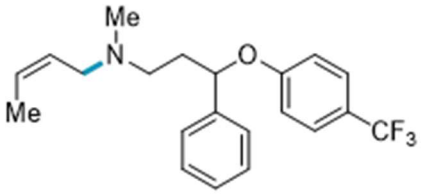

(Z)-N-methyl-N-(3-phenyl-3-(4-(trifluoromethyl)phenoxy)propyl)but-2-en-1-amine (3.33). Prepared from butene and Fluoxetine HCl salt; 97.3 mg (67% yield, 10:1 Z:E) obtained as an oil following General Procedure B and Workup A. **^{1}H NMR** (500 MHz, $CDCl_3$) δ 7.34 (d, J = 8.5 Hz, 2H), 7.30 – 7.21 (m, 4H), 7.21 – 7.13 (m, 1H), 6.82 (d, J = 8.6 Hz, 2H), 5.56-5.46 (m, 1H), 5.41-5.33 (m, 1H), 5.22 (dd, J = 8.3, 4.8 Hz, 1H), 2.96 (d, J = 6.9 Hz, 2H), 2.54-2.47 (m, 1H), 2.44-2.38 (m, 1H), 2.17 (s, 3H), 2.15 – 2.05 (m, 1H), 1.99 – 1.86 (m, 1H), 1.53 (dd, J = 6.9, 1.7 Hz, 3H). Distinctive minor *(E)*-isomer signals observed at δ 2.88 (t, J = 7.4 Hz, 2H), 2.16 (s, 3H). 13C NMR (126 MHz, $CDCl_3$) δ 160.73, 141.18, 128.75, 127.81, 127.40, 126.83, 126.71 (q, J = 3.77 Hz), 125.88, 124.43 (q, J = 271.07Hz), 122.72 (q, J = 32.7 Hz), 115.81, 78.52, 53.90, 53.20, 41.98, 36.48, 13.10. Distinctive minor *(E)*-isomer signals observed at δ 78.42, 59.97, 52.79, 41.85, 36.29, 13.57. **^{19}F NMR** (377 MHz, $CDCl_3$) δ -61.56. **HRMS** (ESI+) Calc: $[M+H]^+$ ($C_{21}H_{24}F_3NO$) 364.1883; measured: 364.1877 = 1.6 ppm difference.

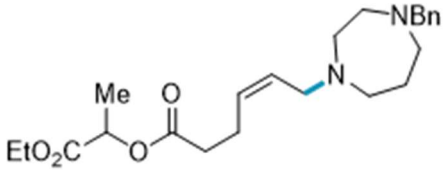

1-ethoxy-1-oxopropan-2-yl (Z)-6-(4-benzyl-1,4-diazepan-1-yl)hex-4-enoate (3.34). Prepared from 1-ethoxy-1-oxopropan-2-yl hex-5-enoate (**S4**) and 1-benzyl-1,4-diazepane; 80.4 mg (50% yield, 4:1 Z:E) obtained as an oil following General Procedure A (using 0.4 mmol, 1 equiv amine) and Workup B. **^{1}H NMR** (500 MHz, $CDCl_3$) δ 7.31 – 7.25 (m, 4H), 7.23 (dt, J = 7.0, 2.9 Hz, 1H), 5.78 – 5.67 (m, 2H), 4.97 (q, J = 7.1 Hz, 1H), 4.12 (qd, J = 6.9, 3.6 Hz, 2H), 3.67 (s, 2H), 3.61 – 3.51 (m, 2H), 3.37 – 2.63 (m, 8H), 2.54 – 2.28 (m, 4H), 2.28 – 1.80 (m, 2H), 1.41 (d, J = 7.0 Hz, 3H), 1.20 (t, J = 7.1 Hz, 3H). Distinct minor *(E)*-isomer signals observed at δ 5.86 – 5.78 (m, 2H), 3.44 (d, J = 7.1 Hz, 2H). **^{13}C NMR** (126 MHz, $CDCl_3$) δ 172.02, 170.64, 136.84, 136.25, 129.19, 128.65, 127.87, 120.95, 68.85, 62.26, 61.44, 54.31, 53.99, 53.52, 52.35, 49.81, 32.89, 23.83, 22.73, 16.90, 14.13. Distinct minor *(E)*-isomer signals observed at δ 171.93, 170.73, 129.15, 68.75, 61.37, 59.41, 52.35, 32.96, 22.23, 14.06. **HRMS** (ESI+) Calc: $[M+H]^+$ ($C_{23}H_{35}N_2O_4$) 403.2591 measured: 403.2585 = 1.5 ppm difference.

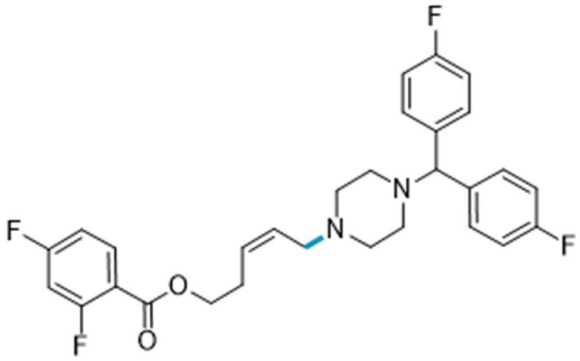

(Z)-5-(4-(bis(4-fluorophenyl)methyl)piperazin-1-yl)pent-3-en-1-yl 2,4-difluorobenzoate (3.35). Prepared from pent-4-en-1-yl 2,4-difluorobenzoate (**S5**) and 1-(bis(4-fluorophenyl)methyl)piperazine; 145.1 mg (71% yield, 2:1 Z:E) obtained as an oil following General Procedure A and Workup B. **^{1}H NMR** (500 MHz, $CDCl_3$) δ 7.96 (qd, J = 8.7, 6.5 Hz, 1H), 7.34 (ddd, J = 8.5, 5.4, 2.8 Hz, 4H), 7.01 – 6.95 (m, 4H), 6.94 – 6.87 (m, 1H), 6.87 – 6.79 (m, 1H), 5.71 – 5.58 (m, 2H), 4.36 (td, J = 6.6, 4.0 Hz, 2H), 4.22 (s, 1H), 3.06 (d, J = 5.3 Hz, 2H), 2.57 (q, J = 6.5 Hz, 1H), 2.68 – 2.09 (m, 7H), 1.68 (s, 2H). Distinct minor *(E)*-isomer signals observed at δ 4.21 (s, 1H), 2.97 (dd, J = 3.9, 1.6 Hz, 2H). **^{13}C NMR** (126 MHz, $CDCl_3$) δ 165.70 (dd, J = 256.5, 12.0 Hz), 163.49 (d, J = 4.1 Hz), 162.83 (dd, J = 263.3, 12.7 Hz), 162.79, 160.84, 138.25 (d, J = 3.3 Hz), 133.85 (dd, J = 10.5, 2.3 Hz), 129.24 (d, J = 7.8 Hz), 129.07, 127.86, 115.38 (d, J = 21.3 Hz), 111.55 (dd, J = 21.5, 4.0 Hz), 105.23 (dd, J = 25.7 Hz), 74.47, 64.55, 54.95, 53.34, 51.70, 31.86, 29.71, 27.16. Distinct minor *(E)*-isomer signals observed at δ 165.67 (dd, J = 256.5, 12.0 Hz), 163.40 (d, J = 4.1 Hz), 115.34 (d, J = 21.3 Hz), 111.52 (dd, J = 21.5, 4.0 Hz), 64.47, 60.63, 53.19, 51.62, 34.13, 30.33. **^{19}F NMR** (377 MHz, $CDCl_3$) δ -101.78 (dd, J = 38.9, 12.3 Hz, 1F), -103.78 (dd, J = 17.2, 12.4 Hz, 1F), -115.75 (d, J = 9.6 Hz, 2F). **HRMS** (ESI+) Calc: $[M+H]^+$ ($C_{29}H_{29}F_4N_2O_2$) 513.2160 measured: 513.2157 = 0.6 ppm difference.

B.6 Vinyl Thianthrenium Salt Mechanistic Studies

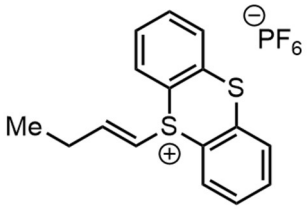

5-(but-1-en-1-yl)-5H-thianthren-5-ium hexafluorophosphate (3.36). Prepared from butene following procedure A except with no amine was added. Reaction was complete within 5 mins; 133.2 mg (32% yield, 1:1 E:Z) obtained as an oil. **^{1}H NMR** (500 MHz, $CDCl_3$) δ 8.16 (dt, J = 7.9, 1.7 Hz, 2H), 7.84 (dt, J = 7.9, 1.4 Hz, 2H), 7.75 (qd, J = 7.6, 1.4 Hz, 2H), 7.64 (tdd, J = 7.7, 4.4, 1.3 Hz, 2H), 7.20 (dt, J = 14.8, 6.3 Hz, 1H), 1H), 6.53 (dt, J = 14.8, 1.7 Hz, 1H), 2.29 (qdd, J = 7.4, 6.2, 1.7 Hz, 2H), 1.00 (t, J = 7.4 Hz, 3H). Distinctive minor *(Z)*-isomer signals observed at δ 6.79 (q, J = 8.0 Hz, 1H), 6.59 (dt, J = 8.6, 1.4 Hz), 2.73 (pd, J = 7.5, 1.4 Hz, 2H), 1.10 (t, J = 7.5 Hz, 2H). **^{13}C NMR** (126 MHz, $CDCl_3$) δ 158.77, 135.62, 134.69, 133.09, 130.38, 130.35, 120.24, 108.70, 53.55, 26.70, 11.29. Distinctive minor *(Z)*-isomer signals observed at δ 157.20, 135.74, 134.58, 132.65, 130.58, 130.36, 120.85, 110.67, 24.01, 12.68. **^{19}F NMR** (377 MHz, $CDCl_3$) δ -71.95, -73.83. **HRMS** (ESI+) Calc: $[M]^+$ ($C_{16}H_{15}S_2$) 271.0610; measured: 271.0605; 1.8 ppm difference.

Subjecting Vinyl-TT+ salt intermediate 35 to Substitution Reaction Conditions (Eq. 3.1)

Dissolved 5-(but-1-en-1-yl)-5H-thianthren-5-ium hexafluorophosphate (**3.36**) (1 equiv) in MeCN (0.05M). Added DIPEA (7 equiv), followed by N-methylbenzylamine (2 equiv). Let stir at room temperature for 3 hrs. Added in CH_2Br_2 as an internal standard and took an NMR aliquot to quantify NMR yield.

B.7 NMR Spectra

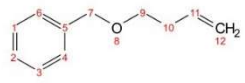

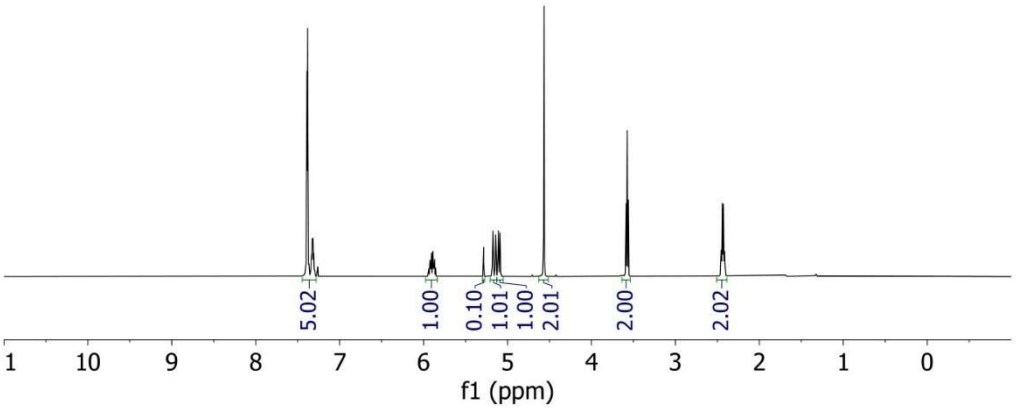
5.02
1.00
0.10
1.01
1.00
2.01
2.00
2.02
1 10 9 8 7 6 5 4 3 2 1 0
f1 (ppm)

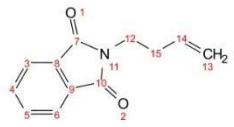

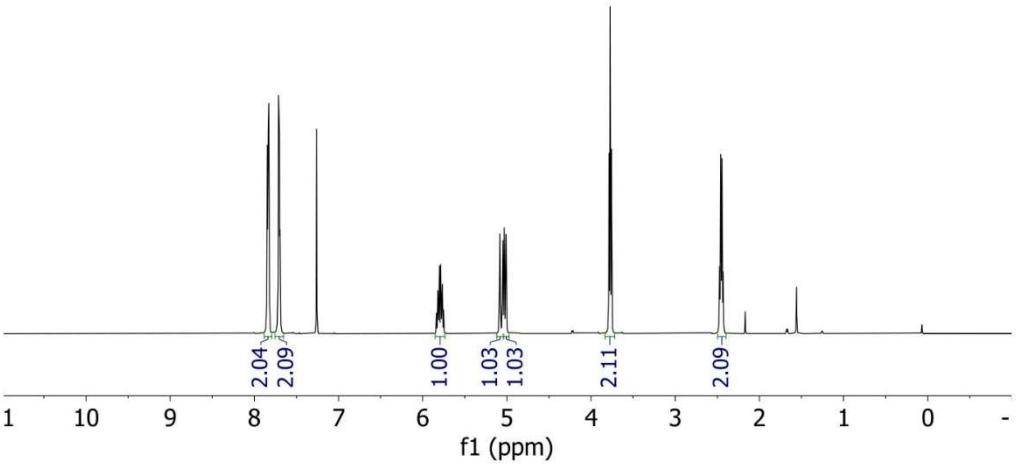
2.04
2.09
1.00
1.03
1.03
2.11
2.09
1 10 9 8 7 6 5 4 3 2 1 0 -
f1 (ppm)

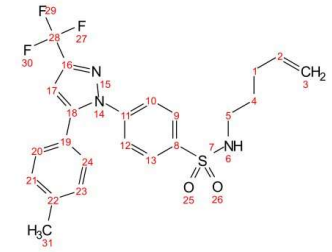

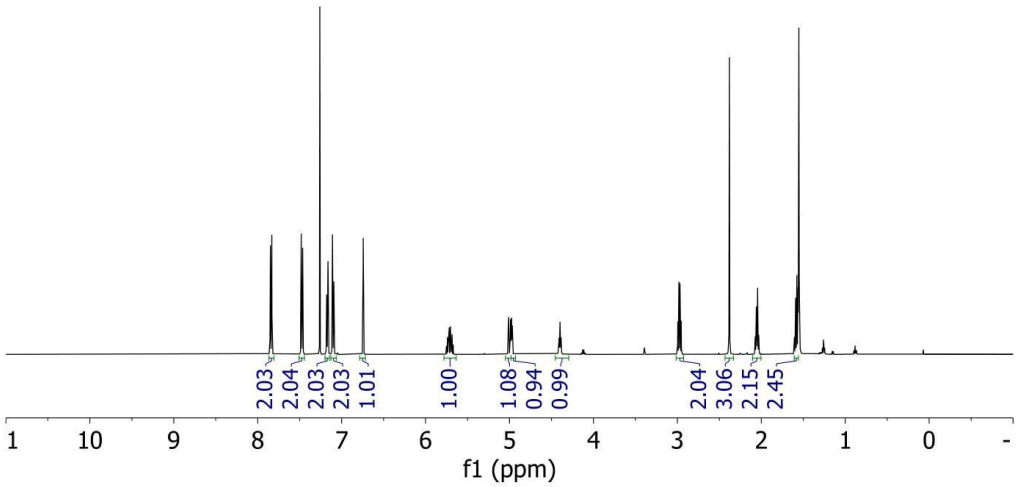
2.03
2.04
2.03
2.03
1.01
1.00
1.08
0.94
0.99
2.04
3.06
2.15
2.45
1 10 9 8 7 6 5 4 3 2 1 0 -
f1 (ppm)

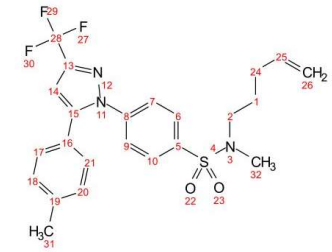

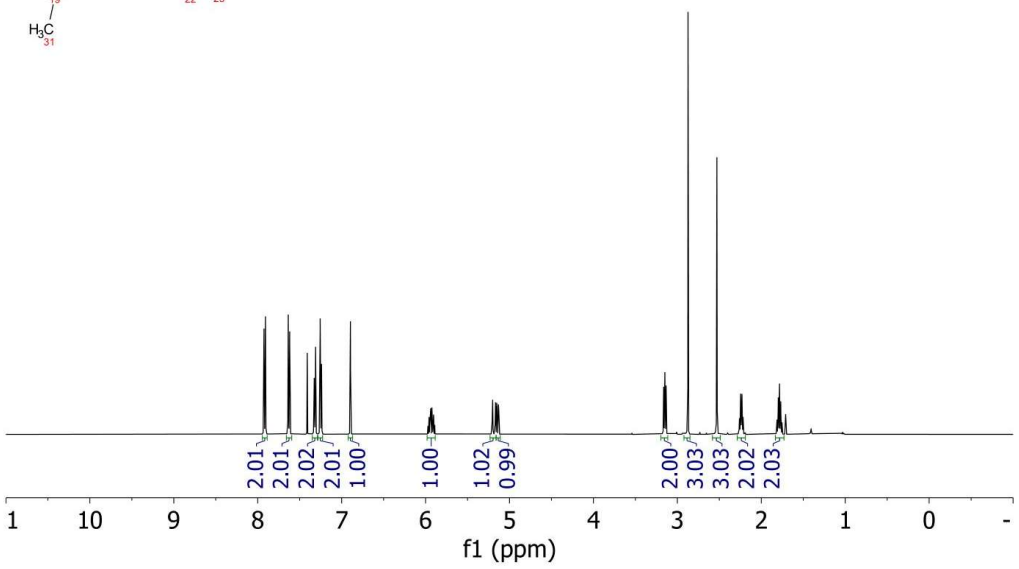
2.01
2.01
2.02
2.01
1.00
1.00
1.02
0.99
2.00
3.03
3.03
2.02
2.03
1 10 9 8 7 6 5 4 3 2 1 0 -
f1 (ppm)

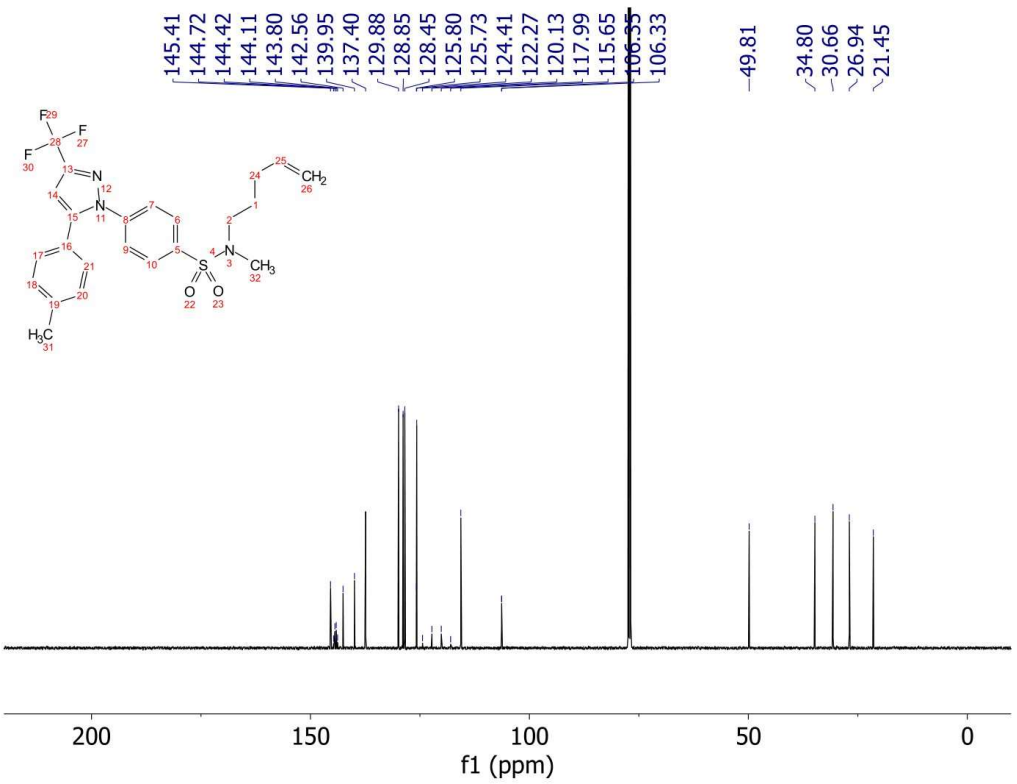
145.41
144.72
144.42
144.11
143.80
142.56
139.95
137.40
129.88
128.85
128.45
125.80
125.73
124.41
122.27
120.13
117.99
115.65
106.33
106.33
49.81
34.80
30.66
26.94
21.45
200
150
100
50
0
f1 (ppm)

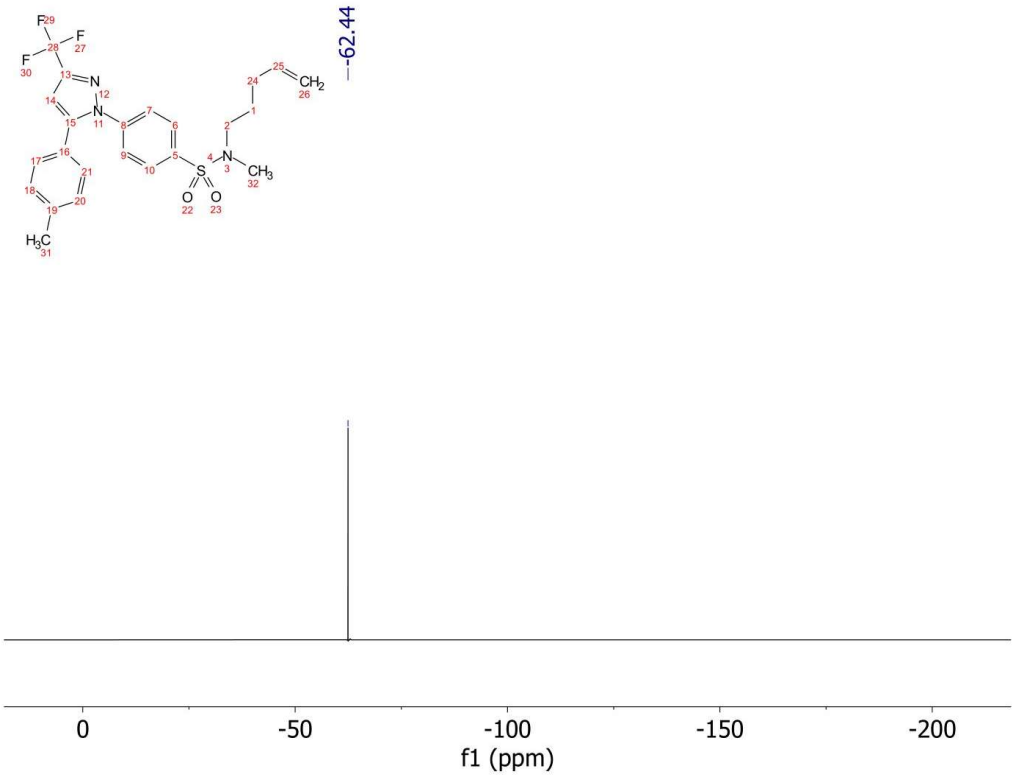
-62.44
0
-50
-100
-150
-200
f1 (ppm)

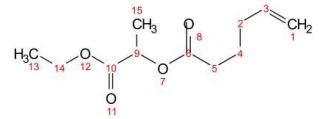

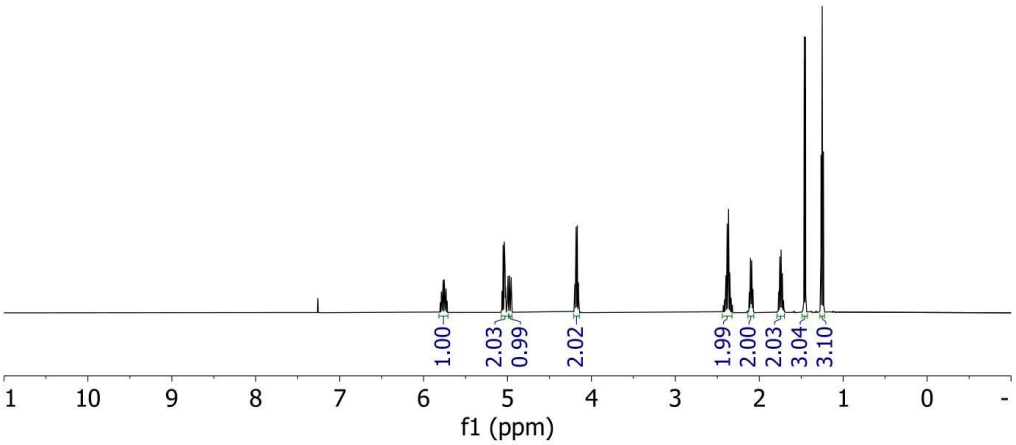

173.02
170.95
137.71
115.51
68.58
61.38
33.29
33.02
24.04
17.01
14.18

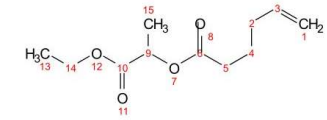

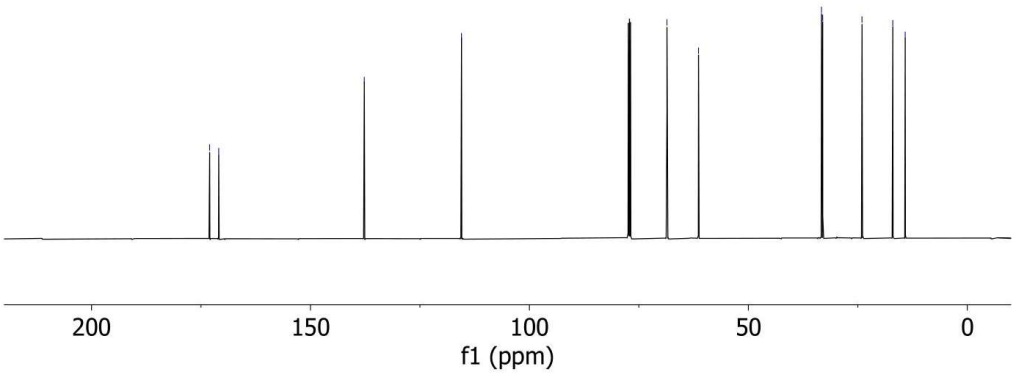

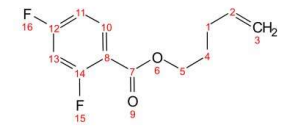
F
16
11
12
10
13
8
14
7
O
6
5
4
1
2
CH2
3
F
15
O
9

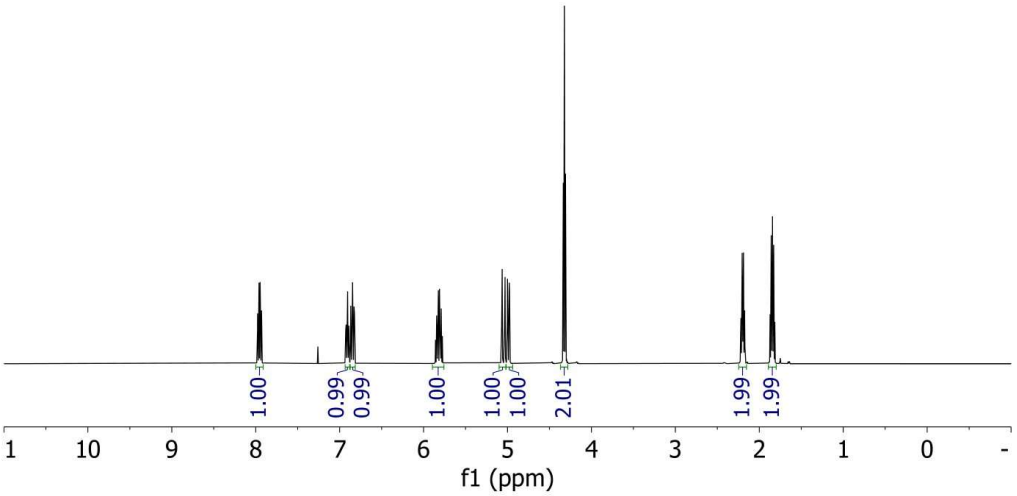
1.00
0.99
0.99
1.00
1.00
1.00
2.01
1.99
1.99
1
10
9
8
7
6
5
4
3
2
1
0
-
f1 (ppm)


166.80
166.71
164.77
164.67
164.02
163.92
163.66
163.62
161.92
161.82
137.43
134.02
134.00
133.94
133.92
115.57
115.54
115.49
115.46
111.70
111.67
111.53
111.50
105.47
105.27
105.26
105.06
64.82
30.13
27.87

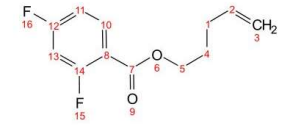
F
16
11
12
10
13
8
14
7
O
6
5
4
1
2
CH2
3
F
15
O
9

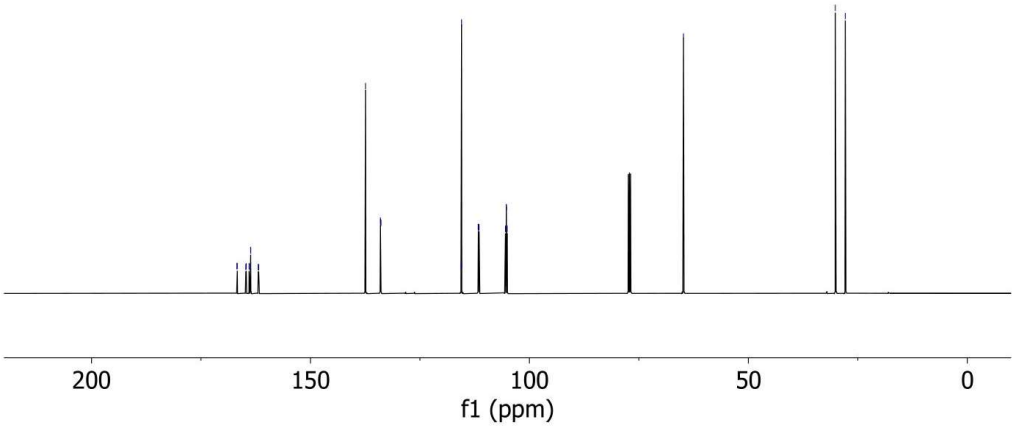
200
150
100
50
0
f1 (ppm)

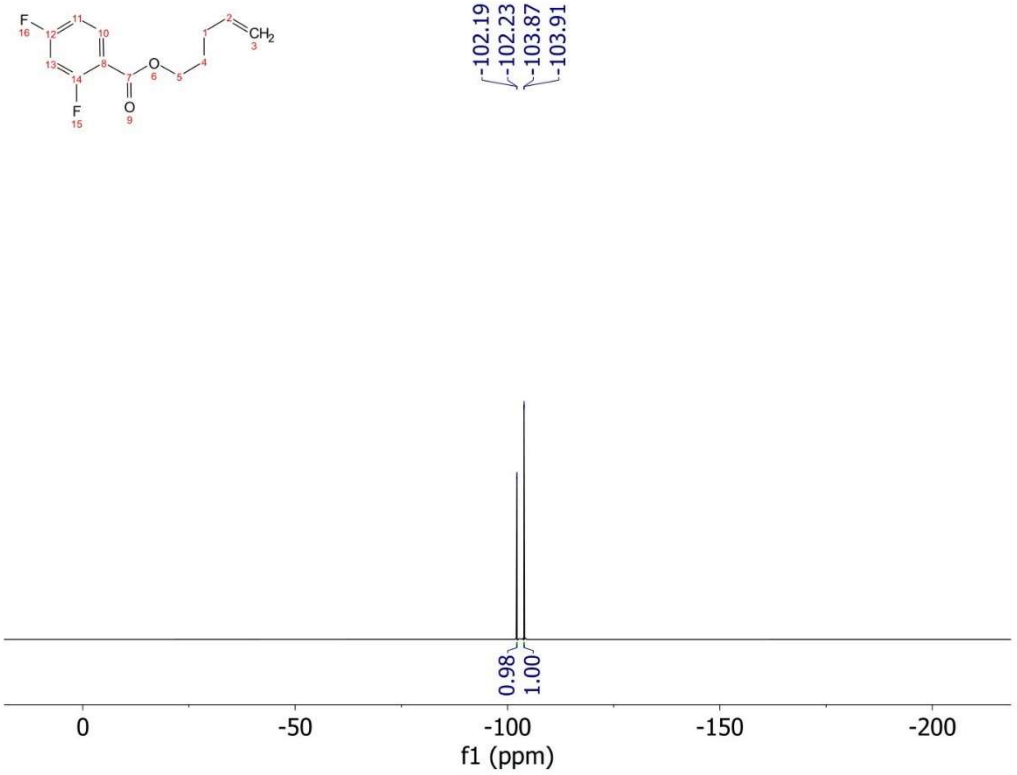
-102.19
-102.23
-103.87
-103.91
0.98
1.00
0
-50
-100
-150
-200
f1 (ppm)
10.40
1.01
0.99
1.68
0.35
1.67
0.37
1.66
0.35
2.51
0.52
1
10
9
8
7
6
5
4
3
2
1
0
f1 (ppm)

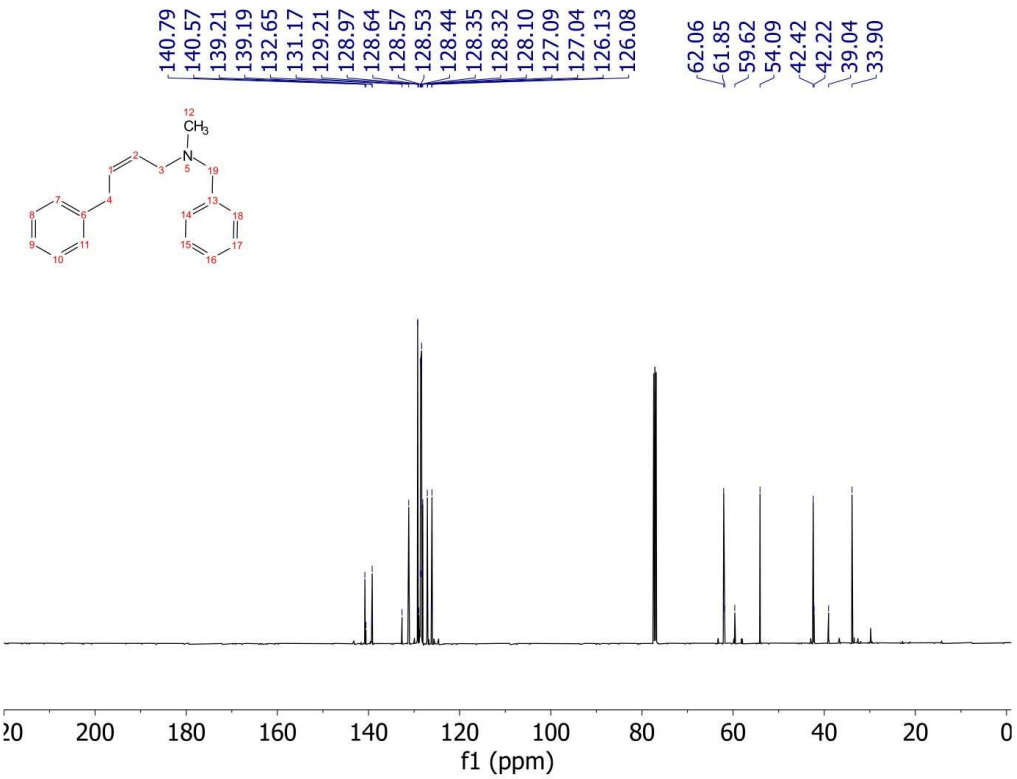
140.79
140.57
139.21
139.19
132.65
131.17
129.21
128.97
128.64
128.57
128.53
128.44
128.35
128.32
128.10
127.09
127.04
126.13
126.08
62.06
61.85
59.62
54.09
42.42
42.22
39.04
33.90
CH3
N
f1 (ppm)

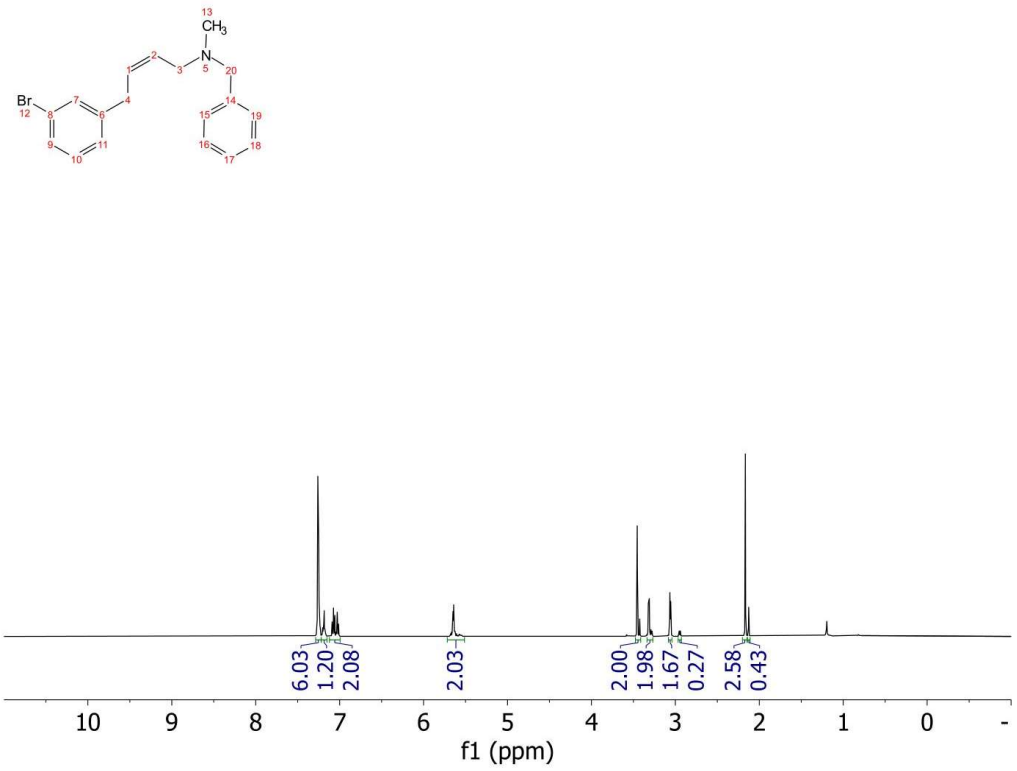
CH3
Br
6.03
1.20
2.08
2.03
2.00
1.98
1.67
0.27
2.58
0.43
f1 (ppm)

143.12
142.92
139.10
139.08
131.73
131.67
131.54
130.22
130.11
130.09
129.76
129.29
129.23
129.22
128.85
128.39
128.36
127.32
127.16
127.10
122.66
122.63
62.11
61.90
59.49
54.00
42.45
42.25
38.61
33.49

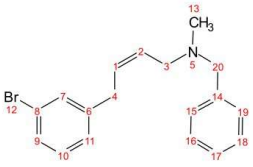

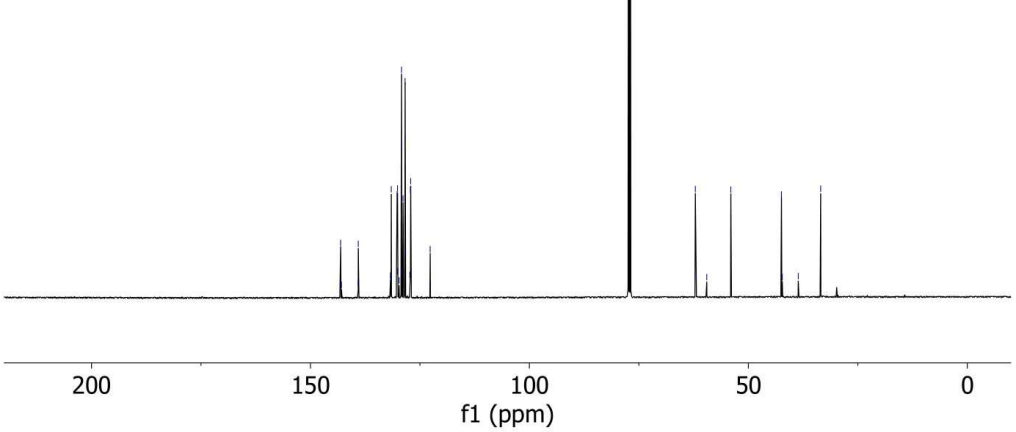

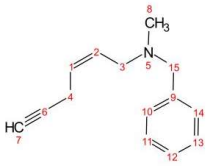

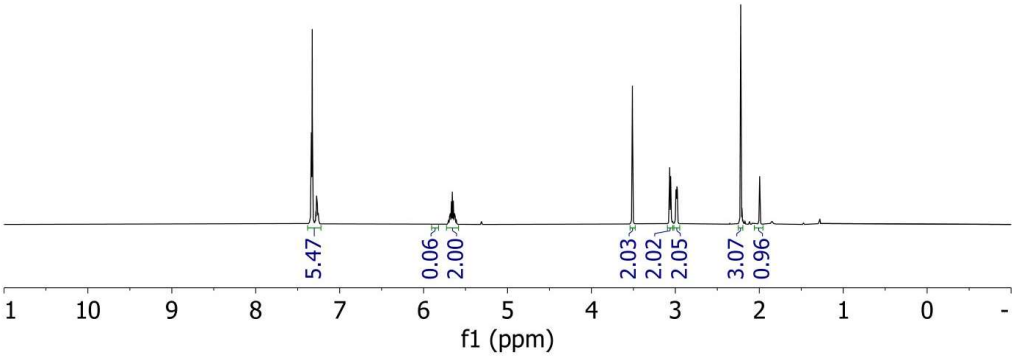

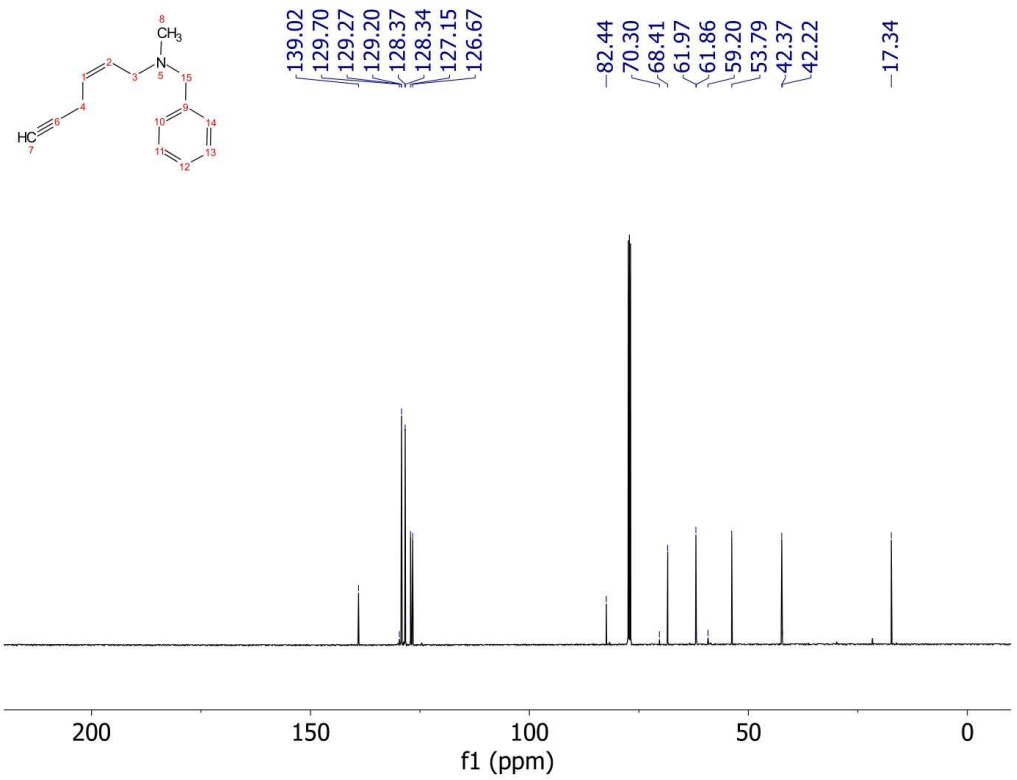
139.02
129.70
129.27
129.20
128.37
128.34
127.15
126.67
82.44
70.30
68.41
61.97
61.86
59.20
53.79
42.37
42.22
17.34
200
150
100
50
0
f1 (ppm)

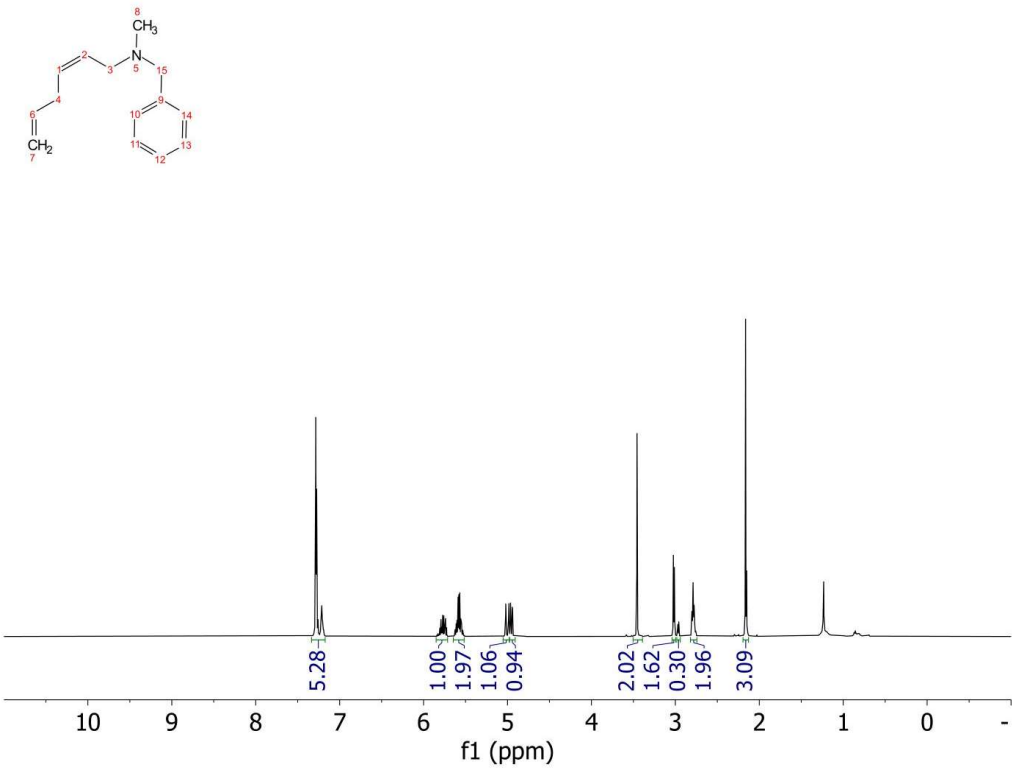
5.28
1.00
1.97
1.06
0.94
2.02
1.62
0.30
1.96
3.09
10
9
8
7
6
5
4
3
2
1
0
-
f1 (ppm)

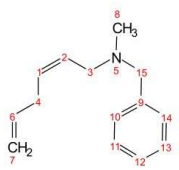


139.25
139.21
136.92
136.60
131.50
129.80
129.21
128.64
128.32
128.17
127.06
127.02
115.34
115.03
61.97
61.81
59.70
53.97
42.35
42.16
36.67
31.89

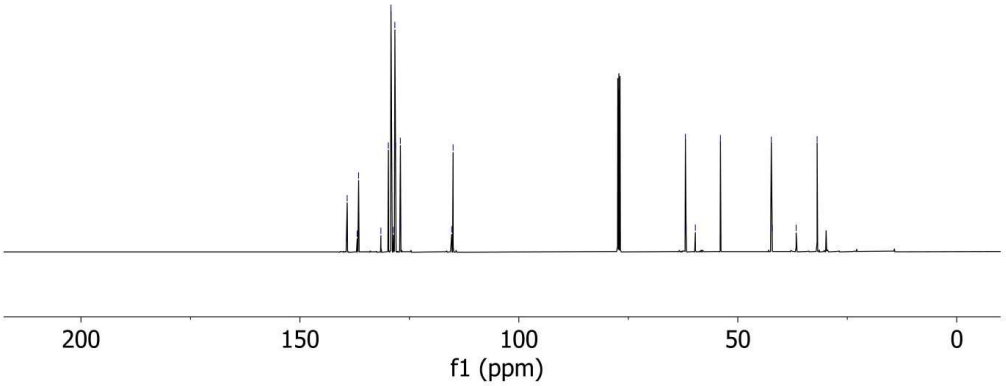
200
150
100
50
0
f1 (ppm)

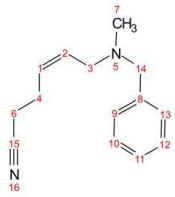

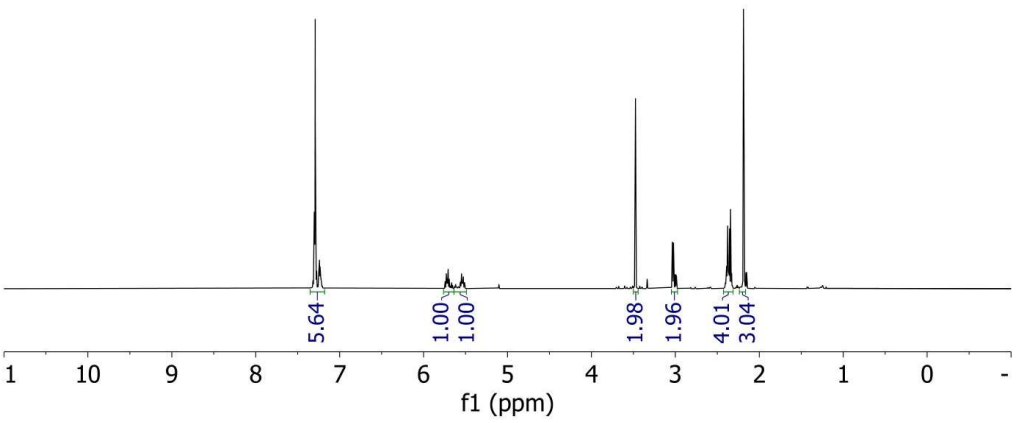
5.64
1.00
1.00
1.98
1.96
4.01
3.04
1
10
9
8
7
6
5
4
3
2
1
0
-
f1 (ppm)

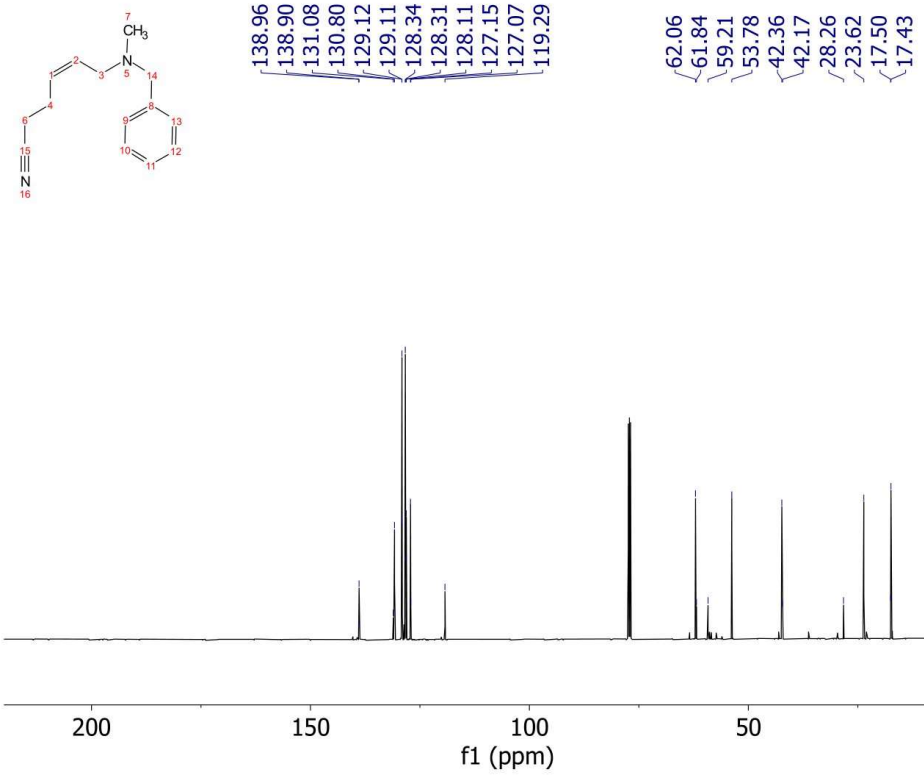
138.96
138.90
131.08
130.80
129.12
129.11
128.34
128.31
128.11
127.15
127.07
119.29
62.06
61.84
59.21
53.78
42.36
42.17
28.26
23.62
17.50
17.43
200
150
100
50
0
f1 (ppm)

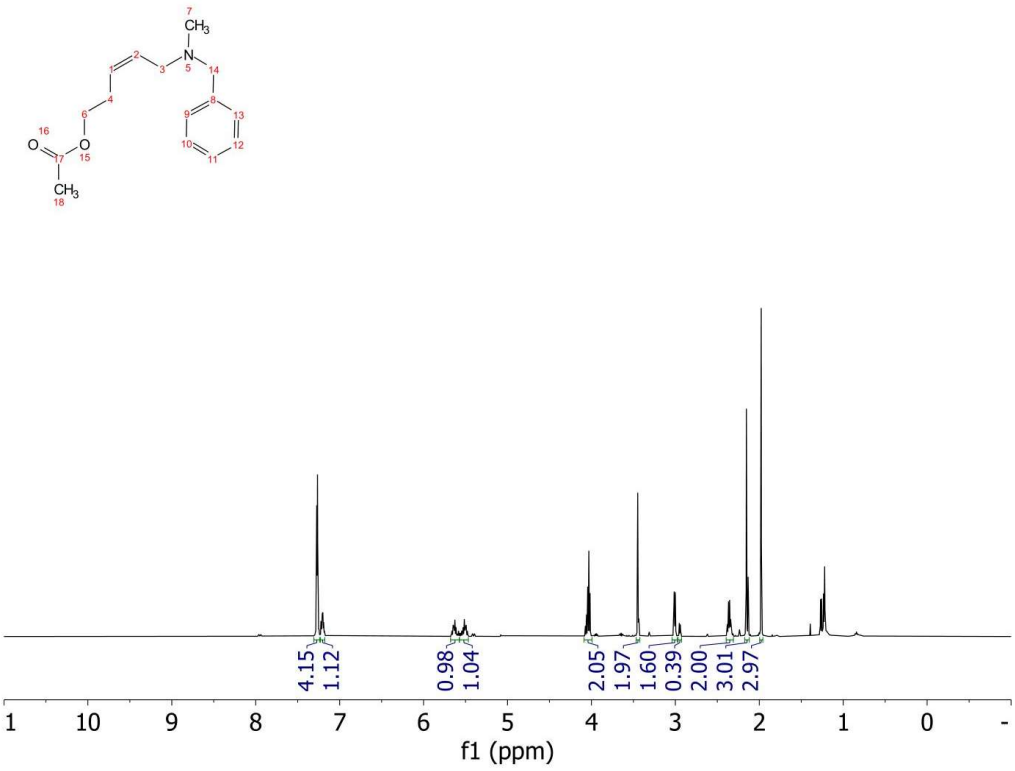
4.15
1.12
0.98
1.04
2.05
1.97
1.60
0.39
2.00
3.01
2.97
1
10
9
8
7
6
5
4
3
2
1
0
-
f1 (ppm)

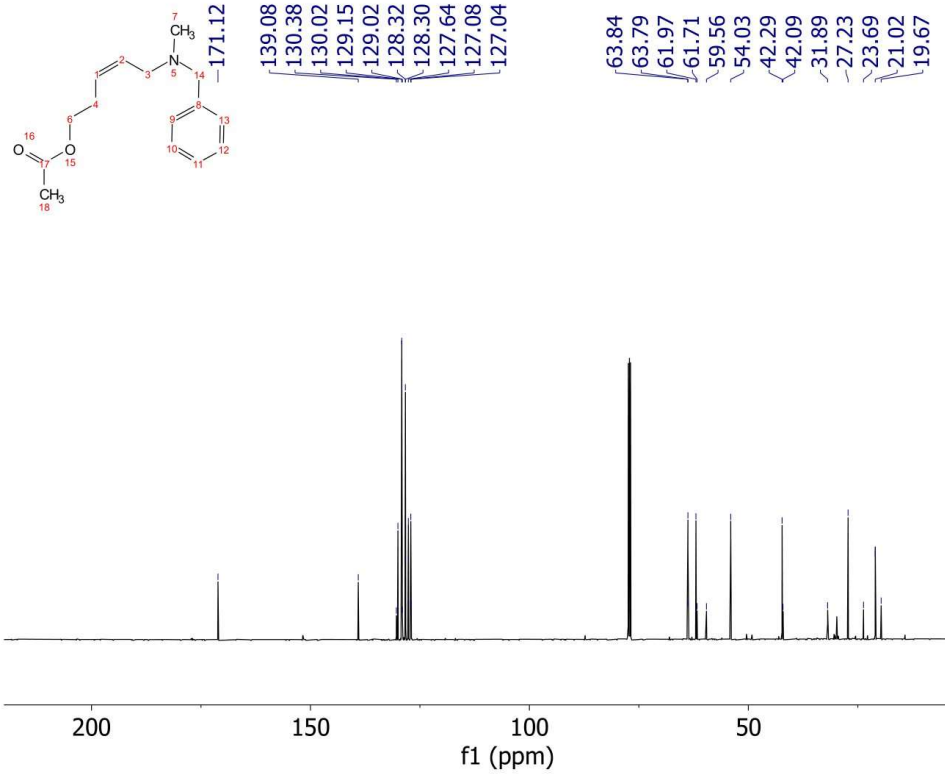
171.12
139.08
130.38
130.02
129.15
129.02
128.32
128.30
127.64
127.08
127.04
63.84
63.79
61.97
61.71
59.56
54.03
42.29
42.09
31.89
27.23
23.69
21.02
19.67
200
150
100
50
0
f1 (ppm)

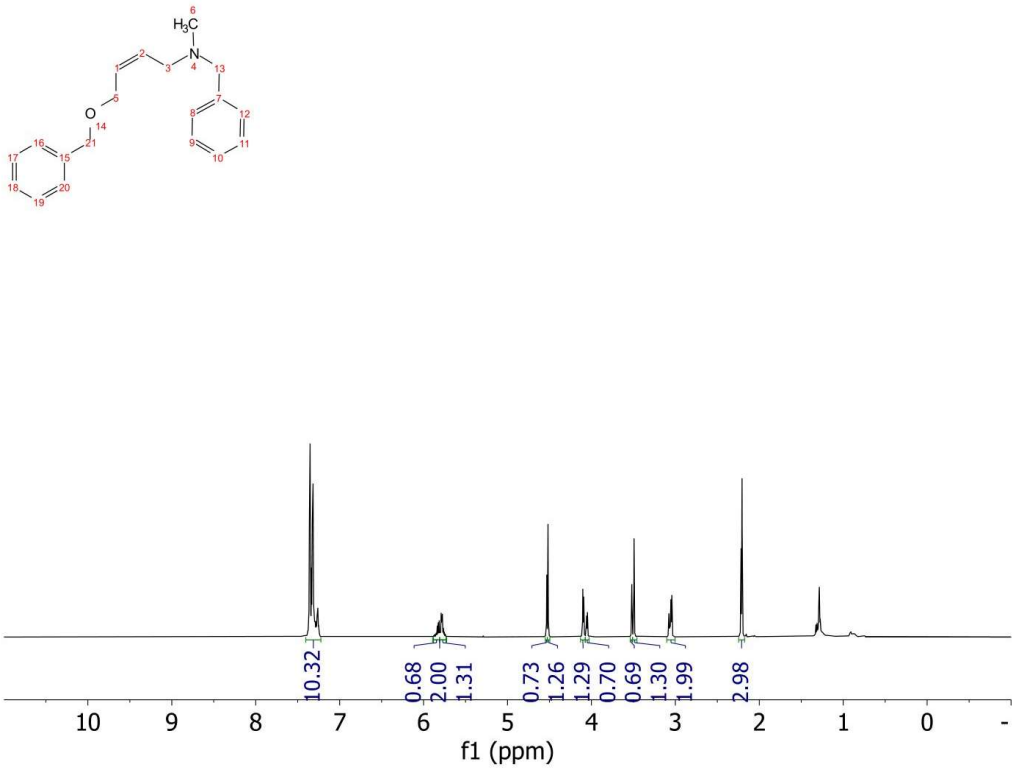
10.32
0.68
2.00
1.31
0.73
1.26
1.29
0.70
0.69
1.30
1.99
2.98
10
9
8
7
6
5
4
3
2
1
0
-
f1 (ppm)

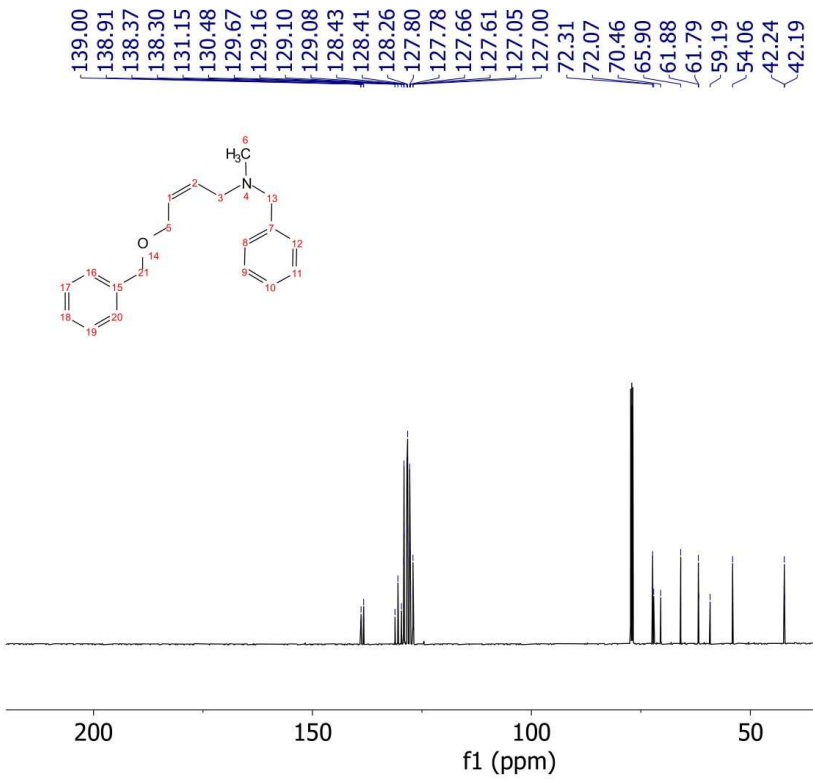
139.00
138.91
138.37
138.30
131.15
130.48
129.67
129.16
129.10
129.08
128.43
128.41
128.26
127.80
127.78
127.66
127.61
127.05
127.00
72.31
72.07
70.46
65.90
61.88
61.79
59.19
54.06
42.24
42.19
200
150
100
50
0
f1 (ppm)

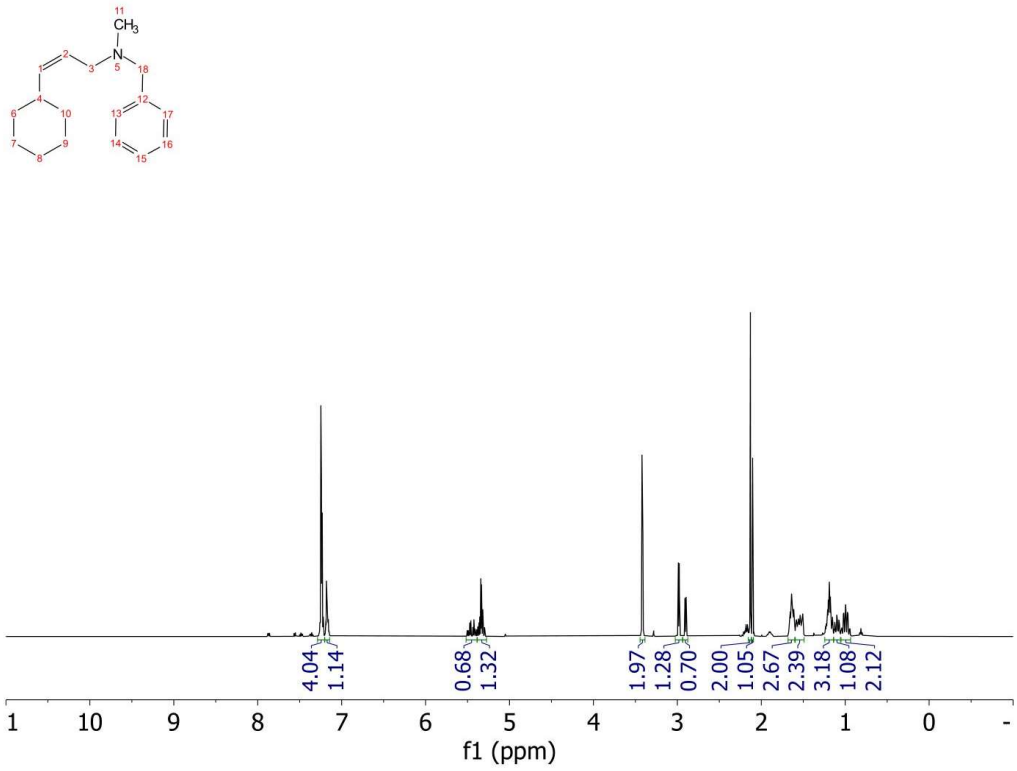
4.04
1.14
0.68
1.32
1.97
1.28
0.70
2.00
1.05
2.67
2.39
3.18
1.08
2.12
1
10
9
8
7
6
5
4
3
2
1
0
-
f1 (ppm)

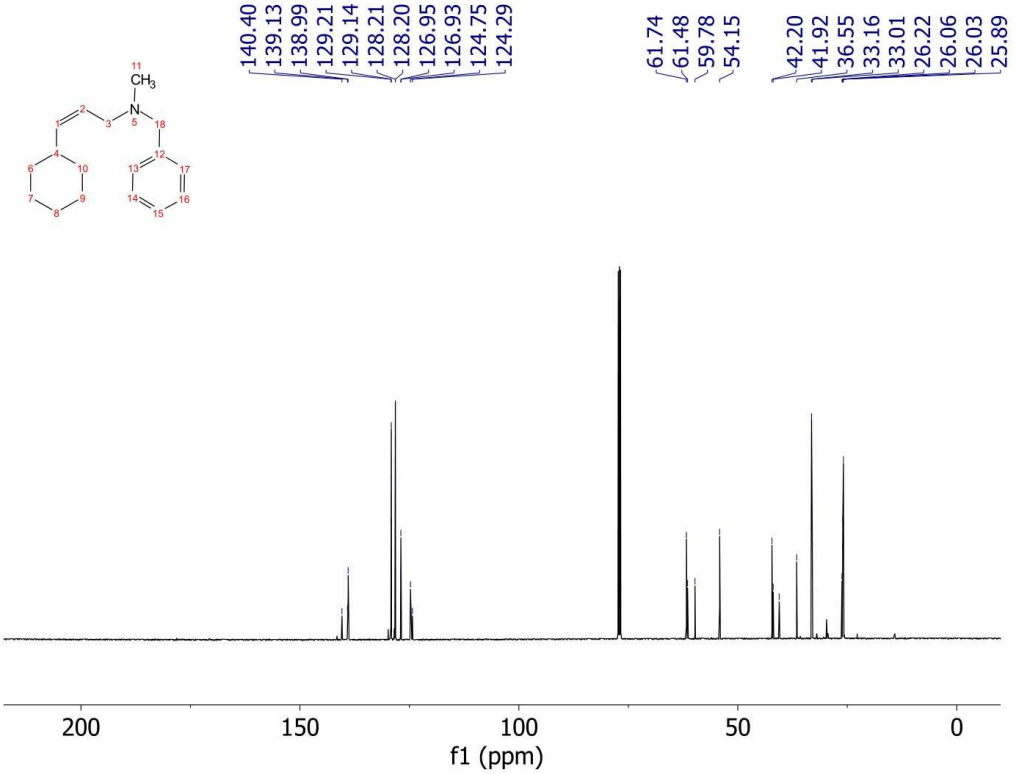
140.40
139.13
138.99
129.21
129.14
128.21
128.20
126.95
126.93
124.75
124.29
61.74
61.48
59.78
54.15
42.20
41.92
36.55
33.16
33.01
26.22
26.06
26.03
25.89
200
150
100
50
0
f1 (ppm)

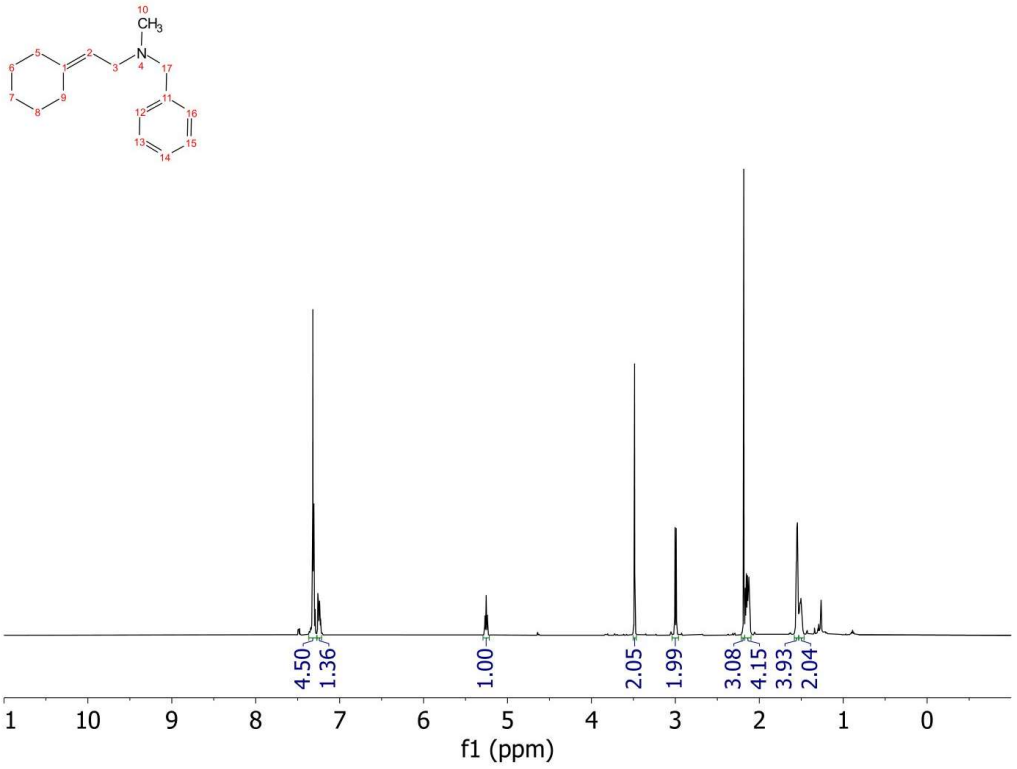
4.50
1.36
1.00
2.05
1.99
3.08
4.15
3.93
2.04
1
10
9
8
7
6
5
4
3
2
1
0
f1 (ppm)

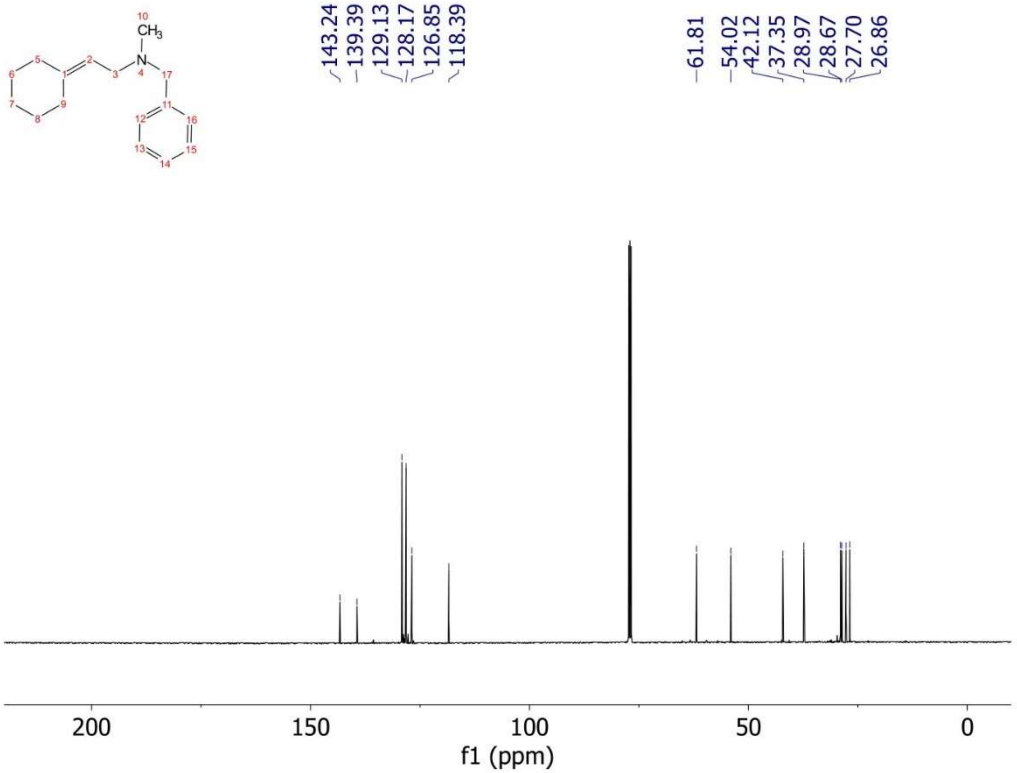
143.24
139.39
129.13
128.17
126.85
118.39
61.81
54.02
42.12
37.35
28.97
28.67
27.70
26.86
200
150
100
50
0
f1 (ppm)

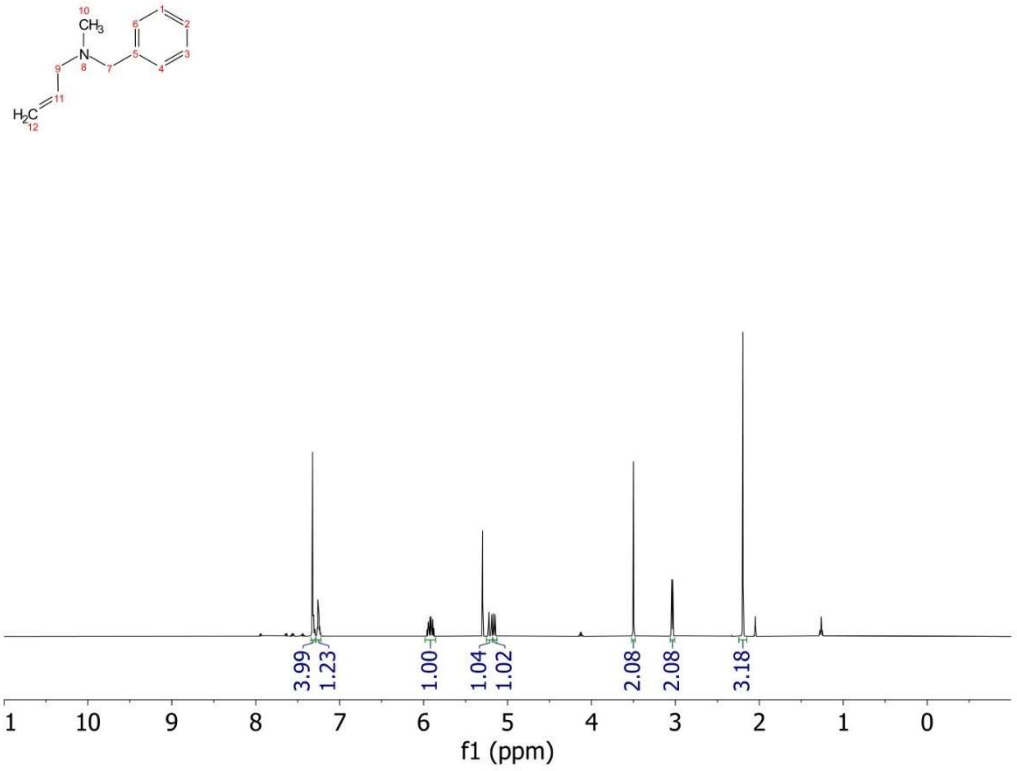
3.99
1.23
1.00
1.04
1.02
2.08
2.08
3.18
1
10
9
8
7
6
5
4
3
2
1
0
f1 (ppm)

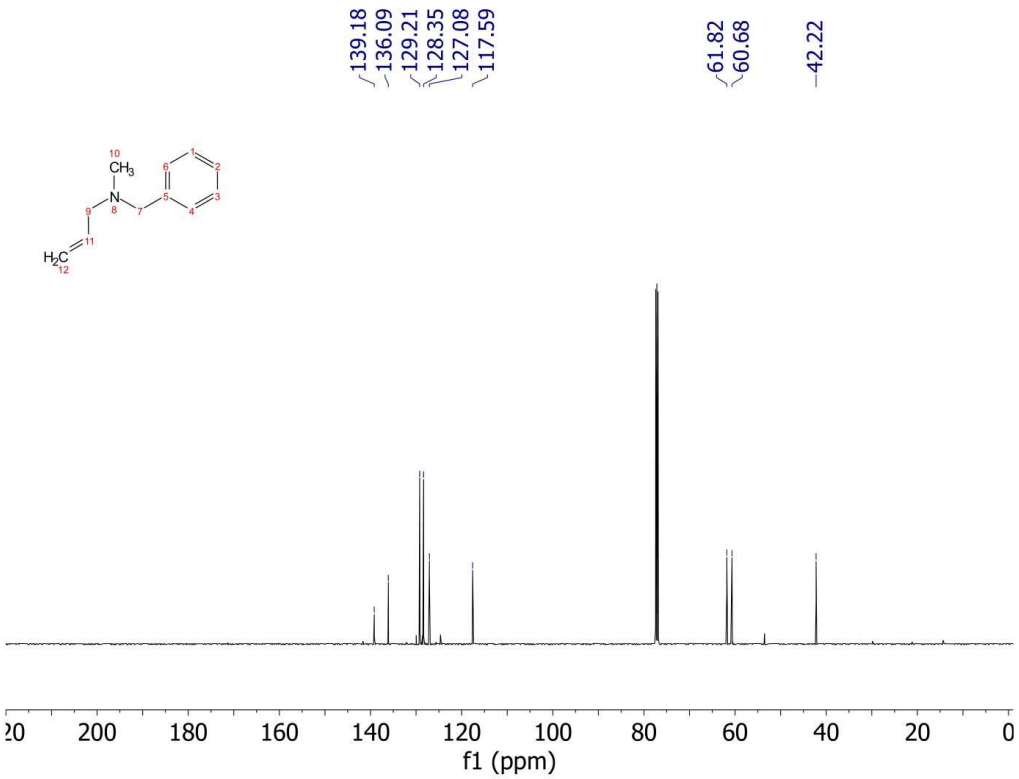
139.18
136.09
129.21
128.35
127.08
117.59
61.82
60.68
42.22
f1 (ppm)

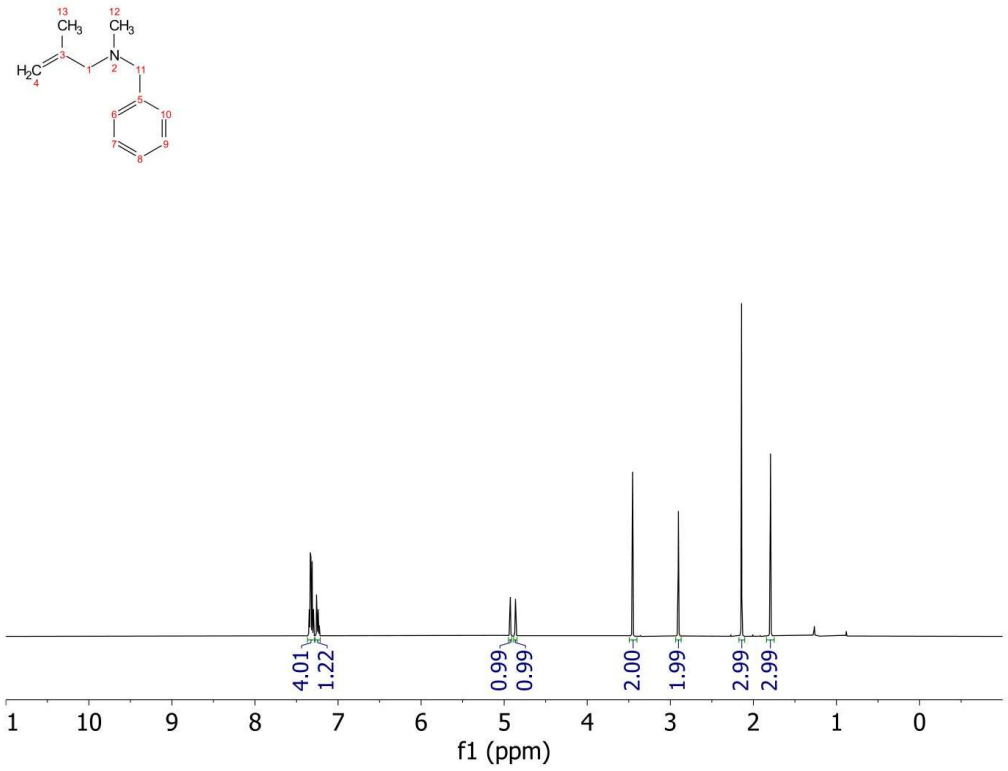
4.01
1.22
0.99
0.99
2.00
1.99
2.99
2.99
f1 (ppm)

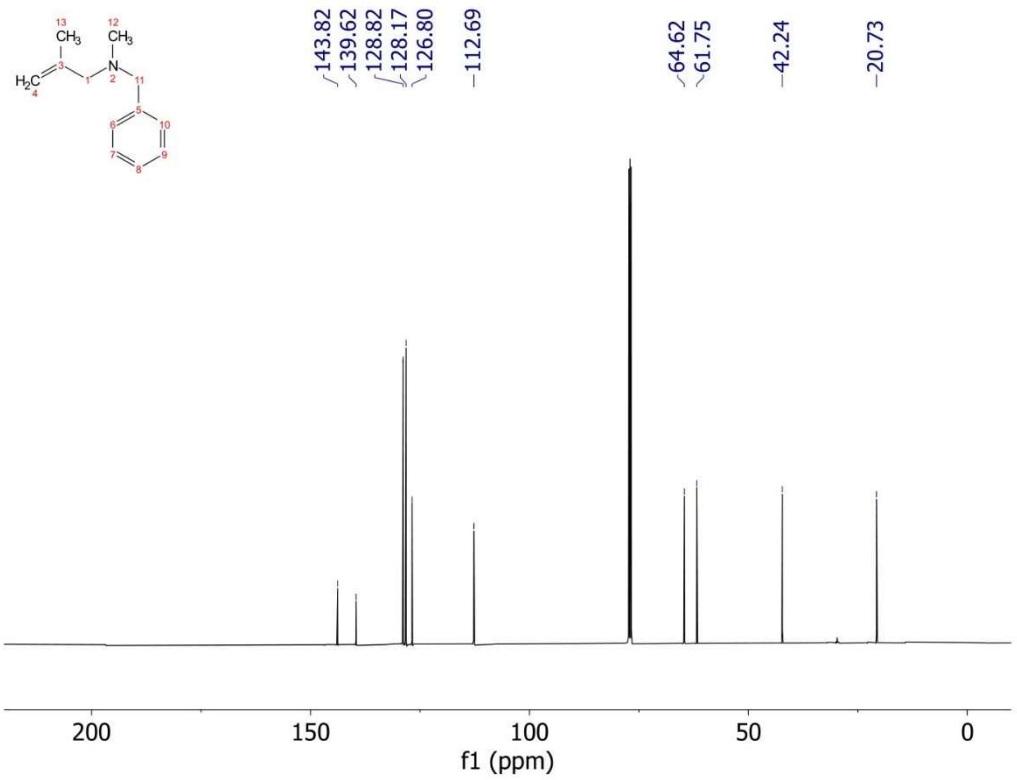
143.82
139.62
128.82
128.17
126.80
112.69
64.62
61.75
42.24
20.73
200
150
100
50
0
f1 (ppm)

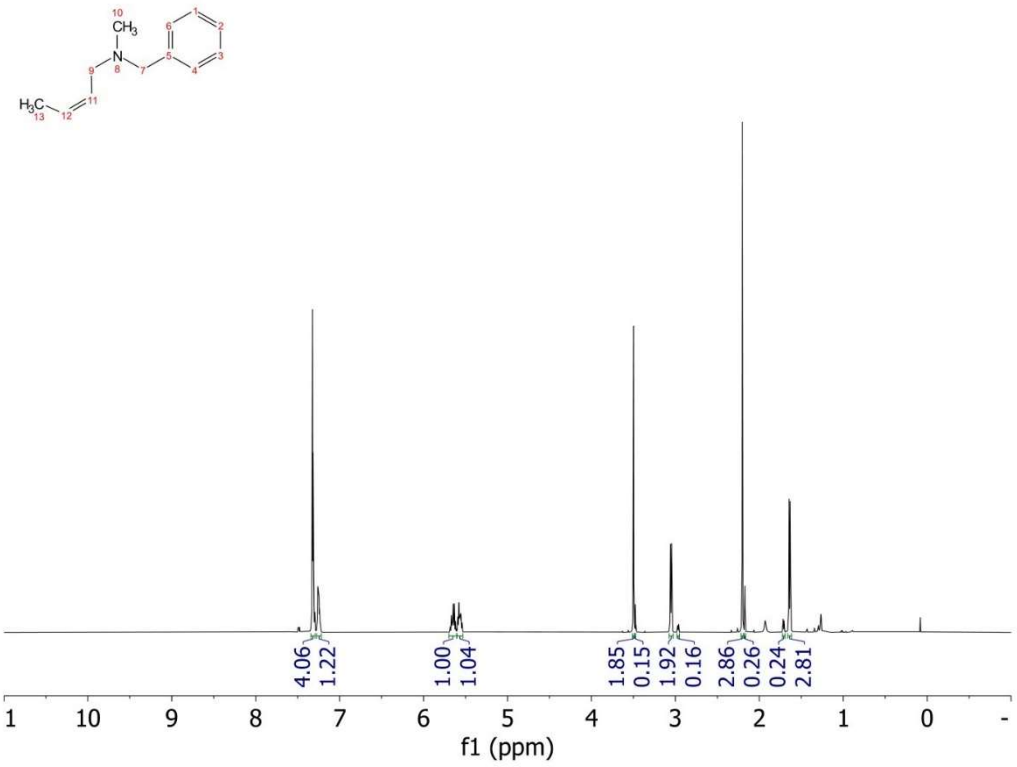
4.06
1.22
1.00
1.04
1.85
0.15
1.92
0.16
2.86
0.26
0.24
2.81
1
10
9
8
7
6
5
4
3
2
1
0
-
f1 (ppm)

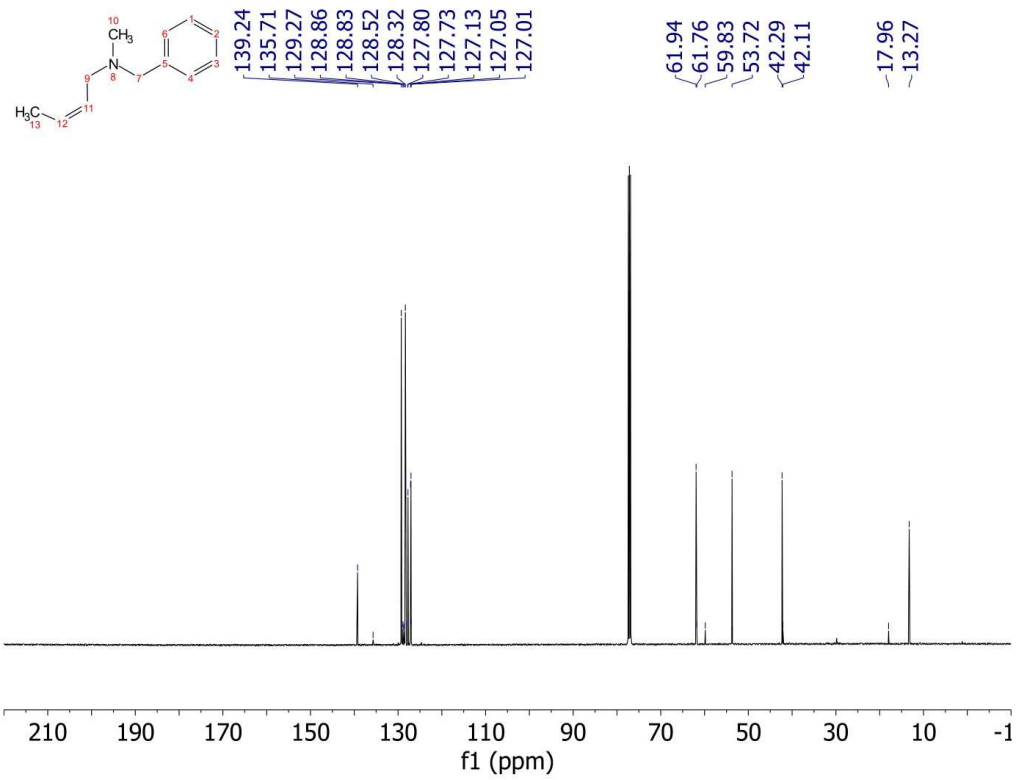
139.24
135.71
129.27
128.86
128.83
128.52
128.32
127.80
127.73
127.13
127.05
127.01
61.94
61.76
59.83
53.72
42.29
42.11
17.96
13.27
210
190
170
150
130
110
90
70
50
30
10
-1
f1 (ppm)

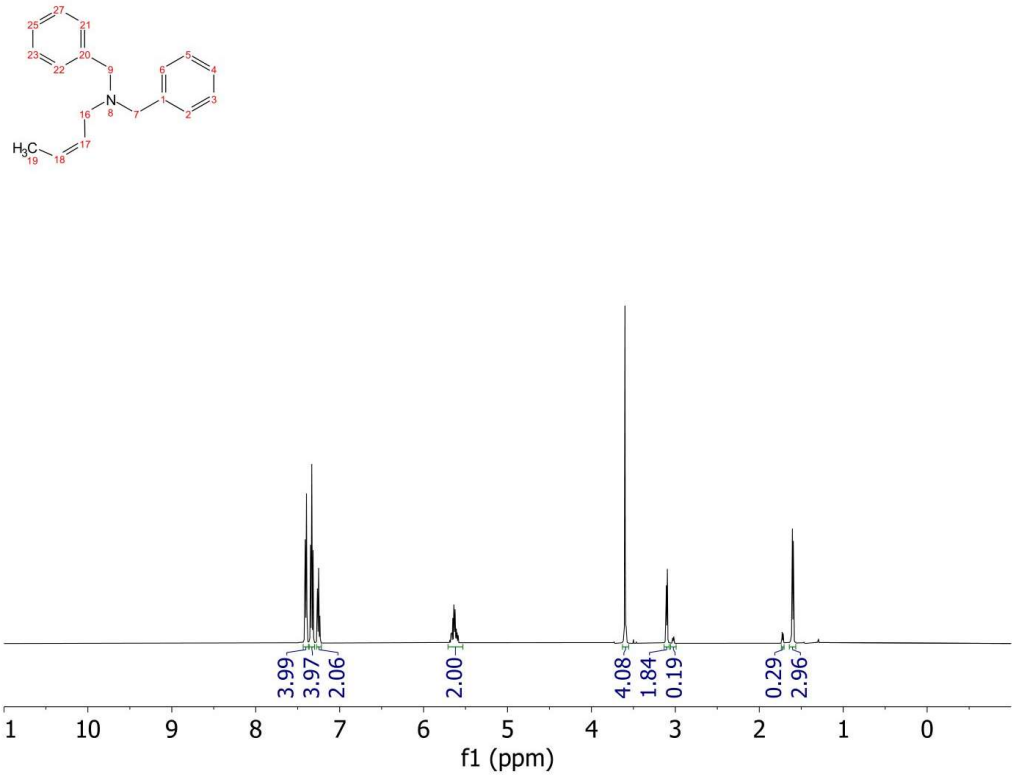
3.99
3.97
2.06
2.00
4.08
1.84
0.19
0.29
2.96
1
10
9
8
7
6
5
4
3
2
1
0
f1 (ppm)

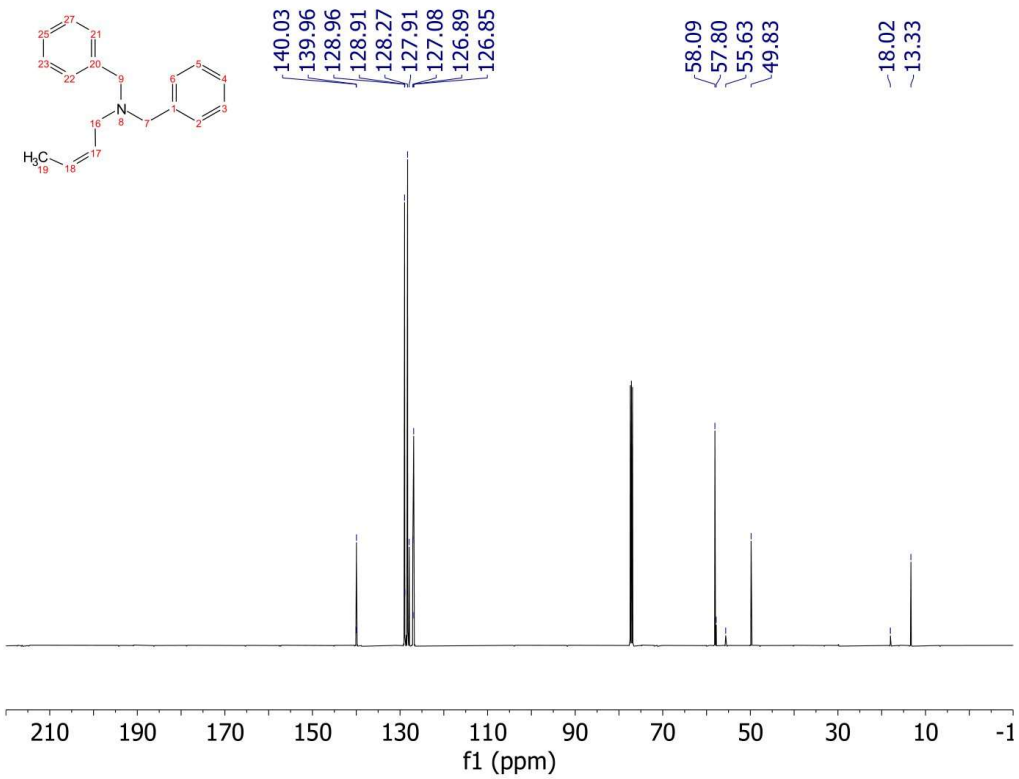
140.03
139.96
128.96
128.91
128.27
127.91
127.08
126.89
126.85
58.09
57.80
55.63
49.83
18.02
13.33
210
190
170
150
130
110
90
70
50
30
10
-1
f1 (ppm)

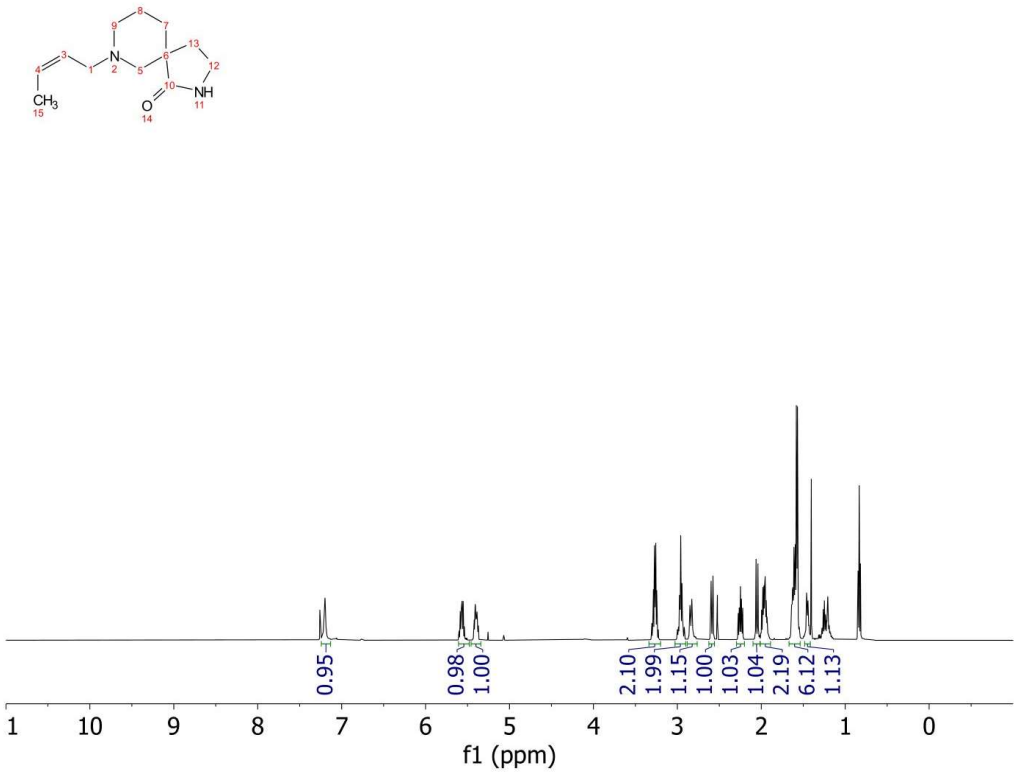
0.95
0.98
1.00
2.10
1.99
1.15
1.00
1.03
1.04
2.19
6.12
1.13
1
10
9
8
7
6
5
4
3
2
1
0
f1 (ppm)

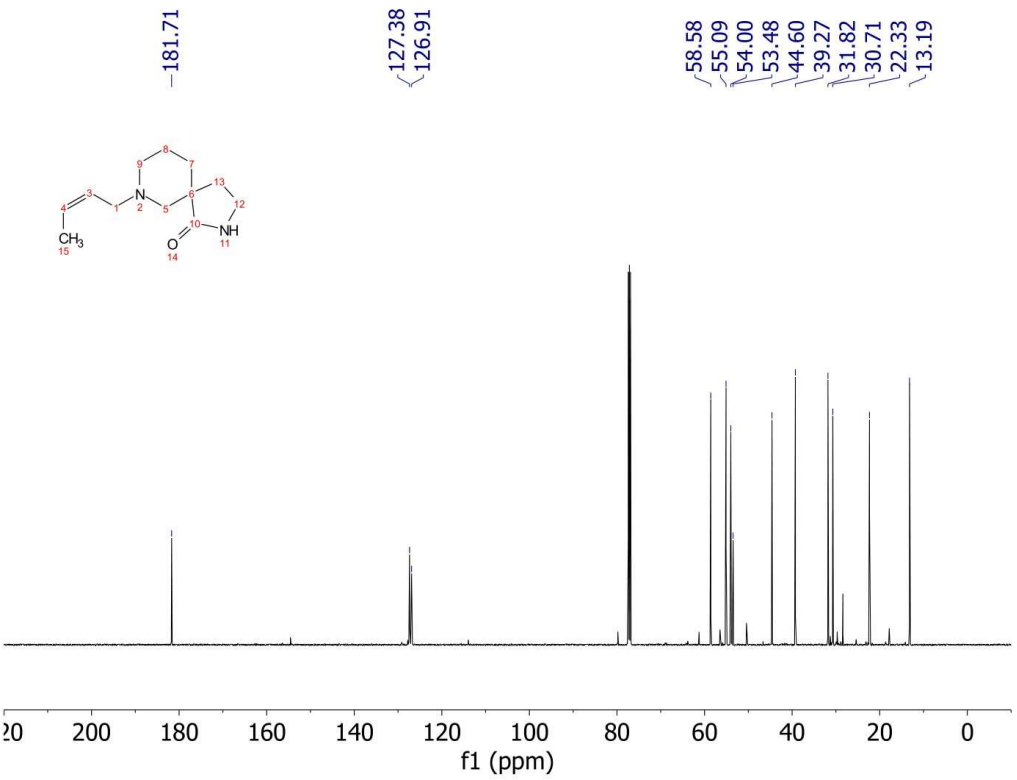
181.71
127.38
126.91
58.58
55.09
54.00
53.48
44.60
39.27
31.82
30.71
22.33
13.19
f1 (ppm)

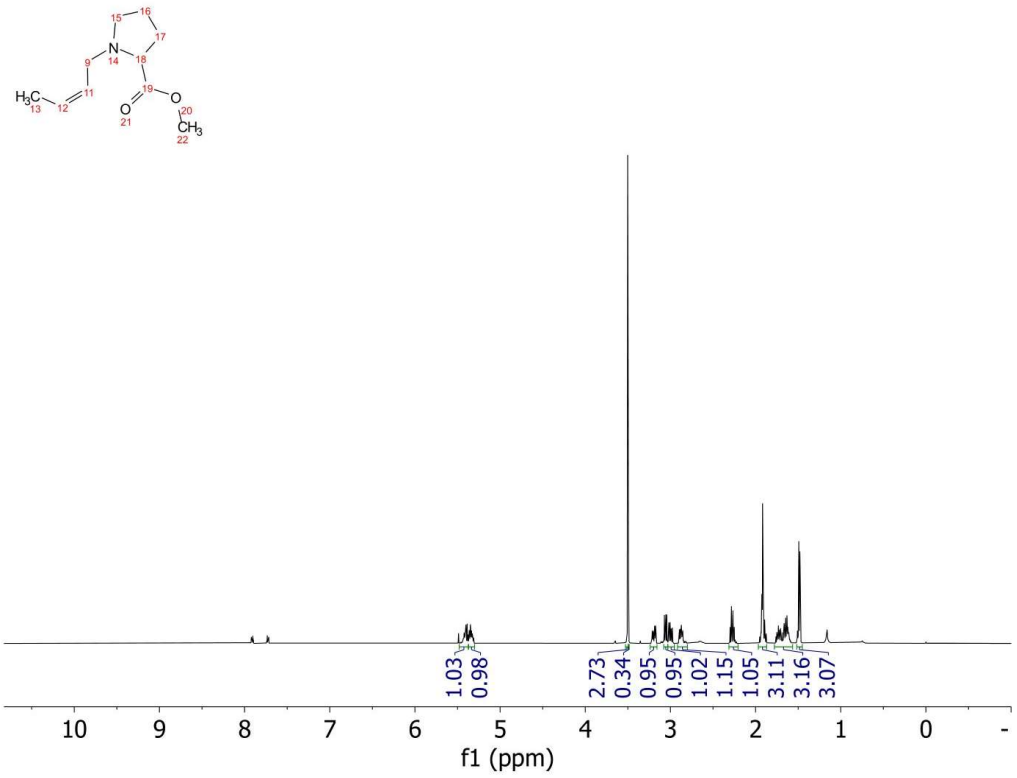
1.03
0.98
2.73
0.34
0.95
0.95
1.02
1.15
1.05
3.11
3.16
3.07
f1 (ppm)

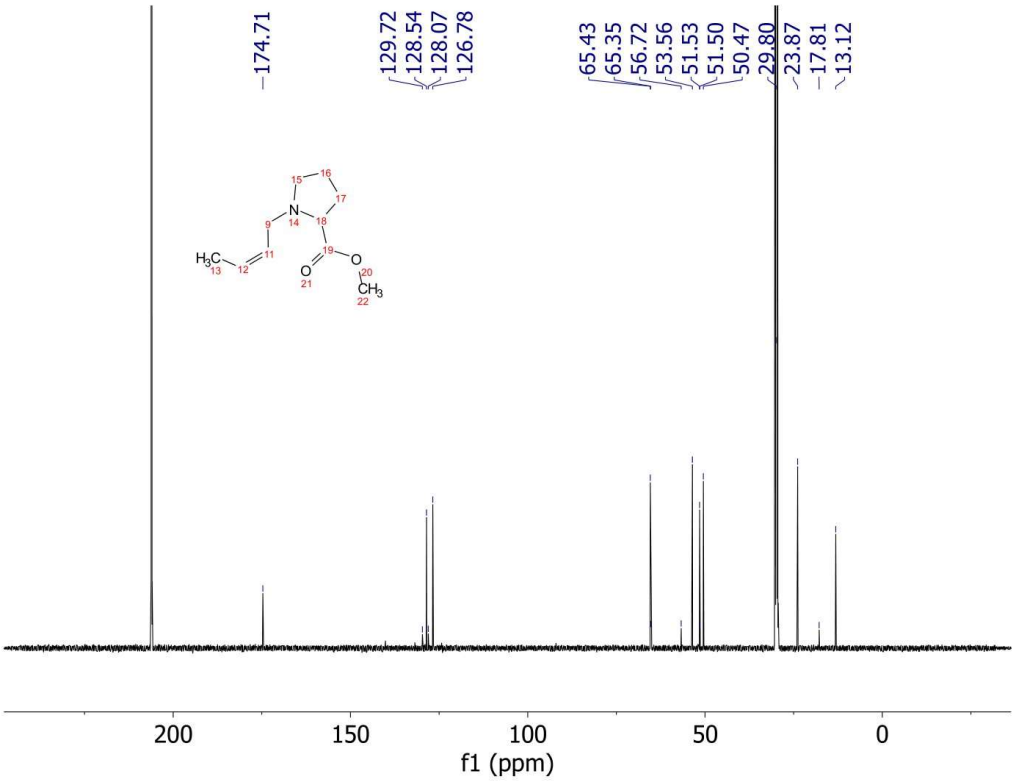
174.71
129.72
128.54
128.07
126.78
65.43
65.35
56.72
53.56
51.53
51.50
50.47
29.80
23.87
17.81
13.12
200
150
100
50
0
f1 (ppm)

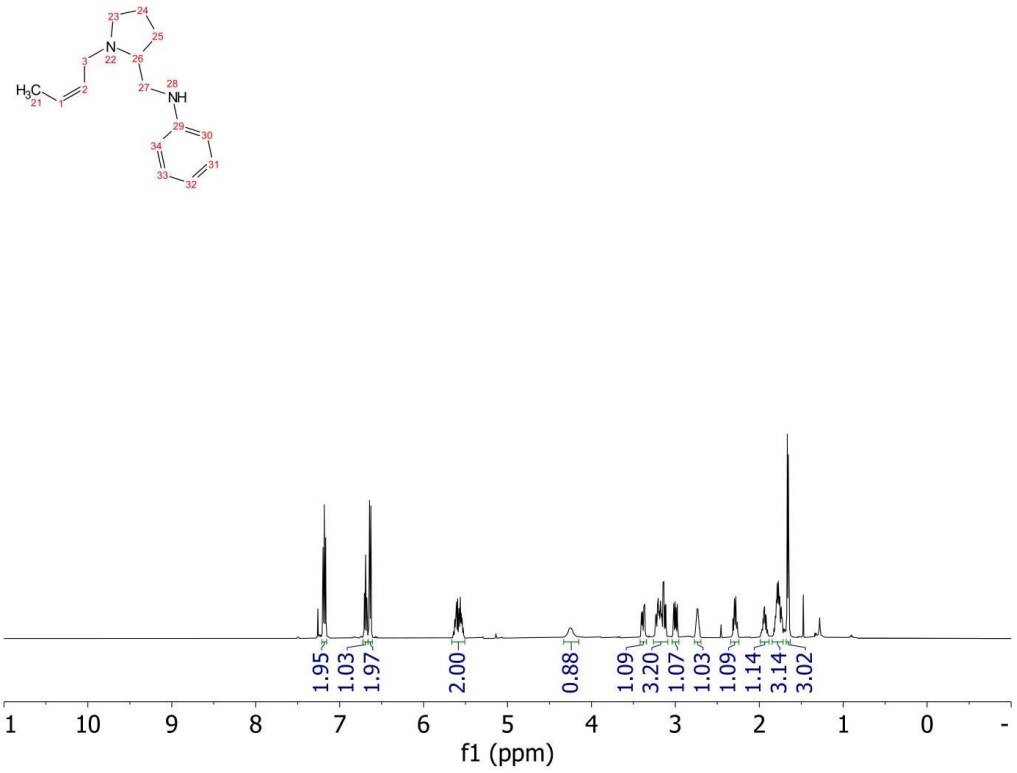
1.95
1.03
1.97
2.00
0.88
1.09
3.20
1.07
1.03
1.09
1.14
3.14
3.02
1
10
9
8
7
6
5
4
3
2
1
0
-
f1 (ppm)

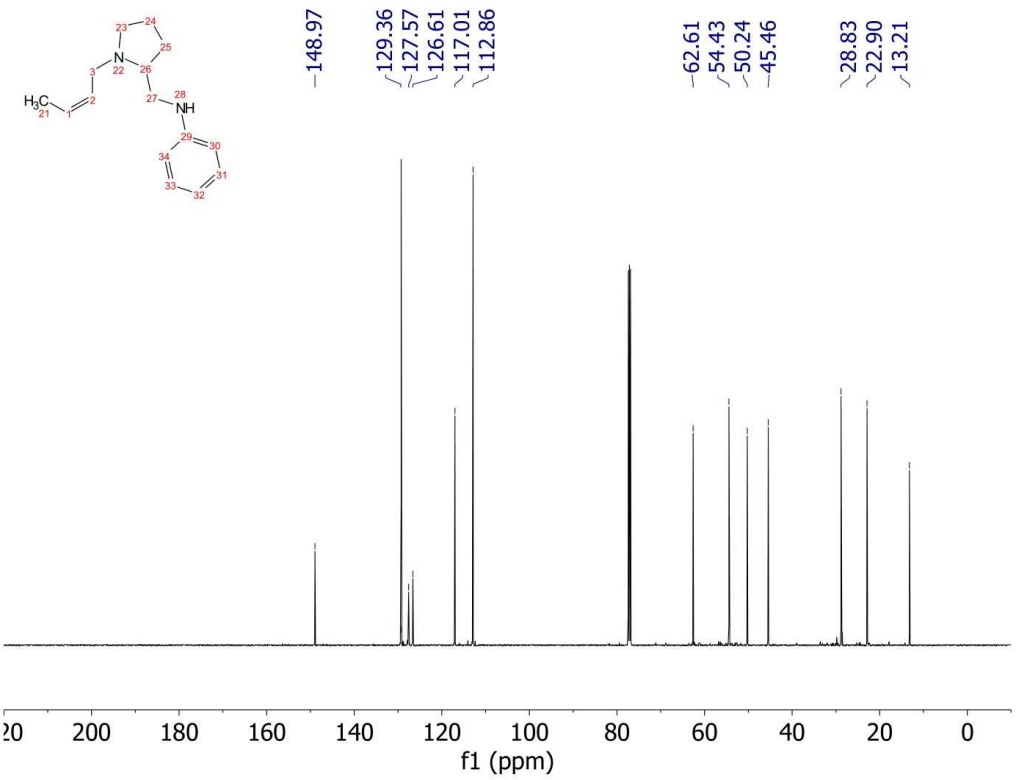
148.97
129.36
127.57
126.61
117.01
112.86
62.61
54.43
50.24
45.46
28.83
22.90
13.21
f1 (ppm)

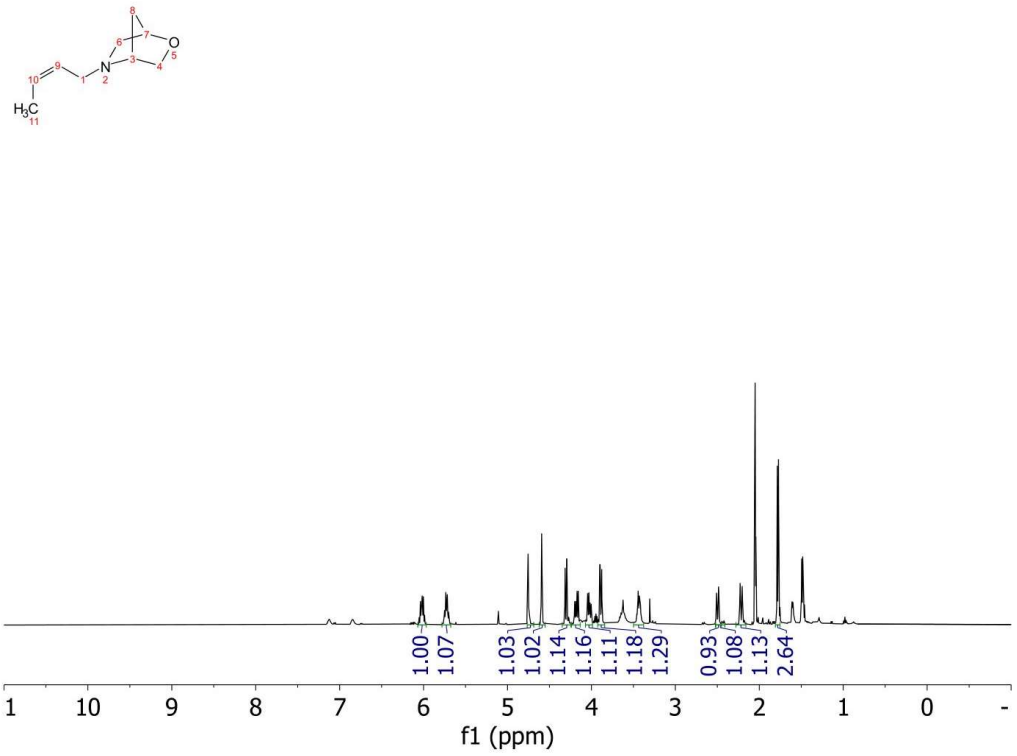
1.00
1.07
1.03
1.02
1.14
1.16
1.11
1.18
1.29
0.93
1.08
1.13
2.64
f1 (ppm)

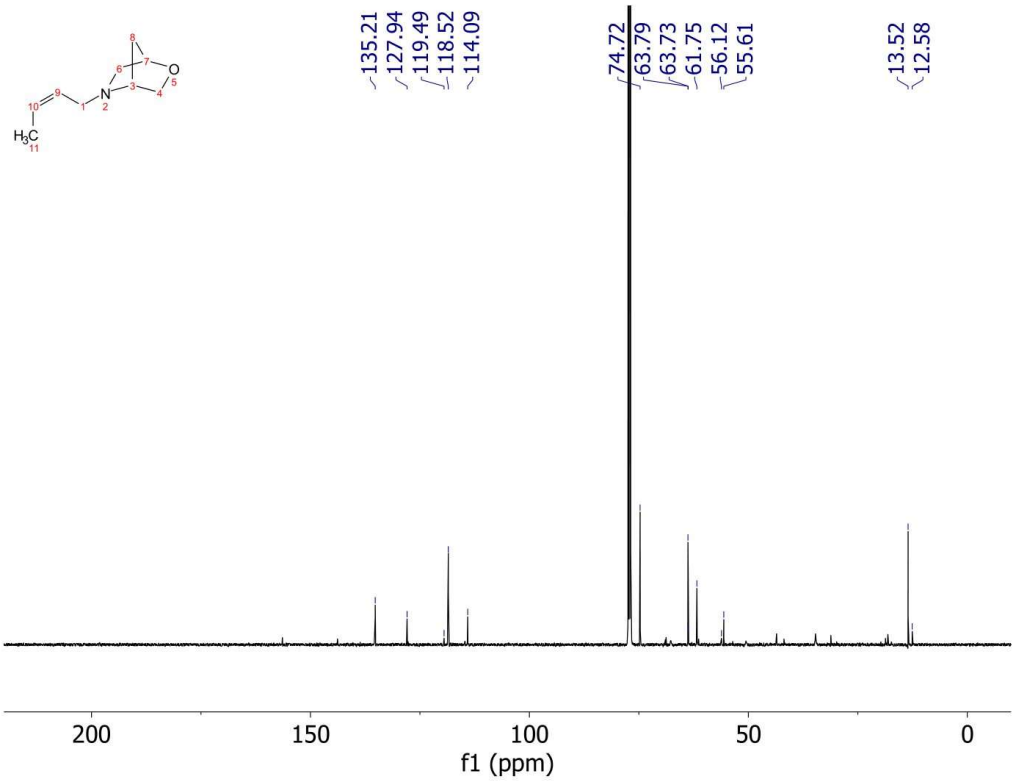
135.21
127.94
119.49
118.52
114.09
74.72
63.79
63.73
61.75
56.12
55.61
13.52
12.58
200
150
100
50
0
f1 (ppm)

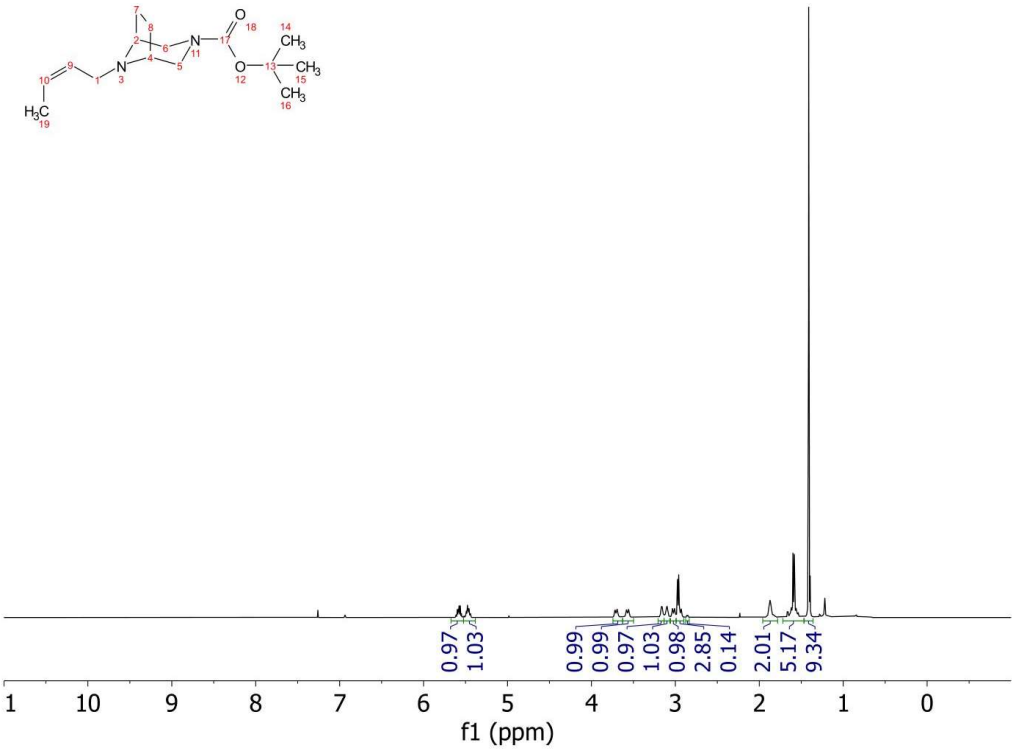
0.97
1.03
0.99
0.99
0.97
1.03
0.98
2.85
0.14
2.01
5.17
9.34
1
10
9
8
7
6
5
4
3
2
1
0
f1 (ppm)

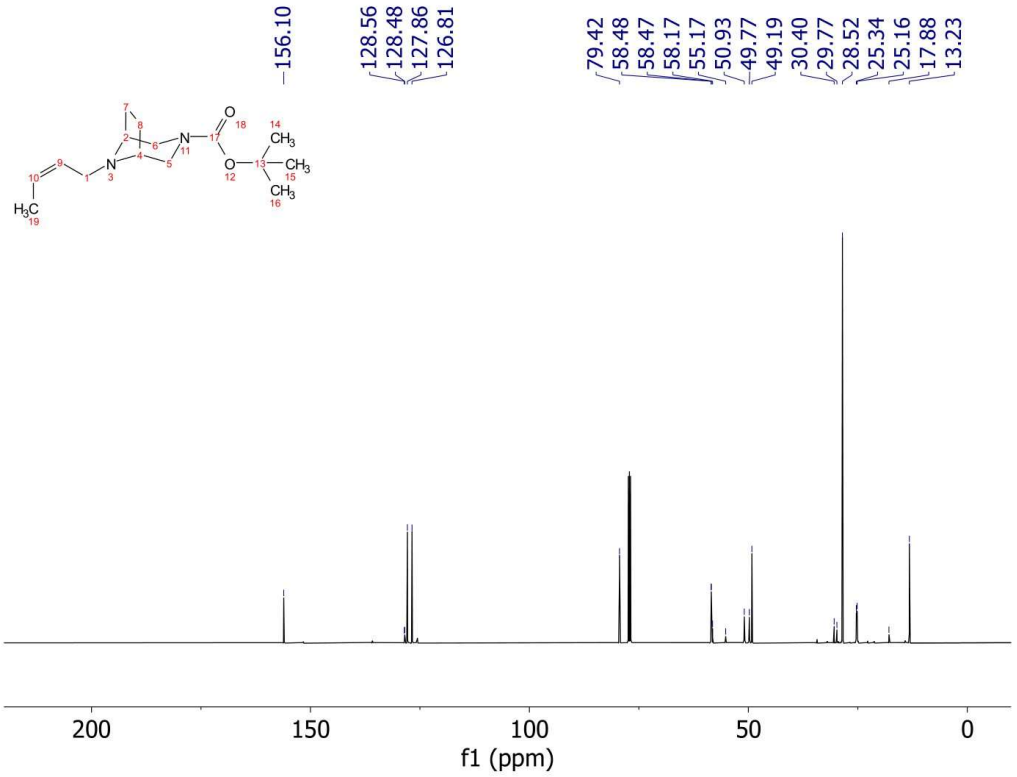
156.10
128.56
128.48
127.86
126.81
79.42
58.48
58.47
58.17
55.17
50.93
49.77
49.19
30.40
29.77
28.52
25.34
25.16
17.88
13.23
200
150
100
50
0
f1 (ppm)

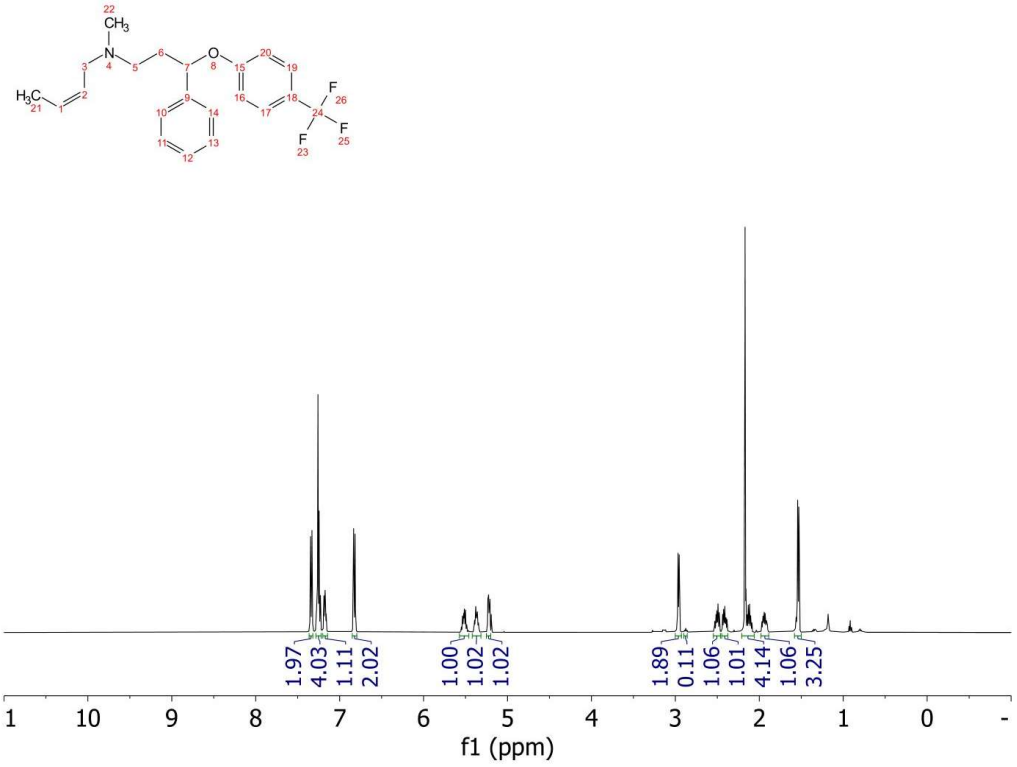
1.97
4.03
1.11
2.02
1.00
1.02
1.02
1.89
0.11
1.06
1.01
4.14
1.06
3.25
1
10
9
8
7
6
5
4
3
2
1
0
-
f1 (ppm)

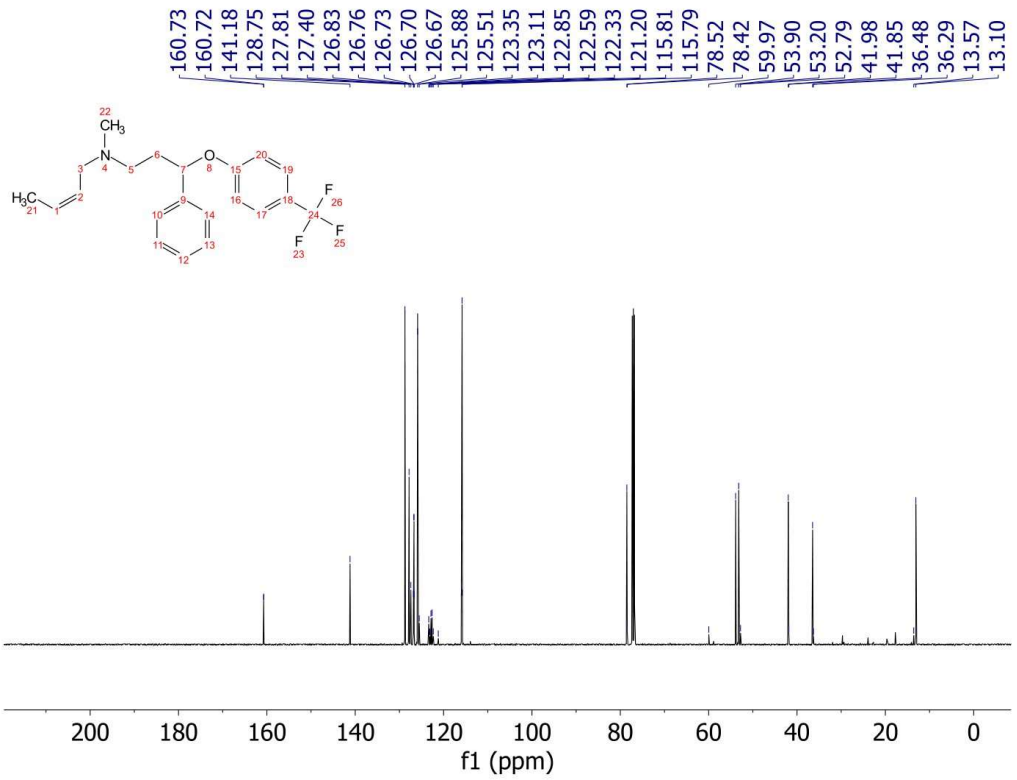
160.73
160.72
141.18
128.75
127.81
127.40
126.83
126.76
126.73
126.70
126.67
125.88
125.51
123.35
123.11
122.85
122.59
122.33
121.20
115.81
115.79
78.52
78.42
59.97
53.90
53.20
52.79
41.98
41.85
36.48
36.29
13.57
13.10
200
180
160
140
120
100
80
60
40
20
0
f1 (ppm)

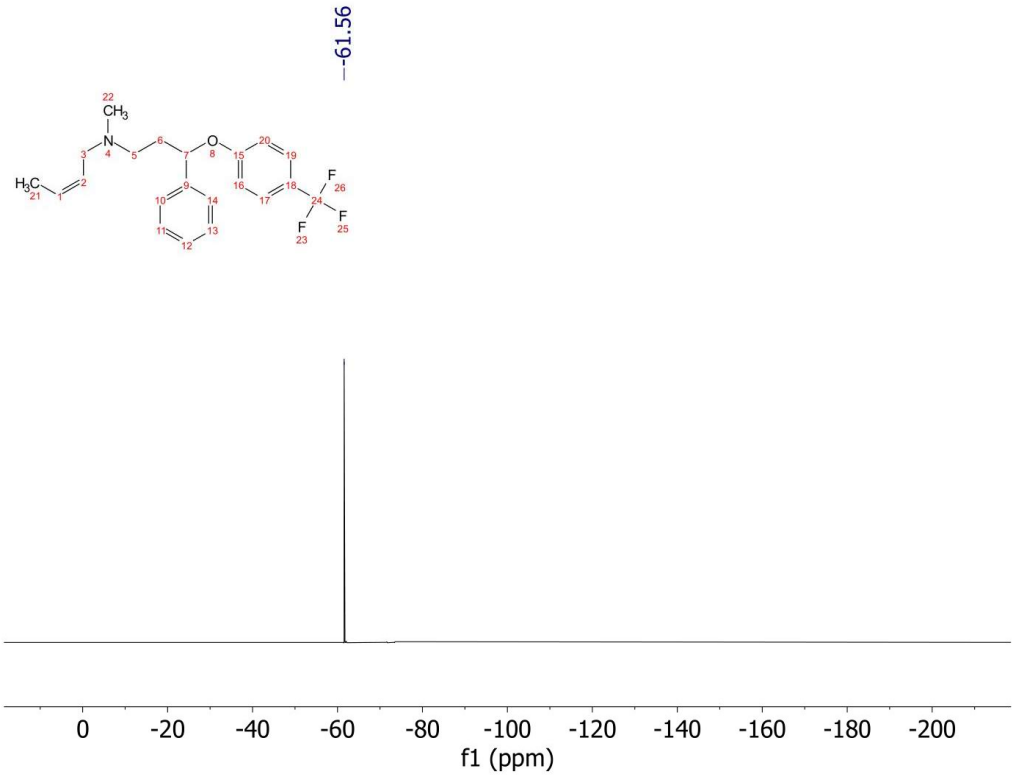
-61.56
0
-20
-40
-60
-80
-100
-120
-140
-160
-180
-200
f1 (ppm)

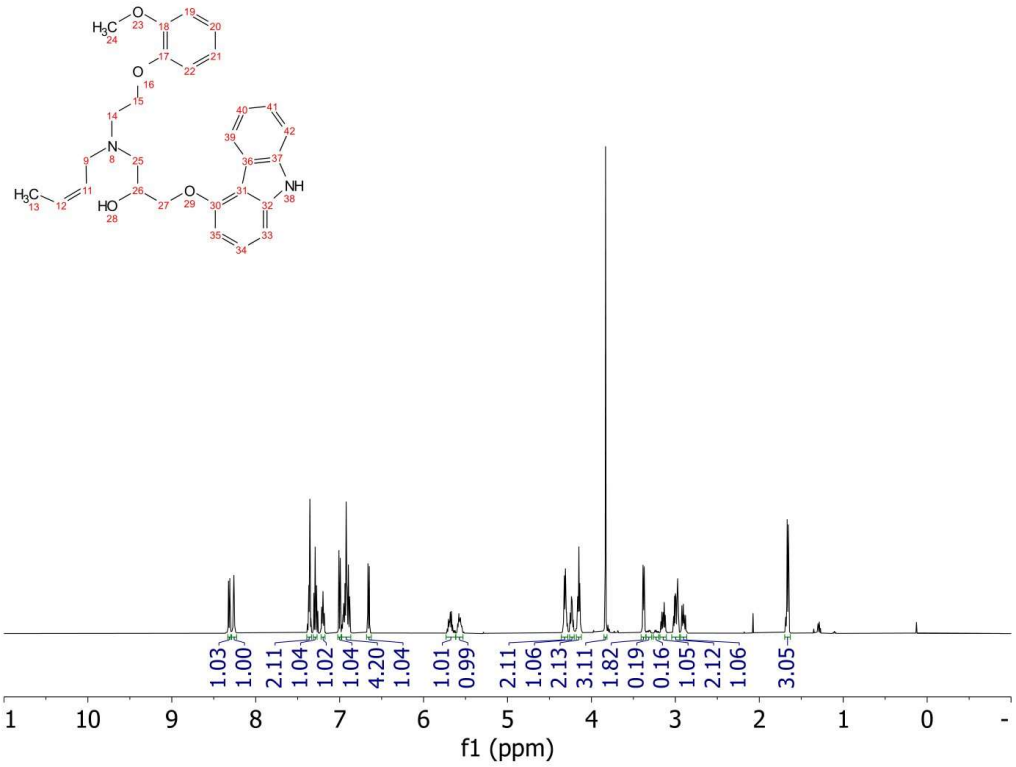
1.03
1.00
2.11
1.04
1.02
1.04
4.20
1.04
1.01
0.99
2.11
1.06
2.13
3.11
1.82
0.19
0.16
1.05
2.12
1.06
3.05
f1 (ppm)

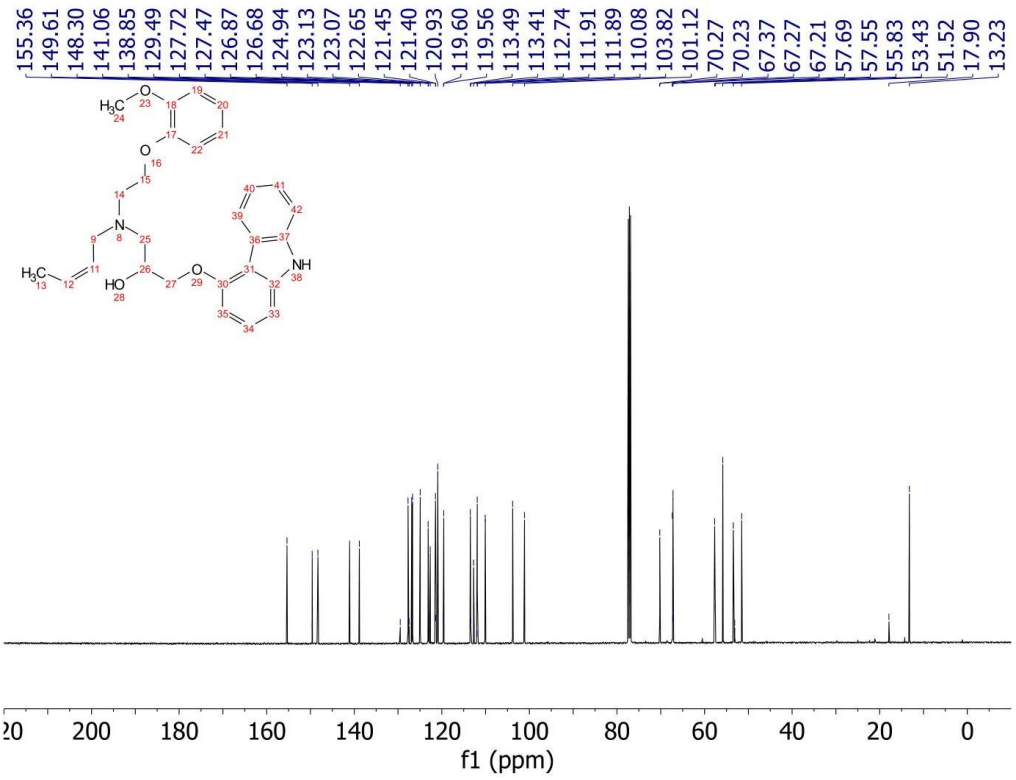
155.36
149.61
148.30
141.06
138.85
129.49
127.72
127.47
126.87
126.68
124.94
123.13
123.07
122.65
121.45
121.40
120.93
119.60
119.56
113.49
113.41
112.74
111.91
111.89
110.08
103.82
101.12
70.27
70.23
67.37
67.27
67.21
57.69
57.55
55.83
53.43
51.52
17.90
13.23
f1 (ppm)

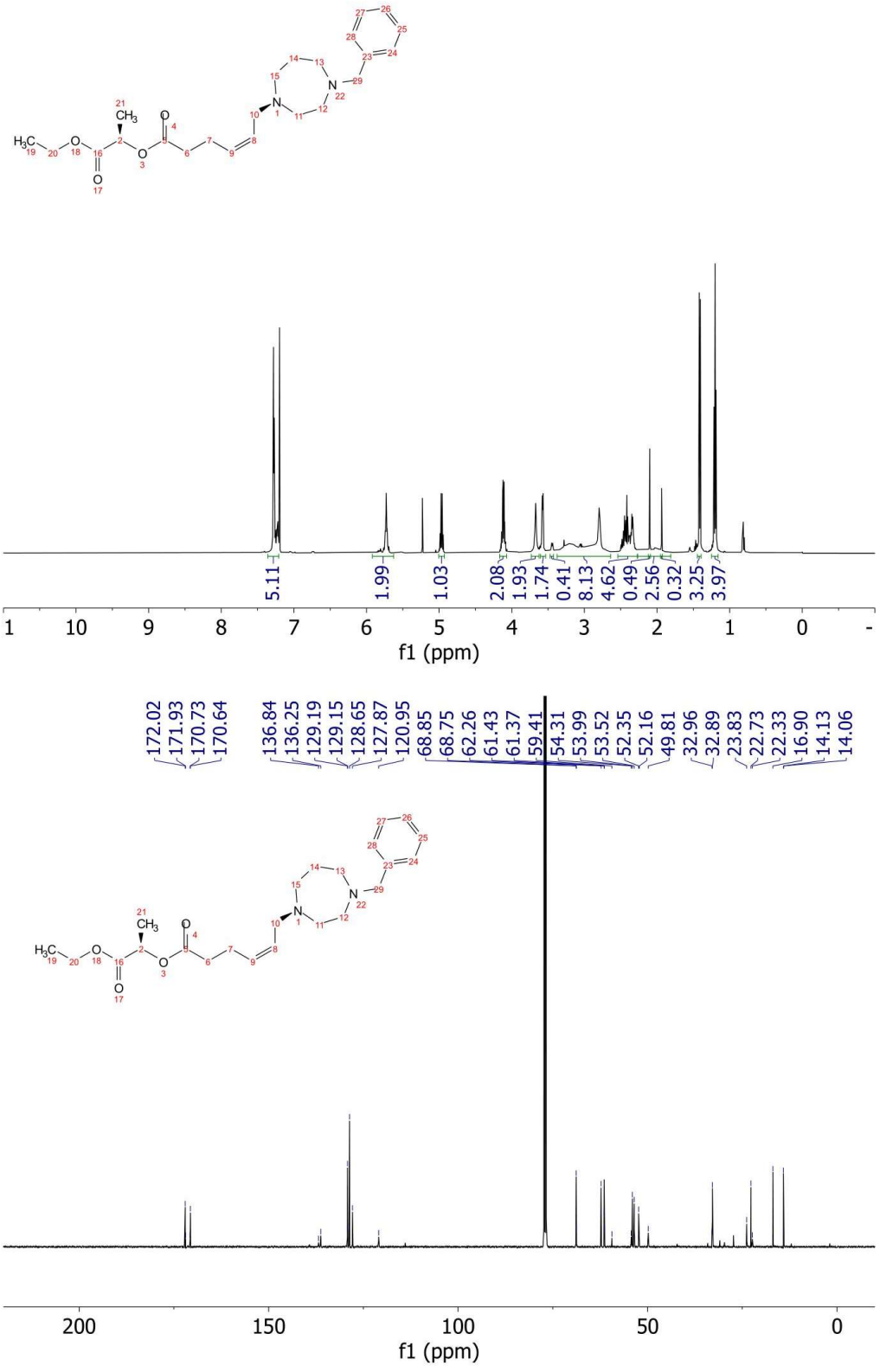
5.11
1.99
1.03
2.08
1.93
1.74
0.41
8.13
4.62
0.49
2.56
0.32
3.25
3.97
f1 (ppm)
172.02
171.93
170.73
170.64
136.84
136.25
129.19
129.15
128.65
127.87
120.95
68.85
68.75
62.26
61.43
61.37
59.41
54.31
53.99
53.52
52.35
52.16
49.81
32.96
32.89
23.83
22.73
22.33
16.90
14.13
14.06
f1 (ppm)

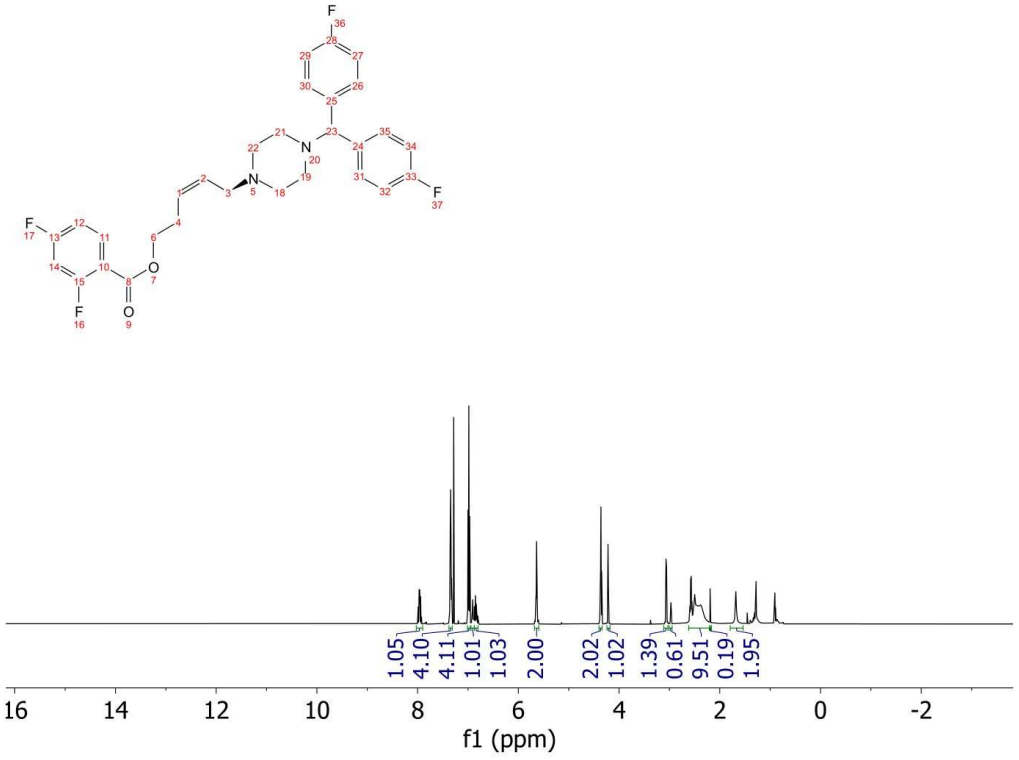
1.05
4.10
4.11
1.01
1.03
2.00
2.02
1.02
1.39
0.61
9.51
0.19
1.95
16
14
12
10
8
6
4
2
0
-2
f1 (ppm)

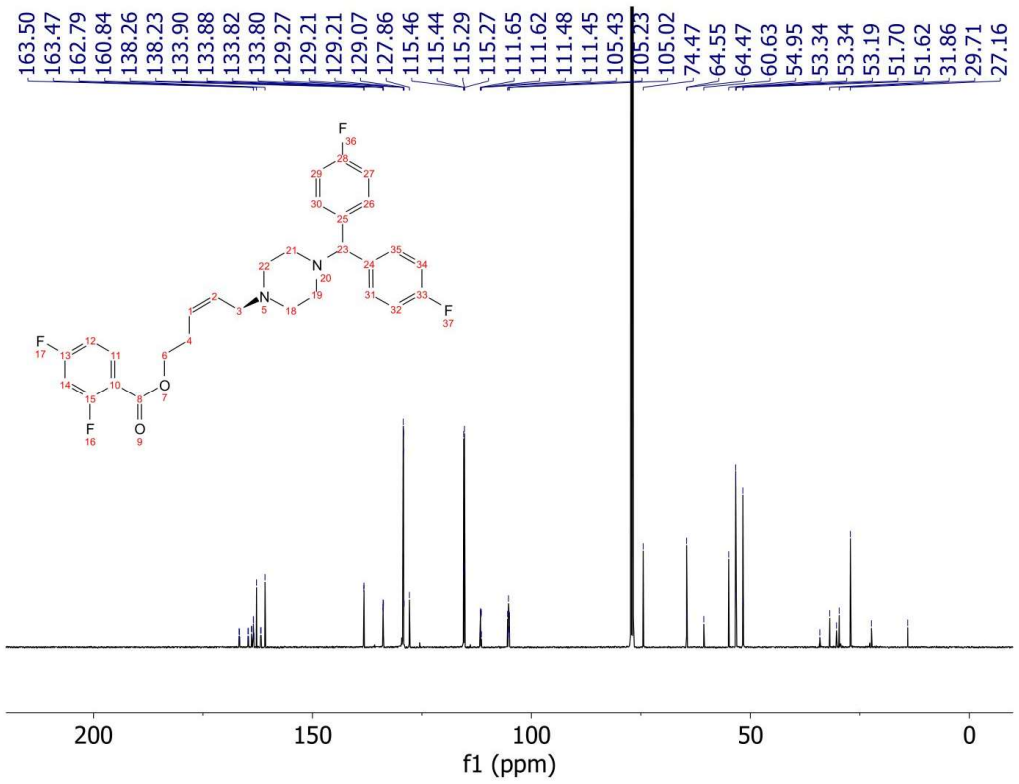
163.50
163.47
162.79
160.84
138.26
138.23
133.90
133.88
133.82
133.80
129.27
129.21
129.21
129.07
127.86
115.46
115.44
115.29
115.27
111.65
111.62
111.48
111.45
105.43
105.23
105.02
74.47
64.55
64.47
60.63
54.95
53.34
53.34
53.19
51.70
51.62
31.86
29.71
27.16
200
150
100
50
0
f1 (ppm)

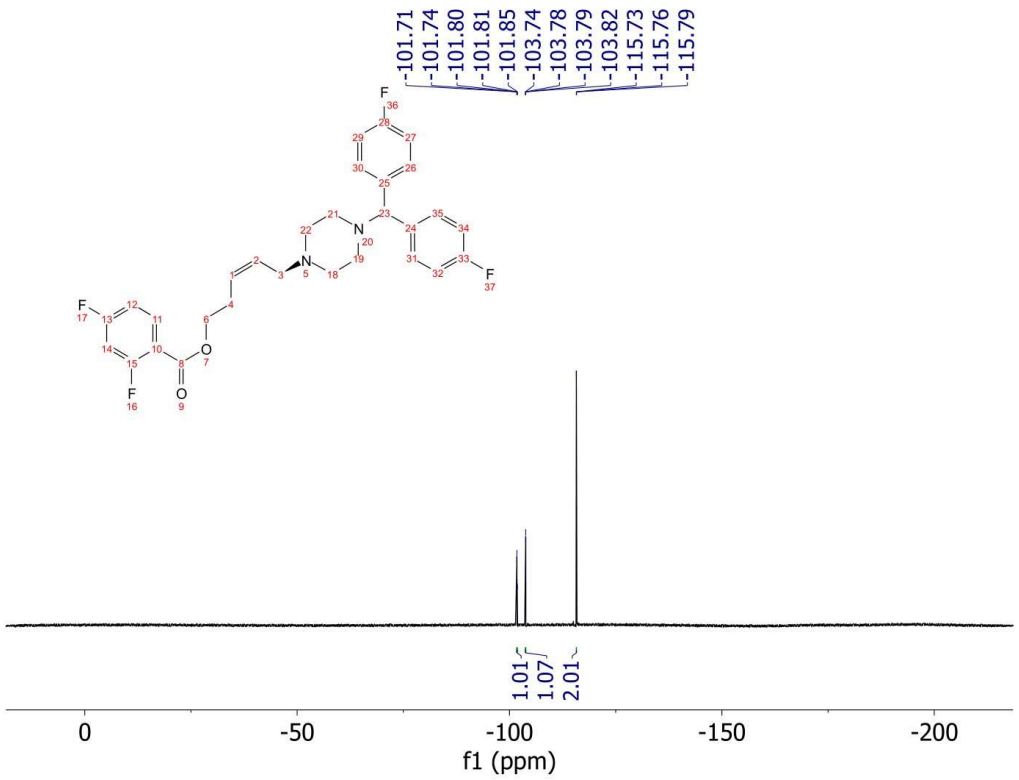
-101.71
-101.74
-101.80
-101.81
-101.85
-103.74
-103.78
-103.79
-103.82
-115.73
-115.76
-115.79
1.01
1.07
2.01
0
-50
-100
-150
-200
f1 (ppm)

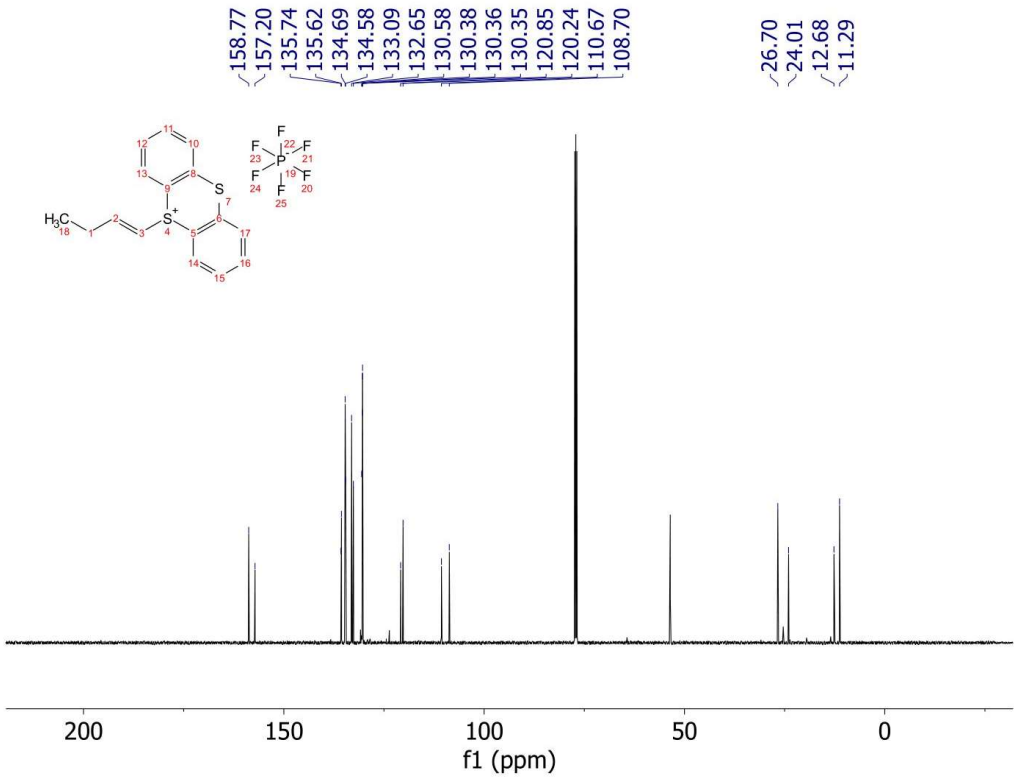
158.77
157.20
135.74
135.62
134.69
134.58
133.09
132.65
130.58
130.38
130.36
130.35
120.85
120.24
110.67
108.70
26.70
24.01
12.68
11.29
200
150
100
50
0
f1 (ppm)

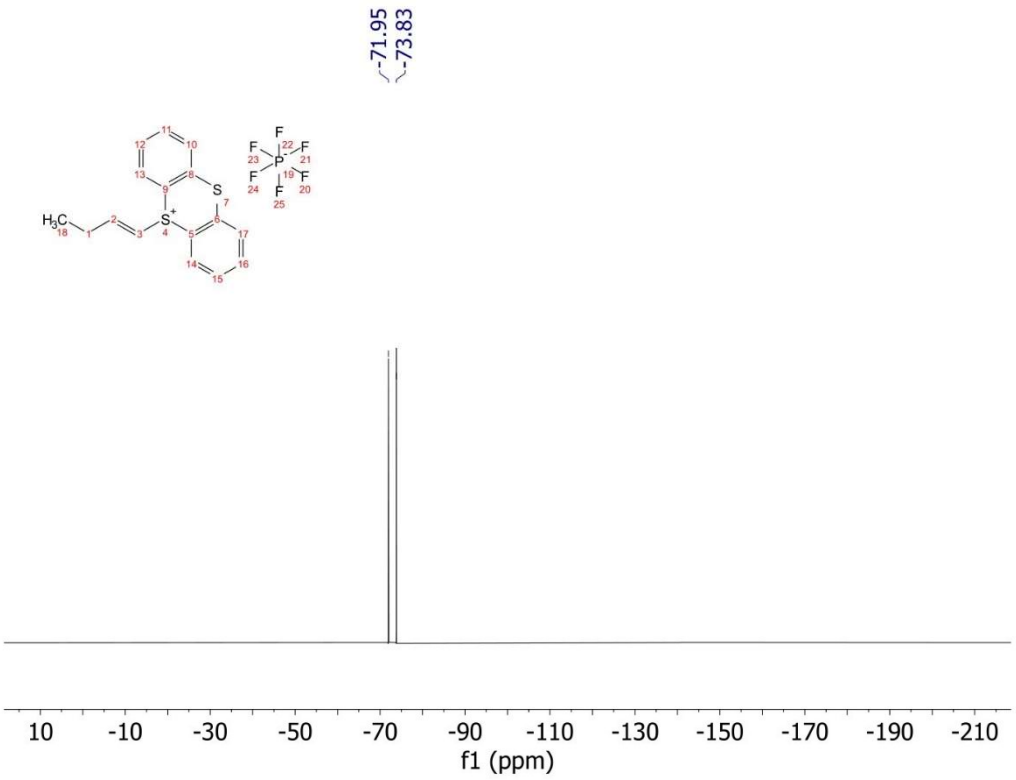
-71.95
-73.83
10
-10
-30
-50
-70
-90
-110
-130
-150
-170
-190
-210
f1 (ppm)

Appendix C: Supporting Information for Chapter 4 (Diastereoselective Synthesis of Cyclopropanes from Carbon Pronucleophiles and Alkenes)

C.1 General Methods and Materials

Unless otherwise noted, reactions were performed under air in an anhydrous solvent. MeCN and toluene were purchased as sureseal bottles and used as is. THF, DMF, DMSO, and DCM were dried by passing through activated alumina columns. Thianthrene was recrystallized from acetone prior to use. *n*-Bu_4NPF_6 was recrystallized three times from EtOAc prior to use. All liquid carbon pronucleophiles were distilled from CaH_2 prior to use. Unless otherwise noted, other commercially available reagents were used as received. Aluminum Oxide (activated, basic, Brockmann I) was purchased from Sigma-Aldrich and used for filtration. Crude reaction mixtures were evaluated by thin-layer chromatography using EMD/Merck silica gel 60 F254 pre-coated plates (0.25 mm) and were visualized by UV and/or Seebach, ninhydrin, or $KMnO_4$ staining. Flash chromatography was performed with a Biotage Isolera One automated chromatography system with re-packed silica columns (technical grade silica, pore size 60 Å, 230 - 400 mesh particle size, 40 - 63 particle size) or pre-packed Biotage Sfär Silica HC Duo 20µm 50g - High Capacity Column columns. Purified materials were dried in vacuo (0.050 Torr) to remove trace solvent. ^{1}H, ^{13}C, ^{19}F, and ^{31}P spectra were taken using a Bruker Avance-400 with a BBFO Probe, a Bruker Avance-500 with a DCH Cryoprobe, a Bruker Avance III HD-500 with a TXO Cryoprobe, or a Bruker Avance-600 with a TCI-F cryoprobe. NMR data are reported relative to residual $CHCl_3$ (1 H, δ = 7.26 ppm), $CDCl_3$ (13 C, δ = 77.16 ppm) or residual C_6H_6 (1 H, δ = 7.16), C_6H_6 (13C, δ = 128.06 ppm). Data for ^{1}H NMR spectra are reported as follows: chemical shift (δ ppm) (multiplicity, coupling constant (Hz), integration). Multiplicity and qualifier abbreviations are as follows: s = singlet, d = doublet, t = triplet, q = quartet, m = multiplet, br = broad. All NMR yields were determined via reference against an internal standard (dibromomethane or mesitylene for 1 H). Mass spectrometry data was collected on a Thermo Scientific Q Exactive Plus Mass Spectrometer. The crystal evaluation and data collections were performed on a Bruker D8 VENTURE PhotonIII four-circle diffractometer with Cu Kα (λ = 1.54178 Å) radiation with the detector to crystal distance of 4.0 cm (Bruker-AXS (2018). APEX3. Version 2018.1-0. Madison, Wisconsin, USA.). The reflections were indexed by an automated indexing routine built in the APEX3 program. Mercury was used for structural visualization.[1]

Abbreviations: OAc—acetate, Aq—aqueous, Boc—*tert*-butyl carbamate, *t*Bu—*tert*-butyl, DBU—1,8-Diazabicycl[5.4.0]undec-7-ene, DC—direct current, DCM— dichloromethane, DMF—dimethyl formamide, DMSO—dimethylsulfoxide, Et—ethyl, EtOAc—ethyl acetate, EtOH—ethanol, Me—methyl, MeCN—acetonitrile, MeOH—methanol, NBS—*N*-bromosuccinimide, NPhth—phthalimide, Ph—phenyl, PTFE—polytetrafluoroethylene, RVC—reticulated vitreous carbon, *n*-Bu_4—tetrabutyl, *n*-Oct_4—tetraoctyl, TBAB—tetrabutylammonium bromide, TEA—triethylamine, TFA— trifluoroacetic acid, THF—tetrahydrofuran, TLC—thin layer chromatography, TT—thianthrene.

Electrochemical Methods and Materials

Bulk constant current electrolysis experiments were driven with a Dr. Meter HY3005M-L DC Power Supply or a custom–made low current power supply which was externally calibrated with a multimeter using a 10 Ohm resistor. Original design and fabrication of low current power supply created by Dr. Blaise J. Thompson. Provides an operational range of ± 0.01 – 9.99 mA, tunable by variable resistor, delivering power to banana socket pair. The power supply is limited to ± 15 V for bulk electrolysis and is powered by an 18 V wall wart. Circuitry is housed within an aluminum enclosure. For additional specifications, see: *J. Am. Chem. Soc.* **2020** 142, 2093-2099 and *Nature* **2021** 596, 74-79.

Divided cell fabricated in house by Tracy Drier. Glass frit purchased from Ace Glass (7176-36). Anode electrode assembled via affixing end of the silver wire (Belden Hook-Up wire, item number 83005 007100) around the pencil (JuneGold 2B graphite 2 mm) and wrapping in teflon tape to prevent exposure, then piercing RVC (8 x 7 x 7 mm, Ultramet, 80 ppi) with pencil. Solvent exposed electrode surface area (22.4 cm^2) was calculated via manufacturer-supplied surface area/volume ratio measurements. Cathode electrode assembled via affixing nickel foam (1.4 x 1.4 cm, or 1.5 x 0.9 cm, MTI Corporation, Surface density: 350g/m^3) to the end of stainless steel wire (Grainger, stainless steel lockwire, 0.025" diameter, item number 16Y043). PTFE tubing (Cole-Parmer; 1/32" ID, 1/16" OD, item number EW-06407-41) connects both sides of the divided cell to normalize pressure. Septa inner diameter 16 mm.

Figure C1. Picture of standard electrochemical H-cell used with electrode setup attached.

C.2 Supplemental Data

C.2.1 Cyclopropanation Comparison with Substitution of Vicinal Dihalide Starting Materials

A literature survey of different conditions varying base, solvents, and use of phase transfer reagents for cyclopropanation of dihaloethanes was found and applied to (3,4-dibromobutyl)benzene as a starting material. Results show minimal formation of cyclopropane product with mass balance favoring elimination side-products. For comparison, substitution of the 4-phenylbutene-derived dicationic adduct results in 85% yield for the desired cyclopropanation product.

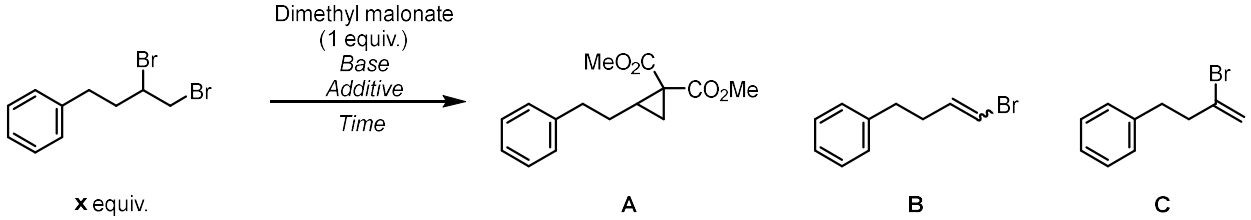

Entry	Base (equiv.)	x equiv.	Additive (equiv.)	Solvent (M)	Time (h)	A (%)	B (%)	C (%)	SM (%)	Source
1	Cs_2CO_3 (2.5)	1.0	--	MeCN (0.3)	2	0	0	0	98*	Our work
2	NaOH (11)	1.5	TBAB (0.2)	Toluene:H_2O (1:1, 0.6)	4	0	54	82	0	Ref. 2
3	NaH (3.0)	1.5	--	DMSO (0.3)	16	0	63	80	0	Ref. 3
4	K_2CO_3 (2.5)	1.4	TBAB (0.05)	DMF (0.3)	16	15	21	26	56	Ref. 4
5	NaOH (25)	1.5	$BnEt_3NCl$ (1)	H_2O (0.5)	16	2	39	54	55	Ref. 5

* No further conversion was observed even after stirring overnight (16 h)

Table C1. Substitution of conventional vicinal dibromide dielectrophile for cyclopropanation.

C.2.2 Cyclopropanation of Vicinal Dibromide Dielectrophiles for Drug Intermediate Analog

Substitution conditions were taken from patent literature prepped by Vertex Pharmaceuticals[6] for the synthesis of 1-(2,2-difluorobenzo[d][1,3]dioxol-5-yl)cyclopropane-1-carbonitrile and applied to vicinal dibromide analogs of alkenes showcased in Scheme 3.

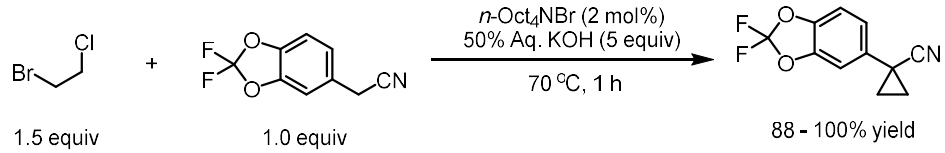

Scheme C1. Patented procedure for cyclopropanation of vicinal dihalide with 2-(2,2-difluorobenzo[d][1,3]dioxol-5-yl)acetonitrile.

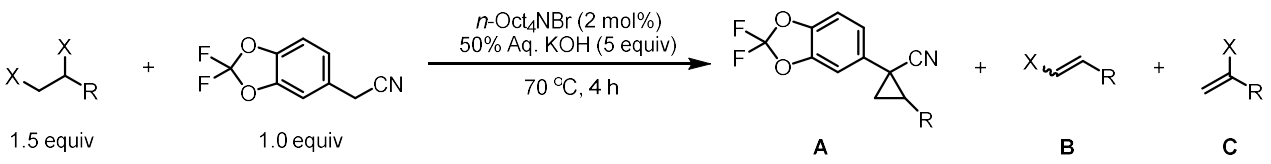

Entry	Substrate	A (%)	B (%)	C (%)	SM (%)
1	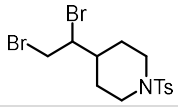	0	32	95	0
2*	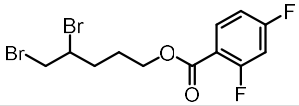	0	33	28	31
3	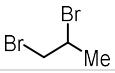	0	58	36	0

*Ester suffered from hydrolysis under basic conditions.

Table C2. Cyclopropanation of vicinal dibromide dielectrophiles targeting drug analog synthesis featured in Scheme 3.

C.3 Reaction Optimization

C.3.1 Experimental Procedures with Cs_2CO_3 Quench

To an oven-dried divided electrochemical cell equipped with magnetic stir bars was added thianthrene (48.7 mg, 0.225 mmol, 1.5 equiv.) to the anode compartment and KPF_6 (110 mg, 0.6 mmol) to both compartments. The cell was equipped with two septa containing a stainless steel wire/Ni foam cathode assembly and a pencil/RVC anode assembly connected together with a teflon tubing to equalize pressure. MeCN (3 mL) was added to the cathode and anode compartments. 4-phenylbutene (23 µL, 0.15 mmol, 1 equiv.) was added to the anode compartment. TFA (116 µL, 1.5 mmol, 10 equiv.) was added to the cathode compartment and both sides of the cell were stirred at 30 °C and electrolyzed under a constant current of 4.5 for 2.5 h (2.5 F/mol). At completion of electrolysis, the electrode leads were disconnected, septa removed, and the anode RVC was pushed off the pencil into the reaction mixture.

Following electrolysis, dibromomethane was added as an internal standard to the anodic compartment. The solution was thoroughly stirred, and 50 µL of mixture mixture was added to an NMR tube prefitted with a glass-sealed NMR insert filled with MeCN-*d3*. The NMR tube was diluted with 0.2 mL MeCN and an NMR of adduct was taken.

The cathode solution was removed from the cell via pipette and a fresh septum was added to the cathode department to prevent equilibration. 2-(6-chloropyridin-3-yl)acetonitrile (22.9 mg, 0.15 mmol, 1 equiv.) was added to the anode compartment followed by Cs_2CO_3 (varying equiv.). To the anode compartment was added a septum pierced with a needle to prevent pressurizing. After pressure equilibration, the needle was removed, and the anode solution was stirred in the cell for 2.5 h.

Following the Cs_2CO_3 quench, upon substitution reaction completion, the reaction mixture was taken up in an NMR tube for NMR yield.

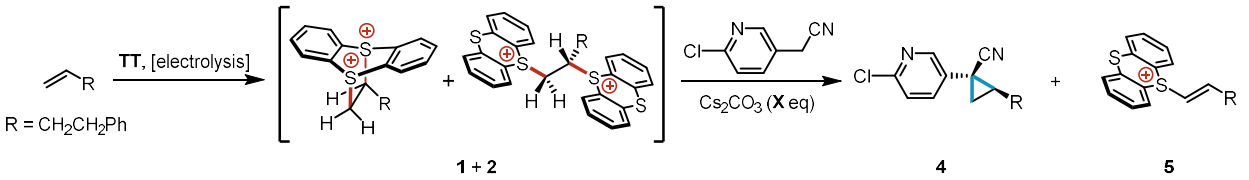

Cs_2CO_3 (equiv.)	1 + 2 (%)	4 (%)	5 (%)
1	88	0	90
2	81	0	83
3	89	5	80
4	85	19	56
5	83	32	43
6	84	67	0
8	78	71	0
10	86	80	0

Table C3. Base equivalence screening yields.

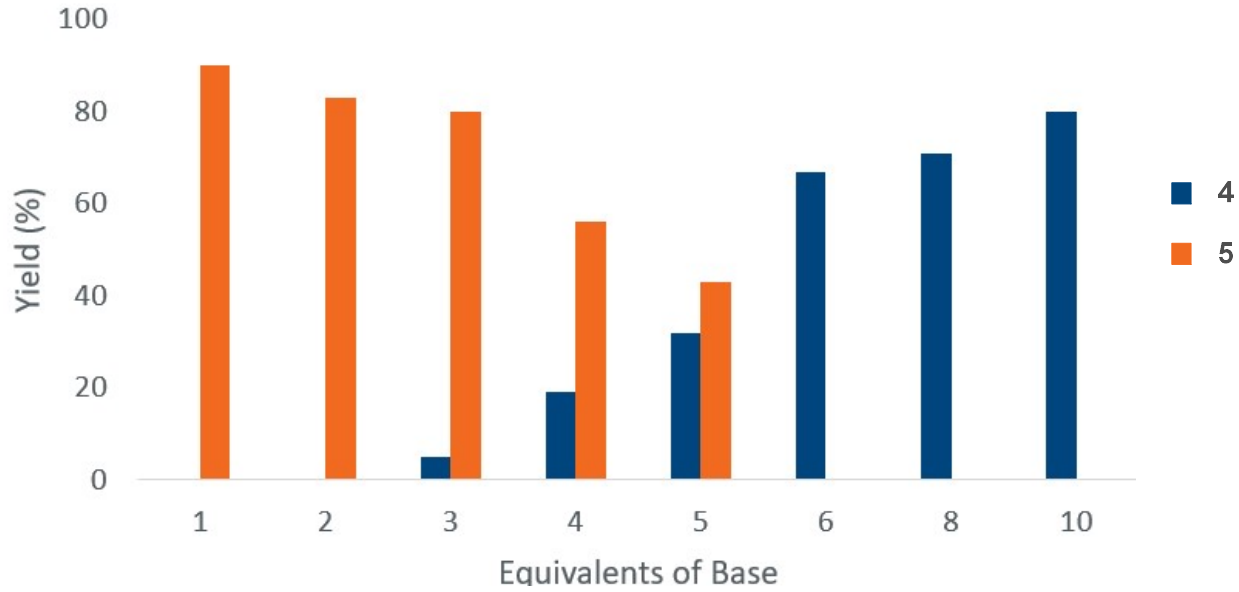

Figure C2. Base equivalence screening for cyclopropanation yield via dication pool.

C.3.2 Experimental Procedures for Reaction Time Course Study for Substitution.

To an oven-dried divided electrochemical cell equipped with magnetic stir bars was added thianthrene (48.7 mg, 0.225 mmol, 1.5 equiv.) to the anode compartment and KPF_6 (110 mg, 0.6 mmol) to both compartments. The cell was equipped with two septa containing a stainless steel wire/Ni foam cathode assembly and a pencil/RVC anode assembly connected together with a teflon tubing to equalize pressure. MeCN-*d3* (3 mL) was added to the cathode and anode compartments. 4-phenylbutene (23 µL, 0.15 mmol, 1 equiv.) was added to the anode compartment. TFA (116 µL, 1.5 mmol, 10 equiv.) was added to the cathode compartment and both sides of the cell were stirred at 30 °C and electrolyzed under a constant current of 4.5 mA for 2.5 h (2.5 F/mol). At completion of electrolysis, the electrode leads were disconnected, and dibromomethane was added as an internal standard and the reaction was stirred for an additional minute. Then, 0.5 mL of the anode solution was transferred to an oven-dried NMR tube directly using a syringe. Initially, the concentration of thianthrenium dicationic adducts was quantified via

^{1}H NMR using dibromomethane as an internal standard (NS = 1, Bruker Avance 600, TCI-F cryoprobe) with shimming. (**Note:** the reaction time was tracked relative to collection of the first spectrum.) Following initial scans, the NMR tube was removed from the spectrometer, and 2-(6-chloropyridin-3-yl)acetonitrile (0.025 mmol, 3.81 mg, 1 equiv. relative to solution in NMR tube) was added to the NMR tube. After a couple shakes, the NMR tube was placed in the NMR spectrometer and a series of spectra were gathered (NS = 1, no lock, no shimming). The NMR tube was again removed from the spectrometer, and Cs_2CO_3 (0.250 mmol, 81.5 mg, 10 equiv. relative to solution in NMR tube) was added to the NMR tube through a glass pipette to prevent solid sticking to the side of the tube. Without mixing, the solid was allowed to sink to the bottom, and the NMR tube was placed in the NMR spectrometer and a series of spectra were gathered (NS = 1, no lock, no shimming). Starting around 18 minutes after initial spectrum was taken, the NMR tube was removed from the spectrometer and mixed by hand in increasing increments of time (0.5, 1, 2, 4 mins). Spectra were collected after each mixing event (NS = 1, no lock, no shimming). Starting around 35 minutes after initial spectrum was taken, the NMR tube was removed from the spectrometer and mixed attached to a rotary evaporator and spun at lowest setting (approximately 10 full revolutions per minute). At varying times during the reaction, mixing was stopped, and spectra were collected to determine the concentration of vinyl thianthenium salt and final cyclopropane product using dibromomethane as an internal standard.

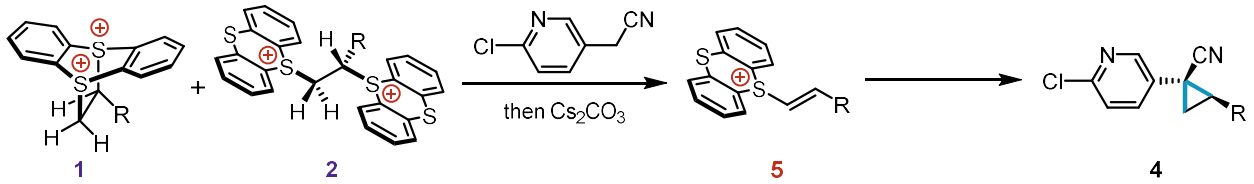

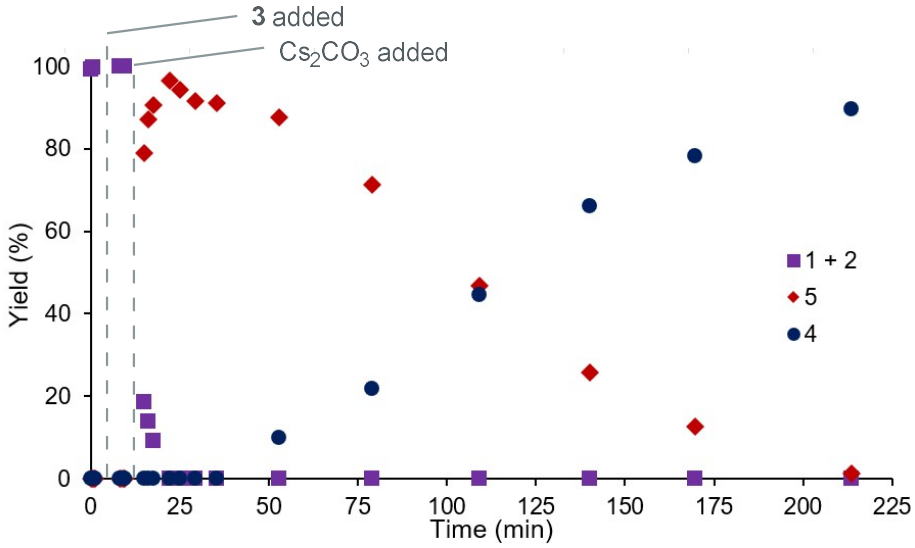

Figure C3. Reaction profile of substitution step with 10 equiv. of Cs_2CO_3. (R = CH_2CH_2Ph)

Time (mins)	1 + 2	5	4
0	99	0	0
9	100	0	0
15	19	79	0
16	14	87	0
18	9	91	0

22	0	96	0
25	0	94	0
29	0	91	0
35	0	91	0
53	0	88	10
79	0	71	22
109	0	47	45
140	0	26	66
170	0	13	78
214	0	1	90

Table C4. Full time course data for cyclopropanation via dication pool.

This ^{1}H NMR time course supports facile elimination of adducts **1** and **2** to form alkenyl thianthrenium **5**, which serves as a key intermediate en route to cyclopropane product **4**. Similarly, mechanistic studies for other transformations via the dication pool also support alkenyl thianthrenium as competent intermediates for both aziridination[7] (see below for data) and allylic amination.[8]

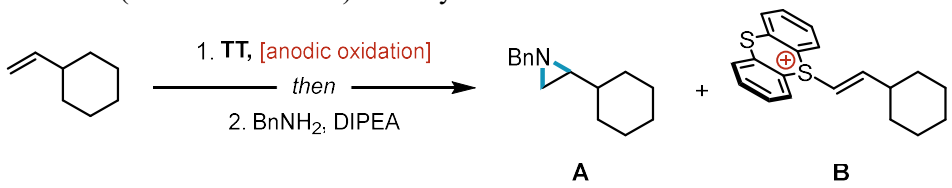

Time (h)	A	B
0.5	17	48
3	23	53
18	0	83

Table C5. Time course of aziridination via the dication pool.

C.3.3 Testing Effect of Nitrile vs Ester Groups on Diastereoselectivity.

To a 1 dram vial was added a stir bar and (*E*)-5-(4-phenylbut-1-en-1-yl)-5H-thianthren-5-ium hexafluorophosphate (43.4 mg, 0.100 mmol) followed by MeCN (2 mL). Then either 2-(6-chloropyridin-3-yl)acetonitrile (15.3 mg, 100 µmol, 1 equiv.) or ethyl-2-(6-chloropyridin-3-yl)acetate (20.0 mg, 15.5 µL, 100 µmol, 1 equiv.) was added, followed by Cs_2CO_3 (65.2 mg, 200 µmol, 2 equiv.). The solution was stirred for 2.5 h. Dibromomethane was added as an internal standard and an aliquot for NMR yield was taken. Cyclopropane coupling product yield and d.r. was determined via ^{1}H NMR. See Reaction Optimization section for characterization of products.

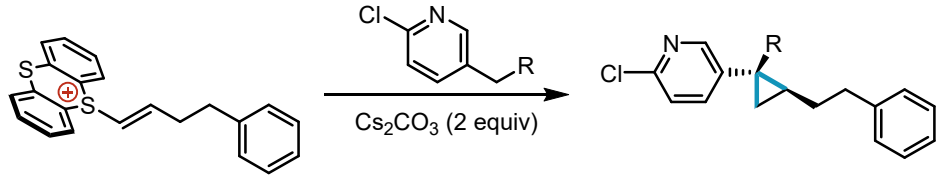

R = CN; 89% yield (**≥20:1 d.r.**)
R = CO_2Et; 56% yield (**2:1 d.r.**)

Scheme C2. Cyclopropanation of vinyl-TT$^+$ as starting material. Distinct d.r. is observed based on steric profile for substituents on acidic methylene carbon pronucleophile.

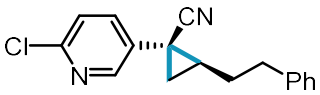

1-(6-Chloropyridin-3-yl)-2-phenethylcyclopropane-1-carbonitrile (C4): Following procedures outlined above afforded an NMR yield of 81% yield, mixture of diastereomers, ≥20:1 d.r. Structural configuration assigned via analogy with compound **25**. **^{1}H NMR** (500 MHz, $CDCl_3$) δ 8.23 (d, *J* = 2.6 Hz, 1H), 7.49 (dd, *J* = 8.4, 2.7 Hz, 1H), 7.29 (dd, *J* = 8.0, 6.3 Hz, 3H), 7.24 – 7.18 (m, 3H), 3.01 – 2.76 (m, 2H), 2.16 – 2.00 (m, 2H), 1.61 (dd, *J* = 8.0, 4.7 Hz, 1H), 1.58 – 1.49 (m, 2H). Distinct minor diastereomer signals observed at δ 8.17 (d, *J* = 2.7 Hz, 0H), 2.58 (td, *J* = 7.9, 4.2 Hz, 1H), 1.74 (dd, *J* = 9.3, 6.3 Hz, 0H), 1.43 (dd, *J* = 7.2, 5.3 Hz, 0H), 1.33 (dd, *J* = 7.4, 5.9 Hz, 1H). **^{13}C NMR** (126 MHz, $CDCl_3$) δ 150.88, 147.18, 140.52, 136.67, 131.74, 128.76, 128.66, 126.52, 124.37, 119.64, 34.90, 33.09, 30.34, 24.20, 17.80. **HRMS** (ESI+) Calc: [M+H]+ (C17H15ClN2) 283.0997, measured: 283.0994; 1.1 ppm difference.

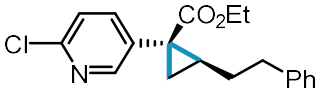

Ethyl 1-(6-chloropyridin-3-yl)-2-phenethylcyclopropane-1-carboxylate (C1): Following procedure outlined above afforded an NMR yield of 56% yield, mixture of diastereomers, 2.4:1 d.r. Structural configuration assigned via analogy with compound **29**. **^{1}H NMR** (500 MHz, $CDCl_3$) δ 8.27 (d, *J* = 2.4 Hz, 1H), 7.51 (dd, *J* = 8.2, 2.6 Hz, 1H), 7.30 (dd, *J* = 8.2, 6.9 Hz, 2H), 7.25 – 7.18 (m, 4H), 4.19 – 4.04 (m, 2H), 2.75 (td, *J* = 7.4, 2.4 Hz, 2H), 2.08 – 1.93 (m, 2H), 1.66 (dd, *J* = 7.5, 4.7 Hz, 1H), 1.55 – 1.45 (m, 1H), 1.28 (dd, *J* = 9.0, 4.7 Hz, 1H), 1.17 (t, *J* = 7.1 Hz, 3H). Distinct minor diastereomer signals observed at δ 8.27 (dd, *J* = 2.5, 0.7 Hz, 1H), 7.51 (dd, *J* = 8.2, 2.4 Hz, 1H), 7.29 – 7.22 (m, 3H), 7.20 – 7.13 (m, 1H), 7.10 – 7.04 (m, 2H), 4.16 – 4.00 (m, 2H), 2.75 – 2.62 (m, 2H), 1.91 (tdd, *J* = 9.2, 6.9, 4.9 Hz, 1H), 1.79 (ddd, *J* = 9.0, 4.4, 0.7 Hz, 1H), 1.67 (dddd, *J* = 13.6, 8.7, 6.8, 4.8 Hz, 1H), 1.16 (t, *J* = 7.1 Hz, 3H), 1.06 (dd, *J* = 6.9, 4.4 Hz, 1H), 0.83 (dtd, *J* = 13.9, 9.0, 6.6 Hz, 1H). **HRMS** (ESI+) Calc: [M+H]+ (C19H20ClNO2) 330.1255, measured: 330.1253; 0.6 ppm difference.

C.3.4 Experimental Procedures with Basic Alumina Filtration Quench.

To an oven-dried divided electrochemical cell equipped with magnetic stir bars was added thianthrene (130 mg, 0.600 mmol, 1.5 equiv.) to the anode compartment and KPF_6 (294 mg, 1.60 mmol) to both compartments. The cell was equipped with two septa containing a stainless steel wire/Ni foam cathode assembly and a pencil/RVC anode assembly connected together with a teflon tubing to equalize pressure. MeCN (8 mL) was added to the cathode and anode compartments. 4-phenylbutene (60 µL, 0.400 mmol, 1 equiv.) was added to the anode compartment. TFA (308 µL, 4.00 mmol, 10 equiv.) was added to the cathode compartment and both sides of the cell were stirred at 30 °C and electrolyzed under a constant current of 12.0 mA for 2.25 h (2.5 F/mol alkene). At completion of electrolysis, the electrode leads were disconnected, septa removed, and the anode RVC was pushed off the pencil into the reaction mixture.

Following electrolysis, dibromomethane was added as an internal standard to the anodic compartment. The solution was thoroughly stirred, and 50 µL of mixture mixture was added to an NMR tube pre-fitted with a glass-sealed NMR insert filled with MeCN-*d3*. The NMR tube was diluted with 0.2 mL MeCN and an NMR of adduct was taken.

The cathode solution was removed from the cell via pipette and a fresh septum was added to the cathode department to prevent equilibration. The anode solution was filtered over a pad of basic alumina (8 g, activated, basic, Brockmann I). The cathode compartment was washed with MeCN (2.0 mL) and pushed across the frit to rinse the frit. The anode compartment was further washed with MeCN (5 x 1.2 mL). The alumina pad was washed with MeCN (2 x 8 mL), taking care to fully disperse the alumina in solution using a spatula. The filtrate was concentrated in vacuo and then resuspended in MeCN (1.5 mL). 2-(6-

chloropyridin-3-yl)acetonitrile or (61.0 mg, 0.400 mmol, 1 equiv.) was added to the reaction mixture followed by Cs_2CO_3 (261 mg, 0.800 mmol, 2 equiv.). The solution was stirred for 2.5 h.

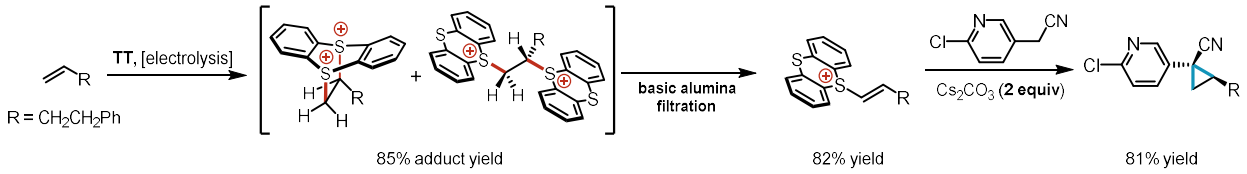

Scheme S3. Cyclopropanation via the dication pool using a basic alumina quench.

C.4 Substrate Preparation

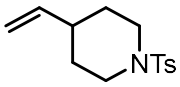

***tert*-Butyl 4-vinylpiperidine-1-carboxylate (C2):** An oven-dried round bottom flask under N_2 was charged with $MePPh_3I$ (28.9 g, 71.5 mmol, 1.3 equiv.) and THF (275 mL, 0.2 M). KOtBu (8.64 g, 77.0 mmol, 1.4 equiv.) was added to the suspension at 0 °C. The resulting mixture was allowed to warm to room temperature and stirred for 1 h. The yellow suspension was then cooled to 0 °C and *tert*-butyl-4-formylpiperidine-1-carboxylate (11.7 g, 55.0 mmol, 1 equiv.) was added. The reaction was allowed to warm to room temperature and stirred overnight. Following completion monitored via TLC, the reaction mixture was concentrated under reduced pressure and then diluted with ether (~ 100 mL) to precipitate triphenylphosphine oxide. The mixture was filtered, and the solid was washed 5x with ether. The filtrate was collected, concentrated under reduced pressure, and the reside was purified via flash column chromatography (EtOAc/hexanes) to give 11.1 g (96%) of **C2** as a liquid. **^{1}H NMR** (400 MHz, $CDCl_3$) δ 5.77 (ddd, J = 17.0, 10.5, 6.4 Hz, 1H), 4.98 (m, 2H), 4.08 (m, 2H), 2.72 (m, 2H), 2.11 (m, 2H), 1.68 (d, J = 13.2, Hz, 2H), 1.45 (s, 9H), 1.28 (m, 2H). **^{13}C NMR** consistent with reported spectra (*Angew. Chem. Int. Ed.* **2018**, 57, 13096-13100).

1-Tosyl-4-vinylpiperidine (C3): An oven-dried round bottom flask was charged with **C2** (9.80 g, 46.4 mmol, 1 equiv.) and 1:1 DCM:TFA (60 mL, 0.8 M). The reaction was stirred at room temperature and monitored for completion via TLC (~ 1 h). Then NEt_3 (70mL), DMAP (567 mg, 4.64 mmol, 0.1 equiv.), and tosyl chloride (10.6 g, 55.7 mmol, 1.2 equiv.) were added to the reaction mixture. The mixture was stirred at room temperature for 16 h. The mixture was then quenched with water (250 mL). The organic layer was separated, and the aqueous layer was extracted with DCM (3 x 250 mL). The combined organic layers were dried over anhydrous Na_2SO_4, filtered, and concentrated under reduced pressure. The residue was purified via flash column chromatography (conditions) to give 10.1 g (82% yield) of **C3** as a solid. **^{1}H NMR** (400 MHz, $CDCl_3$) δ 7.64 (d, J = 8.3 Hz, 2H), 7.32 (d, J = 7.9 Hz, 2H), 5.71 (ddd, J = 17.1, 10.5, 6.4 Hz, 1H), 4.96 (m, 2H), 3.76 (dt, J = 11.9, 3.3 Hz, 2H), 2.43 (s, 3H), 2.28 (td, J = 11.9, 2.6 Hz, 2H), 1.88 (m, 1H), 1.74 (m, 2H), 1.49 (m, 2H). ^{13}C NMR consistent with reported spectra (*Angew. Chem. Int. Ed.* **2018**, 57, 13096-13100.

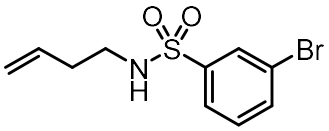

3-bromo-*N*-(but-3-en-1-yl)benzenesulfonamide (C4): To a solution of 3-bromobenzenesulfonyl chloride (2.56 g, 10.0 mmol, 1.1 equiv.) in DCM (10 mL) at 0 °C was added NEt_3 (1.4 mL, 10.0 mmol, 1.1 equiv.) followed by 3-buten-1-amine (0.84 mL, 9.09 mmol, 1 equiv.). The mixture was allowed to warm to room temperature overnight. 1 N HCl (~20 mL) was added to the reaction mixture and the layers were separated. The aqueous layer was extracted with DCM (~40 mL x3). The combined organic layers were dried with anhydrous Na_2SO_4, filtered, and evaporated under reduced pressure. The residue was purified via flash column chromatography (EtOAc/hexanes) to give 2.00 g (76 % yield) of **C4** as a white fluffy solid. **^{1}H NMR** (400 MHz, $CDCl_3$) δ 8.01 (t, J = 1.9 Hz, 1H), 7.79 (ddd, J = 7.9, 1.8, 1.0 Hz, 1H), 7.71 (ddd, J = 8.0, 1.9, 1.0 Hz, 1H), 7.40 (t, J = 7.9 Hz, 1H), 5.63 (ddt, J = 17.1, 10.3, 6.9 Hz, 1H), 5.16 – 5.01 (m, 2H), 4.47 (t, J = 6.4 Hz, 1H), 3.07 (q, J = 6.4 Hz, 2H), 2.28 – 2.20 (m, 2H). ^{13}C NMR consistent with reported spectra (*Nature* **2021**, 596, 74-79.)

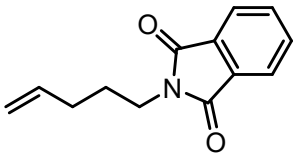

2-(pent-4-enyl)-isoindoline-1,3-dione (C5): To a mixture of potassium phthalimide (11.11 g, 60.0 mmol, 1.5 equiv.) in DMF (80 mL) was added 5-brompent-1-ene (4.74 mL, 40.0 mmol, 1 equiv.). The reaction mixture was heated to 60 °C and stirred overnight (18 h). At completion, the the mixture was cooled to room temperature and poured into a saturated brine solution (~200 mL). The aqueous layer was extracted with Et_2O (3 x 150 mL). The combined organic layers were washed with aqueous 10% LiCl solution (2 x 20 mL), dried over anhydrous Na_2SO_4, filtered, and concentrated under reduced pressure. The residue was purified via flash column chromatography (EtOAc/hexanes) to give 4.66 g (54% yield) of **C5** as a solid. **^{1}H NMR** (500MHz, $CDCl_3$) δ 7.82 (dd, J = 5.4, 3.0 Hz, 2H), 7.69 (dd, J = 5.5, 3.0 Hz, 2H), 5.80 (ddt, J = 16.9, 10.2, 6.6 Hz, 1H), 5.03 (dd, J = 17.1, 1.7 Hz, 1H), 4.96 (dd, J = 10.3, 1.4 Hz, 1H), 3.68 (t, J = 7.4 Hz, 2H), 2.14 – 2.06 (m, 2H), 1.77 (ddd, J = 14.7, 8.1, 6.8 Hz, 2H); ^{13}C NMR consistent with reported spectra (*JACS* **2009**, 131, 9670–9685.)

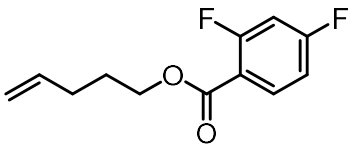

Pent-4-en-1-yl 2,4-difluorobenzoate (C6). A mixture of 2,4-difluorobenzoic acid (1.11 g, 7.0 mmol, 1 equiv.), N-(3-Dimethylaminopropyl)-N′-ethylcarbodiimide hydrochloride (1.74 g, 9.1 mmol, 1.3 equiv.), and 4-(dimethylamino)pyridine (86 mg, 0.7 mmol, 0.1 equiv.) in DCM (28 mL) was stirred at 0 °C for 20 min. Pent-4-en-1-ol (724 mg, 8.4 mmol, 0.87 mL, 1.1 equiv.) was added and the reaction mixture was allowed to warm to room temperature. At completion as monitored by TLC, the mixture was diluted with DCM and extracted with 1N HCl solution (~80 mL). The organic layer was washed with brine solution (~50 mL), dried over anhydrous MgSO4, filtered, and concentrated under reduced pressure. The residue was purified via flash column chromatography (EtOAc/hexanes) to give 1.14 g (72% yield) of **C6** as an oil. **^{1}H NMR** (500MHz, $CDCl_3$) δ 7.95 (td, J = 8.5, 6.5 Hz, 1H), 6.91 (dddd, J = 8.7, 7.6, 2.5, 1.0 Hz, 1H), 6.85 (ddd, J = 11.1, 8.9, 2.5 Hz, 1H), 5.82 (ddt, J = 16.9, 10.2, 6.6 Hz, 1H), 5.05 (dq, J = 17.1, 1.7 Hz, 1H), 5.01 – 4.96 (m, 1H), 4.32 (t, J = 6.5 Hz, 2H), 2.24 – 2.15 (m, 2H), 1.84 (dq, J = 8.1,

6.6 Hz, 2H). ^{13}C NMR consistent with reported spectra (*JACS* **2021**, 143, 21503-21510.)

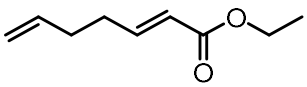

(E)-ethyl hepta-2,6-dienoate (C7): In a flame-dried 1L round-bottom flask, oxalyl chloride (9.77 g, 6.8 mL, 77.0 mmol, 1.1 equiv.) was dissolved in DCM (240 mL). The reaction mixture was cooled to -78 °C. DMSO (13.1 g, 11.9 mL, 168 mmol, 2.4 equiv.) was added, and the reaction was stirred at -78 °C for 10 min. Pent-4-en-1-ol (6.03 g, 7.2 mL, 70.0 mmol, 1 equiv.) was added dropwise, and the reaction was stirred at -78 °C for 30 min before warming to room temperature. (Carbethoxymethylene)triphenylphosphorane (36.6 g, 105 mmol, 1.5 equiv.) dissolved in DCM (55 mL) was added. The reaction was stirred at room temperature for 2 h. Water (100 mL) was added to the reaction mixture and the layers were separated. The aqueous layer was extracted with DCM (50 mL x 3). The combined organic layers were washed with brine (40 mL), dried with anhydrous $MgSO_4$, filtered, and evaporated under reduced pressure. The residue was purified via flash column chromatography (EtOAc/hexanes) to give 8.53 g (79 % yield) of **C7** as an oil. **^{1}H NMR** (400 MHz, $CDCl_3$) δ 6.96 (dt, J = 15.6, 6.7 Hz, 1H), 5.87 – 5.74 (m, 2H), 5.09 – 4.97 (m, 2H), 4.18 (q, J = 7.1 Hz, 2H), 2.35-– 2.36 (m, 2H), 2.25 – 2.18 (m, 2H), 1.28 (t, J = 1.3 Hz, 3H). ^{13}C NMR consistent with reported spectra (*Australian Journal of Chemistry* **2000**, 53, 659-664.)

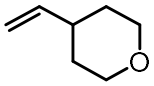

4-vinyltetrahydro-2H-pyran (C8): Sodium hydride (60% oil dispersion, 973 mg, 24 mmol, 1.2 equiv.) was washed with 3 portions of hexanes under an inert atmosphere to remove oil. THF (82 mL) was then added followed by methyltriphenylphosphonium iodide (9.8 g, 24 mmol, 1.2 equiv.). The reaction mixture was then heated to reflux for 2 h. The solution was then cooled to room temperature. Tetrahydro-2H-pyran-4-carbaldehyde (2.3 g, 20 mmol, 1.0 equiv.) was slowly added and the reaction was allowed to stir for an additional 24 h. Upon reaction completion, saturated aqueous $NaHCO_3$ (40 mL) was added and the mixture was extracted with Et_2O (80 mL). The organic layer was then washed with water and brine, dried over $MgSO_4$, and concentrated. (Note: Due to the volatility of the product, the rotavap bath was kept at 0 °C.) The product was purified via column chromatography (Et_2O/pentane) to yield 800 mg (35% yield) of the **C8** as an oil. **^{1}H NMR** (500 MHz, $CDCl_3$) δ 5.78 (ddd, J = 17.0, 10.4, 6.3 Hz, 1H), 5.00 (dt, J = 17.3, 1.6 Hz, 1H), 4.96 (dt, J = 10.5, 1.5 Hz, 1H), 3.97 (ddd, J = 11.5, 4.6, 2.0 Hz, 2H), 3.42 (td, J = 11.7, 2.2 Hz, 2H), 2.26 – 2.15 (m, 1H), 1.63 (ddq, J = 13.2, 4.2, 2.2 Hz, 2H), 1.46 (dtd, J = 13.3, 11.6, 4.4 Hz, 2H). **^{13}C NMR** (126 MHz, CDCl3) δ 142.81, 112.71, 67.70, 38.70, 32.21. HRMS (ESI+) Calc: $[M+H]^+$ ($C_7H_{13}O$) 113.0961, measured: 113.0960.

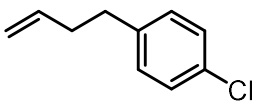

1-(but-3-en-1-yl)-4-chlorobenzene (C9): Allylmagnesium bromide (1 M in THF, 25.8 mL, 25.8 mmol, 1.29 equiv.) was added to a solution of 4-chlorobenzyl bromide (4.11 g, 20 mmol) in Et2O (30 mL) at 0 °C under an inert atmosphere. The reaction was allowed to come to room temperature and stirred for 2 h. Upon reaction completion, the reaction was quenched with saturated aqueous NH_4Cl. The aqueous layer was extracted with DCM, and the combined organic layers were dried over $MgSO_4$, filtered through celite, and concentrated. The crude mixture was purified via flash column chromatography followed by distillation to yield 2.04 g (61% yield) of **C9** as an oil. **^{1}H NMR** (400 MHz, $CDCl_3$) δ 7.27 (dt, *J* = 9.0, 2.1 Hz, 2H), 7.18 – 7.10 (m, 2H), 5.85 (ddt, *J* = 16.9, 10.2, 6.6 Hz, 1H), 5.10 – 4.96 (m, 2H), 2.70 (dd, *J* = 8.8, 6.7 Hz, 2H), 2.37 (tdt, *J* = 7.8, 6.5, 1.4 Hz, 2H). ^{13}C NMR consistent with reported spectra (*Chem. Commun.* **2013**, *49* (95), 11230-11232.)

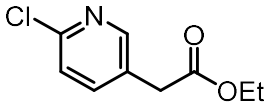

Ethyl 2-(6-chloropyridin-3-yl)acetate (C10): (6-chloropyridin-3-yl)acetonitrile (1.00 g, 6.55 mmol) was added to a mixture of EtOH (12.2 mL) and concentrated sulfuric acid (4.54 mL, 85.2 mmol), and the mixture was stirred under reflux for 45 h. The reaction mixture was slowly added dropwise while stirring to a mixture of $NaHCO_3$ (16.0 g, 190 mmol) and water (100 mL). The aqueous phase was extracted with DCM (5 x 200 mL). The combined organic phases were dried over Na_2SO_4, filtered, and evaporated under reduced pressure. The crude mixture was purified via column chromatography (EtOAC/hexanes) to yield 1.15 g (88% yield) of the **C10** as an oil. ^{1}**H NMR** (500 MHz, $CDCl_3$) δ 8.31 – 8.27 (m, 1H), 7.62 (dd, *J* = 8.2, 2.6 Hz, 1H), 7.30 (dd, *J* = 8.2, 0.6 Hz, 1H), 4.17 (q, *J* = 7.1 Hz, 2H), 3.60 (s, 2H), 1.26 (t, *J* = 7.2 Hz, 3H). ^{13}C NMR consistent with reported spectra (*Chem. Med. Chem.* **2018**, 13 (10), 988–1003.)

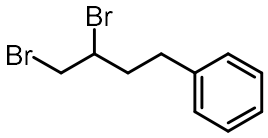

(3,4-Dibromobutyl)benzene (C11): 4-Phenylbutene (5.3 mL, 35.0 mmol, 1.0 equiv.) and DMSO (3.0 mL, 42.0 mmol, 1.2 equiv.) were dissolved in EtOAc (140 mL). The reaction mixture was heated to 60 °C. Aqueous HBr (48%, 9.6 mL, 84.0 mmol, 2.4 equiv.) was added. The reaction was stirred at 60 °C for 30 min. After cooling to room temperature, the reaction mixture was concentrated under reduced pressed. The crude mixture was purified via column chromatography (EtOAc/hexanes) to yield 9.96 g (98% yield) of **C11** as an oil. ^{1}**H NMR** (500 MHz, $CDCl_3$) δ 7.33 (m, 2H), 7.25 (m, 3H), 4.13 (tdd, J = 9.6, 4.5, 3.0 Hz, 1H), 3.87 (dd, J = 10.3, 4.4 Hz, 1H), 3.66 (t, J = 10.0 Hz, 1H), 2.96 (ddd, J = 13.9, 0.3, 4.7 Hz, 1H), 2.78 (ddd, J = 13.8, 9.2, 7.2 Hz, 1H), 2.50 (dddd, J = 14.7, 9.2, 7.2, 3.0 Hz, 1H), 2.11 (dtd, J = 14.3, 9.3, 4.7 Hz, 1H). ^{13}C NMR consistent with reported spectra (*Green Chem.* **2015**, *17*, 3285-3289.)

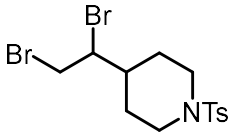

4-(1,2-Dibromoethyl)-1-tosylpiperidine (C12): N-Bromosuccinimide (1.07 g, 6.00 mmol, 3.0 equiv.) and DMSO (0.43 mL, 6.00 mmol, 3.0 equiv.) were dissolved in DCM (24 mL), and the reaction mixture was let stir until NBS completely dissolved. 1-Tosyl-4-vinylpiperidine (**S3**) was added, and the reaction mixture was stirred at room temperature for 30 min. The crude mixture was purified via column chromatography (EtOAc/hexanes) to yield 510 mg (60% yield) of **C12** as a solid. ^{1}**H NMR** (500 MHz, $CDCl_3$) δ 7.65 (d, J = 8.3 Hz, 2H), 7.33 (d, J = 8.1 Hz, 2H), 4.11 (dt, J = 9.7, 4.2 Hz, 1H), 3.93 – 3.85 (m, 2H), 3.82 (dd, J = 10.7, 4.7 Hz, 1H), 3.66 (d, J = 10.7, 9.7 Hz, 1H), 2.42 (s, 3H), 2. 28 (dtd, J = 15.1, 12.1, 2.9 Hz, 2H), 1.88 – 1.70 (m, 3H), 1.67 – 1.53 (m, 2H). ^{13}**C NMR** (126 MHz, CDCl3) δ 143.75, 133.25, 129.83, 127.86, 57.01, 46.07, 45.95, 37.90, 33.72, 30.13, 25.78, 21.67. HRMS (ESI+) Calc: $[M+H]^+$ (C14H19Br2NO2S) 423.9576, measured: 423.9571; 1.2 ppm difference.

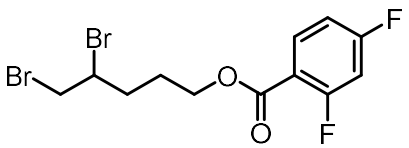

4,5-Dibromopentyl 2,4-difluorobenzoate (C13): N-Bromosuccinimide (1.07 g, 6.00 mmol, 3.0 equiv.) and DMSO (0.43 mL, 6.00 mmol, 3.0 equiv.) were dissolved in DCM (24 mL), and the reaction mixture was let stir until NBS completely dissolved. Pent-4-en-1-yl 2,4-difluorobenzoate (**S6**) was added, and the reaction mixture was stirred at room temperature for 30 min. The crude mixture was purified via column

chromatography (EtOAc/hexanes) to yield 368 mg (48% yield) of **C13** as an oil. **^{1}H NMR** (500 MHz, $CDCl_3$) δ 8.00 – 7.94 (m, 1H), 6.96 – 6.90 (m, 1H), 6.90 – 6.84 (m, 1H), 4.42 – 4.34 (m, 2H), 4.25 – 4.19 (m, 1H), 3.87 (dd, J = 10.3, 4.3 Hz, 1H), 3.63 (t, J = 10.2 Hz, 1H), 2.43 – 2. 31 (m, 1H), 2.13 – 2.02 (m, 1H), 1.98 – 1.85 (m, 2H). **^{13}C NMR** (126 MHz, CDCl3) δ 165.85 (dd, J = 256. 4, 12.0 Hz), 163.60 (d, J = 4.2 Hz), 162.97 (dd, J = 263.4, 12.7 Hz), 134 (dd, J = 10.5, 2.3 Hz), 115.25 (dd, J = 9.9, 3.7 Hz), 111.74 (dd, J = 21.6, 3.9 Hz), 105.38 (t, J = 25.7 Hz), 64.42, 52.04, 36.02, 32.85, 26.26. **^{19}F NMR** (377 MHz, $CDCl_3$) δ -101.73 (d, J = 12.5 Hz, 1F), -103.58 (d, J = 12.6 Hz, 1F).

C.5 General Experimental Procedures

CAUTION: Although there is no known toxicology data on these dicationic adducts and no issues were encountered during these experiments, we suspect, based on analogy to other dielectrophiles, that these adducts are toxic. Isolation or storage of the adducts was avoided.

General Procedure A: Electronically Neutral Alkenes

To an oven-dried divided electrochemical cell equipped with magnetic stir bars was added thianthrene (130 mg, 0.6 mmol, 1.5 equiv.) to the anode compartment and *n*-Bu_4NPF_6 (620 mg, 1.6 mmol, 4 equiv.) to both compartments. The cell was equipped with two septa containing a stainless steel wire/Ni foam cathode assembly and a pencil/RVC anode assembly connected together with a teflon tubing to equalize pressure. MeCN (8 mL) was added to the cathode compartment and the glass frit was allowed to become saturated (<1 min). MeCN (8 mL) was added to the anode compartment, followed by alkene (0.4 mmol, 1 equiv.). (Electrode depth: 2 cm). TFA (306 µL, 4.0 mmol, 10 equiv.) was added to the cathode compartment and both sides of the cell were stirred at 30 °C and electrolyzed under a constant current of 12 mA for 2.25 h (2.5 F/mol). At completion of electrolysis, the electrode leads were disconnected, septa removed, and the anode RVC was pushed off the pencil into the anode reaction mixture. To the anode compartment was added a septum pierced with a needle to prevent pressurizing. After pressure equilibration, the needle was removed, and the cathode solution was removed from the cell via pipette. The anode solution was filtered through activated basic alumina (8 g, Brockmann I). The cathode compartment was washed with MeCN (1 mL) and pushed across the frit to rinse the frit. The anode compartment was further washed with MeCN (5 x 1 mL). The alumina pad was washed with MeCN (3 x 8 mL), taking care to fully disperse the alumina in solution using a spatula. The filtrate was concentrated under reduced pressure. Then a stir bar and MeCN (1.5 mL) was added to the flask, followed by carbon pronucleophile (0.4 mmol, 1 equiv.) then Cs_2CO_3 (326 mg, 1.0 mmol, 2.5 equiv.). The solution was stirred for 2 h. At completion, the mixture was diluted with DCM (60 mL) and water (150 mL). The aqueous layer was extracted with DCM (50 mL x 3). The combined organic layers were washed with saturated NaCl solution (40 mL), dried with anhydrous Na_2SO_4, filtered, and concentrated under reduced pressure. The residue was purified via flash column chromatography to yield the pure cyclopropane product.

General Procedure B: Electron Deficient Alkenes

Followed General Procedure A but modified electrolysis by stirring both sides of the cells and electrolyzing under a constant current of 14.4 mA for 2.25 h (3.0 F/mol). Otherwise, procedure A was followed as written.

General Procedure C: Gaseous Alkenes

To an oven-dried divided electrochemical cell equipped with magnetic stir bars was added thianthrene (216 mg, 1.0 mmol, 2.5 equiv.) to the anode compartment and *n*-Bu_4NPF_6 (620 mg, 1.6 mmol) to both compartments. The cell was equipped with two septa containing a stainless steel wire/Ni foam cathode

assembly and a pencil/RVC anode assembly connected together with a teflon tubing to equalize pressure. In a separate 10 mL-round bottom flask, MeCN (8 mL) was sparged with a balloon of gaseous alkene for 10 min. Alkene-saturated MeCN (4 mL) was transferred to the cathode and anode compartments via Teflon cannula. TFA (460 μL, 6.0 mmol, 15 equiv.) was added to the cathode compartment and both sides of the cell were stirred at ambient temperature and electrolyzed under a constant current of 30.0 mA for 1.5 h (1.7 F/mol TT). At completion of electrolysis, the electrode leads were disconnected, septa removed, and the anode RVC was pushed off the pencil into the reaction mixture. To the anode compartment was added a septum pierced with a needle to prevent pressurizing. After pressure equilibration, the needle was removed, and the cathode solution was removed from the cell via pipette. The anode solution was filtered through activated basic alumina (8 g, Brockmann I). The cathode compartment was washed with MeCN (1 mL) and pushed across the frit to rinse the frit. The anode compartment was further washed with MeCN (5 x 1 mL). The alumina pad was washed with MeCN (2 x 8 mL), taking care to fully disperse the alumina in solution using a spatula. The filtrate was concentrated under reduced pressure. Then a stir bar and MeCN (1.5 mL) was added to the flask, followed by carbon pronucleophile (0.4 mmol, 1 equiv.) then Cs_2CO_3 (261 mg, 0.8 mmol, 2.0 equiv.). The solution was stirred for 16 h. At completion, the mixture was diluted with DCM (60 mL) and water (150 mL). The aqueous layer was extracted with DCM (50 mL x 3). The combined organic layers were washed with saturated NaCl solution (40 mL), dried with anhydrous Na_2SO_4, filtered, and concentrated under reduced pressure. The residue was purified via flash column chromatography to yield the pure cyclopropane product.

General Procedure D: Ethylene

Followed General Procedure C but modified substitution by using DBU (121 μL, 0.8 mmol, 2.0 equiv.) instead of Cs_2CO_3. Otherwise, procedure C was followed as written.

General Procedure E: NMR Yield

Following General Procedure A, but with the following modification: following stirring with carbon pronucleophile and Cs_2CO_3 for 2 h, cyclopropane product yield was determined via ^1H NMR using mesitylene or dibromomethane as an internal standard.

C.6 Product Characterization

Adduct/Vinyl-TT+/Product Yield Breakdown

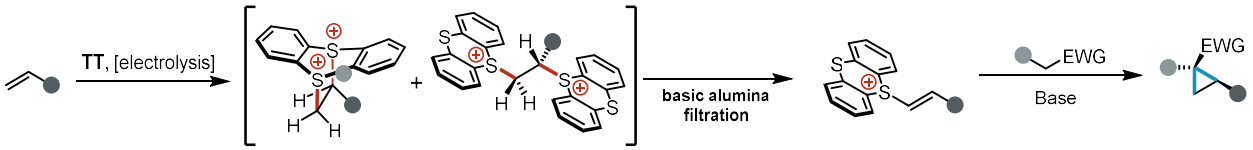

All yields reported relative to carbon pronucleophile as limiting reagent.

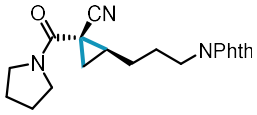

4.6
75% adduct
75% vinyl-TT$^+$
70% product

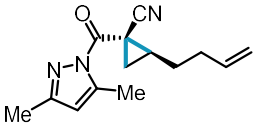

4.7
76% adduct
73% vinyl-TT$^+$
61% product

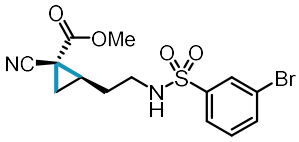

4.8[a]
107% adduct
78% vinyl-TT$^+$
54% product

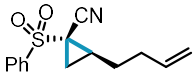

4.9
78% adduct
78% vinyl-TT$^+$
74% product

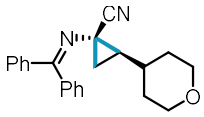

4.10
69% adduct
69% vinyl-TT$^+$
68% product

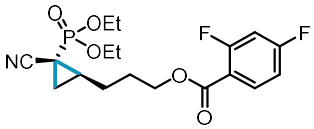

4.11
85% adduct
85% vinyl-TT$^+$
68% product

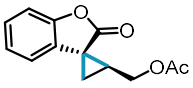

4.12[b]
150% adduct
72% vinyl-TT$^+$
54% product

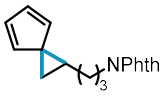

4.13
85% adduct
74% vinyl-TT$^+$
45% product

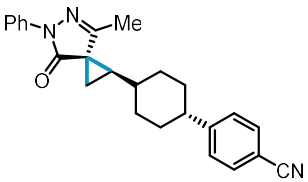

4.14
78% adduct
78% vinyl-TT$^+$
69% product

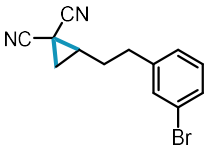

4.15
77% adduct
77% vinyl-TT$^+$
67% product

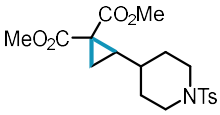

4.16
80% adduct
80% vinyl-TT$^+$
74% product

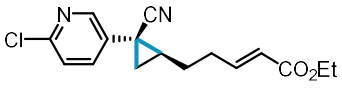

4.17
64% adduct
65% vinyl-TT$^+$
54% product

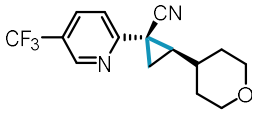

4.18
75% adduct
76% vinyl-TT$^+$
63% product

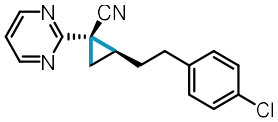

4.19
80% adduct
80% vinyl-TT$^+$
78% product

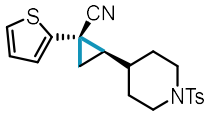

4.20
85% adduct
84% vinyl-TT$^+$
74% product

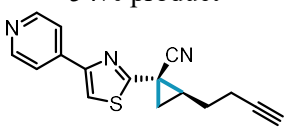

4.21
--
61% vinyl-TT$^+$
61% product

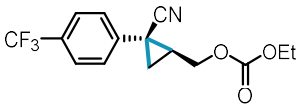

4.22[b]
166% adduct
68% vinyl-TT$^+$
70% product

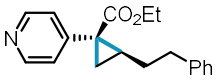

4.23
72% adduct
72% vinyl-TT$^+$
66% product

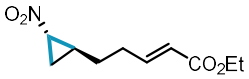

4.24
71% adduct
61% vinyl-TT$^+$
55% product

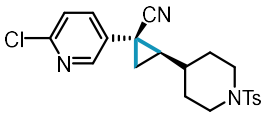

4.25
79% adduct
78% vinyl-TT$^+$
74% product

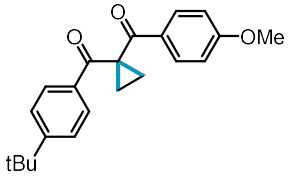

4.26[c]
--
150% vinyl-TT$^+$
76% product

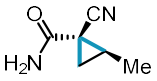

4.27[c]
--
121% vinyl-TT$^+$
74% product

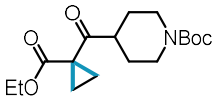

4.28[c]
--
152% vinyl-TT$^+$
95% product

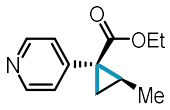

4.29[c]
--
117% vinyl-TT$^+$
83% product

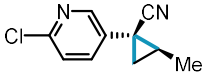

30[c]
--
124% vinyl-TT$^+$
95% product

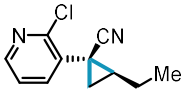

31[c]
--
141% vinyl-TT$^+$
99% product

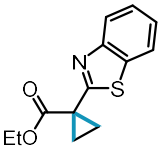

32[c]
--
143% vinyl-TT$^+$
67% product

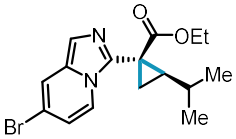

33[c]
--
125% vinyl-TT$^+$
50% product

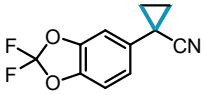

4.34[c]
--
148% vinyl-TT$^+$
87% product

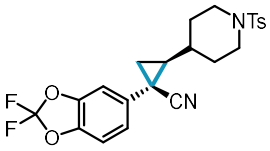

4.35
80% adduct
82% vinyl-TT$^+$
75% product

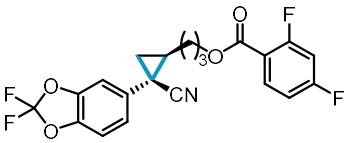

4.36
83% adduct
79% vinyl-TT$^+$
66% product

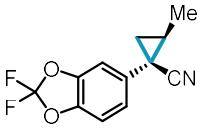

4.37[c]
--
128% vinyl-TT$^+$
74% product

a. 1.5 equiv. alkene used.; b. 2.0 equiv. alkene used.; c. 1 atm alkene used.

Table C6. Telescoped yields for adduct, vinyl-TT$^+$, and cyclopropane yield for each substrate.

Unsuccessful Substrates

Alkenes that failed to form dicationic adduct under electrolysis conditions.

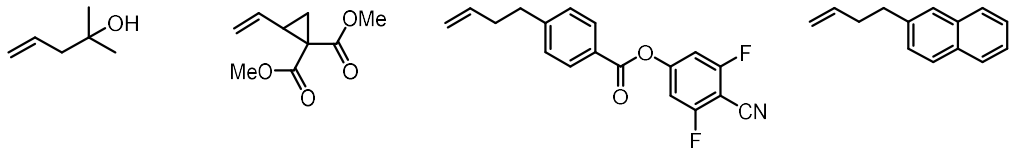

Alkenes that formed adduct but failed to cleanly eliminate to a vinyl thianthrenium salt upon basic workup.

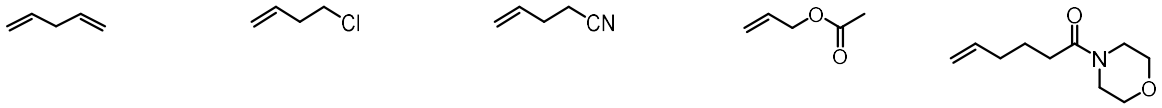

Alkenes that smoothly converted to alkenyl thianthrenium salts but resulted in poor yield of cyclopropane product under substitution conditions.

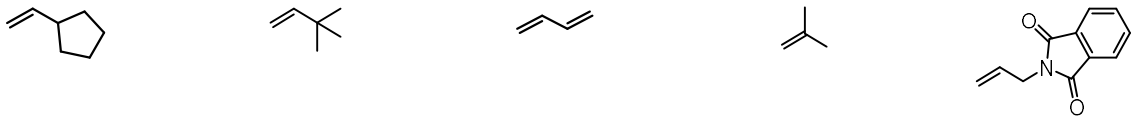

Carbon pronucleophiles that failed to deliver cyclopropane products under substitution conditions.

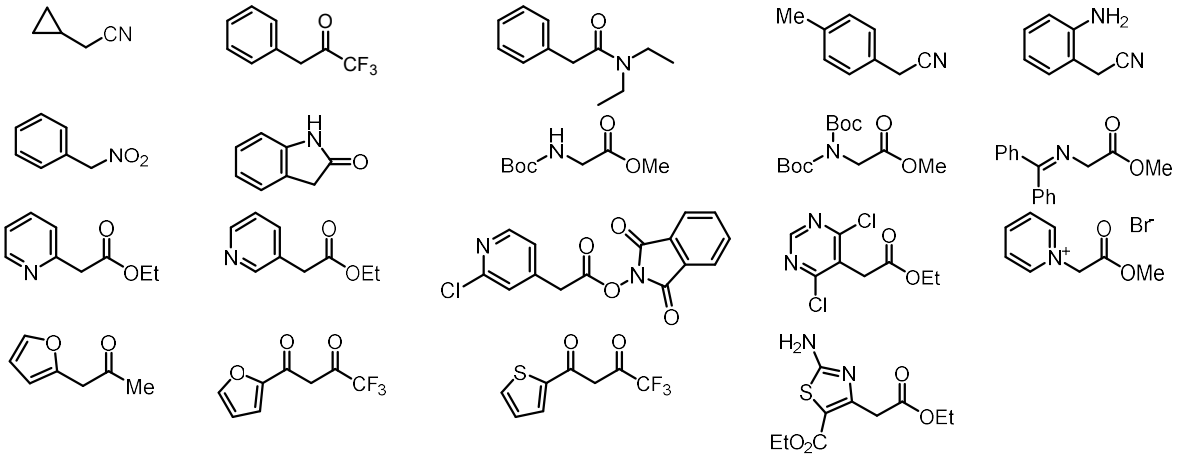

Fig. C4. Alkene and carbon pronucleophile coupling partners that presented challenges for the dication pool.

Product Characterization

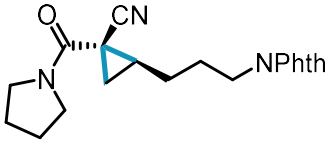

2-(3-(1,3-dioxoisoindolin-2-yl)propyl)-1-(pyrrolidine-1-carbonyl)cyclopropane-1-carbonitrile (4.6). Following General Procedure B afforded one detectable diastereomer in 98.3 mg (70% yield, ≥20:1 d.r.) as an oil. $\mathbf{R_f}$ = 0.14 (20% acetone/hexanes). Structural configuration assigned via analogy with compound **4.27**. **^{1}H NMR** (500 MHz, $CDCl_3$) δ 7.82 (dd, J = 5.4, 3.0 Hz, 2H), 7.70 (dd, J = 5.5, 3.0 Hz, 2H), 3.82 (dt, J = 10.2, 7.0 Hz, 1H), 3.74 (td, J = 7.1, 1.7 Hz, 3H), 3.45 (t, J = 7.0 Hz, 2H), 2.00 (p, J = 6.8 Hz, 2H), 1.95 – 1.79 (m, 6H), 1.77 – 1.68 (m, 1H), 1.67 – 1.58 (m, 1H), 1.23 (q, J = 2.6 Hz, 1H). **^{13}C NMR** (126 MHz, $CDCl_3$) δ 168.41, 162.75, 134.06, 132.14, 123.33, 118.65, 47.74, 47.66, 37.37, 27.85, 27.82, 27.72, 26.55, 24.06, 22.82, 19.83. **HRMS** (ESI+) Calc: $[M+H]^+$ ($C_{20}H_{22}N_3O_3$) 352.1656, measured: 352.1654; 0.6 ppm difference.

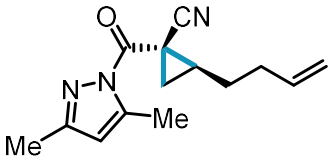

2-(but-3-en-1-yl)-1-(3,5-dimethyl-1H-pyrazole-1-carbonyl)cyclopropane-1-carbonitrile (4.7). Following General Procedure E with KPF_6 instead of *n*-Bu_4NPF_6 afforded an NMR yield of 68%. Structural configuration assigned via analogy with compound **4.27**. **^{1}H NMR** (500 MHz, $CDCl_3$) δ 5.95 (d, *J* = 1.1 Hz, 1H), 5.79 (ddt, *J* = 17.1, 10.2, 6.8 Hz, 1H), 5.00 (dq, *J* = 17.1, 1.7 Hz, 1H), 4.94 (ddd, *J* = 10.2, 2.1, 1.0 Hz, 1H), 2.41 (s, 3H), 2.45 – 2.18 (m, 2H), 2.22 (s, 3H), 2.03 (dd, *J* = 9.0, 5.0 Hz, 1H), 1.90 – 1.72 (m, 3H), 1.37 (dd, *J* = 7.3, 4.7 Hz, 1H). **HRMS** (ESI+) Calc: [M+H]+ (C14H17N3O) 244.1444, measured: 244.1442; 0.8 ppm difference.

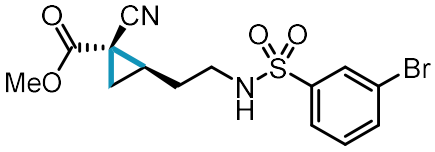

Methyl 2-(2-((3-bromophenyl)sulfonamido)ethyl)-1-cyanocyclopropane-1-carboxylate (4.8). Following General Procedure B using 1.5 equiv. alkene and 21.6 mA for 2.25 h (3.0 F/mol) afforded one detectable diastereomer in 124.5 mg (54% yield, ≥20:1 d.r.) as an oil. $\mathbf{R_f}$ = 0.12 (20% acetone/hexanes). Structural configuration assigned via NOESY. **^{1}H NMR** (500 MHz, $CDCl_3$) δ 8.00 (t, J = 1.9 Hz, 1H), 7.79 (ddd, J = 7.8, 1.8, 1.0 Hz, 1H), 7.71 (ddd, J = 8.0, 1.9, 1.0 Hz, 1H), 7.41 (t, J = 7.9 Hz, 1H), 5.06 (t, J = 6.4 Hz, 1H), 3.81 (s, 3H), 3.15 (q, J = 6.6 Hz, 2H), 1.99 (dtd, J = 8.9, 7.8, 6.4 Hz, 1H), 1.93 – 1.83 (m, 2H), 1.79 (ddt, J = 14.4, 7.9, 6.5 Hz, 1H), 1.39 (dd, J = 7.9, 4.9 Hz, 1H). **^{13}C NMR** (126 MHz, $CDCl_3$) δ 167.93, 141.85, 135.98, 130.93, 130.02, 125.68, 123.32, 117.26, 53.76, 42.02, 30.77, 28.48, 24.76, 19.36. **HRMS** (ESI+) Calc: $[M+NH_4]^+$ ($C_{14}H_{19}BrN_3O_4S$) 404.0274, measured: 404.0273; 0.2 ppm difference.

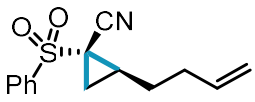

2-(but-3-en-1-yl)-1-(phenylsulfonyl)cyclopropane-1-carbonitrile (4.9). Following General Procedure A afforded one detectable diastereomer in 77.0 mg (74% yield, ≥20:1 d.r.) as an oil. $\mathbf{R_f}$ = 0.34 (20% acetone/hexanes). Structural configuration assigned via NOESY. **^{1}H NMR** (500 MHz, $CDCl_3$) δ 7.96 (dd, J = 8.4, 1.3 Hz, 2H), 7.78 – 7.70 (m, 1H), 7.66 – 7.59 (m, 2H), 5.72 (ddt, J = 17.0, 10.3, 6.7 Hz, 1H), 5.08 – 4.90 (m, 2H), 2.20 (dtd, J = 9.5, 8.1, 6.2 Hz, 1H), 2.11 (dddd, J = 13.2, 8.1, 6.6, 1.4 Hz, 2H), 2.07 – 2.01 (m, 1H), 1.74 (ddt, J = 14.5, 8.0, 6.6 Hz, 1H), 1.55 (dtd, J = 14.3, 8.0, 6.2 Hz, 1H), 1.43 (dd, J = 7.9, 5.6 Hz, 1H). **^{13}C NMR** (126 MHz, $CDCl_3$) δ 137.35, 136.22, 134.92, 129.70, 128.84, 116.44, 114.94, 38.38, 32.17, 29.24, 27.72, 22.25. **HRMS** (ESI+) Calc: $[M+NH_4]^+$ ($C_{14}H_{19}N_2O_2S$) 279.1162, measured: 279.1157; 1.8 ppm difference.

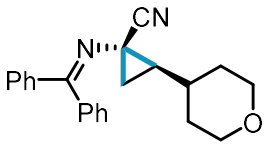

1-((diphenylmethylene)amino)-2-(tetrahydro-2H-pyran-4-yl)cyclopropane-1-carbonitrile (4.10). Following General Procedure A afforded 89.9 mg (68% yield, mixture of diastereomers, 2:1 d.r.) as a solid. $\mathbf{R_f}$ = 0.27 (10:1:89 ethyl acetate:NEt_3:hexanes). Structural configuration assigned via analogy with compound **4.18**. **^{1}H NMR** (500 MHz, $CDCl_3$) δ 7.55 (m, 5H), 7.43 (m, 1H), 7.35 (m, 4H), 4.04 (m, 2H), 3.47 (tdd, J = 11.6, 6.7, 2.4 Hz, 2H), 1.95 (m, 1H), 1.89 (1H), 1.75 (dd, J = 9.3, 5.1 Hz, 1H), 1.63 (m, 4H), 1.27 (dd, J = 7.6, 5.1 Hz, 1H). Distinct minor diastereomer signals observed at δ 3.98 (dddd, J = 13.5, 11.7, 4.7, 2.1 Hz, 2H), 3.37 (tdd, J = 11.7, 5.0, 2.4 Hz, 2H), 1.83 (m, 1H), 1.38 (m, 1H), 1.33 (m, 1H). **^{13}C NMR** (126 MHz, $CDCl_3$) δ 171.91, 139.56, 135.95, 130.83, 129.89, 128.63, 128.60, 128.27, 67. 92, 67.69, 37.52, 37.16, 34.49, 32.42, 32.04, 25.03. Distinct minor diastereomer signals observed at δ 171.16, 139.39, 136.03, 130.80, 129.81, 128.59, 128.57, 128.19, 67.70, 67.52, 37.13, 36.66, 34.20, 31.90, 31.73, 26.34. **HRMS** (ESI+) Calc: $[M+H]^+$ ($C_{22}H_{22}N_2O$) 331.1805, measured: 331.1798; 2.1 ppm difference.

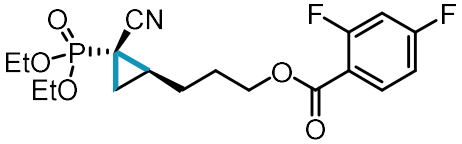

3-(2-cyano-2-(diethoxyphosphoryl)cyclopropyl)propyl 2,4-difluorobenzoate (4.11). Following General Procedure B afforded separable diastereomers, providing 89.2 mg of major diastereomer as an oil and 19.7 mg of minor diastereomer as an oil, 108.9 mg total isolated (68% yield, 5:1 d.r.). Structural configuration assigned via analogy with compound **4.9**.

Major diastereomer: $\mathbf{R_f}$ = 0.19 (20% acetone/hexanes). **^{1}H NMR** (500 MHz, $CDCl_3$) δ 7.98 (td, J = 8.5, 6.5 Hz, 1H), 6.98 – 6.91 (m, 1H), 6.87 (ddd, J = 11.0, 8.8, 2.5 Hz, 1H), 4.40 (t, J = 6.2 Hz, 2H), 4.26 – 4.16 (q, J = 7.1 Hz, 4H), 2.07 – 1.92 (m, 2H), 1.91 – 1.81 (m, 2H), 1.79 – 1.70 (m, 2H), 1.39 (t, J = 7.1 Hz, 6H), 1.29 (ddd, J = 9.1, 6.7, 4.7 Hz, 1H). **^{13}C NMR** (126 MHz, $CDCl_3$) δ 165.91 (dd, J = 256.5, 12.0 Hz), 163.64 (d, J = 4.2 Hz), 163.01 (dd, J = 263.2, 12.7 Hz), 134.12 (dd, J = 10.6, 2.3 Hz), 117.48 (d, J = 4.4 Hz), 115.25 (dd, J = 9.9, 3.7 Hz), 111.79 (dd, J = 21.5, 3.8 Hz), 105.40 (dd, J = 26.0, 25.9 Hz), 64.39, 64.02 (d, J = 6.8 Hz), 63.97 (d, J = 6.8 Hz), 27.72, 27.11 (d, J = 1.3 Hz), 25.46 (d, J = 2.3 Hz), 20.67 (d, J = 3.0 Hz), 16.45 (d, J = 1.9 Hz), 16.47 (d, J = 1.9 Hz), 10.71 (d, J = 200.2 Hz). **^{31}P NMR** (162 MHz, $CDCl_3$) δ 18.64. **^{19}F NMR** (377 MHz, $CDCl_3$) δ -101.76 (d, J = 12.5 Hz), -103.78 (d, J = 12.7 Hz). **HRMS** (ESI+) Calc: $[M+H]^+$ (C18H23F2NO5P) 402.1276, measured: 402.1270; 1.5 ppm difference.

Minor diastereomer: $\mathbf{R_f}$ = 0.16 (20% acetone/hexanes). **^{1}H NMR** (500 MHz, $CDCl_3$) δ 7.98 (td, J = 8.5, 6.5 Hz, 1H), 6.93 (dddd, J = 8.8, 7.6, 2.5, 1.0 Hz, 1H), 6.87 (ddd, J = 11.1, 8.8, 2.5 Hz, 1H), 4.37 (q, J =

6.0 Hz, 2H), 4.23 (ddt, J = 15.2, 8.2, 7.0 Hz, 4H), 2.07 – 1.83 (m, 5H), 1.72 (ddd, J = 8.3, 7.0, 4.5 Hz, 1H), 1.58 (ddd, J = 14.4, 7.2, 4.7 Hz, 1H), 1.41 (t, J = 7.1 Hz, 3H), 1.38 (t, J = 7.1 Hz, 3H). **^{13}C NMR** (126 MHz, $CDCl_3$) δ 165.88 (dd, J = 256.4, 12.0 Hz), 163.67 (d, J = 4.1 Hz), 162.99 (dd, J = 263.2, 12.5 Hz), 134.10 (dd, J = 10.6, 2.4 Hz), 119.79 (d, J = 4.6 Hz), 115.33 (dd, J = 9.9, 3.7 Hz), 111.78 (dd, J = 21.5, 3.8 Hz), 105.27 (dd, J = 26.2, 25.2 Hz), 64.73, 63.88 (d, J = 6.1 Hz), 63.60 (d, J = 6.9 Hz), 29.24 (d, J = 2.4 Hz), 28.17, 24.55 (d, J = 3.5 Hz), 20.96 (d, J = 2.1 Hz), 16.47 (d, J = 6.2 Hz), 16.39, 9.67 (d, J = 199.8 Hz). **^{31}P NMR** (162 MHz, $CDCl_3$) δ 17.87. **^{19}F NMR** (377 MHz, $CDCl_3$) δ -102.91 (d, J = 12.0 Hz), -104.88 (d, J = 12.3 Hz). **HRMS** (ESI+) Calc: $[M+H]^+$ ($C_{18}H_{23}F_2NO_5P$) 402.1276, measured: 402.1273; 0.7 ppm difference.

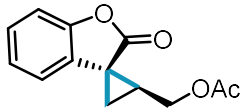

(2-Oxo-2H-spiro[benzofuran-3,1'-cyclopropan]-2'-yl)methyl acetate (4.12). Following General Procedure A using 2.0 equiv. alkene and 29 mA for 2.25 h (3.0 F/mol) afforded 49.7 mg (54% yield, mixture of diastereomers, 6:1 d.r.; estimated 4:1 d.r. in crude ^{1}H NMR spectrum prior to purification) as an oil. **R_f** = 0.30 (20% acetone/hexanes). Structural configuration of major diastereomer assigned via NOESY. **^{1}H NMR** (500 MHz, $CDCl_3$) δ 7.35 – 7.27 (m, 1H), 7.24 – 7.12 (m, 2H), 6.87 (dd, J = 7.5, 1.3 Hz, 1H), 4.70 (ddd, J = 12.0, 6.0, 1.5 Hz, 1H), 4.38 (ddd, J = 12.0, 8.8, 1.1 Hz, 1H), 2.36 (qd, J = 8.5, 5.8 Hz, 1H), 2.04 (s, 3H), 1.92 (d, J = 8.1 Hz, 2H). Distinct minor diastereomer signals observed at δ 7.03 (dd, J = 7.6, 1.4 Hz, 1H), 4.52 (dd, J = 12.3, 6.5 Hz, 1H), 4.21 (dd, J = 12.3, 8.3 Hz, 1H), 2.10 (dd, J = 9.3, 5.0 Hz, 1H), 1.99 (s, 3H), 1.65 (dd, J = 7.8, 5.0 Hz, 1H). **^{13}C NMR** (126 MHz, $CDCl_3$) δ 175.30, 171.04, 153.40, 128.83, 127.98, 124.22, 118.87, 110.80, 61.09, 32.26, 28.29, 24.72, 20.97. Distinct minor diastereomer signals observed at δ 176.75, 170.88, 154.04, 128.19, 125.79, 124.14, 121.09, 111.11, 61.74, 31.37, 29.17, 23.41, 20.83. **HRMS** (ESI+) Calc: $[M+Na]^+$ ($C_{13}H_{12}O_4Na$) 255.0628, measured: 255.0622; 2.4 ppm difference.

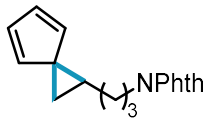

2-(3-(Spiro[2.4]hepta-4,6-dien-1-yl)propyl)isoindoline-1,3-dione (4.13). Following General Procedure B afforded 50.4 mg (45% yield) as a solid. **R_f** = 0.29 (26% Ether/Hexanes).
^{1}H NMR (500 MHz, $CDCl_3$) δ 7.83 (dd, *J* = 5.5, 3.1 Hz, 2H), 7.70 (dd, *J* = 5.5, 3.1 Hz, 2H), 6.54 (ddd, *J* = 5.2, 2.1, 1.4 Hz, 1H), 6.42 (ddd, *J* = 5.0, 2.3, 1.4 Hz, 1H), 6.22 (ddd, *J* = 5.2, 2.1, 1.4 Hz, 1H), 6.05 (dt, *J* = 5.0, 1.8 Hz, 1H), 3.72 – 3.61 (m, 2H), 2.16 – 2.06 (m, 1H), 1.79 (dd, *J* = 8.6, 4.0 Hz, 1H), 1.78 – 1.67 (m, 3H), 1.64 – 1.58 (m, 1H), 1.57 (dd, *J* = 7.3, 4.0 Hz, 1H). **^{13}C NMR** (126 MHz, $CDCl_3$) δ 168.39, 139.83, 135.31, 133.90, 132.15, 130.62, 128.04, 123.19, 42.94, 37.52, 30.04, 28.48, 27.73, 19.98. **HRMS** (ESI+) Calc: [M+H]+ (C18H17NO2) 280.1332, measured: 280.1330; 0.7 ppm difference.

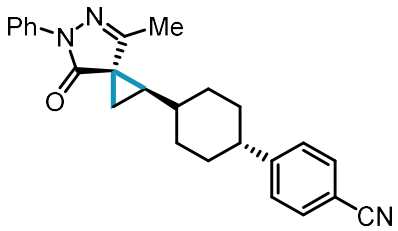

4-(4-(4-methyl-7-oxo-6-phenyl-5,6-diazaspiro[2.4]hept-4-en-1-yl)cyclohexyl)benzonitrile (4.14). Following General Procedure A afforded 105.5 mg (69% yield, mixture of diastereomers, 3:1 d.r.) as a solid. **R_f** = 0.24 (20% ethyl acetate/hexanes). Structural configuration assigned via x-ray crystallography.

^{1}H NMR (500 MHz, $CDCl_3$) δ 7.94 (dd, J = 8.8, 1.2 Hz, 2H), 7.57 (t, J = 8.8 Hz, 2H), 7.42 – 7.37 (m, 2H), 7.29 (d, J = 8.4 Hz, 1H), 7.27 (d, J = 8.4 Hz, 1H), 7.17 (td, J = 7.4, 1.1 Hz, 1H), 2.51 (tt, J = 12.2, 3.4 Hz, 1H), 2.14 – 2.07 (m, 1H), 2.04 – 1.98 (m, 1H), 1.96 (s, 3H), 1.88 (dd, J = 8.5, 3.7 Hz, 1H), 1.85 – 1.73 (m, 3H), 1.72 – 1.60 (m, 1H), 1.52 (dqd, J = 23.3, 12.8, 3.5 Hz, 2H), 1.36 (tt, J = 12.3, 6.3 Hz, 2H), 1.17 (qd, J = 12.7, 3.5 Hz, 1H). Distinct minor diastereomer signals observed at δ 7.95 (dd, J = 8.8, 1.1 Hz, 2H), 2.58 (td, J = 11.5, 9.8, 5.6 Hz, 1H). **^{13}C NMR** (126 MHz, $CDCl_3$) δ 171.53, 159.65, 152.76, 138.95, 132.36, 128.92, 127.77, 124.85, 119.21, 118.89, 109.91, 44.55, 39.88, 37.14, 33.58, 33.47, 33.20, 33.10, 32.96, 32.73, 24.32, 12.60. Distinct minor diastereomer signals observed at δ 172.58, 158.57, 152.31, 138.80, 132.40, 128.95, 127.72, 119.13, 118.65, 110.10, 44.15, 42.82, 38.61, 38.02, 33.50, 33.23, 32.94, 25.70, 16.01. **HRMS** (ESI+) Calc: $[M+H]^+$ ($C_{25}H_{26}N_3O$) 384.2070, measured: 384.2065; 1.3 ppm difference.

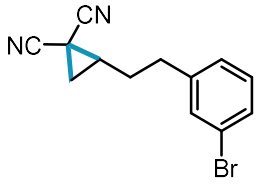

2-(3-bromophenethyl)cyclopropane-1,1-dicarbonitrile (4.15). Following General Procedure A afforded 73.7 mg (67% yield) obtained as an oil. **^{1}H NMR** (400 MHz, $CDCl_3$) δ 7.42 – 7.34 (m, 2H), 7.21 (t, *J* = 7.6 Hz, 1H), 7.17 – 7.12 (m, 1H), 2.84 (tt, *J* = 14.0, 7.6 Hz, 2H), 2.03 – 1.87 (m, 4H), 1.50 (td, *J* = 5.4, 1.3 Hz, 1H). **^{13}C NMR** (126 MHz, $CDCl_3$) δ 141.93, 131.63, 130.51, 130.05, 127.26, 122.98, 115.36, 113.76, 33.91, 31.83, 30.51, 24.73, 4.03. **HRMS** (ESI+) Calc: [M+H]+ (C13H11BrN2) 283.0997, measured: 283.0994; 1.1 ppm difference.

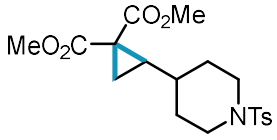

Dimethyl 2-(1-tosylpiperidin-4-yl)cyclopropane-1,1-dicarboxylate (4.16). Following General Procedure B afforded 116.7 mg (74% yield) as a solid. **R_f =** 0.22 (20% acetone/hexanes). **^{1}H NMR** (500 MHz, $CDCl_3$) δ 7.60 (d, J = 8.2 Hz, 2H), 7.30 (d, J = 8.0 Hz, 2H), 3.77 – 3.73 (m, 1H), 3.71 – 3.67 (m, 1H), 3.69 (s, 3H), 3.68 (s, 3H), 2.42 (s, 3H), 2.20 (td, J = 11.8, 2.7 Hz, 1H), 2.11 (td, J = 11.8, 2.7 Hz, 1H), 1.82 – 1.66 (m, 3H), 1.59 – 1.45 (m, 2H), 1.34 (ddd, J = 20.5, 8.4, 4.7 Hz, 2H), 0.74 (qt, J = 11.1, 3.7 Hz, 1H). **^{13}C NMR** (126 MHz, $CDCl_3$) δ 170.36, 168.71, 143.59, 133.05, 129.70, 127.74, 52.76, 52.62, 46.15, 46.02, 35.37, 33.79, 33.26, 31.14, 30.84, 21.56, 19.88. **HRMS** (ESI+) Calc: $[M+H]^+$ ($C_{19}H_{26}NO_6S$) 396.1475, measured: 396.1471; 1.0 ppm difference.

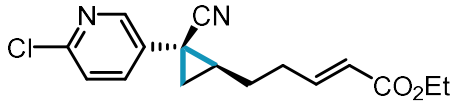

Ethyl (E)-5-(2-(6-chloropyridin-3-yl)-2-cyanocyclopropyl)pent-2-enoate (4.17). Following Following General Procedure B afforded one detectable diastereomer with an NMR yield of 54%. Structural configuration assigned via analogy with compound **4.25**. **^{1}H NMR** (500 MHz, $CDCl_3$) δ 8.27 (d, J = 2.7 Hz, 1H), 7.56 (dd, J = 8.4, 2.7 Hz, 1H), 7.31 (d, J = 8.5 Hz, 1H), 7.01 – 6.92 (m, 1H), 5.86 (dq, J = 15.6, 1.5 Hz, 1H), 4.17 (q, J = 7.1 Hz, 2H), 2.54 – 2.38 (m, 2H), 1.96 – 1.88 (m, 2H), 1.74 – 1.61 (m, 1H), 1.60 – 1.48 (m, 2H), 1.27 (t, J = 7.1 Hz, 3H). Distinct minor diastereomer signals observed at δ 6.77 (m, 1H), 5.75 (m, 1H). **HRMS** (ESI+) Calc: [M+H]+ (C16H14ClN3) 305.1051, measured: 305.1049; 0.7 ppm difference.

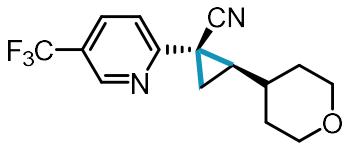

2-(Tetrahydro-2H-pyran-4-yl)-1-(5-(trifluoromethyl)pyridin-2-yl)cyclopropane-1-carbonitrile (4.18). Following General Procedure B afforded one detectable diastereomer in 74.7 mg (63% yield, ≥20:1 d.r.) as a solid. $\mathbf{R_f}$ = 0.26 (10% acetone/hexanes). Structural configuration assigned via x-ray crystallography. **^{1}H NMR** (500 MHz, $CDCl_3$) δ 8.73 – 8.69 (m, 1H), 7.92 (dd, *J* = 8.3, 2.5 Hz, 1H), 7.83 (d, *J* = 8.2 Hz, 1H), 4.03 (ddd, *J* = 11.6, 4.6, 2.4 Hz, 1H), 3.97 (ddd, *J* = 11.3, 4.3, 2.4 Hz, 1H), 3.49 – 3.39 (m, 2H), 2.06 (dd, *J* = 8.7, 4.4 Hz, 1H), 1.98 – 1.91 (m, 1H), 1.87 (dq, *J* = 9.6, 2.3 Hz, 1H), 1.80 – 1.73 (m, 1H), 1.69 – 1.58 (m, 2H), 1.58 – 1.46 (m, 2H). **^{13}C NMR** (126 MHz, $CDCl_3$) δ 158.94, 146.78 (q, J = 4.1 Hz), 134.11 (q, J = 3.5 Hz), 125.21 (q, J = 33.2 Hz), 123.53 (q, J = 272.2 Hz), 120.51, 119.93, 67.73, 67.60, 38.49, 38.09, 32.20, 32.02, 26.02, 21.42. **^{19}F NMR** (377 MHz, $CDCl_3$) δ -62.28. **HRMS** (ESI+) Calc: [M+H]+ (C15H15F3N2O) 297.1209, measured: 297.1206; 1.0 ppm difference.

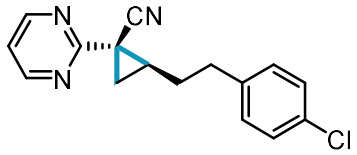

2-(4-Chlorophenethyl)-1-(pyrimidin-2-yl)cyclopropane-1-carbonitrile (4.19). Following General Procedure A afforded one detectable diastereomer in 84.8 mg (75% yield, ≥20:1 d.r.) as an oil. $\mathbf{R_f}$ = 0.29 (30% EtOAC/Hexanes). Structural configuration assigned via analogy with compound **4.18**. **^{1}H NMR** (500 MHz, C_6D_6) δ 7.97 (d, *J* = 4.9 Hz, 2H), 7.03 (d, *J* = 8.4 Hz, 1H), 6.70 (d, *J* = 8.3 Hz, 2H), 6.11 (t, *J* = 4.9 Hz, 1H), 2.46 (ddd, *J* = 14.0, 8.6, 5.6 Hz, 1H), 2.33 (ddd, *J* = 13.7, 8.2, 6.6 Hz, 1H), 1.82 – 1.60 (m, 4H), 1.04 (dd, *J* = 6.7, 4.2 Hz, 1H).). Distinct minor diastereomer signals observed at δ 6.53 (d, *J* = 8.3 Hz, 1H). **^{13}C NMR** (126 MHz, $CDCl_3$) δ 166.10, 156.95, 139.67, 132.14, 130.17, 128.79, 128.25, 128.06, 127.87, 119.04, 118.87, 34.18, 32.68, 32.24, 26.37, 24.23. **HRMS** (ESI+) Calc: [M+H]+ (C16H14ClN3) 284.0949, measured: 284.0944; 1.8 ppm difference.

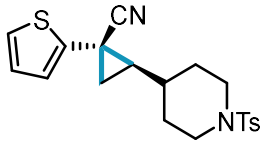

1-(Thiophen-2-yl)-2-(1-tosylpiperidin-4-yl)cyclopropane-1-carbonitrile (4.20). Following General Procedure B afforded separable diastereomers, providing 101.9 mg of major diastereomer as a solid and 12.4 mg of minor diastereomer as a solid, 114.3 mg total isolated (74% yield, 8:1 d.r.). Structural configuration assigned via analogy with compound **22**.

Major diastereomer: $\mathbf{R_f}$ = 0.22 (20% acetone/hexanes). **^{1}H NMR** (500 MHz, $CDCl_3$) δ 7.68 – 7.60 (m, 2H), 7.37 – 7.29 (m, 2H), 7.19 (dd, *J* = 5.2, 1.2 Hz, 1H), 6.99 (dd, *J* = 3.6, 1.3 Hz, 1H), 6.93 (dd, *J* = 5.2, 3.7 Hz, 1H), 3.85 (ddd, *J* = 7.0, 4.7, 2.4 Hz, 2H), 2.44 (s, 3H), 2.25 (dtd, *J* = 22.1, 12.1, 2.8 Hz, 2H), 2.12 (d, *J* = 13.4 Hz, 1H), 1.84 (d, *J* = 13.3 Hz, 1H), 1.70 – 1.57 (m, 3H), 1.46 – 1.35 (m, 2H), 1.15 – 1.03 (m, 1H). **^{13}C NMR** (126 MHz, $CDCl_3$) δ 143.83, 140.25, 132.85, 129.84, 127.86, 127.42, 126.02, 120.25, 46.31 (d, *J* = 1.9 Hz), 38.51, 36.15, 30.81, 30.58, 24.56, 21.66, 15.72. **HRMS** (ESI+) Calc: $[M+NH4]^+$ (C20H22N2O2S2) 404.1461, measured: 404.1460; 0.2 ppm difference.

Minor diastereomer: $\mathbf{R_f}$ = 0.20 (20% acetone/hexanes). **^{1}H NMR (**500 MHz, $CDCl_3$) δ 7.58 (d, *J* = 8.2 Hz, 2H), 7.28 (d, *J* = 8.2 Hz, 2H), 7.21 (dd, *J* = 5.2, 1.4 Hz, 1H), 6.99 (dd, *J* = 3.5, 1.4 Hz, 1H), 6.94 (dd, *J* = 5.2, 3.5 Hz, 1H), 3.72 (dtd, *J* = 11.7, 3.9, 1.9 Hz, 1H), 3.64 (dtd, *J* = 11.7, 3.9, 1.9 Hz, 1H), 2.41 (s, 3H), 2.16 (td, *J* = 11.7, 3.1 Hz, 1H), 1.99 (td, *J* = 11.8, 2.9 Hz, 1H), 1.81 (dd, *J* = 9.3, 5.6 Hz, 2H), 1.70 – 1.46

(m, 4H), 1.31 (dd, *J* = 7.5, 5.6 Hz, 1H), 0.58 (dtd, *J* = 15.1, 11.1, 4.0 Hz, 1H). **^{13}C NMR** (126 MHz, $CDCl_3$) δ 143.65, 135.73, 133.37, 129.78, 128.62, 127.49, 126.18, 122.22, 45.96, 45.70, 34.90, 34.44, 30.72, 30.45, 20.38, 14.12. **HRMS** (ESI+) Calc: $[M+H]^+$ ($C_{20}H_{22}N_2O_2S_2$) 387.1196, measured: 387.1194; 0.5 ppm difference.

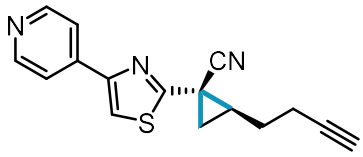

2-(But-3-yn-1-yl)-1-(4-(pyridin-4-yl)thiazol-2-yl)cyclopropane-1-carbonitrile (4.21). Following General Procedure A afforded an NMR yield of 61% (5:1 d.r.). Structural configuration assigned via analogy with compound **4.18**. **^{1}H NMR** (500 MHz, $CDCl_3$) δ 8.66 (d, *J* = 5.4 Hz, 2H), 7.71 (d, *J* = 6.1 Hz, 2H), 7.61 (s, 1H), 2.48 (tdd, *J* = 6.9, 2.6, 1.0 Hz, 2H), 2.37 – 2.25 (m, 1H), 2.22 (m, 1H), 2.11 – 1.99 (m, 2H), 1.99 – 1.89 (m, 0H), 1.82 – 1.68 (m, 1H). **HRMS** (ESI+) Calc: [M+H]+ ($C_{16}H_{14}ClN_3$) 280.0903, measured: 280.0902; 0.4 ppm difference.

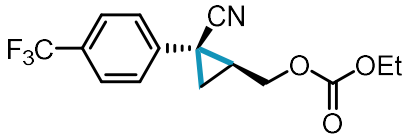

(2-Cyano-2-(4-(trifluoromethyl)phenyl)cyclopropyl)methyl ethyl carbonate (4.22). Following General Procedure A using 2.0 equiv. alkene and 29 mA for 2.25 h (3.0 F/mol) afforded one detectable diastereomer in 88.4 mg (70% yield, ≥20:1 d.r.) as an oil. **R_f** = 0.24 (20% acetone/hexanes). Structural configuration assigned via NOESY. **^{1}H NMR** (500 MHz, $CDCl_3$) δ 7.62 (d, J = 8.1 Hz, 2H), 7.42 (d, J = 8.1 Hz, 2H), 4.55 (dd, J = 12.0, 6.0 Hz, 1H), 4.29 (dd, J = 12.0, 8.4 Hz, 1H), 4.23 (q, J = 7.1 Hz, 2H), 2.10 – 2.01 (m, 1H), 1.77 – 1.70 (m, 2H), 1.32 (t, J = 7.2 Hz, 3H). **^{13}C NMR** (126 MHz, $CDCl_3$) δ 154.93, 139.33 (q, *J* = 1.5 Hz), 130.50 (q, *J* = 32.9 Hz), 126.40, 126.17 (q, *J* = 3.7 Hz), 123.87 (q, *J* = 272.2 Hz), 119.15, 67.40, 64.62, 28.45, 22.05, 19.82, 14.32. **^{19}F NMR** (377 MHz, $CDCl_3$) δ -62.73. **HRMS** (ESI+) Calc: $[M+Na]^+$ ($C_{15}H_{14}F_3NO_3Na$) 336.0818, measured: 336.0813; 1.5 ppm difference.

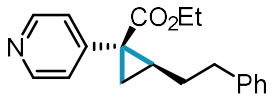

Ethyl 2-phenethyl-1-(pyridin-4-yl)cyclopropane-1-carboxylate (4.23). Following General Procedure A afforded 77.8 mg (66% yield, mixture of diastereomers, 3:1 d.r.) as an oil. **R_f** = 0.31 (20% acetone/hexanes). Structural configuration assigned via analogy with compound **4.29**. **^{1}H NMR** (500 MHz, $CDCl_3$) δ 8.54 – 8.51 (m, 2H), 7.37 – 7.13 (m, 7H), 4.16 (dddd, J = 17.9, 10.9, 7.1, 3.8 Hz, 2H), 2.81 – 2.73 (m, 2H), 2.05 – 1.93 (m, 2H), 1.67 (dd, J = 7.4, 4.7 Hz, 1H), 1.59 (dq, J = 9.1, 7.2 Hz, 1H), 1.29 (dd, J = 8.9, 4.7 Hz, 1H), 1.23 – 1.10 (m, 3H). Distinct minor diastereomer signals observed at δ 8.58 – 8.56 (m, 2H), 7.09 – 6.99 (m, 2H), 4.10 – 4.05 (m, 1H), 2.72 – 2.63 (m, 2H), 1.74 (dd, J = 9.0, 4.5 Hz, 1H), 1.13 (dd, *J* = 6.9, 4.5 Hz, 1H), 0.89 (dtd, J = 13.9, 9.0, 6.7 Hz, 1H). **^{13}C NMR** (126 MHz, $CDCl_3$) δ 171.09, 149.90, 149.65, 141.53, 128.55, 128.54, 126.14, 124.88, 61.42, 35.69, 34.05, 29.56, 29.12, 20.79, 14.31. Distinct minor diastereomer signals observed at δ 173.02, 149.56, 145.47, 141.43, 128.49, 128.46, 126.50, 126.10, 35.34, 33.39, 32.33, 28.42, 20.67, 14.19. **HRMS** (ESI+) Calc: $[M+H]^+$ ($C_{19}H_{22}NO_2$) 296.1645, measured: 296.1642; 1.0 ppm difference.

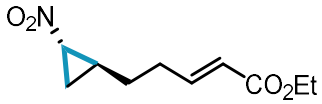

Ethyl (*E*)-5-(2-nitrocyclopropyl)pent-2-enoate (4.24). Following General Procedure B afforded one detectable diastereomer in 41.9 mg (49% yield) obtained as an oil and afforded an NMR yield of 55%. Structural configuration assigned via NOESY. **^{1}H NMR** (400 MHz, $CDCl_3$) δ 6.92 (dt, *J* = 15.6, 7.0 Hz, 1H), 5.85 (dt, *J* = 15.7, 1.6 Hz, 1H), 4.19 (q, *J* = 7.2 Hz, 2H), 4.10 – 4.03 (m, 1H), 2.35 (qd, *J* = 7.3, 1.6 Hz, 2H), 1.99 (dqd, *J* = 10.2, 7.3, 2.9 Hz, 1H), 1.86 (ddd, *J* = 10.2, 5.8, 3.5 Hz, 1H), 1.66 – 1.41 (m, 3H), 1.29 (t, *J* = 7.1 Hz, 3H), 1.08 (td, *J* = 7.3, 5.8 Hz, 1H). **^{13}C NMR** (126 MHz, $CDCl_3$) δ166.46, 146.77, 122.79, 60.56, 59.79, 31.22, 29.91, 25.60, 18.54, 14.44. **HRMS** (ESI+) Calc: [M+Na]+ (C10H15NO4) 236.0893, measured 236.0890; 1.3 ppm difference.

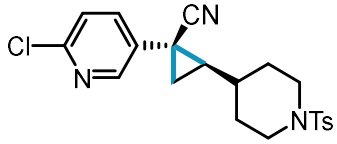

1-(6-chloropyridin-3-yl)-2-(1-tosylpiperidin-4-yl)cyclopropane-1-carbonitrile (4.25). Following scaleup setup and procedures afforded 3.3 g (72% yield, ≥20:1 d.r.) as solid. **R_f** = 0.32 (15% EtOAC/Hexanes). Structural configuration assigned via NOESY. **^{1}H NMR** (500 MHz, $CDCl_3$) δ 8.28 (d, J = 2.7 Hz, 1H), 7.63 (d, J = 8.3 Hz, 2H), 7.52 (dd, J = 8.4, 7.8 Hz, 1H), 3.92 – 3.79 (m, 2H), 2.44 (s, 3H), 2.25 (dtd, J = 15.0, 12.0, 2.8 Hz, 2H), 2.11-2.04 (m, 1H), 1.90-1.83 (m, 1H), 1.68-1.55 (m, 3H), 1.49 (dd, J = 7.4, 5.9 Hz, 1H), 1.35 (ddd, J = 10.1, 8.7, 7.4 Hz, 1H), 1.15 (ddt, J = 15.3, 11.4, 5.8 Hz, 1H). Distinct minor diastereomer signals observed at δ 8.26 (d, J = 2.8 Hz, 1H), 7.69 (dd, J = 8.3, 2.7 Hz, 1H), 7.55 (d, J = 8.2 Hz, 2H), 3.73 (d, J = 12.2 Hz, 1H), 3.59 (d, J = 12.0 Hz, 1H), 2.41 (s, 3H). **^{13}C NMR** (126 MHz, $CDCl_3$) δ 151.22, 147.43, 143.89, 136.66, 132.80, 131.17, 129.85, 127.83, 124.57, 119.56, 46.26, 46.21, 38.60, 35.23, 30.84, 30.60, 23.04, 21.65, 17.26. **HRMS** (ESI+) Calc: $[M+Na]^+$ (C21H22ClN3O2S) 438.1013, measured: 438.1011; 0.5 ppm difference.

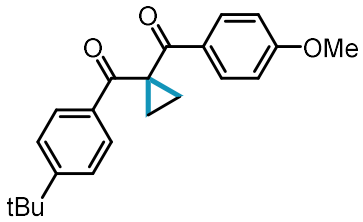

(1-(4-(*tert*-butyl)benzoyl)cyclopropyl)(4-methoxyphenyl)methanone (4.26). Following General Procedure D afforded 102.3 mg (76% yield) obtained as an oil. **R_f** = 0.27 (5% EtOAc/hexanes). **^{1}H NMR** (500 MHz, $CDCl_3$) δ 7.81 (d, J = 8.9 Hz, 2H), 7.76 (d, J = 8.6 Hz, 2H), 7.30 (d, J = 8.6 Hz, 2H), 6.76 (d, J = 8.9 Hz, 2H), 3.77 (s, 3H), 1.66 (s, 4H), 1.24 (s, 9H). **^{13}C NMR** (126 MHz, $CDCl_3$) δ 197.80, 196.42, 164.30, 157.65, 135.72, 132.13, 131.46, 129.74, 126.41, 114.66, 56.35, 41.44, 36.01, 31.94, 16.43. **HRMS** (ESI+) Calc: [M+H]+ (C22H24O3) 359.1618, measured: 359.1612; 1.7 ppm difference.

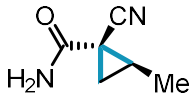

1-cyano-2-methylcyclopropane-1-carboxamide (4.27). Following General Procedure C afforded one detectable diastereomer in 36.8 mg (74% yield, ≥20:1 d.r.) obtained as an white solid. **R_f** = 0.25 (50% EtOAc/hexanes). Structural configuration assigned via x-ray crystallography. **^{1}H NMR** (500 MHz, $CDCl_3$) δ 6.42 (br s, 1H), 6.21 (br s, 1H), 1.95 (ddq, J = 8.8, 7.7, 6.2 Hz, 1H), 1.83 (dd, J = 8.8, 4.3 Hz, 1H), 1.36 (d, J = 6.2 Hz, 3H), 1.25 (dd, J = 7.8, 4.4 Hz, 1H). **^{13}C NMR** (126 MHz, $CDCl_3$) δ 168.17, 119.00, 25.62,

25.27, 20.31, 15.22. **HRMS** (ESI+) Calc: [M+H]+ (C6H8N2O) 147.0529, measured: 147.0527; 1.4 ppm difference.

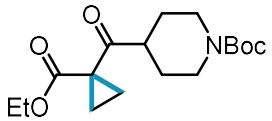

***tert*-Butyl 4-(1-(ethoxycarbonyl)cyclopropane-1-carbonyl)piperidine-1-carboxylate (4.28)**. Following General Procedure D afforded 123.3 mg (95% yield) obtained as an oil. $\mathbf{R_f}$ = 0.29 (10% EtOAc/hexanes). **^{1}H NMR** (500 MHz, $CDCl_3$) δ 4.17 (q, J = 7.2Hz, 2H), 4.04 (br s, 2H), 3.29 (tt, J = 11.3, 3.6Hz, 1H), 2.75 (t, J = 12.7Hz, 2H), 1.80 (d, J = 13.2Hz, 2H), 1.48 (dtd, J = 13.4, 11.8, 4.3Hz, 1H), 1.40 (s, 9H), 1.24 (t, J = 7.1Hz, 3H). **^{13}C NMR** (126 MHz, $CDCl_3$) δ 206.71, 171.00, 154.62, 79.46, 61.26, 47.12, 33.76, 28.37, 18.18, 14.07. **HRMS** (ESI+) Calc: [M+H]+ (C17H27NO2) 326.1962, measured: 326.1955; 2.1 ppm difference.

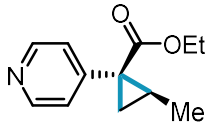

Ethyl 2-methyl-1-(pyridin-4-yl)cyclopropane-1-carboxylate (4.29). Following General Procedure C afforded 70.76 mg (67.7% yield, mixture of diastereomers, 4:1 d.r.) as an oil. $\mathbf{R_f}$ = 0.21 (70% Et_2O/hexanes). Structural configuration assigned via NOESY. **^{1}H NMR** (500 MHz, $CDCl_3$) δ 8.51 (m, 2H), 7.21 (m, 2H), 4.14 (m, 2H), 1.60 (m, 2H), 1.30 (d, J = 5.8 Hz, 2H), 1.26 (m, 1H), 1.19 (t, J = 7.1 Hz, 3H). Distinct minor diastereomer signals observed at δ 8.56 (m, 2H), 7.18 (m, 2H), 4.06 (m, 2H), 1.93 (m, 1H), 1.75 (dd, J = 9.0, 4.4 Hz, 1H), 1.15 (t, J = 7.1 Hz, 3H), 1.08 (dd, J = 6.8, 4.4 Hz, 1H), 0.80 (d, J = 6.3 Hz, 3H). **^{13}C NMR** (126 MHz, $CDCl_3$) δ 171.04, 150.05, 149.79, 124.61, 61.32, 34.32, 23.57, 14.38, 13.12. Distinct minor diastereomer signals observed at δ 173.29, 149.65, 145.48, 126.71, 61.37, 33.36, 23.13, 22.00, 15.32, 14.23. **HRMS** (ESI+) Calc: $[M+H]^+$ (C12H15NO2) 206.1176, measured: 206.1176; <0.1ppm ppm difference.

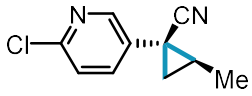

1-(6-chloropyridin-3-yl)-2-methylcyclopropane-1-carbonitrile (4.30). Following General Procedure C afforded one detectable diastereomer in 73.3 mg (95% yield, ≥20:1 d.r.) obtained as an oil. $\mathbf{R_f}$ = 0.25 (10% acetone/hexanes). Structural configuration assigned via analogy with compound **25**. **^{1}H NMR** (500 MHz, $CDCl_3$) δ 8.39-8.36 (m, 1H), 7.65 (dd, J = 7.6, 2.2Hz, 1H), 7.27-7.23 (m, 1H) 1.59-1.48 (m, 5H), 1.48-1.43 (m, 1H). **^{13}C NMR** (126 MHz, $CDCl_3$) δ 153.40, 149.54, 139.68, 131.34, 122.66, 119.20, 23.13, 23.09, 19.12, 15.62. **HRMS** (ESI+) Calc: [M+H]+ (C10H9ClN2) 193.0527, measured: 193.0527; <0.1 ppm difference.

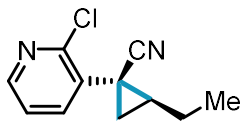

1-(2-chloropyridin-3-yl)-2-ethylcyclopropane-1-carbonitrile (4.31). Following General Procedure C afforded one detectable diastereomer in 82.1 mg (99% yield, ≥20:1 d.r.) obtained as an oil. $\mathbf{R_f}$ = 0.23 (15% acetone/hexanes). Structural configuration assigned via analogy with compound **25**. **^{1}H NMR** (500 MHz, $CDCl_3$) δ 8.31 (dd, J = 4.8, 1.9Hz, 1H), 7.62 (dd, J = 7.6, 1.9Hz, 1H), 7.21 (dd, J = 7.6, 4.7Hz, 1H), 1.84 (dq, J = 14.4, 7.2Hz, 1H), 1.66 (tt, J = 14.2, 7.3Hz, 1H), 1.52-1.39 (m, 3H), 1.16 (t, J = 7.4Hz, 3H). **^{13}C**

NMR (126 MHz, $CDCl_3$) δ 152.99, 149.49, 139.93, 131.24, 122.78, 119.35, 29.90, 24.41, 22.34, 18.71, 13.03. **HRMS** (ESI+) Calc: [M+H]+ (C9H7ClN2) 207.0684, measured: 207.0681; 1.4 ppm difference.

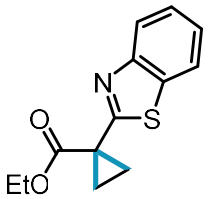

***tert*-butyl 4-(1-(ethoxycarbonyl)cyclopropane-1-carbonyl)piperidine-1-carboxylate (4.32)**. Following General Procedure C afforded 67.1 mg (68% yield) obtained as an oil. $\mathbf{R_f}$ = 0.39 (5% acetone/hexanes). **^{1}H NMR** (500 MHz, $CDCl_3$) δ 7.90 (dt, J = 8.1, 0.9Hz, 1H), 7.86 (dt, J = 7.9, 1.0Hz, 1H), 7.43 (ddd, J = 8.3, 7.2, 1.3Hz, 1H), 7.34 (ddd, J = 8.2, 7.2, 1.2Hz, 1H), 4.27 (q, J = 7.1Hz, 2H), 1.94 (m, 4H), 1.31 (t, J = 7.1Hz, 3H). **^{13}C NMR** (126 MHz, $CDCl_3$) δ 171.86, 168.75, 151.86, 135.94, 125.72, 124.52, 122.44, 121.21, 61.57, 27.89, 22.76, 14.14. **HRMS** (ESI+) Calc: [M+H]+ (C13H13NO2S) 248.0740, measured: 248.0734; 2.4 ppm difference.

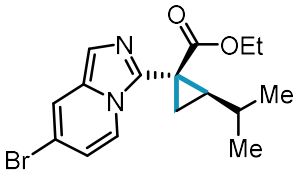

Ethyl 1-(7-bromoimidazo[1,5-a]pyridin-3-yl)-2-isopropylcyclopropane-1-carboxylate (4.33). Following General Procedure C afforded one detectable diastereomer in 70.76 mg (50% yield, ≥20:1 d.r.) obtained as a solid. $\mathbf{R_f}$ = 0.28 (20% EtOAc/hexanes). Structural configuration assigned via analogy with compound **4.18**. **^{1}H NMR** (500 MHz, $CDCl_3$) δ 8.23 (dd, J = 2.0, 0.9 Hz, 1H), 7.74 (d, J = 7.7, 0.7 Hz, 1H), 7.42 (dt, J = 9.5, 0.9 Hz, 1H), 7.17 (dd, J = 9.5, 1.9 Hz, 1H), 4.15 (m, 2H), 1.81 (dd, J = 7.5, 4.1 Hz, 1H), 1.75 (dd, J = 9.1, 4.1 Hz, 1H), 1.67 (td, J = 9.3, 7.5, 1H), 1.23 (t, J = 7.1 Hz, 3H), 0.97 (t, J = 6.3 Hz, 3H), 0.91 (m, 1H), 0.80 (d, J = 6.3 Hz, 3H). **^{13}C NMR** (126 MHz, $CDCl_3$) δ 173.59, 143.13, 142.22, 127.35, 125.43, 118.05, 113.64, 106.79, 61.10, 39.50, 29.18, 28.01, 22.47, 21.78, 20.41, 14.36. **HRMS** (ESI+) Calc: [M+H]+ (C16H19BrN2O2) 351.0703, measured: 351.0699; 1.1 ppm difference.

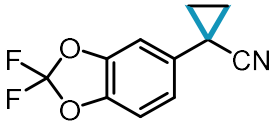

1-(2,2-difluorobenzo[d][1,3]dioxol-5-yl)cyclopropane-1-carbonitrile (4.34). Following General Procedure D afforded 82.9 mg (87% yield) obtained as an white solid. $\mathbf{R_f}$ = 0.25 (40% Et_2O/hexanes). **^{1}H NMR** (500 MHz, $CDCl_3$) δ 7.08 (dd, J = 8.4, 1.9 Hz, 1H), 7.03 (m, 2H), 1.73 (m, 2H), 1.37 (m, 2H). **^{13}C NMR** (126 MHz, $CDCl_3$) δ145.18, 144.28, 133.31, 132.66 (t, J = 256.4Hz), 123.03, 110.67, 108.98, 18.86, 14.81. **^{19}F NMR** (376 MHz, $CDCl_3$) δ -49.90. **HRMS** (ESI+) Calc: [M+H]+ (C11H7F2NO2) 224.0518, measured: 225.0515; 1.3 ppm difference.

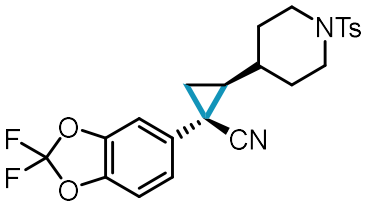

1-(2,2-Difluorobenzo[d][1,3]dioxol-5-yl)-2-(1-tosylpiperidin-4-yl)cyclopropane-1-carbonitrile (4.35). Following General Procedure B afforded one detectable diastereomer in 138.2 mg (74% yield, ≥20:1 d.r.)

as a solid. $\mathbf{R_f}$ = 0.34 (20% acetone/hexanes). Structural configuration assigned via NOESY. **^{1}H NMR** (500 MHz, $CDCl_3$) δ 7.64 (d, *J* = 8.4 Hz, 2H), 7.36 – 7.31 (m, 2H), 7.05 – 6.97 (m, 2H), 6.96 (d, *J* = 1.7 Hz, 1H), 3.86 (dddt, *J* = 9.3, 6.6, 4.1, 2.4 Hz, 2H), 2.44 (s, 3H), 2.25 (dtd, *J* = 20.3, 12.1, 2.7 Hz, 2H), 2.10 (ddd, *J* = 13.0, 3.7, 2.1 Hz, 1H), 1.86 (ddd, *J* = 13.1, 3.8, 2.2 Hz, 1H), 1.68 – 1.57 (m, 2H), 1.55 (dd, *J* = 5.6, 3.1 Hz, 1H), 1.40 (dd, *J* = 7.2, 5.7 Hz, 1H), 1.29 (ddd, *J* = 10.2, 8.7, 7.3 Hz, 1H), 1.12 (tdt, *J* = 11.6, 9.9, 3.7 Hz, 1H). **^{13}C NMR** (126 MHz, $CDCl_3$) δ 144.38, 143.87, 143.51, 133.86, 132.82, 132.36, 131.82, 129.85, 129.77, 127.86, 122.14, 120.50, 109.93, 108.19, 46.33, 46.29, 38.57, 34.96, 30.93, 30.66, 22.80, 21.66, 19.70. **^{19}F NMR** (377 MHz, $CDCl_3$) δ -49.83. **HRMS** (ESI+) Calc: [M+H]+ ($C_{23}H_{22}F_2N_2O_4S$) 461.1341, measured: 461.1335; 1.3 ppm difference.

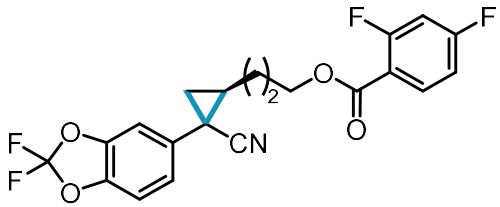

3-(2-cyano-2-(2,2-difluorobenzo[d][1,3]dioxol-5-yl)cyclopropyl)propyl 2,4-difluorobenzoate (4.36). Following General Procedure B afforded one detectable diastereomer in 110.9 mg (66% yield, ≥20:1 d.r.) as a solid. $\mathbf{R_f}$ = 0.43 (20% acetone/hexanes). Structural configuration assigned via analogy with compound **4.35**. **^{1}H NMR** (500 MHz, $CDCl_3$) δ 7.98 (td, J = 8.6, 6.5 Hz, 1H), 7.07 – 6.98 (m, 3H), 6.93 (dddd, J = 8.8, 7.6, 2.4, 1.0 Hz, 1H), 6.86 (ddd, J = 11.1, 8.8, 2.5 Hz, 1H), 4.43 (td, J = 6.2, 1.0 Hz, 2H), 2.08 (dtd, J = 14.0, 6.4, 2.3 Hz, 1H), 2.05 – 1.98 (m, 1H), 1.96 – 1.84 (m, 2H), 1.62 – 1.54 (m, 2H), 1.52 – 1.45 (m, 1H). **^{13}C NMR** (126 MHz, $CDCl_3$) δ 165.92 (dd, J = 256.6, 12.0 Hz), 163.71 (d, J = 4.2 Hz), 162.98 (dd, J = 263.2, 12.5 Hz), 144.35 (t, J = 1.1 Hz), 143.33 (t, J = 1.1 Hz), 134.11 (dd, J = 10.5, 2.3 Hz), 132.85, 131.81 (t, J = 256.4 Hz), 121.88, 120.43, 115.24 (dd, J = 9.9, 3.7 Hz), 111.81 (dd, J = 21.5, 3.8 Hz), 109.81, 107.87, 105.40 (dd, J = 26.2, 25.7 Hz), 64.68, 30.04, 28.16, 27.90, 24.08, 20.18. **^{19}F NMR** (377 MHz, $CDCl_3$) δ 49.89, -101.67 (d, J = 12.7 Hz), -103.75 (d, J = 12.5 Hz). **HRMS** (ESI+) Calc: $[M+NH_4]^+$ ($C_{21}H_{19}F_4N_2O_4$) 439.1276, measured: 439.1270; 1.4 ppm difference.

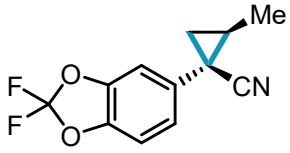

1-(2,2-difluorobenzo[d][1,3]dioxol-5-yl)-2-methylcyclopropane-1-carbonitrile (4.37). Following General Procedure C afforded 72.0 mg (74% yield, ≥20:1 d.r.) obtained as an oil. Structural configuration assigned via analogy with compound **4.35**. $\mathbf{R_f}$ = 0.25 (40% Et_2O/hexanes). **^{1}H NMR** (500 MHz, $CDCl_3$) δ 7.05 (dd, J = 8.4, 1.8Hz, 1H), 7.02 (d, J = 7.0Hz, 1H), 6.99 (d, J = 1.9Hz, 1H), 1.59-1.52 (m, 2H), 1.48 (d, J = 5.6Hz, 3H), 1.43-1.37 (m, J = 1H). **^{13}C NMR** (126 MHz, $CDCl_3$) δ144.17, 143.07, 133.05, 131.66 (t, J = 256.3Hz), 121.59, 120.40, 109.59, 107.65, 25.08, 25.00, 20.43, 15.92. **^{19}F NMR** (376 MHz, $CDCl_3$) δ -49.95. **HRMS** (ESI+) Calc: $[M+H]^+$ ($C_{12}H_9F_2NO_2$) 238.0674, measured: 238.0670; 1.7 ppm difference.

C.7 Scale-Up Batch Electrolysis Setup and Procedures

Figure C4. Left: Large scale divided cell batch assembly prior to addition of solvent. **Right:** Large scale divided cell batch assembly 5 minutes into electrolysis.

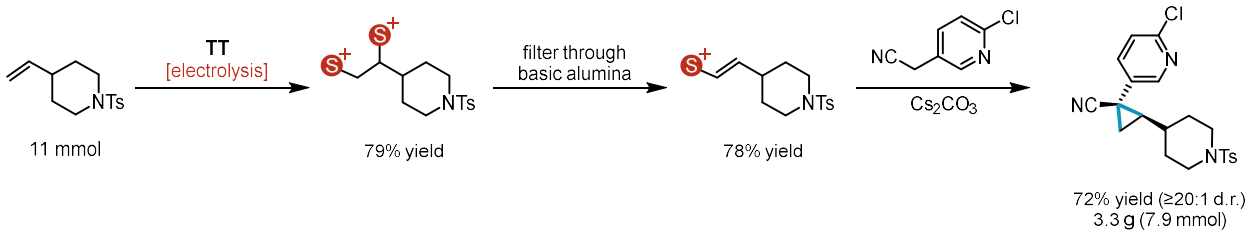

Scheme C4. Scale-up reaction for cyclopropanation via dication pool.

Procedure (11 mmol scale) - To an oven-dried large scale divided electrochemical cell equipped with magnetic stir bars was added thianthrene (3.57 g, 16.5 mmol, 1.5 equiv.), 1-tosyl-4-vinylpiperidine (2.92 g, 11 mmol, 1 equiv.), and *n*-Bu_4NPF_6 (17.0 g, 44.0 mmol, 4.0 equiv.) to the anode compartment and *n*-Bu_4NPF_6 (8.50 g, 22 mmol, 2.0 equiv.) to the cathode compartment. The cell was equipped with two septa containing a large scale stainless steel wire/Ni foam cathode assembly (electrode dimensions: 8x4.5 cm, rolled into a tube) and a pencil/RVC anode assembly (electrode dimensions: 8.5x1x1 cm) connected together with a teflon tubing to equalize pressure. MeCN (46 mL) and TFA (8.5 mL, 110 mmol, 10 equiv.) was added to the cathode compartment at the same time that MeCN (110 mL) was added to the anode compartment as to equalize solvent level in both compartments. The cathode septa was pierced with an outlet needle to avoid pressurization from hydrogen evolution. Both sides of the cell were then stirred at 30 °C and electrolyzed under a constant current of 175 mA for 5.1 h (3.0 F/mol). At completion of electrolysis, the electrode leads were disconnected, septa removed, and the anode RVC was pushed off the pencil into the reaction mixture. Dibromomethane was added as an internal standard and an NMR aliquot was taken to assess adduct formation. To the anode compartment was added a septum pierced with a needle to prevent pressurizing. After pressure equilibration, the needle was removed, and the cathode solution was removed from the cell via pipette. The anode solution was filtered through activated basic alumina (110 g, Brockmann I). The cathode compartment was washed with MeCN (40 mL) and pushed across the frit to rinse the frit. The anode compartment was further washed with MeCN (5 x 40 mL). The alumina pad was washed with MeCN (3 x 320 mL), taking care to fully disperse the alumina in solution using a spatula. The filtrate was concentrated under reduced pressure until ~50mL MeCN

remains. Mesitylene was added as an internal standard and an NMR aliquot was taken to assess vinyl-TT+ yield. Then a stir bar was added to the flask, followed by 2-chloro-5-(cyanomethyl)pyridine (1.68 g, 11.0 mmol, 1 equiv.) then Cs_2CO_3 (8.96 g, 27.5 mmol, 2.5 equiv.). The solution was stirred for 16 h. At completion, the mixture was diluted with DCM (200 mL) and water (600 mL). The aqueous layer was extracted with DCM (200 mL x 3). The combined organic layers were dried with anhydrous Na_2SO_4, filtered, and concentrated under reduced pressure. The residue was purified via flash column chromatography to yield the pure cyclopropane product.

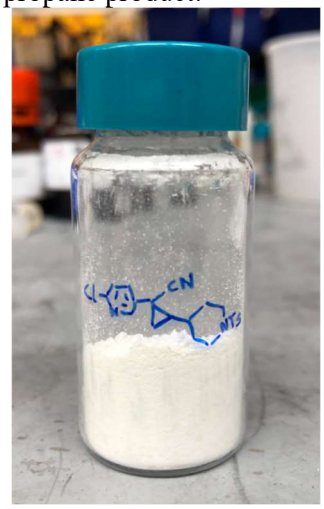

Figure C5. Gram-scale synthesis of cyclopropane via dication pool.

C.8 X-Ray Diffraction Data

Data Collection (4.18)

A colorless crystal with approximate dimensions 0.18 × 0.18 × 0.15 mm^3 was selected under oil under ambient conditions and attached to the tip of a MiTeGen MicroMount©. The crystal was mounted in a stream of cold nitrogen at 100(1) K and centered in the X-ray beam by using a video camera.

The crystal evaluation and data collection were performed on a Bruker D8 VENTURE PhotonIII four-circle diffractometer with Cu Kα (λ = 1.54178 Å) radiation and the detector to crystal distance of 4.5 cm.[9]

The initial cell constants were obtained from a 180° φ scan conducted at a 2θ = 50° angle with an exposure time of 1 second per frame. The reflections were successfully indexed by an automated indexing routine built into the APEX3 program. The final cell constants were calculated from a set of 9394 strong reflections from the actual data collection.

The data were collected by using a full sphere data collection routine to survey reciprocal space to the extent of a full sphere to a resolution of 0.78 Å. A total of 24922 data were harvested by collecting 22 sets of frames with 1.0º scans in ω and φ with exposure times of 0.75–4 sec per frame. These highly redundant datasets were corrected for Lorentz and polarization effects. The absorption correction was based on fitting a function to the empirical transmission surface as sampled by multiple equivalent measurements.[10]

Structure Solution and Refinement (4.18)

The systematic absences in the diffraction data were uniquely consistent for the space group $P2_1/c$ that yielded chemically reasonable and computationally stable results of refinement.[11–16]

A successful solution by intrinsic phasing provided most non-hydrogen atoms from the *E*-map. The remaining non-hydrogen atoms were located with an alternating series of least-squares cycles and difference Fourier maps. The atomic structure factors were determined by DFT calculations, using the B3LYP hybrid functional and the 6-31G(d) basis set, in the NoSpherA2 extension of the olex2.refine program.[17–19] All atoms were refined with anisotropic displacement coefficients.

In the stereoisomer shown in Figure 1 both chiral centers (C7 and C10) are *R*. The *S,S*-stereoisomer is also present in the crystal structure. The *R,R* molecule was chosen arbitrarily.

The final least squares refinement of 325 parameters against 3021 data resulted in residuals *R* (based on F^2 for $I \geq 2\sigma$) and *wR* (based on F^2 for all data) of 0.0216 and 0.0478, respectively. The final difference Fourier map was featureless.

Data Collection (4.14)

A colorless crystal with approximate dimensions 0.168 × 0.08 × 0.076 mm^3 was selected under oil under ambient conditions and attached to the tip of a MiTeGen MicroMount©. The crystal was mounted in a stream of cold nitrogen at 100(1) K and centered in the X-ray beam by using a video camera.

The crystal evaluation and data collection were performed on a Bruker D8 VENTURE PhotonIII four-circle diffractometer with Cu Kα (λ = 1.54178 Å) radiation and the detector to crystal distance of 4.5 cm.[9]

The initial cell constants were obtained from a 180° φ scan conducted at a 2θ = 50° angle with the exposure time of 1 second per frame. The reflections were successfully indexed by an automated indexing routine built in the APEX3 program. The final cell constants were calculated from a set of 9365 strong reflections from the actual data collection.

The data were collected by using the full sphere data collection routine to survey the reciprocal space to the extent of a full sphere to a resolution of 0.80 Å. A total of 128377 data were harvested by collecting 34 sets of frames with 0.9º scans in ω and φ with an exposure time 1–6 sec per frame. These highly redundant datasets were corrected for Lorentz and polarization effects. The absorption correction was based on fitting a function to the empirical transmission surface as sampled by multiple equivalent measurements.[10]

Structure Solution and Refinement (4.14)

The systematic absences in the diffraction data were uniquely consistent for the space group $P2_1/n$ that yielded chemically reasonable and computationally stable results of refinement.[11–16]

A successful solution by intrinsic phasing provided most non-hydrogen atoms from the *E*-map. The remaining non-hydrogen atoms were located in an alternating series of least-squares cycles and difference Fourier maps. All non-hydrogen atoms were refined with anisotropic displacement coefficients. All hydrogen atoms were included in the structure factor calculation at idealized positions and were allowed to ride on the neighboring atoms with relative isotropic displacement coefficients.

The compound crystallizes as a racemate. The enantiomer shown in Figure 1 (C8 – *S*, C12 – *S*) was chosen arbitrarily.

There are two symmetry-independent molecules with identical compositions, handedness, and very similar conformations in the asymmetric unit.

The final least-squares refinement of 525 parameters against 8466 data resulted in residuals *R* (based on F^2 for $I \geq 2\sigma$) and *wR* (based on F^2 for all data) of 0.0371 and 0.0990, respectively. The final difference Fourier map was featureless.

Data Collection (4.27)

A colorless crystal with approximate dimensions 0.09 x 0.07 x 0.06 mm^3 was selected under oil under ambient conditions and attached to the tip of a MiTeGen MicroMount©. The crystal was mounted in a stream of cold nitrogen at 100(1) K and centered in the X-ray beam by using a video camera.

The crystal evaluation and data collection were performed on a Bruker D8 VENTURE PhotonIII four-circle diffractometer with Cu Kα (λ = 1.54178 Å) radiation and the detector to crystal distance of 4.5 cm.[9]

The initial cell constants were obtained from a 180° φ scan conducted at a 2θ = 50° angle with an exposure time of 1 second per frame. The reflections were successfully indexed by an automated indexing routine built into the APEX3 program. The final cell constants were calculated from a set of 9522 strong reflections from the actual data collection.

The data were collected by using a full sphere data collection routine to survey reciprocal space to the extent of a full sphere to a resolution of 0.80 Å. A total of 11798 data were harvested by collecting 20 sets of frames with 0.9º scans in ω and φ with exposure times of 10-30 sec per frame. These highly redundant datasets were corrected for Lorentz and polarization effects. The absorption correction was based on fitting a function to the empirical transmission surface as sampled by multiple equivalent measurements[10]

Structure Solution and Refinement (4.27)

The systematic absences in the diffraction data were uniquely consistent for the space group $P2_1/n$ that yielded chemically reasonable and computationally stable results of refinement.[11–16]

A successful solution by intrinsic phasing provided most non-hydrogen atoms from the *E*-map. The remaining non-hydrogen atoms were located with an alternating series of least-squares cycles and difference Fourier maps. All atoms were refined with anisotropic displacement coefficients. The atomic form factors were computed with NoSpherA2[17] at the B3LYP/def2-SVP level of theory.

This compound crystallizes as a racemate. The molecule shown in the first diagram was chosen arbitrarily, with chiral atoms C2 and C4 in the *S*,*S* conformation. However, the *R*,*R* enantiomer is also present in the structure.

The final least-squares refinement of 154 parameters against 1309 data resulted in residuals *R* (based on F^2 for $I \geq 2\sigma$) and *wR* (based on F^2 for all data) of 0.0157 and 0.0393, respectively. The final difference Fourier map was featureless.

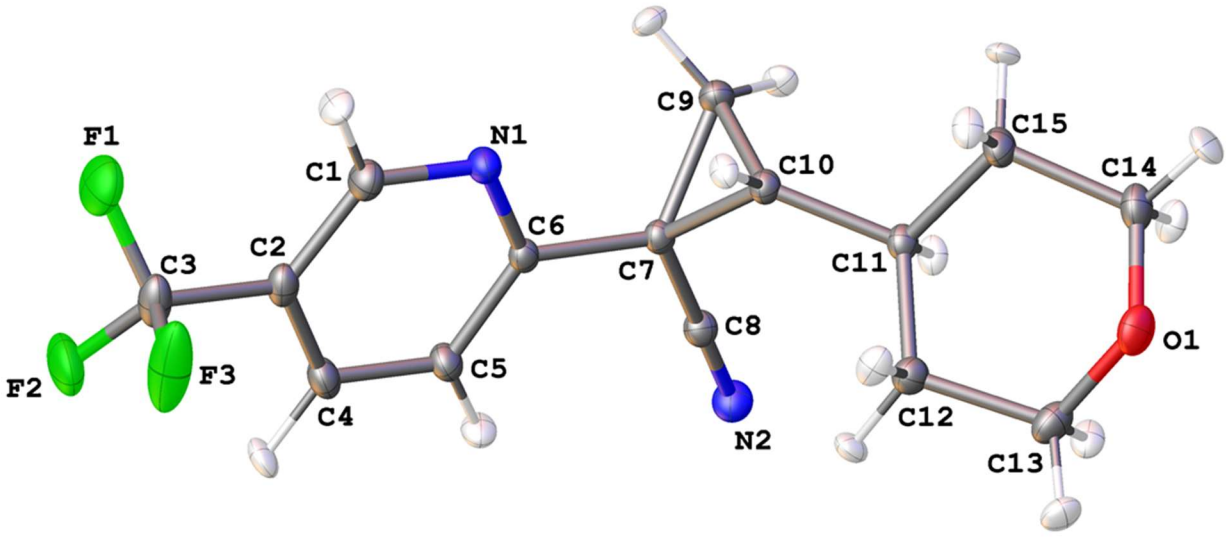

Figure C6. A molecular drawing of the asymmetric unit in compound **4.18** shown with 50% probability ellipsoids.

Table C7 Crystal data and structure refinement for (4.18)

Identification code	wickens06
Empirical formula	$C_{15}H_{15}F_3N_2O$
Formula weight	296.294
Temperature/K	100.00
Crystal system	monoclinic
Space group	$P2_1/c$
a/Å	6.1884(5)
b/Å	9.2955(10)
c/Å	24.5282(19)
α/°	90
β/°	91.250(5)
γ/°	90
Volume/Å^3	1410.6(2)
Z	4
ρ_{calc}g/cm^3	1.395
μ/mm^{-1}	0.993
F(000)	618.5
Crystal size/mm^3	0.18 × 0.18 × 0.15
Radiation	Cu Kα (λ = 1.54178)
2Θ range for data collection/°	7.2 to 158.26
Index ranges	$-7 \leq h \leq 7$, $-11 \leq k \leq 11$, $-31 \leq l \leq 27$
Reflections collected	24922
Independent reflections	3021 [R_{int} = 0.0236, R_{sigma} = 0.0151]
Data/restraints/parameters	3021/0/325
Goodness-of-fit on F^2	1.101
Final R indexes [I>=2σ (I)]	R_1 = 0.0216, wR_2 = 0.0475
Final R indexes [all data]	R_1 = 0.0221, wR_2 = 0.0478
Largest diff. peak/hole / e Å^{-3}	0.36/-0.26

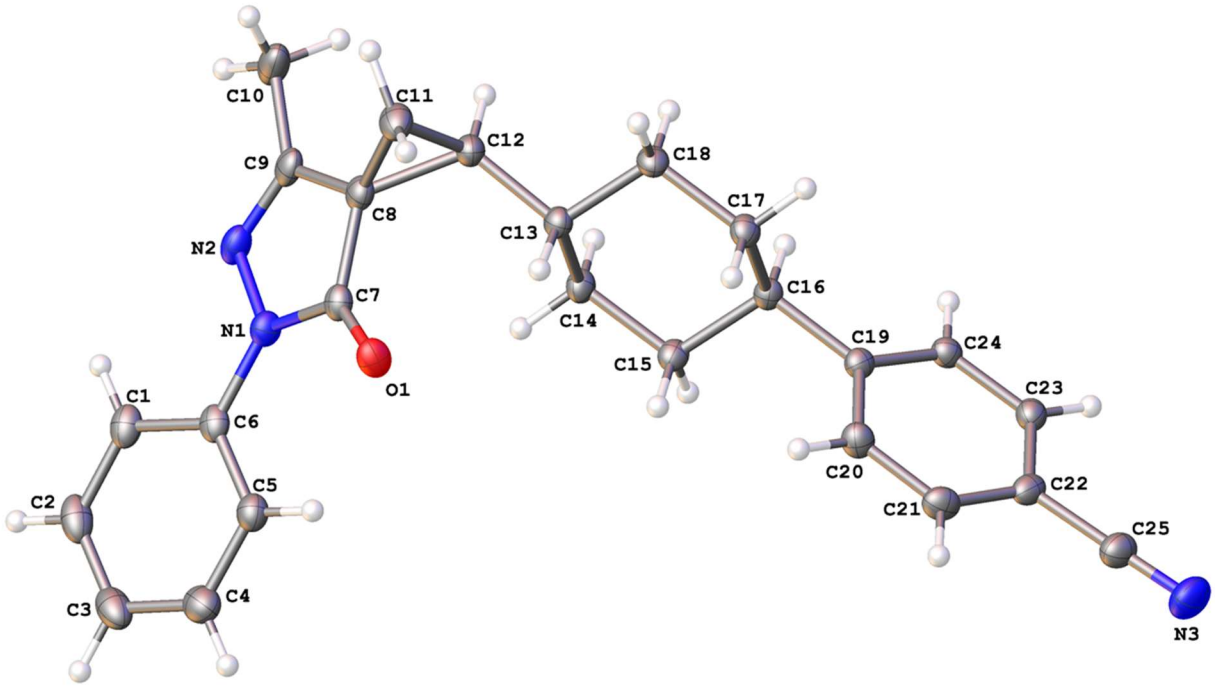

Figure C7. A molecular drawing of the first symmetry-independent molecules of compound **4.14** shown with 50% probability ellipsoids.

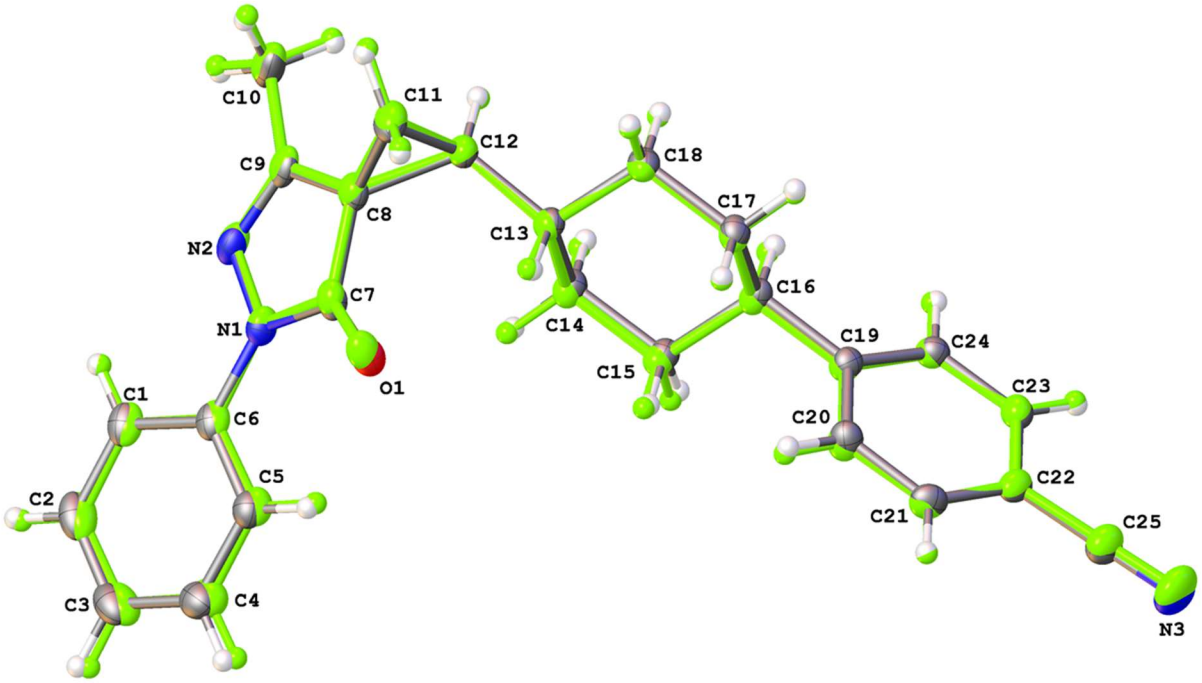

Figure C8. A superposition of the two symmetry-independent molecules of compound **4.14** shown with 50% probability ellipsoids. The second molecule is green.

Table C8 Crystal data and structure refinement for (4.14).

Identification code	Wickens07
Empirical formula	$C_{25}H_{25}N_3O$
Formula weight	383.48
Temperature/K	100.00
Crystal system	monoclinic
Space group	$P2_1/n$
a/Å	15.3630(10)
b/Å	10.4765(6)
c/Å	26.2845(17)
α/°	90
β/°	99.916(5)
γ/°	90
Volume/Å^3	4167.3(5)
Z	8
ρ_{calc}g/cm^3	1.222
μ/mm^{-1}	0.593
F(000)	1632.0
Crystal size/mm^3	0.168 × 0.08 × 0.076
Radiation	Cu Kα (λ = 1.54178)
2Θ range for data collection/°	6.236 to 149.198
Index ranges	$-19 \leq h \leq 19$, $-13 \leq k \leq 12$, $-32 \leq l \leq 32$
Reflections collected	128377
Independent reflections	8466 [R_{int} = 0.0331, R_{sigma} = 0.0126]
Data/restraints/parameters	8466/0/525
Goodness-of-fit on F^2	1.086
Final R indexes [I>=2σ (I)]	R_1 = 0.0371, wR_2 = 0.0974
Final R indexes [all data]	R_1 = 0.0393, wR_2 = 0.0990
Largest diff. peak/hole / e Å^{-3}	0.28/-0.21

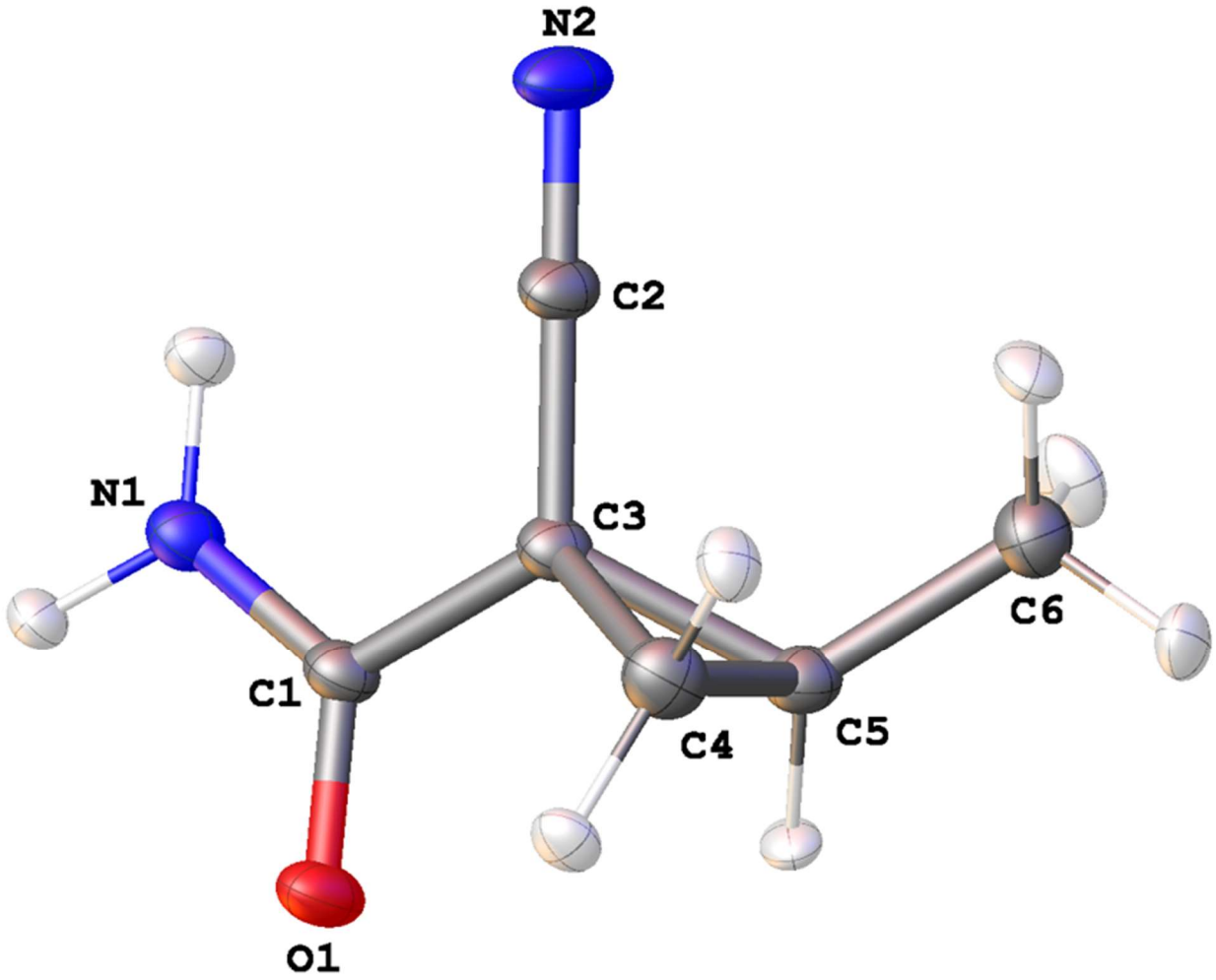

Figure C9. A molecular drawing of the molecule in compound **4.27** shown with 50% probability ellipsoids. The molecule shown was chosen arbitrarily, with chiral atoms C2 and C4 in the S,S conformation. However, this compound crystallizes as a racemate, thus the R,R enantiomer is also present.

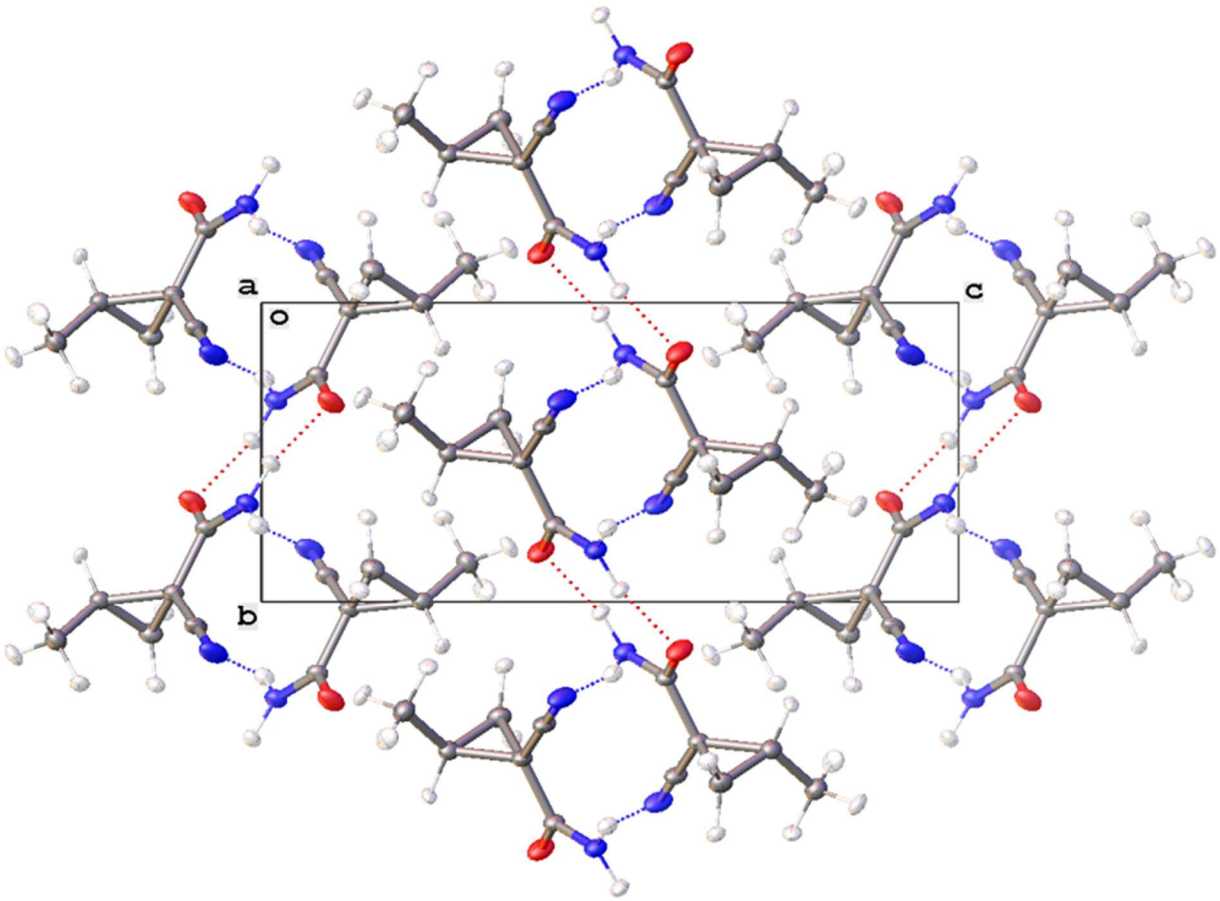

Figure C10. A packing diagram of compound **4.27** shown along the a axis with 50% probability ellipsoids.

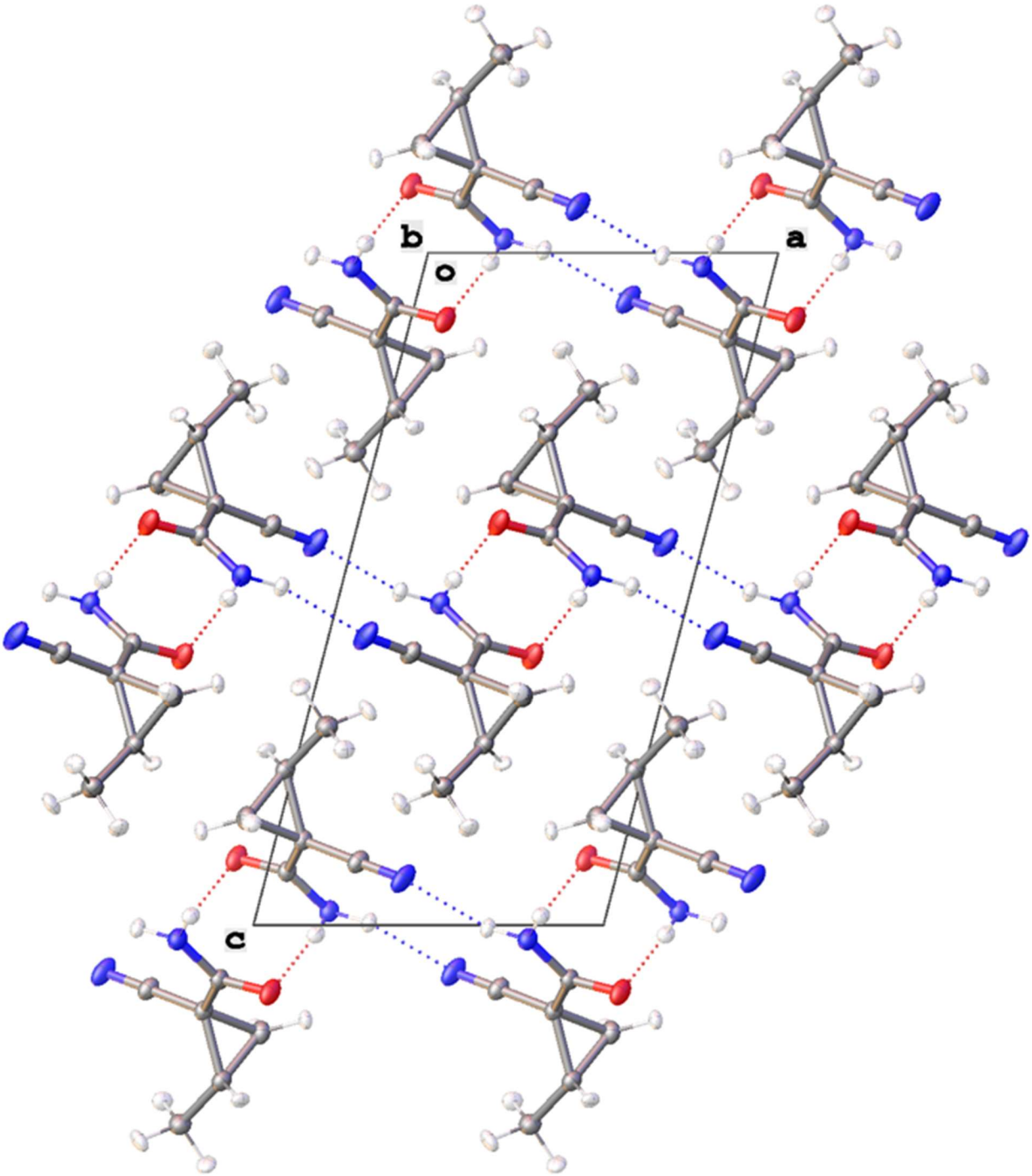

Figure C11. A packing diagram of compound **4.27** shown along the b axis with 50% probability ellipsoids.

Table C9 Crystal data and structure refinement for compound 4.27.

Identification code	wickens08
Empirical formula	$C_6H_8N_2O$
Formula weight	124.143
Temperature/K	100.00
Crystal system	monoclinic
Space group	$P2_1/n$
a/Å	7.4137(7)
b/Å	6.1089(6)
c/Å	14.7286(14)
α/°	90
β/°	104.550(4)
γ/°	90
Volume/Å^3	645.66(11)
Z	4
ρ_{calc}g/cm^3	1.277
μ/mm^{-1}	0.740
F(000)	264.9
Crystal size/mm^3	0.09 × 0.07 × 0.06
Radiation	Cu Kα (λ = 1.54178)
2Θ range for data collection/°	12.34 to 149.06
Index ranges	$-9 \leq h \leq 9$, $-7 \leq k \leq 7$, $-18 \leq l \leq 18$
Reflections collected	11382
Independent reflections	1309 [R_{int} = 0.0259, R_{sigma} = 0.0180]
Data/restraints/parameters	1309/0/154
Goodness-of-fit on F^2	1.296
Final R indexes [I>=2σ (I)]	R_1 = 0.0157, wR_2 = 0.0389
Final R indexes [all data]	R_1 = 0.0165, wR_2 = 0.0393
Largest diff. peak/hole / e Å^{-3}	0.11/-0.08

C.9 References

(1) Macrae, C. F.; Edgington, P. R.; McCabe, P.; Pidcock, E.; Shields, G. P.; Taylor, R.; Towler, M.; Streek, J. van de. Mercury: Visualization and Analysis of Crystal Structures. *J Appl Cryst* **2006**, *39* (3), 453–457. https://doi.org/10.1107/S002188980600731X.

(2) Peretto, I.; Radaelli, S.; Parini, C.; Zandi, M.; Raveglia, L. F.; Dondio, G.; Fontanella, L.; Misiano, P.; Bigogno, C.; Rizzi, A.; Riccardi, B.; Biscaioli, M.; Marchetti, S.; Puccini, P.; Catinella, S.; Rondelli, I.; Cenacchi, V.; Bolzoni, P. T.; Caruso, P.; Villetti, G.; Facchinetti, F.; Del Giudice, E.; Moretto, N.; Imbimbo, B. P. Synthesis and Biological Activity of Flurbiprofen Analogues as Selective Inhibitors of β-Amyloid1-42 Secretion. *J. Med. Chem.* **2005**, *48* (18), 5705–5720. https://doi.org/10.1021/jm0502541.

(3) Okaniwa, M.; Hirose, M.; Imada, T.; Ohashi, T.; Hayashi, Y.; Miyazaki, T.; Arita, T.; Yabuki, M.; Kakoi, K.; Kato, J.; Takagi, T.; Kawamoto, T.; Yao, S.; Sumita, A.; Tsutsumi, S.; Tottori, T.; Oki, H.; Sang, B.-C.; Yano, J.; Aertgeerts, K.; Yoshida, S.; Ishikawa, T. Design and Synthesis of Novel DFG-Out RAF/Vascular Endothelial Growth Factor Receptor 2 (VEGFR2) Inhibitors. 1. Exploration of [5,6]-Fused Bicyclic Scaffolds. *J. Med. Chem.* **2012**, *55* (7), 3452–3478. https://doi.org/10.1021/jm300126x.

(4) Chang, X.-W.; Han, Q.-C.; Jiao, Z.-G.; Weng, L.-H.; Zhang, D.-W. 1-Aminoxymethylcyclopropanecarboxylic Acid as Building Block of β N–O Turn and Helix: Synthesis and Conformational Analysis in Solution and in the Solid State. *Tetrahedron* **2010**, *66* (51), 9733–9737. https://doi.org/10.1016/j.tet.2010.10.037.

(5) Rancourt, J.; Cameron, D. R.; Gorys, V.; Lamarre, D.; Poirier, M.; Thibeault, D.; Llinàs-Brunet, M. Peptide-Based Inhibitors of the Hepatitis C Virus NS3 Protease: Structure−Activity Relationship at the C-Terminal Position. *J. Med. Chem.* **2004**, *47* (10), 2511–2522. https://doi.org/10.1021/jm030573x.

(6) Altshuler, D. M.; Anderson, C. D.; Chen, W. G.; Clemens, J. J.; Cleveland, T.; Coon, T. R.; Frieman, B.; GROOTENHUIS (deceased), P.; Ruah, S. S. H.; Hare, B. J.; KEWALRAMANI, R.; Mccartney, J.; Miller, M. T.; PARASELLI, P.; Pierre, F.; ROBERTSON, S. M.; SOSNAY, P. R.; SWIFT, S. E.; Zhou, J. Methods of Treatment for Cystic Fibrosis. WO2020102346A1, May 22, 2020. https://patents.google.com/patent/WO2020102346A1/en?oq=WO2020%2f102346 (accessed 2022-12-30).

(7) Holst, D. E.; Wang, D. J.; Kim, M. J.; Guzei, I. A.; Wickens, Z. K. Aziridine Synthesis by Coupling Amines and Alkenes via an Electrogenerated Dication. *Nature* **2021**, *596* (7870), 74–79. https://doi.org/10.1038/s41586-021-03717-7.

(8) Wang, D. J.; Targos, K.; Wickens, Z. K. Electrochemical Synthesis of Allylic Amines from Terminal Alkenes and Secondary Amines. *J. Am. Chem. Soc.* **2021**, *143* (51), 21503–21510. https://doi.org/10.1021/jacs.1c11763.

(9) *Bruker-AXS (2019). APEX3. Version 2019.11-0. Madison, Wisconsin, USA.*

(10) Krause, L.; Herbst-Irmer, R.; Sheldrick, G. M.; Stalke, D. Comparison of Silver and Molybdenum Microfocus X-Ray Sources for Single-Crystal Structure Determination. *J Appl Cryst* **2015**, *48* (1), 3–10. https://doi.org/10.1107/S1600576714022985.

(11) *Sheldrick, G. M. (2013b). XPREP. Version 2013/1. Georg-August-Universität Göttingen, Göttingen, Germany.*

(12) *Sheldrick, G. M. (2013a). The SHELX homepage, http://shelx.uni-ac.gwdg.de/SHELX/.*

(13) Sheldrick, G. M. SHELXT – Integrated Space-Group and Crystal-Structure Determination. *Acta Cryst A* **2015**, *71* (1), 3–8. https://doi.org/10.1107/S2053273314026370.

(14) Sheldrick, G. M. Crystal Structure Refinement with SHELXL. *Acta Cryst C* **2015**, *71* (1), 3–8. https://doi.org/10.1107/S2053229614024218.

(15) Dolomanov, O. V.; Bourhis, L. J.; Gildea, R. J.; Howard, J. a. K.; Puschmann, H. OLEX2: A Complete Structure Solution, Refinement and Analysis Program. *J Appl Cryst* **2009**, *42* (2), 339–341. https://doi.org/10.1107/S0021889808042726.

(16) *Guzei, I. A. (2007-2022). Programs Gn. University of Wisconsin-Madison, Madison, Wisconsin, USA.*

(17) Kleemiss, F.; Dolomanov, O. V.; Bodensteiner, M.; Peyerimhoff, N.; Midgley, L.; Bourhis, L. J.; Genoni, A.; Malaspina, L. A.; Jayatilaka, D.; Spencer, J. L.; White, F.; Grundkötter-Stock, B.; Steinhauer, S.; Lentz, D.; Puschmann, H.; Grabowsky, S. Accurate Crystal Structures and Chemical Properties from NoSpherA2. *Chem. Sci.* **2021**, *12* (5), 1675–1692. https://doi.org/10.1039/D0SC05526C.

(18) Bourhis, L. J.; Dolomanov, O. V.; Gildea, R. J.; Howard, J. a. K.; Puschmann, H. The Anatomy of a Comprehensive Constrained, Restrained Refinement Program for the Modern Computing Environment – Olex2 Dissected. *Acta Cryst A* **2015**, *71* (1), 59–75. https://doi.org/10.1107/S2053273314022207.

(19) Neese, F. Software Update: The ORCA Program System, Version 4.0. *WIREs Computational Molecular Science* **2018**, *8* (1), e1327. https://doi.org/10.1002/wcms.1327.

C.10 NMR Spectra

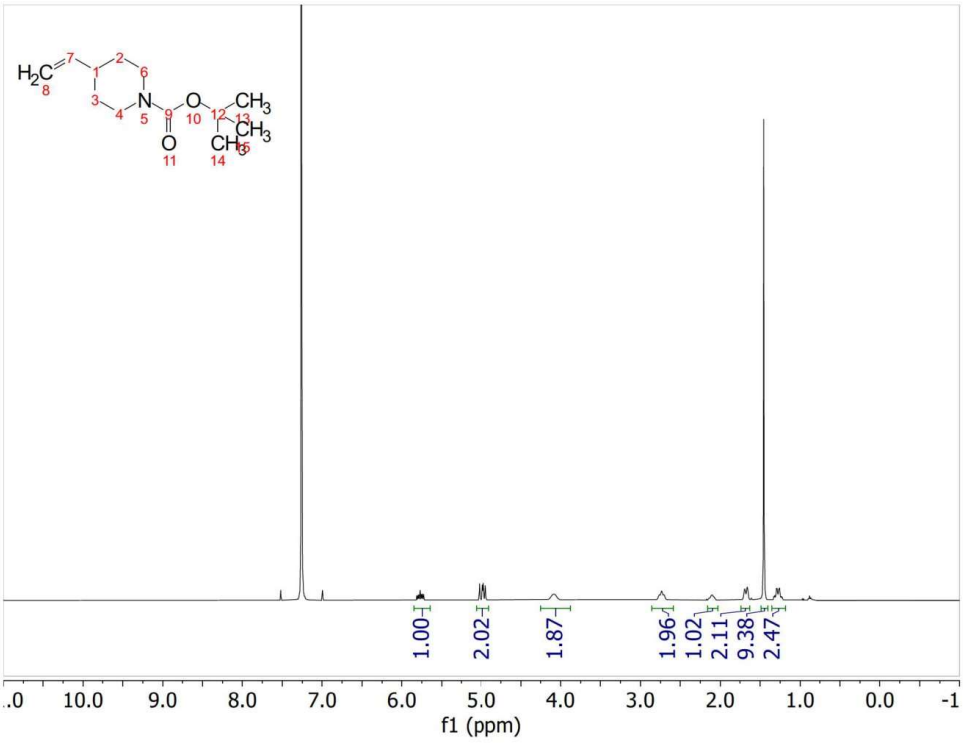

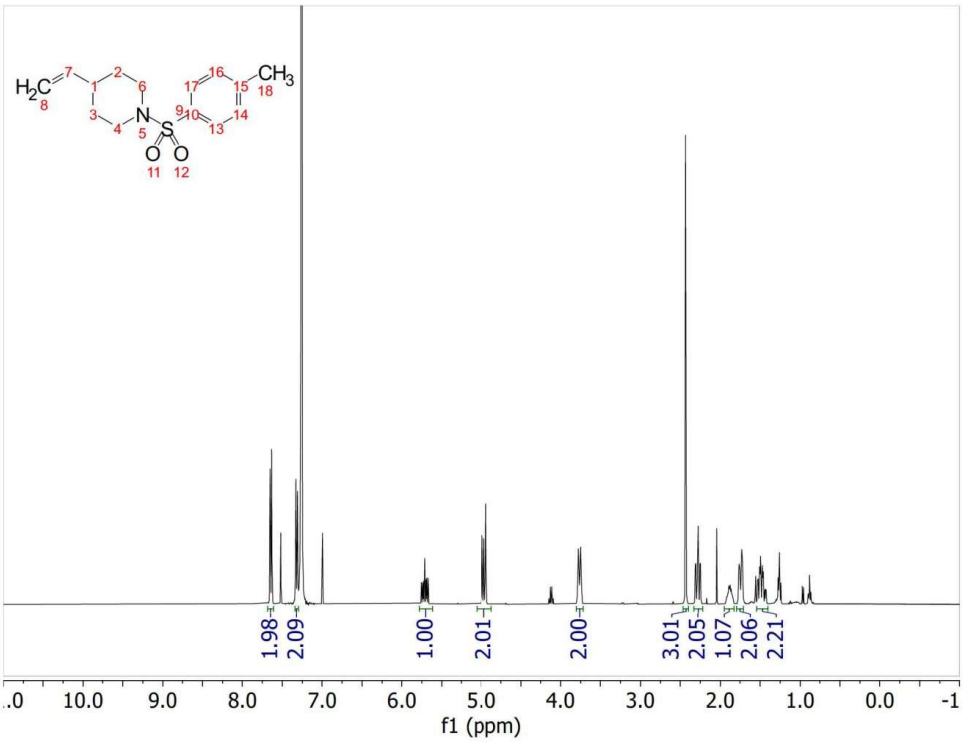

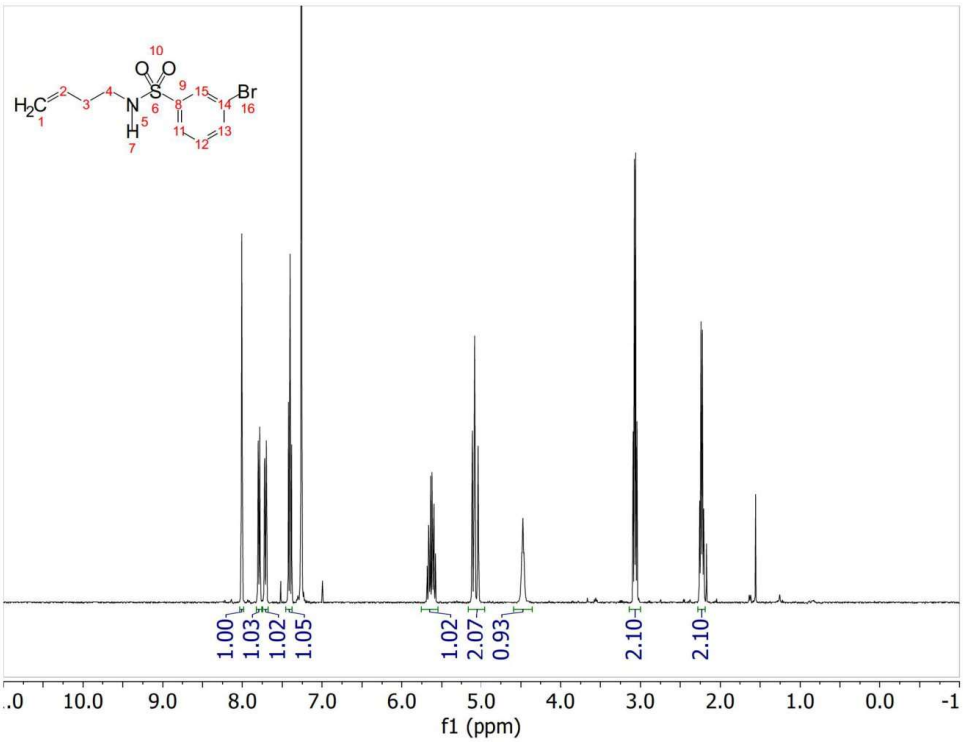
1.00
1.03
1.02
1.05
1.02
2.07
0.93
2.10
2.10
f1 (ppm)

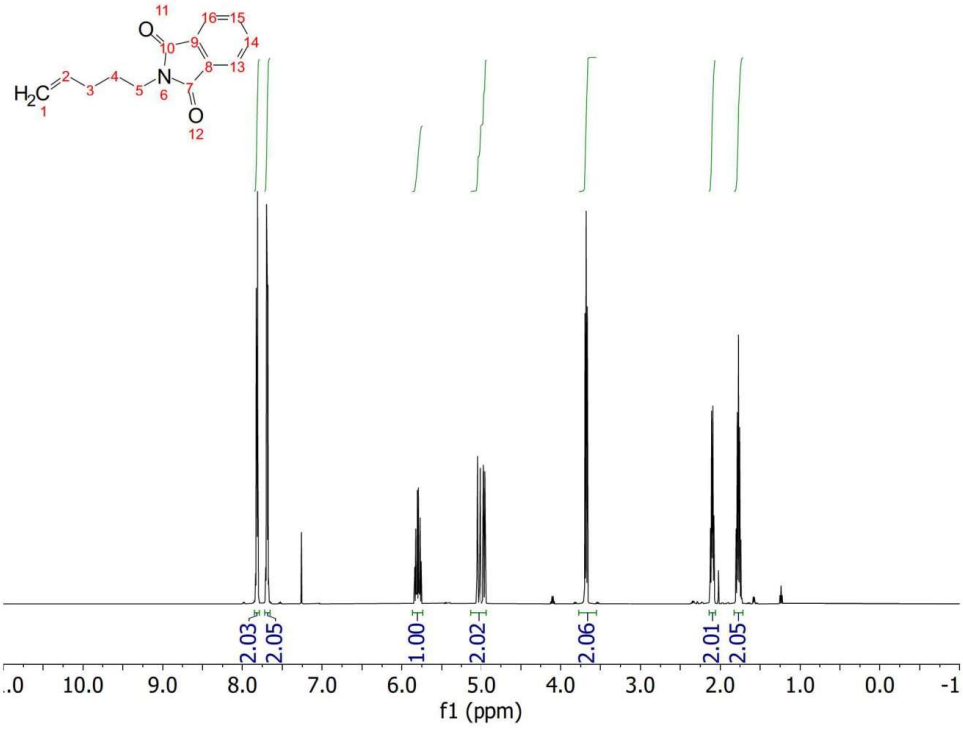
2.03
2.05
1.00
2.02
2.06
2.01
2.05
f1 (ppm)

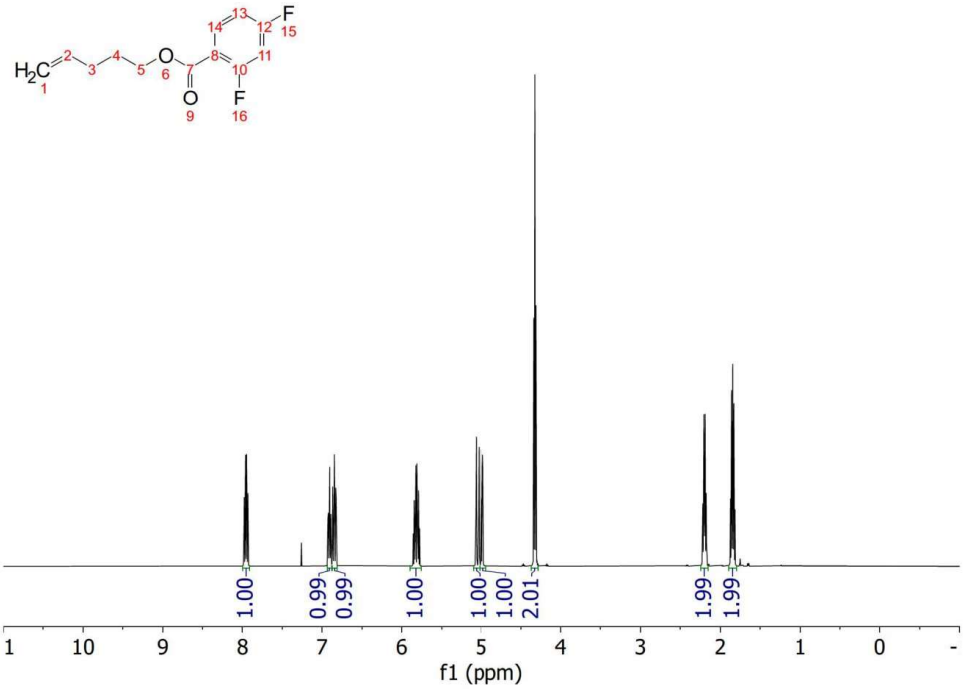
1.00
0.99
0.99
1.00
1.00
1.00
2.01
1.99
1.99
f1 (ppm)

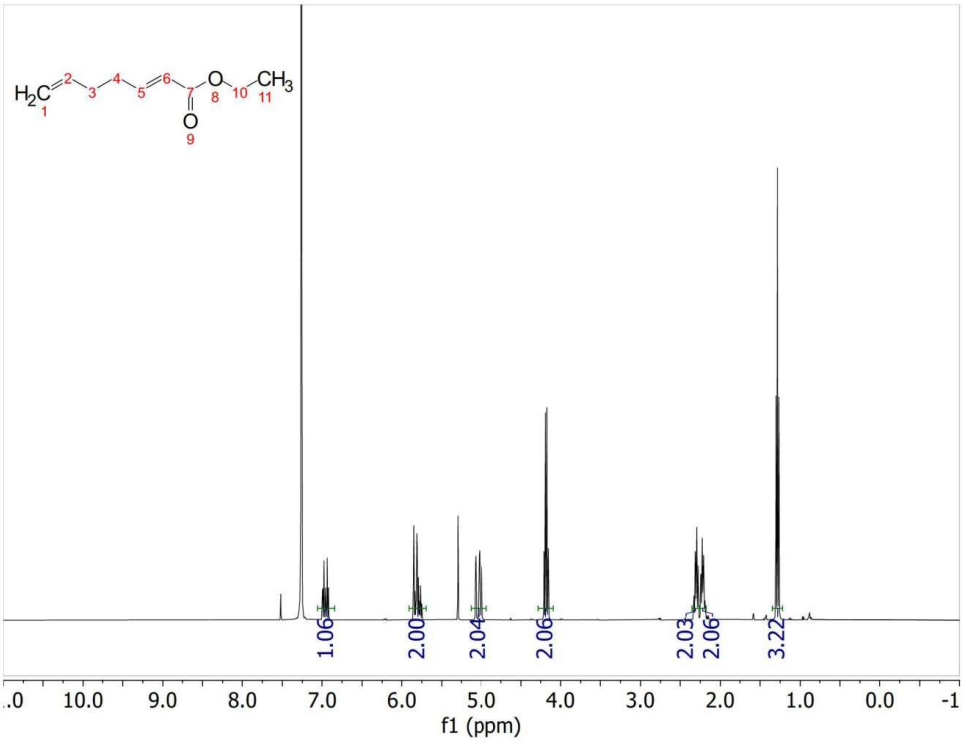
1.06
2.00
2.04
2.06
2.03
2.06
3.22
f1 (ppm)

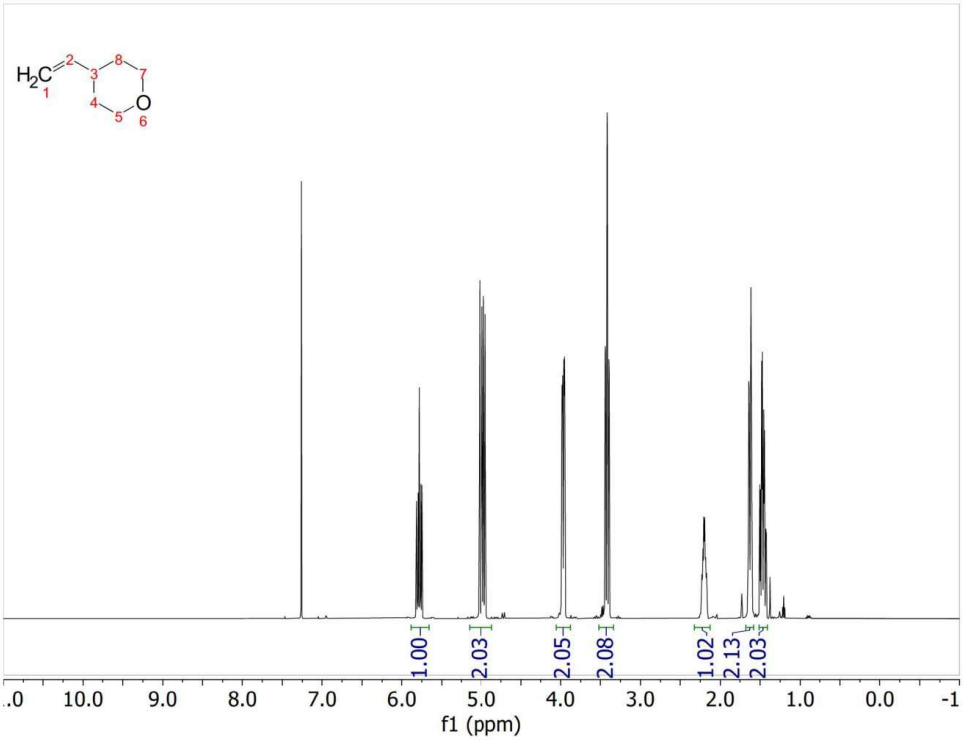
1.00
2.03
2.05
2.08
1.02
2.13
2.03
10.0
9.0
8.0
7.0
6.0
5.0
4.0
3.0
2.0
1.0
0.0
f1 (ppm)

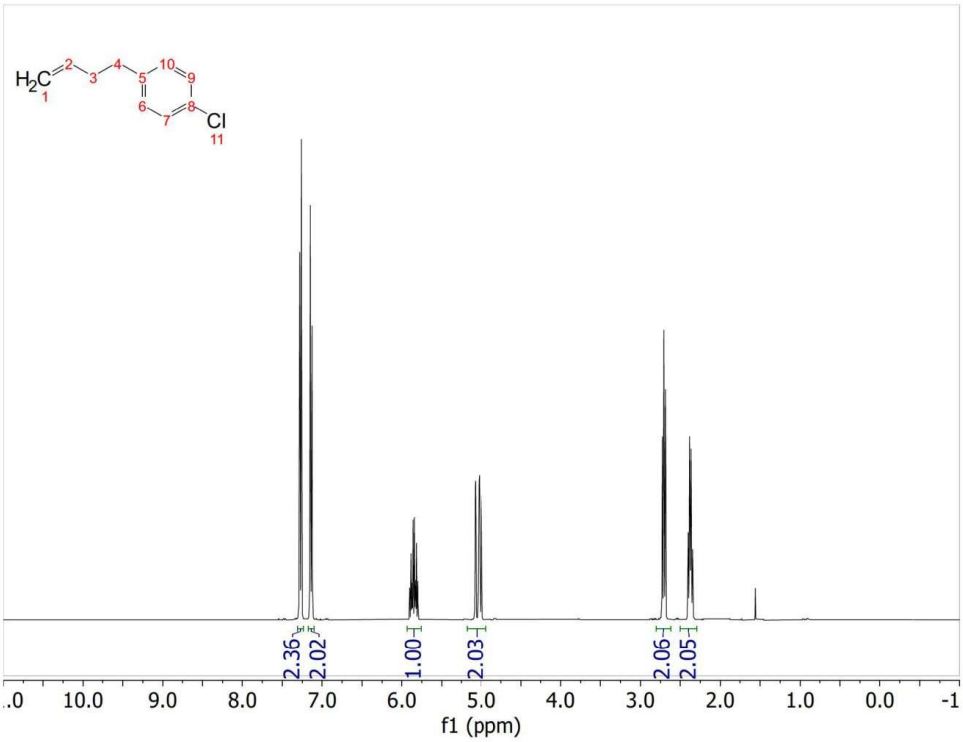
Cl
2.36
2.02
1.00
2.03
2.06
2.05
10.0
9.0
8.0
7.0
6.0
5.0
4.0
3.0
2.0
1.0
0.0
f1 (ppm)

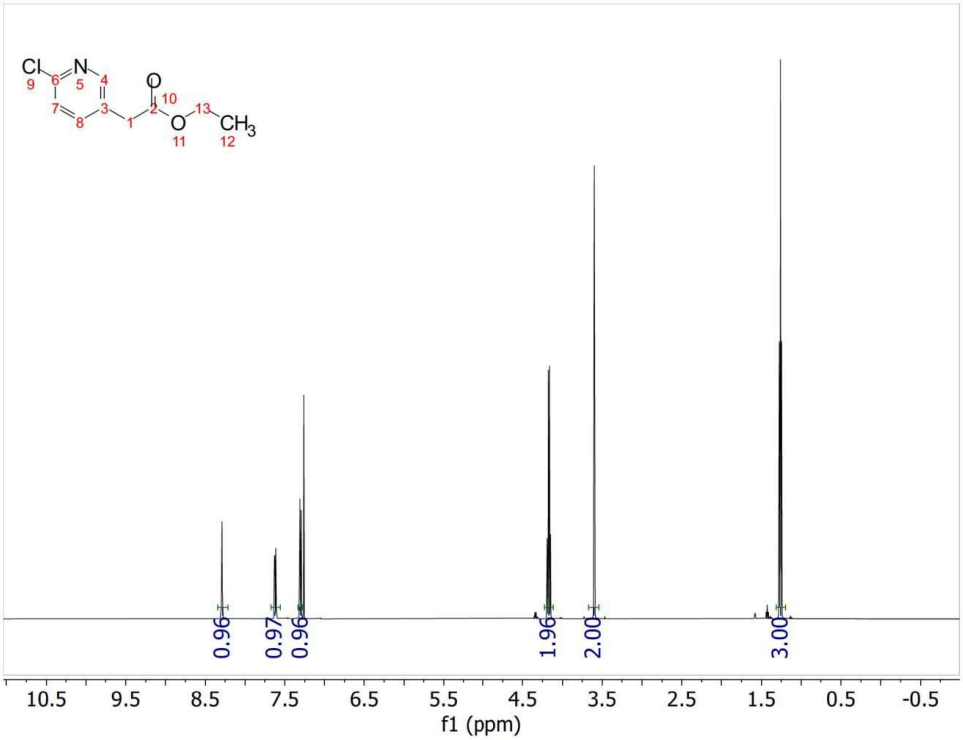
Cl
N
O
O
CH3
0.96
0.97
0.96
1.96
2.00
3.00
10.5
9.5
8.5
7.5
6.5
5.5
4.5
3.5
2.5
1.5
0.5
-0.5
f1 (ppm)

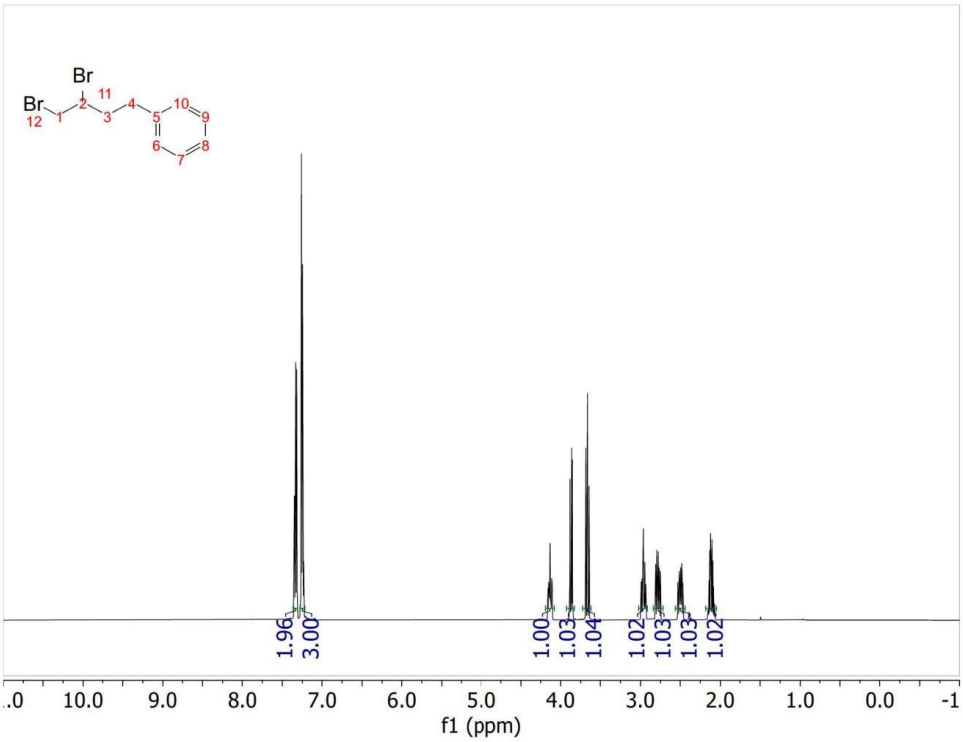
Br
Br
1.96
3.00
1.00
1.03
1.04
1.02
1.03
1.03
1.02
10.0
9.0
8.0
7.0
6.0
5.0
4.0
3.0
2.0
1.0
0.0
-1
f1 (ppm)

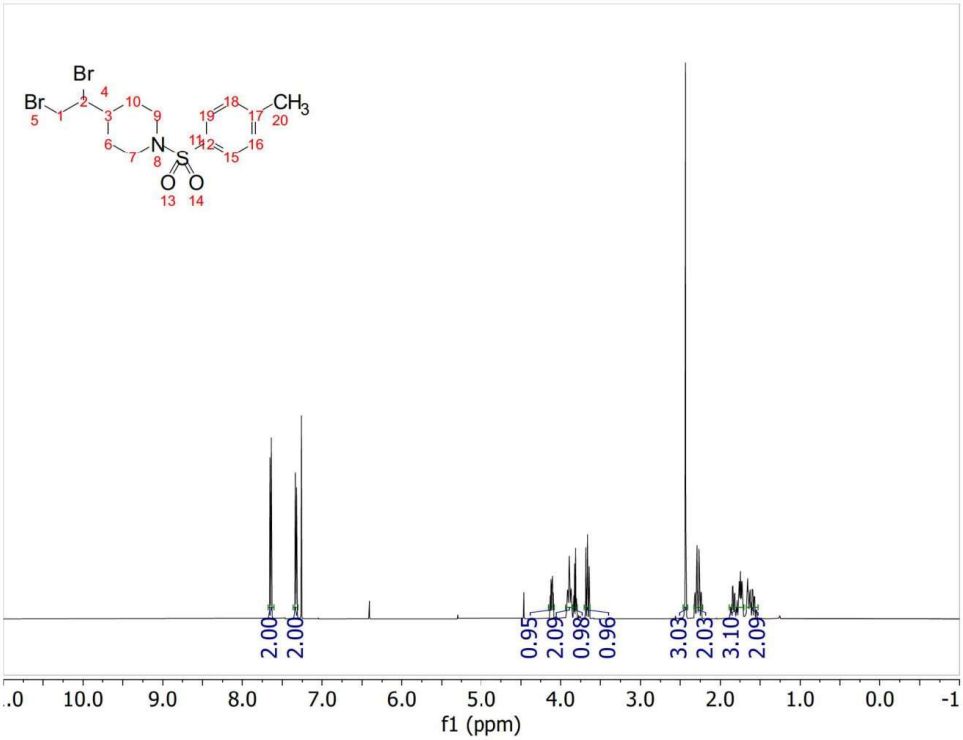
Br
Br
5
1
2
4
3
10
9
6
7
N
8
S
O
O
13
14
18
19
17
CH3
20
11
12
15
16
2.00
2.00
0.95
2.09
0.98
0.96
3.03
2.03
3.10
2.09
10.0
9.0
8.0
7.0
6.0
5.0
4.0
3.0
2.0
1.0
0.0
f1 (ppm)

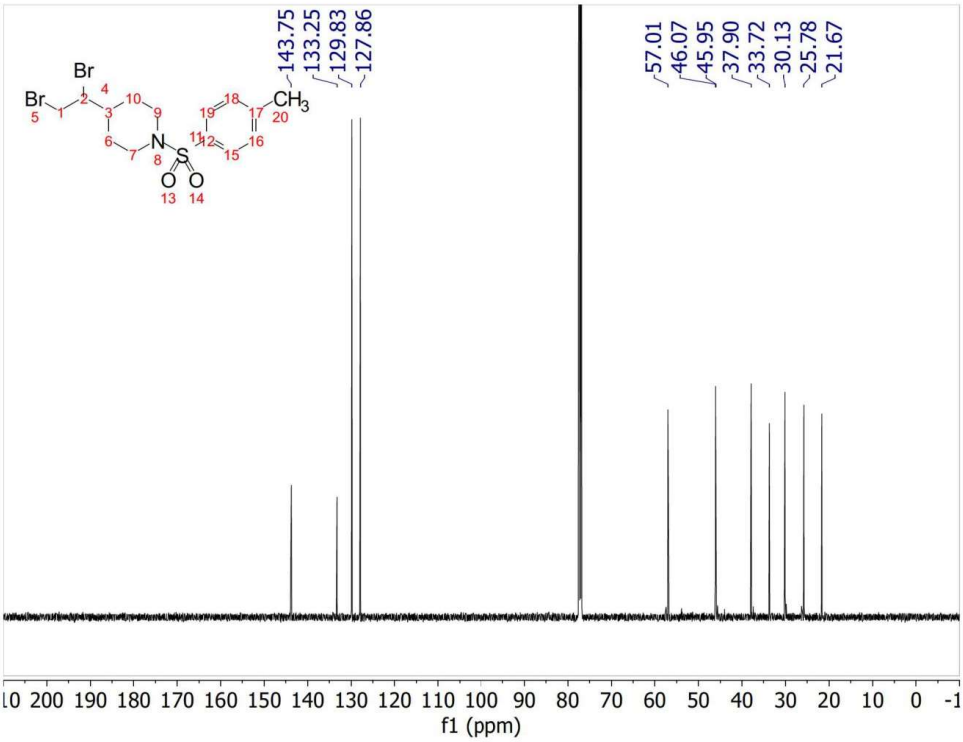
143.75
133.25
129.83
127.86
57.01
46.07
45.95
37.90
33.72
30.13
25.78
21.67
f1 (ppm)

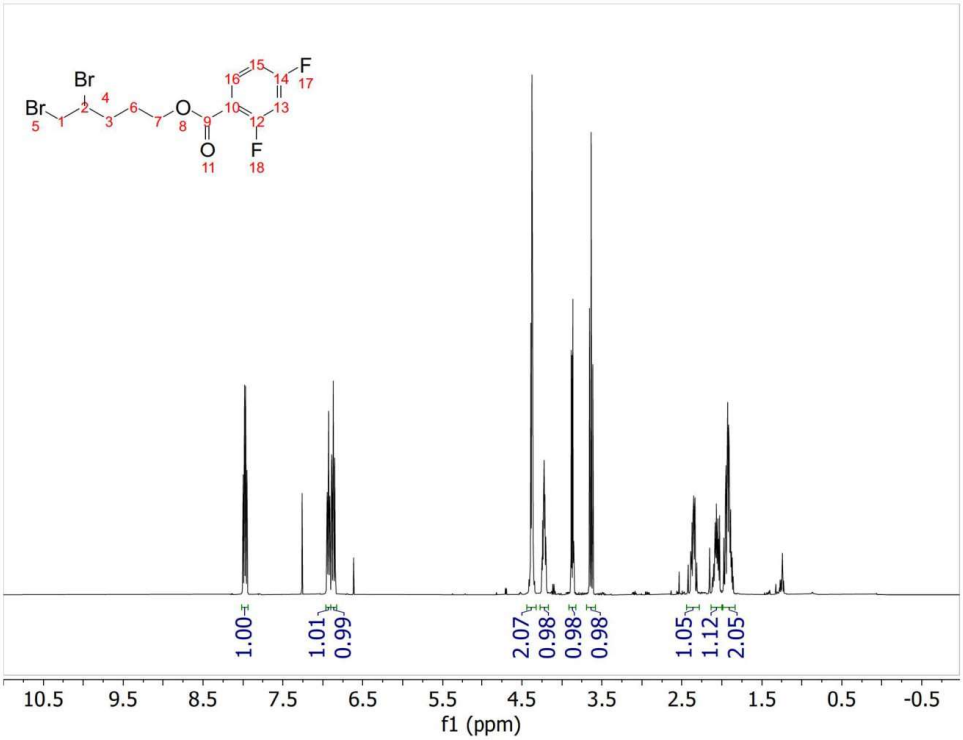
Br
Br
O
O
F
F
1.00
1.01
0.99
2.07
0.98
0.98
0.98
1.05
1.12
2.05
10.5 9.5 8.5 7.5 6.5 5.5 4.5 3.5 2.5 1.5 0.5 -0.5
f1 (ppm)

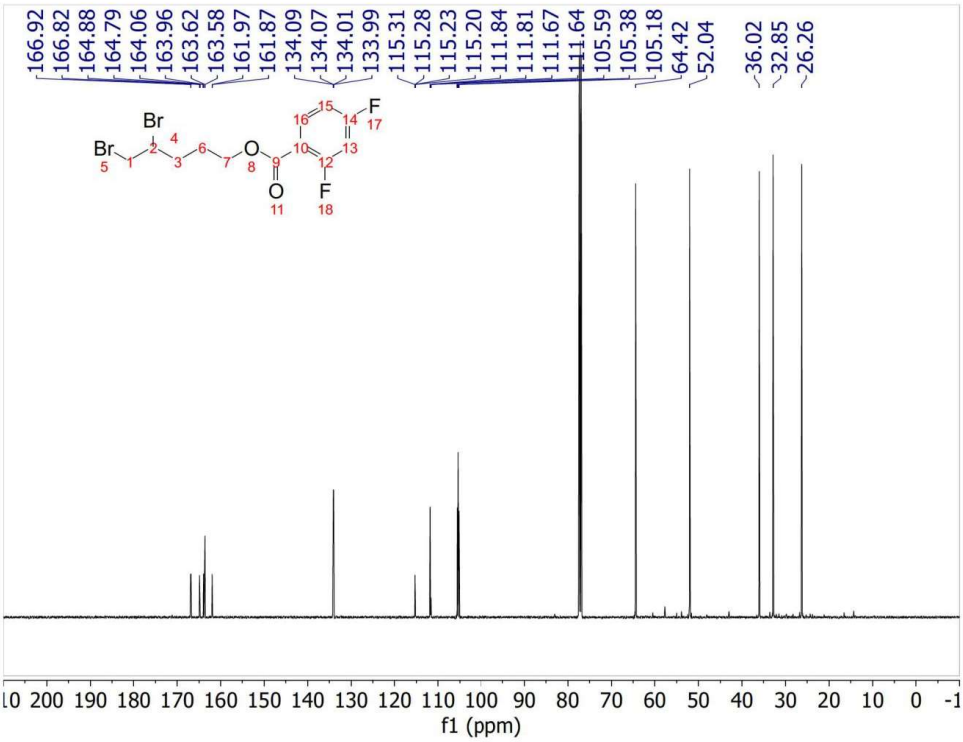
166.92
166.82
164.88
164.79
164.06
163.96
163.62
163.58
161.97
161.87
134.09
134.07
134.01
133.99
115.31
115.28
115.23
115.20
111.84
111.81
111.67
111.64
105.59
105.38
105.18
64.42
52.04
36.02
32.85
26.26
Br
Br
O
O
F
F
f1 (ppm)

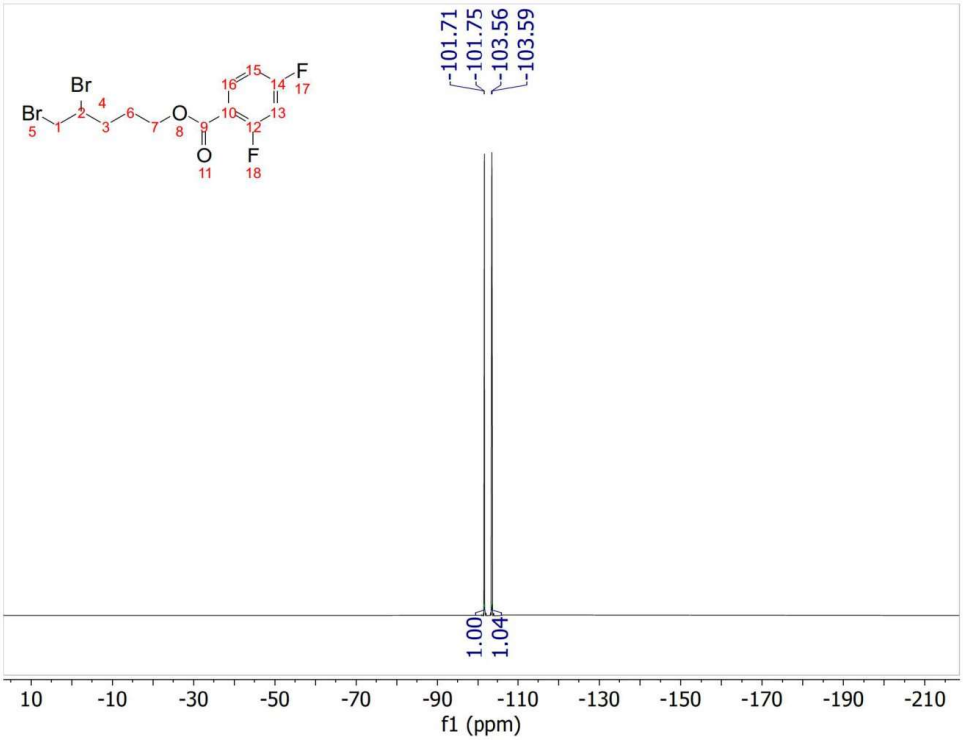
-101.71
-101.75
-103.56
-103.59
1.00
1.04
10 -10 -30 -50 -70 -90 -110 -130 -150 -170 -190 -210
f1 (ppm)

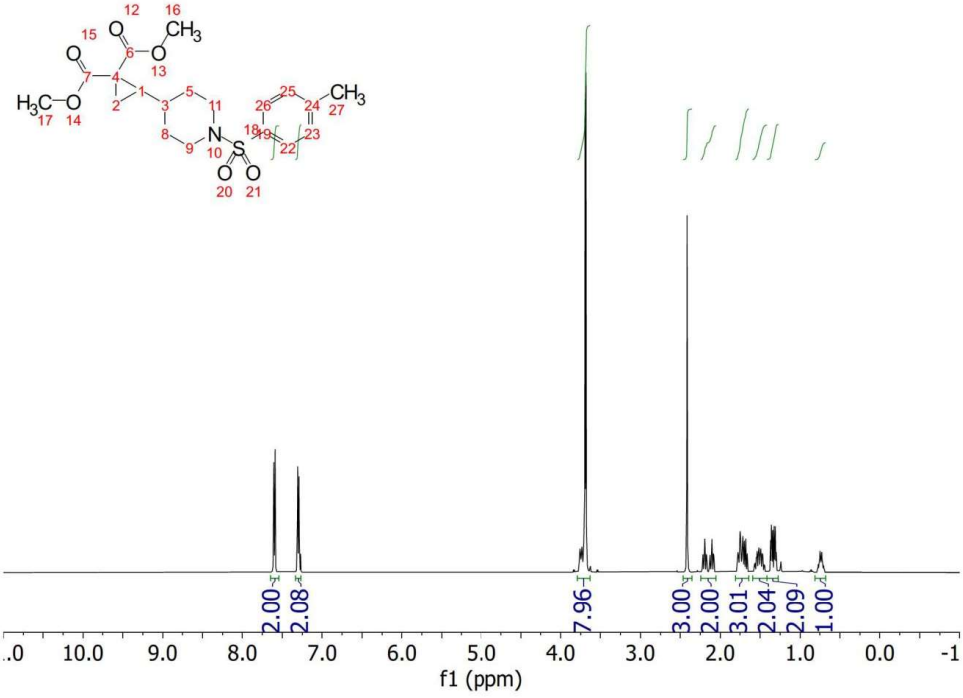
2.00
2.08
7.96
3.00
2.00
3.01
2.04
2.09
1.00
.0 10.0 9.0 8.0 7.0 6.0 5.0 4.0 3.0 2.0 1.0 0.0 -1
f1 (ppm)

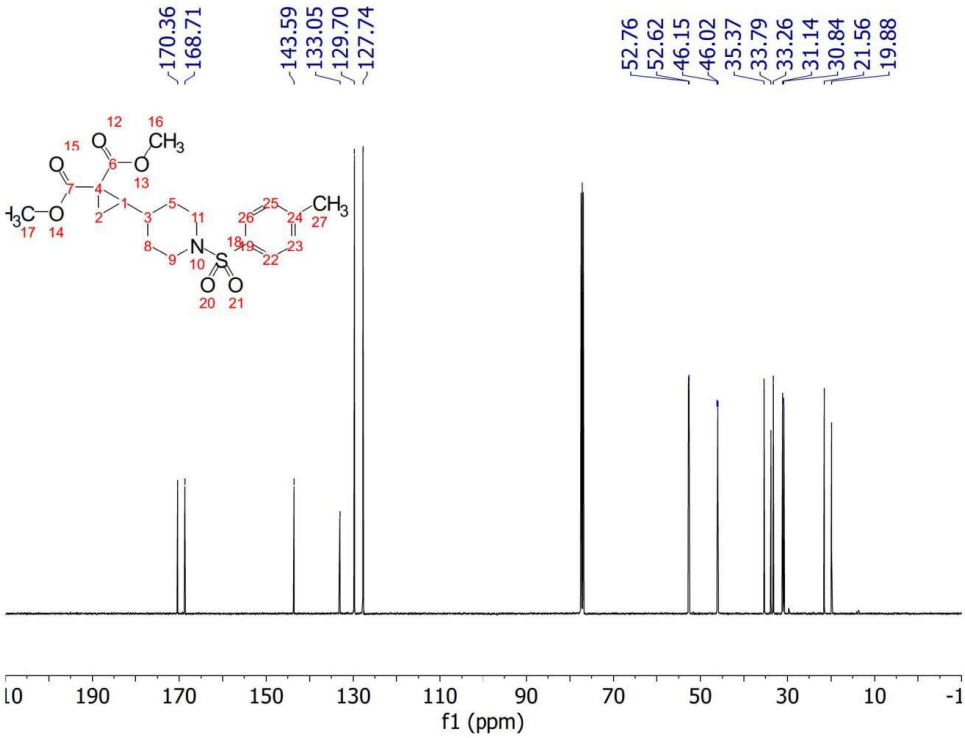
170.36
168.71
143.59
133.05
129.70
127.74
52.76
52.62
46.15
46.02
35.37
33.79
33.26
31.14
30.84
21.56
19.88
f1 (ppm)

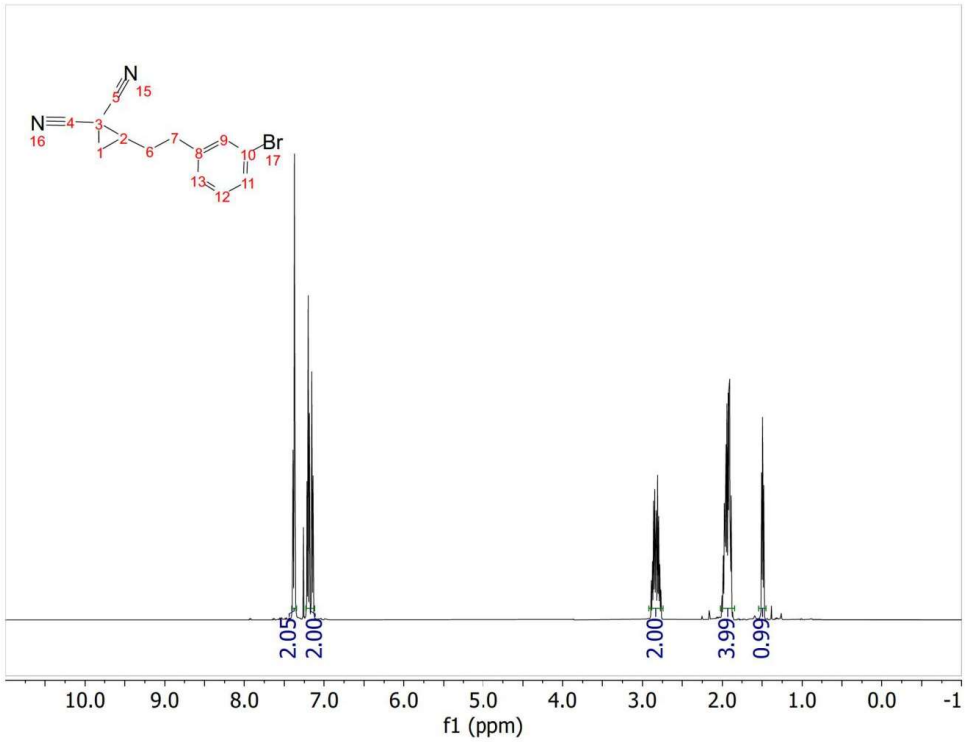
2.05
2.00
2.00
3.99
0.99
f1 (ppm)

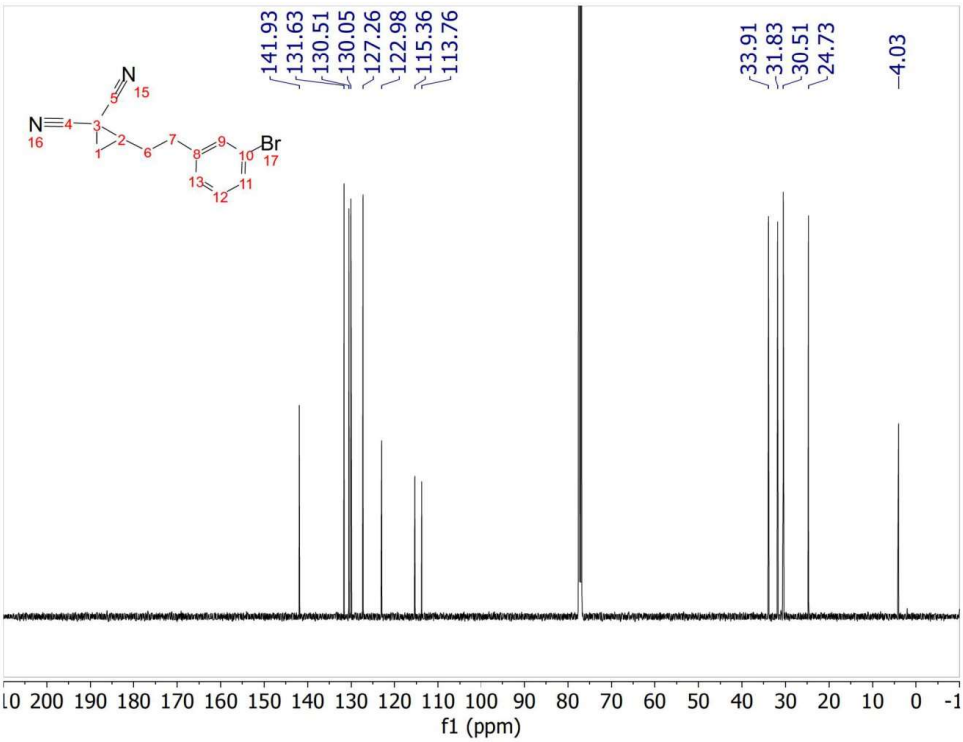
141.93
131.63
130.51
130.05
127.26
122.98
115.36
113.76
33.91
31.83
30.51
24.73
4.03
f1 (ppm)

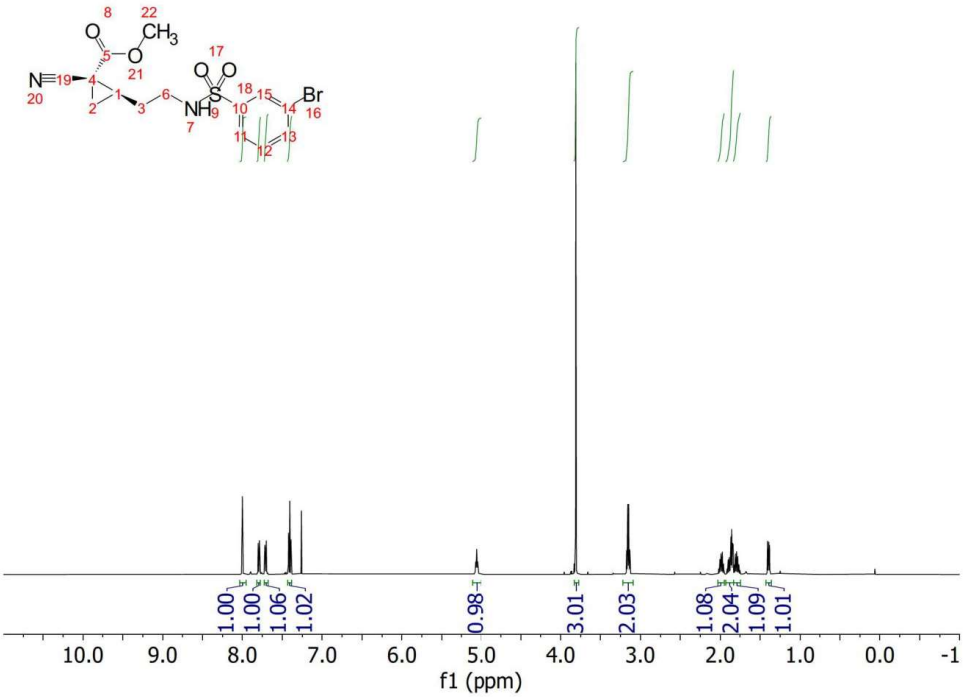
1.00
1.00
1.06
1.02
0.98
3.01
2.03
1.08
2.04
1.09
1.01
f1 (ppm)

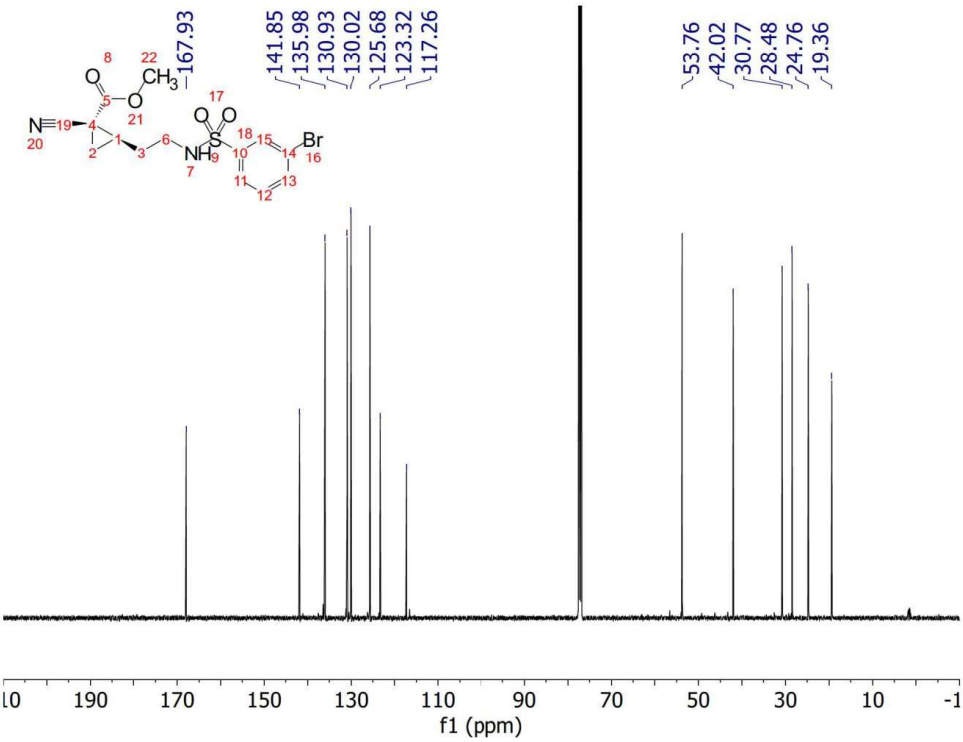
167.93
141.85
135.98
130.93
130.02
125.68
123.32
117.26
53.76
42.02
30.77
28.48
24.76
19.36
f1 (ppm)

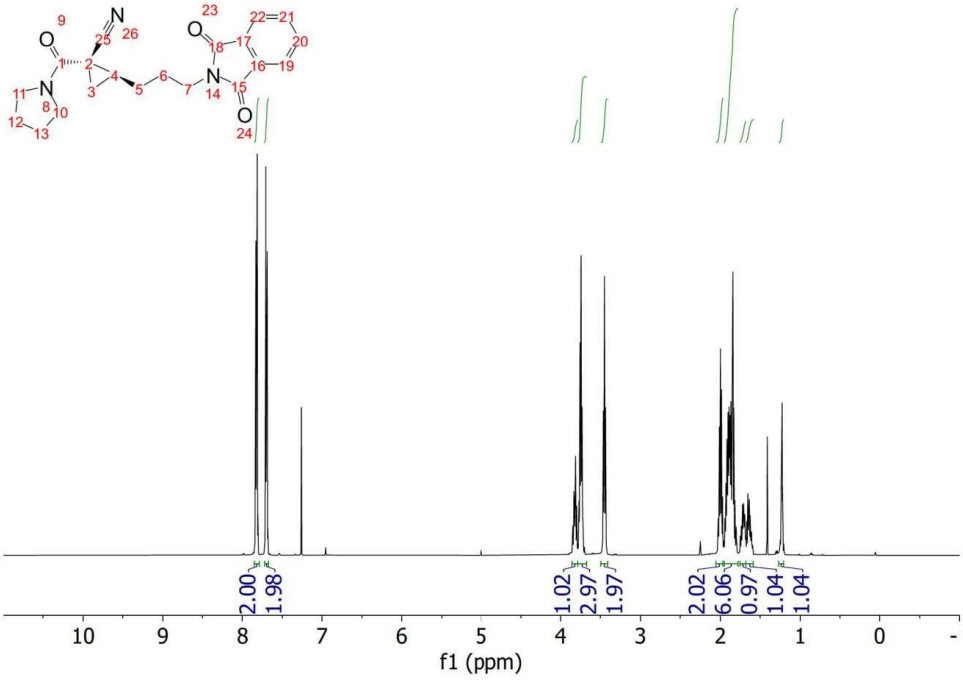
2.00
1.98
1.02
2.97
1.97
2.02
6.06
0.97
1.04
1.04
f1 (ppm)

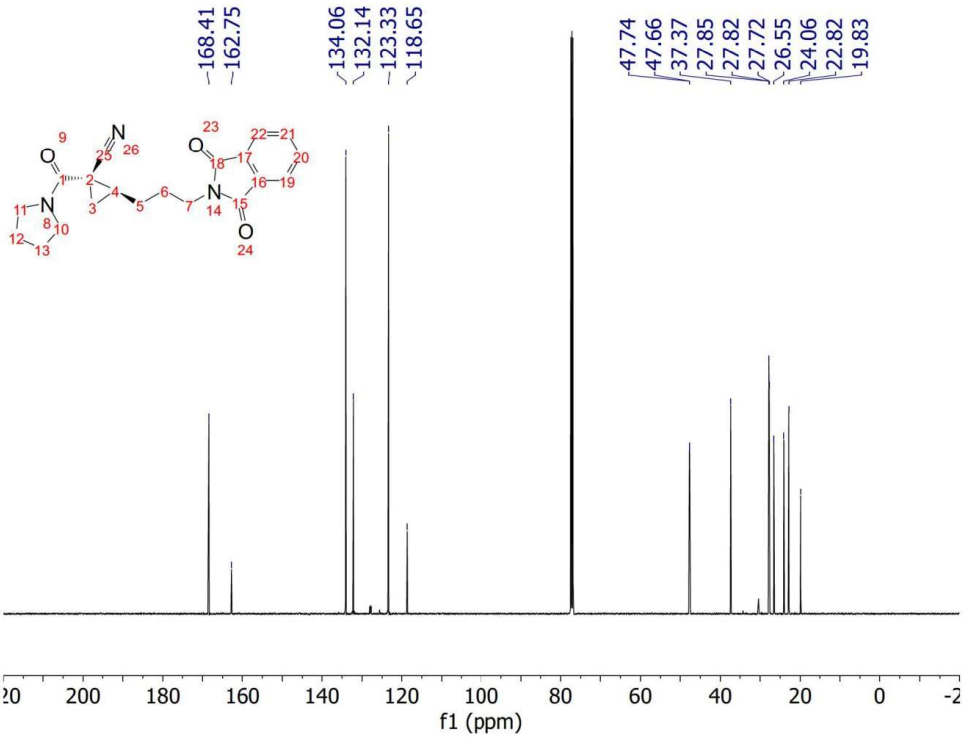
168.41
162.75
134.06
132.14
123.33
118.65
47.74
47.66
37.37
27.85
27.82
27.72
26.55
24.06
22.82
19.83
f1 (ppm)

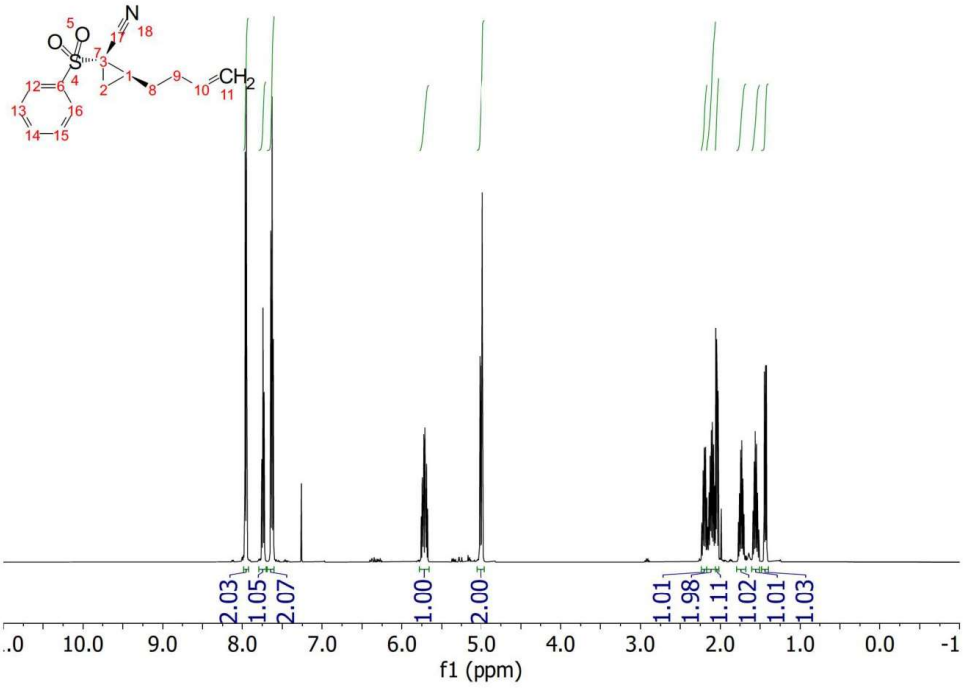
2.03
1.05
2.07
1.00
2.00
1.01
1.98
1.11
1.02
1.01
1.03
f1 (ppm)

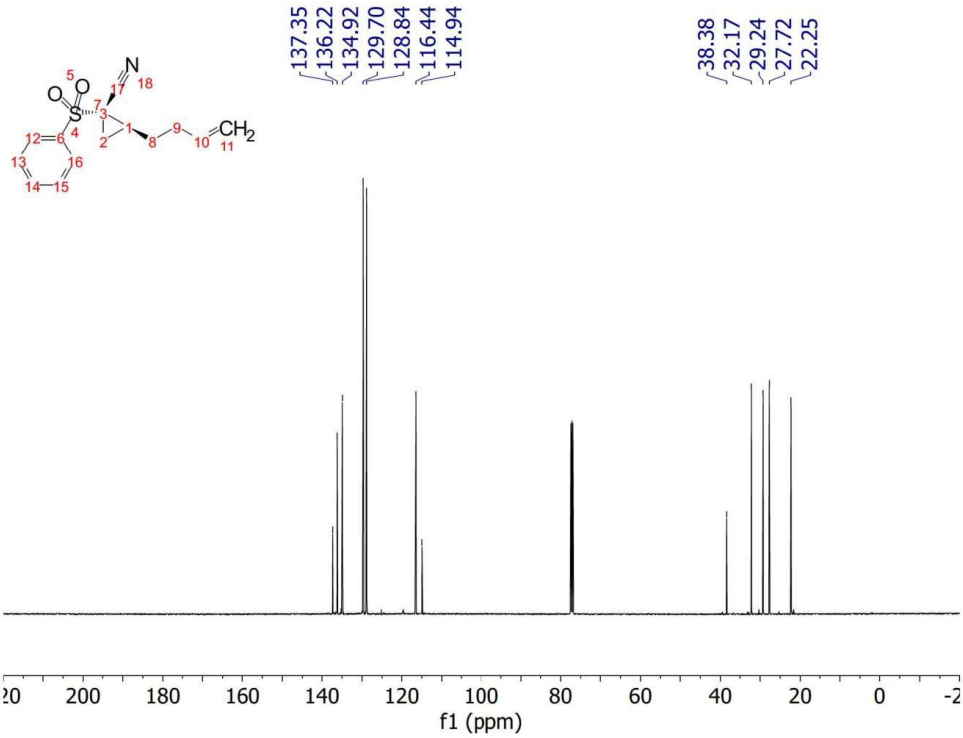
137.35
136.22
134.92
129.70
128.84
116.44
114.94
38.38
32.17
29.24
27.72
22.25
f1 (ppm)

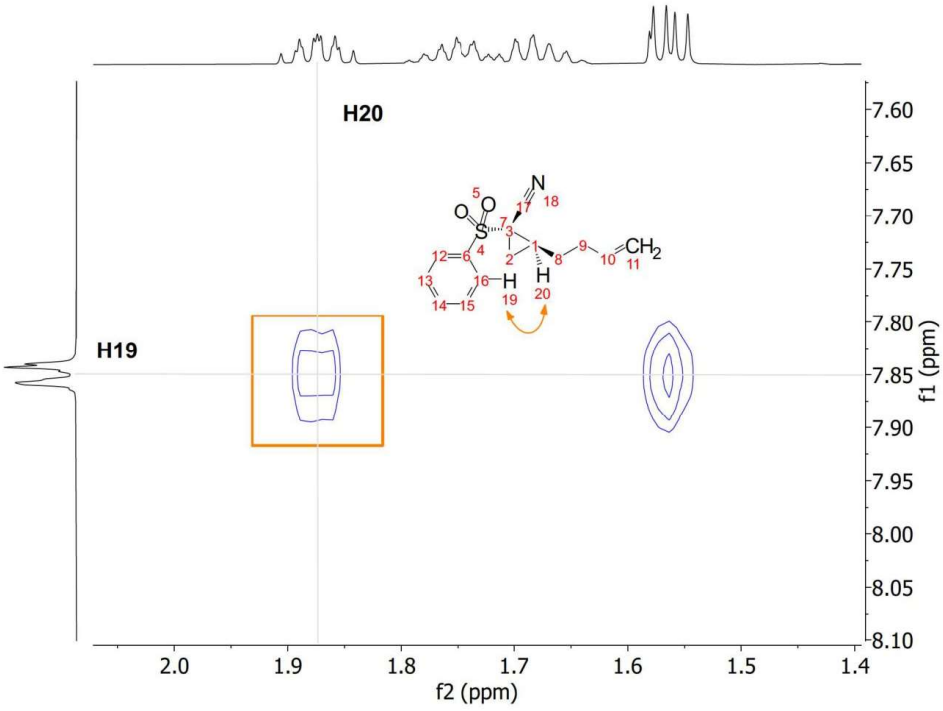
H20
H19
f2 (ppm)
f1 (ppm)

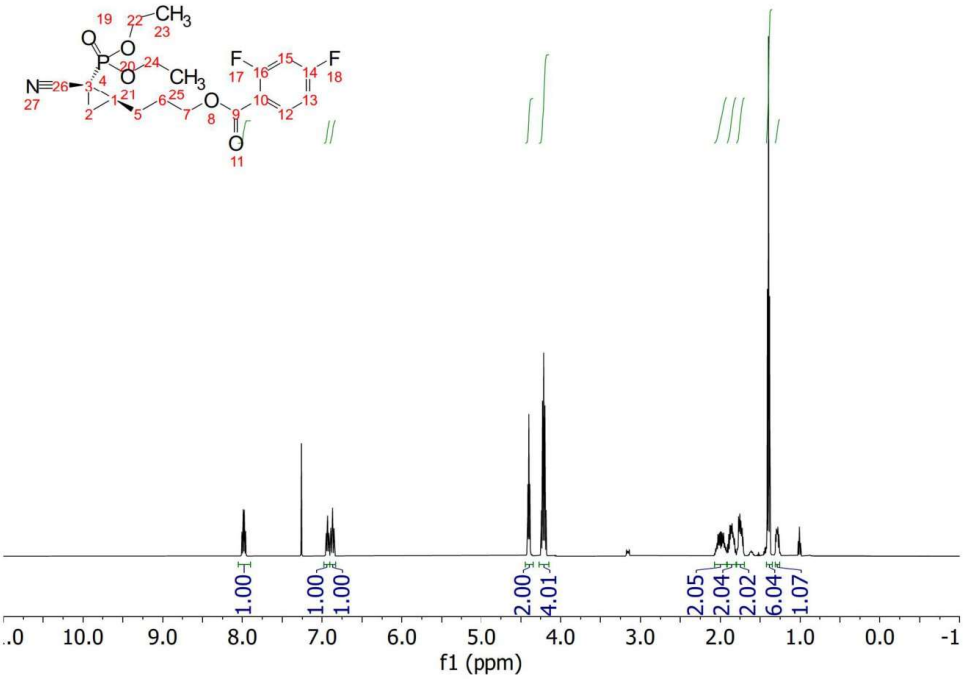
1.00
1.00
1.00
2.00
4.01
2.05
2.04
2.02
6.04
1.07
10.0
9.0
8.0
7.0
6.0
5.0
4.0
3.0
2.0
1.0
0.0
f1 (ppm)

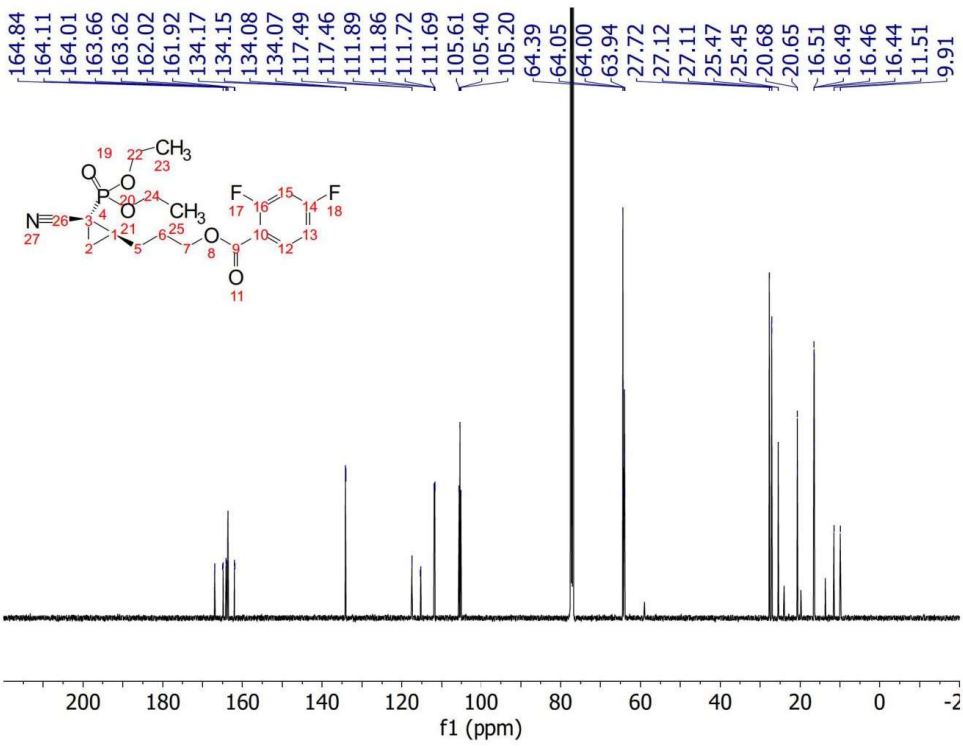
164.84
164.11
164.01
163.66
163.62
162.02
161.92
134.17
134.15
134.08
134.07
117.49
117.46
111.89
111.86
111.72
111.69
105.61
105.40
105.20
64.39
64.05
64.00
63.94
27.72
27.12
27.11
25.47
25.45
20.68
20.65
16.51
16.49
16.46
16.44
11.51
9.91
200
180
160
140
120
100
80
60
40
20
0
f1 (ppm)

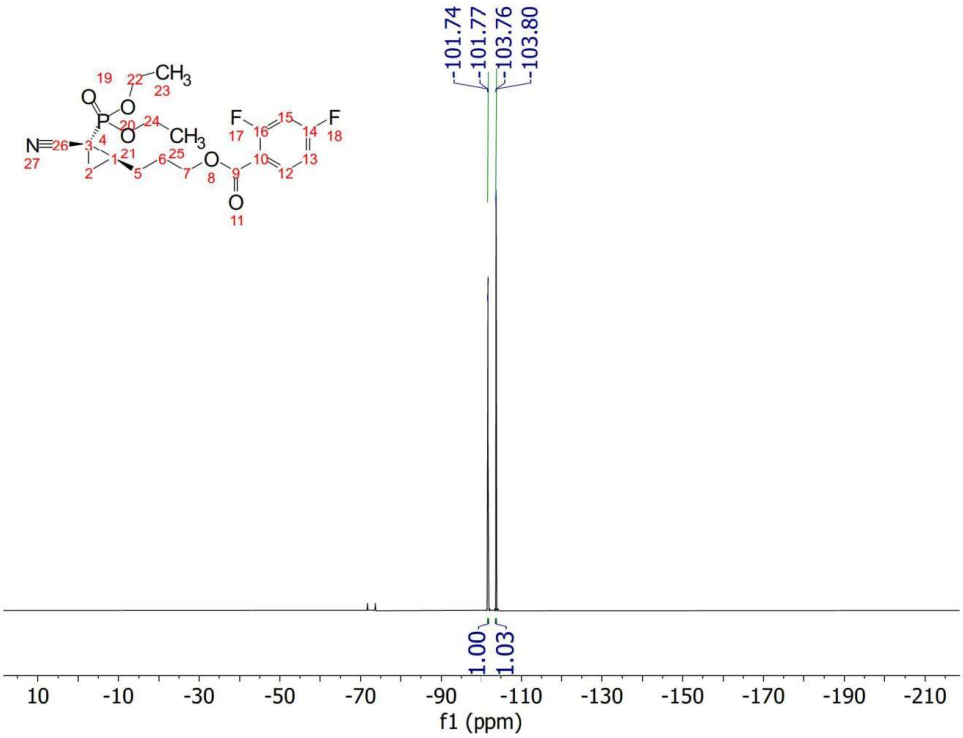
-101.74
-101.77
-103.76
-103.80
1.00
1.03
10
-10
-30
-50
-70
-90
-110
-130
-150
-170
-190
-210
f1 (ppm)

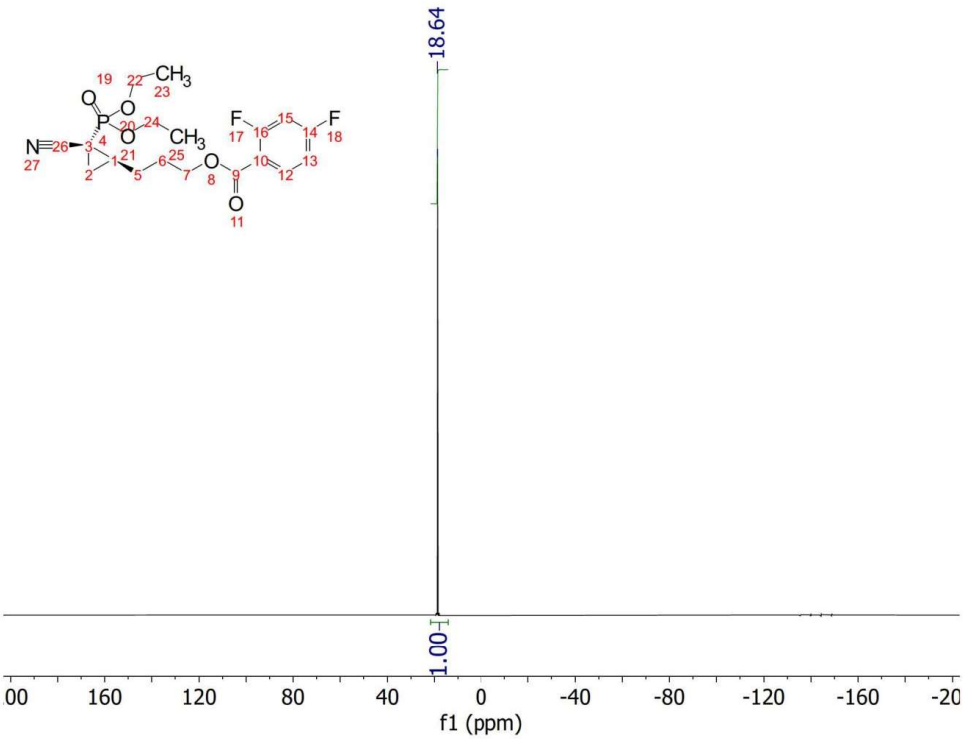
18.64
1.00
00
160
120
80
40
0
-40
-80
-120
-160
-20
f1 (ppm)

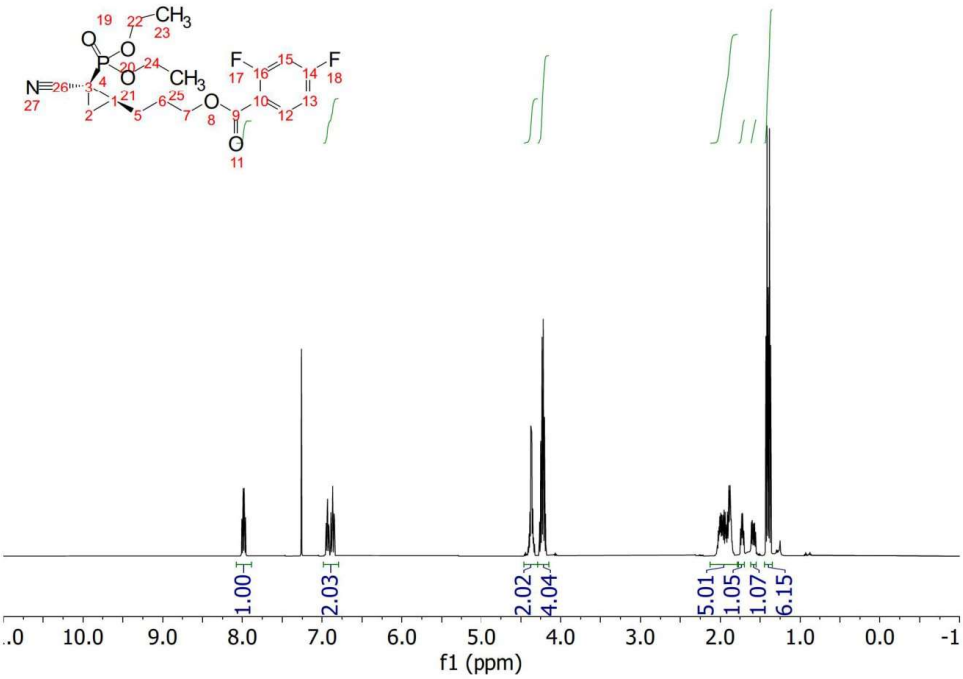
1.00
2.03
2.02
4.04
5.01
1.05
1.07
6.15
f1 (ppm)

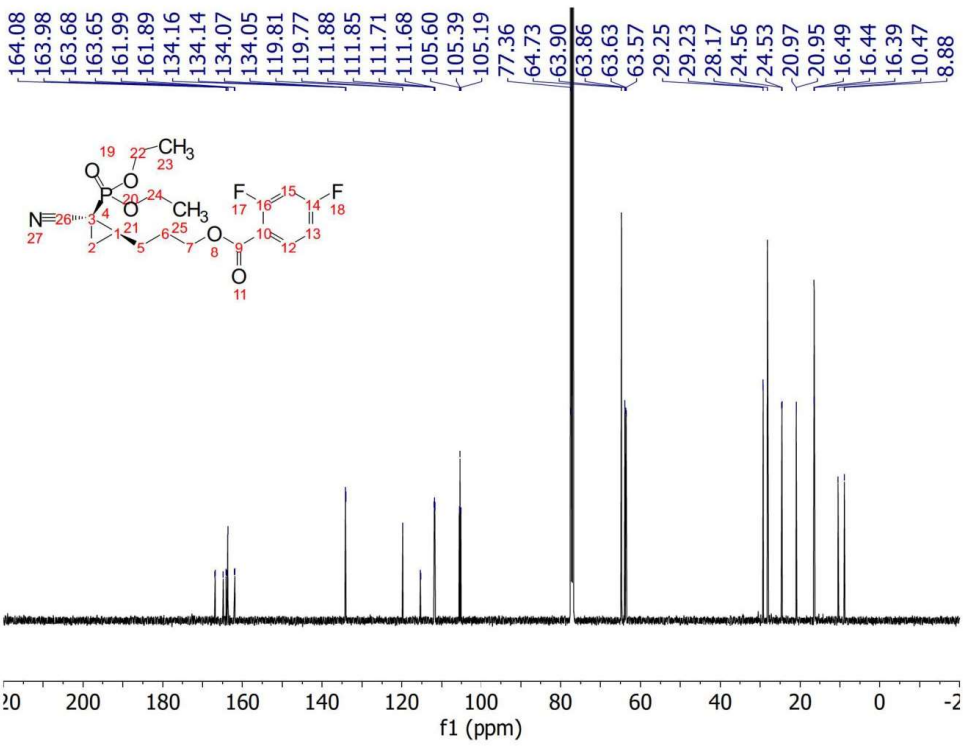
164.08
163.98
163.68
163.65
161.99
161.89
134.16
134.14
134.07
134.05
119.81
119.77
111.88
111.85
111.71
111.68
105.60
105.39
105.19
77.36
64.73
63.90
63.86
63.63
63.57
29.25
29.23
28.17
24.56
24.53
20.97
20.95
16.49
16.44
16.39
10.47
8.88
f1 (ppm)

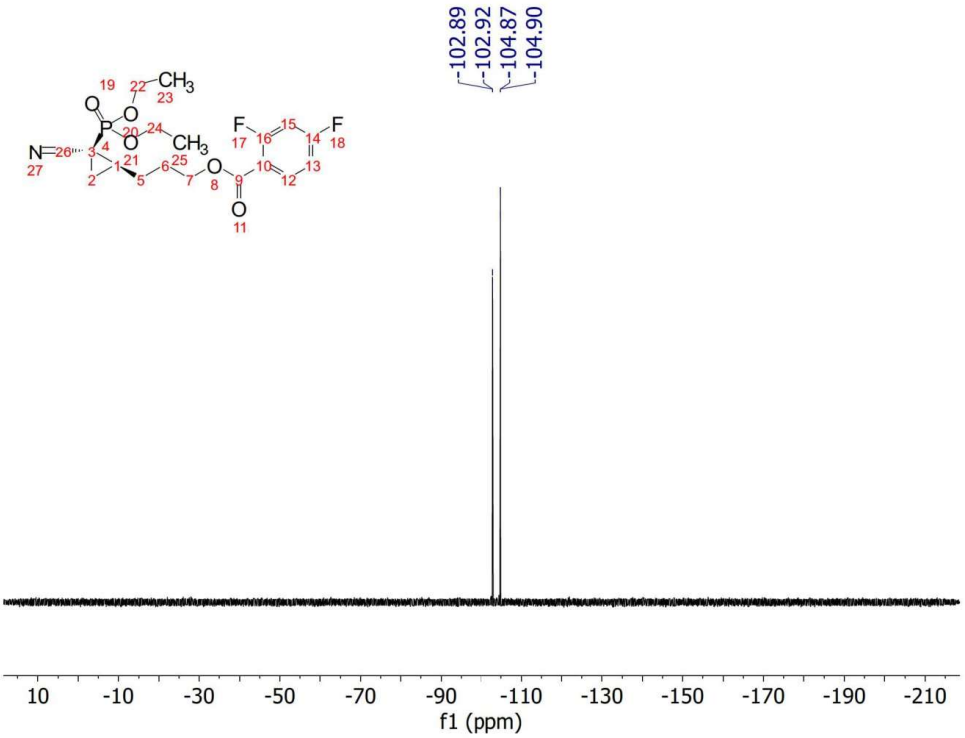
-102.89
-102.92
-104.87
-104.90
10
-10
-30
-50
-70
-90
-110
-130
-150
-170
-190
-210
f1 (ppm)

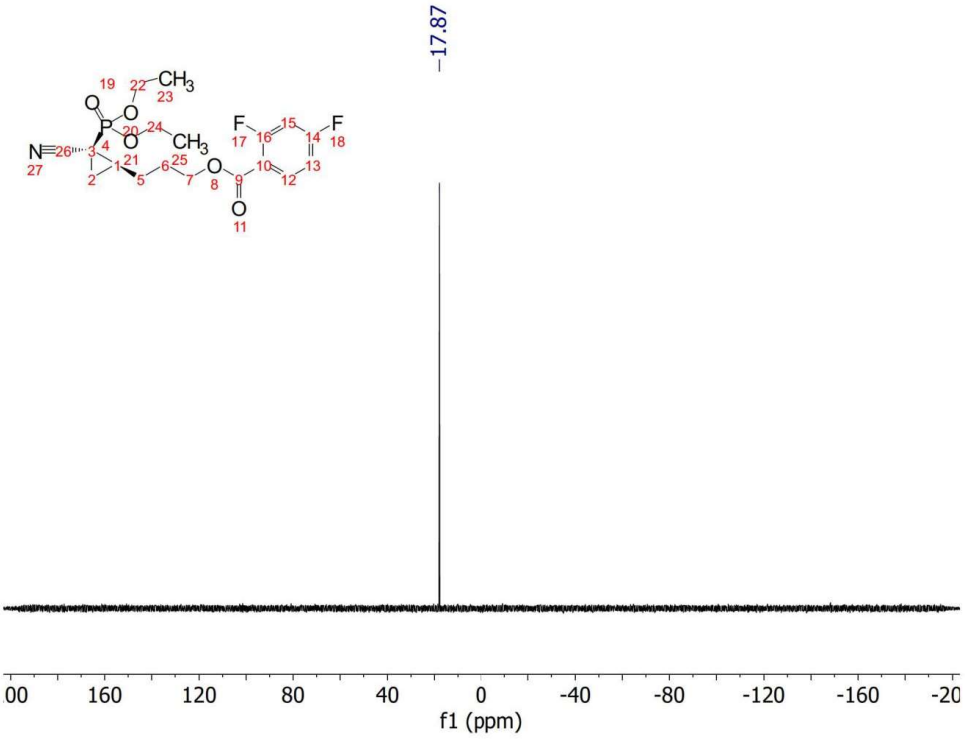
-17.87
00
160
120
80
40
0
-40
-80
-120
-160
-20
f1 (ppm)

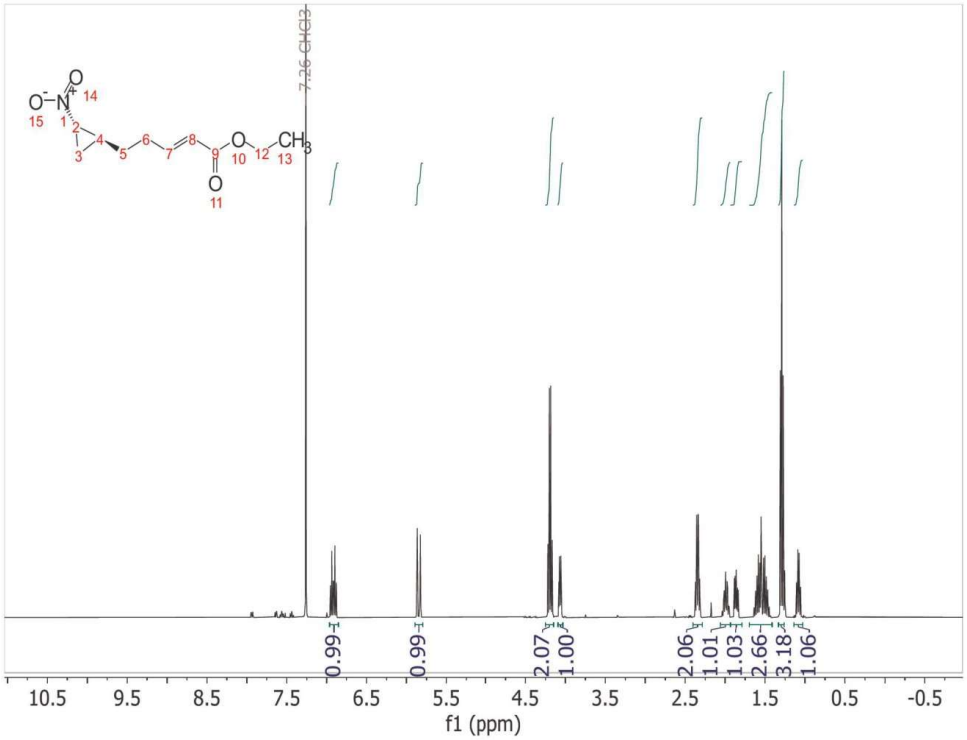
7.26 CHCl3
0.99
0.99
2.07
1.00
2.06
1.01
1.03
2.66
3.18
1.06
10.5 9.5 8.5 7.5 6.5 5.5 4.5 3.5 2.5 1.5 0.5 -0.5
f1 (ppm)

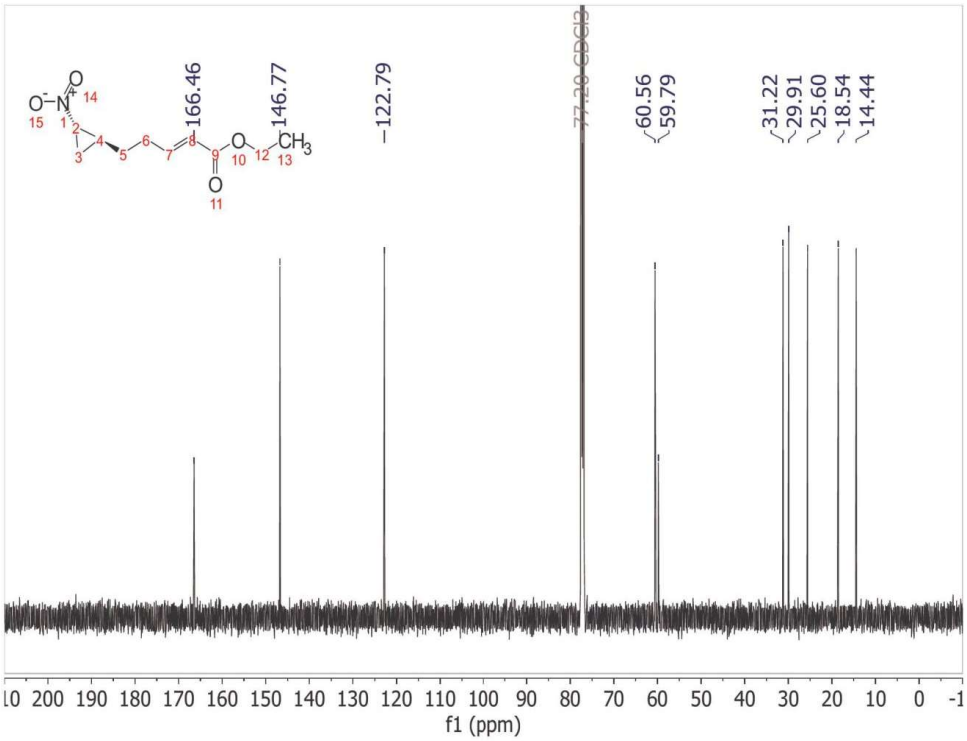
166.46
146.77
122.79
77.20 CDCl3
60.56
59.79
31.22
29.91
25.60
18.54
14.44
f1 (ppm)

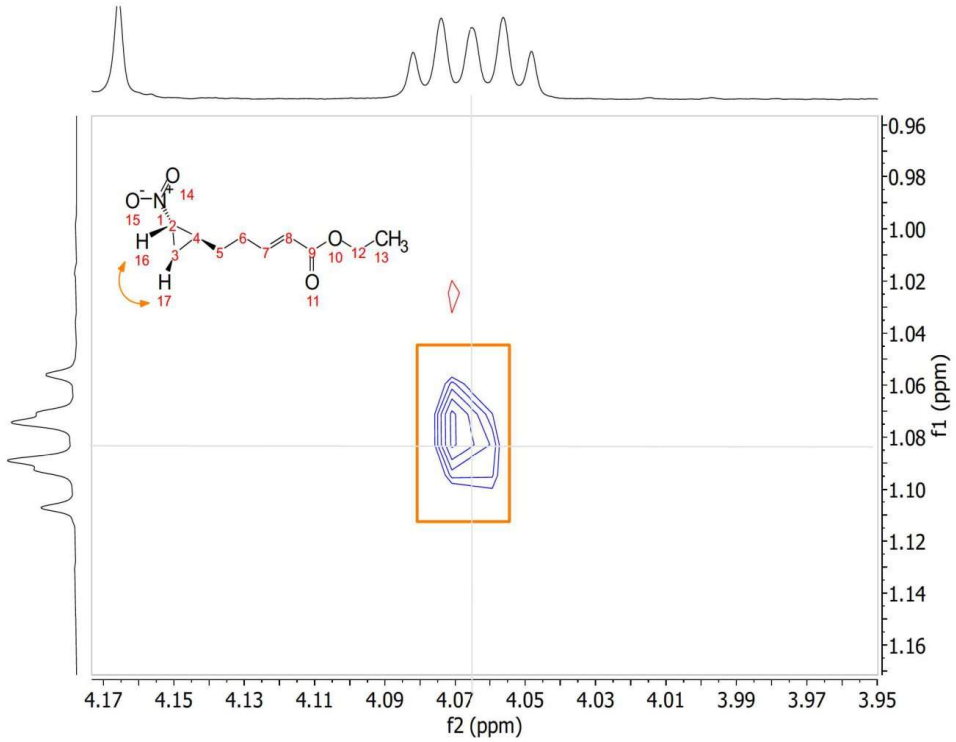
0.96
0.98
1.00
1.02
1.04
1.06
1.08
1.10
1.12
1.14
1.16
f1 (ppm)
4.17
4.15
4.13
4.11
4.09
4.07
4.05
4.03
4.01
3.99
3.97
3.95
f2 (ppm)

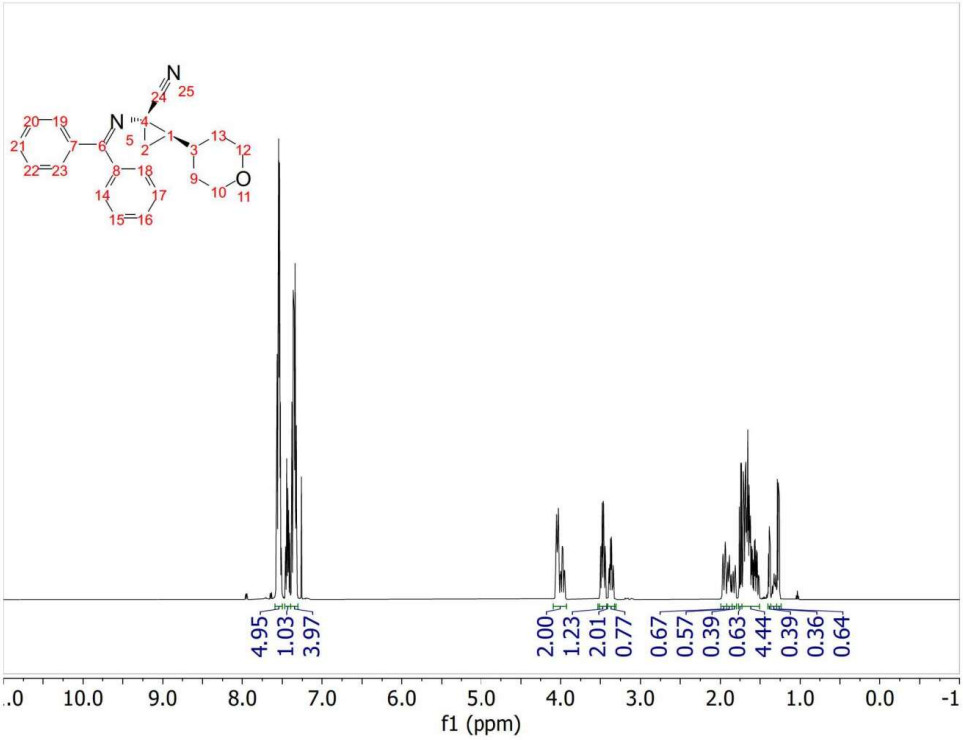
4.95
1.03
3.97
2.00
1.23
2.01
0.77
0.67
0.57
0.39
0.63
4.44
0.39
0.36
0.64
10.0
9.0
8.0
7.0
6.0
5.0
4.0
3.0
2.0
1.0
0.0
-1
f1 (ppm)

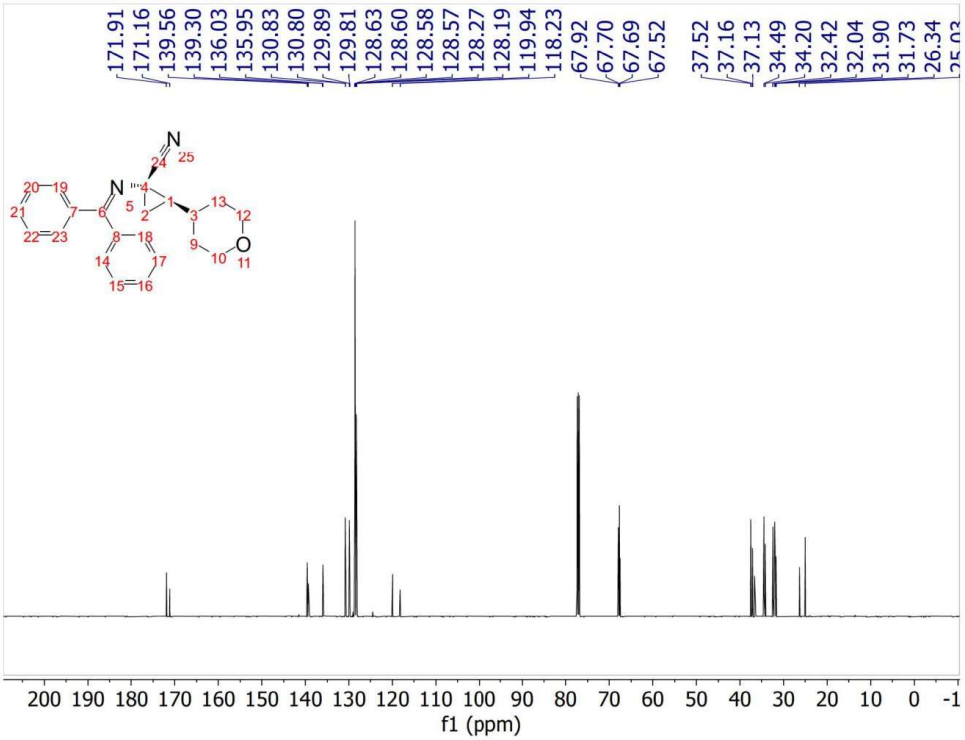
171.91
171.16
139.56
139.30
136.03
135.95
130.83
130.80
129.89
129.81
128.63
128.60
128.58
128.57
128.27
128.19
119.94
118.23
67.92
67.70
67.69
67.52
37.52
37.16
37.13
34.49
34.20
32.42
32.04
31.90
31.73
26.34
200 190 180 170 160 150 140 130 120 110 100 90 80 70 60 50 40 30 20 10 0 -1
f1 (ppm)

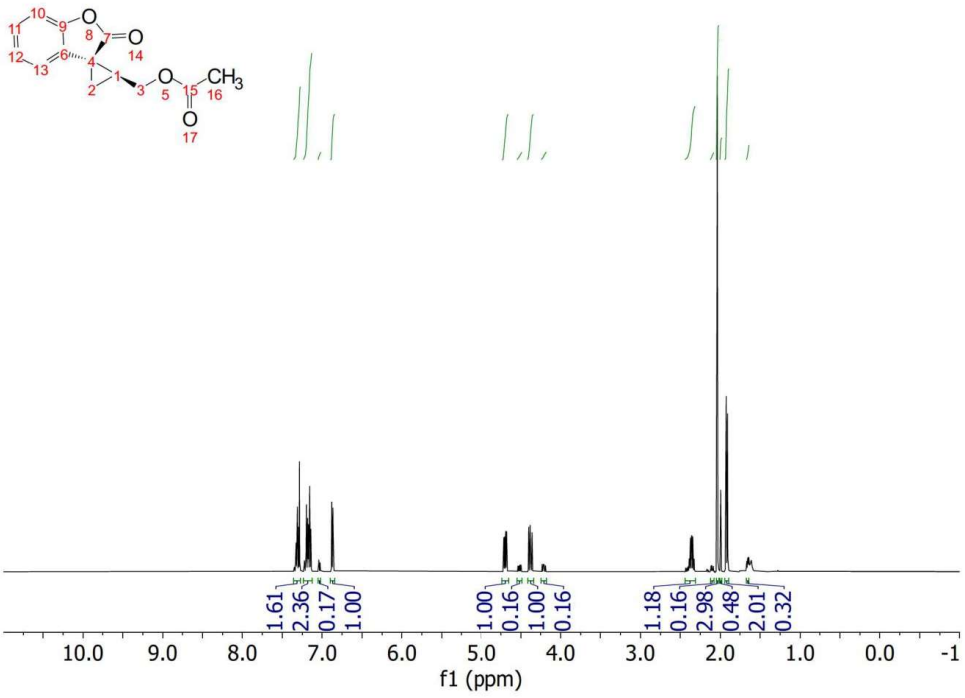
1.61
2.36
0.17
1.00
1.00
0.16
1.00
0.16
1.18
0.16
2.98
0.48
2.01
0.32
10.0 9.0 8.0 7.0 6.0 5.0 4.0 3.0 2.0 1.0 0.0 -1
f1 (ppm)

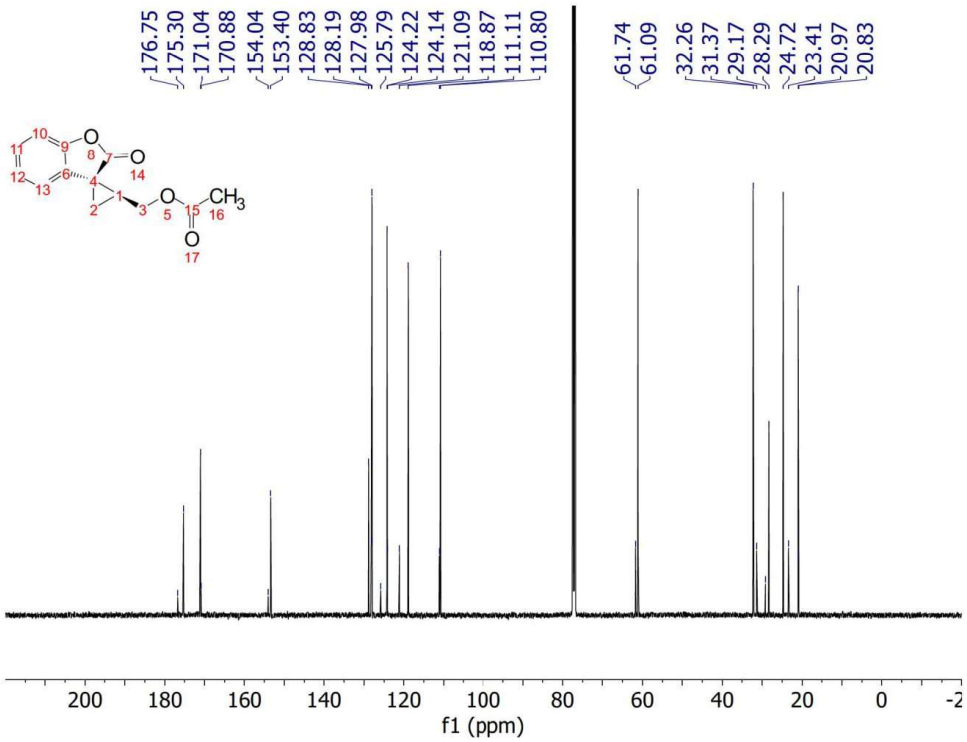
176.75
175.30
171.04
170.88
154.04
153.40
128.83
128.19
127.98
125.79
124.22
124.14
121.09
118.87
111.11
110.80
61.74
61.09
32.26
31.37
29.17
28.29
24.72
23.41
20.97
20.83
200
180
160
140
120
100
80
60
40
20
0
f1 (ppm)

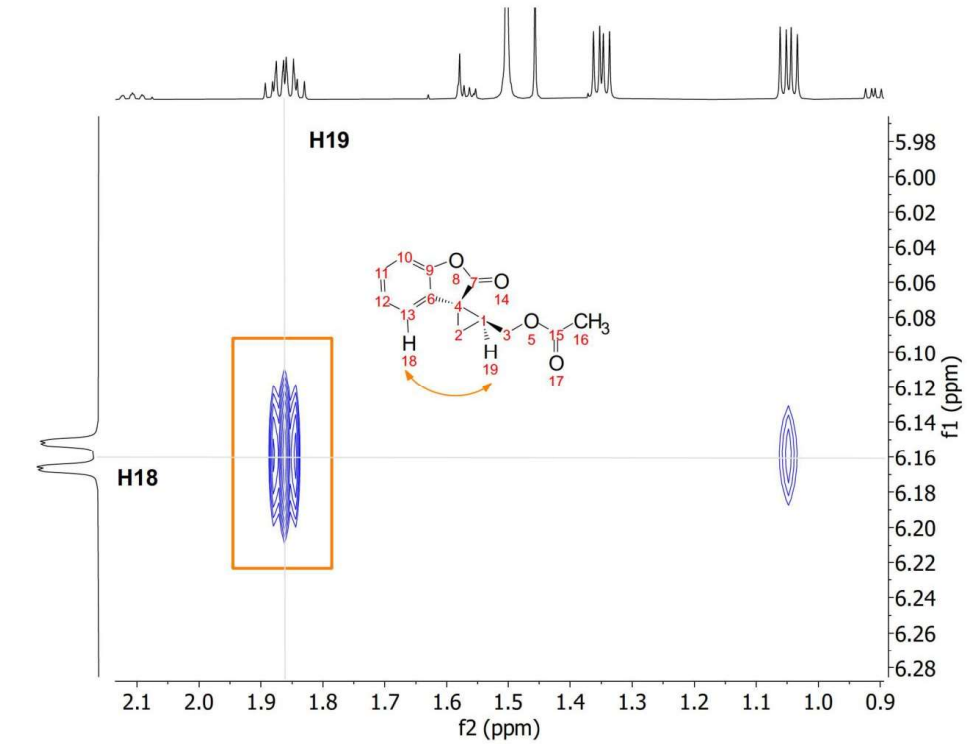
H19
H18
5.98
6.00
6.02
6.04
6.06
6.08
6.10
6.12
6.14
6.16
6.18
6.20
6.22
6.24
6.26
6.28
f1 (ppm)
2.1
2.0
1.9
1.8
1.7
1.6
1.5
1.4
1.3
1.2
1.1
1.0
0.9
f2 (ppm)

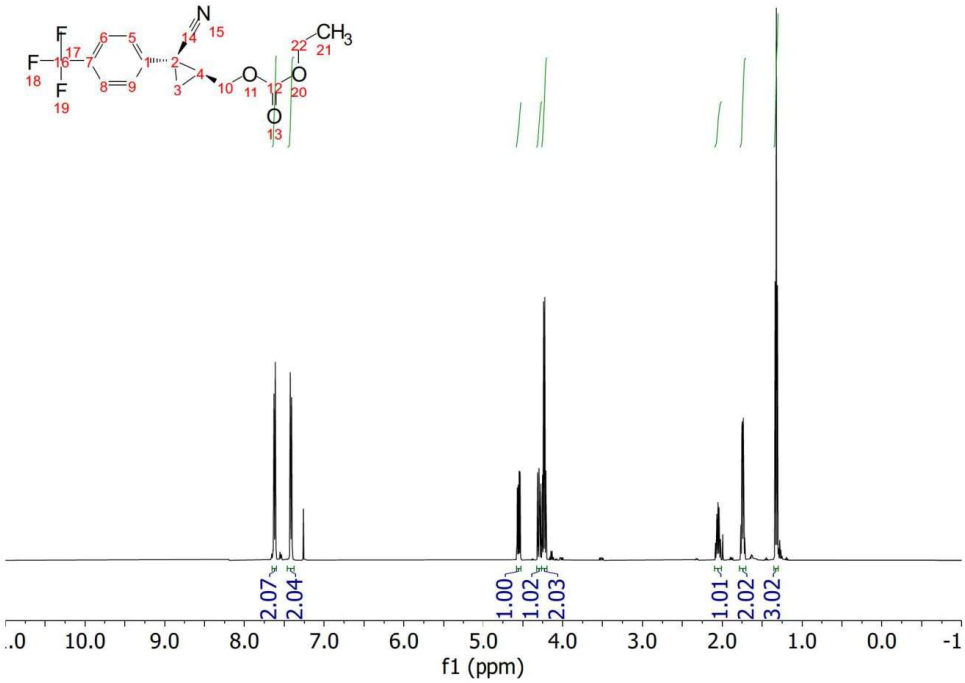
2.07
2.04
1.00
1.02
2.03
1.01
2.02
3.02
f1 (ppm)

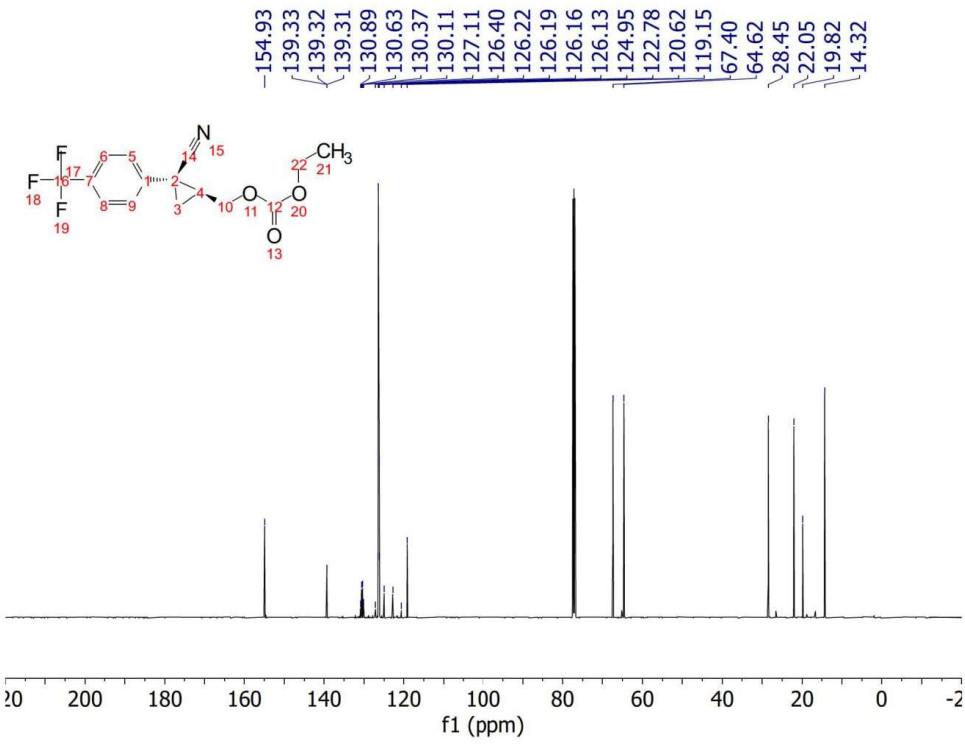
154.93
139.33
139.32
139.31
130.89
130.63
130.37
130.11
127.11
126.40
126.22
126.19
126.16
126.13
124.95
122.78
120.62
119.15
67.40
64.62
28.45
22.05
19.82
14.32
f1 (ppm)

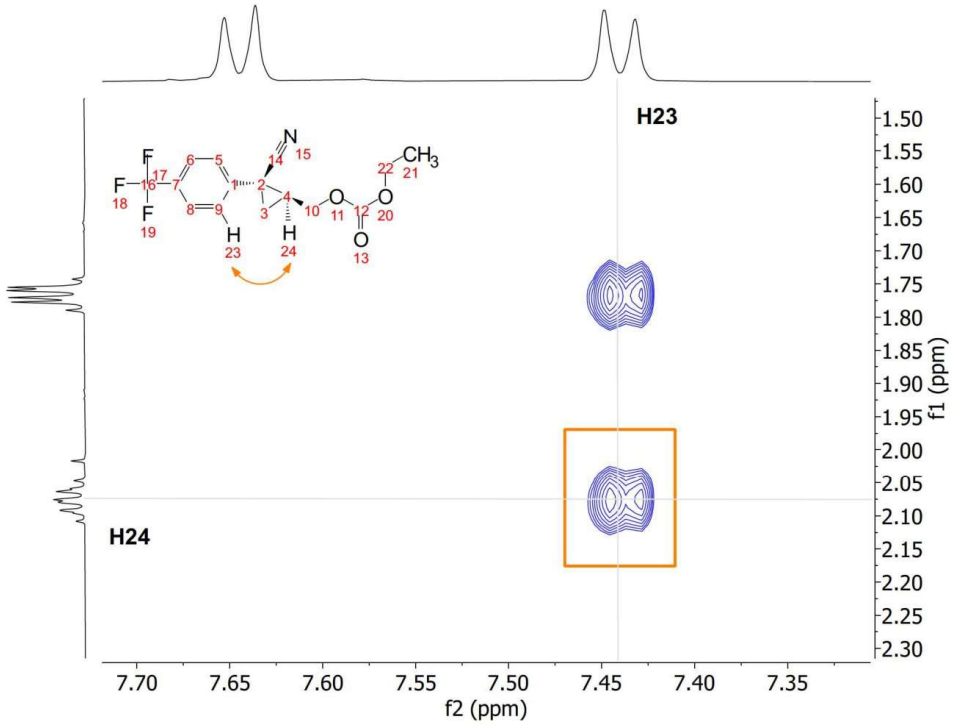
H23
H24
f2 (ppm)
f1 (ppm)

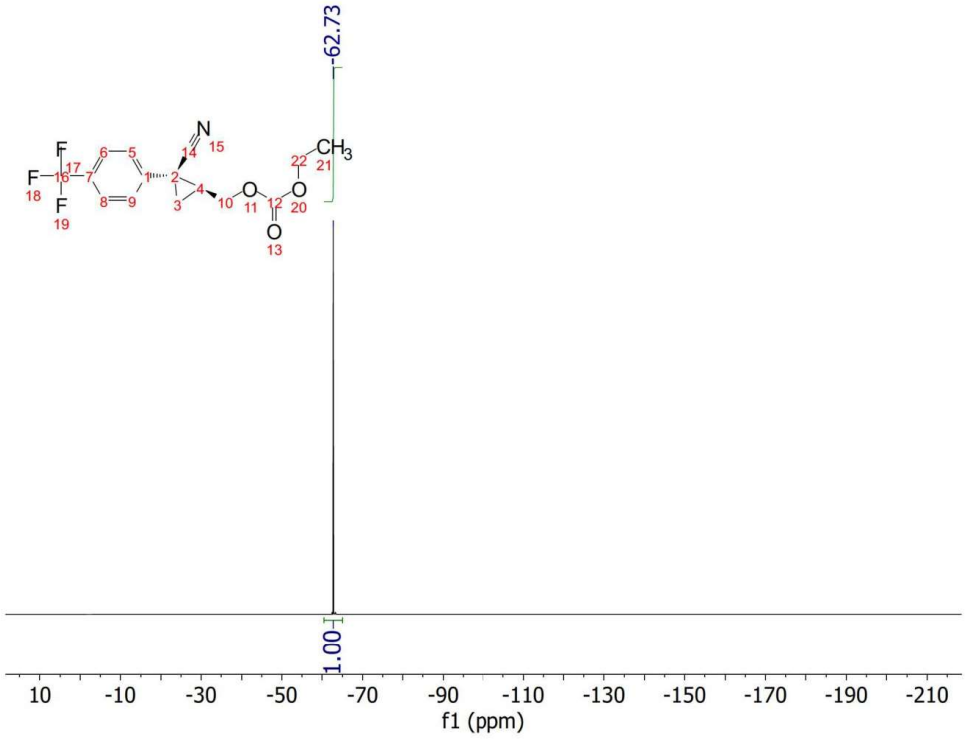
-62.73
1.00
f1 (ppm)

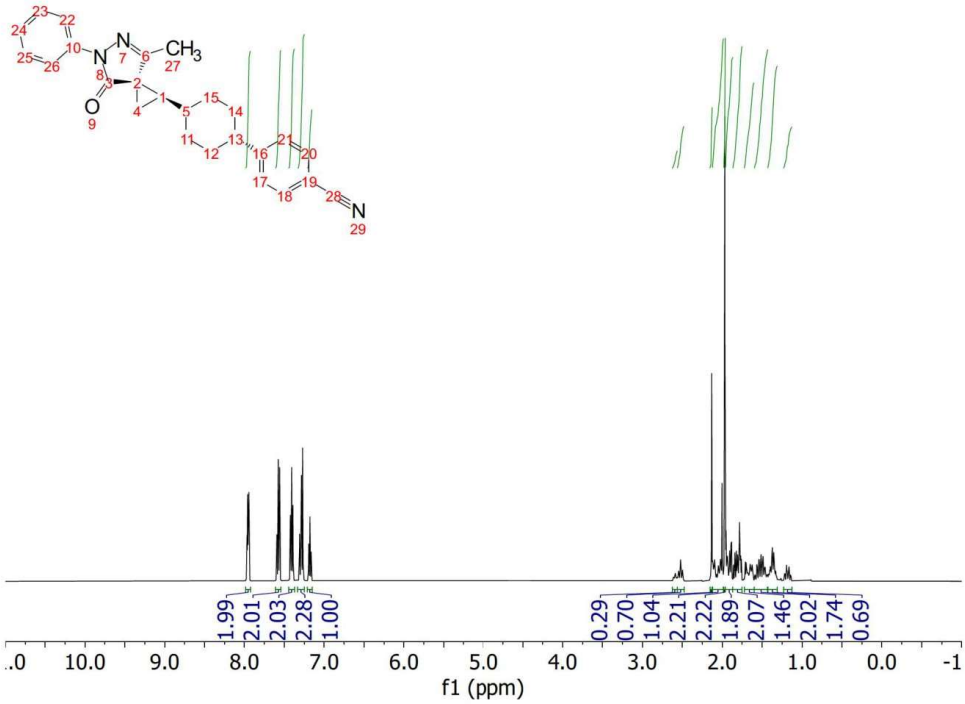
1.99
2.01
2.03
2.28
1.00
0.29
0.70
1.04
2.21
2.22
1.89
2.07
1.46
2.02
1.74
0.69
10.0
9.0
8.0
7.0
6.0
5.0
4.0
3.0
2.0
1.0
0.0
f1 (ppm)

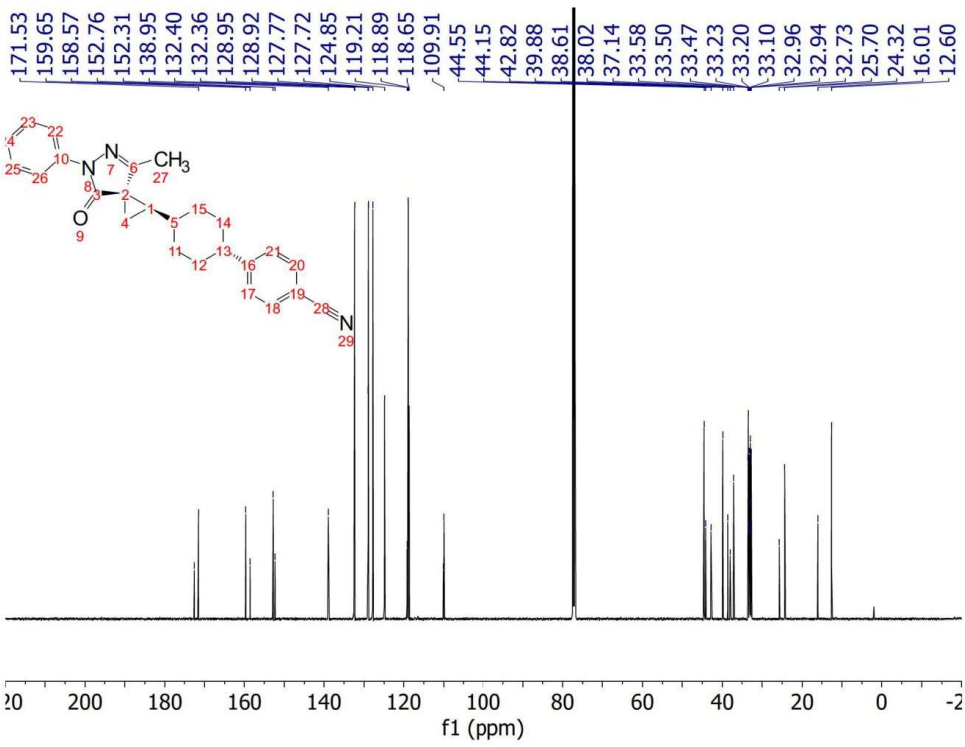
171.53
159.65
158.57
152.76
152.31
138.95
132.40
132.36
128.95
128.92
127.77
127.72
124.85
119.21
118.89
118.65
109.91
44.55
44.15
42.82
39.88
38.61
38.02
37.14
33.58
33.50
33.47
33.23
33.20
33.10
32.96
32.94
32.73
25.70
24.32
16.01
12.60
200
180
160
140
120
100
80
60
40
20
0
f1 (ppm)

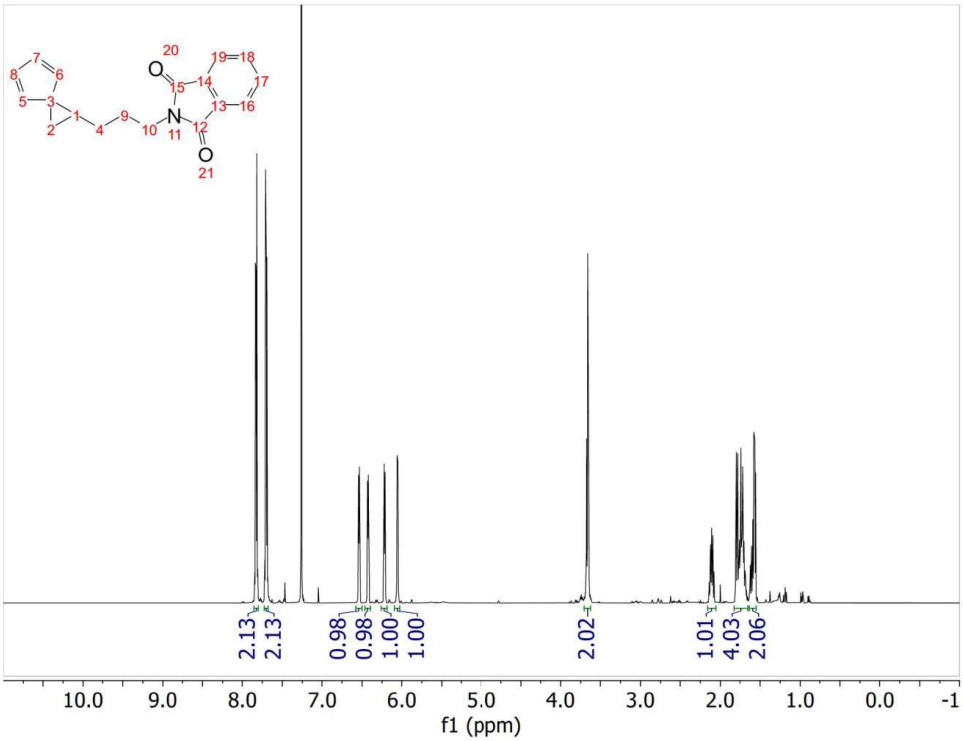
2.13
2.13
0.98
0.98
1.00
1.00
2.02
1.01
4.03
2.06
10.0 9.0 8.0 7.0 6.0 5.0 4.0 3.0 2.0 1.0 0.0 -1
f1 (ppm)

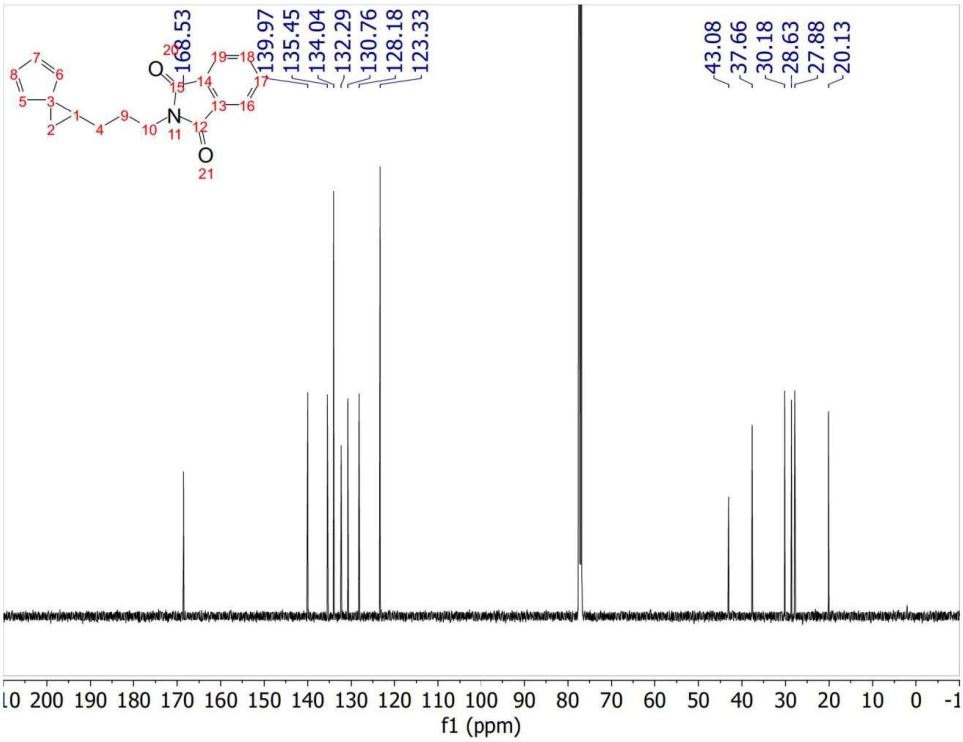
168.53
139.97
135.45
134.04
132.29
130.76
128.18
123.33
43.08
37.66
30.18
28.63
27.88
20.13
10 200 190 180 170 160 150 140 130 120 110 100 90 80 70 60 50 40 30 20 10 0 -1
f1 (ppm)

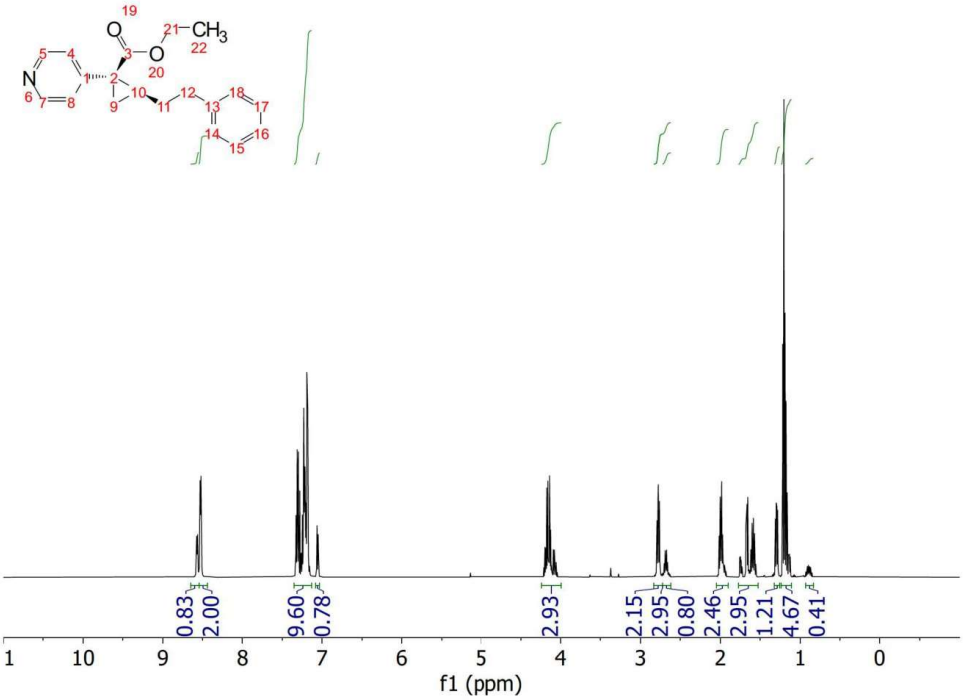
0.83
2.00
9.60
0.78
2.93
2.15
2.95
0.80
2.46
2.95
1.21
4.67
0.41
f1 (ppm)

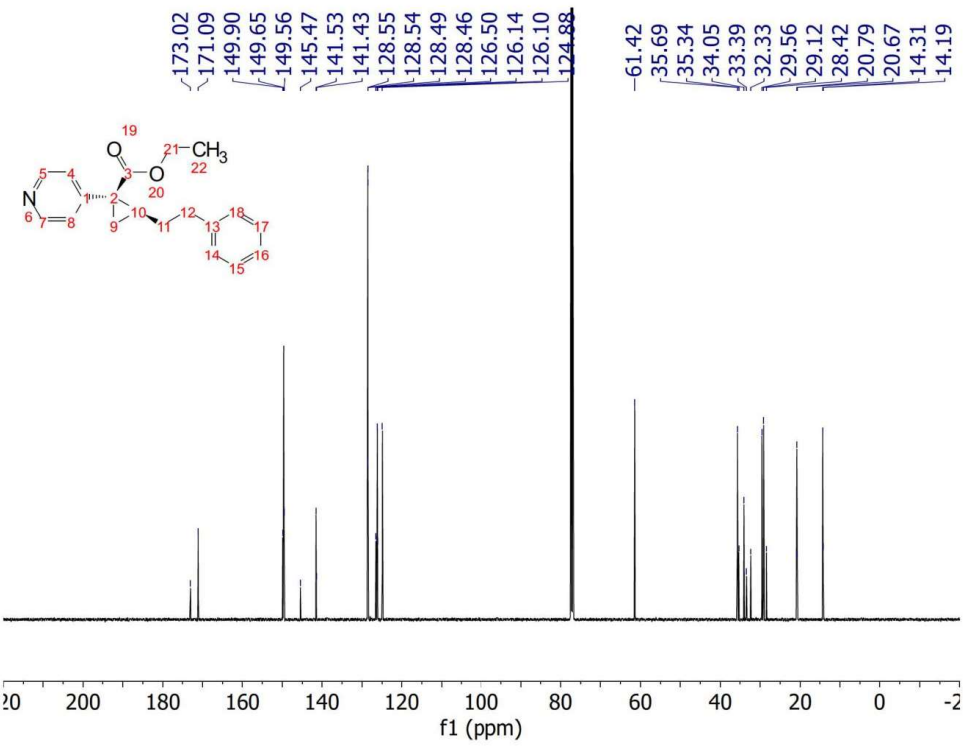
173.02
171.09
149.90
149.65
149.56
145.47
141.53
141.43
128.55
128.54
128.49
128.46
126.50
126.14
126.10
124.88
61.42
35.69
35.34
34.05
33.39
32.33
29.56
29.12
28.42
20.79
20.67
14.31
14.19
f1 (ppm)

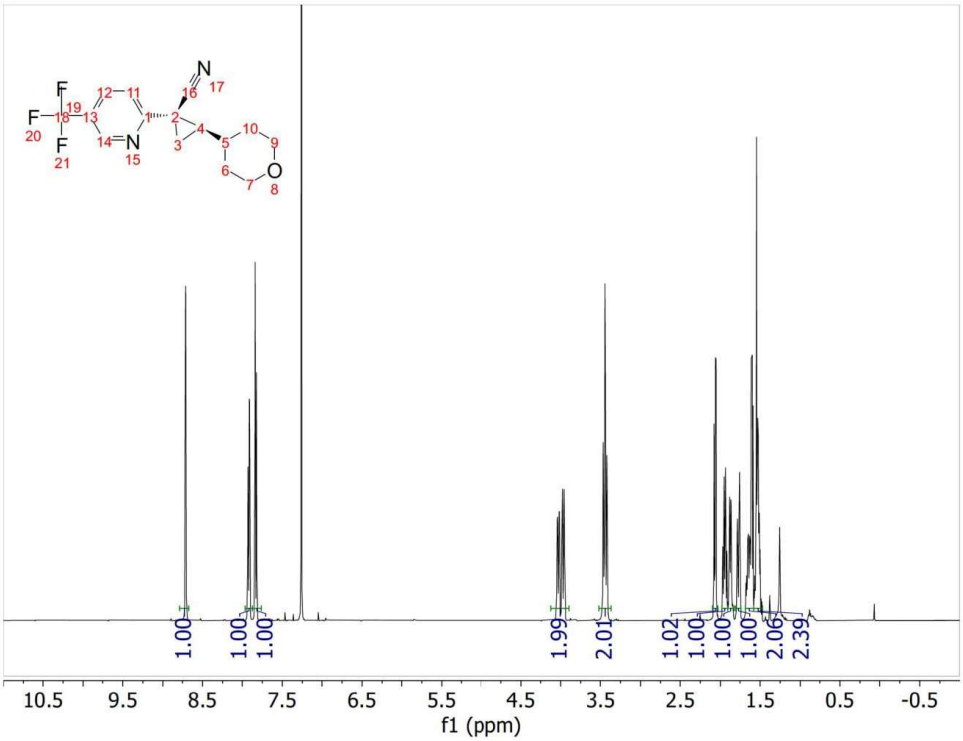
1.00
1.00
1.00
1.99
2.01
1.02
1.00
1.00
1.00
2.06
2.39
10.5
9.5
8.5
7.5
6.5
5.5
4.5
3.5
2.5
1.5
0.5
-0.5
f1 (ppm)

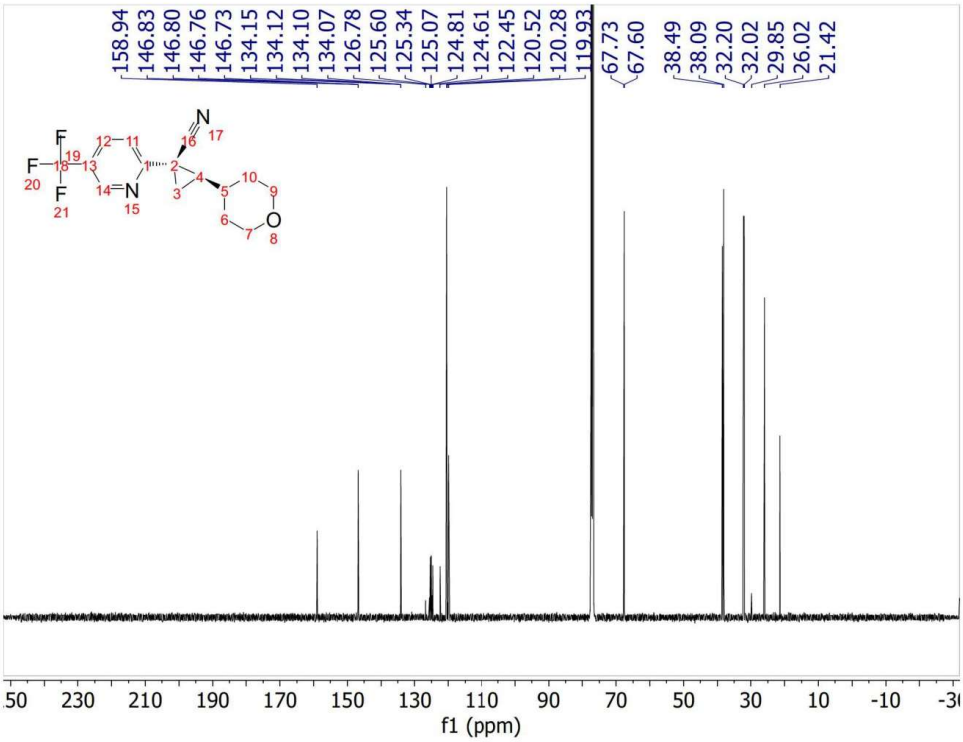
158.94
146.83
146.80
146.76
146.73
134.15
134.12
134.10
134.07
126.78
125.60
125.34
125.07
124.81
124.61
122.45
120.52
120.28
119.93
67.73
67.60
38.49
38.09
32.20
32.02
29.85
26.02
21.42
f1 (ppm)

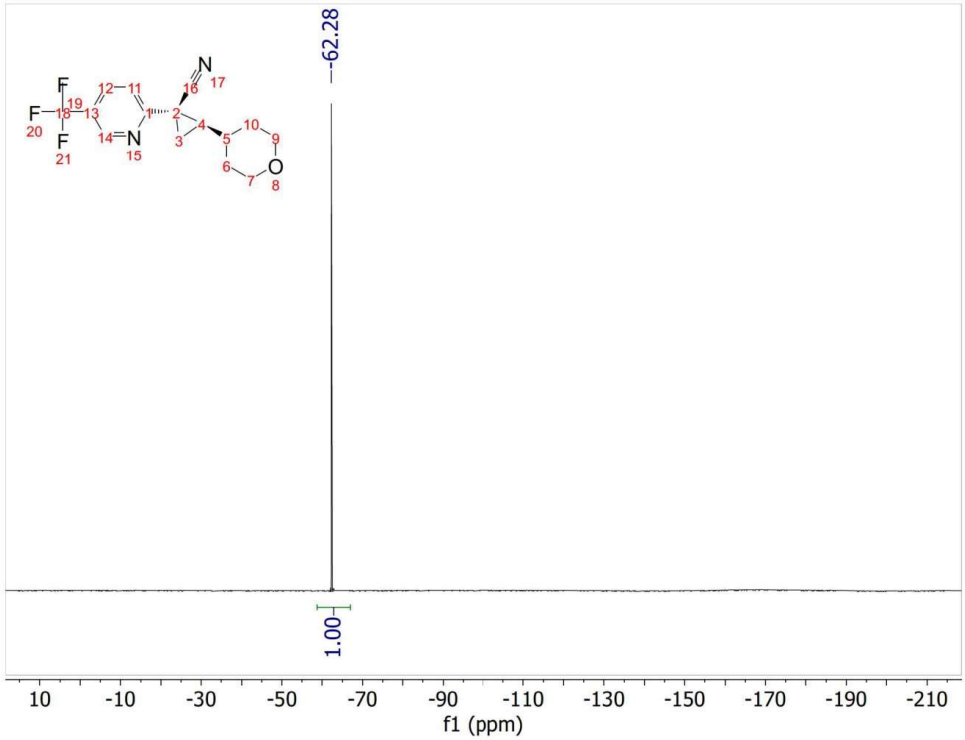
-62.28
1.00
10
-10
-30
-50
-70
-90
-110
-130
-150
-170
-190
-210
f1 (ppm)

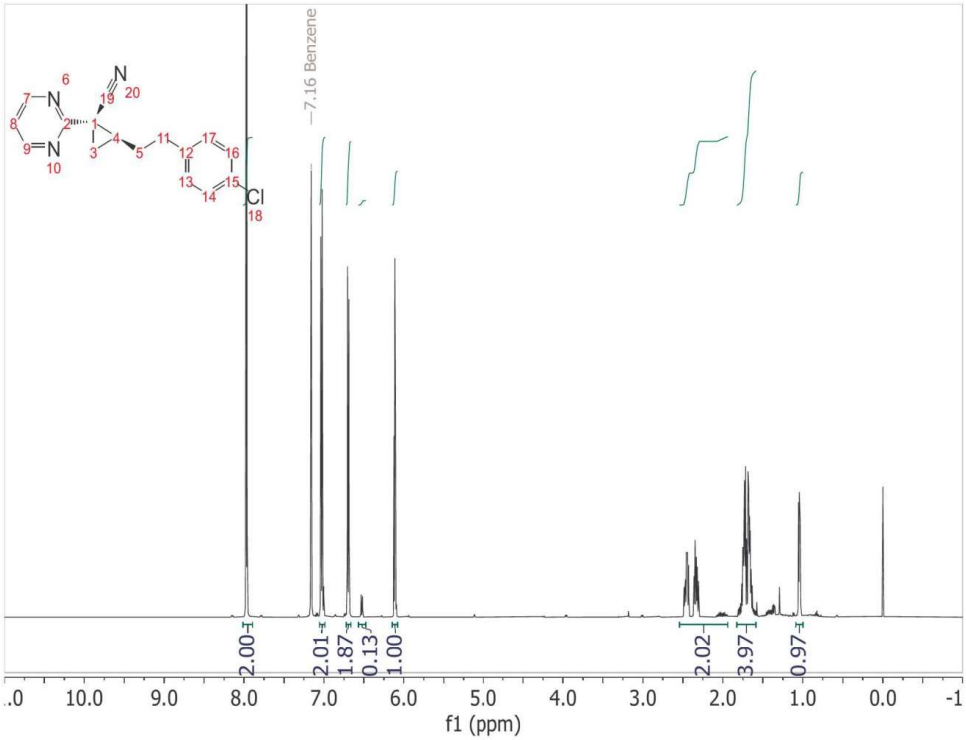
7.16 Benzene
2.00
2.01
1.87
0.13
1.00
2.02
3.97
0.97
10.0
9.0
8.0
7.0
6.0
5.0
4.0
3.0
2.0
1.0
0.0
f1 (ppm)

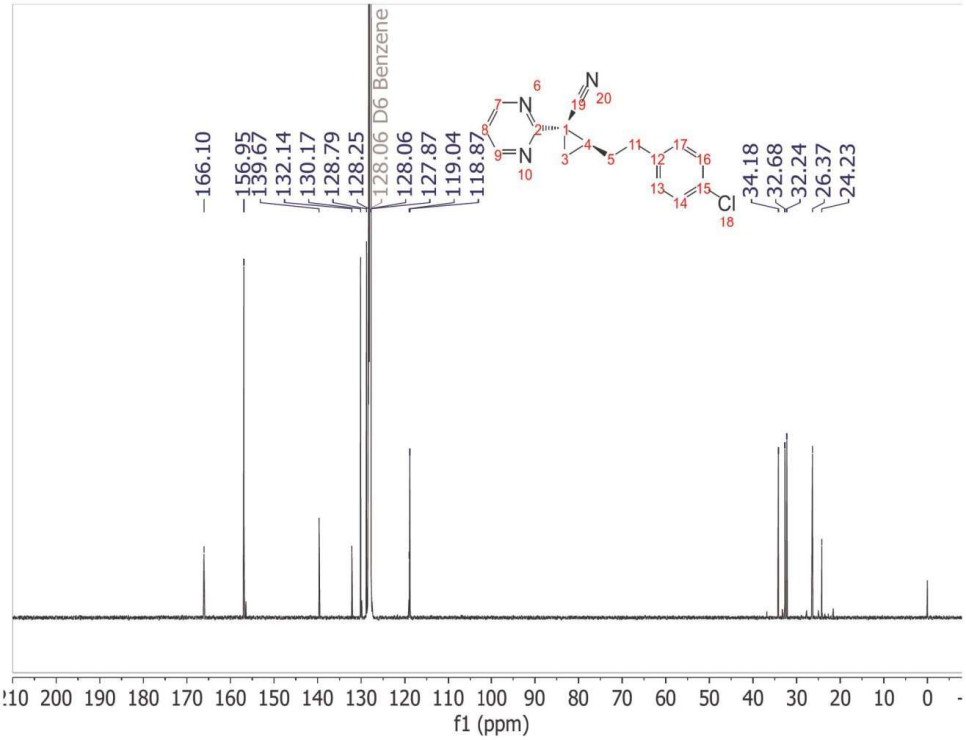
166.10
156.95
139.67
132.14
130.17
128.79
128.25
128.06 D6 Benzene
128.06
127.87
119.04
118.87
34.18
32.68
32.24
26.37
24.23
f1 (ppm)

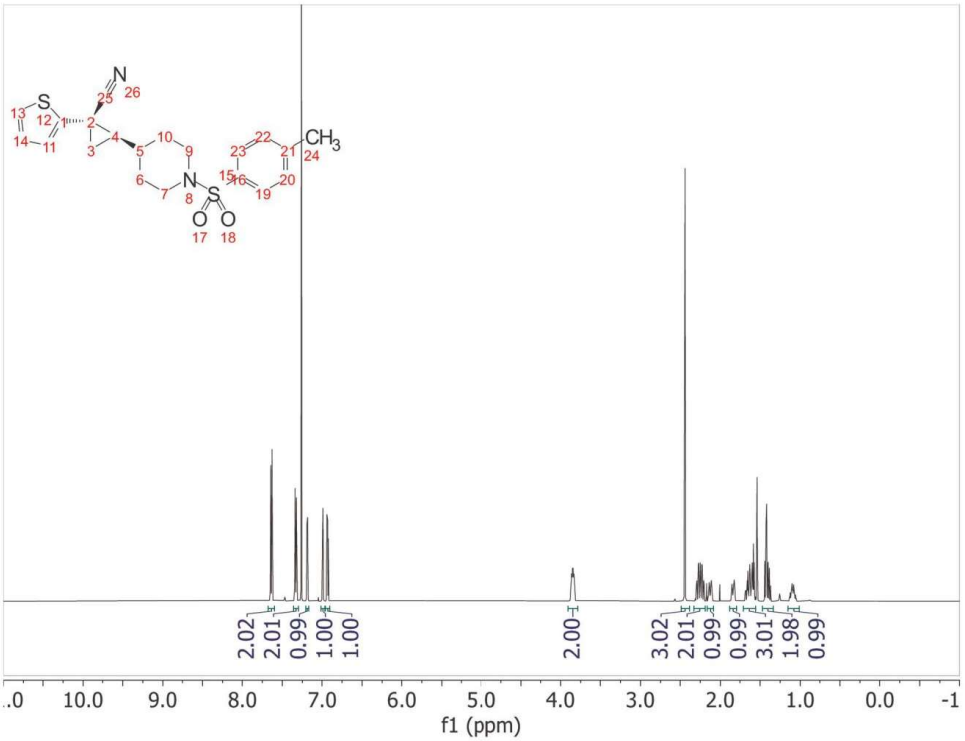
2.02
2.01
0.99
1.00
1.00
2.00
3.02
2.01
0.99
0.99
3.01
1.98
0.99
f1 (ppm)

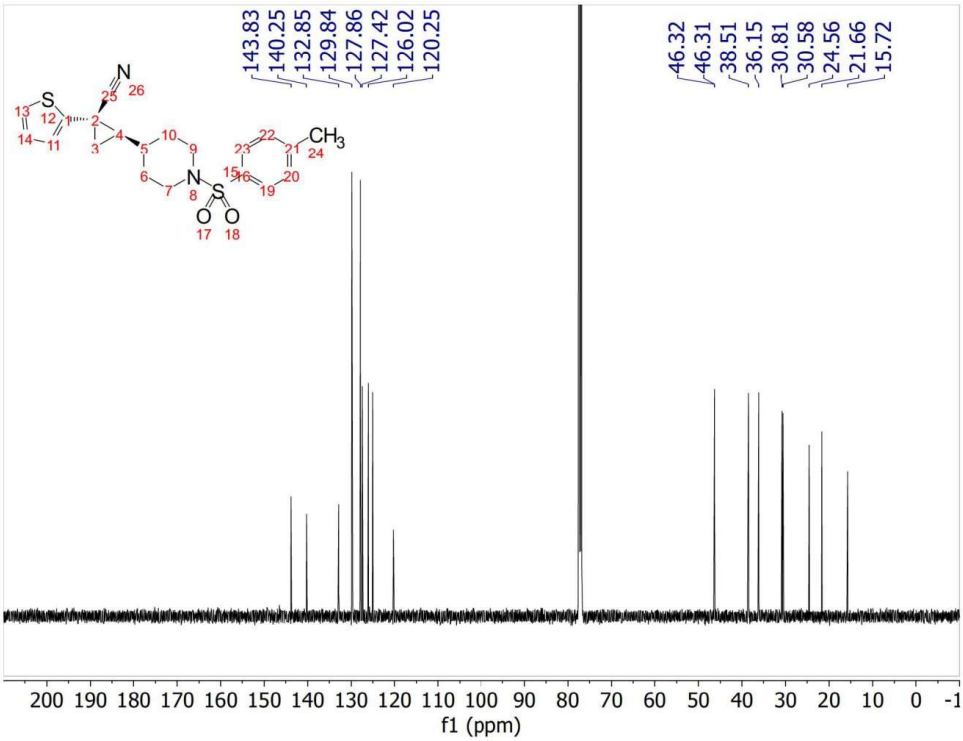
143.83
140.25
132.85
129.84
127.86
127.42
126.02
120.25
46.32
46.31
38.51
36.15
30.81
30.58
24.56
21.66
15.72
200 190 180 170 160 150 140 130 120 110 100 90 80 70 60 50 40 30 20 10 0 -1
f1 (ppm)

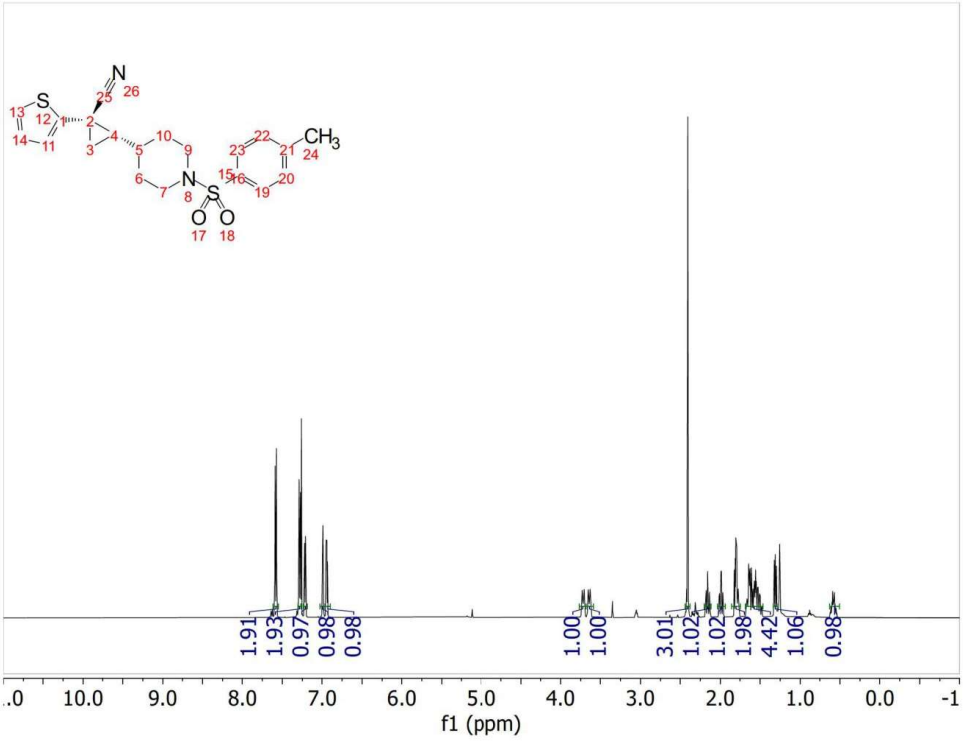
1.91
1.93
0.97
0.98
0.98
1.00
1.00
3.01
1.02
1.02
1.98
4.42
1.06
0.98
.0 10.0 9.0 8.0 7.0 6.0 5.0 4.0 3.0 2.0 1.0 0.0 -1
f1 (ppm)

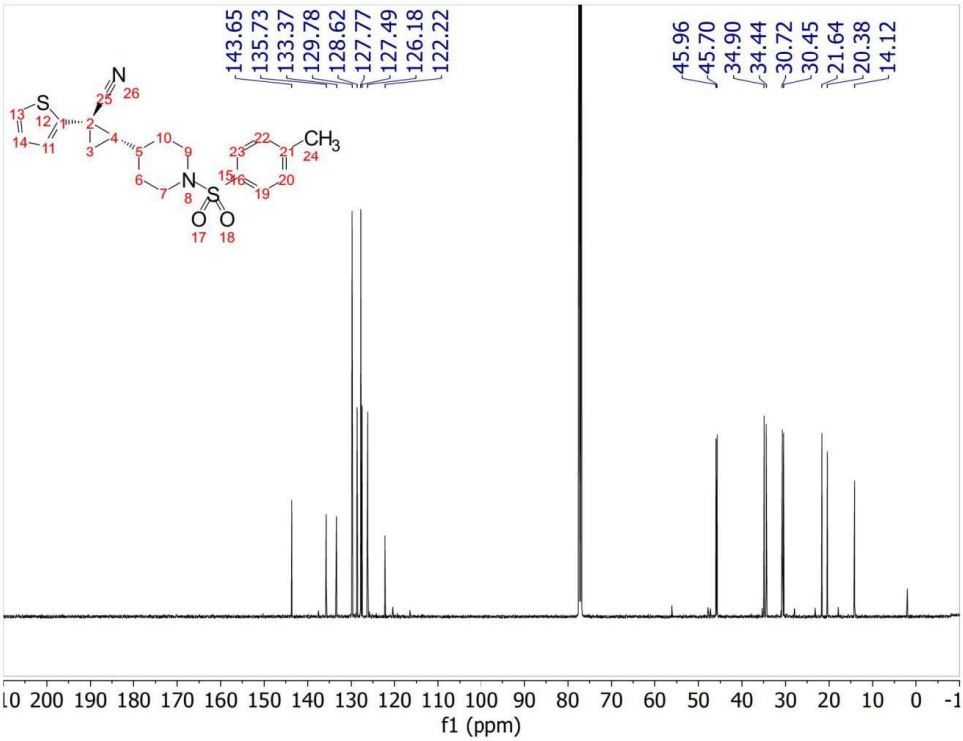
143.65
135.73
133.37
129.78
128.62
127.77
127.49
126.18
122.22
45.96
45.70
34.90
34.44
30.72
30.45
21.64
20.38
14.12
f1 (ppm)

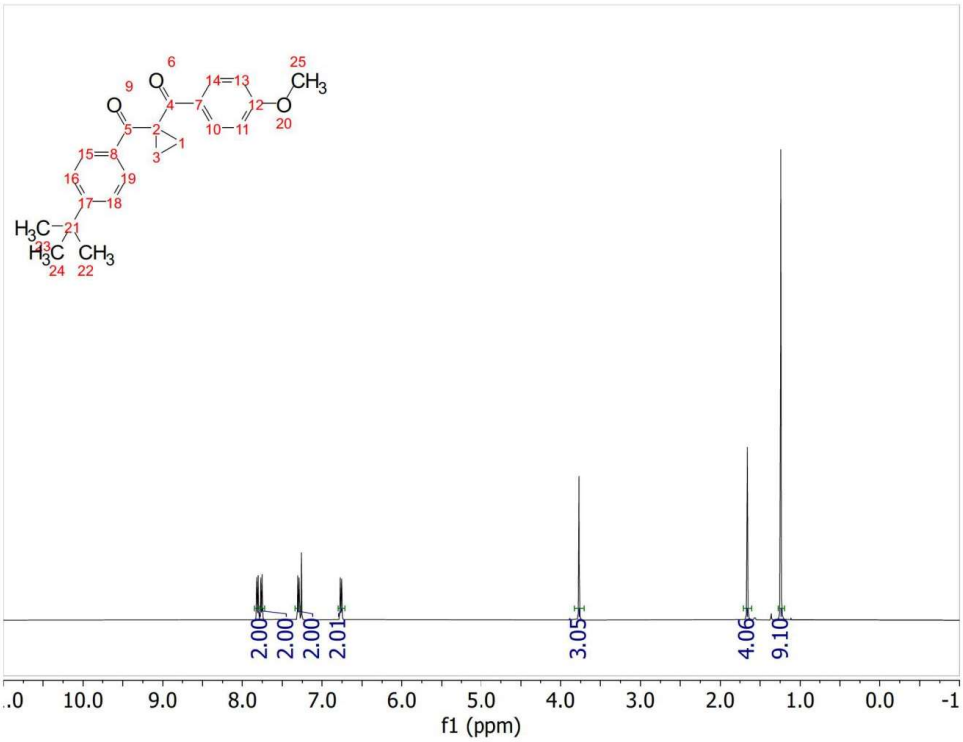
2.00
2.00
2.00
2.01
3.05
4.06
9.10
f1 (ppm)

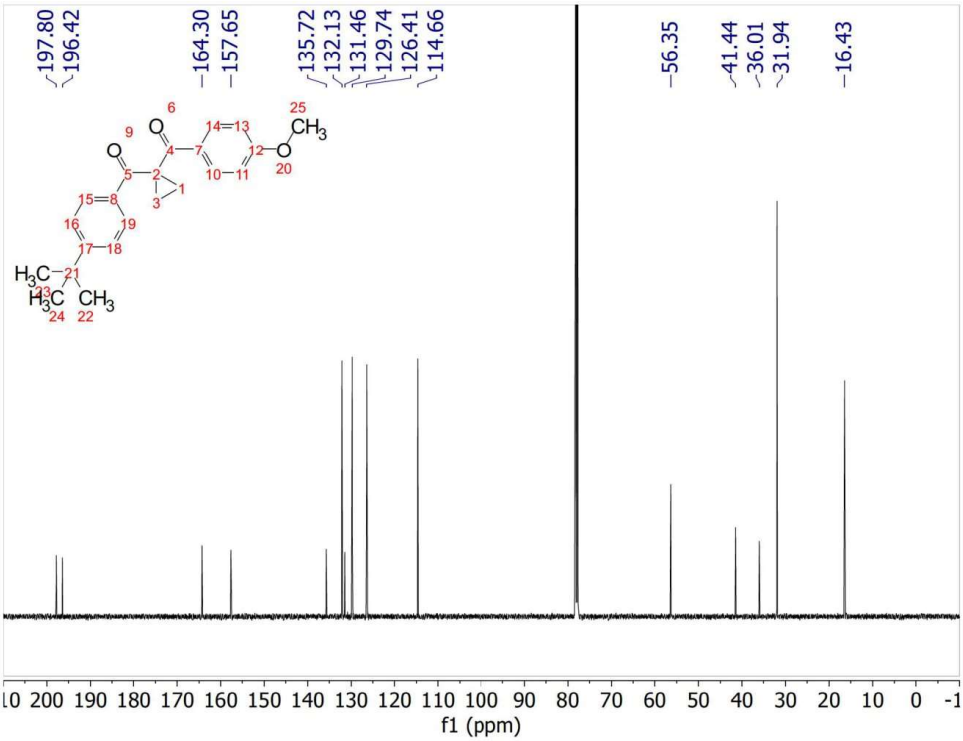
197.80
196.42
164.30
157.65
135.72
132.13
131.46
129.74
126.41
114.66
56.35
41.44
36.01
31.94
16.43
f1 (ppm)

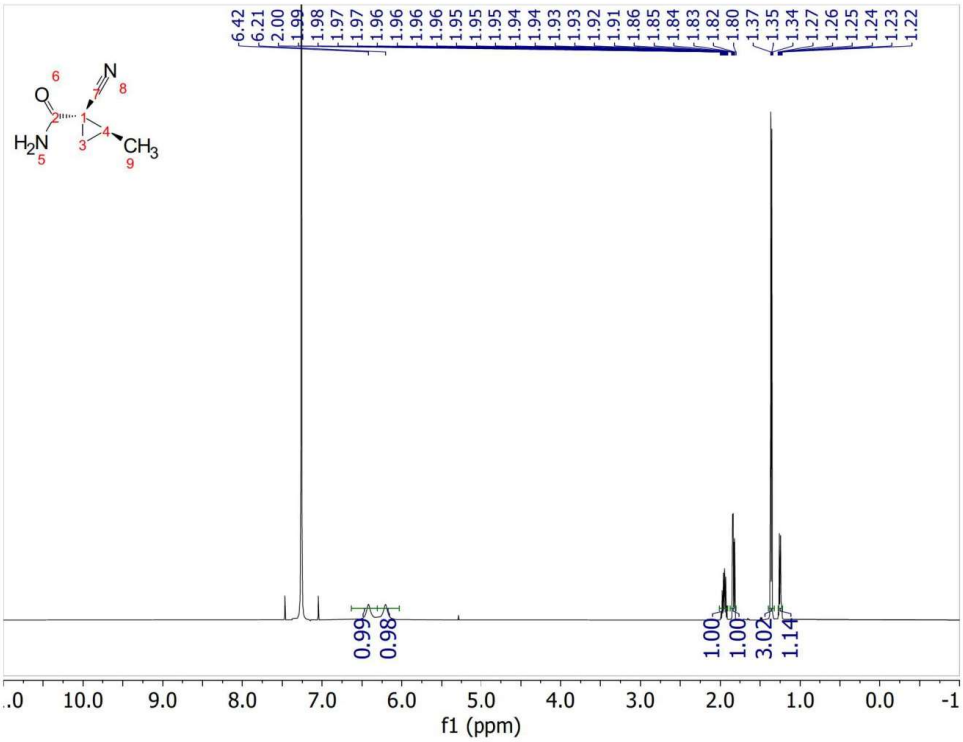
6.42
6.21
2.00
1.99
1.98
1.97
1.97
1.96
1.96
1.96
1.96
1.95
1.95
1.95
1.94
1.94
1.93
1.93
1.92
1.91
1.86
1.85
1.84
1.83
1.82
1.80
1.37
1.35
1.34
1.27
1.26
1.25
1.24
1.23
1.22
0.99
0.98
1.00
1.00
3.02
1.14
f1 (ppm)

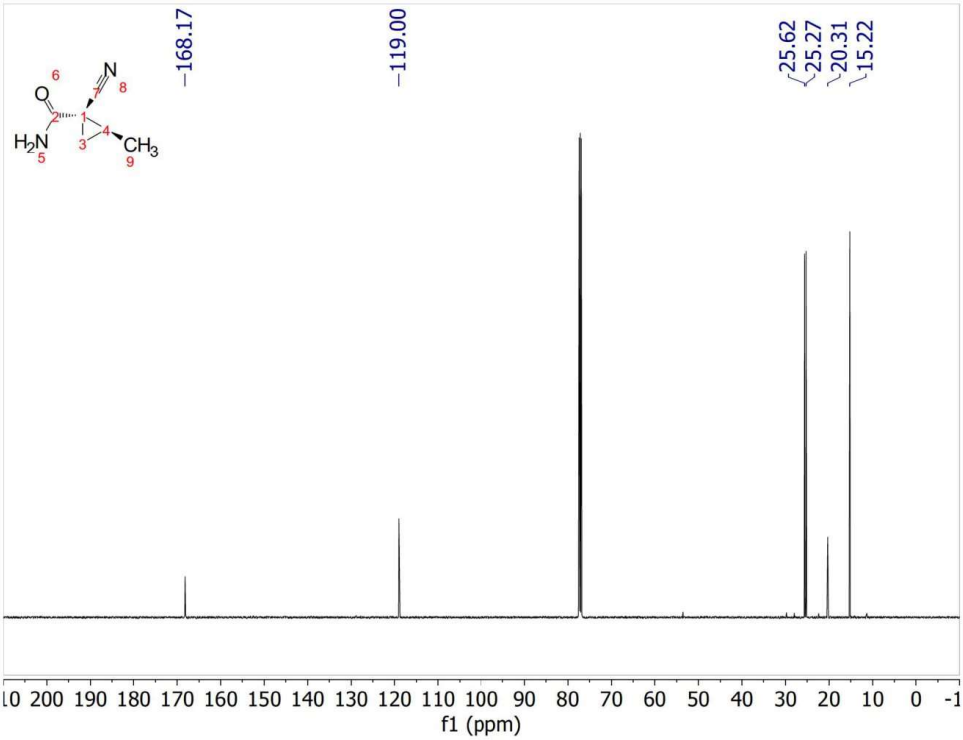
168.17
119.00
25.62
25.27
20.31
15.22
f1 (ppm)

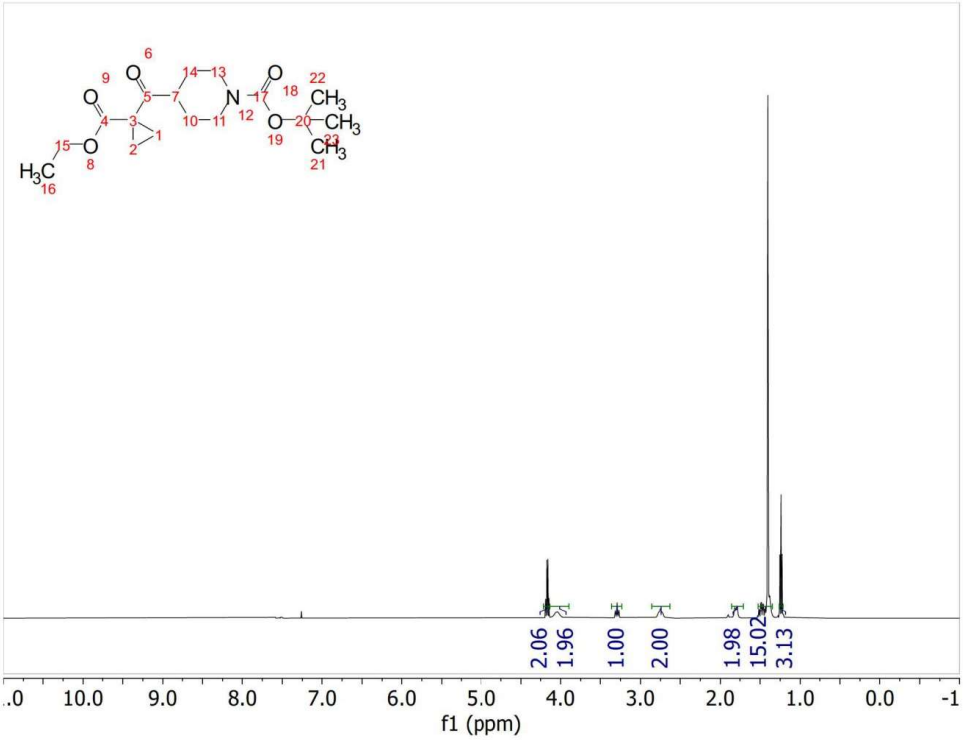
2.06
1.96
1.00
2.00
1.98
15.02
3.13
f1 (ppm)

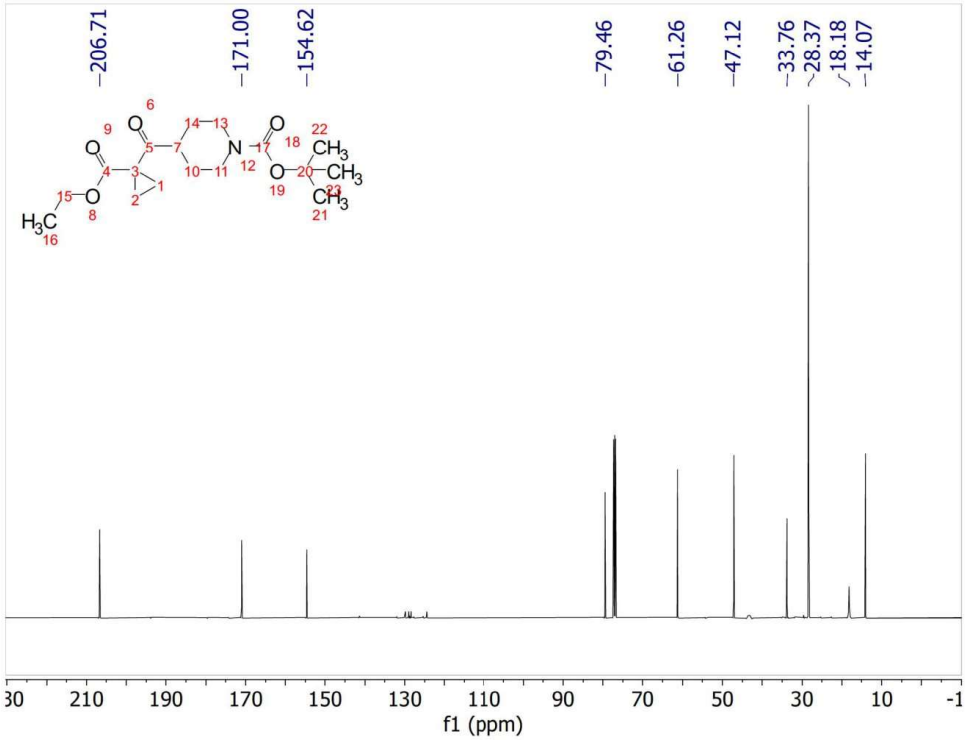
206.71
171.00
154.62
79.46
61.26
47.12
33.76
28.37
18.18
14.07
f1 (ppm)

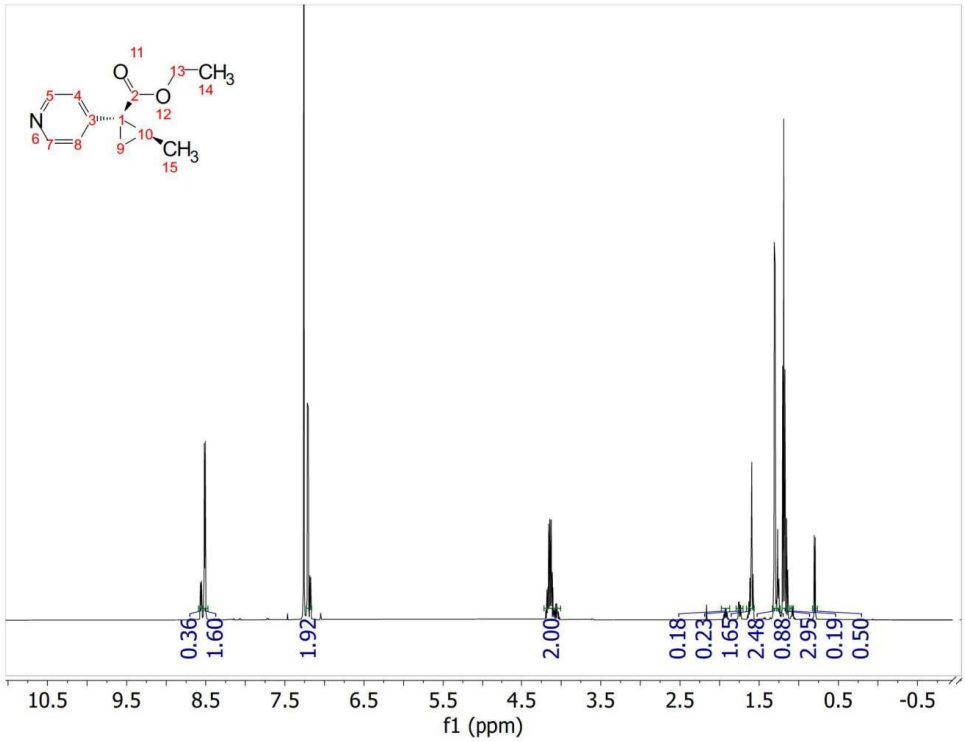
0.36
1.60
1.92
2.00
0.18
0.23
1.65
2.48
0.88
2.95
0.19
0.50
f1 (ppm)

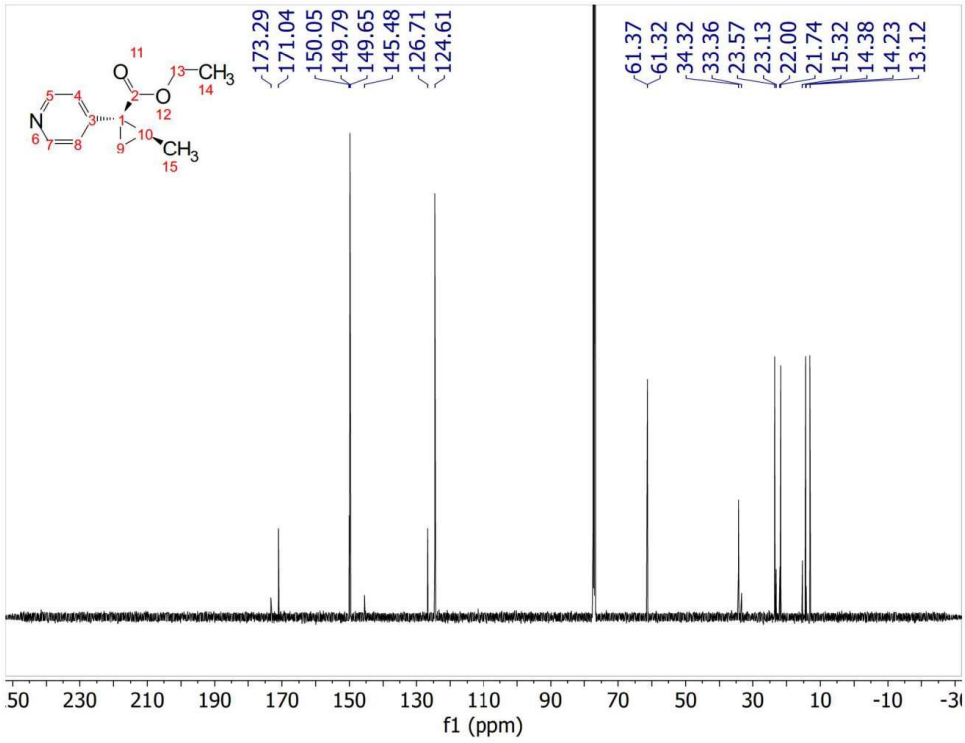
173.29
171.04
150.05
149.79
149.65
145.48
126.71
124.61
61.37
61.32
34.32
33.36
23.57
23.13
22.00
21.74
15.32
14.38
14.23
13.12
f1 (ppm)

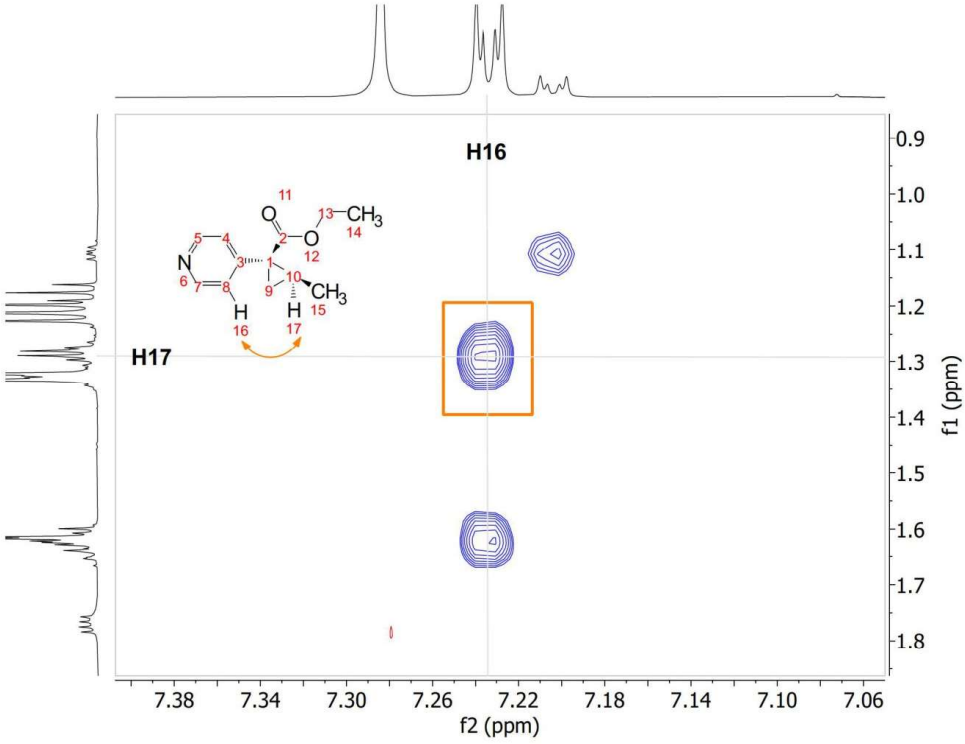
H16
H17
f2 (ppm)
f1 (ppm)

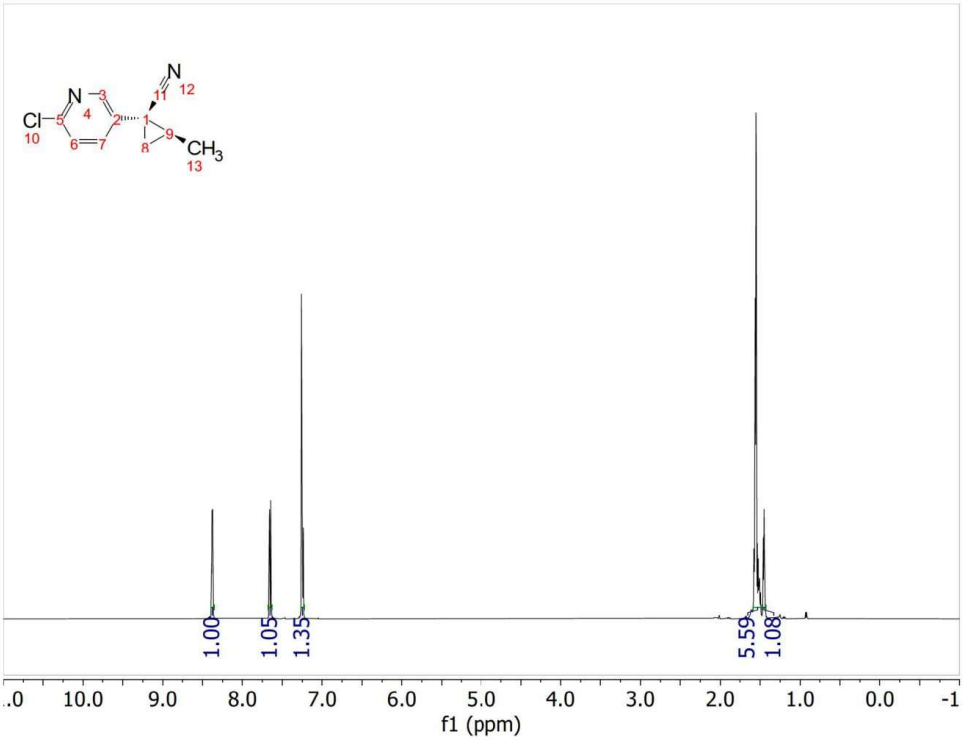
1.00
1.05
1.35
5.59
1.08
f1 (ppm)

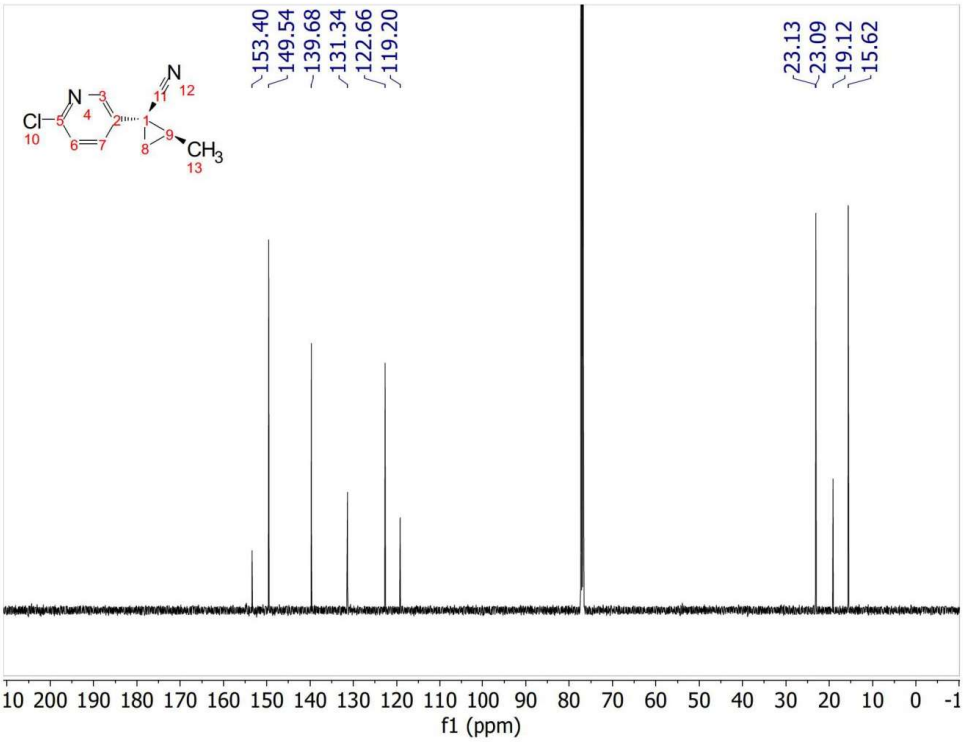
153.40
149.54
139.68
131.34
122.66
119.20
23.13
23.09
19.12
15.62
f1 (ppm)

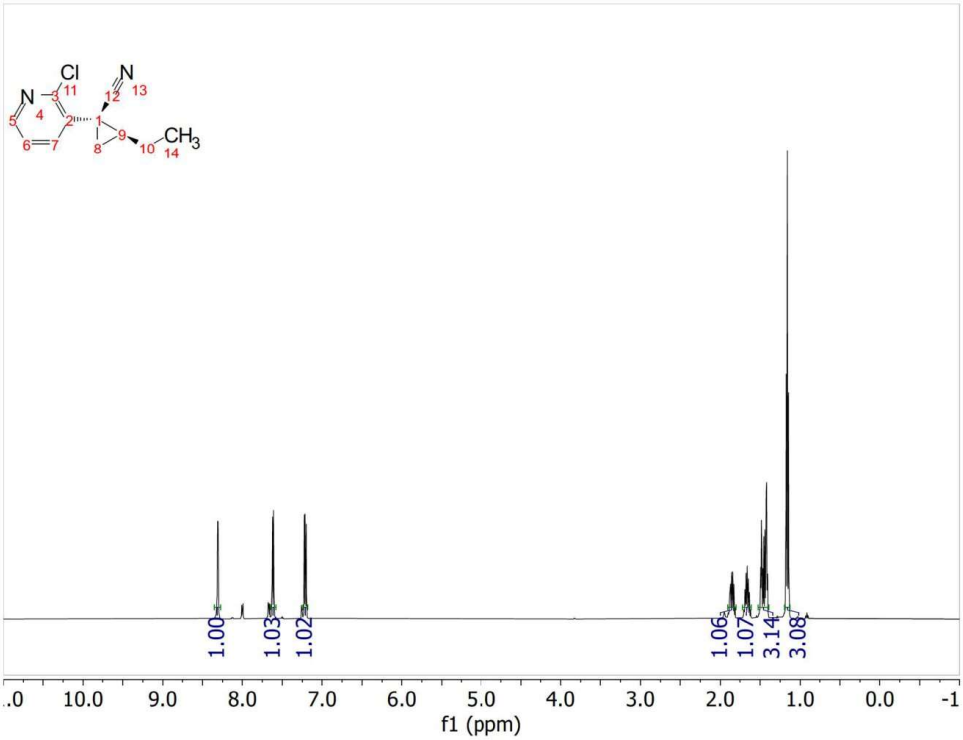
Cl
N
N
CH3
1.00
1.03
1.02
1.06
1.07
3.14
3.08
f1 (ppm)

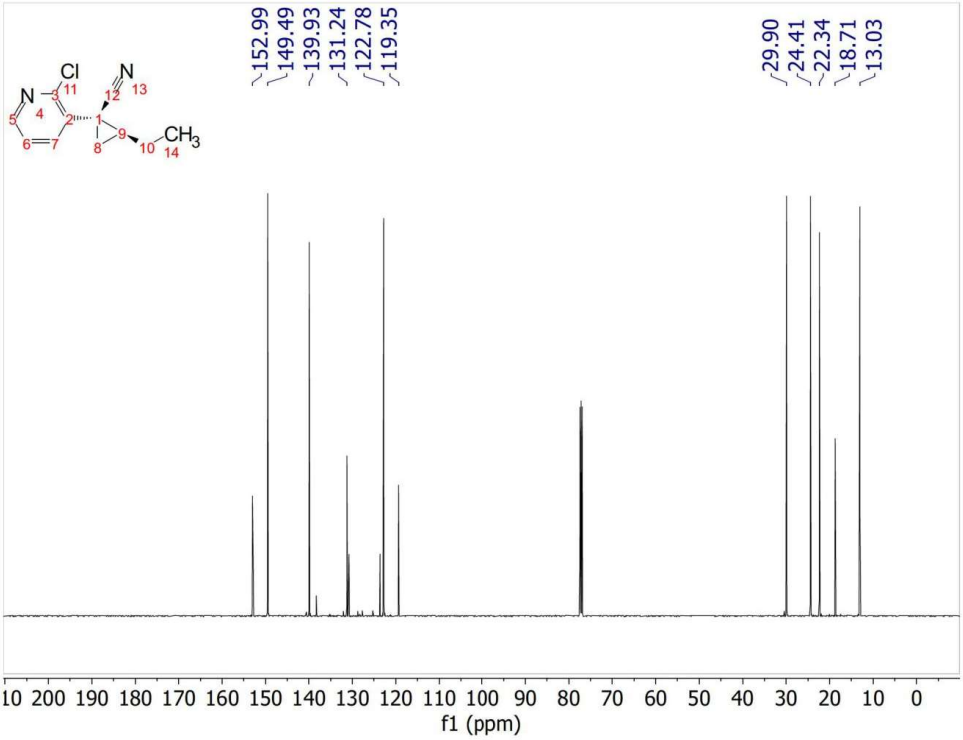
Cl
N
N
CH3
152.99
149.49
139.93
131.24
122.78
119.35
29.90
24.41
22.34
18.71
13.03
f1 (ppm)

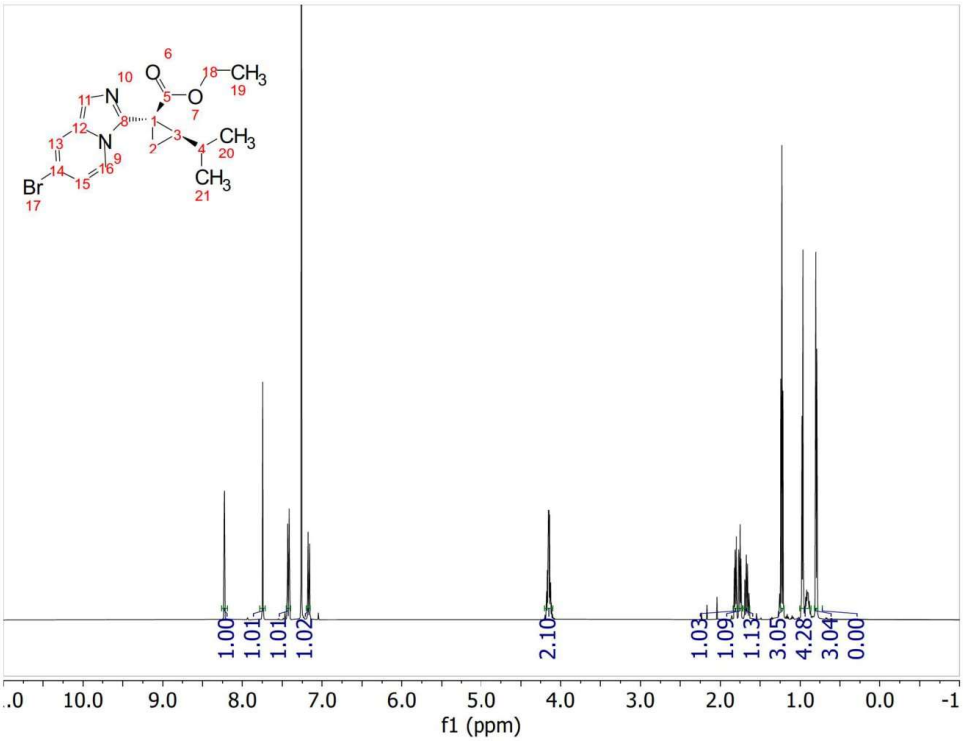
1.00
1.01
1.01
1.02
2.10
1.03
1.09
1.13
3.05
4.28
3.04
0.00
f1 (ppm)

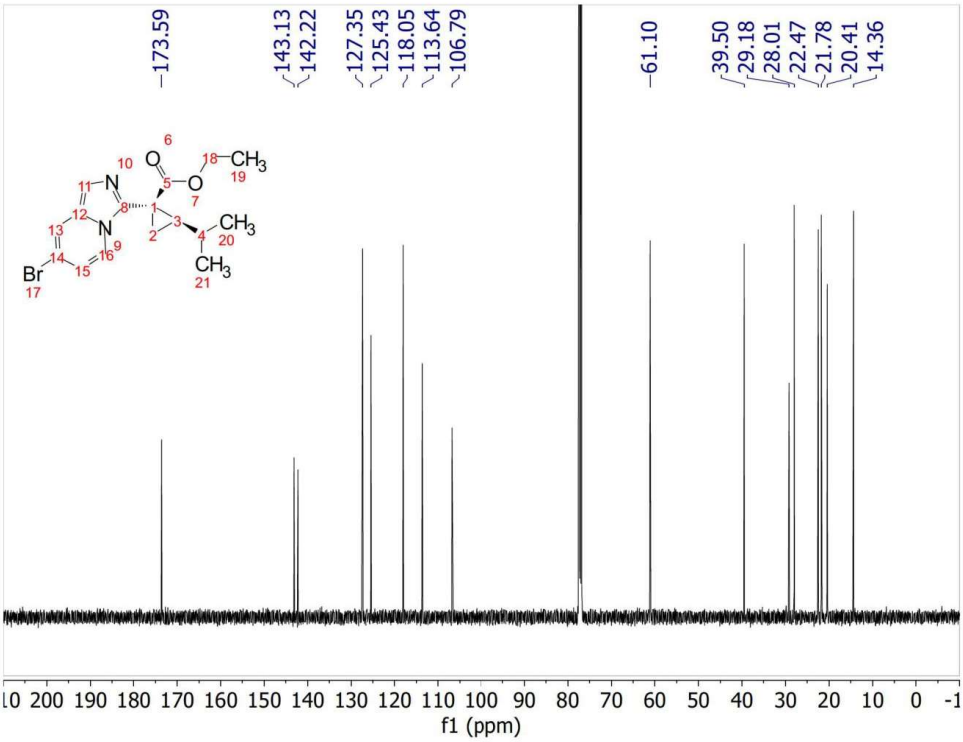
173.59
143.13
142.22
127.35
125.43
118.05
113.64
106.79
61.10
39.50
29.18
28.01
22.47
21.78
20.41
14.36
f1 (ppm)

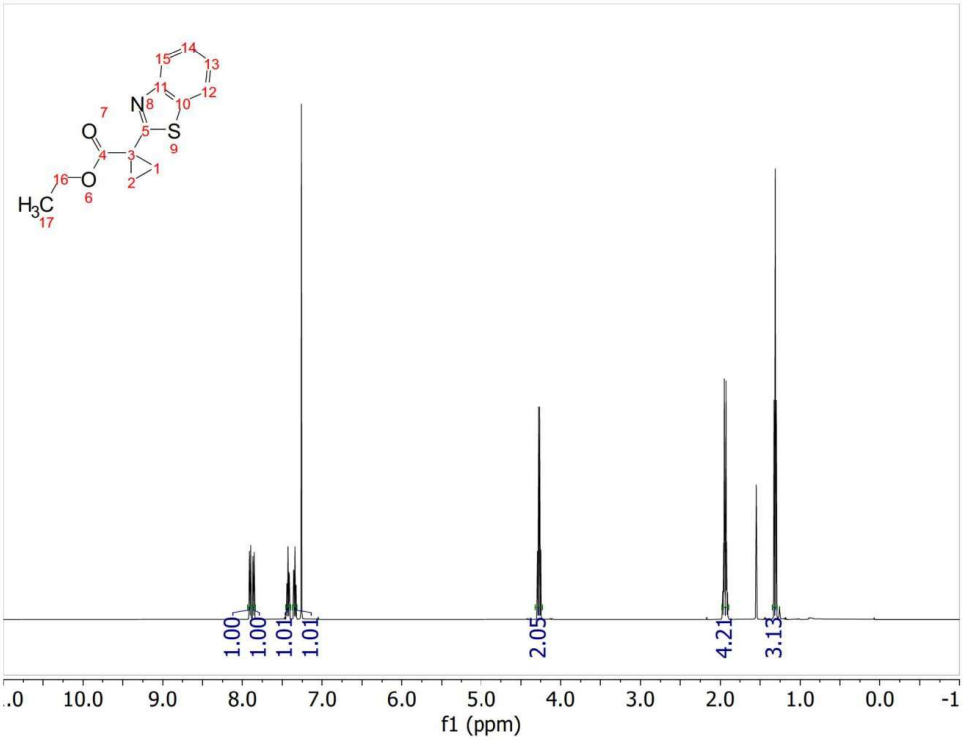
1.00
1.00
1.01
1.01
2.05
4.21
3.13
f1 (ppm)

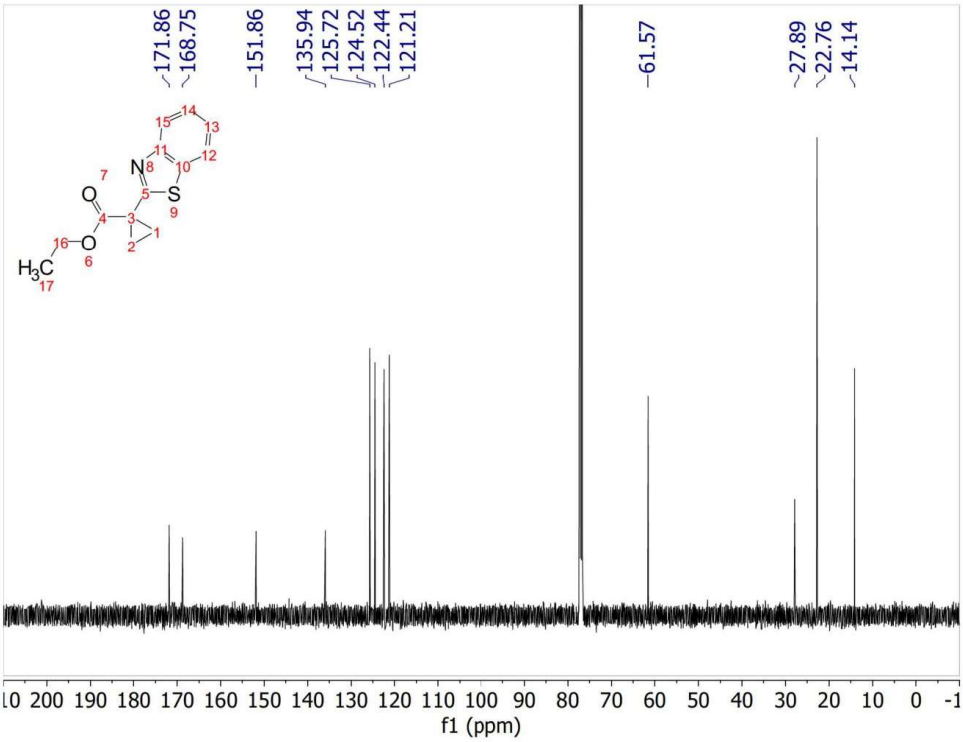
171.86
168.75
151.86
135.94
125.72
124.52
122.44
121.21
61.57
27.89
22.76
14.14
f1 (ppm)

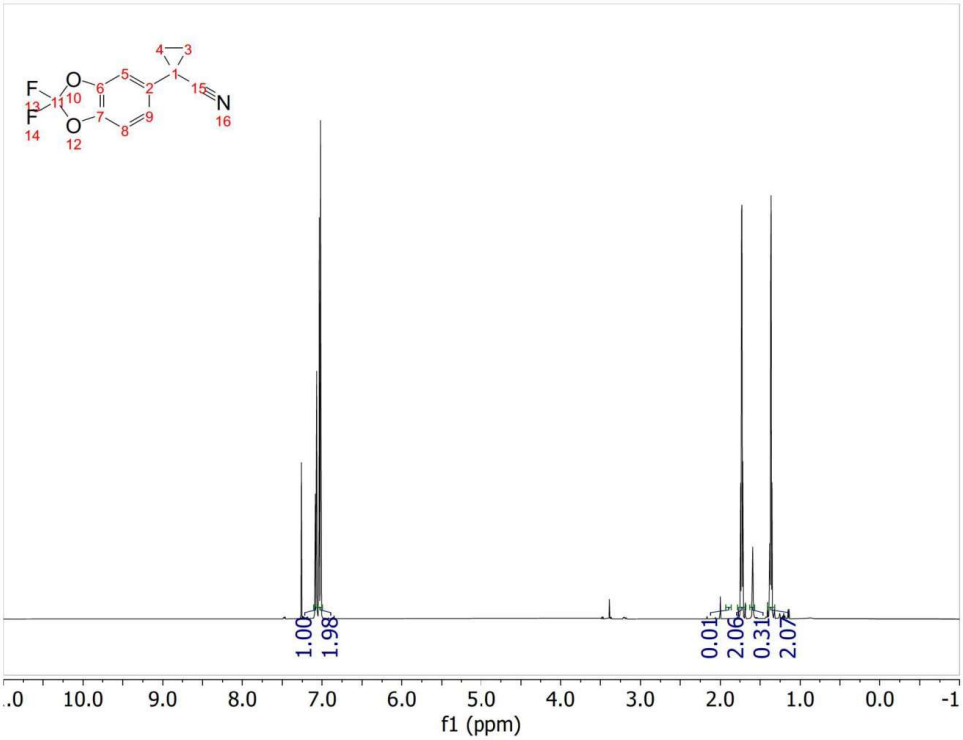
1.00
1.98
0.01
2.06
0.31
2.07
f1 (ppm)

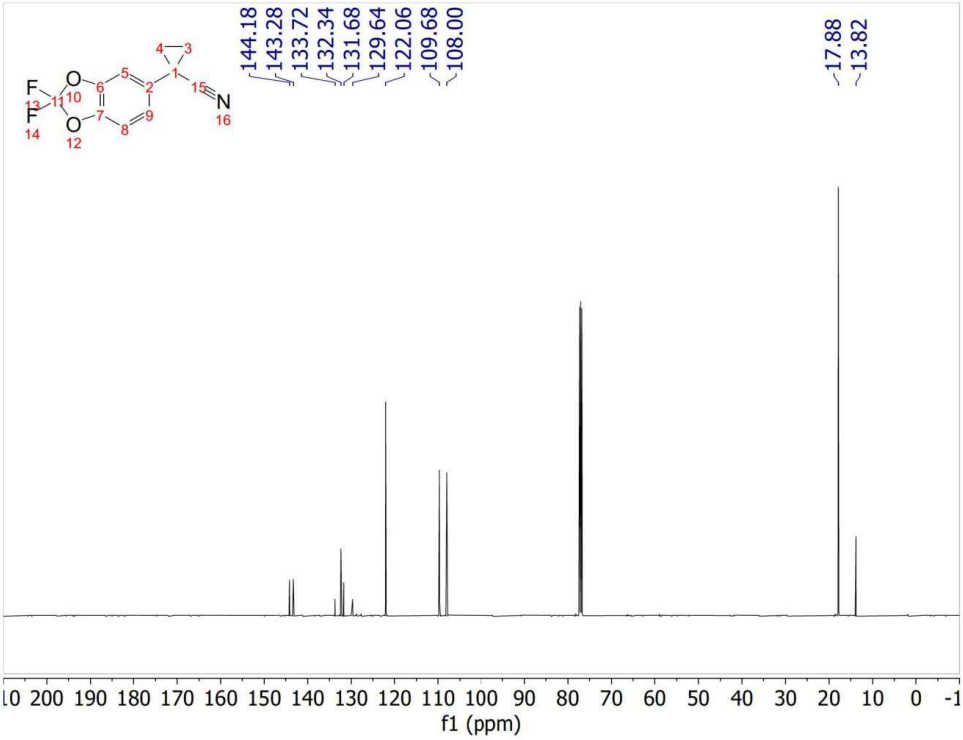
144.18
143.28
133.72
132.34
131.68
129.64
122.06
109.68
108.00
17.88
13.82
f1 (ppm)

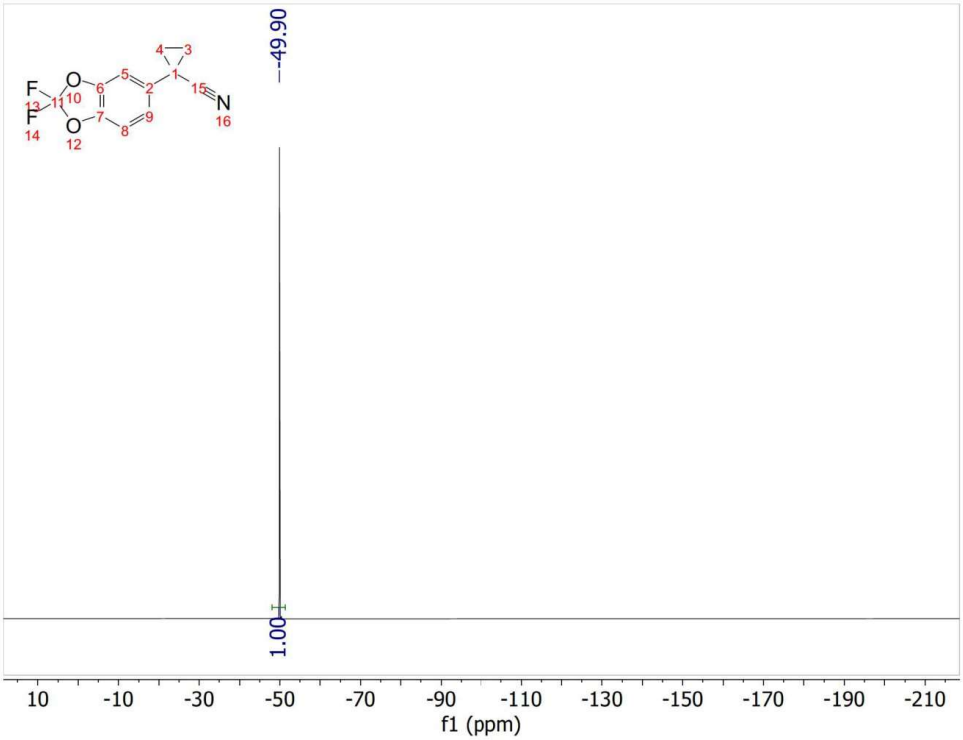
-49.90
1.00
10
-10
-30
-50
-70
-90
-110
-130
-150
-170
-190
-210
f1 (ppm)

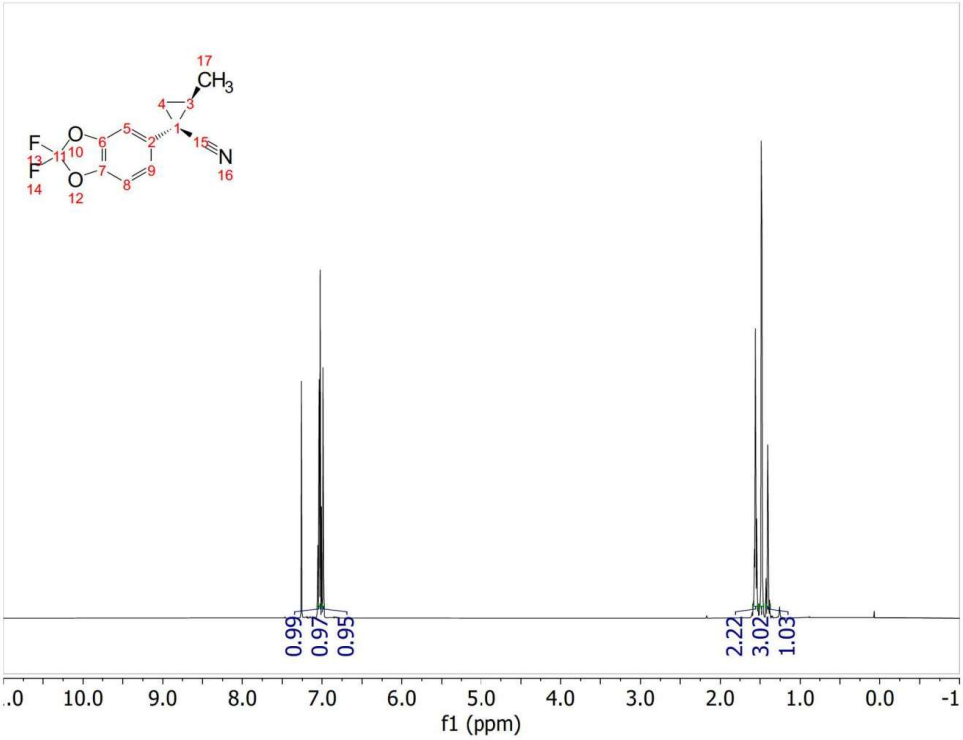
0.99
0.97
0.95
2.22
3.02
1.03
10.0
9.0
8.0
7.0
6.0
5.0
4.0
3.0
2.0
1.0
0.0
f1 (ppm)

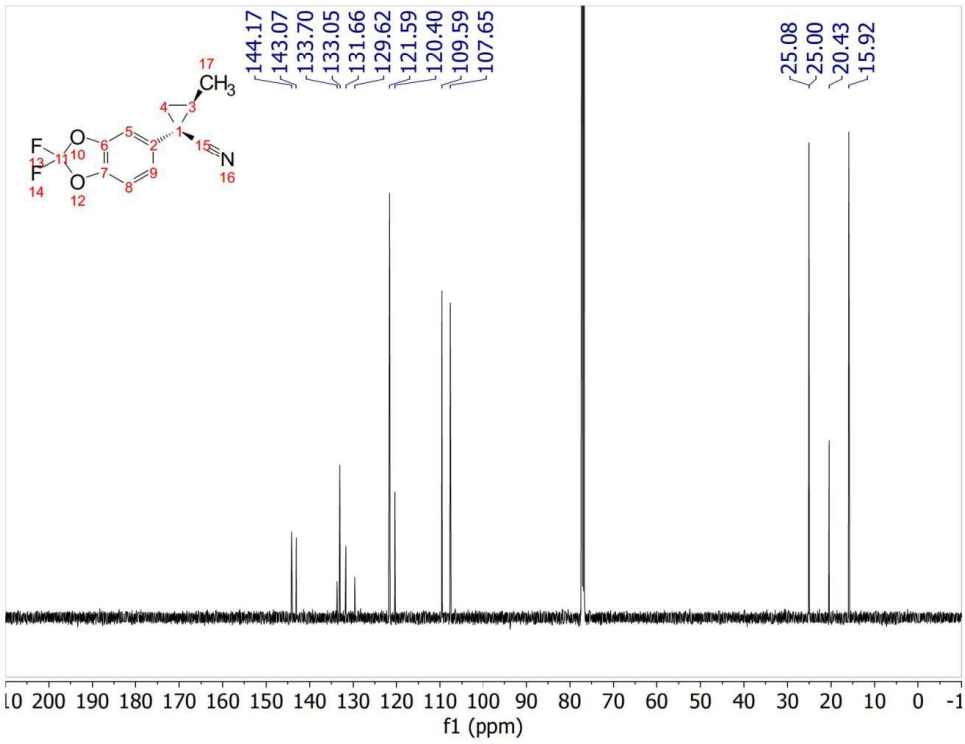
144.17
143.07
133.70
133.05
131.66
129.62
121.59
120.40
109.59
107.65
25.08
25.00
20.43
15.92
f1 (ppm)

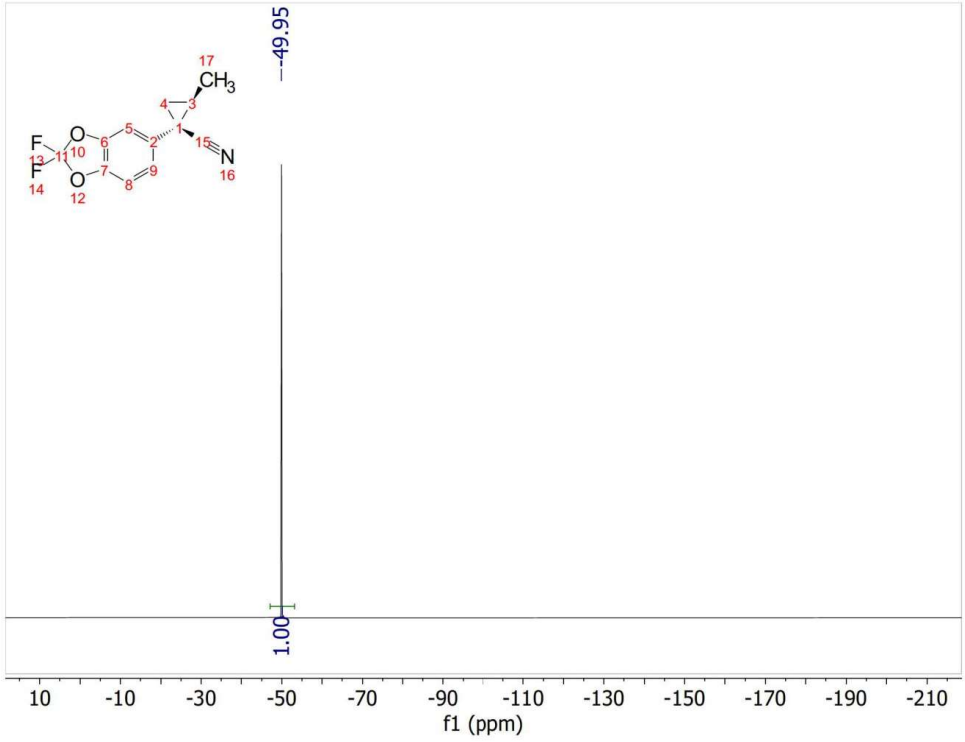
-49.95
1.00
f1 (ppm)

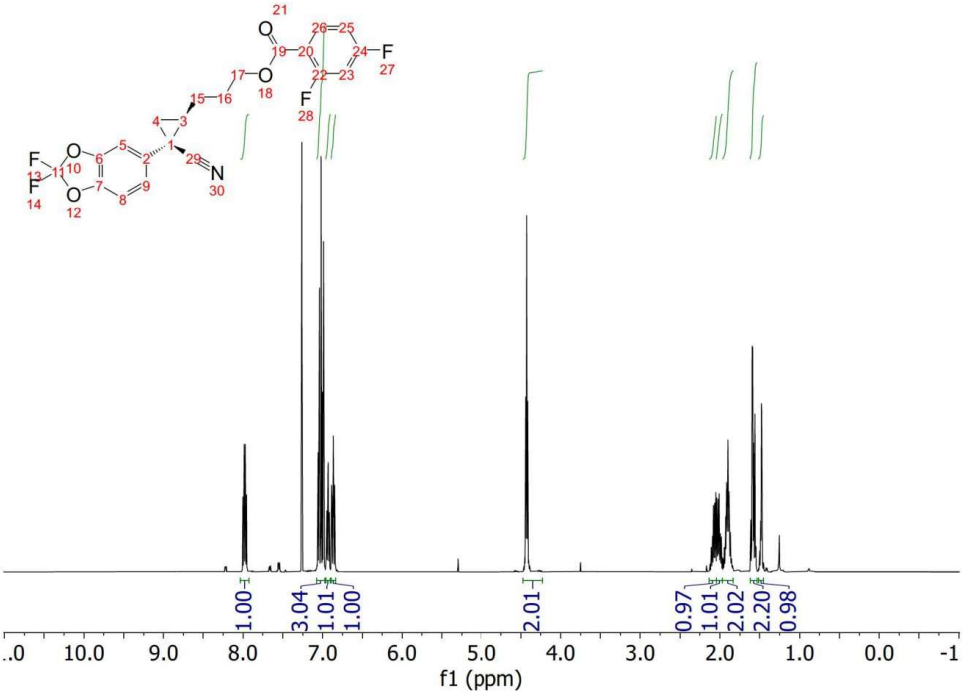
1.00
3.04
1.01
1.00
2.01
0.97
1.01
2.02
2.20
0.98
f1 (ppm)

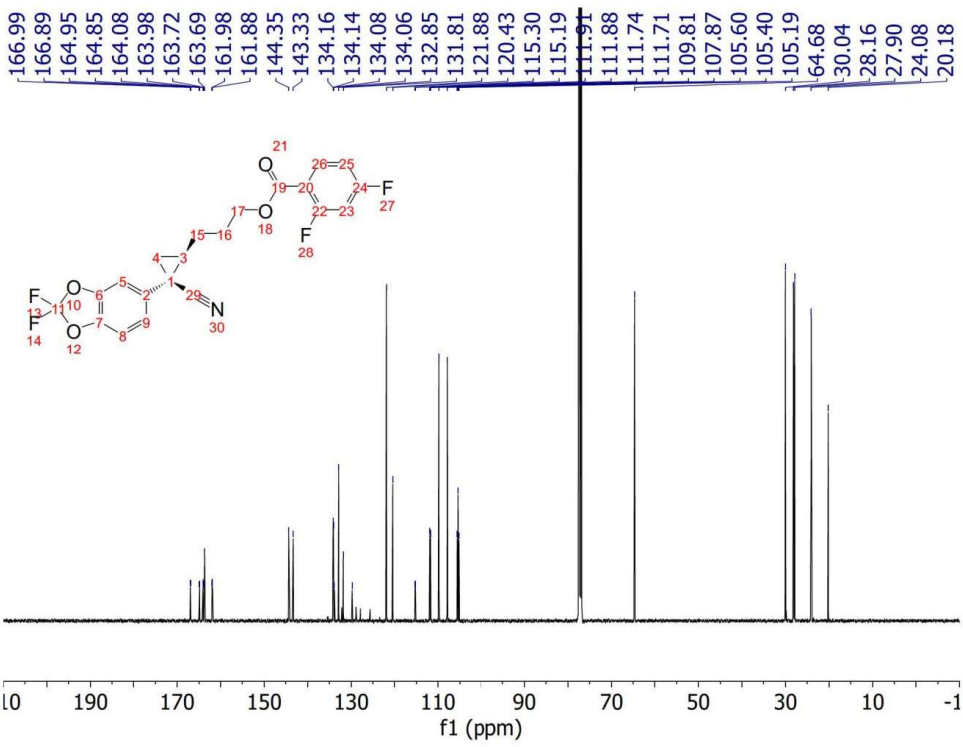
166.99
166.89
164.95
164.85
164.08
163.98
163.72
163.69
161.98
161.88
144.35
143.33
134.16
134.14
134.08
134.06
132.85
131.81
121.88
120.43
115.30
115.19
111.91
111.88
111.74
111.71
109.81
107.87
105.60
105.40
105.19
64.68
30.04
28.16
27.90
24.08
20.18
f1 (ppm)

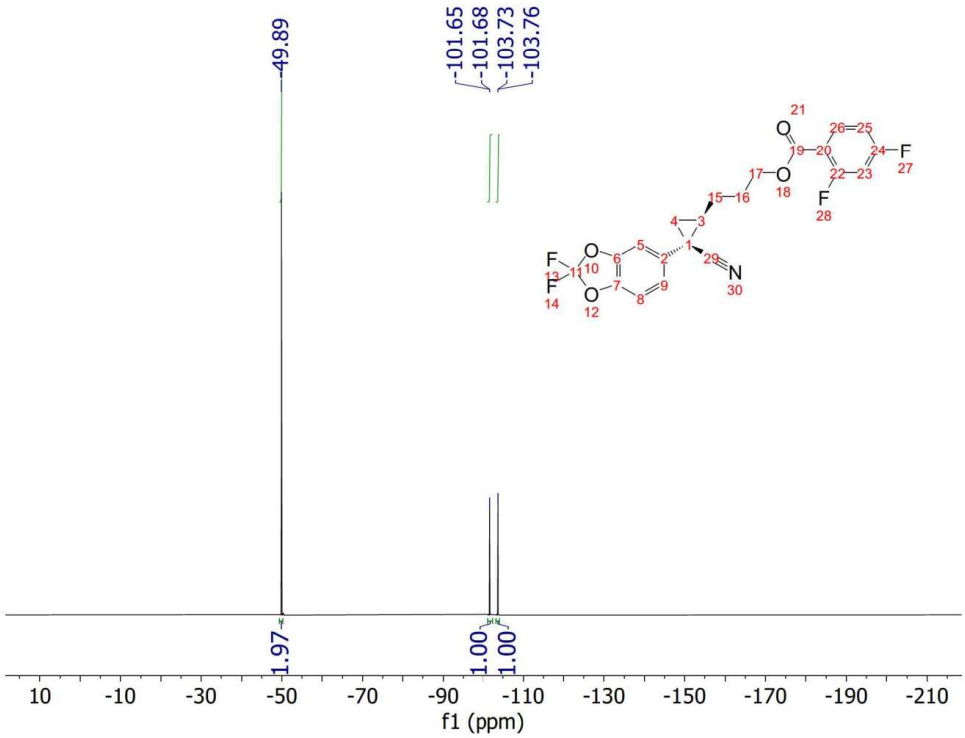
-49.89
-101.65
-101.68
-103.73
-103.76
1.97
1.00
1.00
10 -10 -30 -50 -70 -90 -110 -130 -150 -170 -190 -210
f1 (ppm)

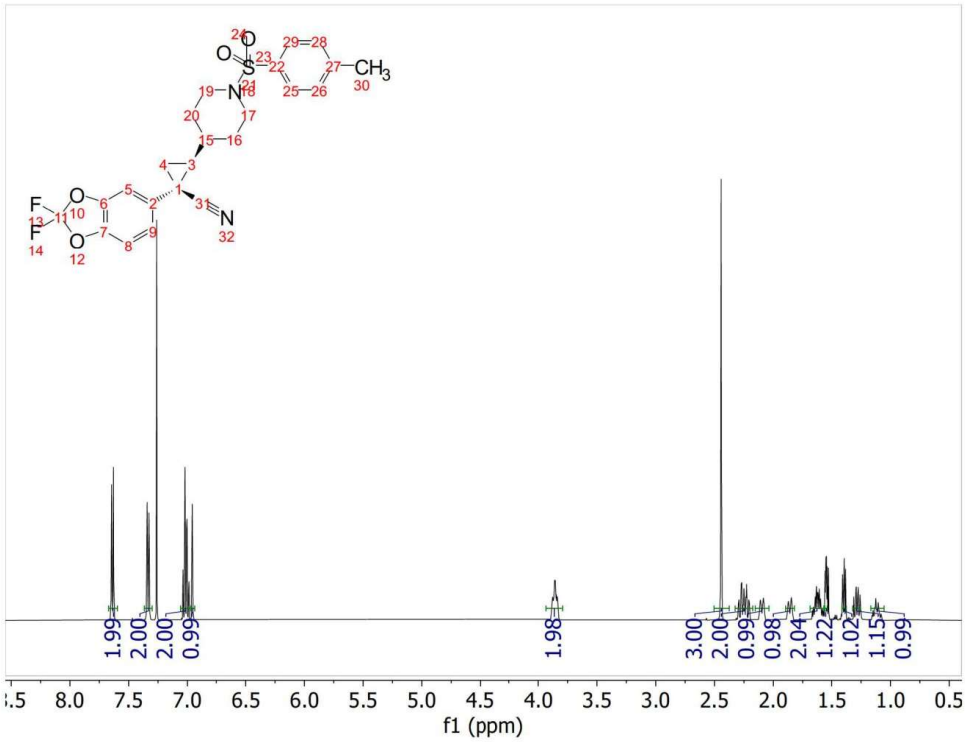
1.99
2.00
2.00
0.99
1.98
3.00
2.00
0.99
0.98
2.04
1.22
1.02
1.15
0.99
8.0 7.5 7.0 6.5 6.0 5.5 5.0 4.5 4.0 3.5 3.0 2.5 2.0 1.5 1.0 0.5
f1 (ppm)

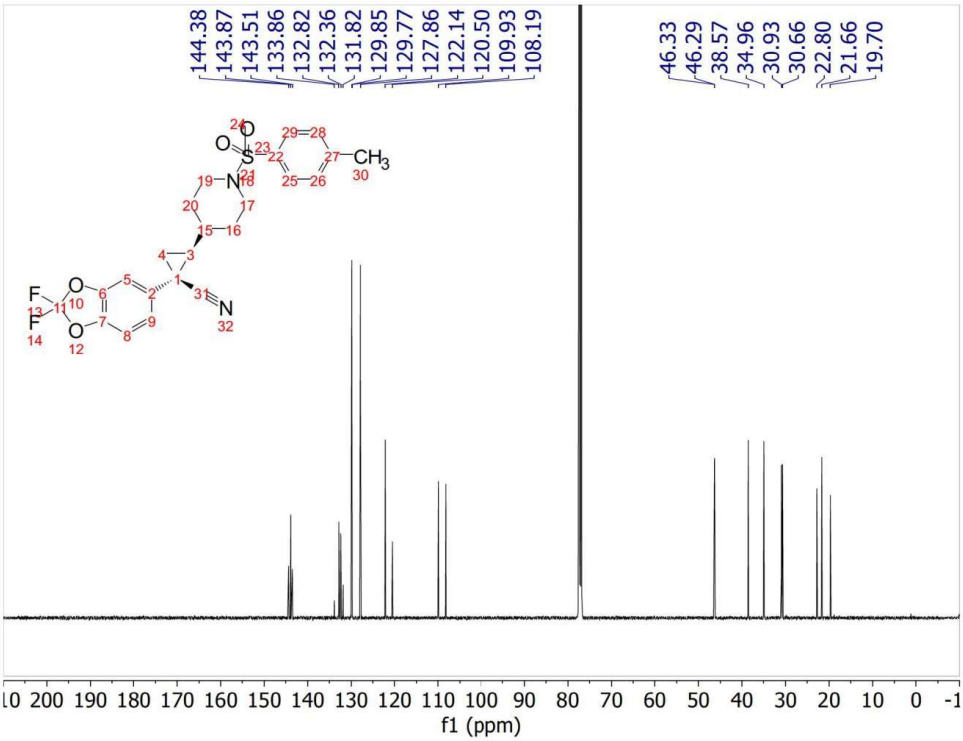
144.38
143.87
143.51
133.86
132.82
132.36
131.82
129.85
129.77
127.86
122.14
120.50
109.93
108.19
46.33
46.29
38.57
34.96
30.93
30.66
22.80
21.66
19.70
f1 (ppm)

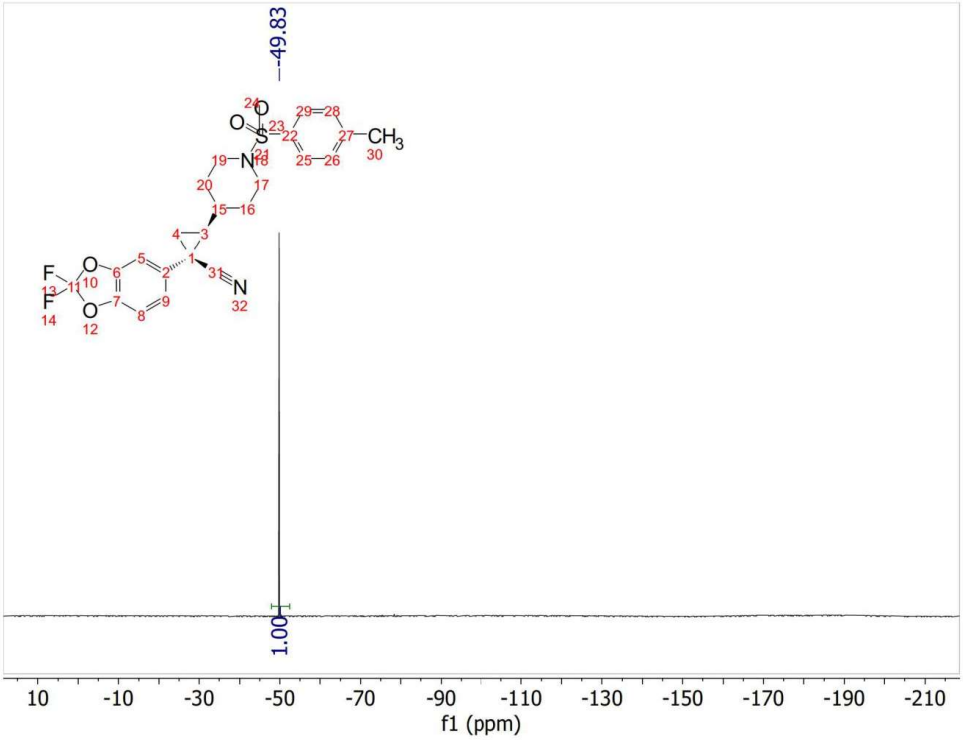
-49.83
1.00
f1 (ppm)

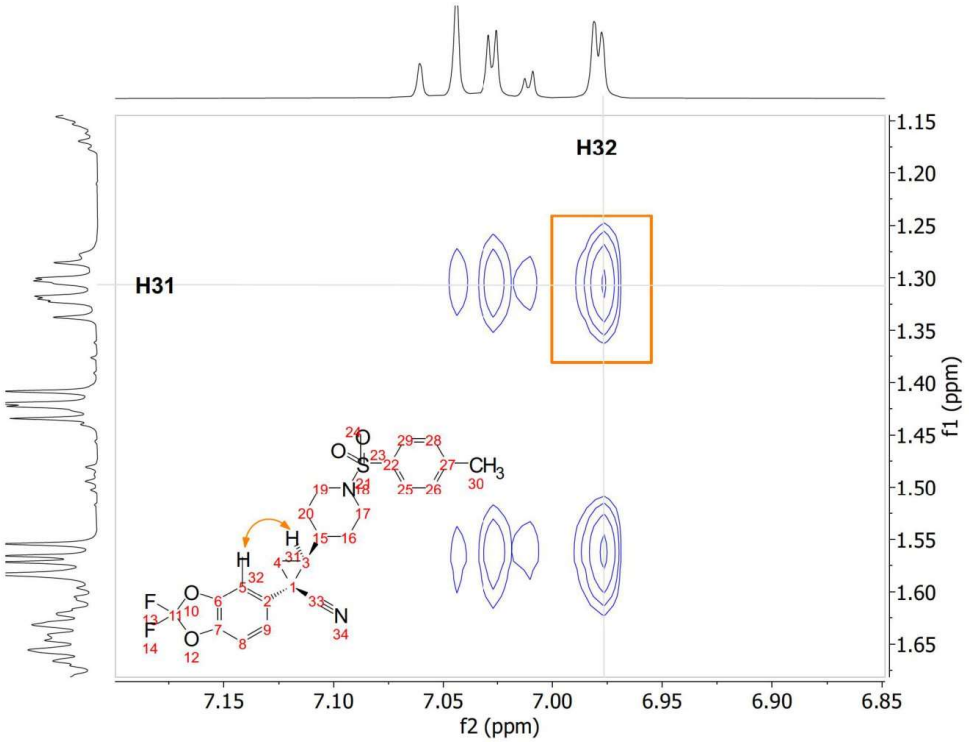
H32
H31
f2 (ppm)
f1 (ppm)
7.15
7.10
7.05
7.00
6.95
6.90
6.85
1.15
1.20
1.25
1.30
1.35
1.40
1.45
1.50
1.55
1.60
1.65

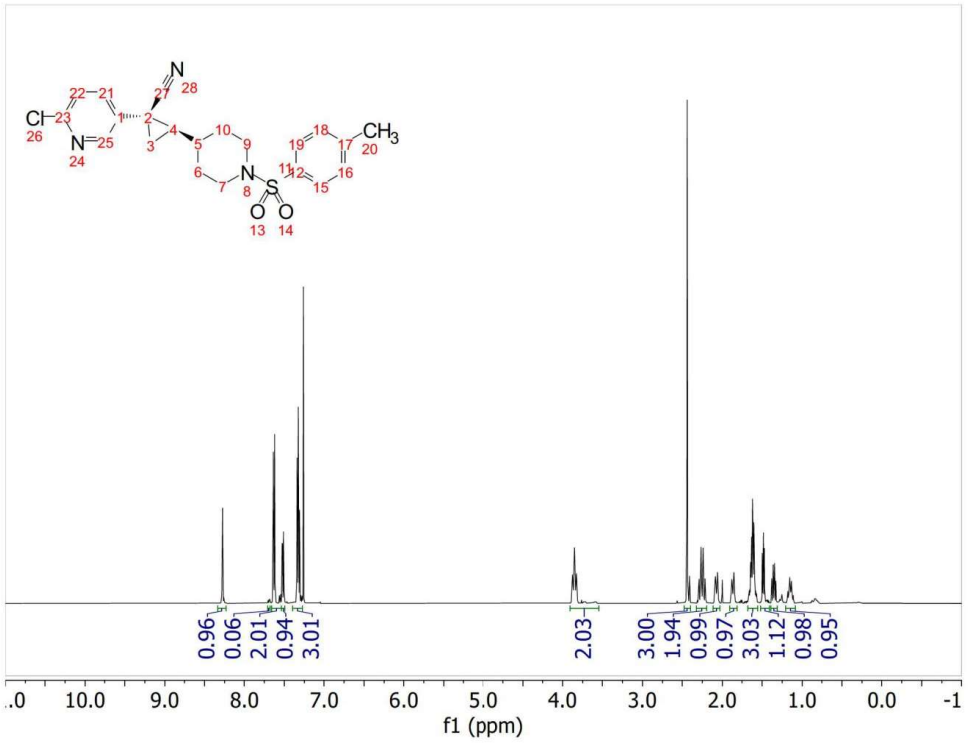
0.96
0.06
2.01
0.94
3.01
2.03
3.00
1.94
0.99
0.97
3.03
1.12
0.98
0.95
f1 (ppm)

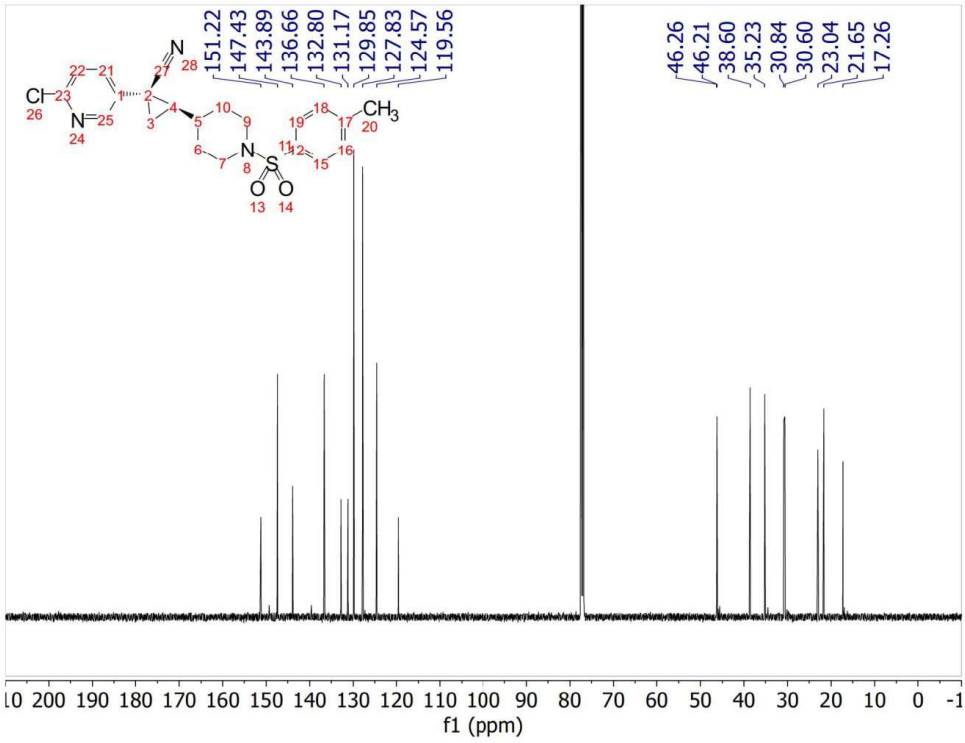
151.22
147.43
143.89
136.66
132.80
131.17
129.85
127.83
124.57
119.56
46.26
46.21
38.60
35.23
30.84
30.60
23.04
21.65
17.26
f1 (ppm)

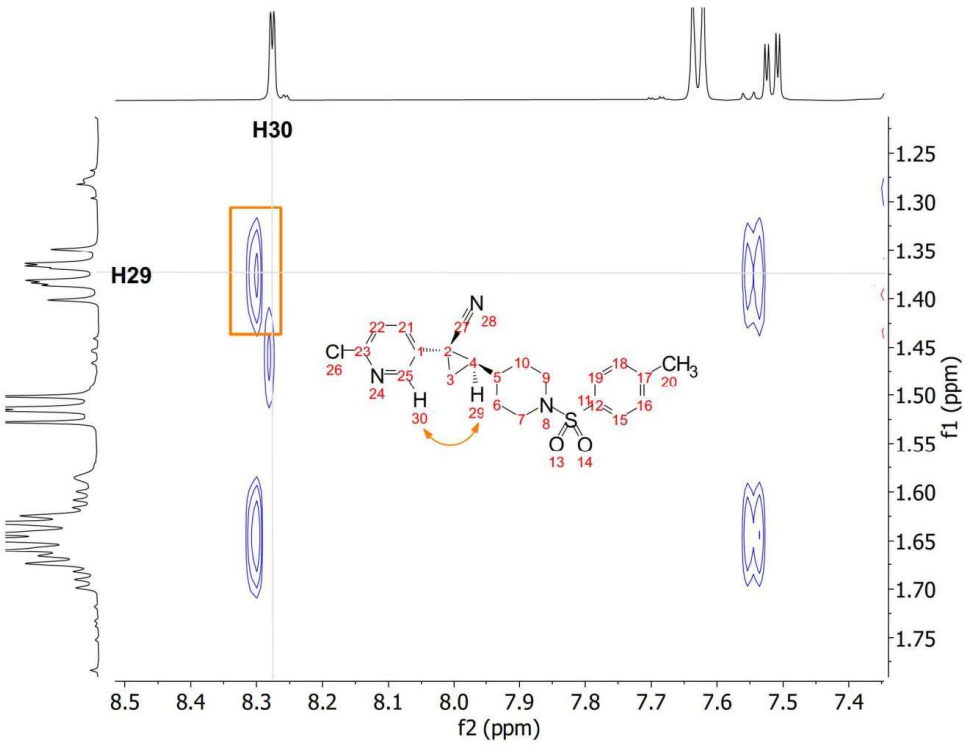
H30
H29
f2 (ppm)
f1 (ppm)